



Waste Isolation Pilot Plant Technical Assessment Team Report

March 17, 2015

SRNL-RP-2014-01198

Revision 0



DISCLAIMER

This work was prepared under an agreement with and funded by the U.S. Government. Neither the U.S. Government or its employees, nor any of its contractors, subcontractors or their employees, makes any express or implied:

1. warranty or assumes any legal liability for the accuracy, completeness, or for the use or results of such use of any information, product, or process disclosed; or
2. representation that such use or results of such use would not infringe privately owned rights; or
3. endorsement or recommendation of any specifically identified commercial product, process, or service.

Any views and opinions of authors expressed in this work do not necessarily state or reflect those of the United States Government, or its contractors, or subcontractors.

Printed in the United States of America

**Prepared for
U.S. Department of Energy**

**Keywords: Waste Isolation Pilot Plant,
WIPP, transuranic, TRU, drum**

Retention: *Permanent*

Waste Isolation Pilot Plant Technical Assessment Team Report

SRNL-RP-2014-01198

Revision 0

SIGNATURES

WPP TECHNICAL ASSESSMENT TEAM

David L. Wilson, Savannah River National Laboratory

 Date 3/18/15

Michael L. Baker, Oak Ridge National Laboratory


 Date 3/18/15

Bradley R. Hart, Lawrence Livermore National Laboratory

 Date 3/18/15

John E. Harris, Savannah River National Laboratory

 Date 3/18/15

Jon M. Schwartz, Pacific Northwest National Laboratory

 Date 3/19/15

Paul E. Stover, Sandia National Laboratory

 Date 3/19/2015

REVIEWER
 Michael Kneek, Deputy Under Secretary for Science and Energy
 United States Department of Energy

 Date 3/23/15

APPROVAL
 Terry A. Michalske, Director
 Savannah River National Laboratory

 Date 3/24/15

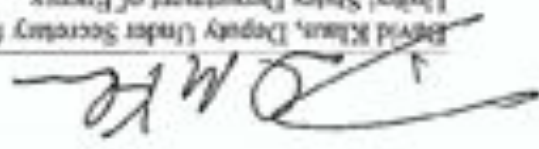
David Klaus, Deputy Under Secretary for Management and Performance
 United States Department of Energy

 Date 3/26/15

TABLE OF CONTENTS

LIST OF FIGURES	6
LIST OF TABLES	10
LIST OF ABBREVIATIONS AND ACRONYMS	12
1.0 EXECUTIVE SUMMARY	13
2.0 BACKGROUND	14
3.0 WIPP TAT ASSESSMENT STRATEGY	17
3.1 TAT INVESTIGATIVE CONSTRAINTS	17
3.2 TAT TECHNICAL ASSESSMENT AREA OBJECTIVES	18
3.3 TAT METHODS OF INQUIRY	19
3.4 UTILIZATION OF NATIONAL LABORATORY EXPERIENCE AND EXPERTISE	22
4.0 OVERARCHING CONCLUSION AND KEY JUDGMENTS	23
4.1 CONTENTS OF 68660 WERE CHEMICALLY INCOMPATIBLE.	23
4.2 DRUM 68660 BREACHED AS THE RESULT OF INTERNAL CHEMICAL REACTIONS THAT GENERATED HEAT AND PRODUCED GASES THAT BUILT UP PRESSURE SUFFICIENT TO OVERCOME THE DRUM VENT AND SEAL	27
4.3 DRUM 68660 WAS THE SOURCE OF THE CONTAMINATION IN WIPP P7R7	33
4.4 INITIATION OF THE THERMAL RUNAWAY WAS INTERNAL AND NOT CAUSED BY PHENOMENA OUTSIDE DRUM 68660.	34
4.5 THERMAL AND MECHANICAL EFFECTS RESULTED IN THE MOVEMENT OF MATERIAL DURING THE RELEASE EVENT AND CAUSED THE DAMAGE OBSERVED IN P7R7; THE RELEASE DID NOT RESULT FROM A DETONATION.	36
5.0 SUMMARY	38
APPENDIX A. TAT APPROACH TO MITIGATING UNCERTAINTIES	39
APPENDIX B. SAMPLING INTEGRATED SUMMARY REPORT	42
APPENDIX C. ANALYSIS INTEGRATED SUMMARY REPORT	48
APPENDIX D. MODELING INTEGRATED SUMMARY REPORT	76
APPENDIX E. DRUM CHARACTERIZATION INTEGRATED SUMMARY REPORT	150
APPENDIX F. REACTION CHEMISTRY AND HYPOTHESES	182
APPENDIX G: SUMMARY OF REACTIVITY TESTING	202
ATTACHMENT 1. TAT MEMBER QUALIFICATIONS	228
ATTACHMENT 2. WASTE ISOLATION PILOT PLANT (WIPP) FEBRUARY 14, 2014 EVENT TECHNICAL ASSESSMENT TEAM (TAT) CHARTER	257
ATTACHMENT 3. WASTE ISOLATION PILOT PLANT EVENT TECHNICAL ASSESSMENT TEAM PROJECT PLAN	260

LIST OF FIGURES

Figure 2-1. Panel 7 Room 7 configuration	14
Figure 2-2 Visual evidence of breach of drum located at position 16-4 in P7R7 at WIPP	15
Figure 3-1 Notional depiction of WIPP TAT investigative strategy to reduce uncertainty in event analysis	22
Figure 4-1. Processing of parent Drum S855793 to produce sibling Drums 68660 and 68685	24
Figure 4-2.TAT Model of Drum 68660 contents and distribution based on x-rays of Drum 68660	25
Figure 4-3. Calculated temperature profiles in Drum 68660 after 70 days.	29
Figure 4-4. Thermogravimetric-mass spectroscopy (TG-MS) analysis of debris from the release	30
Figure 4-5. Analysis results for case with original estimate of properties and “slow” loading (left) matches observed damage seen in post-event photograph of Drum 68660 showing discoloration and lid displacement (right).	32
Figure 4-6. Fire and radiological event locations within WIPP	35
Figure A-1. Notional depiction of WIPP TAT investigative strategy to reduce uncertainty in event analysis	41
Figure B-1. Swiffer multi-sampler, PVC sampler, and Multi-sampler device being deployed on a fifty-foot rod to sample 15-5.	43
Figure B-2. Delrin®/Teflon® sampler, shown with Teflon® vial in the collector and with Teflon® vial sealed for sample transport.	44
Figure C-1. SEM (A) and EDS (B) analysis of the debris from the parent drum.	53
Figure C-2. (a) Particle under white light and a 10x objective. (b) Particle illuminated by an excitation band of 375-425 nm observing the emission of 475 nm and longer. (c) The emission spectra of particle (blue) overlaid with the typical kitty litter (red).	56
Figure C-3. Optical microscopy of R15 C5 particles.	57
Figure C-4. Optical Microscopy of R15 C5 particles.	57
Figure C-5. (a) SEM image of particles collected from R15 C5 and (b) Representative EDS of sample.	57
Figure C-6. (a) SEM of small particles from R15 C5 and (b) EDS of particles.	57
Figure C-7. Elongated piece of steel from the sample collected from the lip of R16 C4.	58
Figure C-8. Polarized light microscopy image of (a) salt-like particles from R15 C5 and (b) “hairy” particle from R15 C5.	58
Figure C-9. SEM analysis of salt particles from R16 C4.	59
Figure C-10. SEM-EDS of small Pu particle associated with hairy salt particle from R16 C4.	59
Figure C-11. SEM-EDS of a small particle of Pb associated with the hairy salt particle from R16 C4.	59
Figure C-12. Radiograph of job control solid waste layer in Drum 68660 showing the glove-box glove.	60
Figure C-13. SEM-EDS analysis of sample from the lip of R16 C4 showing a bismuth particle.	61
Figure C-14. XRD analysis of the R15 C5 sample.	62
Figure C-15. TG-MS analysis of debris from R15 C5 under argon	63
Figure C-16. MS analysis of the evolved gases from the decomposition of R15 C5 under argon.	63
Figure C-17. FTIR spectra of the solid R15 C5 sample compared to Swheat Scoop®	64
Figure C-18. (a) Pictures of where ATR-IR data was collected on black particle 4 (blue dot) and black particle 5 (red dot) in subsample R16 C4. (b) Overview picture of subsample R16 C4, loose powder that was collected from the Swiffer sampler that was landed near the lip of the drum that breached (R16 C4). (c) IR spectra of black particle 4 (blue) and black particle 5 (red).	65
Figure C-19. FTIR spectra of cellulose (chromatography paper) and nitrocellulose at room temperature. [Coatas, 2014]	66
Figure C-20. FTIR of the CH ₂ Cl ₂ extract of R15 C5.	67
Figure C-21. FTIR spectrum of a particle collected from the methylene chloride extract of R15 C5 compared to cellulose and Swheat Scoop®. Particle is similar to cellulose.	67
Figure C-22. MgO collected from R14 C2.	70
Figure C-23. Sample collected from R16 C4 using Swiffer head.	70
Figure C-24. MgO sample collected from super sack in Panel 7 Room 7.	70
Figure C-25. Dark particles found in the MgO samples from R14.	71
Figure C-26. XRD of MgO from R14 C2, R14 C4 and a reference MgO sample.	71

Figure C-27. XRD of MgO from super sack sampled at the surface.	72
Figure C-28. FTIR spectra from MgO from R14 C2, C4, and C8.	72
Figure C-29. FTIR spectrum of MgO from sack at face of room 7 panel 7.	72
Figure D-1. TAT Model of Drum 68660 contents and distribution based on x-rays of Drum 68660	87
Figure D-2. Waste equilibrium composition at 1 atm for waste processed with A) Swheat Scoop® and B) zeolite.	88
Figure D-3. A) 2D axisymmetric mesh with reflection about X axis and B) temperature profiles after 70 days. Model parameters are in Table 9.	88
Figure D-4. A) Axial centerline temperature, B) radial temperatures at 0.41 m, C) pressure, and decomposition gas mass in drum #68660.	89
Figure D-5. Adiabatic flame temperature and gas compositions for various mixtures of air with the decomposition gases predicted from Drum 68660.	90
Figure D-6. Calculated thermal runaway time with a hot radiation boundary temperature.	90
Figure D-7. The effect of thermal runaway of Drum 68660 on a nearby victim drum: A) fast thermal runaway of victim drum and B) slow thermal runaway of Drum 68660.	91
Figure D-8. Drum 68660 in WIPP.	93
Figure D-9. Skolnik CQ5508 Drum CAD geometry	95
Figure D-10. Tested Closure Ring Engineering Stress-Percent Strain Curves for a drum obtained from LANL.	96
Figure D-11. Tested Drum Lid Engineering Stress-Percent Strain Curves for a drum obtained from LANL.	96
Figure D-12. Slower ramped loading form for analyses (referred to as “Slow” load)	98
Figure D-13. Faster ramped loading form (and unloading) for analyses (referred to as “Fast” load)	98
Figure D-14. Analysis results for case with original estimate of properties and “fast” loading.	99
Figure D-15. Comparison of tested drum at LANL (Larranaga et al., 1999) left, and analysis results, right.	99
Figure D-16. Section showing lid deformation for initial property estimates and “fast” loading case.	100
Figure D-17. Analysis results for case with original estimate of properties and “slow” loading.	101
Figure D-18. As opening (Figure 1 has it after it is open)	101
Figure D-19. Analysis results for case with original estimate of properties, “slow” loading, and surrogate cask on top.	102
Figure D-20. Analysis results for case with test properties and “fast” loading.	103
Figure D-21. Analysis results for case with test properties and “slow” loading.	104
Figure D-22. Analysis results for case with test properties, “slow” loading with maximum ramp pressure of 50 psi, and surrogate cask on top.	105
Figure D-23. Analysis results for case with test properties, “slow” loading with maximum ramp pressure of 75 psi, and surrogate cask on top.	105
Figure D-24. Analysis results for case with test properties, “fast” loading with maximum ramp pressure of 75 psi, and surrogate cask on top.	106
Figure D-25. Permanently deformed lid from fire test (reproduced from Hasegawa et al. 1993)	108
Figure D-26. Optical image of Drum 68660 taken after the breach.	113
Figure D-27. Metal drum coupons exposed to a temperature of 300C in air.	114
Figure D-28. Metal drum coupons exposed to a temperature of 400C in air.	115
Figure D-29. Metal drum coupons exposed to a temperature of 500C in air.	115
Figure D-30. Metal drum coupons exposed to a temperature of 700C in air.	116
Figure D-31. Curves showing paint degradation kinetics. Time-to-blacken data are plotted as blue diamonds. Time-to- peel data are presented as red squares.	116
Figure D-32. Results of heating using a propane torch and heat gun.	117
Figure D-33. Images of polymers exposed to elevated temperatures.	119
Figure D-34: Salt hauling truck after the fire	121
Figure D-35: Fire and radiological event locations	121
Figure D-36: Smoke exiting the salt shaft	123
Figure D-37: Temperature near the top of the salt handling shaft on February 5th and 6th	124
Figure D-38: Carlsbad temperatures in early February	124

Figure D-39: Plan view showing principal mine relationships of air inlet shaft, truck fire, and P7R7	125
Figure D-40: WIPP flow model schematic	126
Figure D-41: Geometry of an axial segment in transient conduction model.	127
Figure D-42: Post-fire predicted mass flow rates and temperatures	130
Figure D-43: Vertical temperature profiles: air and shaft wall temperatures in AIS and SHS one hour after fire onset	132
Figure D-44: Predicted temperature versus depth into wall at tops and bottoms of AIS and SHS one hour after fire onset	132
Figure D-45: Predicted buoyancy-driven flows and 1st-law consistent flow for specified SHS base temperatures	133
Figure D-46: Total emittance of water vapor	135
Figure D-47: Carlsbad weather conditions between fire and release events	136
Figure D-48: Illustration of finite element model of MgO sack	138
Figure D-49: Bag surface temperature as a function of incident heat flux and time	139
Figure D-50: Approximate geometry of waste array in P7R7 (dimensions in feet)	140
Figure D-51: Results of CFD simulation (upper temperature bound)	141
Figure D-52: Results of CFD simulation (lower temperature bound)	142
Figure D-53: Waste Face at Panel 7 Room 7	143
Figure D-54: Transient Count Record from CAM151	144
Figure D-55: Plot of panel 7 airflow from Ted Wyka supplied spreadsheet (Wyka)	146
Figure D-56: Summary of flow-wise dispersion coefficients from various investigators	146
Figure D-57: Predicted transient concentration at CAM151 for various release time intervals	147
Figure D-58: Beta and alpha counts from filters at the surface in days following the release	148
Figure E-1. Processing of parent Drum S855793 to produce sibling Drums 68660 and 68685	151
Figure E-2. Flow chart showing processing of Drum 68660	152
Figure E-3. Timeline for Drum 68660 from inception to the release event.	152
Figure E-4. TAT Model of Drum 68660 contents and distribution based on x-rays of Drum 68660	153
Figure F-1. Schematic representations of amylose and amylopectin	185
Figure F-2. Oxidation of Glucose to Produce Trihydroxyglutaric Acid and Tartaric Acid	188
Figure G-1. Cutaway illustration of the Sandia Instrumented Thermal Ignition (SITI) experiment. Insulation is not shown.	205
Figure G-2. Thermocouple placement during Medium Scale experiments	208
Figure G-3. Comparison of ARC-measured self-heating rates for undried and dried 3.5 M HNO ₃ / Swheat Scoop®	210
Figure G-4. New Bomb	211
Figure G-5. ARC Bomb after 7.5 g 16 h dried 3.5 M HNO ₃ / Swheat Scoop® Experiment	211
Figure G-6. ARC Bomb after 7 g 7-day dried 3.5 M HNO ₃ / Swheat Scoop® Experiment	211
Figure G-7. ARC-measured thermal behavior of 3.5 g dried (H,Pb,Fe)TEAN after drying at 50-60°C for 2-4 hours	212
Figure G-8. ARC-measured thermal behavior of 7 g of (H,Pb,Fe)TEAN/ Swheat Scoop® dried at 50°C for 5.5 hours in bomb	213
Figure G-9. Exp386 temperature and pressure data. Contents were Swheat Scoop® and water. The vessel was sealed.	214
Figure G-10. (a) Exp386 video frame showing steam escaping after vessel seal failure. (b) Exp386 post-test debris.	214
Figure G-11. Exp388 temperature data. Contents were neutralized acid and Swheat Scoop®.	215
Figure G-12. Frames from Exp388 video showing two jets	215
Figure G-13. Exp388 post-test residue	215
Figure G-14. Exp390 temperature data. Contents were neutralized acid, Swheat Scoop®, magnesium nitrate hexahydrate, and sodium nitrate.	216
Figure G-15. Images from video of Exp390. Left: pressure-burst event accompanied by loud report, and right: decaying jet that followed the pressure-burst event.	216

Figure G-16. Exp390 post-test residue.	216
Figure G-17. Exp396 temperature data. Contents were over-neutralized acid, Swheat Scoop®, magnesium nitrate hexahydrate, and sodium nitrate.	217
Figure G-18. Image from video of Exp396.	217
Figure G-19. Post-test debris from Exp396.	217
Figure G-20. Exp401 initial ramp and hold at 105°C.	218
Figure G-21. Exp401 second part - reheated and held at 105°C for about 4 hours, then heated at 5°C/min.	218
Figure G-22. Image from video of Exp401.	218
Figure G-23. Post-test debris from Exp401.	218
Figure G-24. Temperature data from Exp403. Contents were based on the LANL WB-4 mix: Ca nitrate, Cr nitrate, Fe nitrate, Mg nitrate, Na nitrate, Pb nitrate, oxalic acid, and Swheat Scoop®. No liquids were added.	219
Figure G-25. Image from video of Exp403.	219
Figure G-26. Post-test images from Exp403. The left image shows that a substantial amount of material was expelled through the vent. The right image shows that the O-ring failed.	220
Figure G-27. Temperature data collected for Drum F over the course of the experiment. Thermocouples correspond to the arrangement shown in figure 2.	221
Figure G-28 Comparison of thermocouple 3 for each drum over the course of the experiment. “Drum A Pad” was the name given to the thermocouple measuring the ambient temperature immediately outside Drum A.	221
Figure G-29. Drum C headspace gas composition as a function of time.	222

LIST OF TABLES

Table 3 1. Samples collected in WIPP and LANL for TAT analysis	19
Table 3 2. TAT analytical techniques used to examine WIPP samples	20
Table B-1. Samples collected in WIPP in May 2014	43
Table B-2. Samples collected in WIPP in August 2014	44
Table B-3. Samples collected from parent drum S855973 at LANL on August 7, 2014	45
Table B-4. Analytical techniques used to examine WIPP samples	46
Table C-1. Composition of salts in 68660 (as described in the Model Section)	51
Table C-2. DSC data for reaction between lignocellulosics and various nitrate salts. [Wu, 1986]	54
Table C-3. Ratio of metal cations relative to sodium from the debris on R15 C5 and the parent drum.	69
Table D-1. Parent and sibling drum mass balance	83
Table D-2. Assumptions regarding Swheat Scoop® and neutralized liquids	83
Table D-3. Processed salts in 68660a	84
Table D-4. Processed liquids in 68660a,b	84
Table D-5. Drum 68660 with zeolite instead of Swheat Scoop®	84
Table D-6. Volumes and masses used to calculate zeolite mass	84
Table D-7. Various oxygen balances and reaction energies in 68660	85
Table D-8. Possible reactions in 68660 at 1 atm and 500 K	85
Table D-9. Model parameters for 68660	86
Table D-10. Result exploring maximum ramp pressure vs. time to maximum pressure.	107
Table D-11. Paint degradation kinetics obtained from analysis of thermal test results.	117
Table E-1. Parent and sibling drum mass balance	155
Table E-2. Assumptions regarding Swheat and processed liquids	156
Table E-3. Processed Salts in 68660 ^a	157
Table E-4. Processed liquids in 68660 ^{a,b}	157
Table E-5. MIN02 Salts in S855793 (Daughters 68660 and 68685)	157
Table E-6. Inventory of Nitrate Salt Types in Drum 68660	158
Table E-7. Pu and Am Inventory and Radiolytic Heat Generation from the Salts in Drum 68660	158
Table E-8. Am and Pu Activity Concentration Analyzed in the Liquids Phases after Flash Evaporation	159
Table E-9. Ranges for Pu and Am Inventory and Radiolytic Heat Generation in Drum 68660 Processed Liquid	160
Table E-10. Drums with processed liquid in them and whose parents contained oxalate salts	161
Table E-11. Drums with processed liquids and glove box gloves and whose parents contained oxalate salts	161
Table E-12. Drums with glove box gloves	161
Table E-13. Drums 60% full or less	161
Table E-14. Material Types (grams)	162
Table E-15. Processed LANL Waste Drums in Panel 7	163
Table E-16. Waste Drum Am241/Am243 Content Based on FRAM Using CCP Gamma Spectra	166
Table E-17. SRNL and PNNL Post-event Am and Pu Ratios	167
Table E-18. Calculated Average Pu and Am Ratios for all PNNL and SRNL Samples and their 2-sigma Uncertainties	168
Table E-19. Analytical Pu and Am Isotopic Data for MT52 Salts in S842528	169
Table E-20. LANL Processed Drums in Panel 7 Whose Parent Drums Contained MT42 Salts	169
Table E-21. Material Types in Parent Drum S846088	170
Table E-22. Remaining Eight Drums with MT52:MT53:MT54 Salt Mixtures	171
Table E-23. Analytical Am and Pu Isotopic Data for Salts in S844689 (Daughters 68647 and 68649)	172
Table E-24. Analytical Am and Pu Isotopic Data for Salts in S816692 (Daughter 68581)	172
Table E-25. Analytical Am and Pu Isotopic Data for Salts in S852895 (Daughters 68555 and 68609)	172
Table E-26. Analytical Am and Pu Isotopic Data for Salts in S833846 (Daughter 68653)	173
Table E-27. Analytical Am and Pu Isotopic Data for Salts in S845072 (Daughter 68666)	173
Table E-28. Analytical Am and Pu Isotopic Data for Salts in S855793 (Daughter 68660)	174

Table E-29. Daughters' Mixed Salts Pu240/Pu239 and Am241/Pu239 Ratios and FRAM Am241/Am243 Ratios	174
Table F-1. Melting Points of Selected Hydrated Metal Nitrates [Weast 1984]	192
Table G-1. Summary of tests and test parameters. Swheat Scoop® used in all tests. Unless noted, all tests were vented and heated at 5°C/min.	206
Table G-2. LANL WB-4 mixture and Exp403 target mass percentages	219
Table G-3. Drum C headspace gas composition data	223

LIST OF ABBREVIATIONS AND ACRONYMS

AIB	Accident Investigation Board
AIChE	American Institute of Chemical Engineers
Am	americium
APTAC	Automatic Pressure Tracking Adiabatic Calorimetry
ARC	accelerating rate calorimetry
atm	atmosphere
CAM	constant air monitor
CBFO	Carlsbad Field Office
CCP	Central Characterization Program
CCPS	Center for Chemical Process Safety
CFD	computational fluid dynamics
DOE	Department of Energy
EM	Office of Environmental Management
FAS	fixed air sampler
FTIR	Fourier transform infrared [spectroscopy]
HENC	high efficiency neutron counter
HEPA	high efficiency particulate air [filter]
IC	ion chromatography
INL	Idaho National Laboratory
LAFO	Los Alamos Field Office
LANL	Los Alamos National Laboratory
LCMS	liquid chromatography-mass spectrometry
LLNL	Lawrence Livermore National Laboratory
MT	material type
ORNL	Oak Ridge National Laboratory
P7R7	Panel 7 Room 7
PNNL	Pacific Northwest National Laboratory
Pu	plutonium
PVC	polyvinyl chloride
RTR	Real Time Radiography/Radiograph
SEM-EDS	scanning electron microscopy-energy dispersive x-ray fluorescence spectroscopy
SITI	Sandia Instrumented Thermal Ignition
SNL	Sandia National Laboratories
SRNL	Savannah River National Laboratory
SRNS	Savannah River Nuclear Solutions, LLC.
SWB	standard waste box
TAA	Technical Assessment Area
TAT	Technical Assessment Team
TG/DTA	thermogravimetric and differential thermal analysis
TEA	triethanolamine
TEAN	triethanolammonium nitrate
TG-MS	thermogravimetric- mass spectroscopy analysis
TRU	transuranic
U	uranium
W	watt
WCRR	Waste Characterization, Reduction, and Repackaging [facility]
WIPP	Waste Isolation Pilot Plant
XRD	x-ray diffraction [spectroscopy]

1.0 EXECUTIVE SUMMARY

This report provides the results of the Waste Isolation Pilot Plant (WIPP) technical assessment led by the Savannah River National Laboratory and conducted by a team of experts in pertinent disciplines from SRNL and Lawrence Livermore National Laboratory (LLNL), Oak Ridge National Laboratory (ORNL), Pacific Northwest National Laboratory (PNNL), and Sandia National Laboratories (SNL).

The charter of the WIPP Technical Assessment Team (TAT) was to determine to the extent feasible the mechanisms and chemical reactions that may have resulted in the breach of at least one waste drum and release of waste material in WIPP on February 14, 2014.

The TAT undertook an extensive process of historical data review, sample collection and analysis, laboratory testing, and computational modeling to understand the release event in WIPP P7R7. Investigative constraints, such as incomplete documentation of the processes used to create the drum that breached and the physical inaccessibility of the breached drum in WIPP, created uncertainties, which made collection and interpretation of scientific data alone insufficient to reconstruct the event fully. However, the TAT evaluated the uncertainties and utilized expert assessments of available information and analytical data to fulfill its charter.

Using this strategy, the TAT reached its overarching conclusion and five associated key judgments.

The TAT's *overarching conclusion* is that chemically incompatible contents of Drum 68660 from Los Alamos National Laboratory in combination with physical conditions (e.g., the configuration of the materials in the drum) supported exothermic chemical reactions leading to a thermal runaway; the consequent build-up of gases within the drum displaced the drum lid, venting radioactive materials and hot matter that further reacted with air or other materials outside the drum to cause the damage observed in WIPP P7R7.

The following key judgments led to and support that conclusion:

Key Judgment 1: Contents of Drum 68660 were chemically incompatible.

Key Judgment 2: Drum 68660 breached as the result of internal chemical reactions that generated heat and produced gases that built up pressure sufficient to overcome the drum vent and seal.

Key Judgment 3: Drum 68660 was the source of the radiological contamination in WIPP.

Key Judgment 4: Initiation of the thermal runaway was internal and not caused by phenomena outside Drum 68660.

Key Judgment 5: Thermal and pressure effects resulted in the movement of material during the release event and caused the damage observed in WIPP P7R7; the release did not result from a detonation.

2.0 BACKGROUND

WASTE ISOLATION PILOT PLANT

The mission of the Department of Energy's (DOE's) Waste Isolation Pilot Plant (WIPP) near Carlsbad, New Mexico is to provide permanent, underground disposal of defense-related transuranic (TRU) and TRU-mixed wastes (wastes that also have hazardous chemical components). WIPP is a deep geologic repository mined out of a thick bed of salt for the disposal of TRU waste generated primarily from the clean-up of DOE sites historically associated with the construction and maintenance of the nation's nuclear weapons stockpile. TRU waste typically consists of clothing, tools, debris, and inorganic salts left from the research and production of nuclear weapons. TRU waste is contaminated with small amounts of plutonium and other TRU radioactive elements. Over its lifetime, WIPP is expected to receive approximately 175,000 cubic meters of TRU waste from various DOE sites.

For the purposes of this report, the WIPP Technical Assessment Team (TAT) has adopted the nomenclature used by WIPP to describe the underground waste disposal units. Figure 2-1 depicts the configuration of waste drums and other materials in WIPP Panel 7 Room 7 (P7R7). Each WIPP disposal room consists of a series of rows and columns of waste with the waste containers placed in staggered positions to maximize disposal capacity. When referring to a location within the panel, the TAT uses a designation first of the row and second of the column within the room. For example, the location of Drum 68660 is Row 16, Column 4, which is abbreviated to 16-4.

Also depicted in Figure 2-1 are the locations of magnesium oxide (MgO) supersacks. The purpose of the MgO is to provide an engineered barrier that decreases the solubilities of the actinide elements in transuranic waste in any brine present in the post-closure repository; MgO will decrease actinide solubilities by sequestering carbon dioxide (CO₂) that would be produced should microbial activity consume the cellulosic, plastic, and rubber materials in the TRU waste. MgO supersacks were placed in every location annotated with a number (3000 or 4200) on top of a hexagonal shape. In the locations noted in beige, the supersack bags burned or melted during the release event. [DOE-CFO 2009]

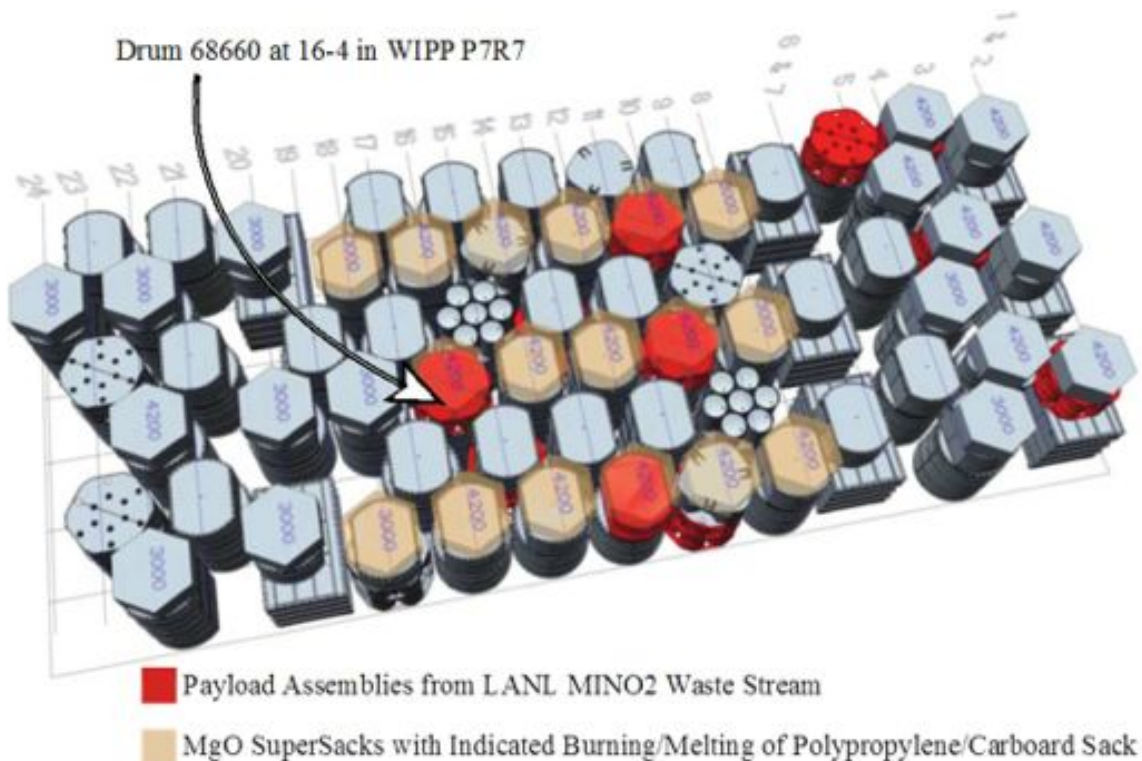


Figure 2-1. Panel 7 Room 7 configuration

WIPP RADIOACTIVE MATERIAL RELEASE EVENT

On Friday, February 14, 2014, an incident in P7R7 of the WIPP underground repository resulted in the release of radioactive material into the environment. No personnel were in the repository during the event, and no personnel were determined to have received external contamination; however, twenty-one individuals were identified through bioassay to have low-level amounts of internal contamination, and trace amounts of radioactive material were detected off-site following the incident. [AIB, April 2014]

WIPP ACCIDENT INVESTIGATION BOARD

On February 27, 2014, Matthew Moury, the Deputy Assistant Secretary for Safety, Security, and Quality Programs, DOE Office of Environmental Management (EM), formally appointed an Accident Investigation Board (AIB) to investigate the WIPP release in accordance with DOE Order 225.1B, *Accident Investigations*. That charge expanded the AIB's original scope to investigate the February 5, 2014 salt-hauling truck fire in the WIPP underground. The scope of the AIB's investigation is broad and includes identifying all relevant facts; determining direct, contributing, and root causes; developing conclusions; and determining measures to prevent recurrence. The scope of the AIB's investigation includes DOE programs and oversight activities. [Moury, March 2014]

The AIB's Phase 1 Investigation Report released in April 2014 concludes that the direct cause of the event was the "breach of at least one transuranic (TRU) waste container in the underground which resulted in airborne radioactivity escaping to the environment downstream of the HEPA filters." That conclusion is based on direct evidence of a breach of the drum located in the top of position of 16-4 in P7R7 (subsequently identified as Drum 68660 from LANL), as shown in Figure 2-2. The Phase 1 Investigation Report notes that "the exact mechanism of container failure . . . is unknown at this time and must be determined once access to the underground is restored. This will be investigated in Phase 2." [AIB, April 2014]



Figure 2-2. Visual evidence of breach of drum located at position 16-4 in P7R7 at WIPP

WIPP TECHNICAL ASSESSMENT TEAM

To complement the AIB investigation, on May 27, 2014, DOE established the TAT to determine to the extent feasible the particular mechanism(s) and chemical reactions that may have resulted in the failure of the waste drum and release of material in WIPP. This narrowly defined scope allowed the TAT to confine its investigation to the technical aspects of the release while the AIB conducted its broader investigation.

The TAT was chaired by the Savannah River National Laboratory (SRNL) and composed of members from SRNL and Lawrence Livermore National Laboratory (LLNL), Oak Ridge National Laboratory (ORNL), Pacific Northwest National Laboratory (PNNL), and Sandia National Laboratories (SNL).^a The TAT's national-laboratory team approach provided scientific and technical rigor and credibility needed to assess the event and support DOE's implementation of a WIPP recovery plan.

The TAT chairperson coordinated with the AIB Chair and reported to the DOE Deputy Under Secretary for Management and Performance (S-3). The Deputy Under Secretary for Science and Energy (S-4) served as the Technical Task Monitor of the TAT. The Assistant Secretary for Environmental Management (EM-1) was also a key stakeholder of the TAT activities. The TAT maintained independent authority to direct activities within its charter.^b

REFERENCES

1. [AIB, April 2014] Accident Investigation Board. April 2014. *Phase 1 Accident Investigation Report Radiological Release Event at the Waste Isolation Pilot Plant on February 14, 2014*. Office of Environmental Management. Department of Energy.
2. [DOE-CFO 2009] Appendix MgO-2009: Magnesium Oxide as an Engineered Barrier. Title 40 CFR Part 191 Subparts B and C: Compliance Recertification Application for the Waste Isolation Pilot Plant. United States Department of Energy Waste Isolation Pilot Plant. Carlsbad Field Office. Carlsbad, New Mexico.
3. [Moury, March 2014] Moury, Matthew. March 4, 2014. "Radiological Incident into the February 14, 2014 Event at the Waste Isolation Pilot Plant." Department of Energy. Office of Environmental Management. Department of Energy. Washington, DC.

^a See Attachment 3 to this report, *Waste Isolation Pilot Plant Event Technical Assessment Team Project Plan*, Attachment 2: "TAT Scope Overview by Laboratory."

^b See Attachment 2 to this report, "Waste Isolation Pilot Plant (WIPP) February 14, 2014 Event Technical Assessment Team (TAT) Charter."

3.0 WIPP TAT ASSESSMENT STRATEGY

DOE and the TAT recognized from the start that the TAT's retrospective evaluation of hypotheses as to the mechanism(s) that had caused the WIPP release might not lead to a definitive conclusion. However, DOE and the TAT also recognized that eliminating hypotheses from further consideration could be important to informing decisions about future WIPP operation.^c

To achieve the most technically definitive and defensible results from its sampling, analysis, modeling, testing, activities, the TAT planned and executed its work using accepted principles of forensic science and analytical chemistry, including traceability, quality control and assurance, and peer review.

However, collection and interpretation of scientific data alone were insufficient to reconstruct the event fully. In addition to evaluating the scientific data, the TAT evaluated uncertainties and utilized expert opinions to arrive at an overarching conclusion and key judgments regarding the mechanism(s) and chemical reactions that resulted in the drum failure and release of material in WIPP.

The TAT's assessment strategy included these components:

- Identification and acknowledgement of *constraints* to the investigation
- Establishment of *objectives* specifically designed to fulfill the TAT's charter
- Development and execution of *methods of inquiry* to meet the TAT's objectives while mitigating to the extent feasible the investigative constraints
- Use of the *scientific and technical experience and expertise* of the TAT members and the DOE national laboratories both to perform the TAT's investigative activities and to provide expert opinions to support its conclusions.

3.1 TAT INVESTIGATIVE CONSTRAINTS

The TAT recognized that identification and acknowledgement of constraints to the investigation were as important to accomplishing the TAT's mission as collecting and interpreting available data.

Initial visual imagery obtained by the AIB showed that one waste drum within WIPP P7R7 was breached. This confirmed that the release was due to an internal reaction in a drum and not an external event such as a roof collapse or bolt failure. The waste drum, identified as Drum 68660 (located at position 16-4), had been packaged at Los Alamos National Laboratory (LANL) and contained nitrate and oxalate salt TRU waste. Once the drum was identified as breached, a number of possible mechanisms were identified and were investigated during the course of the TAT's work. While the TAT was able to reach key judgments concerning the release, determining the exact cause was hindered by three principal constraints to the investigation:

1. **Access to the area in which the release occurred was limited.** Soon after the release, examination of the affected area was performed using remote tools and cameras. LANL Drum 68660 is nominally 32 feet from the "waste face," that is, the last row of waste emplaced in P7R7. Visual evidence that Drum 68660 was breached was obtained using a small camera mounted on a boom arm. Samples for laboratory analyses were collected remotely using the same boom arm. The results of Project REACH, the remote visual examination of P7R7 in January 2015, provided confirmation of the TAT's key judgment that Drum 68660 was the cause of the radiological release and the initiation of the resulting thermal event that consumed much of the available^d combustible material between rows 8 and 18 in P7R7. (See Figure 2-1.)
2. **Contents and configuration of the reactant mixture could not be exactly described.** LANL waste stream LA-MIN02-V.001 was generated in the 1970s and 1980s and generally resulted from plutonium (Pu)

^c See Attachment 2 to this report, "Waste Isolation Pilot Plant (WIPP) February 14, 2014 Event Technical Assessment Team (TAT) Charter."

^d Packaging material, primarily polymeric material used for waste package assembly and MgO containment, available to participate in subsequent spread of combustion.

recovery operations. Those recovery operations were accomplished using nitric acid digestion with Pu recovery and purification by ion exchange and oxalate precipitation. Following Pu removal, the liquid residues were evaporated and the evaporator bottoms cooled to precipitate the metal nitrate salts. Nitrate salts derived from ion-exchange effluents were washed with concentrated nitric acid, air dried, and packaged for storage. Nitrate salts derived from oxalate precipitation effluents also contained oxalate salts and were washed with water prior to air drying and packaging for storage. While process knowledge aided in understanding the composition of the waste, characterization data of the material placed in the parent drum of Drum 68660 are limited. Additionally, during processing operations, the waste from parent drums was distributed among multiple sibling drums, and other items (e.g., worn gloves, lead shielding, other job waste) often were added to the waste drums with limited characterization and documentation.

3. **Details about the nitrate salt waste processing operations were not fully documented.** The procedures used to process the drums in the LANL Waste Characterization, Reduction, and Repackaging (WCRR) facility produced limited and inconsistent documentation. For example, liquids recovered from the parent waste drums were characterized using pH-indicating paper and then “neutralized” by adding neutralizing agent. The material was then mixed and the resultant pH again measured with pH-indicating paper. In many cases, neither the initial nor final pH was recorded. Additionally, both the “neutralized” liquid and the nitrate salts were mixed with the absorbent Swheat Scoop® (“kitty litter”) at a target volume ratio of 3:1 Swheat Scoop®:waste material. Actual measurements of the salt volume/weight or the quantity of Swheat Scoop® used were not recorded. Ultimately, the goal of the WCRR operation is to produce drums suitable for shipment to WIPP, that is, meeting the requirements of “no prohibited materials” and “no free liquid” while staying within the allowed content window as determined by gross radioassay.

Those conditions constrained the TAT’s ability to obtain data that would support definitive conclusions as to the cause of the release. They did not, however, prevent the TAT from reaching an overarching conclusion and associated key judgments.

3.2 TAT TECHNICAL ASSESSMENT AREA OBJECTIVES

The TAT pursued objectives in four inter-related technical assessment areas (TAAs) to determine the mechanism(s) and chemical reactions that resulted in the drum breach and release of material in WIPP.

Those objectives were

1. **Site Assessment and Sampling:** Work closely with the AIB to assess sites pertinent to the TAT mission (in WIPP and LANL); identify, collect, and preserve samples from the sites; and distribute the samples to the national laboratories for analyses.^e
2. **Analysis and Characterization:** Develop and implement a strategy for characterization and analysis of collected samples and interpretation of resulting data.^f
3. **TRU Drum Processes and Practices:** Assemble information about the history of the suspect drum, characterization of TRU drums generally, and characterization of the bags containing magnesium oxide (MgO) in the WIPP underground to familiarize the TAT with waste form processes, history, and materials related to the containers in WIPP and LANL.^g
4. **Mechanism, Hypothesis, and Technical Integration:** Evaluate potential reaction chemistry and release mechanisms that could explain the WIPP release and associated observations; use available data and analyses from other TAAs to determine whether the WIPP event was due to a single drum failure or whether additional drums were involved; and present options to guide future inspection, sampling, and analysis programs to prove

^e For details about TAT Site Assessment and Sampling activities and conclusions, see Appendix B, Sampling Integrated Summary Report.”

^f For details about TAT Analysis and Characterization activities and conclusions, see Appendix C, “Analysis Integrated Summary Report.”

^g For details about TAT TRU Drum Processes and Practices activities and conclusions, see Appendix E, “Drum Characterization Integrated Summary Report.”

or disprove postulated reactions. Interface directly with LANL’s team of scientists as needed to understand LANL’s investigation of waste compatibility and reaction energetics.^{h, i}

3.3 TAT METHODS OF INQUIRY

The TAT developed and executed the following methods of inquiry to meet its objectives while mitigating to the extent feasible the investigative constraints and maximizing the usefulness of available information:

1. **Visual examination and sample analyses.** The TAT relied heavily on visual documentation obtained by the AIB. Given the limited access to the breached drum, this visual observation provided important information to allow the TAT to assess potential reaction mechanisms and sequences. In addition to the visual observation, the TAT did have access to samples collected during the event (e.g., fixed air sampler, or FAS, and constant air monitor, or CAM, filters and cartridges) and material recovered from the area near the breached drum. Analyses of these samples provided important insights into the event. Table 3-1 lists samples collected for TAT analysis, and Table 3-2 lists the variety of analytical methods the TAT used to interrogate samples.^j

Table 3-1. Samples collected in WIPP and LANL for TAT analysis

Chain of Custody	Sample Location	Sample Type	Date Collected
14-0183	None (clean blanks)	PVC, smears, sticky tape	May 2014
14-0183	15-5 SWB	Ejected debris from multi-sampler	May 2014
14-0183	16-4 drum lip	MgO from multi-sampler	May 2014
14-0182	16-4	MgO from sticky pad	May 2014
14-0182	14-4	Bulk MgO from PVC sampler	May 2014
14-0182	14-6	Bulk MgO from PVC sampler	May 2014
14-0182	14-2	Bulk MgO from PVC sampler	May 2014
9572 Sample #1	16-4 drum	MgO from Delrin [®] sampler	August 2014
9572 Sample #2	15-5 SWB	Ejected debris from Delrin [®] sampler	August 2014
9572 Sample #3	15-5 SWB	Ejected debris from Delrin [®] sampler	August 2014
9572 Sample #6	Front of Panel 7	Bulk MgO from Delrin [®] sampler	August 2014
9572 Sample #7	Front of Panel 7	Bulk MgO from Delrin [®] sampler	August 2014
69120 (from parent drum S855793)	Authentic	Glass filter	August 7, 2014
	Quality control	Clean, glass filter taken into contaminated area	August 7, 2014
	Quality control	Clean, glass filter (transport blank)	August 7, 2014
	Authentic	Solid debris in Teflon bottle	August 7, 2014
	Quality control	Clean, empty Teflon bottle taken into contaminated area	August 7, 2014
	Quality control	Clean, empty Teflon bottle (transport blank)	August 7, 2014
	Authentic	IAEA wipe sample	August 7, 2014
	Quality control	Clean, IAEA wipe taken into contaminated area	August 7, 2014

^h For details about TAT Mechanism, Hypothesis, and Technical Integration activities and conclusions, see Appendix F, “Reaction Chemistry and Hypotheses.”

ⁱ Additional detail about the TAT objectives may be found in Attachment 3 to this report, *Waste Isolation Pilot Plant Event Technical Assessment Team Project Plan*, Section 3.0: “Primary Technical Assessment Areas.”

^j See Appendix B, “Sampling Integrated Summary Report,” and Appendix C, “Analysis Integrated Summary Report.”

Chain of Custody	Sample Location	Sample Type	Date Collected
	Authentic (Archive)	Glass filter	August 7, 2014
	Quality control (Archive)	Clean, glass filter taken into contaminated area	August 7, 2014
	Quality control (Archive)	Clean, glass filter (transport blank)	August 7, 2014
	Authentic (Archive)	Solid debris in Teflon bottle	August 7, 2014
	Quality control (Archive)	Clean, empty Teflon bottle	August 7, 2014
	Quality control (Archive)	Clean, empty Teflon bottle opened in contaminated area	August 7, 2014
	Authentic (Archive)	IAEA wipe sample	August 7, 2014
	Quality control (Archive)	Clean, IAEA wipe taken into contaminated area	August 7, 2014

Table 3-2. TAT analytical techniques used to examine WIPP samples

Analysis	What's Detected?	Questions Addressed
Gamma analysis	Radioactivity	<ul style="list-style-type: none"> Where in WIPP did contamination spread? Do isotopes observed in the environment reflect the expected contents of the Drum 68660?
Optical microscopy	Sample morphology	<ul style="list-style-type: none"> Is the sample homogeneous? Are Swheat Scoop® particles present in the sample?
Scanning electron microscopy (SEM)	Particles	<ul style="list-style-type: none"> Particle morphology Are Swheat Scoop® particles present in the sample? When combined with energy dispersive spectroscopy, provide particle composition (detected lead, sodium, chloride, magnesium, and potassium)
Fourier Transform infrared spectroscopy (FTIR)	Non-destructive technique; identifies bulk materials	<ul style="list-style-type: none"> Are oxidized organics (carbohydrates) and nitrated organics present? Are nitrates, nitrites, carbonates, and metal oxides present? Distinguish MgO, Mg(OH)₂, and MgCO₃ to determine whether MgO was exposed to significant amounts of water or CO₂
RAMAN Spectroscopy	Non-destructive technique; identifies bulk materials	<ul style="list-style-type: none"> Are nitrates, nitrites, phosphates, or chlorates present? Is carbonaceous soot present?
X-ray fluorescence (XRF)	Non-destructive determination of elemental composition	<ul style="list-style-type: none"> Are metals present that might have catalyzed chemical reactions?
X-ray diffraction (XRD)	Atomic and molecular structure of a crystal	<ul style="list-style-type: none"> Are crystalline reaction products in the debris? Distinguish MgO, Mg(OH)₂, and MgCO₃ to determine whether MgO was exposed to significant amounts of water or CO₂

Analysis	What's Detected?	Questions Addressed
Ion chromatography (IC)	Anions and cations	<ul style="list-style-type: none"> • Are nitrates, nitrites, chloride, sulfate, fluoride, oxalate, or other anions observed in the sample? • Presence of nitrite and carbonate consistent with hypothesis of reaction of Swheat Scoop® and metal nitrate salts
Inductively coupled plasma mass spectrometry (ICP/MS)	Inorganic elements at trace concentrations	<ul style="list-style-type: none"> • What is the elemental composition? • Are metals present that might catalyze chemical reactions?
Gas chromatography/ mass spectrometry (GC/MS)	Semi-volatile organic compounds at trace concentrations	<ul style="list-style-type: none"> • Can organic chemicals that were contained in the waste drum be detected? • Are any products of possible oxidation or nitration chemistry observed?
Liquid chromatography/ mass spectrometry (LC/MS)	Non-volatile organic compounds at trace concentrations	<ul style="list-style-type: none"> • Are organic chemicals indicative of reacted Swheat Scoop® (e.g., carbohydrates, sugars) observed? • Are any products of possible oxidation or nitration chemistry reactions observed?
Thermogravimetric-mass spectroscopy (TG-MS)	Volatile organics are detected as a function of temperature	<ul style="list-style-type: none"> • Thermal stability of the debris and decomposition products

2. **Chemical reactivity studies and experiments.** As discussed above, the knowledge of the Pu recovery processes used by LANL provided a general “compositional window” of the contents of the known breached drum (Drum 68660). This knowledge allowed a series of tests to be performed to evaluate potential matrices for reactivity in order to better assess potential initiation and reaction pathways. The TAT also assessed LANL small-scale tests to evaluate potential reactivity within the MIN02 waste. While it was not possible to design a single test to definitively determine the specific conditions that resulted in the breach of Drum 68660, the small-scale tests did provide meaningful insights that supported the TAT’s assessment.^k
3. **Computational modeling and engineering analysis.** In the absence of direct access to Drum 68660 and extensive sampling and analysis of the contents, the TAT relied on modeling to describe key physical, thermal, and chemical characteristics of the breach of Drum 68660. The modeling allowed evaluation of both potential chemical reaction scenarios and the physical aspects of the breach such as pressure-time scenarios that could result in the observed drum breach. When combined, the chemical and physical models provided insights into the evolution of the event, from initiation to the observed damage in the room.^l

Figure 3-1 depicts the TAT’s approach to addressing uncertainties, which is discussed in detail in Appendix A.

^k See Appendix F, “Reactivity and Hypotheses.”

^l See Appendix D, Modeling Integrated Summary Report.”

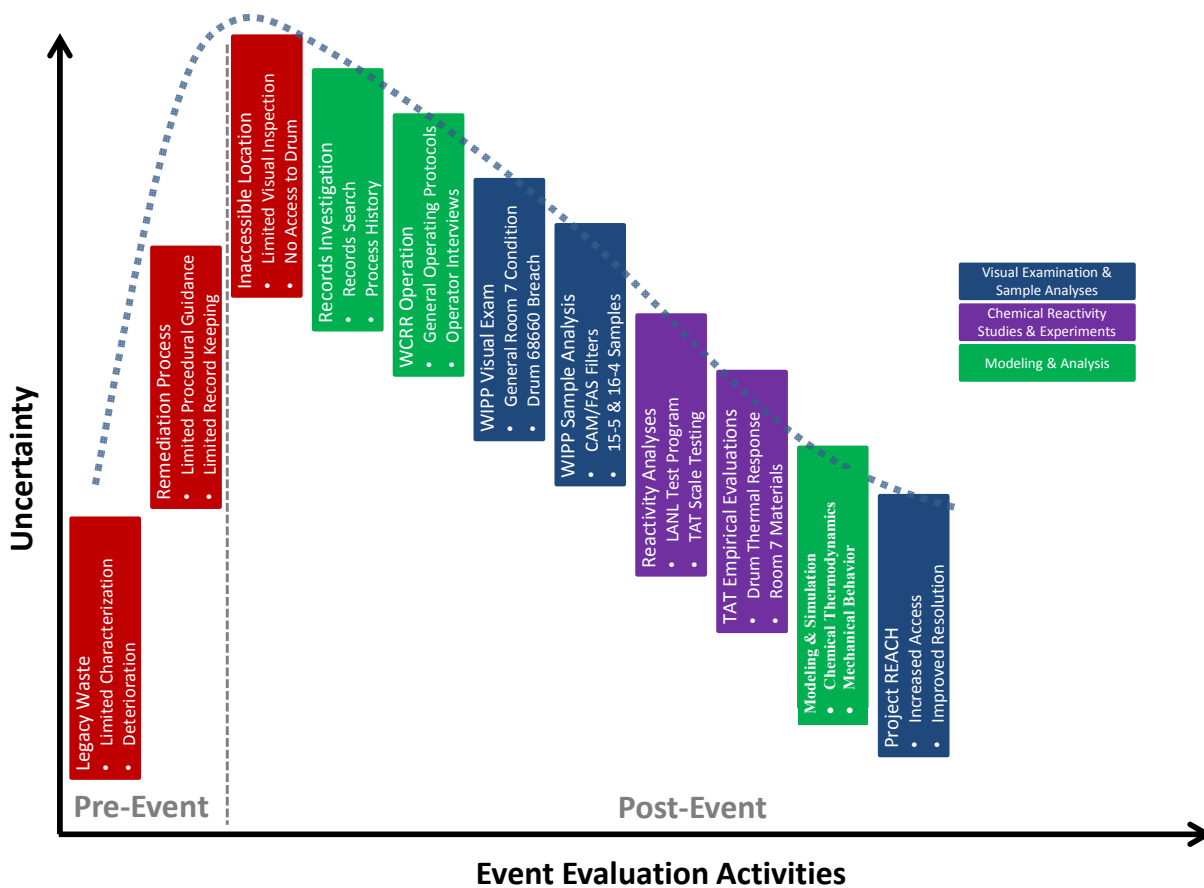


Figure 3-1. Notional depiction of WIPP TAT investigative strategy to reduce uncertainty in event analysis

3.4 UTILIZATION OF NATIONAL LABORATORY EXPERIENCE AND EXPERTISE

Not only are the national laboratory personnel selected as members of the TAT expert and accomplished in disciplines pertinent to the TAT mission, but DOE's constitution of the TAT as a national laboratory team has enabled the TAT to utilize the broader experience, expertise, and capabilities of the member laboratories and to reach out to other national laboratories for support as needed.^m For example, the TAT identified and solicited support from national laboratory experts in appropriate disciplines who were not members of the TAT to perform independent peer reviews of the TAT's interpretations and observations.

Application of that national laboratory experience and expertise in forensic science also has enabled the TAT to extrapolate from the known and the uncertain to the likely and to articulate sound reasoning bridging those information gaps. Using the collective experience and expertise of the US national laboratories has enabled the TAT to provide the level of technical rigor needed to ensure the credibility of its data collection and interpretation activities.

^m See Attachment 1 to this report, "TAT Member Qualifications," for summaries of the qualifications specifically pertinent to the TAT mission of TAT members and other supporting the TAT from national laboratories.

4.0 OVERARCHING CONCLUSION AND KEY JUDGMENTS

This chapter summarizes the TAT's overarching conclusion and set of accompanying key judgments. Appendices to this report describe in more detail the investigative activities and technical assessments leading to and supporting the TAT's overarching conclusion and key judgments.

The TAT's *overarching conclusion* is that chemically incompatible contents of LANL Drum 68660 in combination with physical conditions (e.g., the configuration of the materials in the drums) supported exothermic chemical reactions leading to a thermal runaway; the consequent build-up of gases within the drum displaced the drum lid, venting radioactive materials and hot matter that further reacted with air or other materials outside the drum to cause the damage observed in WIPP P7R7.

A thermal runaway is reached when dissipation of energy to surrounding regions cannot keep up with the production of energy by exothermic chemical reactions.

The following key judgments led to and support that conclusion:

Key Judgment 1: Contents of Drum 68660 were chemically incompatible.

Key Judgment 2: Drum 68660 breached as the result of internal chemical reactions that generated heat and produced gases that built up pressure sufficient to overcome the drum vent and seal.

Key Judgment 3: Drum 68660 was the source of the radiological contamination in WIPP P7R7.

Key Judgment 4: Initiation of the thermal runaway was internal and not caused by phenomena outside Drum 68660.

Key Judgment 5: Thermal and pressure effects resulted in the movement of material during the release event and caused the damage observed in WIPP P7R7; the release did not result from a detonation.

4.1 CONTENTS OF 68660 WERE CHEMICALLY INCOMPATIBLE.

Production of Drum 68660

The TAT estimated the content and distribution of material within Drum 68660 based on multiple sources of information, including LANL records related to the content and processing of its parent drum and x-ray video of Drum 68660 taken prior to its transport to WIPP.

The LANL parent drum of Drum 68660 contained nitrate salt residues from plutonium processing at LANL. Records of the original processing operations indicate that the parent drum, Drum S855793, contained 14 plastic bags of salt waste. Ten of those bags contained acidic nitrate salts, and four contained a mixture of nitrate and oxalate salts. During processing of Drum S855793, the contents were repackaged into two new sibling drums, Drum 68660 and Drum 68685; processing involved neutralization of acidic liquid contents, sorption of the neutralized liquid, and admixture of acidic nitrate salts to meet the waste acceptance criteria for disposal at WIPP.

Approximately two gallons of free liquids (reported to have a pH of 0), which contained water, nitric acid, and dissolved metal nitrates, were drained from the parent steel drum and plastic bags and neutralized to a target pH of approximately 7 with an undocumented volume of KolorSafe® (which contains triethanolamine, or TEA, water, and an indicator dye). The neutralized liquids were then sorbed onto Swheat Scoop®, a 100% wheat product.ⁿ The neutralized liquids sorbed to Swheat Scoop® were placed on top of job control solid waste (e.g., plastic bags, empty KolorSafe® bottle, a glove-box glove) in Drum 68660. Like all drums processed through the WCCR facility, Drum 68660 was lined with fiberboard and a vented polyvinyl chloride (PVC) bag.

The remaining moist, acidic nitrate salts from the parent drum were mixed with the remaining mass of Swheat

ⁿ The Swheat Scoop®-to-liquid volume ratio was assumed to be 3:1 based on TAT evaluations regarding the quantity of Swheat Scoop® required to fully absorb liquids.

Scoop®. The nitrate-salt admixture was distributed between Drum 68660 and Drum 68685.^o In Drum 68660, the nitrate salt admixture was placed on top of the layer of neutralized and sorbed liquid. Sibling Drum 68685 did not contain a layer of neutralized and sorbed liquid, so the nitrate salt admixture was placed directly into the bottom of the drum; a lead blanket from the parent drum was placed on top of the nitrate salt admixture in Drum 68685.

The two sibling drums contained all the processed waste from parent drum S855793 as well as external material added to the parent waste during the WCRR operation, including an empty neutralizer bottle and approximately 11 kilograms of job control solid waste. After Drum 68660 was filled to about 65% capacity, the PVC bag was taped closed and the vented drum lid installed on December 4, 2013. Drum 68660 was shipped to WIPP on January 29, 2014 and underwent the internal chemical reactions that led to the release of material in WIPP on February 14, 2014. Drum 68685 remains at LANL. Drum 68685 is isolated in a standard waste box (SWB) at LANL and periodically monitored for temperature and the composition of head-space gases.

Figure 4-1 provides a schematic representation of the processing of Drum S855793 to produce Drum 68660 and Drum 68685.

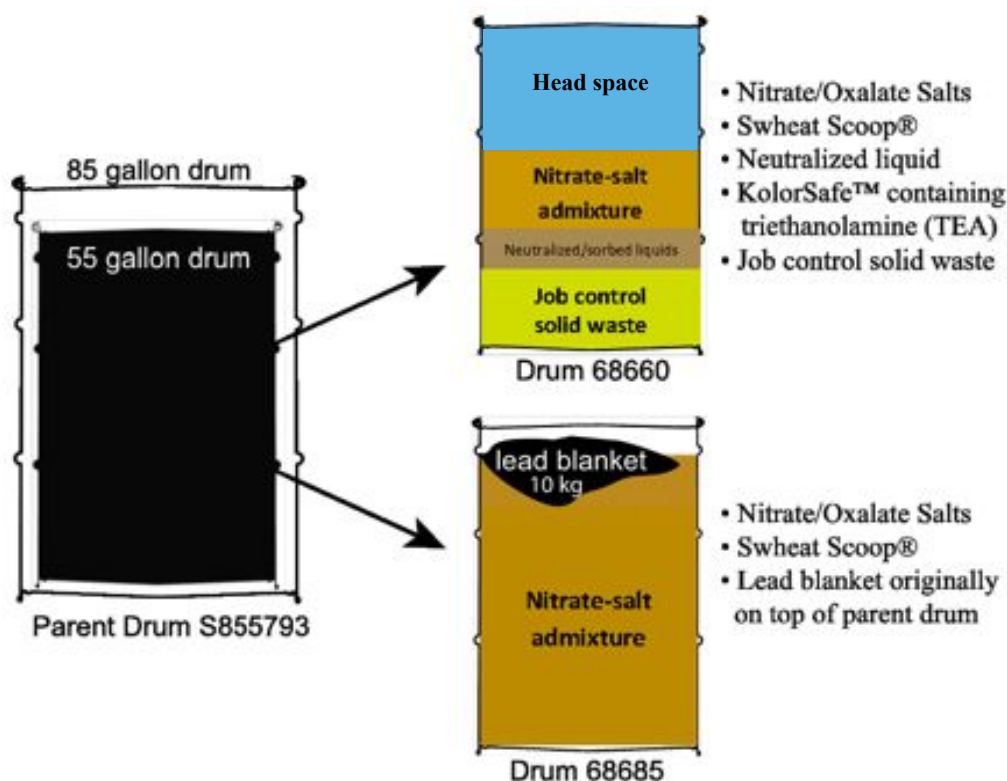


Figure 4-1. Processing of parent Drum S855793 to produce sibling Drums 68660 and 68685

Using x-ray images of Drum 68660 taken prior to its transport to WIPP, the TAT constructed a model of the drum contents and distribution and used this configuration to support its assessment. Since there are no documented records detailing the loading of Drum 68660, the TAT used WCRR process knowledge to estimate the drum configuration. The model includes the bottom layer of job control solid waste, the layer of neutralized and sorbed liquid, the nitrate-salt admixture layer, and a head-space layer. (See Figure 4-2.)

^o The Swheat Scoop®-to-nitrate-salt volume ratio was determined to be 0.7:1 based on TAT calculations of overall mass balance using the measured parent drum mass and both sibling drum masses.

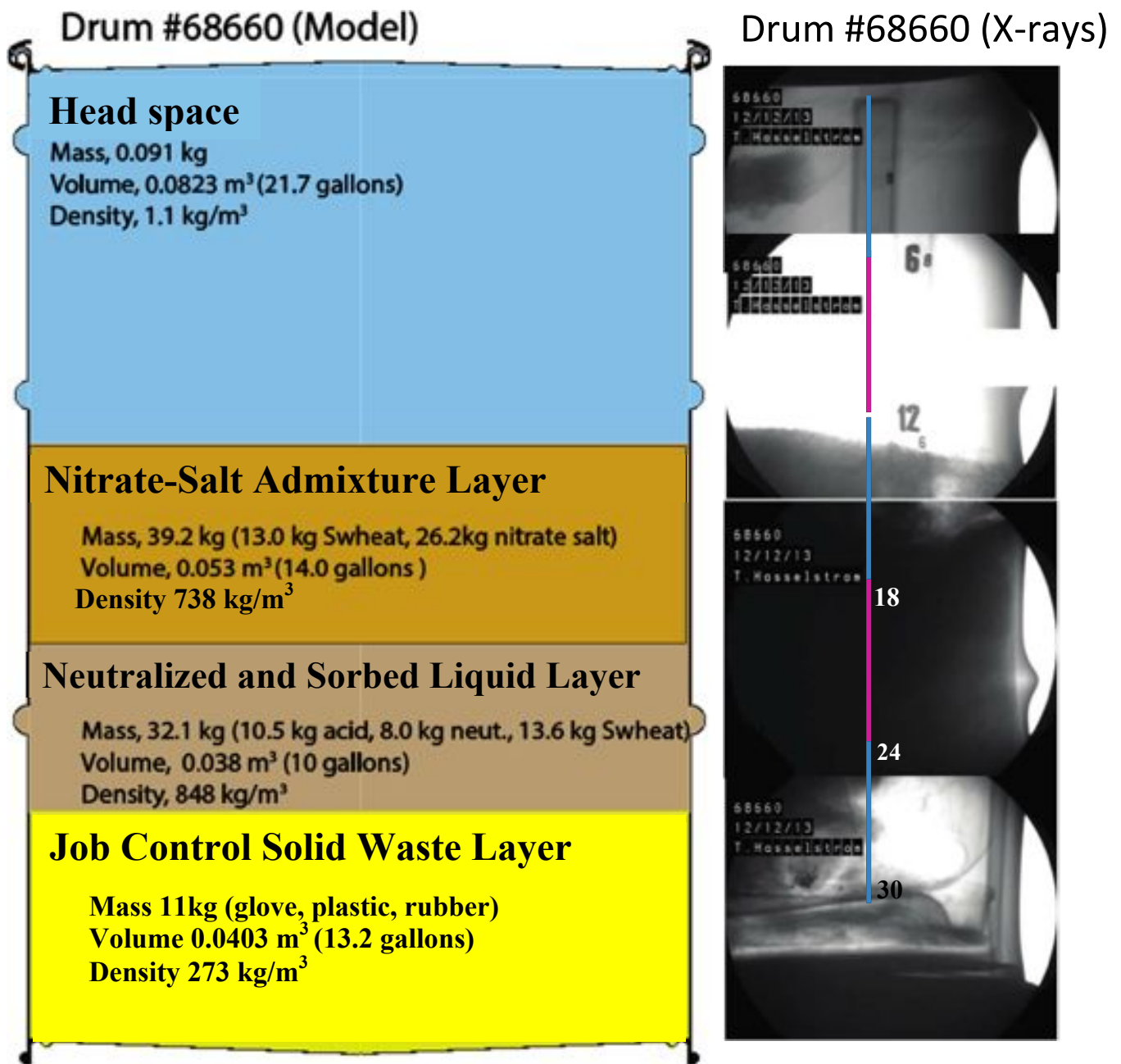


Figure 4-2. TAT Model of Drum 68660 contents and distribution based on x-rays of Drum 68660

Chemical Reactivity within Drum 68660

Based on the chemical components and physical configuration of the contents of Drum 68660 and upon review of chemical literature and results of laboratory testing, the TAT assessed possible chemical reactions that could have occurred in Drum 68660.

The combination of the nitrate salt residues, organic sorbent (Swheat Scoop®), and neutralizing agent (TEA) represents a potentially reactive chemical mixture of fuels and oxidizers. The potential role of each of the contents in the release is described below.

Role of Metal Nitrate Salts

Metal nitrates and nitric acid that are present in the MIN02 waste stream serve as the oxidizing and nitrating reagents.

Documentation of the original, detailed chemical composition of the nitrate salt waste contained in Drum 68660 does not exist. From the analysis of samples taken from two unprocessed drums as part of the LANL investigation as well as information from the characterization of process streams in the plutonium processing facility from which the nitrate salt waste stream originated, the predominant metals expected to be in Drum 68660 as metal nitrates include iron, aluminum, sodium, potassium, magnesium, and calcium. Other metals that would be expected to be present in lower concentrations include lead, chromium, nickel, zinc, and uranium. The nitric acid content in the moist metal nitrate salt waste is not precisely known but would be expected to be appreciable since the free liquid isolated from the parent drum was reported to have a pH of 0. A portion of this acidic liquid would have been retained with the solid nitrate salts and subsequently combined with the Swheat Scoop® sorbent during the processing operation.

Role of Absorbent

The Swheat Scoop® line of absorbents produced by Pet Care Systems (Detroit Lakes, MN) are 100% wheat products primarily composed of starch (65-70% dry weight) and proteins (14 wt%) with smaller amounts of lignin, lipids, and other polymeric carbohydrates including cellulose, and minerals.^p

According to the manufacturer, the production process exposes the starch of the grain from inside the kernel of the wheat, which serves as the clumping agent upon contact with liquids. Given the high weight fraction of starch in the sorbent, starch would be expected to serve as the predominant fuel component in Drum 68660. In addition to the starches and other organic components, according to the manufacturer, Swheat Scoop® is known to harbor an indigenous natural microbial population, which is the source of the product's enzymes claimed in the patent to degrade animal residues and associated odorous compounds.^q

All of the organic compounds present in the Swheat Scoop® sorbent would be subject to and could participate in oxidation and nitration reactions under opportune conditions.

Further support for the hypothesis of the oxidation of carbohydrate (i.e., Swheat-Scoop®) by nitrate salts is provided by the identification of significant levels of sodium carbonate in samples obtained from the ejected contents of Drum 68660. Sodium carbonate was *not* present in the original waste stream. Therefore, the TAT has concluded that it is most likely a product of an oxidation reaction.

Role of Neutralization Reagent

KolorSafe® containing TEA was used to neutralize the acidic free liquid isolated from the parent drum of Drum 68660. KolorSafe® is a color-indicating neutralizing agent used to facilitate operations (i.e., the color change indicates when the acid is neutralized). The neutralization of nitric acid with TEA produces the corresponding nitrate salt, triethanolammonium nitrate, or TEAN. TEA may also form complexes with metal ions that are present in the free liquid. TEAN has a melting point of 80 °C and decomposes exothermically beginning at about 250 °C, which is about 85 °C below the boiling point of TEA.

TEAN is potentially more reactive than TEA since the fuel (organic) and oxidizer (nitrate) are present together in the same molecule.

Role of Physical Configuration of Waste within Drum 68660

As shown in Figure 4-2, Drum 68660 was packaged in such a manner that there are four distinct regions: (1) job control solid waste layer, (2) layer of neutralized and sorbed liquid, (3) nitrate-salt admixture layer, and (4) drum

^p See Appendix F. References: *Swheat Scoop* 2014, Saldek 1997, Shewry 2013, Sramkova 2009.

^q See Appendix F. Reference: Saldek 1997.

head space. Consequently, there are a number of interfacial regions: (1) job control solid waste and neutralized/sorbed liquid, (2) neutralized/sorbed liquid and nitrate-salt admixture, (3) neutralized/sorbed liquid and fiber board liner, (4) nitrate-salt admixture and fiber board liner, and (5) nitrate-salt admixture and drum head space. The chemical and physical forms of these layers and interfaces are different in chemical reactivity and thermal conductivity. The degree of mixing between the layer of neutralized and sorbed liquid and the layer of nitrate-salt admixture is not known.

The physical configuration at the interface of the neutralized-and-sorbed liquid/Swheat Scoop® and the nitrate-salt admixture/Swheat Scoop® layers may have formed a localized region of reactivity leading to the thermal-runaway event.

4.2 DRUM 68660 BREACHED AS THE RESULT OF INTERNAL CHEMICAL REACTIONS THAT GENERATED HEAT AND PRODUCED GASES THAT BUILT UP PRESSURE SUFFICIENT TO OVERCOME THE DRUM VENT AND SEAL.

The physical evidence from P7R7, combined with thorough analysis of available sample data, chemical reactivity testing^f, and analytical modeling, indicates that Drum 68660 breached as a result of internal reactions that were exothermic in nature. The TAT hypothesizes that a sequence of exothermic chemical reactions led to a thermal runaway, which resulted in solids, radioactivity, and hot gases being released from the drum.

The thermal runaway process was a localized, complex, highly exothermic event occurring within the contents of the drum. The event resulted in chemical reactions and physical changes, both of which accelerated with increased temperature. When the energy-release rate of the process exceeded the rate of thermal conduction, the process transitioned into a deflagration phase that released gases in a relative short time. The process was highly localized and resulted in temperature gradients within the drum from ambient to high temperatures. Significant pressure build-up from evolved gases in the drum resulted in a breach, allowing gases, and most likely solid matter, to be ejected from the drum.

Continued deflagration after a runaway is not uncommon. The extent of reaction of both the retained and the released contents of Drum 68660 likely ranged from fully reacted to non-reacted states.

The sequence of chemical conditions that led to a runaway reaction system and release of drum contents into P7R7 in the WIPP facility cannot be quantitatively determined because of the previously described constraints but can be generalized as follows:

- A combination of exothermic chemical reactions and radioactive decay heated the drum contents in localized regions of Drum 68660. Exothermic chemical reactions produced the bulk of the initial heat as radioactive decay would be small due to the low radioactivity content in the drum and because biotic activity in the Wheat Scoop® material would be minimal.
- Localized removal of water by hydrolysis reactions with carbohydrates and evaporation increased the concentration of nitric acid and increased the reactivity of the nitrate/organic mixtures. Localized melting of hydrated metal nitrate salts may have occurred, providing for the release of water from crystalline phases and the increased transport of reactive species. Energy released from exothermic reactions continued to heat the drum contents. As the temperature increased, the concentration of nitric acid in the gas phase also increased, which may have led to greater reactivity as nitric acid is more reactive in the gas phase.
- Heat from the exothermic chemical reactions continued to increase the temperature of the drum contents, which in turn increased the reaction rates and the production rate of gaseous products and initiated chemical reactions with higher activation energies.
- Ultimately, a self-heating condition was achieved such that the dissipation of energy and the release of gases to surrounding regions of the drum could not keep up with their production by the exothermic chemical reactions.

^f See Appendix G, "Summary of Reactivity Testing."

- Heat and gas production ultimately proceeded at such a rate as to pressurize the drum and overcome the venting and drum ring enclosure.
- The reaction of the contents of the drum that were released into the larger environment of P7R7 was likely quenched as the conditions favorable for the runaway suddenly diminished, and the reaction of materials remaining in the drum likely continued until the materials were depleted or the drum contents cooled.

TAT Testing and Modeling Results

Thermochemical Calculation

Thermal runaway of Drum 68660 was modeled using a heat source determined by a simple global reaction rate, which represents the waste decomposing into products such as H₂, CO, CO₂, and various carbonates. The TAT used existing information to determine the composition of the waste in Drum 68660 and an equilibrium code to determine the products. The reaction energy was calculated based on the given product composition and the calculated equilibrium composition. The rate of energy release was prescribed in the model by having the thermal runaway occur close to the observed 72-day birth-to-breach of Drum 68660.

The TAT utilized the thermoequilibrium code CTH-TIGER^s to determine the potential decomposition species in Drum 68660 based on the estimated contents of the drum. CTH-TIGER also was used to determine what the products would have been if Drum 68660 had been processed with an inorganic sorbent such as zeolite rather than the organic Swheat Scoop®. The equilibrium compositions of the mixtures were 1) the contents of Drum 68660 processed with organic Swheat Scoop® and 2) Drum 68660 contents processed with inorganic zeolite. Both these mixtures were evaluated at 1 atmosphere (atm) pressure with temperatures ranging from room temperature to the adiabatic flame temperature, which is the temperature that the equilibrium products reach with no loss of energy to the outside environment (that is, the maximum potential temperature).

The adiabatic flame temperature for the waste processed with the organic Swheat Scoop® was calculated to be approximately 618 °C at 1 atm. In contrast, the model showed that the adiabatic flame temperature for Drum 68660 waste processed with inorganic zeolite would have been slightly below 100 °C. An adiabatic flame temperature less than the boiling point of water (100 °C) is a strong indicator that the zeolite-processed waste would not have produced thermal runaway. The energy that generated the elevated temperature in the waste processed with Swheat Scoop® came from the initial energy available in the organic material. The calculated high adiabatic flame temperature for the Swheat Scoop®-processed waste is consistent with the observed thermal runaway of Drum 68660.

To determine the rate of energy release, the TAT used a simple kinetic model that prescribed 70 days as the period of time to achieve thermal runaway. Seventy days is within the time interval between December 4 when Drum 68660 left Los Alamos and February 14 when Drum 68660 breached at WIPP. Figure 4-3 shows modeling results with high temperatures in the middle of the drum and cooler temperatures towards the edges of the drum. In fact, the edges of the drum are close to ambient conditions at the time of thermal runaway.

^s CTH-TIGER is a thermochemical code that can predict equilibrium compositions for any two thermodynamic states such as temperature and pressure given an appropriate equation of state and large enough product species database. The code can also predict flame temperatures and detonation states for given initial conditions. The code was initially developed at the Stanford Research Institute and further developed at the Sandia National Laboratories.

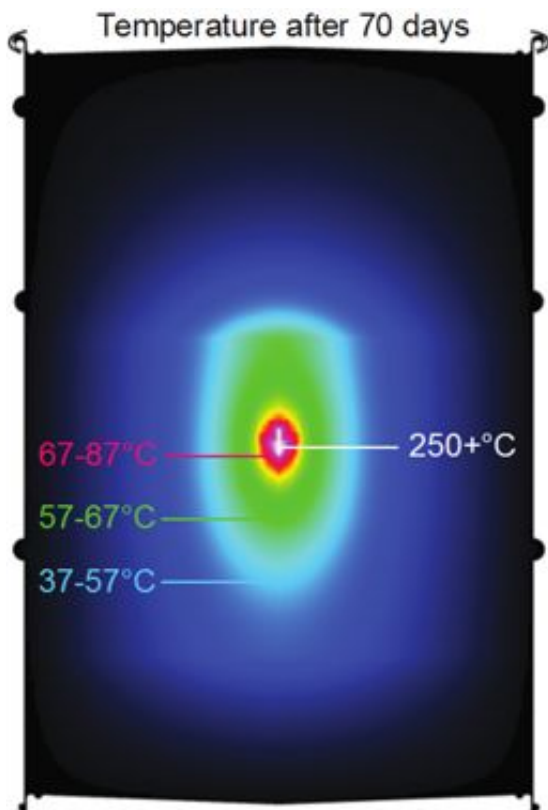


Figure 4-3. Calculated temperature profiles in Drum 68660 after 70 days.

Once thermal runaway is reached, the temperatures of the gases approach the adiabatic flame temperature, and rapid reaction of the waste material begins. The model demonstrates that at these higher temperatures, the organic Swheat Scoop® starts to gasify and the equilibrium composition becomes fuel-rich. Since the TAT did not have direct access to the reacted drum, the extent of reaction is not precisely known. However, in Drum 68660, the calculated composition of the gases at the adiabatic flame temperature included 33 mol% H₂ and 9 mol% CO fuels. The predicted hot decomposition products likely continued to gasify the remainder of the waste to produce fuel-rich gases that mixed with air and may have reached even higher temperatures as fuels such as H₂ and CO reacted with air. Pressurization and effluent predictions from this thermal model were used in other models such as the drum breach model and the room model.

Chemical analysis of the debris ejected from 68660 identified carbonate (CO₃²⁻) and nitrite (NO₂⁻) anions, which is consistent with nitrate salt oxidation of the Swheat Scoop®. Thermal analysis of the debris shows weight loss above 150 °C (Figure 4-4), which indicates that the debris did not experience high temperatures or that the exposure to high temperature was brief (<seconds) and insufficient to consume the material. If the exothermic oxidation reactions occurred in the middle of the drum, for example, pressure could build up from the gaseous products and could eject the unreacted top layer of Swheat Scoop®/nitrate salt out of the drum along with hotter matter that further reacted with the air or other materials outside the drum. Consistent with the nitrate salt layer being ejected, nitrate, nitrite, and oxalate salts were found in the debris and on the constant air monitor (CAM) filters. Moreover, nitrite and oxalate salts are not stable over 400 °C and 500 °C, respectively, and oxalic acid starts to decompose above 150 °C in the gas phase, and its calculated half-life at 250 °C is 3 seconds (s). Thus, it can be concluded that the collected materials ejected from the drum either did not experience high temperatures (over 400 °C) or that their exposure to elevated temperatures was very limited in duration (<seconds), resulting in the observation of nitrite and oxalate salts in the collected samples.[†]

[†] See Appendix C. References: Stern, 1972 & Oza, 1950 ; Gadalla, 1984; Lapidus, 1964

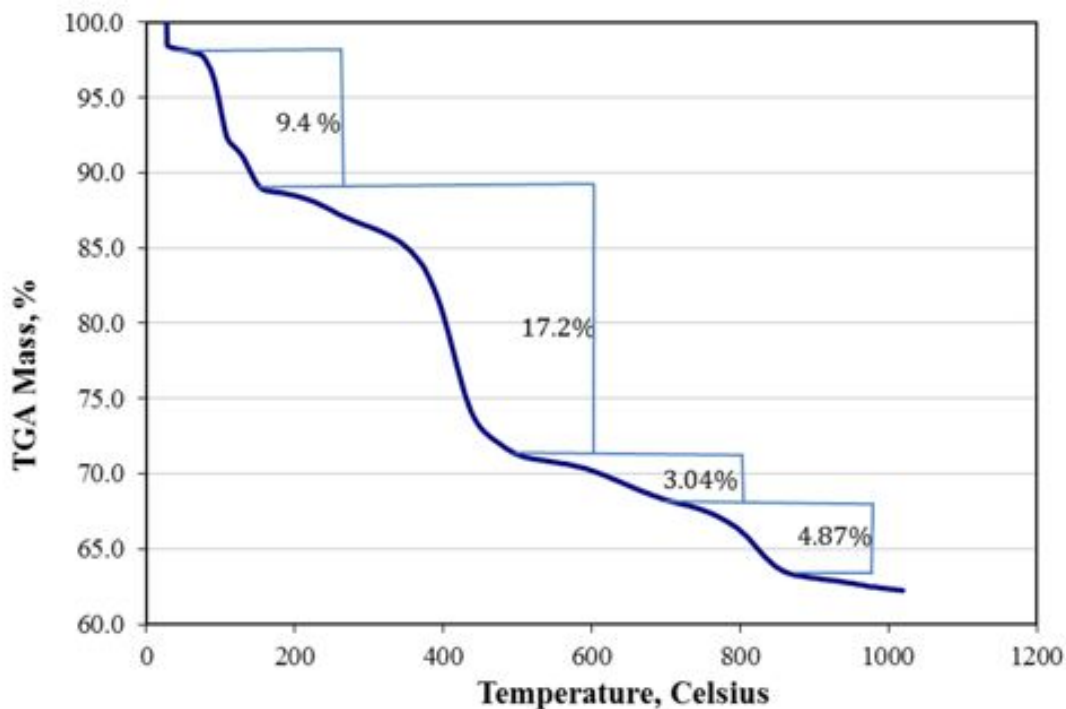


Figure 4-4. Thermogravimetric-mass spectroscopy (TG-MS) analysis of debris from the release

Laboratory Testing

The TAT performed an evaluation of the condition of Drum 68660 after the breach (using remote visual imagery obtained by the AIB) and compared that visual evaluation to the results of laboratory testing that exposed material obtained from a prototypic drum to a variety of temperatures and atmospheres.

Results of that testing suggest that the hottest portion of the drum was in the layer of neutralized and sorbed liquid. Due to uncertainties associated with the processing of the drum (i.e., precise records as to how Drum 68660 was packed do not exist) and inaccessibility of the drum (i.e., only remote imagery is available), the TAT's assessment of the initiation point of the reaction cannot be definitive; however, the analyses suggest that temperatures in the layer of neutralized and sorbed liquid of the drum were the highest.

To further evaluate the material compatibility and energetics of the subsequent reaction(s), the TAT evaluated Automatic Pressure Tracking Adiabatic Calorimetry (APTAC) experiments performed by LANL using a variety of chemical compositions reflecting various combinations of Swheat Scoop®, metal nitrate salts, nitric acid, and oxalate. These experiments were designed to offer insight into potential sympathetic reactions as well as evidence of material decomposition and off-gassing through pressure rise. The results of these experiments clearly show that self-heating of some of these mixtures can occur at low onset temperatures (i.e., below 100 °C). Using accelerating rate calorimetry (ARC), PNNL found that 1) a mixture of 3 volume parts Swheat Scoop® and 1 volume part 3.5 M HNO₃ dried in air at room temperature overnight begin reacting at 30 °C and continued to react until reaching 80 °C when the reaction rate accelerated into thermal runaway and 2) a mixture of 3 volume parts Swheat Scoop and 1 volume part KolorSafe®-neutralized 3.5 M HNO₃ began a sustainable self-heating reaction near 140 °C. SNL conducted bench-scale-thermal-runaway tests of Swheat Scoop® mixed with water and nitrated salts representative of Drum 68660. The heating of few-gram samples at 1 °C/minute show little exothermic behavior with Swheat Scoop® and water, but adding neutralized acid and nitrate salts results in significant reactivity leading to thermal runaway. This behavior is suppressed by liquid water, and a thermal runaway occurs after the water has fully vaporized, although it is not clear from this experiment whether runaway occurs quickly because of the relatively high wall temperature at the end of the vaporization process. The PNNL and SNL data suggest that the dry materials are highly reactive with one another but that the reactivity is suppressed in the presence of liquid water.

From the reaction chemistry discussed above, oxidation products from the Swheat Scoop® and/or nitration products were predicted. To determine whether these materials were present, the debris from 15-5 was analyzed by Fourier transform infrared (FTIR) spectroscopy. The FTIR spectra are complex and show a mixture of organic materials similar to Swheat Scoop® as well as inorganic materials. By comparing the FTIR spectra to information obtained using a full suite of analysis methods (e.g., scanning electron microscopy-energy dispersive x-ray fluorescence spectroscopy, or SEM-EDS; x-ray diffraction, or XRD; and ion chromatography, or IC), the TAT found the data to be consistent with a mixture of Swheat Scoop® or other carbohydrates, such as those potentially found in the cardboard liner, with nitrate, nitrite, oxalate, and carbonate salts. Organic material consistent with these results also was observed by liquid chromatography mass spectrometry (LC-MS). Since the extent of reaction in the drum is unknown and limited samples were obtained from the reaction area, the TAT cannot rule out the presence of nitrate esters or other nitrated organic compounds, which are known to be reactive.

Modeling and Simulation

To better understand the mechanical behavior of the drum, a finite element model was developed to simulate the pressurization during the runaway reaction within the drum. The transient temperatures in Drum 68660 were calculated by assuming a background heat source of 0.12 Watt (W) in the nitrate-salt admixture layer and 0.17 W in the neutralized and sorbed liquid layer.^u The decay heat is based on radiological calculations using isotopes of Pu and Americium (Am). More decay energy is deposited in the neutralized and sorbed liquid layer due to higher concentrations of Am in the 2 gallons of decanted liquid (Appendix D). The background heat source was estimated to be representative of the heat generated by radioactive decay in Drum 68660.

Under these conditions, thermal runaway occurred in the model after 70 days, similar to the observed drum behavior. Gas pressure at runaway was predicted to be 340 psig with a sealed drum (no vent). Furthermore, the predicted wall temperature increased by only about 1 °C, demonstrating that heating would not be apparent prior to runaway. The analysis also suggests that assuming that the neutralized/sorbed liquid waste and solid waste had similar reactivity, the initiation location was about 0.4 meters above the bottom center portion of the drum. Only about 3.4 kg (out of 71.3 kg total) was converted into decomposition gases in the thermal runaway model, suggesting that material ejected during the burst was likely unreacted. Modeling of the contents remaining in the drum was not a part of the thermal runaway modeling effort

Additional mechanical modeling was undertaken to aid in understanding the conditions required to cause drum breach.^v A variety of scenarios were evaluated in an attempt to reproduce the observed behavior. In the case most reproducing observed drum damage, the load was ramped to 50 psi in 0.1 seconds to represent a relatively slow pressurization representing non-detonation gas generation from reactions in the drum. That loading resulted in the drum lid opening at the top edge of the drum at the end opposite the flanges on the closure ring at approximately 35 psi (see Figure 4-5, *left*). Analyses comparing the loading with and without the potential weight of the MgO on the lid of the drum showed no significant influence on the pressure at which the drum opened or on the displacement mode of the drum opening. These analyses included constant pressure on the inside bottom of the drum to represent the weight of the contents.

To benchmark the models used, the results of experimental data, including results of LANL pressurization tests published in 1998-9 and results of SRNL pressurization tests published in 1991, were considered. The various pressurization scenarios modeled showed that the drum lid would open if the internal pressure were sufficiently high (e.g., 75 PSI for a “fast” load case, 35 PSI for a “slow” load case, and 46 PSI for a “slow” load case with the weight of another drum on top); the sidewalls of the drum did not rupture. This is consistent with published experimental data and consistent with the photographic evidence of the breach of Drum 68660. The extent and behavior of displacement of the lid was found to depend on the rate of pressurization of the drum; however, all

^u See Appendix D, “Thermal Activity in Drum.”

^v See Appendix D, “Thermal Response of Dru.”

scenarios tested resulted in the displacement of the drum's lid. These historical results are consistent with the TAT evaluation.

The slower pressurization scenario compares favorably to post-event photographs of Drum 68660 (Figure 4-5, *right*). These results support the conclusion that the thermal runaway reactions within the drum led to a relatively slow pressurization of the drum rather than a rapid pressurization or detonation. This slow pressurization was sufficient to overcome the drum vent.

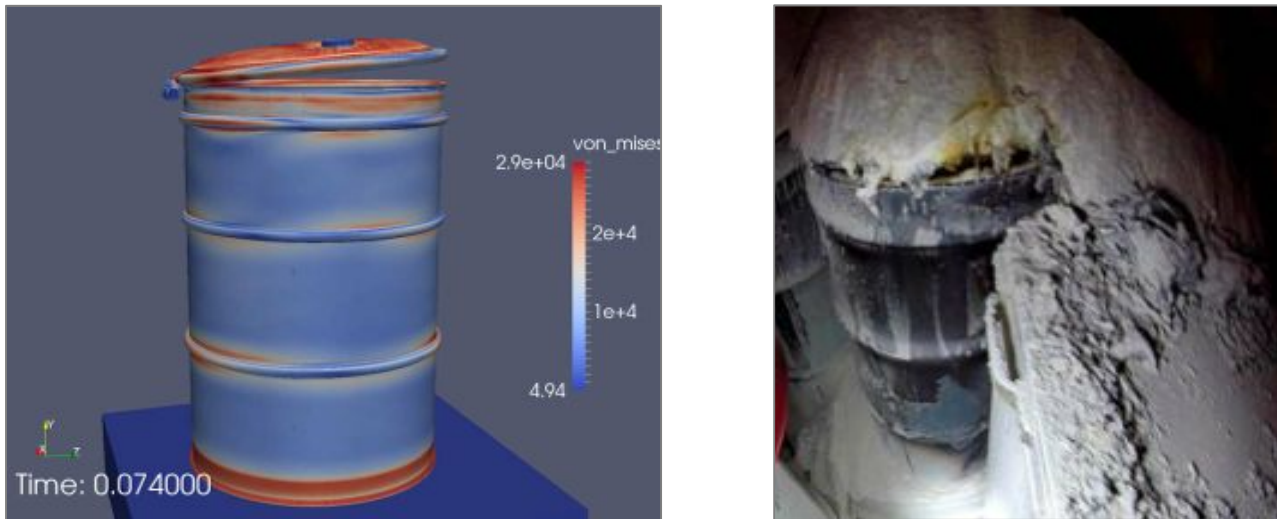


Figure 4-5. Analysis results for case with original estimate of properties and “slow” loading (left) matches observed damage seen in post-event photograph of Drum 68660 showing discoloration and lid displacement (right).

4.3 DRUM 68660 WAS THE SOURCE OF THE CONTAMINATION IN WIPP P7R7.

Based on the available photographic and video information, there is no evidence that any drum other than Drum 68660 breached or had compromised seals. This observation is supported by data from a series of non-destructive measurements made of the drum contents for acceptance into the WIPP facility and destructive analytical measurements obtained from a variety of sample locations in the facility, which includes debris from 15-5 and 16-4, surface smears, and constant air monitor (CAM) filters within WIPP as well as sampling of the Station A fixed air sampler (FAS) high efficiency particulate air (HEPA) filter. When this data set was compared to historical analytical data for the Pu and Am isotopic content for the processed wastes of the LANL drums stored in P7R7, it was determined to be consistent with a release from Drum 68660. Although when accounting for the analytical uncertainties inherent in the isotopic measurements, it cannot be concluded that no other drum contributed to the isotopic signature, from these data it can be stated that the dominant source of radioactivity was Drum 68660. Therefore, based on the evidence—photography and video; parent drum historical Uranium (U), Pu, and Am data for all LANL material types stored in P7R7; Central Characterization Program (CCP) gamma spectra for key LANL drums in P7R7 using high efficiency neutron counters (HENCs); and U, Pu, and Am isotopic measurements on post-event samples—it has been concluded that Drum 68660 was the source of the post-event radioactive contamination at the WIPP facility.

Early post-event sampling and analysis of Station A FAS exhaust HEPA filter detected Pu240/Pu239 mass ratios consistent with those established for material types 52 (MT52) and 53 (MT53) and Am241/Pu239 activity ratios generally associated with the material types (MT52 and MT53) in parent drum S855798. It should be noted that the Am/Pu ratio is a result of the way those MTs were processed to recover plutonium and is not necessarily a characteristic for classification of material type. Also, that ratio cannot be used as an absolute signature for the recovered plutonium since the chemistry used in the recovery process varied by salt batch. Based on early analyses of these two signature actinide isotopic ratios performed by the WIPP onsite laboratory and LANL analytical lab, a release of radiological material from 68660 was confirmed.

To verify this initial finding, the TAT conducted an exhaustive study based on the criteria outlined above that included all waste items in P7R7 to confirm that Drum 68660 was the dominant contributor of the radiological material distributed throughout the facility. Based on that comprehensive analysis, it was determined that Drum 68660 was the dominant and maybe the sole contributor to the radiological contamination sampled in the facility as it is the only drum which contains homogenized salts with both Am241/Am243 and Pu240/Pu239 mass ratios within the ranges of those measured in the post-event samples by SRNL and PNNL.^w

The TAT also performed transport modeling of the release from P7/R7 for a range of release durations and possible contaminant deposition rates. Model results for an initial default release of 1 Ci were then scaled to estimate release amounts that could explain the radioactivity observed in the exhaust by the Panel 7 CAM and the Station A FAS. For airborne release fractions consistent with a significant over-pressure event with fire affecting the entire contents of the radioactive inventory in a container, the resulting source terms were consistent with estimates of the total radioactivity contained in Drum 68660 (Hunter and Viner, 2015). The model-derived source term values contain uncertainty, in part due to the lack of representative information on potential deposition of Americium along the exhaust path.

Based on the information available, the TAT has determined with a high degree of confidence that the dominant source of the radioactive contamination observed in WIPP was Drum 68660.

^w The analysis is detailed in the ‘Systematic Evaluations and Discussions for Source Term’ section of Appendix E, “Drum Characterization Integrated Summary Report.”

4.4 INITIATION OF THE THERMAL RUNAWAY WAS INTERNAL AND NOT CAUSED BY PHENOMENA OUTSIDE DRUM 68660.

Key Judgment 2 is that the breach of Drum 68660 was the result of exothermic reactions within the drum. The TAT also considered a number of different potential initiation hypotheses that involved heating from unknown external sources (Appendix F). Throughout this process, analyses were performed to assess the plausibility of each hypothesis. Although some evidence of potential fire damage on nearby drums was observed, this damage was likely caused by hot matter and gases released from Drum 68660 that reacted with air or other materials outside the drum. Experimental studies concluded that the condition and/or damage of the paint on the drum exterior is consistent with that surface being heated in an oxidizing environment and not the result of heating in a reducing environment (a direct flame impingement).^x Possible external energy sources considered included the carbonation or hydration of the MgO, energy exchange between adjacent drums, and ignition of flammable gases accumulated within the waste pack. None of these mechanisms was found to be a likely source of external heating that would have caused the initiation of Drum 68660. Additional exploratory analyses were performed to attempt to better quantify various aspects of the release event as they relate to initiation. Based on these analyses, the TAT concluded that the initiation of Drum 68660 was not the result of heating from heat sources external to the drum.

The TAT considered several possible external heating hypotheses, including effects of the February 5 salt-haul truck fire, drum-to-drum heating, and combustion of flammable gases in Room 7. Specially, several hypotheses regarding the potential involvement of the February 5, 2014 truck fire in the February 14, 2014 release were evaluated:

- A thermal pulse from the truck fire event reached P7R7.
- Combustion products from the truck fire reached P7R7.
- Exothermic reactions of H₂O and CO₂ (which are expected by-products from the fire) with MgO resulted in elevated temperatures in P7R7 or in the observed damage to the MgO bags.
- Reduced ventilation in P7R7 following the truck fire influenced the release event.

For approximately 12 hours following the truck fire, the flow data indicate that the flow through Panel 7 was reduced. Figure 4-6 shows the locations of the P7R7 and the truck fire. Flow between the truck fire location and P7R7 was modeled to estimate transport of energy and combustion products to P7R7 and potential temperature and humidity increase in P7R7 due to the fire. Although the fire temperature is not established, estimates of the air temperature just downstream from the fire were computed based on measured temperature and air flowrate data. Based on calculations for a range of airflows, the maximum air temperature increase in P7R7 was less than 5°C as a result of the truck fire. Likewise, calculations of the potential humidity increase in Room 7 due to the salt truck fire showed only a small rise in humidity. The observed absence of thermal damage near the face of P7R7 also confirms that elevated temperatures did not occur in this area.

^x See Appendix D, “Thermal Response of Drum.”

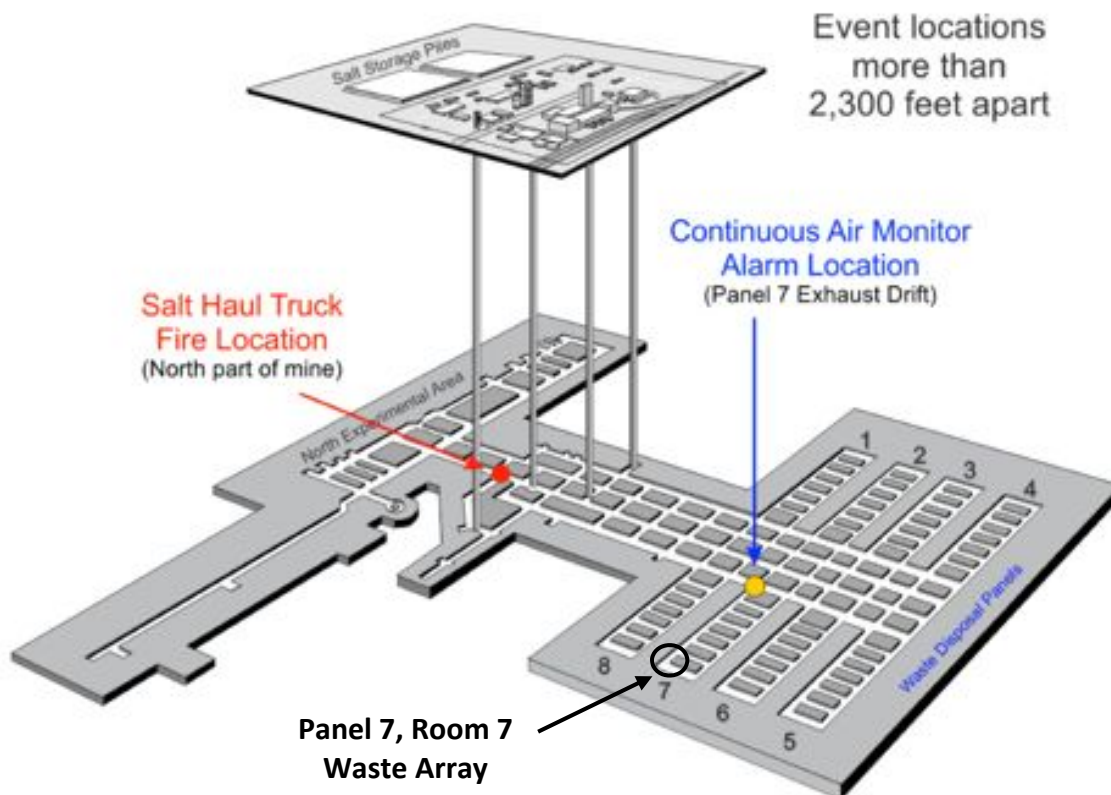


Figure 4-6. Fire and radiological event locations within WIPP

Independent of the expected air composition in P7R7, the potential for H₂O or CO₂ to react with the MgO was analyzed. Bounding calculations for the energy liberated due to the reaction of H₂O and/or CO₂ with the MgO concluded that the maximum increase in MgO temperature rate is less than 4°C per day, which is easily mitigated by heat transferred to the room ventilation air. Additionally, analyses of MgO samples taken from the damaged MgO bags did not show any evidence of reaction with either H₂O or CO₂. Consequently, the potential of these reactions to have caused significant heating of waste drums leading to initiation and/or damage to the MgO bags was ruled out. (Appendix D)

The potential for external heating of Drum 68660 to lead to an internal thermochemical response was examined. Calculations for radiative heat transfer between adjacent drums indicated that this is an ineffective mode of heat transfer and it was not a mechanism for transferring heat from drum-to-drum in the waste pack. The possibility of the accumulation and ignition of heavier-than-air flammable gases within the waste pack was considered. Based on the best estimate of the chemical composition of Drum 68660, no heavier-than-air flammable gases were identified through modeling in the reaction products that might vent. Consequently, there is no evidence that any of the potential external heat sources considered had sufficient energy and duration to initiate the thermal runaway of Drum 68660.

Additionally, a set of experiments was designed and conducted to investigate the exterior drum discoloration of WIPP waste Drum 68660 following the event on February 14, 2014. Remote visual imagery obtained by the AIB (e.g., photographic evidence) indicated the majority of Drum 68660 had become black (top 2/3) and the bottom portion (bottom 1/3) appears to transition from black to brown to tan to white (the original drum color). The drum material discolorations from these photos provide insight into the temperature the WIPP waste drum may have experienced and whether the heat source was internal or external to the drum. The experimental data are consistent with an internal temperature source causing the observed drum discoloration.^y It was also determined

^y See Appendix D, "Thermal Response of Drum."

that all gradients of observed exterior paint color occurred experimentally when the drum exterior sections were in oxidizing environments, such as air. The results also indicated that drum blackening did not result from external flame impingement. The experiments established that a direct impingement of flame (reducing environment) on the exterior surface caused white paint to peel, but it did not change the exterior paint from white to brown to black.

After an evaluation of both thermal and humidity impacts on the waste array resulting from the February 5, 2014 truck fire, it was concluded that the release event of February 14, 2014 was not initiated by the truck fire. TAT analyses identified no potential external heat scenarios that would have contributed to the initiation of Drum 68660. Based on these analyses, the TAT concluded that the initiation of Drum 68660 was not the result of heating from sources external to the drum.

4.5 THERMAL AND MECHANICAL EFFECTS RESULTED IN THE MOVEMENT OF MATERIAL DURING THE RELEASE EVENT AND CAUSED THE DAMAGE OBSERVED IN P7R7; THE RELEASE DID NOT RESULT FROM A DETONATION.

As discussed above, the runaway reaction overcame the drum vent and seal, resulting in the breach and the release of hot gases and other materials to the room. While the composition of the gases released may have been combustible, the TAT cannot quantitatively determine whether combustion occurred.

Visual observation suggests that the MgO supersacks in 17 locations were damaged during or after the release event. The observed damage likely occurred from polypropylene supersacks igniting and burning or from their being exposed to a heat flux large enough to thermally damage them without igniting. The undisturbed piles of MgO imply relatively benign flow conditions and further support the key judgment that the release was not a detonation. An experimental investigation into the flammability of the polypropylene material used in the supersacks and the polyethylene material used in the slip sheets demonstrated that both materials readily ignited when exposed to a flame and that both were capable of sustaining a flame. ^z

Simulations using the thermal-runaway model predict an adiabatic flame temperature for the waste in Drum 68660 of 618 °C at a pressure of 1 atm. This is the maximum internal temperature expected following thermal runaway and is determined from energy within the solid waste that contains both oxidizers and fuels. Following thermal runaway, the hot decomposition gases vent from Drum 68660. The blackbody emissive power at this temperature is approximately 30 kW/m². This represents an upper bound on the radiative heat flux. The combined convective and radiative heating could be significantly higher. Simulations of the MgO supersacks exposed to various heating rates show that even for heat fluxes as high as 80 kW/m², several minutes would be required to raise the surface temperature of the MgO supersacks sufficient to result in thermal damage without ignition.

The equilibrium composition of gases released from Drum 68660 at the adiabatic flame conditions is 34.1% H₂, 24.5% H₂O, 10.6% CO, 21.4% CO₂, 4.8% N₂, 4.5% CH₄, and other minor species. The hydrogen composition is within the flammability limit for hydrogen air mixtures, which is 4-75% by volume. The estimated hydrogen percent in the drum (34.1% by volume) at a temperature of 618 °C is close to the stoichiometric hydrogen composition (29.7 volume %). The auto ignition temperature for hydrogen in air is 520-750 °C, depending on the hydrogen percentage in the air. The decomposition products in Drum 68660 could have ignited when mixed with air, causing the external flame temperature to be as high as 1500 °C.

The exact external temperature in P7R7 would depend on factors such as heat loss to the surroundings and mixing with the external air. At the high end of this temperature range (1500 °C), the heat flux on the MgO supersacks if the gases ignited is predicted to be more than an order of magnitude larger and would have resulted in rapid thermal damage to the polypropylene. Additionally, these temperatures would imply the presence of an external flame, which likely would ignite the exposed supersacks and slip sheets.

^z See Appendix D, "Thermal Response of Drum."

The TAT performed simplified computational fluid dynamics (CFD) modeling of a release from position 16-4 in P7R7 with the characteristics described above. A simplified geometric configuration of P7R7 was used in the CFD modeling.^{aa} A detailed replication of the best-estimate geometry is unlikely to result in increased fidelity of the results. The simplified CFD simulations of the air flow within P7R7 show a predicted region of elevated temperature that roughly corresponds to the observed damage footprint. However, due to uncertainties in the waste array geometry, release flow rate, and release duration, it is difficult to support further conclusions.

A precise description of fire characteristics cannot be established. Visual evidence from the January 2015 REACH investigation suggested that in some areas, fire propagated along regions of combustible material but that multiple, apparently isolated, ignitions of combustible material also occurred. These may have resulted from hot or burning embers discharged during the release. CFD calculations cannot fully recreate flow conditions as too many important conditions are unknown. However, modeling efforts do reflect flow features including unsteady stagnation and recirculation regions that occur for a flow driven over a complicated geometry. The flow would be expected to provide favorable conditions for random deposition of embers that may have been ejected from the drum. The potential trajectory of ejected materials will depend on the velocity, shape, and weight of embers as well as the overall flow conditions within P7R7.

^{aa} See Appendix D, “Thermal Damage Footprint External to Drum.”

5.0 SUMMARY

As discussed, the TAT has undertaken a deliberative investigation process to understand and determine the cause of the February 14, 2014 WIPP release event. Uncertainties about the processing of the waste and inaccessibility of Drum 68660 constrained the TAT's ability to determine definitively the initiator of the release. The TAT has concluded that chemically incompatible contents of LANL Drum 68660 in combination with physical conditions (e.g., the configuration of the materials in the drum) supported exothermic chemical reactions leading to a thermal runaway; the consequent build-up of gases within the drum displaced the drum lid, venting radioactive materials and hot matter that further reacted with air or other materials outside the drum to cause the damage observed in WIPP P7R7

Through a combination of review of the available visual imagery of P7R7, evaluation of the results of chemical reactivity testing, and modeling of the event and material behavior, the TAT arrived at a number of key judgments that led to and support the overarching conclusion:

Key Judgment 1: Contents of Drum 68660 were chemically incompatible.

Key Judgment 2: Drum 68660 breached as the result of internal chemical reactions that generated heat and produced gases that built up pressure sufficient to overcome the drum vent and seal.

Key Judgment 3: Drum 68660 was the source of the radiological contamination in WIPP P7R7.

Key Judgment 4: Initiation of the thermal runaway was internal and not caused by phenomena outside Drum 68660.

Key Judgment 5: Thermal and pressure effects resulted in the movement of material during the release event and caused the damage observed in WIPP P7R7; the release did not result from a detonation.

APPENDIX A. TAT APPROACH TO MITIGATING UNCERTAINTIES

DISCUSSION OF PROBLEM

Investigation of nuclear process upsets, particularly those involving complex matrices of potential reactants, can be difficult and constrained. The root cause of such events can potentially be determined quickly by examining process histories, the environment and the contents of the reactant mixture. With respect to the LANL MIN02 waste stream, it can be generally stated that combining potentially acidic nitrate salts (i.e., a strong oxidizing agent) with organic matter (i.e., a fuel) will yield potentially incompatible mixtures. At the highest level, this analysis can provide insights into the nature of the event (i.e., whether the event was caused by mechanical or chemical effects) and can greatly simplify the investigatory process. In the case of the release from WIPP Panel 7, Room 7, there are three broad areas of uncertainty that greatly limit the ability to draw exact conclusions on the cause of the event:

1. **Contents and distribution of the reactant mixture cannot be exactly described.** Handling of the MIN02 waste stream from LANL has been the primary suspect in the investigation since the identification of the Drum 68660 breach. This waste was generated in the 1970's and 1980's and generally resulted from Pu recovery operations. Those recovery operations were accomplished using nitric acid digestion with Pu recovery and purification by ion exchange and oxalate precipitation. Following Pu removal, the chemical residues were evaporated and the evaporator bottoms cooled to produce metal nitrate salts. Nitrate salts derived from ion-exchange effluents were washed with concentrated nitric acid, air dried, and packaged for storage. Nitrate salts derived from oxalate precipitation effluents also contained oxalate salts and were washed with water prior to air drying and packaging for storage. While process knowledge aids in understanding the composition of the waste, precise characterization data of the material recovered are limited. Additionally, during processing operations, other items (e.g., worn gloves, lead shielding, other job waste, etc.) were often added to the waste drum with limited characterization and documentation.
2. **MIN02 waste processing operations did not document process details.** The procedures used by LANL to process the drums at the Waste Characterization, Reduction, and Repackaging (WCRR) facility produced limited and inconsistent documentation describing the detailed processes used. For example, liquids recovered from the original waste drums were characterized using pH-indicating paper and "neutralized" by adding a neutralizing agent. The material was then mixed and the resultant pH again measured with pH-indicating paper. In many cases the initial pH was not recorded. Additionally, both the "neutralized" liquid and the nitrate salts are mixed with Swheat Scoop® ("kitty litter") at a nominal volume of 3:1 Swheat Scoop®:waste material. Actual measurements of Swheat Scoop® used were not recorded. Ultimately, the goal of the WCRR operation is to produce drums suitable for shipment to WIPP; meeting the requirements of no prohibited materials and "no free liquid" while staying within the allowed content window as determined by gross radioassay are the primary considerations.
3. **Access to the reacted drum is limited.** Visual observation of LANL Drum 68660 confirms that the drum is breached. Drum 68660 is nominally 32 feet (roughly 10 meters) from the access point in P7R7 (i.e., the "waste face"), and examination of the affected area has required remote tools and cameras; initial confirmation of the breach was obtained by visual evidence using a small camera rotated on a boom arm. Samples for laboratory analyses were collected remotely using this same mechanism.

These broad uncertainties and limited information constrict the investigation and constrain the ability to draw exact conclusions on the cause of the release. The limitations do not, however, prevent substantive conclusions from being drawn that will identify the primary cause of the release and identify actions required to prevent recurrence.

INVESTIGATIVE STRATEGY

The uncertainties and limitations described above require an approach that relies on three primary areas.

1. **Visual examination and sample analyses.** The TAT is relying heavily on visual documentation obtained by the Accident Investigation Board (AIB). Given the limited access to the breached drum, this visual observation provides important information to allow the TAT to identify potential reaction mechanisms and sequences. In addition to the visual observation, the TAT does have access from limited samples obtained during the event (e.g., fixed air sampler and constant air monitor filters and cartridges) and material recovered from the area near the breached drum. These samples, while limited, provide important insight into the event. Samples also were obtained from the parent drum.
2. **Chemical reactivity studies and experiments.** As discussed above, the knowledge of the Pu recovery processes used by LANL provide a general ‘compositional window’ of the contents of the known breached drum (Drum 68660). This knowledge allowed a series of tests to be performed to evaluate potential matrices for reactivity and susceptibility in order to better assess potential initiation and reaction pathways. The TAT also interfaced with LANL as they conducted small-scale tests to evaluate potential reactivity within the MINO2 waste. While it was not possible to design a single test to definitively determine the specific conditions that resulted in the breach of Drum 68660, the small-scale tests did provide meaningful insights that supported the TAT’s assessment.
3. **Computational modeling and engineering analysis.** In the absence of direct access to Drum 68660 and extensive sampling and analysis, the TAT relied on modeling to describe key mechanical, thermal, and chemical characteristics of the breach of Drum 68660. The modeling allowed evaluation of both potential chemical reaction scenarios and the mechanical aspects of the breach such as the pressure-time scenario that could result in drum breach. When combined, the chemical and mechanical models provide an overall description of the evolution of the event, from initiation to the observations made in the room.

These three investigative areas provide information required to reduce the uncertainties inherent to this assessment and to evaluate the hypotheses proposed by the TAT.

Management of uncertainty in the investigation was a critical component of the TAT effort and provides varying levels of confidence in the key judgments developed by the TAT. The approach to managing uncertainty is notionally illustrated in Figure A-1. The lack of detailed information about the waste being processed and the details of the process raise the initial uncertainty level considerably. The inability to examine the reacted drum raises this uncertainty level further. Working with the DOE Accident Investigation Board (AIB) and the investigation team at the Los Alamos National Laboratory (LANL), the TAT undertook a systematic process to reduce uncertainty. This process described above does not completely eliminate the impacts of the initial uncertainties discussed above, but it does inform the analysis and enable key judgments regarding the nature of event.

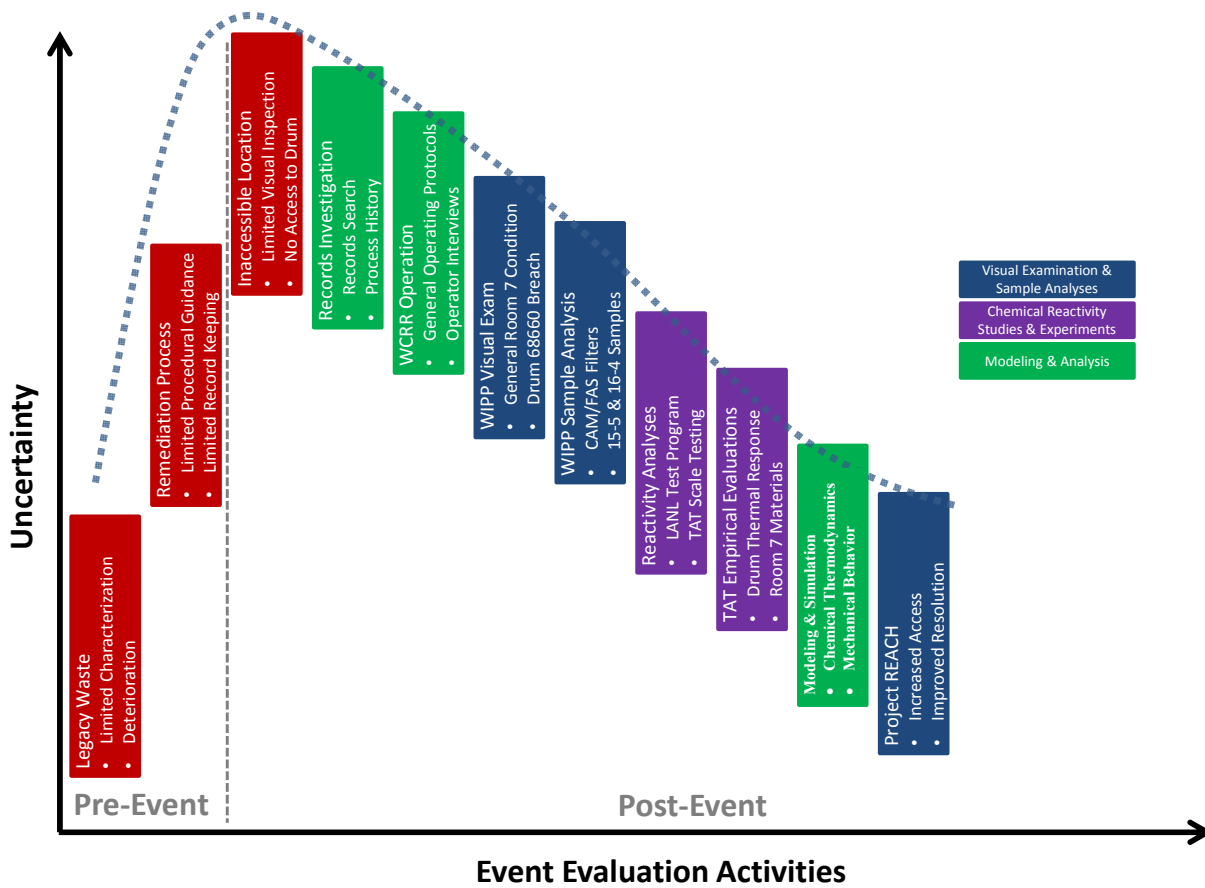


Figure A-1. Notional depiction of WIPP TAT investigative strategy to reduce uncertainty in event analysis

The investigative strategy and approach used by the TAT is discussed in detail in subsequent sections of this report. The systematic approach employed by the TAT maximizes the use of available information and combines this information with targeted experimental programs and modeling analyses to develop conclusions regarding the nature of the reaction(s) responsible for the radiological release. Ultimately, the TAT used this information to arrive at key judgments concerning the causes of the likely scenarios.

APPENDIX B. SAMPLING INTEGRATED SUMMARY REPORT

The goal of sampling and analysis activities in support of WIPP TAT was to discover evidence that indicated the cause of the drum breach. Sampling is the process by which evidence is collected. Analysis is the process by which pieces of evidence, or collected samples, are prepared and interrogated by a variety of instrumental techniques that provide chemical information. Data are produced as the result of these analyses. Such data can only be evaluated and interpreted with an understanding of the analysis process and its limitations and with an understanding of the sampling process and its limitations. For these reasons, sampling and analysis are considered together. The quality of data produced must be assessed by considering both sampling and analysis together – analytical results are only as good as the samples that can be provided.

Questions and hypotheses guided the sampling and analysis process; however, the reality of the harsh environment of WIPP limited the manner in which sampling could be conducted. To look for evidence of what caused the drum breach, the optimum place to sample would be inside Drum 68660 itself. However, given the configuration of the drums in the WIPP facility, this was not possible. The next best place to look for evidence would be near the drum — assuming that the drum contents spewed during the breach. But, collecting samples from outside of the drum complicates data interpretation, as signals from the background environment must also be considered, and there can be no expectation that the samples that are collected will be homogeneous in composition. And, to make the job more difficult, sampling could only be performed using a fifty-foot pole to hold a sampling device; thus, this introduced some uncertainty in understanding the precise location of the sample collection. Out of necessity, the sampling strategy became to sample what was easily-available for collection and to interrogate the sample with as many different techniques as possible, with the hopes of obtaining useful information. Once data from initial sampling and analysis were available, subsequent analyses could be targeted with the goal of addressing specific questions.

Prior to collecting samples from the immediate vicinity of Drum 68660, many samples, including filters from constant air monitors and swipes, were collected from May–June 2014 from various locations in WIPP to measure radioactivity. The major goals of these sampling activities were to make a physical assessment of the situation and to determine the extent of the contamination by swiping various locations and monitoring the swipes for radioactivity. In addition, air filters from early entries into WIPP were collected and analyzed to determine the identity of the element(s) responsible for the airborne activity and for the presence of other trace elements, anions, and organic compounds. Ultimately, Am and Pu isotope ratios were measured and used to support the hypothesis that the release came from a single drum and that the isotopic ratios were consistent with those expected to be present in Drum 68660.

The next stage of sampling was to collect as much evidence as possible from the environment around Drum 68660, with the goal of collecting samples that might provide insight into the cause of the drum breach. The initial sample collection activity would provide experience and information that could inform subsequent sampling and analysis efforts. The first sampling activity near Drum 68660 occurred in May 2014, with limited guidance from the WIPP TAT. The main concern during this sampling was to use a collector that would fit on the end of a fifty-foot, titanium/aluminum pole and that was made of a material that would not generate sparks. Due to the harsh environment, samplers were required to wear bulky PPE and standard operating procedures limited the activities of the WIPP operators and the time they could remain on station. Additionally, the area around Drum 68660 could not be directly accessed; sampling was performed remotely, with limited control and visibility of the actual collection operation.

Two sampling configurations were used during this collection. The first was a “Swiffer® multi-sampler,” which consisted of four Rad Con disc smears on the top section, a Velcro® strip on the bottom section, and a narrower Velcro® strip (in the center) with the adhesive tape exposed (Figure B-1, top left). This sampler could be easily deployed on the end of a sampling pole. It was hoped that the Swiffer® multi-sampler would collect particles (primarily MgO) with both the exposed adhesive and the Velcro. The second sampler was a scoop made of PVC

pipe, which also could be deployed at the end of a pole (Figure B-1, top right). This sampler was used to collect bulk material (primarily MgO).

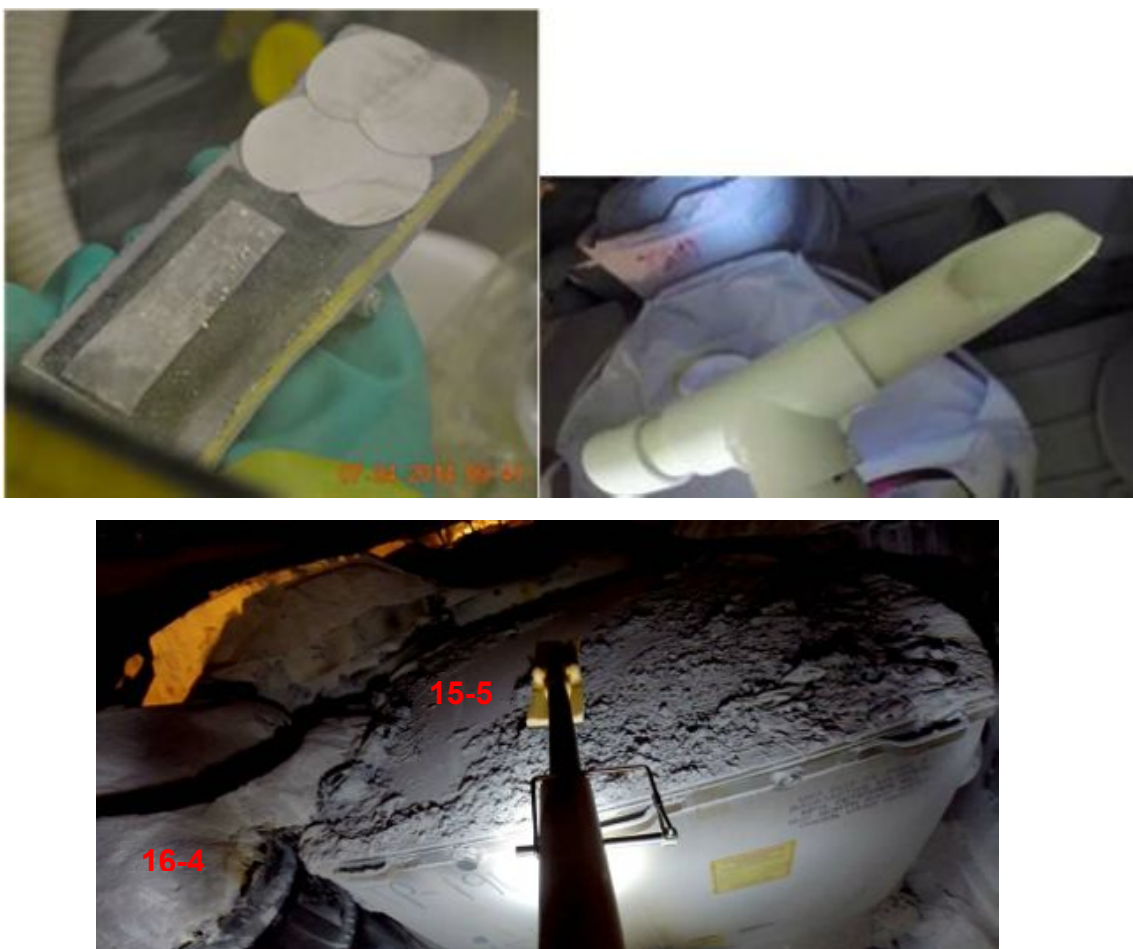


Figure B-1. Swiffer multi-sampler, PVC sampler, and Multi-sampler device being deployed on a fifty-foot rod to sample 15-5.

Using these tools, several samples were collected in May 2014. Collected samples are summarized in Table B-1.

Table B-1. Samples collected in WIPP in May 2014.

Chain of Custody	Sample Location	Sample Type
14-0183	None (clean blanks)	PVC, smears, sticky tape
14-0183	15-5 SWB	Ejected debris from multi-sampler
14-0183	16-4 drum lip	MgO from multi-sampler
14-0182	16-4	MgO from sticky pad
14-0182	14-2	Bulk MgO from PVC sampler
14-0182	14-4	Bulk MgO from PVC sampler
14-0182	14-6	Bulk MgO from PVC sampler

While the May sample collection yielded some useful analytical data, it also provided insight as to how to improve the next sample collection. For example, the materials that were used for sample collection (the Velcro[®], the tape, and the PVC) contributed a background of organic contamination to the samples. This is not an ideal situation when a goal of sampling is to determine the presence of organic compounds. In addition, the Swiffer[®] sampler did not collect a sufficient quantity of material/debris. Thus, when sampling was performed in August 2014, a new sampler was designed by a team of LLNL and WIPP staff and fabricated at LLNL. The new sampler

consisted of Delrin[®] and Teflon[®] parts so that it would not add to contamination of the samples; see Figure B-2. The edge of this sampler was machined to optimize the potential for large amounts of MgO to be collected (up to 5 g) and directly transferred into a Teflon sampling container. Additionally, the Teflon[®] sampling vials, which were cleaned of inorganic and organic contaminants, were fitted with Teflon[®] plugs to restrict their volume such that no more than 5 grams of sample were collected; this was necessary to ensure that the collected mass of the sample did not exceed that of the approved safety basis. Once the sample has been taken, the vial can be removed and sealed for transport.



Figure B-2. Delrin[®]/Teflon[®] sampler, shown with Teflon[®] vial in the collector and with Teflon[®] vial sealed for sample transport.

The new sampler was used to collect samples on August 15, 2014. The sampling team first attempted to obtain a representative sample of the discolored MgO on top of the Drum 68660 — the breached drum appeared to have released material all around the 16-4 area, including on the top of the 15-5 SWB. While it had been expected that the MgO would be a powder that would be easy to sample, the material in the area of 16-4 was instead very hard, crusty, and nearly impossible to sample. As a result, only a small amount of material was collected. Next, the material on the top of the 15-5 SWB sampled. It was found to be thin with crusted/hard mounds in several locations and this limited the ability to obtain homogeneous samples. To assess background chemicals and contaminants, two samples were also taken from unused MgO bags that were located in the front of the Panel 7 (after row 24). Although the MgO bags were present during the event, these bags did not exhibit any damage (their polypropylene/ cardboard outer containment was intact). The samples were closed and brought to the surface where chain of custody was initiated and the samples sealed with tamper-evident tape. The samples were then placed in coolers that were also sealed with tamper-evident tape and sent to SRNL for distribution and analysis. Samples that were collected in August 2014 are summarized in Table B-2.

Table B-2. Samples collected in WIPP in August 2014.

Chain of Custody	Sample Location	Sample Type
9572 Sample #1	16-4 drum	MgO from Delrin [®] sampler
9572 Sample #2	15-5 SWB	Ejected debris from Delrin [®] sampler
9572 Sample #3	15-5 SWB	Ejected debris from Delrin [®] sampler
9572 Sample #6	Front of Panel 7	Bulk MgO from Delrin [®] sampler
9572 Sample #7	Front of Panel 7	Bulk MgO from Delrin [®] sampler

Because the configuration of WIPP prevented samples from being collected inside of Drum 68660, the next best option was to sample its “parent” drum (S855793), which resided at LANL. This sampling was conducted on August 6–7, 2014. Sampling of the parent drum was performed under the assumption that the parent drum still

contained residues that could be detected and that would reflect the composition of materials in the breached drum. The advantages of sampling the parent drum included that it could be easily accessed and sampled and that additional analytical techniques could be used while sampling this drum that could not be used at WIPP (for example, headspace gases could be sampled). However, sampling the parent drum posed the limitation that there was much less material to sample, because the drum is considered to be empty. In addition, it was found that the gasket of the parent drum was missing; thus, organic solvents would be expected to have volatilized from the drum during storage and would not be available for detection.

The first sampling activity performed in investigating the parent drum was to sample the headspace of the 85-gallon over pack drum, in which the drum was nested. A special sampling port was inserted through both the lid of overpack and into drum S855793 to detect, in near-real-time, headspace gases (H₂, CO, CO₂, N₂O and volatile organic compounds) in the parent drum using gas chromatography/mass spectrometry. In addition, two samples were collected in 100-mL, gas-tight syringes; one sample was immediately sent for laboratory analysis at LANL, and the other was transferred to an evacuated 200-mL Summa canister for future TAT laboratory analysis (in addition, a field blank was collected in a 50-mL Summa canister for the TAT).

The second sampling activity focused on the collection of solid and liquid residue samples from the parent drum S855793 (although no free liquids were found in the parent drum). Samples collected included IAEA swipes for radiological analysis, glass swipes for organic analysis, and debris for targeted analysis. Each sample was placed in a primary container, which was placed inside of two re-sealable plastic bags, the outer of which was sealed with a tamper-evident seal. Each sample was documented with COC paperwork. Samples collected from the parent drum are summarized in Table B-3.

Table B-3. Samples collected from parent drum S855793 at LANL on August 7, 2014 for analysis by the TAT laboratories.

Chain of Custody	Sample Type	Comment
69120 (from parent drum S855793)	Authentic	Glass filter
	Quality control	Clean, glass filter taken into contaminated area
	Quality control	Clean, glass filter (transport blank)
	Authentic	Solid debris in Teflon bottle
	Quality control	Clean, empty Teflon bottle taken into contaminated area
	Quality control	Clean, empty Teflon bottle (transport blank)
	Authentic	IAEA wipe sample
	Quality control	Clean, IAEA wipe taken into contaminated area
	Authentic (Archive)	Glass filter
	Quality control (Archive)	Clean, glass filter taken into contaminated area
	Quality control (Archive)	Clean, glass filter (transport blank)
	Authentic (Archive)	Solid debris in Teflon bottle
	Quality control (Archive)	Clean, empty Teflon bottle
	Quality control (Archive)	Clean, empty Teflon bottle opened in contaminated area
Authentic (Archive)	IAEA wipe sample	
Quality control (Archive)	Clean, IAEA wipe taken into contaminated area	

Once samples were collected, entered into chain-of-custody, and distributed to the various laboratories, sample analysis activities could begin. Initial analyses were guided by the desire to glean as much information as possible from each sample (e.g. sample morphology and metals, anions, and organic compounds present). In general, the strategy of analysis was adopted such that non-destructive analyses (e.g. microscopy) were performed first and destructive analyses (e.g. gas chromatography/mass spectrometry) were performed later. Each analytical technique performed provided different information; see Table B-4. Once initial data were obtained as a result of chemical analyses, these were used to ask additional questions, refine hypotheses, develop subsequent analysis plans, and improve future sampling strategies. Integration from data from all analytical techniques allows the story of Drum 68660 to emerge. As this section was intended to provide an overview of the sampling and analysis strategy, specific analytical results will be discussed in the relevant sections of this report.

Table B-4. Analytical techniques used to examine WIPP samples.

Analysis	What's Detected?	Questions Addressed
Gamma analysis	Radioactivity	<ul style="list-style-type: none"> • Where in WIPP did contamination spread? • Do isotopes observed in the environment reflect the expected contents of the Drum 68660?
Optical microscopy	Sample morphology	<ul style="list-style-type: none"> • Is the sample homogeneous? • Are Swheat Scoop® particles present in the sample?
Scanning electron microscopy (SEM)	Particles	<ul style="list-style-type: none"> • Examines particle morphology • Are Swheat Scoop® particles present in the sample? • When combined with energy dispersive spectroscopy, can provide particle composition (detected lead, sodium, chloride, magnesium, and potassium)
Fourier Transform infrared spectroscopy (FTIR)	Non-destructive technique; identifies bulk materials	<ul style="list-style-type: none"> • Are oxidized organics (carbohydrates) and nitrated organics present? • Are nitrates, nitrites, carbonates, and metal oxides present? • MgO, Mg(OH)₂, and MgCO₃ can be distinguished to determine whether MgO was exposed to significant amounts of water or CO₂
RAMAN Spectroscopy	Non-destructive technique; identifies bulk materials	<ul style="list-style-type: none"> • Are nitrates, nitrites, phosphates, or chlorates present? • Is carbonaceous soot present?
X-ray fluorescence (XRF)	Non-destructive determination of elemental composition	<ul style="list-style-type: none"> • Are metals present that might have catalyzed chemical reactions?
X-ray diffraction (XRD)	Atomic and molecular structure of a crystal	<ul style="list-style-type: none"> • Are crystalline reaction products in the debris? • MgO, Mg(OH)₂, and MgCO₃ can be distinguished to determine whether MgO was exposed to significant amounts of water or CO₂
Ion chromatography (IC)	Anions and cations	<ul style="list-style-type: none"> • Are nitrates, nitrites, chloride, sulfate, fluoride, oxalate, or other anions observed in the sample? • Presence of nitrite and carbonate would be consistent with hypothesis of reaction of Swheat Scoop® and metal nitrate salts
Inductively coupled plasma mass spectrometry (ICP/MS)	Inorganic elements at trace concentrations	<ul style="list-style-type: none"> • What is the elemental composition of the samples? • Are metals present that might catalyze chemical reactions?
Gas chromatography/ mass spectrometry (GC/MS)	Semi-volatile organic compounds at trace concentrations	<ul style="list-style-type: none"> • Can organic chemicals that were contained in the waste drum be detected? • Are any products of possible oxidation or nitration chemistry observed?

Analysis	What's Detected?	Questions Addressed
Liquid chromatography/ mass spectrometry (LC/MS)	Non-volatile organic compounds at trace concentrations	<ul style="list-style-type: none"> • Are organic chemicals indicative of reacted Swheat Scoop® (e.g., carbohydrates, sugars) observed? • Are any products of possible oxidation or nitration chemistry reactions observed?
Thermogravimetric-mass spectroscopy (TG-MS)	Volatile organics are detected as a function of temperature	<ul style="list-style-type: none"> • Thermal stability of the debris and decomposition products

APPENDIX C. ANALYSIS INTEGRATED SUMMARY REPORT

SUMMARY OF CONCLUSIONS

Nondestructive and destructive analytical methods were used to analyze samples of debris collected from the top of R15 C5, the lip of R16 C4, the parent drum, and the constant air monitor (CAM) and fixed air sample (FAS) filters in addition to MgO samples collected from the tops of R14 C2, R14 C4, R14 C6 and R16 C4. The analytical evidence supports the conclusion that an exothermic oxidation reaction of Swheat Scoop® by metal nitrate salts produced gases that contributed to the breach of Drum 68660. The metals and the acidic environment found in Drum 68660 are known to accelerate these oxidation reactions. Moreover, the ratio of metal nitrate salts in Drum 68660 was in a range in which a low melting eutectic mixture could form, which would also accelerate the oxidation reactions. Nitrated organics were not detected and they are not necessary to produce the exothermic reaction leading to the breach of Drum 68660. All the contents of the drum were not consumed and the material ejected from Drum 68660 either did not experience temperatures over 200 °C, or their exposure to elevated temperatures was very limited in duration (<seconds). These findings are based on the details described below.

- Metals and acid were present that would accelerate the oxidation reactions:
 - The metals found in the debris and the acidic environment of Drum 68660 are known to accelerate the decomposition of the organic materials comprising the Swheat Scoop®.
 - Trivalent nitrate salts, i.e., iron and aluminum, react at lower temperature with ligocellulosics than mono or divalent nitrate salts (i.e., Na, K, Mg, Ca, and Pb).
 - Metals (Bi, W, and La) from the glovebox glove were not involved in the reaction.
 - Other than one particle of Bi found on the lip of R16 C4, no Bi, W or La were found in the samples from R15 C5, R16 C4 or the CAM filters.
 - At the time of the Real Time Radiography (RTR) of Drum 68660 performed at LANL, the glovebox glove was in the job control solid waste layer at the bottom of the drum physically separated from the neutralized liquid/Swheat Scoop® layer^{bb}; though unlikely, physical contact may have occurred to some degree during transportation of the drum to WIPP.
- Reaction products are from metal nitrate oxidation of organics:
 - Significant levels of nitrite and carbonate salts were found in the samples that were not present in the original waste stream. These compounds are products from the oxidation of carbohydrates (Swheat Scoop®) by metal nitrate salts.
- Reaction inside the drum did not go to completion:
 - Materials ejected from the drum either did not experience temperatures over 200 °C, or their exposure to elevated temperatures was very limited in duration (<seconds), resulting in the observation of thermally sensitive materials in the collected samples.
 - Thermally sensitive materials (i.e., oxalate and nitrite salts) were found in ejected material that would not have survived a high temperature reaction.
 - Triethanolamine (TEA), a component of Kolorsafe® liquid acid neutralizer, was tentatively identified in a sample of the debris collected from R15 C5.
- Oxidation products were observed in the debris but nitration products were not detected:
 - Nonextractable oxidation products were detected but no lower molecular weight oxidation products were found.
 - Formation of nitrated (i.e., nitrate esters or nitro-containing) compounds cannot be ruled out but if they are present, they are in low concentration.
 - Formation of nitrated compounds is not necessary to produce an exothermic reaction, which could produce sufficient quantities of gas to cause the breach of Drum 68660.
 - The absence of triethanolammonium nitrate (TEAN) and TEAN decomposition products indicates the material potentially was consumed in the reaction.
- Eutectic mixture of nitrate salts could form:

^{bb} See Appendix E, Addendum A, “Expert Interpretation Of Real Time Radiographic Recordings,” for details.

- Although an exact ratio of the salts is not known, they are in a range in which a eutectic mixture of Mg, Na, Ca, and K nitrate salts could form. While the melting temperature of the potential eutectic mixture is not precisely known, these results indicate that a liquefied eutectic mixture was possible in the drum environment, which could accelerate the oxidation reactions.
- Gases from truck fire did not cause the damage to the super sacks:
 - No evidence to support the presence of Mg(OH)₂, MgCO₃ or other metastable hydrous carbonate species that would be expected if the material in the super sacks was exposed to significant quantities of CO₂ and/or H₂O combustion products.
 - The low radioactivity on the exposed MgO on the adjacent drums indicates that the event was of short duration (seconds).

SUMMARY OF ANALYTICAL PROCESS

Samples collected from WIPP (as described in Appendix B, “Sampling Integrated Summary Report”) were sent to Pacific Northwest National Laboratory (PNNL), Savannah River National Laboratory (SRNL), and Lawrence Livermore National Laboratory (LLNL) for analysis. PNNL received the samples from the lip of R16 C4 and the top of standard waste box (SWB) R15 C5 taken on May 30, 2014 using the multi-sampler device. The bulk MgO samples from R14 C2, R14 C4, and R14 C6 and the MgO sample taken from the top of R16 C4 using the multi-sampler device were sent to SRNL. The second set of samples from the lip of R16 C4 and two samples from R15 C5 taken on August 15, 2014 were sent to SRNL for analysis, and a subsample of R15 C5 was sent to LLNL for LC-MS analysis. Samples of the debris and swipes from the parent drum were sent to SRNL for analysis.

The analytical approach for the samples was determined at the first meeting of the TAT on June 3-4, 2014 and followed standard practices for identification of unknown samples. [Magnuson, 2012] Analysis initially started with nondestructive analysis (optical and gamma analysis, XRD/XRF, SEM-EDS, Raman and/or FTIR) followed by destructive analysis (ICP-EOS, ICP-MS, IC, extraction/GC-MS, LC-MS, and TG-MS). Sets of instructions (called R&D Directions at SRNL, Test Instructions at PNNL, Sample Preparation and Analysis Plan at LLNL) were prepared describing how the samples would be handled and analyzed. These instructions built off the existing analytical procedures and quality control documents already in place at PNNL, SRNL, and LLNL. These instructions were circulated to the WIPP TAT for review, comments were addressed and the final revised documents were approved by unanimous vote of the TAT. Work did not start until TAT approval was obtained. Each lab assigned its samples a unique sample (and tracking) number including all sample splits and sample transfers, which were tracked with a chain of custody form. The samples were photographed during all aspects of unpacking and transfer, and the samples were qualitatively surveyed for radioisotopes by nondestructive gamma analysis. An archive sample was maintained from all samples for future reference. The analytical details for each analysis and the raw data are presented in the Appendix (Analytical Results from PNNL, SRNL, and LLNL). A full discussion of the radiochemical analysis is presented in the Source Term Section and is not discussed here. Below is a high level summary of the analytical results followed by a discussion of how the analytical data supports the key judgments.

SUMMARY OF ANALYTICAL RESULTS

The analytical efforts focused on the materials ejected onto the SWB R15 C5 to determine the reactions that occurred in Drum 68660 that led to the breach. The samples from the lip of R16 C4 were much smaller and primarily contained MgO. Overall, the debris from R15 C5 was very heterogeneous and predominantly contained a mixture of inorganic salts. The primary metals identified were consistent with what was known to be in Drum 68660 [see Thermal Modeling Section] (Mg, Na, Ca, Fe, Al, K, and Ni, note – Cr was observed in XRF but not in the ICP-OES,) while trace quantities (typically <0.02 wt%) of other metals (Ba, Mn, Ti, and Zn) not noted in the original drum contents were observed. No Bi, W, or La (from a glovebox glove) was detected by SEM-EDS, ICP-OES, ICP-MS, or micro-XRD analysis of the R15 C5 samples. The phosphorus observed in the R15 C5 samples most likely originated from the Swheat Scoop®, which contains about 0.5 wt% phosphorus. Lead was ubiquitous and in a R15 C5 sample, it was found in concentrations over 100-fold greater than that predicted from the drum

contents. This most likely arises from nitric acid leaching of the lead drum liner present within the parent drum during the decades of storage before processing. In addition to the anions expected based on the drum contents (NO_3^- , F^- , and oxalate), new anions were found in the debris including NO_2^- , CO_3^{2-} , and Cl^- . The nitrite and carbonate are consistent with products expected from the reaction of carbohydrates with metal nitrate salts (see below). Significantly more metal cations were found than anions indicating that metal oxides are present in the debris. The debris from R15 C5 contained a small number of methylene chloride extractable organic compounds (and no additional compounds were observed after derivatization, reporting limit 2ppm). A few low molecular weight organic acids (formic, acetic and oxalic) were observed in the water extract of R15 C5, but these acids were also found in the Swheat Scoop®. FTIR and micro-fluorescence microscopy analyses of the debris and the methylene chloride extract were very complex and showed the presence of organic material that resembled Swheat Scoop® (i.e., carbohydrates) and inorganics materials (nitrates and carbonates). Oxidized materials were also identified in the FTIR spectra (by both bulk and micro-techniques) but no other degradation products of Swheat Scoop® or triethanolamine (TEA) could be identified. No nitrated organics or triethanolamine were detected by GC-MS or FTIR analysis. A sample of R15 C5 was sent to LLNL to analyze for polar, high molecular material by LC-MS using a high-resolution mass spectrometer capable of tandem mass spectrometry in positive electrospray mode. Unlike, GC-MS, no LC-MS libraries are available to assist in the identification of unknown compounds; however, by exploiting exact mass measurements, the presence of targeted compounds can be detected. Using this type of targeted analysis, triethanolamine was tentatively identified in the sample. TG-MS analysis of the debris from R15 C5 under argon showed unreacted material was present. The debris showed a total weight loss of 9.4% at 200 °C, 17% at 400 °C and a final weight loss of 35.1% at 1000 °C indicating the material did not experience high temperatures. Gases evolved below 200 °C included m/z 16 (CH_4), m/z 18 (H_2O), m/z 30 (NO and CH_2O) and m/z 44 (CO_2 and/or N_2O), and m/z 46 (NO_2 , and other materials), which is consistent with the decomposition of organics and metal nitrate salts.

The sample from the lip of R16 C4 was primarily MgO. The metals found in the sample were consistent with what was found in R15 C5 except the Pb was found in significantly lower concentrations. SEM analysis found pieces of steel in the sample (which could have originated from the drum). Although it was anticipated that organics would be present on the lip of 68660 since it was discolored, hard and crusty, only minor amounts of organic residues (such as carboxylic acids) were detected by micro-FTIR ATR, and no detectable amounts of organics were found in the methylene chloride extract. No triethanolamine or nitrated organics were detected by GC-MS or FTIR analysis. It is postulated that high molecular weight (methylene chloride insoluble) organic compounds derived from the Swheat Scoop® are responsible for the material on the lip of R16 C4 being hard and crusty.

The debris from parent drum S855793 was expected to be acidic based on the drum history and a water extract of the debris was found to be slightly acidic (pH was 3.8, with a total acid content of 0.0157 N). The anions in the water extract were consistent with the known contents of the waste stream (nitrate, fluoride, and sulfate) and the extractable anions from the Swheat Scoop® (formate, acetate, oxalate, chloride, sulfate, and phosphate). Since phosphorous was not in significant concentration in the waste stream (<0.01 wt%), it is a good indicator of Swheat Scoop®. The metals found in the debris were consistent with the drum contents (Mg, Na, Ca, Al, Fe, and K) except for the high concentrations of lead (11.7 wt%). The IAEA swipes only contained a trace amount of lead. No significant amount of organics was found from the methylene chloride extracts of the glass swipes by GC-MS (reporting limit 20 ppm). FTIR analysis of the extract detected inorganic material including carbonates and nitrates. Extraction of the debris with methylene chloride found long chain fatty acids (linoleic and palmitic acids), which are known to be present in Swheat Scoop®. [Sramkova, 2009]

Many of the major materials found in the debris on R15 C5 were also found on the CAM and FAS filters. The materials on the CAM filters include anions (nitrate, nitrite, oxalate, acetate, formate, chloride, fluoride, and sulfate), metals (Mg, Na, Ca, Fe, Al, and Pb), and organics (that have an FTIR spectra similar to Swheat Scoop®). The materials on the FAS filters also include anions (nitrate, nitrite, formate, chloride, fluoride, and sulfate) and metals (Mg, Na, Fe, Al, and Pb). This indicates the material ejected from the drum formed aerosol particles that moved through the room and drift and were collected by the CAM and the FAS filters. This observation is

supported by optical microscopy and SEM-EDS measurements of small salt particles on R15 C5 and R16 C4. Extremely small Pu and Pb particles (too small to be accurately measured by SEM but well below 100 nm in diameter) were found associated with larger, high-surface-area “hairy” salt particles. The morphology and chemical makeup of these salts were significantly different from that naturally expected from the mine, and consistent with a rapid precipitation mechanism out of the entrained liquid known to be present within Drum 68660.

Magnesium oxide was collected from on top of adjacent drums (R14 C2, R14 C4, and R14 C6) and a reference sample was collected from an intact bag of MgO located on the floor at the waste face. The samples were white or beige colored and were composed of powder and pellets with an occasional dark particle. The MgO samples had low radioactivity, which indicated that the event was of short duration. If the radioactive material was slowly ejected from 68660 over a time frame of minutes, more radioactivity would be expected on the adjacent drum. XRD and FTIR analysis of the MgO from the drums indicated that no Mg(OH)₂, MgCO₃ or other metastable hydrous carbonate species was present that would be expected if the material in the super sacks was exposed to significant quantities of CO₂ and/or H₂O combustion products from the truck fire. Therefore, it is concluded that the truck fire event did not cause the damage observed in Panel 7 Room 7.

Parent Drum: Contents, Acidity and Metals

In the Reaction Chemistry and Hypothesis discussion (Appendix F), it is proposed that a series of internal exothermic reactions produced sufficient gas pressure to breach Drum 68660. These reactions could have been initiated by a combination of chemical and/or radiolytically induced reactions between nitric acid, nitrate salts, metals, triethanolamine (TEA)/triethanolammonium nitrate (TEAN), and Swheat Scoop®. It is important to define the contents of Drum 68660 since these materials should be found in the debris on R15 C5 and the lip of R16 C4, and these materials are responsible for the exothermic reactions and the corresponding reaction products.

The contents of Drum 68660 were estimated by Weisbrod starting from the Veazey salt analysis as described in the Thermal Modeling Section. The drum had a layer of job control solid waste (plastic/rubber) on the bottom, processed liquid layer consisting of Swheat Scoop®/nitric acid/Kolorsafe® liquid acid neutralizer (i.e., triethanolamine, water and Alizarin, an indicator dye), and a metal nitrate salt layer mixed with Swheat Scoop®. The Swheat Scoop® was mixed with the liquids in a 3:1 volume ratio while Swheat Scoop® was mixed with the nitrate salts in a 0.7:1 volume ratio. The molarity of the acid in the liquid layer and the interstitial liquid in the nitrate salts was 3.3M. [Clark, 2015] The estimated composition of the nitrate salt layer is shown in Table C-1. Note the initial Pb content is very small and no nitrites or carbonates were present.

Table C-1. Composition of salts in 68660 (as described in the Thermal Runaway Model Section)

Component	Wt%
Mg(NO ₃) ₂ • 6 H ₂ O	62.3
NaNO ₃	13.7
Ca(NO ₃) ₂ • 4 H ₂ O	9.47
Fe(NO ₃) ₃ • 9 H ₂ O	6.45
Al(NO ₃) ₃ • 9 H ₂ O	2.38
KNO ₃	2.08
(COOH) ₂	1.53
HNO ₃	1.53
H ₂ O (with trace elements)	0.20
NaF	0.18
Cr(NO ₃) ₂ • 9H ₂ O	0.13
Ni(NO ₃) ₂ • 6 H ₂ O	0.06
Pb(NO ₃) ₂	0.01

Acidity of Parent Drum (S855793): The acidity of the waste stream is important in determining potential reaction chemistry. Swheat Scoop® is derived from the whole grain of wheat, which is primarily composed of starch (65-70% dry weight) and proteins (14%) with smaller amounts of lignin, lipids, other polymeric carbohydrates including cellulose, and minerals. Dilute nitric acid is known to hydrolyze and oxidize hemicellulose, starch, and amorphous regions of cellulose to monosaccharides, polysaccharides, carboxylic acids (including acetic and oxalate acid [Sullivan, 1983]) and aldehydes (like hydroxymethyl furfural). [Rodriguez-Choong, 2004; Bensah, 2013; Fontana, 2008] Concentrated nitric acid or a combination of nitric acid with a dehydrating reagent like sulfuric acid leads to nitration reactions to form nitrate esters and nitro compounds [Olah, 1989]. Heating concentrated (69%) nitric acid to 180 °C can result in complete mineralization of the primary components of biomass (carbohydrates, carboxylic acids). [Würfels, 1989] In test reactions run at LANL [Clark, 2015], it was also shown that nitric acid lowers the temperature where decomposition and/or exothermic reactions can occur for both Swheat Scoop® and TEA. Thus, the acidity of the waste stream can contribute to the degradation of the Swheat Scoop®.

During processing of the parent drum (S855793), it was documented that approximately 2 gallons of liquid was collected with a pH of 0, measured by pH paper, and neutralized with Kolersafe®. Based on process knowledge, the nitrate salts from the ion exchange process were washed with 3.3M nitric acid, while nitrate salts from the oxalate filtrates were not washed with bulk acid because it would accelerate decomposition of the oxalic acid present in the salts. [Clark, 2015] Typically, after emptying a drum and processing its contents, a little adsorbent, Swheat Scoop®, was added into the empty drum to adsorb any residual liquids. The parent drum (S855793) of 68660 was sampled as described in the Appendix B (Sampling Integrated Summary Report) to learn more about the contents of the drum. The dry solid debris was extracted with water and the total acid content was determined to be 0.0157 N by titration. The total acid content for a water extract of Swheat Scoop® was 0.0050 N. The free acid available in the solid, which represents the free H⁺ concentration (in 20 mL of solution) relative to the mass of the sample (0.6901g), is 0.455 mol/Kg, which is similar to quantities measured by LANL for samples taken from other empty parent drums with acidic liquid [Martinez, 2014]. Although it is not possible to back calculate the acidity of the original drum, this does confirm the materials in the parent drum were acidic.

The water extract from the debris from the parent drum was also analyzed by ion chromatography. As expected, the dominant anions were nitrate (12.6 wt%) and oxalate (0.264 wt%) with smaller amounts of chloride (899 µg/g), sulfate (290 µg/g), and formate (638 µg/g). Fluoride and acetate also were observed but could not be quantitated because they co-eluted. Swheat Scoop® was also found to contain water extractable ions including small amounts (<0.05 wt%) of chloride (480 µg/g), formate (332 µg/g), nitrate (240 µg/g), oxalate (240 µg/g), and sulfate (435 µg/g). Phosphate was found in higher concentrations (0.50 wt%), and since it is not found in significant concentrations in the waste stream (<0.01 wt%), phosphate can be used as a signature of Swheat Scoop® in the debris. Overall, the anions detected in the parent drum were consistent with the content of 68660 and Swheat Scoop®.

Metals in Parent Drum (S855793): Metals could potentially act as catalyst to accelerate the decomposition of the organic materials as discussed in the Reaction Chemistry and Hypothesis appendix (Appendix F). Thus, the metals in the parent drum were qualitatively analyzed by SEM-EDS, and quantitated by ICP-OES and ICP-MS using a mixed acid (HNO₃/HCl/HF in a 2:1:1 volume ratio) digestion and peroxide (Na₂O₂) fusion (which is more aggressive and can provide a higher recovery of the metals). Since Swheat Scoop® was added to the empty parent drum to adsorb any residual liquids, the metals found in the debris are representative of the metals in the liquid, except for the pieces of metal from the drum. SEM-EDS analysis of the chunks of debris from the parent drum were found to contain predominately Pb with smaller amounts of Na, Mg, Al, K, Ca and K (see Figure C-1). Quantitative analyses of one sample found 11.7 wt% Pb and 2.8 wt% Na. Other metals detected which were expected based on drum contents included Al (9050 ppm), Fe (7300 ppm), Mg (5010 ppm), K (1270 ppm), Ca (573 ppm), Cr (843 ppm), and Ni (343 ppm). Additional metals detected include U (3540 ppm), Ba (1610 ppm), Zn (643 ppm), Cu (290 ppm), Mn (23 ppm), and Sr (19 ppm). Some of these metals were also found in the Swheat Scoop® including Na, Al, K, P, Mg, Ca, and Si. There are no significant amounts of metal in the debris that are unexpected based on the contents of 68660 except for the high lead concentration. Martinez and

Chamberlin reported similar results in the analysis of other parent drums in which high Pb (19-42 wt%) and sodium (1.7-3.7 wt%) concentrations were observed and similar metals were found. [Martinez, 2014]

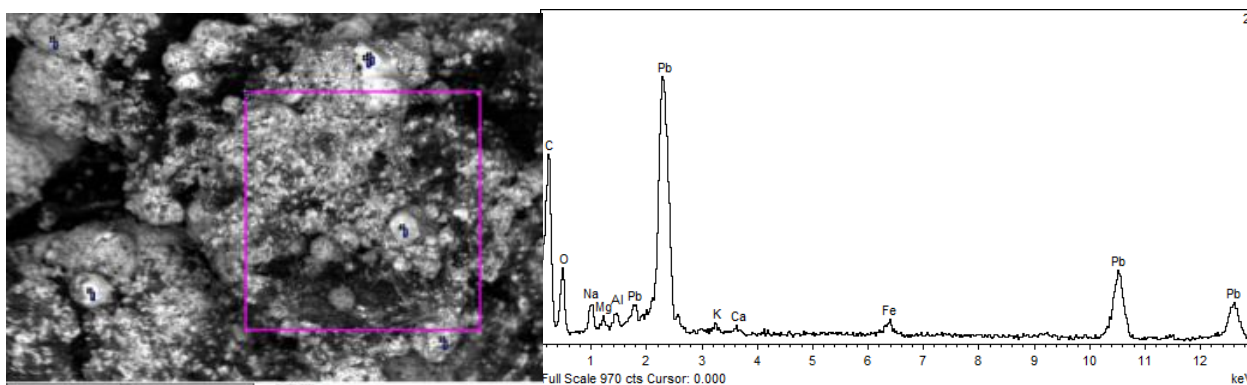


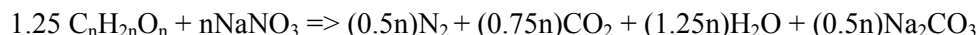
Figure C-1. SEM (A) and EDS (B) analysis of the debris from the parent drum.

Conclusions from Analysis of the Parent Drum: The metals found in the debris and the acidic environment found in the parent drum are known to accelerate the decomposition of the organic materials found in Sweat Scoop®. The metals were consistent with the drum history except for the high levels of lead, which most likely arise from nitric acid leaching of the lead drum liner present within the parent drum during the decades of storage before processing. Since phosphorus is not found in high concentration in the waste stream, phosphorus can be used to identify the presence of Sweat Scoop® in the debris samples.

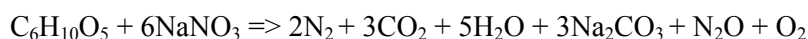
Exothermic Oxidation of Organics by Nitrate Salts

Predicted Reaction Products: The potential reactions that could lead to a series of internal exothermic reactions and produce sufficient gas pressure to breach Drum 68660 are discussed in Appendix F, "Reaction Chemistry and Hypotheses." In all cases, these reactions would produce specific products indicative of the reaction history. Thus, reaction products could arise from: (a) the hydrolysis, oxidation, and nitration of Sweat Scoop® (or more specifically carbohydrates) by nitric acid and/or metals; (b) the reaction of the metal nitrate salts and Sweat Scoop® (as discussed below); (c) the decomposition of the TEAN/Sweat Scoop® layer; (d) ionizing radiation from the radioactive decay of the transuranic elements in the waste; or/and (e) biotic reactions. Thus, the debris on the standard waste box R15 C5 and the material on the lip of breached drum were analyzed for potential reaction products from the materials in Drum 68660.

Nitrate salts are known to react with organics to produce inorganics products and volatile gases. For example, PNNL investigated the use of carbohydrates (sugars) to denitrate low-activity waste, which was acidic and high in nitrates and alkali metals [Smith, 1999]. The goal of PNNL studies was to remove the nitrates at modest temperatures (250-400 °C) and make N₂ rather than nitrogen oxides (NO₂, NO, N₂O). The denitration reaction proceeded as follows:

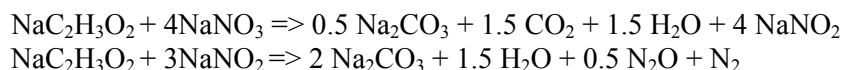


Depending on the ratio of organic (fuel) to nitrate salt (oxidizer), a range of products including CO, N₂O or NO could be formed. For example, for the reaction of cellulose with sodium nitrate at a 1:1 C:N ratio, the products are:



Carboxylic acids, from the acid hydrolysis of Sweat Scoop®, could react with nitrate salts to form similar products. Kozlowski and Bartholomew [1968] studied the decomposition of sodium formate and sodium acetate

in molten sodium nitrate and sodium nitrite at 320 °C. The products from the reaction were similar to those found in the reaction of carbohydrates except sodium nitrite was found as a reaction intermediate (as shown below).



These reactions were very vigorous and produced large amounts of gas. In general, it was observed that the lower the concentration of organic, the higher the allowable operating temperatures. It was also noted that sodium hydroxide could be formed in the reaction but it would rapidly react with the CO₂ in the melt producing Na₂CO₃ and H₂O.

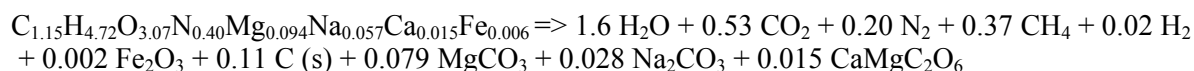
Magnesium nitrate has been shown to reduce the decomposition temperature of amylose from 280 °C to ca. 150 °C. [Desai, 1972] It was proposed that NO₂, generated at low temperature, was responsible for the low temperature oxidation of the amylose. Wu and Zavarin [1986] investigated the reaction of 20 different inorganic nitrate salts with lignocellulosic materials (including wood flour, cellulose, lignin, and xylan) and proposed that the exotherms between 100-200 °C most likely arose from the NO₂ oxidation of lignocellulosics (to form NO and carboxylate salts). They also found that the first exothermic peak in the DSC of a mixture of nitrate-lignocellulose materials decreased as the acidity of the nitrate salt increased (as shown in Table C-2). Kochkar et al. [2001] also reported the oxidation of starch by NO₂ at 70 °C produced carboxylic acids. Solid state ¹³C NMR showed that the primary -CH₂OH group in starch was oxidized while the secondary carbons were less affected.

Table C-2. DSC data for reaction between lignocellulosics and various nitrate salts. [Wu, 1986]

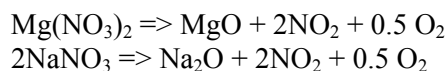
Nitrate Salt	pH of 1N solution	Wood Flour (°C) ^a	Xylan (°C) ^a	Microcrystalline Cellulose (°C) ^a
Fe(NO ₃) ₃	1.11	96	123	154
Al(NO ₃) ₃	2.24	126	147	178
Pb(NO ₃) ₂	3.45	202	207	185
Mg(NO ₃) ₂	4.61	200	190	215
Ca(NO ₃) ₂	5.13	217	232	247
NaNO ₃	6.52	260	NM	276

^aPeak temperature for the first oxidation exotherm in the DSC (800psi, N₂). NM- not measured

For the materials in Drum 68660, the potential decomposition products were determined by the thermoequilibrium code CTH-TIGER (Thermal Modeling Appendix). This model includes the Swheat Scoop®/processed liquid layer (TEAN) and the Swheat Scoop®/nitrate salt layer (see Table C-1) but does not include the plastic/rubber job waste on the bottom of the drum. The model predicts an exothermic reaction (-2.17 x 10⁶ J/kg) producing the equilibrium composition of products at 227 °C at 1 atmosphere, as shown below.

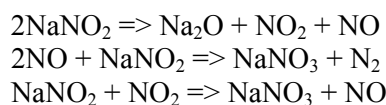


In addition to the nitrate salts reacting with organics, the salts can decompose depending on the reaction temperature. [Stern, 1972]. In general, divalent nitrate salts (Mg and Ca) decompose at a lower temperature than the monovalent nitrate salts (Na and K) to form the metal oxide as shown below. These decomposition products can then oxidize and/or nitrate organics materials (as previously discussed).

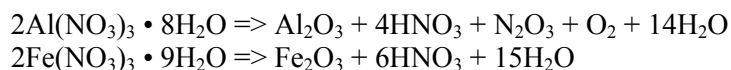


Most ionic salts melt to form liquids stable to various degrees before decomposition. Mg(NO₃)₂ and Ca(NO₃)₂ are stable up to about 325 °C and 425 °C, respectively while NaNO₃ and KNO₃ decomposes around 600 °C and 650 °C, respectively. However, the decomposition depends on the reaction environment. For example, it has been

reported that $\text{Mg}(\text{NO}_3)_2$ decomposed (to $\text{Mg}(\text{NO}_2)_2$) at 125 °C in a NO atmosphere. [Stern, 1972] In general, nitrite salts are less stable than nitrate salts. For example, NaNO_2 has been reported to be unstable above 330 °C, and KNO_2 is unstable above 410 °C. [Stern, 1972] The decomposition of nitrites and nitrates depend on the environment as shown below.



The trivalent metal nitrates, i.e., iron and aluminum, have a different decomposition pathway than that of the mono- and di-valent nitrate salts and produce HNO_3 , rather than NO_2 , as the major product at temperatures around 150 °C. [Wieczorerk-Ciurowa, 1999; Keely, 1963; Melnikov, 2013]



Triethanolammonium nitrate (TEAN) is an organic nitrate salt that melts at 80 °C and has a broad exotherm (in the DSC) with an onset temperature of 251 °C. [Bracuti, 1992] Pyrolysis of the liquid propellant LGP1845, which is composed of hydroxylammonium nitrate (63.2 wt%), TEAN (20 wt%) and water (16.8 wt%), produced NO , N_2O , N_2 , CO_2 , CO , H_2O , HCN , and C_2H_4 at temperatures between 130-540 °C. [Chang, 2001] Pyrolysis of TEAN (under 200 psi Ar and a heating rate of 175 °C s^{-1}) exhibited an exotherm at 250-325 °C and the formation of CO_2 , N_2O , CO , NO , NH_3 , and HCN . [Cronin, 1988] Laser heating of TEAN under argon produced water as the dominate product, and a series of other products similar to previous reported study including HCN , NH_3 , NO , H_2CO , CH_3CHO , CO , H_2 , CO_2 , CH_4 , C_2H_4 , CH_3CN , N_2O , and NO_2 . [Lee, 1999] Overall, the decomposition products from TEAN are gaseous.

Triethanolamine (TEA) can form complexes with metal ions through the oxygen and/or nitrogen atoms. [Naiini, 1997; Masoud, 2002] Thus, the free hydroxyl groups of TEAN could complex metals. Thermal analysis (DTA/TG/DTG) of TEA metal complexes typically showed an endotherm (melting) followed by an exotherm accompanied by weight loss. For example, $\text{Fe}(\text{TEA})_2\text{Cl}_3$ shows an endotherm corresponding to melting (165 °C) immediately followed by an exotherm (ranging from 187-273 °C and 273-302 °C but centered at 251 °C and 287 °C, respectively). [Içbudak, 1996] Similar behavior was also noted for TEA complexes with metal saccharinates in which an exotherm was measured at 150-300 °C with mass loss before or after melting. [Yilmaz, 2002] Unfortunately, there are few studies on the solid products formed from the thermal degradation of TEA metal complexes at temperatures between 150 – 500 °C, which would help guide the search for products in the debris on R15 C5.

Conclusion: From the reactions described above, the primary products expected from the oxidation of Sweat Scoop® by metal nitrate salts are volatile gases (N_2O , N_2 , CO_2 , NO), combustible gases (CH_4 , H_2 , and CO), inorganic salts (Na_2CO_3 , NaNO_2 , MgCO_3 and CaMgC_2O_6), carbon, water and nitric acid. The trivalent nitrate salts (Fe and Al) appears to be more reactive than the divalent (Mg, Ca, and Pb) and monovalent nitrate salts (Na and K). Depending on the reaction temperature, the nitrate salts could decompose and release reactive species, i.e., O_2 and NO_2 , that would accelerate the decomposition of Sweat Scoop®.

Optical and Electron Microscopy of WIPP Samples: The samples from R15 C5 were heterogeneous containing a variety of large (cm-mm) and small (μm -nm) sized particles, which contained a complex mixture of organic and inorganic materials. Although visual inspection of the particles for the two R15 C5 samples did not reveal any Sweat Scoop® present, micro-fluorescence, an empirical technique, identified particles with a spectrum similar to that of unreacted Sweat Scoop® (see Figure C-2). It is possible that the Sweat Scoop® could be coated in salt (Figure C-3) or degraded (Figure C-4), obscuring its identity. Many small particles ranging in size from 1-10 μm were observed by SEM-EDS (see Figures C-5 and C-6). These particles predominately contained Mg, O and Na with small amounts of K, Ca, and Cl. Magnesium and sodium rich areas were found throughout the samples. In

backscatter imaging, Pb was observed in almost all the samples with smaller amounts of Al, P, Fe and occasional Si. Small pieces of steel, most likely from the drum were found on the lip of R16 C4 (see Figure C-7). Micro-XRF analysis was also performed on small samples taken from R15 C5 and R16 C4. Those analyses were not quantifiable, due to limitations caused by the presence of a slip cover required to manage radioactive contamination risks, but K, Ca, Cr, Fe, Zn, Cu, Pb, and Mo were commonly identified in most scans. The elements La, W, and Bi, from a glovebox glove, were not observed in scans of over 100 randomly chosen particles. ICP-OES quantitated the Pb as 0.57 and 0.77 wt% in the two R15 C5 samples, which is about 100-fold more concentrated than the Pb in the waste stream (see Table C-1). This high Pb concentration must arise from nitric acid leaching of the Pb liner in the parent drum over the past 28 years of storage before processing. Overall, the elements Mg, Na, K, Ca, Al, and Fe are consistent with what is known to be in Drum 68660 (Table C-1) while Cl and Si could arise from the WIPP salt or the MgO. The phosphorous most likely arises from the Swheat Scoop® because phosphorous is not present in significant concentration (<0.01 wt%) in the waste stream but it is found in the native Swheat Scoop® (0.5 wt%).

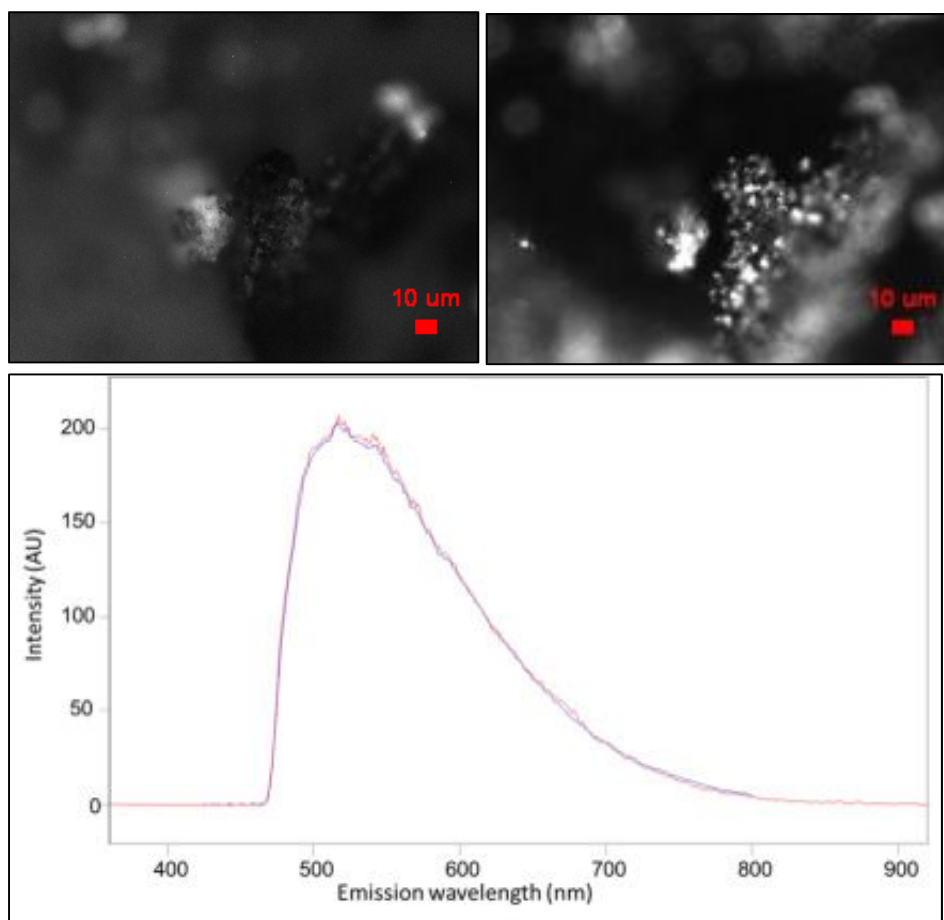


Figure C-2. (a) Particle under white light and a 10x objective. (b) Particle illuminated by an excitation band of 375-425 nm observing the emission of 475 nm and longer. (c) The emission spectra of particle (blue) overlaid with the typical kitty litter (red).

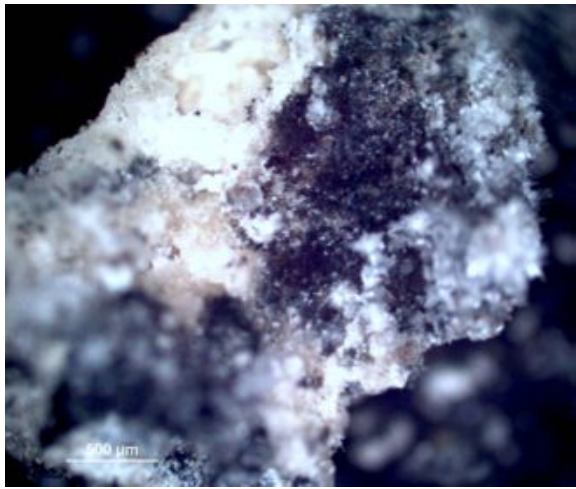


Figure C-3. Optical microscopy of R15 C5

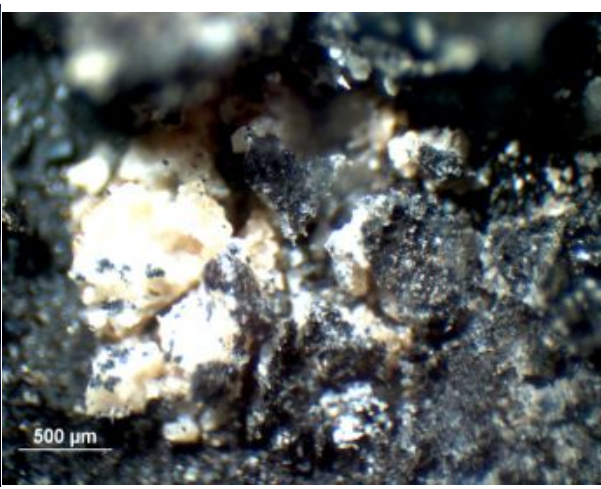


Figure C-4. Optical Microscopy of R15 C5

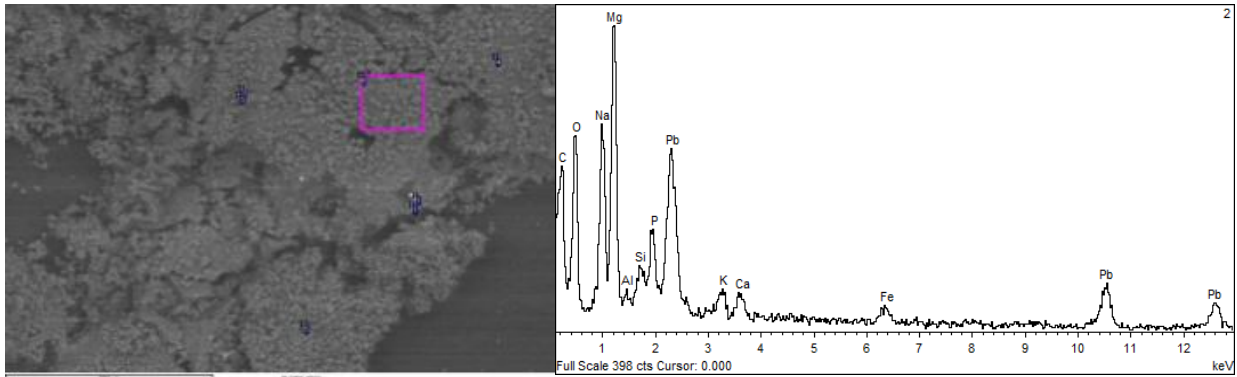


Figure C-5. (a) SEM image of particles collected from R15 C5 and (b) Representative EDS of sample.

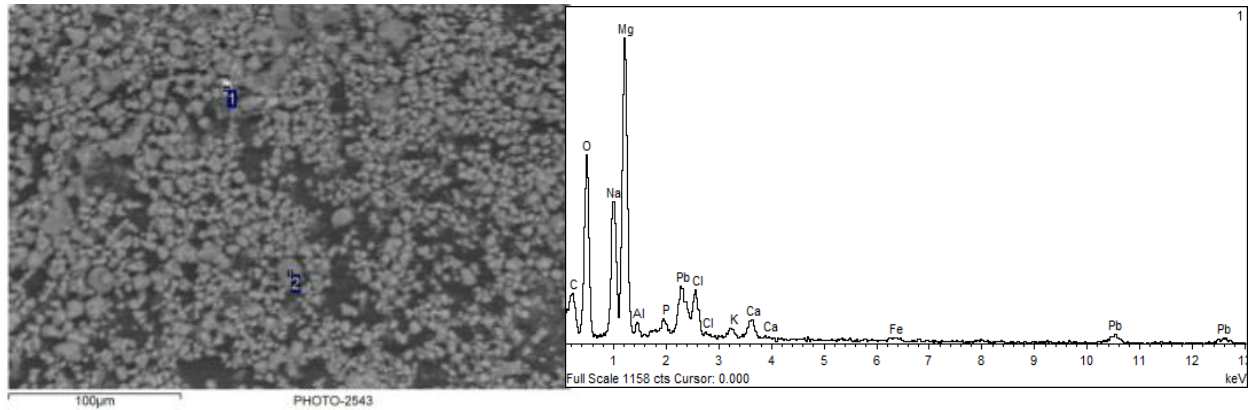


Figure C-6. (a) SEM of small particles from R15 C5 and (b) EDS of particles

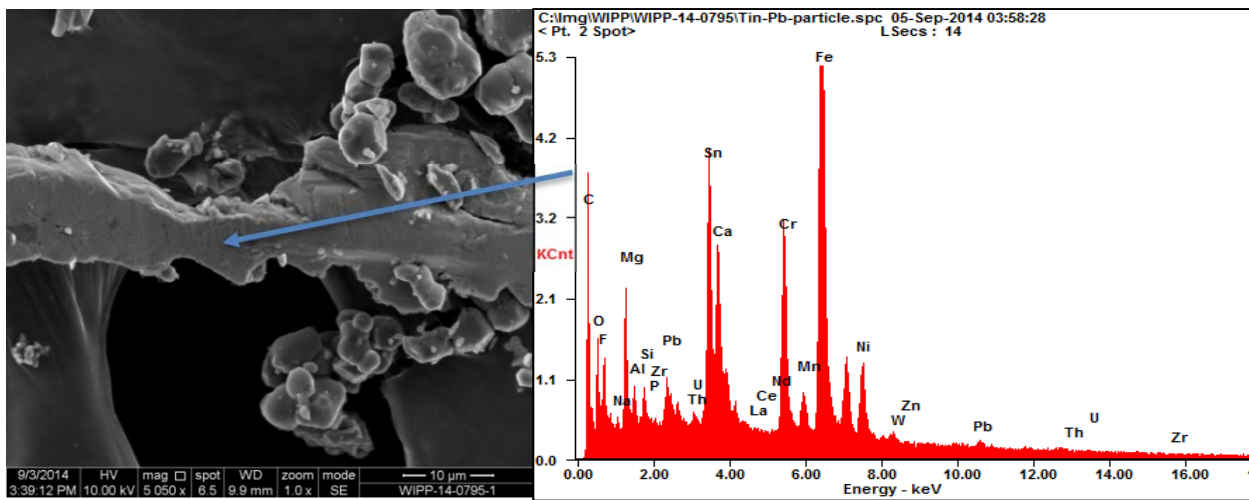


Figure C-7. Elongated piece of steel from the sample collected from the lip of R16 C4

Optical microscopy and SEM analysis of the R15 C5 samples showed salt particles that could have originated from the mine or the drum (see Figure C-8). The Carlsbad salt is a well-described material. It is a Precambrian mineral, 250 million years old and tends to contain numerous inclusions. Figure C-8a shows a salt particle with a morphology and characteristics (inclusions, etc.) indicative of the Precambrian salt from the mine. This spiny or whisker-like material shown in Figure C-8b was found infrequently, but was observed in all the samples. A similar type of phase was observed during the SEM examination of the R16 C4 lip sample, but it was not identified during the optical microscopy examination of the same sample.

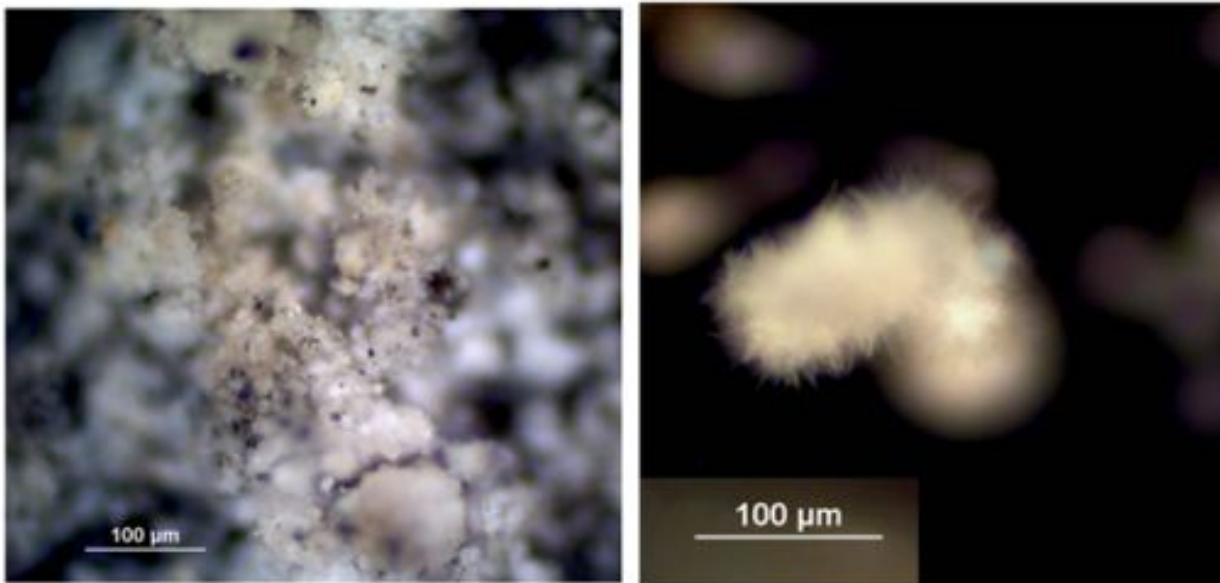


Figure C-8. Polarized light microscopy image of (a) salt-like particles from R15 C5 and (b) “hairy” particle from R15 C5

SEM-EDS images of salt particles from R16 C4, which are thought to be similar to those pictured in the optical microscopy in Figure C-8b, are pictured in Figure C-9. These “hairy” sodium bearing particles were also found to be closely associated with submicron Pb and Pu particles. Based upon SEM-EDS, we believe these Na bearing particle are likely associated with CO_3 , which is consistent with FTIR results that identified particles of sodium carbonate (see below). The hairy like structure of the Na-bearing particles is indicative of kinetically unstable solid phases that have rapidly formed from solution. Submicron particles of Pu and Pb are closely associated with

these hair-type of particles (See Figures C-10 and C-11). The Pu and U-bearing particles were not associated with the MgO indicating the MgO on the lip of R16 C4 did not come from inside the drum (but from the broken super sack).

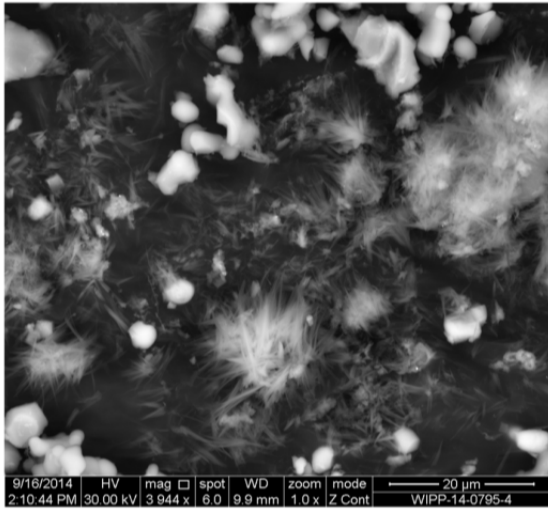


Figure C-9. SEM analysis of salt particles from R16 C4

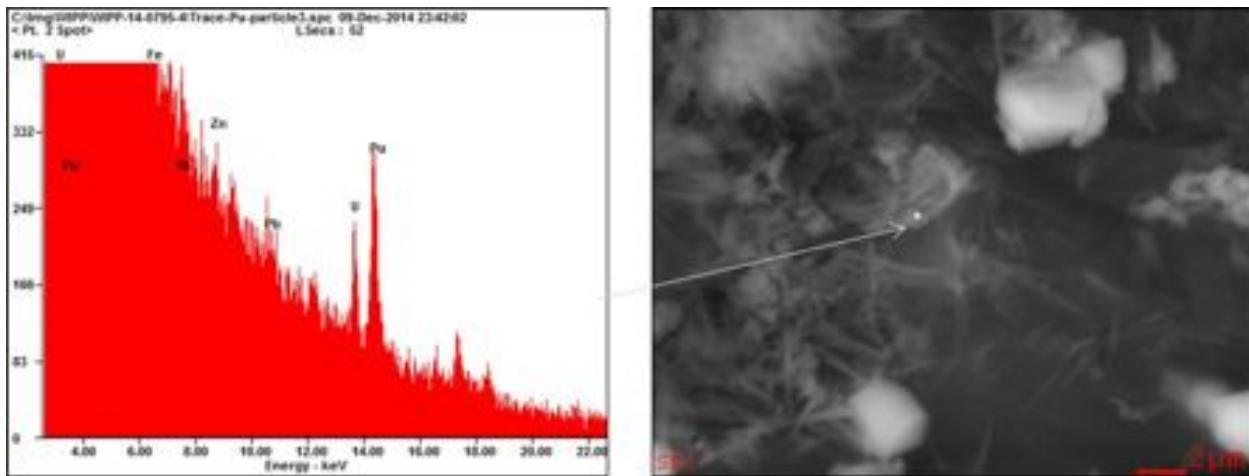


Figure C-10. SEM-EDS of small Pu particle associated with hairy salt particle from R16 C4

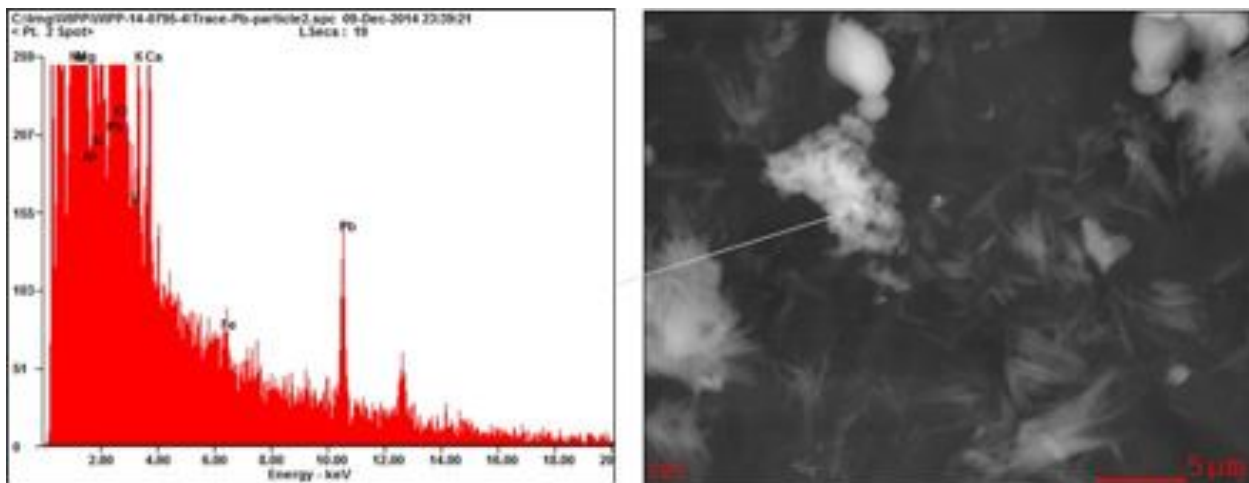


Figure C-11. SEM-EDS of a small particle of Pb associated with the hairy salt particle from R16 C4

Conclusion: High concentration of Pb found in the debris was attributed to nitric acid leaching of the lead liner in the parent during over the 28 years before processing. Other metals detected were consistent with the known content of the waste stream. Phosphorous can be used as an indicator for the presence of Swheat Scoop® since it is not found in high concentration in the waste stream. Some of the sodium containing salt particles in the debris have a morphology consistent with rapid precipitation from solution. This could have occurred as the liquids were ejected from 68660.

Glovebox Glove Did Not Participate in the Oxidation Reactions: It was proposed that the metals (Bi, W, and La) in a tungsten-lined glovebox glove, which was added to Drum 68660 as process waste, could be a reaction initiator. LANL studies showed that a piece of tungsten-lined glovebox glove in concentrated nitric acid with Swheat Scoop® and NaNO₃ provided a low temperature exotherm around 100 °C in a DSC experiment. [Clark, 2015] RTR of Drum 68660 at LANL confirmed that a glove was in the bottom job control solid waste layer (Figure C-12). The glove appears to be near the interface of the job control solid waste layer and the neutralized liquid/Swheat Scoop® layer, but there appears to be a “barrier” between the glove and the neutralized liquid/Swheat Scoop®, i.e., discarded plastic within the job control solid waste layer.



Figure C-12. Radiograph of job control solid waste layer in Drum 68660 showing the glovebox glove

Although the exact concentration of metals in the gloves is proprietary, from the company’s patent on radiation attenuation elastomeric materials [Larmigny, 2012], it can be determined that the inorganic matrix contains 70-90 wt% bismuth trioxide (Bi₂O₃) (with a preferable composition of 80±2 wt%) and 5-15 wt% of tungsten trioxide (WO₃) and lanthanum oxide (La₂O₃) (with a preferable composition of 10±1 wt% for each oxide). The preferred size range of the oxides is from 1 to 100 micrometers, with 80% of the particles less than 50 micrometers. The mass of the neoprene elastomer represents 15 to 35 wt% of the layer within the glove construction with the remaining 65 to 85 wt% composed of the inorganic oxides. The metal oxide/elastomer layer is inserted between two other elastomeric layers in the final glove. An order of magnitude calculation on the mass of rubber and inorganic oxide in one glove is: ~300g of rubber, 100-125 g Bi₂O₃, 10-13 g WO₃ and 9.5-12.5 g La₂O₃. Since the mass of the contents of the drum is 82.3 Kg (Thermal Model), the wt% Bi, W, and La in the drum is approximately 0.12 wt%, 0.012 wt%, and 0.011 wt%, respectively. If the gloves were involved in the oxidation reactions, it is proposed that the metals would be ejected and found in the debris on R15 C5, the lip of R16 C4 or on the CAM filters. ICP-OES and ICP-MS analysis of the two R15 C5 samples and the sample from the lip of R16 C4 showed no Bi, W or La within detection limits (ppm). SEM-EDS and micro-XRF analysis of over 100 randomly selected particles from R15 C5 showed no Bi, W, or La. However, one bismuth particle was found on the lip of R16 C4 by SEM-EDS analysis but no W and La was observed (see Figure C-13). Additional analysis did not find any other Bi particles. Micro-XRF analysis of the Velcro tape sample containing particles from R15 C5 did not reveal any Bi, W, or La particles. ICP-MS analysis of the CAM filters also did not show any Bi, W, or La particles. Thus, it is unlikely that the tungsten-lined glovebox glove participated in the reaction because of the

physical separation of the glove from the waste in the bottom (job control solid waste layer) of the drum and the lack of significant analytical evidence for Bi, W, or La found in the collected samples.

Conclusion: The glovebox glove did not participate in the reaction in Drum 68660 because it was physically separated from the Swheat Scoop®-processed liquid layer and Bi, W, or La was not found in R15 C5 or the CAM filters. The metals in the glove were in high enough concentration that they should have been seen if they were ejected from the drum.

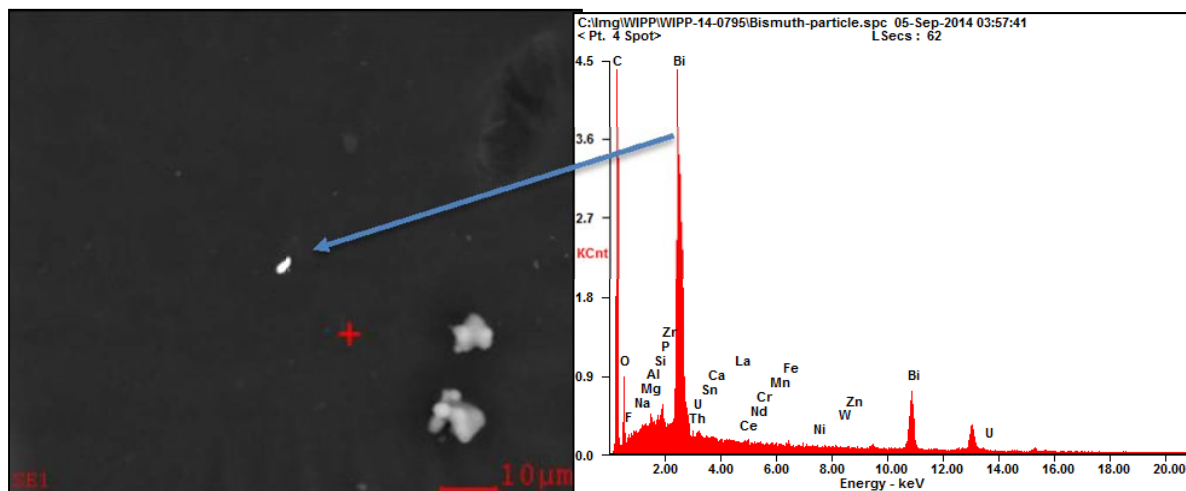


Figure C-13. SEM-EDS analysis of sample from the lip of R16 C4 showing a bismuth particle

Reaction Products from Metal Nitrate Salt Oxidation of Swheat Scoop®: The debris found on R15 C5 and the material on the lip of R16 C4 were analyzed to determine whether any reaction products (described above) could be found to support the proposed reaction pathways. X-ray diffraction (XRD) analysis of a ground sample of the debris from R15 C5 was measured and search match identification was performed with Jade software from Materials Data Inc. and the International Centre of Diffraction Database (see Figure C-14). The sample was found to contain NaNO_3 (nitratine), MgO , and $\text{Na}_3\text{H}(\text{CO}_3)_2 \cdot 2\text{H}_2\text{O}$ (Trona). Ion chromatography (IC) analysis of a water extract of the debris from R15 C5 also showed carbonate (but not quantitated by IC because of the peak shape and resolution) and nitrate (34,600 mg/Kg) in addition to nitrite (13,100 mg/Kg) and oxalate (13,100 mg/Kg). The total inorganic carbon in the water extract of R15 C5, determined by acidification and sparging using a Total Carbon Analyzer, was 43,600 mg/Kg while the Swheat Scoop® water extraction and water blanks only contained 342mg/Kg and 389 mg/Kg inorganic carbon. The water extract was also basic (pH 10.8). Sodium carbonate and nitrite salts were not present in the original waste stream, nor were they present in the MgO from the super sacks (see discussion on MgO), or in the Swheat Scoop® and are believed to be a product from the reaction of nitrate salts with Swheat Scoop®.

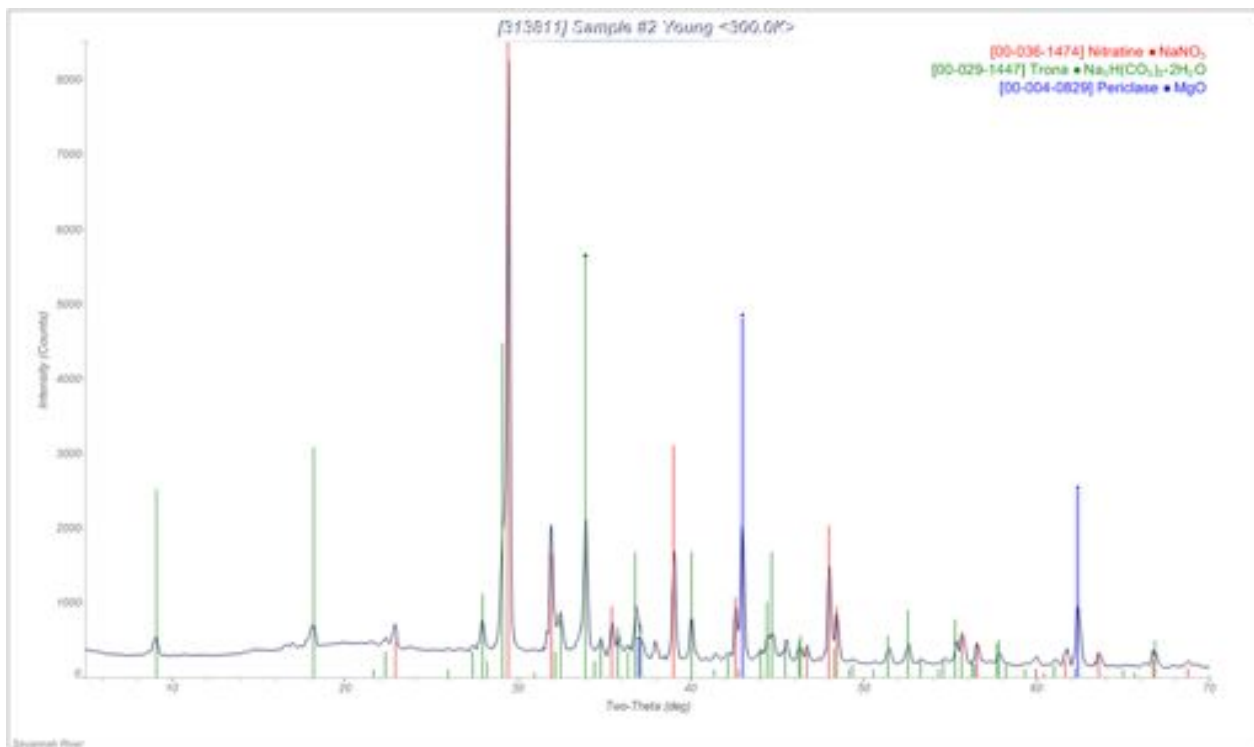


Figure C-14. XRD analysis of the R15 C5 sample

The origin of the MgO in the debris from R15 C5 is less clear. MgO could arise from the broken super sack or from the thermal degradation or chemical degradation of the $\text{Mg}(\text{NO}_3)_2$. From the pictures of the orientation of the debris on top of SWB R15 C5, it is unlikely that the majority of the MgO is from the super sack. $\text{Mg}(\text{NO}_3)_2$ can thermally decompose to form MgO but temperatures above 325 °C are needed. Since it is known that $\text{Mg}(\text{NO}_3)_2$ can oxidize organics, [Cembella, 1986; Desai, 1972; Wu, 1986] the MgO in the debris from R15 C5 most likely arises from the $\text{Mg}(\text{NO}_3)_3$ oxidation of Swheat Scoop®.

Conclusion: The material ejected from Drum 68660 was from the metal nitrate salt oxidation of Swheat Scoop®. Carbonate and nitrite were not found in the original waste stream and are known oxidation product from the reaction of nitrate salts with carbohydrates.

Reactions Inside 68660 Did Not Go to Completion: TG-MS analysis (under argon) of the debris from R15 C5 shows weight loss starting at 70 °C and a total weight loss of 9.4%, 11.4 %, 17.3%, 26.6% and 35.1% at 200, 300, 400, 500 and 1000 °C, respectively (Figure C-15). If the sample had experienced temperatures above 200 °C in the drum, no weight loss should be seen until after 200 °C. Mass spectrometry analysis of the evolved gases below 400 °C showed m/z 16 (CH_4), m/z 18 (H_2O), m/z 44 (CO_2 and/or N_2O), m/z 30 (NO and CH_2O) and m/z 46 (NO_2) were present which is consistent with the decomposition of organics and nitrate salts (Figure C-16). Since m/z 30 is the base peak (i.e., 100% abundance) for NO_2 in the mass spectrum and m/z 30 and 46 peaks do not overlay, it indicates another material is responsible for the m/z 46 peak at temperatures below 150 °C. Oxygen (m/z 32) evolution starts at 560 °C and reaches a maximum at 620 °C consistent with decomposition of NaNO_3 . The TG-MS results indicate that the materials ejected from the drum either did not experience temperature temperatures over 200 °C or that their exposure to elevated temperature was very limited in duration (<seconds). If the oxidation reactions occurred in the middle of the drum, for example, pressure could build up from the gaseous products and eject the unreacted top layer of Swheat Scoop®/nitrate salt out of the drum. Nitrate (3.5 wt%), nitrite (1.3 wt%), and oxalate (1.3 wt%) salts were found in the debris on R15 C5 as well as on the CAM filters consistent with the salt layer being ejected. Since magnesium and calcium nitrite salts are unstable above 400 °C [Stern, 1972; Oza, 1950] and magnesium and calcium oxalate salts are unstable above 500 °C [Gadalla, 1984], this indicates that the reaction temperature in the drum did not exceed these temperatures for an extended

period. Moreover, oxalic acid starts to decomposes above 150 °C in the gas phase and its calculated half-life at 250 °C is 3 s. [Lapidus, 1964] Thus, it can be concluded that the materials ejected from the drum either did not experience high temperatures (over 400 °C) or that their exposure to elevated temperatures was very limited in duration (<seconds) resulting in the observation of nitrite and oxalate salts in the collected samples. LC-MS data are consistent with presence of triethanolamine, further supporting that reactions did not go to completion.

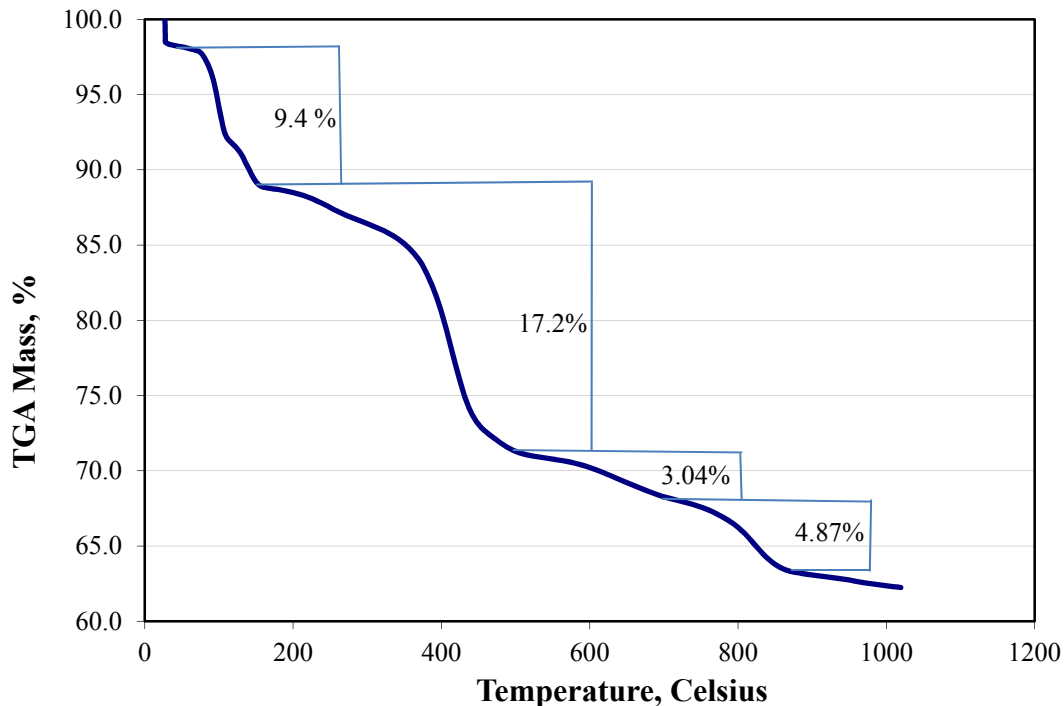


Figure C-15. TG-MS analysis of debris from R15 C5 under argon

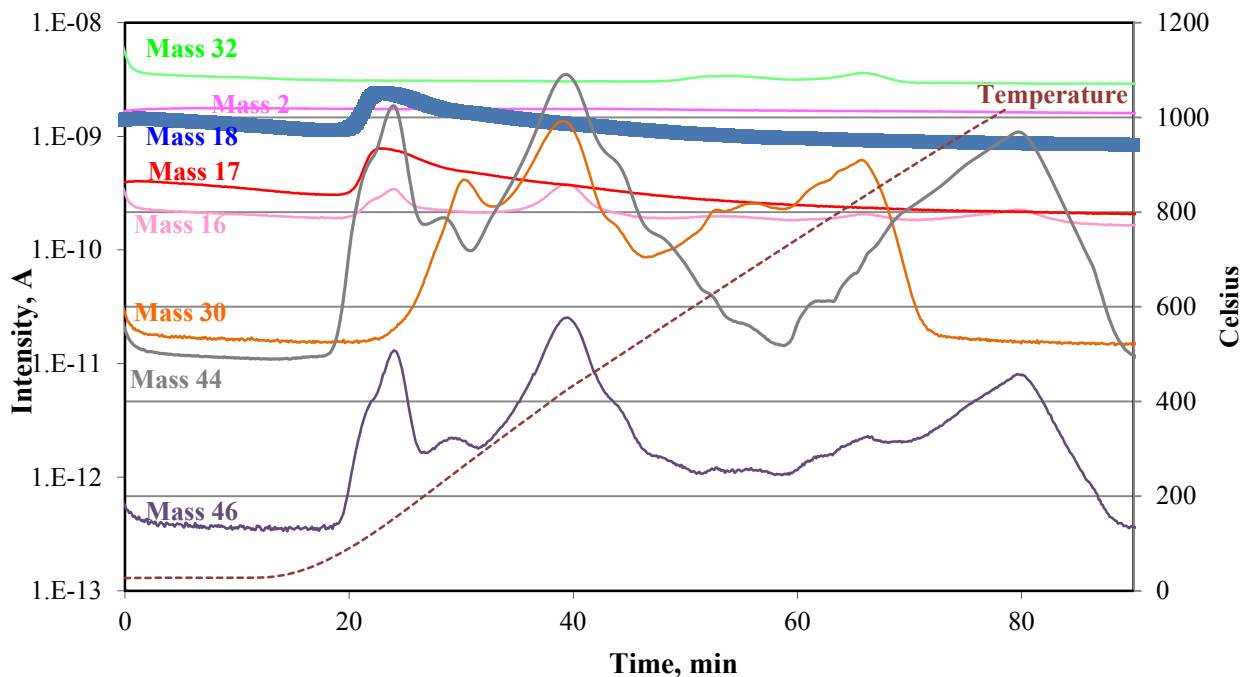


Figure C-16. MS analysis of the evolved gases from the decomposition of R15 C5 under argon

Conclusion: The reactions inside Drum 68660 did not go to completion and the material ejected from the drum did not experience temperatures over 200 °C or their exposure to elevated temperatures was of short duration (seconds). This hypothesis is supported by the unreacted material and thermally sensitive materials found in the debris.

Oxidation Products Found in Debris but Nitration Products Were Not Detected: From the reaction chemistry discussed above, oxidation and nitration products from *Swheat Scoop*® are predicted. To analyze for these materials, the debris from R15 C5 was placed between KBr discs and analyzed by FTIR microscopy (Figure C-17). The FTIR spectra are very complex and show a mixture of organic materials (identified by C-H stretches centered at 2935 cm^{-1}) and inorganic materials. By comparing the results from SEM-EDS, XRD, and IC with the FTIR spectra, the data is consistent with a mixture of *Swheat Scoop*® (or other carbohydrates) with nitrate, nitrite, oxalate, and carbonate salts. The broad peak at 3000 – 3700 cm^{-1} is from hydroxyl groups and hydrogen bonded hydroxyls (and water) associated with the organics or inorganic salts. Amines (N-H stretches) also come in this region (3200- 3400 cm^{-1}) and they have additional N-H bends and C-N stretches between 1000-1600 cm^{-1} . Nitrate salts (Na, K, Ma, Ca, Fe, and Pb) all have very strong bands at 1350-1380 cm^{-1} and weaker bands at 815-835 cm^{-1} (while nitrate salts with divalent cations have an additional strong peak at 1430-1480 cm^{-1}). [Miller, 1952] Nitrite salts have very strong bands at 1235-1250 cm^{-1} and medium intensity bands at 1328-1380 and 820-835 cm^{-1} . Carbonates have very strong stretches at 1410-1450 cm^{-1} . [Miller, 1952] Oxalate salts (Na, Ca, Mg, and K) have very strong stretches at 1605-1640 cm^{-1} and 1320-1370 cm^{-1} [Pedersen, 1967] while salts of aliphatic carboxylates have strong stretches at 1538-1580 cm^{-1} and 1405-1470 cm^{-1} . All these peaks are found in the spectra. The small peak at 2174 cm^{-1} could be from a nitrile group and will be discussed in more detail later.

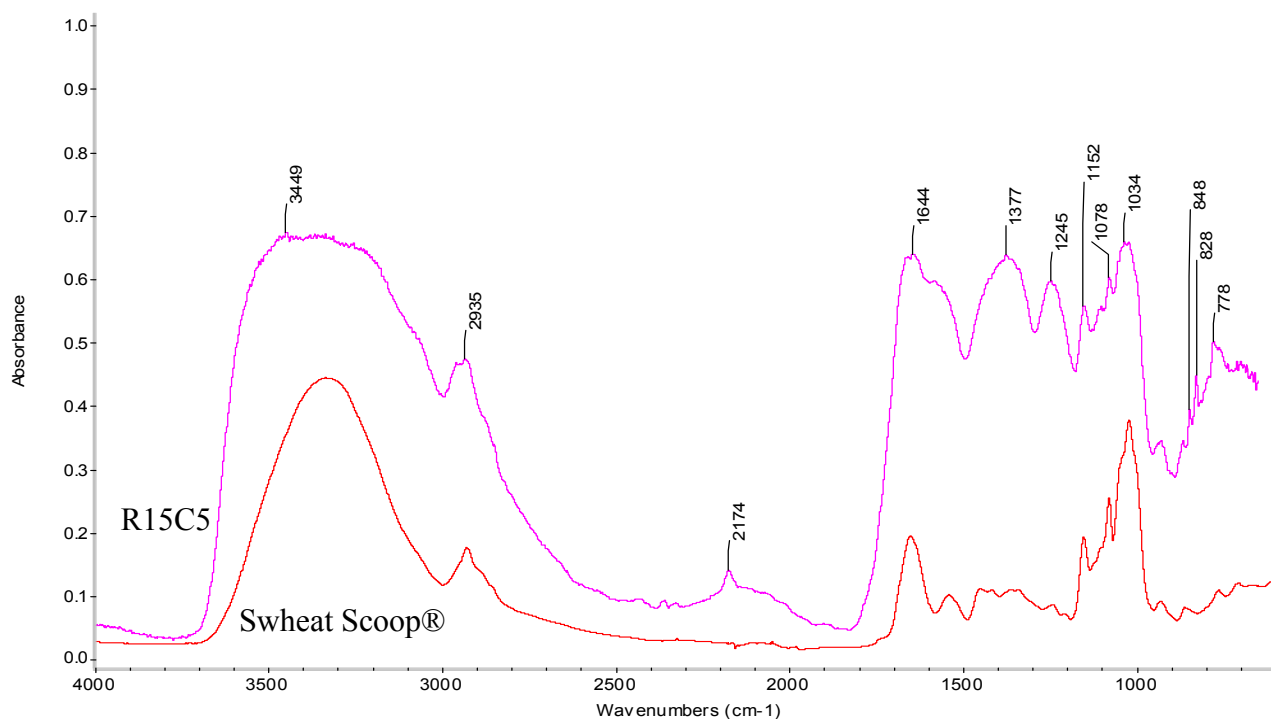


Figure C-17. FTIR spectra of the solid R15 C5 sample compared to *Swheat Scoop*®

FTIR microscopy of particles from the lip of R16 C4 showed similar spectra containing a mixture of inorganic and organic materials. For example, FTIR microscopy of the black particle in Figure C-18a has spectral signatures indicative of an aliphatic carboxylic acid (1703 cm^{-1}), carboxylate salts (1581 cm^{-1}), nitrates, nitrites, carbonates, and nitrile (2214 cm^{-1}). The upper spectrum (and optical microscope image) is consistent with nylon from the Velcro (showing N-H stretch at 3298 cm^{-1} and amide bands at 1637 cm^{-1} and 1537 cm^{-1}).

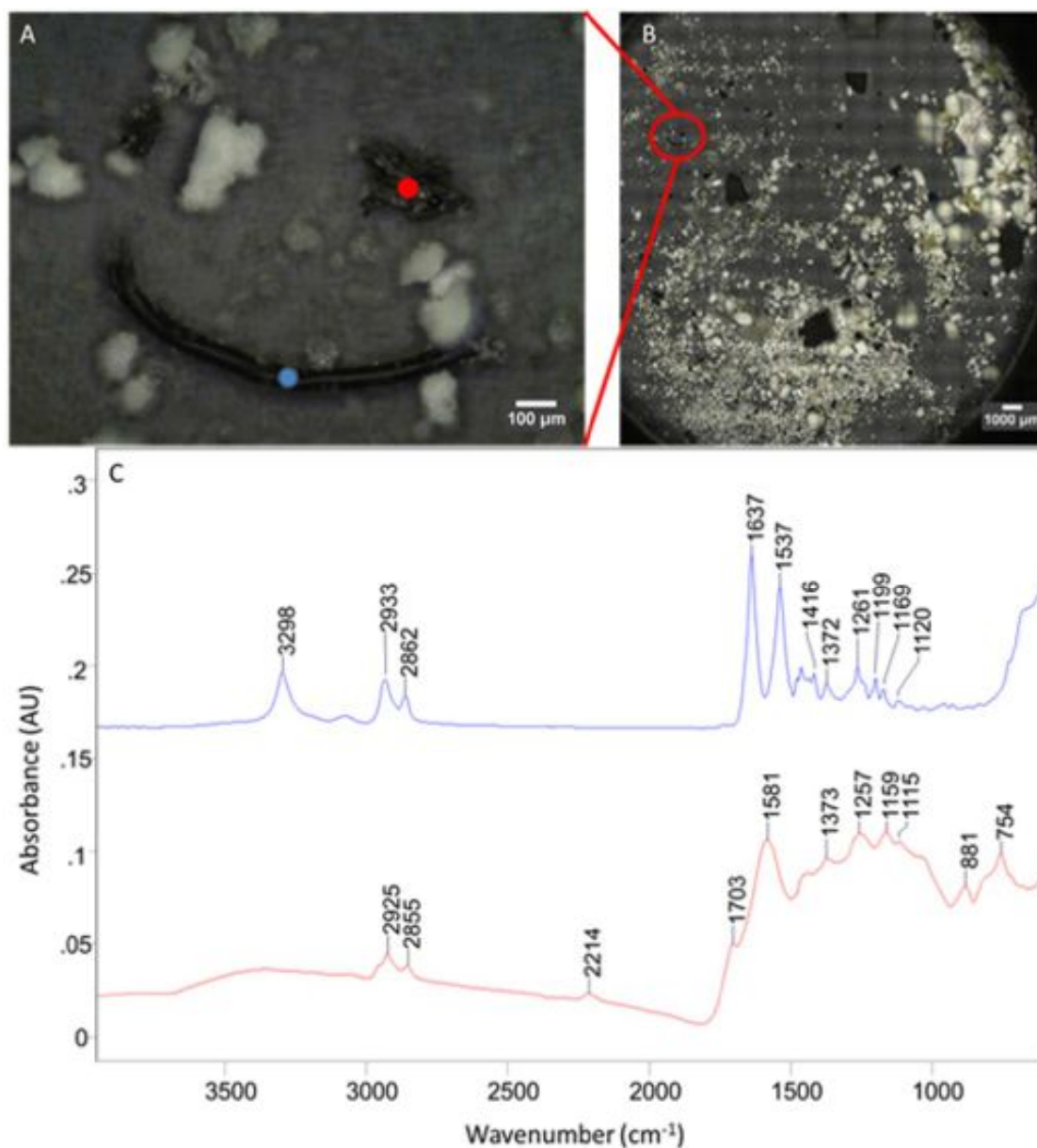


Figure C-18. (a) Pictures of where ATR-IR data was collected on black particle 4 (blue dot) and black particle 5 (red dot) in subsample R16 C4. (b) Overview picture of subsample R16 C4, loose powder that was collected from the Swiffer sampler that was landed near the lip of the drum that breached (R16 C4). (c) IR spectra of black particle 4 (blue) and black particle 5 (red).

It is difficult to determine whether nitrate esters, which have characteristic NO₂ stretches at 1625-1660 cm⁻¹, 1275-1380 cm⁻¹, and 840-880 cm⁻¹ [Suppes, 2003; López-López, 2010] and aliphatic nitro group, which have stretches at 1540-1575 cm⁻¹, and 1350-1375 cm⁻¹, [Lambert 1987] are present in the sample because these peaks overlap with other materials in the sample. The FTIR spectrum of nitrocellulose is shown in Figure C-19 to highlight the strong NO₂ bands at 1660 and 1280 cm⁻¹, and NO stretch at 840 cm⁻¹ compared to cellulose. If nitrate esters were in high concentrations, they could be easily observed by FTIR (or Raman spectroscopy).

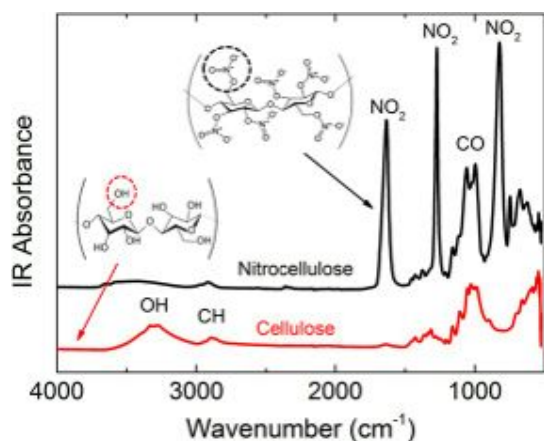


Figure C-19. FTIR spectra of cellulose (chromatography paper) and nitrocellulose at room temperature [Coatas, 2014]

Particles of R15 C5 stuck to the Velcro tape were analyzed by Raman microscopy using an incident frequency of 1064 nm. Many attempts were made to visually identify and measure particles that could yield useful Raman spectra, i.e., particles that were not black. These particles included tan and bluish-gray particles and particle aggregates of varying sizes. These particles and aggregates were interrogated with the very lowest levels of laser power that were required to maintain a stable laser beam. The results of the Raman analyses did not provide any useful vibrational information about the residues. Instead, spectra from the WIPP samples were overwhelmed with blackbody emission and sometimes with fluorescence emission. In many cases, the interrogated particles were obliterated from the surface of the Velcro adhesive backing when exposed to the excitation laser.

The debris from R15 C5 was also extracted with CH_2Cl_2 and the solvent evaporated onto KBr discs and analyzed by FTIR microscopy to look for nitrated or oxidized organics. A representative spectrum is shown in Figure C-20. The sample contains organic residue (C-H stretches present 2960 and 2876 cm^{-1}) and potentially carboxylic acids or esters based on the peaks above 1700 cm^{-1} . Carboxylic acids have been observed from the nitrate salt oxidation of lignocellulosic materials and the carbonyl bands appeared around $1700\text{--}1725\text{ cm}^{-1}$. [Wu, 1986] Oxalic acid has C=O stretches at 1745 cm^{-1} and O-C-O stretch at 1224 cm^{-1} while the mono ($1745, 1623, 1394, 1245\text{ cm}^{-1}$) and dicarboxylate salts ($1569, 1305\text{ cm}^{-1}$) have stretches at lower frequencies. [Jung, 2003] The peaks above 3100 cm^{-1} can be attributed to --OH from acids or alcohols, hydrogen bonded water or amines. The peaks at $1227, 1133$ and 1069 cm^{-1} are an indication the sample contains carbohydrates, since typical C-O stretches in carbohydrates are found between $1000\text{--}1250\text{ cm}^{-1}$. [Tipson, 1968] As previously discussed, it is difficult to determine whether nitrate esters or nitro groups are present in the sample because the characteristic stretching frequencies overlap with other materials. If nitrate esters are present, they are in low concentration. Some entrained particles were also present that had FTIR spectra similar to cellulose (see Figure C-21), sodium oxalate and sodium carbonate. Although Swheat Scoop® particles are not clearly visible, there is insoluble organic material resembling Swheat Scoop® in most FTIR spectra of the samples from R15 C5, R16 C4 and the CAM filters.

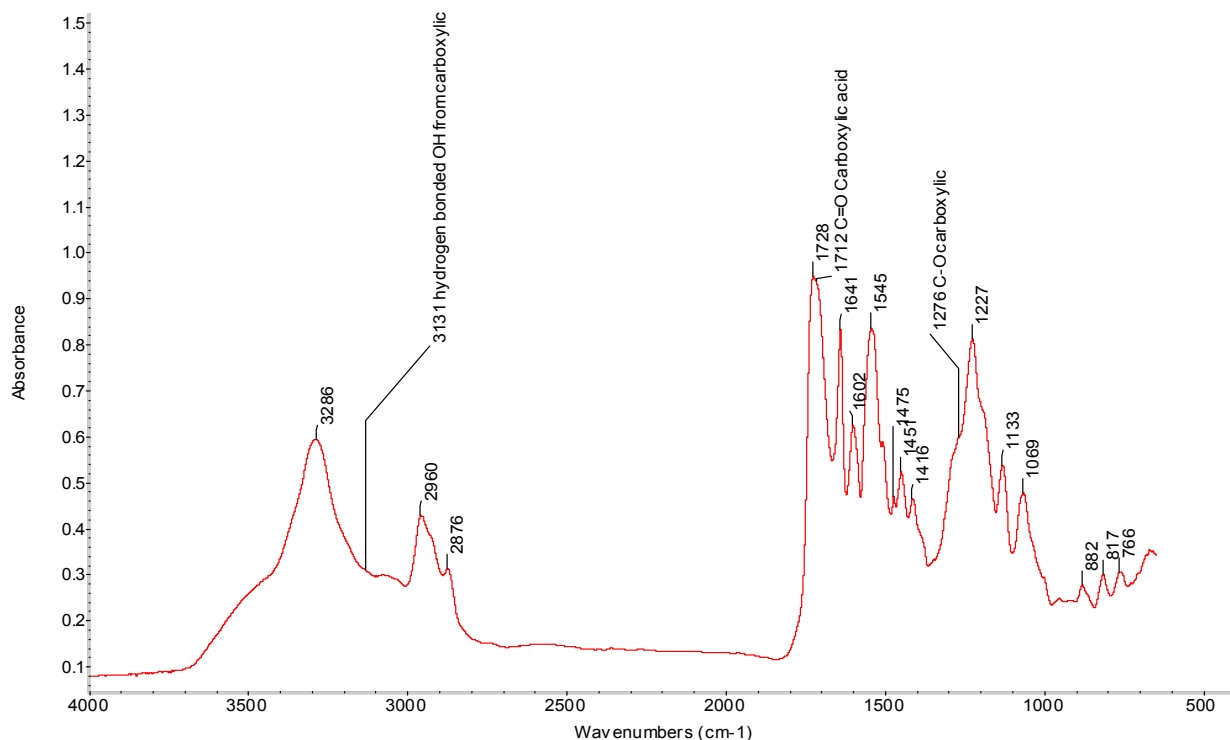


Figure C-20. FTIR of the CH₂Cl₂ extract of R15 C5.

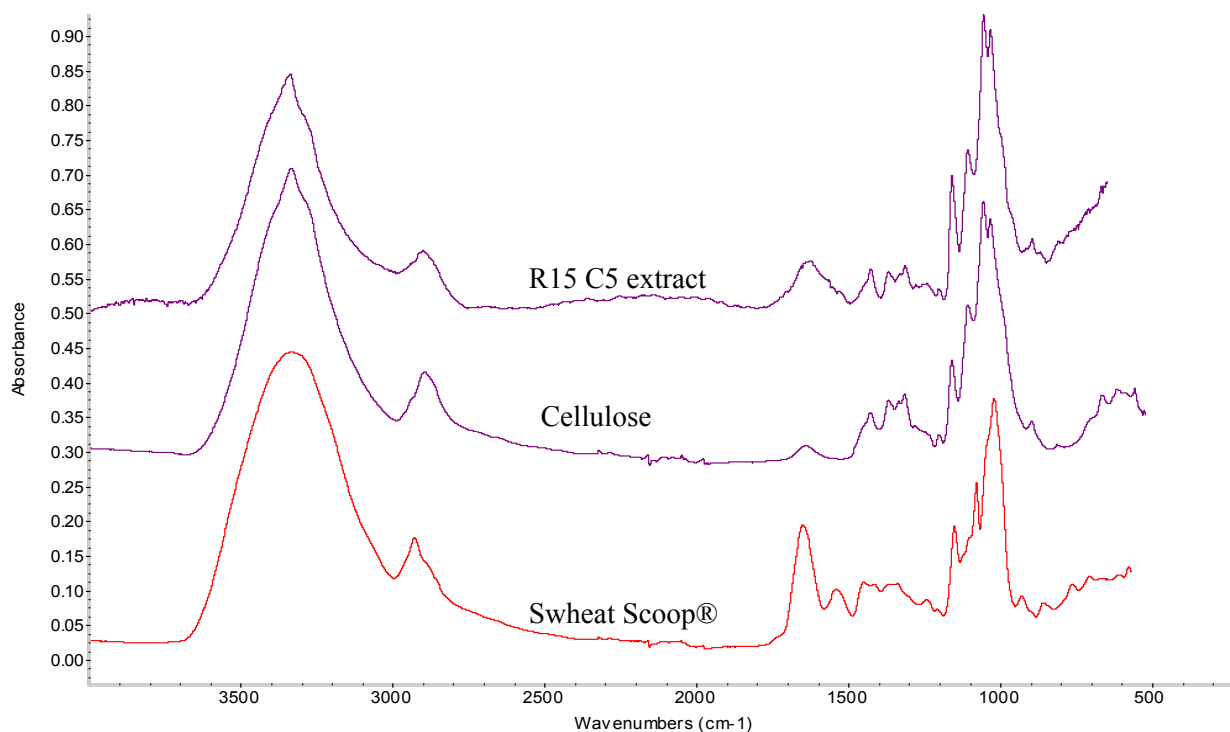


Figure C-21. FTIR spectrum of a particle collected from the methylene chloride extract of R15 C5 compared to cellulose and Sweat Scoop®. Particle is similar to cellulose.

The methylene chloride extracts were also analyzed by GC-MS and very few organic compounds were observed (ppm detection limits). No oxidized materials (i.e., small carboxylic acids or sugars), triethanolamine (TEA), or nitrate esters (i.e., no materials with a nitronium ($m/z = 46$, NO_2^+) fragment) were observed. Since TEA is a high

boiling (335 °C) liquid, an authentic sample was analyzed on the GC-MS, using the same method that was used for the methylene chloride extracts, to confirm its retention time and mass spectrum. Selective ion monitoring at m/z 118 (the base peak for TEA in the mass spectrum) did not find any TEA. Since many of the expected reaction products are polar (sugars, carboxylic acids, and alcohols) and might not make it through the GC, the extracts were derivatized with N-methylbis(trifluoroacetamide) (MBTFA), which is best for trifluoroacetylating carbohydrates and sugars, and BF_3 /butanol, which is best for esterifying carboxylic acids. No new materials, other than decomposition products from the reagents, were observed. Since the residue from R15 C5 was basic, some of the organics could be tied up as salts and are not extractable in organic solvent. For example, oxalate, formate, and acetate were found in the water extract of the debris but these products were not observed in the methylene chloride extract by GC-MS. A water extract of the debris from R15 C5 found organic carbon (TOC 23,280 mg/Kg) was present in the water. However, it is known that Swheat Scoop® has cold-water solubility [Sladek, 1997] and a water extract of Swheat Scoop® contained 46,700 mg/Kg of organic carbon. Since the water extract from R15 C5 also contained phosphate (1610 mg/Kg), Swheat Scoop® is present in the sample and could be contributing to the measured carbon.

To analyze for polar organics, the R15 C5 samples was extracted with methanol and analyzed by LC-MS using a high resolution mass spectrometer capable of tandem mass spectrometry experiments, in positive electrospray mode. Unlike, GC-MS, no LC-MS libraries are available to assist in the identification of unknown compounds; however, by exploiting exact mass measurements, the presence of targeted compounds can be detected. Using this type of targeted analysis, triethanolamine was tentatively identified in the sample.

Conclusion: Oxidation products (i.e., carboxylic acids) were found in the debris from Drum 68660 consistent with oxidation reactions but nitrated organic products were not observed in the debris from 68660 (but could not be ruled out). The gases from the nitrate salt oxidation of Swheat Scoop® can produce sufficient quantities of gas to cause the breach of 68660. Unreacted organic materials still remain in the debris from R15 C5 indicating the reaction did not go to completion.

No Products from Decomposition of TEAN were Observed: As previously discussed, TEAN decomposes above 250 °C to gaseous products including, HCN, NH_3 , NO, H_2CO , CH_3CHO , CO, H_2 , CO_2 , CH_4 , C_2H_4 , CH_3CN , N_2O , and NO_2 , [Lee, 1999] which, due to their high volatilities, would not be observed in the debris except maybe unreacted TEA (which has a bp 335 °C). No TEA or TEA degradation products were observed in the methylene chloride extracts of R15 C5 but TEA was potentially identified in the LC-MS analysis. Since the debris from R15 C5 was basic, the HCN could potentially react with a base and form a cyanide salt. Nitriles have strong unique stretches in the FTIR with sodium and potassium cyanide having stretches at 2080 and 2070 cm^{-1} respectively, and $\text{Fe}(\text{CN})_6^{3-}$ having a stretch at 2100 cm^{-1} . [Miller, 1952] For R15 C5, R16 C4, and the CAM filter, peaks in the FTIR were observed at 2174 cm^{-1} , 2214 cm^{-1} and 2236 cm^{-1} , respectively. These peaks are too high for metal cyanides and are more consistent with alkyl nitriles, which have CN stretches between 2190-2260 cm^{-1} , [Scorates, 1994] or alkynes, which have weak stretches between 2100-2260 cm^{-1} . The most likely origin of the nitriles is from the thermal decomposition of the proteins (ca. 14 wt%) in Swheat Scoop®. It is known that pyrolysis of proteins will produce nitriles. [Moldoveanu, 1998]

Conclusion: The contribution of TEAN to the breach of Drum 68660 cannot be determined because no unreacted TEAN or its decomposition products were observed. However, if the reaction temperature in the drum around the TEAN exceeded 250 °C, it would be consumed by exothermic degradation to gaseous products.

Low Melting Eutectic Mixture of Salts Could Form: One hypothesis is that a low melting eutectic mixture of salts was formed that increased the transport of reactive materials and accelerated the oxidation reactions. It is well known that binary or ternary mixtures of Na, K, Ca, and Mg nitrates form low melting (<150 °C) eutectics. [Janz, 1972] For example, a mixture of 67-71 wt% $\text{Mg}(\text{NO}_3)_2 \cdot 6 \text{H}_2\text{O}$, 23-26 wt% KNO_3 , and 6-8 wt% NaNO_3 melts at 65 °C ($\text{Mg}/\text{Na} = 3.5$, $\text{K}/\text{Na} = 5$) while a 91-94 wt% $\text{Mg}(\text{NO}_3)_2 \cdot 6 \text{H}_2\text{O}$ and 6-9 wt% NaNO_3 has a melting point of 83 °C ($\text{Mg}/\text{Na} = 4$). [Hammond, 1998] To determine whether a eutectic mixture of metal salts could be present, exact composition and concentrations of the salts would be needed since the melting point is dependent

on these variables. Although the concentrations of metals from the materials on R15 C5 can be determined by ICP-OES, it is difficult to determine whether the Na and Mg came from 68660 or the salt mine and broken super sacks, respectively. Nevertheless, the ratio of the primary metal ions in the two samples from R15 C5 and the sample from the parent drum was measured by ICP-EOS after either mixed acid digestion or peroxide fusion. The R16 C4 lip sample was not included because the material appeared to be predominately MgO from the super sack from the photographs (see Sampling section), and SEM-EDS analysis. The ICP-OES results are shown in Table C-3 as a ratio of salts normalized to sodium along with the expected ratio of salts from the estimated contents in Drum 68660 (Table C-3). Although the ratio of salts varied significantly between the two R15 C5 samples, the salt ratios are in a range in which a eutectic mixture of Mg, Na, Ca, and K nitrates salts could form. While the melting temperature of the potential eutectic mixture is not precisely known and will depend on the water of hydration, these results indicate that a liquefied eutectic mixture was possible in the drum environment. These numbers were also examined to help determine the ratio of salts to use in the 10-gallon drum tests.

Table C-3. Ratio of metal cations relative to sodium from the debris on R15 C5 and the parent drum.

	68660	R15 C5 Sample 2	R15 C5 Sample 3	Parent Drum
Component (X)	X/Na	X/Na	X/Na	X/Na
Mg	1.6	0.60	3.2	0.18
Na	1.0	1.0	1.0	1.0
Ca	0.26	0.015	0.083	0.075
Fe	0.11	0.005	0.017	0.26
K	0.18	0.042	0.12	0.16

Conclusion: The composition and concentration of metal nitrate salts in Drum 68660 were in a range where a low melting eutectic mixture could form which would accelerate the oxidation reactions.

MgO Did Not React with CO₂ or H₂O

If MgO in the super sacks reacted with CO₂ and H₂O from the truck fire, the products of this reaction would be Mg(OH)₂ (brucite), MgCO₃ (magnesite) and potentially other metastable hydrous carbonates including (Mg₅(CO₃)₄(OH)₂ • 4H₂O) (hydromagnesite), Mg₂CO₃(OH)₂ • 3H₂O (artinite), and MgCO₃ • H₂O (nesquehonite). These reactions are exothermic and the products have a lower bulk density than MgO and could cause the super sack to expand and break. To investigate this scenario, samples of MgO were obtained from WIPP and analyzed for products from the hydration and/or carbonation of MgO. The rates and heat of hydration were also determined (Room External Model Report) and found to be too low to generate enough heat to melt the polypropylene (i.e., super sack) bags.

MgO Samples: MgO samples were collected from the broken super sacks on top of waste drums R14 C2, R14 C4, and R14 C6 in Room 7 of Panel 7 on May 30, 2014 with a PVC pipe type collection apparatus as previously discussed. The samples contained powder and small pellets as shown in Figure C-22. An addition MgO sample was also taken from the top of R16 C4 using a multi-sampler device constructed from a Swiffer® head containing 4 disc smears, a Velcro strip and a Velcro strip with the adhesive tape exposed (as described in the Sampling Integrated Summary Report in Appendix B, see Figure C-23). Low levels of Am-241 were found by gamma analysis for R14 C2 (1100 dpm), R14 C4 (1200 dpm), R14 C6 (<260 dpm) and R16 C4 (3700 dpm). Results of this analysis were qualitative since calibrated geometries for these samples were not available. Interestingly, the R14 C6 sample had the lowest activity even though the material ejected from R16 C4 would have moved toward R14 C6. However, if the material (and radioactivity) was quickly released from R16 C4 in the direction of the super sack on top of R14 C6 and caused the super sack to fail, then most of the radioactivity would be buried under the MgO and relatively clean MgO from the interior of the super sack would be exposed and sampled. Since all of the MgO samples from the top of the waste drums had low levels of radioactivity, this implies that the radioactive release was fast and the airflow carried the materials out of Room 7. If radioactive material was slowly released (i.e., over minutes) from Drum 68660, more radioactivity would have deposited on the surrounding MgO sacks.

Two additional MgO samples were collected (August 15, 2014) from an intact bag of MgO located on the floor at the waste face (upstream from the event). One sample was taken at the MgO surface inside the bag and the other at a depth of 6 inches. Both samples were surveyed for radioactivity and were found to have less than $1.71E2$ dpm/sample of Am-241. Finally, a sample of MgO that had not been placed in the mine (and was not radioactive) was collected from the WIPP site. This sample was used as a reference. All samples were white or beige colored and consisted of powder and pellets (see Figures C-22 through C-24). In R14 C6 and R14 C2, dark colored particles (4 and 1, respectively) were found (about 1-mm in diameter). They were physically separated and analyzed (see Figure C-25).



Figure C-22. MgO collected from R14 C2.

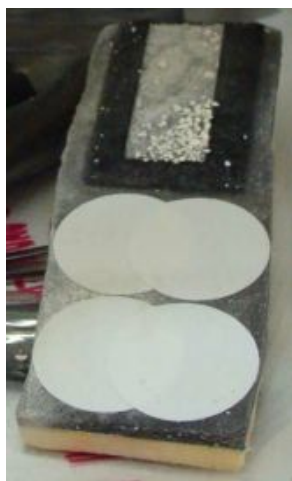


Figure C-23. Sample collected from R16 C4 using Swiffer head.



Figure C-24. MgO sample collected from super sack in Panel 7 Room 7.

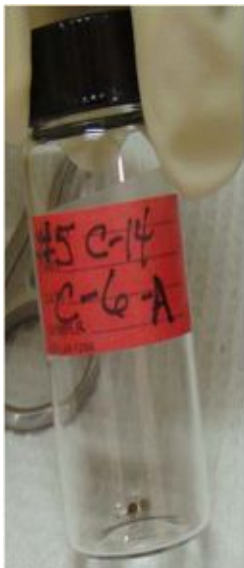


Figure C-25. Dark particles found in the MgO samples from R14.

Analytical Results: Specification for the MgO (Specification for Prepackaged MgO backfill: Specification D-0101 Revision 8, 02/11/09) to be emplaced in the underground areas at the WIPP states that “the sum of magnesium oxide (MgO) plus calcium oxide (CaO) shall be a minimum of 95%, with the MgO being no less than 90%.” Other materials that could be present in the MgO based on sample analysis (Attachment D to Specification document) include SiO₂, Al₂O₃, and Fe₂O₃.

All MgO samples were analyzed by X-ray diffraction (XRD) and FTIR microscopy to determine whether the MgO had reacted with water and/or CO₂ to produce Mg(OH)₂, MgCO₃ and/or other metastable hydrous carbonates. [Xiong, 2008] X-ray diffraction pattern provides information mostly from the bulk sample while FTIR provides information about the surface of the sample. XRD patterns of the samples obtained from WIPP were compared to the reference MgO samples and search match identification was performed with Jade software from Materials Data Inc. and the International Centre of Diffraction Database. FTIR spectra of the WIPP MgO samples were compared to reference spectra of potential reaction products (such as Mg(OH)₂ and MgCO₃) or from the literature. [Miller, 1952; Hanna, 1965; Kwon, 2009; Zhang, 2006] Since the samples contained both powder and pellets, as shown in Figures C-22 through C-24, both morphologies were independently examined by XRD. The X-ray diffraction patterns show the material from R14 and the two bags of MgO from Room 7 contained primarily MgO (see Figures C-26 and C-27) while extended analysis showed a small amount (< a few %) of CaCO₃ was present. No bulk Mg(OH)₂, MgCO₃ or other products from the reaction of MgO with H₂O and/or CO₂ were observed in the samples.

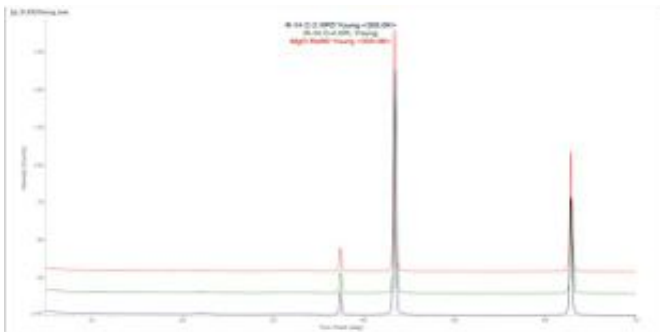


Figure C-26. XRD of MgO from R14 C2, R14 C4 and a reference MgO sample.

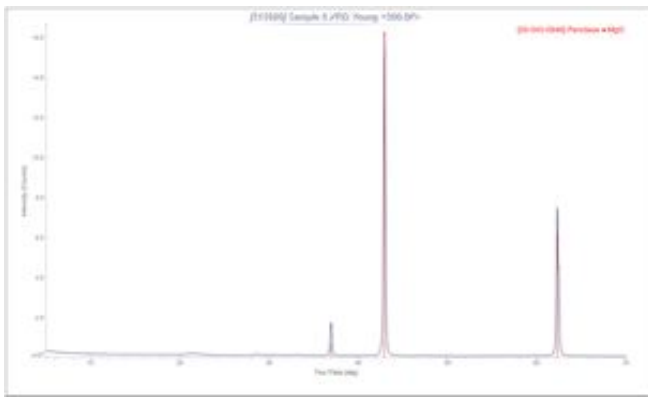


Figure C-27. XRD of MgO from super sack sampled at the surface.

FTIR microscopy showed the samples predominately contained MgO (see Figures C-28 and C-29). [Hanna, 1965] No OH stretches were observed at 3700 cm^{-1} (isolated OH) and $3650\text{-}3350\text{ cm}^{-1}$ (H-bonded OH) for $\text{Mg}(\text{OH})_2$ [Kwon, 2009] and no strong CO_2 stretches were observed at 1485 and 1420 cm^{-1} for $\text{MgCO}_3 \cdot 3\text{H}_2\text{O}$. [Zhang, 2006] Samples from the surface of the sack in Room 7 showed small amounts of carbonates and silicates on the surface while samples taken from 6" deep had fewer surface species. Monodentate surface carbonates on MgO can be identified by stretches at $1510 - 1550$, $1390 - 1410$, $1035 - 1050$, and $860 - 865\text{ cm}^{-1}$ while bicarbonates carbonates and bidentate carbonates show stretches at higher frequencies ($1655\text{-}1670\text{ cm}^{-1}$). [Kwon, 2009] Silicates and magnesium silicates have stretches in the region from $1000 - 1300\text{ cm}^{-1}$. [Kalampounias, 2011] SEM-EDS analysis of the samples also showed Mg, Ca and Si are present in the MgO. XRF analysis of the R14 MgO samples showed Fe, Ca with Ni, Cr, Ti and Zn and trace amounts of 4f and 5d elements (such as Pb).

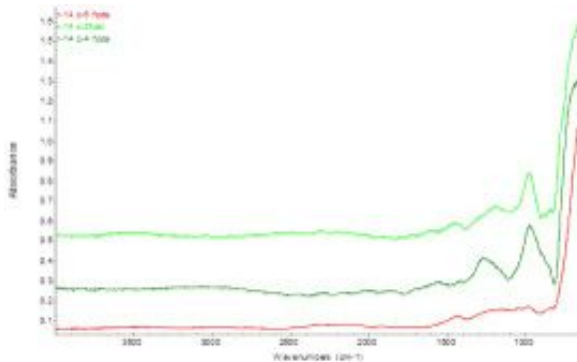


Figure C-28. FTIR spectra from MgO from R14 C2, C4, and C8.

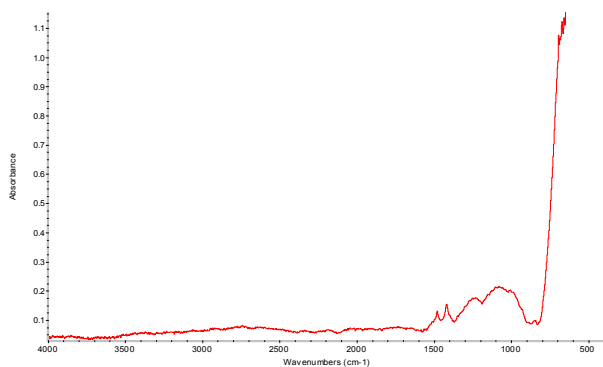


Figure C-29. FTIR spectrum of MgO from sack at face of room 7 panel 7.

The dark colored particles in the R14 MgO samples were physically separated from the MgO and analyzed by FTIR and SEM-EDS. Similar dark particles were found in the reference MgO sample and the MgO specification

indicate other material could be in the sample. SEM-EDS analysis showed elements including Ti, Si, Al, Fe, and Mn and FTIR analysis showed carbonates, sulfates, nitrates, iron oxide and silica were present.

Conclusion: Analysis of MgO samples obtained from Room 7 Panel 7 provided no evidence to support the presence of Mg(OH)₂, MgCO₃ or other metastable hydrous carbonate species that would be expected if the material in the super sacks was exposed to significant quantities of CO₂ and/or H₂O combustion products. Therefore it is concluded that the truck fire event did not cause the damage observed in Panel 7 Room 7. It is also concluded that the duration of the event was short which limited the radioactivity found on the MgO on the adjacent drums.

REFERENCES

1. Bensah, E. C.; Mensah, M. Chemical Pretreatment Methods for the Production of Cellulosic Ethanol: Technologies and Innovation. *Int. J. Chem. Eng.* **2013**, Article ID 719607.
2. Bracuti, A. J. *The Crystal and Molecular Structure of Triethanolammonium Nitrate*. Technical Report ARAED-TR-92026; U. S. Army, December 1992.
3. Cembella, A. D.; Antia, N. J.; Taylor, F. J. R. The Determination of Total Phosphorous in Seawater by Nitrate Oxidation of the Organics Component. *Wat. Res.* **1986**, *20*, 1197-1199.
4. Chang, Y.-P.; Boyer, E.; Kuo, K. K. Combustion Behavior and Flame Structure of XM46 Liquid Propellant. *J. Propulsion Power* **2001**, *17*, 800-808.
5. Clark, D. L.; Funk, D. J. Waste Isolation Pilot Plant (WIPP): Chemical Reactivity and Recommended Remediation Strategy for Los Alamos Remediated Nitrate Salts (RNL) Waste. Los Alamos, NM. 2015. LA-CP-15-20082.
6. Costas, M. N.; Veigas, B.; Jacob, J. M.; Santos, D. S.; Gomes, J.; Baptista, P. V.; Martins, H.; Inácio, J.; Fortunato, F. *Nanotech.* **2014** *25*, 94006.
7. Cronin, J. T.; Brill, T. B. Thermal Decomposition of Energetic Materials 29- The Fast Thermal Decomposition of Characteristics of a Multicomponent Material: Liquid Gun Propellant 1845. *Combust. Flame* **1988**, *74*, 81-89.
8. Desai, D. H.; Patel, C. K.; Patel, K. C.; Patel, R. D. The Effect of Some Nitrate Salts on the Thermal Behaviour of Amylose. *Die Stärke* **1972**, 42-45.
9. Fontana, J. D.; Mitchell, D. A.; Molina, O. E.; Gaitan, A.; Bonfim, T. M. B.; Adelman, J.; Grzybowski, A.; Passos, M. Starch Depolymerization with Dilute Phosphoric Acid and Application of the Hydrolysate in Astaxanthin Fermentation. *Food Technol. Biotechnol.* **2008**, *46*, 305-310.
10. Gadalla, A. M. M. Kinetics of the Decomposition of Hydrated Oxalates of Calcium and Magnesium in Air. *Thermochimica Acta* **1984**, *74*, 255-272.
11. Hammond, M. J. Reversible Liquid/Solid Phase Change Compositions. US Patent 5,785,884, July 28, 1998.
12. Hanna, R. Infrared Properties of Magnesium Oxide. *J. Am. Chem. Soc.* **1965**, *48*, 376.
13. Içbudak, H.; Yilmaz, V. T.; Ölmez, H. Thermal Decomposition Behavior of Some Trivalent Transition and Inner-Transition Metal Complexes of Triethanolamine. *Thermochimica Acta* **1996**, *289*, 23-32.
14. Janz, G. J.; Krebs, U.; Siegenthaler, H. F.; Tomkins, R. P. T. Molten Salts: Volume 3, Nitrates, Nitrites and Mixtures. *J. Phys. Chem. Ref. Data* **1972**, *1*, 581-746.
15. Jung, Y. M. Characterization of pH-Dependent IR Spectra of Oxalic Acid: Comparison of Self-Modeling Curve Resolution Analysis with Calculation of IR Frequencies. *Bull. Korean Chem. Soc.* **2003**, *24*, 1410-1412.
16. Kalampounias, A. G. IR and Raman Spectroscopic Studies of Sol-Gel Derived Alkaline-Earth Silicate Glasses. *Bull. Mater. Sci.* **2011**, *34*, 299-303.
17. Keely, W. M.; Maynor, H. W. Thermal Studies of Nickel, Cobalt, Iron, and Copper Oxides and Nitrates. *J. Chem. Eng. Data* **1963**, *8*, 297-300.
18. Kochkar, H.; Morawietz, M.; Hölderich, W. F. *Appl. Catal., A.* **2001**, *210*, 325-328.
19. Kozłowski, T. R.; Bartholomew, R. F. Reactions between Sodium Carboxylic Acids Salts and Molten Sodium Nitrate and Sodium Nitrite. *Inor. Chem.* **1968**, *7*, 2247-2254.

20. Kwon, H.; Park, D. G. Infra-Red Study of Surface Carbonation of Polycrystalline Magnesium Hydroxide. *Bull. Korean Chem. Soc.* **2009**, *30*, 2567-2573.
21. Lambert, J. B.; Shurvell, H. F.; Cooks, R. G. *Introduction to Organic Spectroscopy*; Macmillan: New York, 1987; p 175. Lapidus, G.; Barton, D.; Yankwich, P. E. Kinetics and Stoichiometry of the Gas-Phase Decomposition of Oxalic Acid. *J. Phys. Chem.* **1964**, *68*, 1863-1865.
22. Larmigny, J.-P.; Mathieu, J.-P.; Guerin, D.; Dobrowolski, A. Radiation attenuation elastomeric material, a multilayer glove for protection against ionizing radiation and their uses. US Patent 20120217423 A1; August 30, 2012.
23. Lee, Y. J.; Litzinger, T. A. Combustion Chemistry of HAN, TEAN, and XM46. *Combustion Sci. Tech.* **1999**, *141*, 19-36.
24. López-López, M.; Fernández de la Ossa, M. A.; Galindo, J. S.; Ferrando, J. L.; Vega, A.; Torre, M.; García-Ruiza, C. New Protocol for the Isolation of Nitrocellulose from Gunpowders: Utility in their Identification. *Talanta* **2010**, *81*, 1742-1749.
25. Magnuson, M. L.; Satzger, D.; Alcaraz, A.; Brewer, J.; Fetterolf, D.; Harper, M.; Hrynchuk, R.; Mcally, M. F.; Montgomery, M.; Nottingham, E.; Peterson, J.; Rickenbach, M.; Seidel, J. L.; Wolnik, K. Guidelines for the Identification of Unknown Samples for Laboratories Performing Forensic Analyses for Chemical Terrorism. *J. Forensic Sci.* **2012**, *57*, 636-642.
26. Martinez, P. T.; Chamberlin, R. M. Analytical Chemistry and Materials Characterization Results for Debris Recovered from Four Nitrate Salt Waste Drums. LANL, October 24, 2014.
27. Masoud, M. S.; Abou El-Enein, S. A.; Abed, I. M.; Ali, A. E. Synthesis and Characterization of Amino Alcohol Complexes. *J. Coord. Chem.* **2002**, *55*, 153-178.
28. Melnikov, P.; Nascimento, V. A.; Arkhangelsky, I. V.; Zaroni Consolo, L. Z. Thermal Decomposition Mechanism of Aluminum Nitrate Octahydrate and Characterization of Intermediate Products by the Technique of Computerized Modeling. *J. Therm. Anal. Calorim.* **2013**, *111*, 543-548.
29. Miller, F. A.; Wilkins, C. H. Infrared Spectra and Characteristic Frequencies of Inorganics Ions. *Anal. Chem.* **1952**, *24*, 1253-1294.
30. Moldoveanu, S. C. *Analytical Pyrolysis of Natural Organic Polymers*. Elsevier: Amsterdam, 1998; Chapter 12. Analytical Pyrolysis of Proteins, p 373- 396.
31. Naiini, A. A.; Young, Jr., V. G.; Verkade, J. G. Alkali and Alkaline Earth Metal Chloride Complexes of Triethanolamine: The Structure of [Sr(TEA)₂]Cl₂. *Polyhedron* **1997**, *16*, 2087-2092.
32. Olah, G. Malhotra, R.; Narang, S. C. Nitration: Methods and Mechanisms. Wiley 1989.
33. Oza, T. M.; Dipali, N. L. The Thermal Decomposition of Magnesium Nitrite. *J. Indian Chem. Soc.* **1950**, *27*, 305-316.
34. Pedersen, B. F. Interpretation of Infrared Spectra of Solid Alkali Metal Oxalates, and their Hydrates and Perhydrates. *Acta Chemica Scandinavica* **1967**, *21*, 801-811.
35. Rodríguez-Chong, A.; Ramírez, J. A.; Garrote, G.; Vazquez, M. Hydrolysis of Sugar Cane Bagasse using Nitric Acid: A Kinetic Assessment. *J. Food Eng.* **2004**, *61*, 143-152.
36. Sladek, J. H. Method for Sorbing Liquid Using Ground Wheat Grain Litter. U. S. Patent 5,690,052, November 25, 1997.
37. Socrates, G. *Infrared Characteristic Group Frequencies*; Wiley: West Sussex, England, 1994; p 54.
38. Smith, H. D.; Jones, E. O.; Schmidt, A. J.; Zacher, A. H.; Brown, M. D.; Elmore, M. R. Gano, S. R. Denitration of High Nitrate Salts Using Reductants. PNNL-12144, Pacific Northwest National Laboratory, Richland, Washington, 1999.
39. Sramkova, Z.; Gregova, E.; Sturdik, E. Chemical Composition and Nutritional Quality of Wheat Grain. *Acta Chimica Slovaca* **2009**, *2*, 115-138.
40. Stern, K. H. High Temperature Properties and Decomposition of Inorganic Salts Part 3. Nitrates and Nitrites. *J. Phys. Chem. Ref. Data* **1972**, *1*, 747-772.
41. Sullivan, J. M.; Williard, J. W.; White, D. L.; Kim, Y. K. Production of Oxalic Acid via the Nitric Acid Oxidation of Hardwood (Red Oak) Sawdust. *Ind. Eng. Chem. Prod. Res. Dev.* **1983**, *22*, 699-709.
42. Suppes, G. J.; Dasari, M. Synthesis and Evaluation of Alkyl Nitrates from Triglycerides as Cetane Improvers. *Ind. Eng. Chem. Res.* **2003**, *42*, 5042-5053.

43. Tipson, R. S. *Infrared Spectroscopy of Carbohydrates. A Review of the Literature*; National Bureau of Standards Monograph 110; U. S. Government Printing Office: Washington, DC, 1968.
44. Veazey, G. W.; Schake, A. R.; Shalke, P. D.; Romero, D. A.; Smith, C. A. *Waste-form Development for Conversion to Portland Cement at Los Alamos National Laboratory (LANL) Technical Area 55 (TA-55)*, LA-13125 (1996)
45. Wieczorek-Ciurowa, K.; Kozak, A. J. The Thermal Decomposition of $\text{Fe}(\text{NO}_3)_3 \cdot 9\text{H}_2\text{O}$. *J. Therm. Anal. Calorim.* **1999**, *58*, 647-651.
46. Wu, K.-T.; Zavarin, E. Thermal Analysis of Mixtures of Nitrates and Lignocellulosics Materials. *Thermochimica Acta* **1986**, *107*, 131-148.
47. Würfels, W.; Jackwerth, E. Residues from Biological Materials after Pressure Decomposition with Nitric Acid. *Analytica Chimica Acta* **1989**, *226*, 1-16.
48. Xiong, Y.; Lord, A. S. Experimental Investigation of the Reaction Path in the $\text{MgO-CO}_2\text{-H}_2\text{O}$ System in Solution with Various Ionic Strengths, and their Application to Nuclear Waste Isolation. *Appl. Geochem.* **2008**, *23*, 1634-1659.
49. Yilmaz, V. T.; Topcu, Y.; Karadag, A. Thermal Decomposition of Triethanolamine and Monoethanolethylenediamine Complexes of Some Transition Metal Saccharinates. *Thermochimica Acta* **2002**, *383*, 129-135.
50. Zhang, Z.; Zheng, Y.; Ni, Y.; Liu, Z.; Chen, J.; Liang, X. Temperature- and pH-Dependent Morphology and FT-IR Analysis of Magnesium Carbonate Hydrates. *J. Phys. Chem. B* **2006**, *110*, 12969-12973.

APPENDIX D. MODELING INTEGRATED SUMMARY REPORT

Description of Appendix:

Appendix D contains the reports describing a more detailed account of the modeling activities and the experimental results applied to support the modeling activities. The contents are arranged as follows:

- Thermal Activity in Drum: modeling of thermal excursion in Drum 68660
- Mechanical Response of Drum: modeling of drum behavior when pressurized
- Thermal Response of Drum: experimental observations supporting thermal model
- Thermal Damage Footprint External to Drum: models for thermal transport in P7R7

THERMAL ACTIVITY IN DRUM: MODELING OF THERMAL EXCURSION IN DRUM 68660

Summary

Information provided to the WIPP Technical Assessment Team (TAT) was used to describe the approximate content of the drum, which included an organic cat litter (Swheat Scoop®) composed of 100% wheat products. The drum also contained various nitrate salts, oxalic acid, and a nitric acid solution that was neutralized with triethanolamine (TEA). The waste in Drum 68660 was partitioned between a processed salt layer, containing nitrate salts and Swheat Scoop®, and a processed liquid layer containing nitric acid, dissolved nitrate salts, a neutralizer, and Swheat Scoop®. Equilibrium calculations were made with the approximate drum contents to predict the products of an exothermic reaction within the drum. If an inorganic adsorbent such as zeolite had been used in lieu of the Swheat Scoop®, the overall reaction would have been endothermic.

A finite element model was used to calculate the pressurization and thermal runaway of the drum. The transient temperatures in Drum 68660 were calculated by assuming a background heat source of 0.12 W in the processed salt layer and 0.17 W in the processed liquid layer. The heat source was representative of heat generated by radioactive decay. The drum achieved thermal runaway after about 70 days. Gas generation at thermal runaway was predicted to be 340 psig with a sealed drum (no vent). At thermal runaway, the wall temperature increases modestly by about 1 °C, demonstrating that heating would not be apparent prior to thermal runaway. The thermal runaway location was predicted to be about 0.41 meters above the bottom center portion of the drum. At thermal runaway, only about 3.4 kg (out of 71.3 kg total) was converted into decomposition gases, indicating that most of the material remained available for reaction.

Introduction

Drum 68660 was produced as part of the processing of parent drum S855793. Drum S855793 was a 55-gallon drum containing wet nitrate salts contaminated with radioactive waste from 1985. Drum S855793 was in an 85-gallon overpack used as a precaution for leakage. Radiography indicated the presence of liquids that required processing. Processing included decanting the liquid, neutralizing the liquid, and adsorbing the liquid in Swheat Scoop®. The Swheat Scoop® was also mixed with the remaining wet nitrate salts. A 9.98 kg lead blanket was on top of the 55-gallon drum and is considered part of the parent waste.

Two sibling drums (68660 and 68685) were produced during processing of the parent drum. These two sibling drums contained all of the waste in the parent drum S855793 as well as external material added to the parent waste: TEA neutralizer, Swheat Scoop®, and 11 kg of room job control solid waste. Drum 68660 (65% full) was shipped to WIPP and experienced thermal runaway on February 14, 2014. Drum 68685 (85% full) remains at Los Alamos.

Drum contents

The content of Drum 68660 shown in Figure D-1 was determined with an overall material balance as given in Table D-1 using the assumptions listed in Table D-2. Table D-1 show the net weight, which is the total mass minus the container mass composed of the drum steel, a plastic liner bag, and a fiberboard. The combined volumes of the processed layers were estimated from X-rays, which are partially shown in Figure D-1. The X-ray image in Figure D-1 was stitched together from an X-ray video and only shows the edge of Drum 68660. The combined processed salt and liquid layer volume probably ranges between 0.08-0.10 m³ since the layer interfaces are not sharp. The Swheat Scoop® bulk density is higher than the optimal density mentioned in the Swheat Scoop® patent (550 kg/m³) and is closer to 600 kg/m³ based on measurements of large quantities of Swheat Scoop®. The higher density is due to settling in the larger volumes. The Swheat Scoop® moisture content is typically between 10-13% at the manufacturing facility and loses about 2% moisture when it is shipped to dry environments such as New Mexico. This would make the moisture content range between 8 to 11% on a mass basis. We have chosen 10% to be the moisture content in Swheat Scoop®. An overall mass balance was used to determine the total mass of Swheat Scoop® used to process the waste in the parent drum.

Two gallons of liquids were decanted from the nitrate salts in parent drum S855793. The two gallons of decanted liquids were composed of 3.3-molar nitric acid with dissolved nitrate salts. The two gallons of decanted liquids were neutralized with 2 gallons of 3.3-molar TEA making a total of 0.015 m³ (4 gallons) of liquid that was absorbed using Swheat Scoop®. The *Swheat Scoop® to liquid* volume ratio was assumed to be 3:1 based on experience in our laboratory where large amounts of Swheat Scoop® were required to fully absorb liquid. The remaining mass of Swheat Scoop® was mixed with the nitrate salts that were distributed between sibling drums 68660 and 68685 giving a *Swheat Scoop® to nitrate salt* volume ratio of 0.7:1. This ratio is lower than the specification of 1.2:1 for zeolite absorbents.

The 11 kg of nonreactive job control solid waste was added to the bottom of Drum 68660 and included a tungsten-lined glove, at least one empty TEA bottle, and plastic bags. The “waste” above the job control solid waste layer in 68660 is subdivided into two reactive layers: a *processed liquid layer* directly above the job control solid waste layer and a *processed nitrate salt layer* above the processed liquid layer. The space above the processed nitrate salt layer is filled with air. The volume and density of each of these layers is given in Figure D-1. The estimated contents of the processed salt layer and processed liquid layer are given in Tables D-3 and D-4, respectively. Table D-3 has a detailed description of the composition of the nitrate salts. Weisbrod estimated the composition of the nitrate salts by starting with Veazey salt analysis. Weisbrod conducted a series of evaporation simulations using Stream Analyzer© from OLI Systems. Table D-3 also lists a more simple composition for the nitrate salts. Measured solubility data at our laboratory was used with this simple composition to determine the amount of nitrate salts that were dissolved into the decanted liquid as shown in Table D-4.

Table D-5 shows the theoretical contents of Drum 68660 with zeolite substituted for the Swheat Scoop®. Analcite, NaAlSi₂O₆·H₂O with a density of 2265 kg/m³ was chosen as a representative zeolite. The rest of the composition is the same as in 68660 as given in Tables D-3 and D-4, excluding the Swheat Scoop®. This composition was determined to show that the overall equilibrium reaction with the zeolite would be endothermic and that this mixture would not produce a thermal runaway as the actual mixture in Drum 68660 with the organic wheat-based adsorbent. The volume of zeolite added to the liquids was based on a 3:1 volume ratio. The amount of zeolite added to the nitrate salts was based on a 1:1 volume ratio. Table D-6 shows the volumes and masses used to calculate the zeolite mass.

Equilibrium calculations

CTH-TIGER was used to determine the potential decomposition species in Drum 68660. CTH-TIGER is a thermoequilibrium code that can predict equilibrium compositions given any two thermodynamic states such as temperature and pressure by assuming an appropriate equation of state (EOS) and using a large product species database. The JCZS2i equation of state library with 1757 potential product species was used in all of the equilibrium calculations in the current work. The JCZS2i database contains the same species found in the NASA-CEA ideal gas code. CTH-TIGER code predicts both ideal and non-ideal gas states. Since the pressures within the

drum are relatively low, the ideal gas EOS is suitable and either the NASA code or CTH-TIGER code could have been used for these calculations. We checked selected equilibrium points with both codes and concluded that either code is suitable. The calculations shown in the current work are from CTH-TIGER.

The heat of formation, density, and elemental composition of each of the components in the processed liquid and processed salt layers are needed for the equilibrium calculations. All of these components with parameters can readily be found in the literature except for Swheat Scoop®, which is 100% wheat. Swheat Scoop® is assumed to have the same elemental composition as wheat flour. LECO Corporation sells a wheat flour standard sample with an elemental composition of C 45.0 wt%, H 6.5 wt%, O 45.3 wt%, S 0.2 wt%, and N 3.0 wt%. The oxygen content is determined by difference. This gives a generic formula for the dry wheat with a molecular weight of 160.11 g/mol, $C_6H_{10.4}O_{4.53}S_{0.01}N_{0.34}$. Note that the molecular formula for cellulose is $C_6H_{10}O_5$, which is close to the wheat formula. The heat of combustion of wheat is 19.25×10^6 J/kg or 3080 kJ/mol. The heat of combustion can be used with the generic wheat formula ($C_6H_{10.4}O_{4.53}S_{0.02}N_{0.34} + 6.345O_2 \rightarrow 6CO_2 + 5.2 H_2O + 0.17 N_2 + 0.01 SO_2 + 3080$ KJ/mol exothermic) along with Hess' law to determine enthalpy of formation for the wheat, -3.38×10^6 J/kg.

Table D-7 gives various oxygen balances and reaction energies for the reactive layers in Drum 68660 at 1 atm pressure and 500 K. Equilibrium reactions showing final products are shown in Table D-8. The oxygen balance represents the number of moles of oxygen that are excess or deficient for 100 grams of a compound. The oxygen balance was calculated as $OB\% = (-1600/Mw_{waste}) \times (2C + 0.5H - O + Mg + 0.5Na + Ca + 1.5Al + 2Si)$, where Mw_{waste} is the molecular weight of the mixture and C, H, O, Mg, Na, Ca, Al, and Si are the number of atoms of these elements in the mixture, respectively. The reactive layers include 1) the processed salt layer, 2) the processed liquid layer, 3) the combined processed salt and liquid layer, and 4) the combined layers using zeolite as the absorbent instead of Swheat Scoop®. The composition of layers processed with Swheat Scoop® are given in Tables D-3 and D-4. Table D-5 gives the composition using zeolite as the absorbent. For all of these compositions, calculations were performed for both a "dry" and a "wet" composition. The "dry" composition does not include the moisture in the Swheat Scoop®, acid, or the neutralizer, whereas, the "wet" composition includes all of the water. The dry reactions (1) and (3) in Table D-8 form the basis of the simple chemistry model. Water in the Swheat Scoop®, acid, and neutralizer is assumed to evolve from the system using a simple desorption mechanism.

Figure D-2 shows the effect of temperature on the equilibrium composition at 1 atm pressure for the processed waste in Drum 68660. The compositions in Figure D-2.A were calculated with the combined processed waste with Swheat Scoop® given in Tables D-3 and D-4. The compositions in Figure D-2.B were determined from the processed waste with zeolite given in Table D-5. The adiabatic flame temperature for the Swheat Scoop® processed waste is 864 K at 1 atm as shown in Figure D-2.A. The adiabatic flame temperature for the waste processed with zeolite is only 371 K. The adiabatic flame temperature is the temperature that the equilibrium products reach with no loss of energy to the outside environment. The energy used to raise the products to this temperature originates from the initial energy available in the processed waste. An adiabatic flame temperature that is less than the boiling point of water is a strong indicator that the zeolite processed waste will not ignite. Similar conclusions were drawn from Table D-7, which shows that the reaction enthalpy at 500 K and 1 atm is endothermic.

The high adiabatic flame temperature for the Swheat Scoop® processed waste supports the observed thermal runaway of Drum 68660. There is sufficient energy in processed waste in 68660 to produce thermal runaway in the waste mixture. Thermal runaway occurs when energy is being produced faster than can be dissipated. The rate of energy production is a kinetic process and cannot be calculated by equilibrium considerations. The kinetics are addressed in the following section. However, once thermal runaway is reached, the temperatures of the gases *inside Drum 68660* will approach the adiabatic flame temperature and burning of the waste material begins. At these higher temperatures, the equilibrium composition becomes fuel rich. For example, the composition of the gases at the adiabatic flame temperature includes 33 mol% H_2 and 9 mol% CO as shown in Figure D-2.A. The hot gases can continue to gasify the remainder of the waste to produce fuel rich gases that mix with air external to the

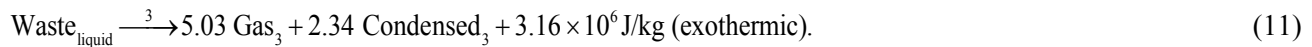
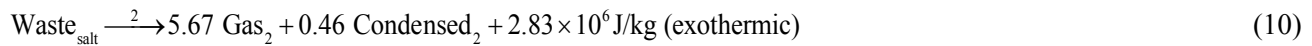
drum and may reach higher temperatures as the H₂ and CO react with oxygen in the air that is external to the drum.

Thermal Runaway Chemistry Model

We have modeled the thermal runaway of the waste by solving the conductive energy equation using a volumetric source for chemical reactions. Three reactions were considered in the current paper.: 1) a drying reaction, 2) a reaction of the dry waste in the processed salt layer, and 3) a reaction of the dry waste in the processed liquid layer. The first reaction is water desorption:



This desorption reaction is for the water associated with the moisture in the Swheat Scoop® as well as the water associated with the acid and neutralizer. The “dry processed salts” and the “dry processed liquid” reactions can be modeled with Eqn. (1) and (3) in Table D-8. The reactions can be simplified as follows:



Waste_{salt} and Waste_{liquid} represent the dry processed salt waste and the dry processed liquid waste respectively. The molecular weights of Waste_{salt} and Waste_{liquid} are 185.5 and 152.5 g/mol, respectively. Gas₂ and Gas₃ represent the average gas in reaction 2 and 3 with a molecular weight of 24.3 and 23.9 g/mol, respectively.

The reaction rates assumed for the three reactions in Eqns. (12)-(14) are:

$$r_1 = A_1 \exp\left(\frac{-E_1 + \xi\sigma_1}{RT}\right) [H_2O_a] \quad (12)$$

$$r_2 = A_2 \exp\left(\frac{-E_2 + \xi\sigma_2}{RT}\right) [Waste_{\text{salt}}] \quad (13)$$

$$r_3 = A_3 \exp\left(\frac{-E_3 + \xi\sigma_3}{RT}\right) [Waste_{\text{liq}}], \quad (14)$$

where the concentration are in brackets with units kmol/m³. The form of the rate expression with distributed activation energy can lead to accelerating reaction rates, where a long induction time is followed by a rapid increase leading to thermal runaway. In the current work, the reaction rates are assumed to be pressure independent. Thus the reaction rates will be the same whether or not the drum was plugged or the vent remained open. The gas concentrations can be determined by solving the following equations.

$$\frac{d[H_2O_g]}{dt} = +r_1, \quad \frac{d[gas_1]}{dt} = +5.67 r_2, \quad \text{and} \quad \frac{d[gas_3]}{dt} = +5.03 r_3. \quad (15)$$

and the number of moles of gas generated by the reaction in can be determined by simple integration:

$$n_{\text{gas}} = \int_{\text{waste}} [H_2O_a] + [gas_1] + [gas_2] dV \quad (16)$$

The pressure can then be determined by the ideal equation of state using the average temperature of the waste and initial air in the system. The pressure is determined by assuming the system is sealed. If the system were vented the gauge pressure would be zero.

Finite Element Model

A finite element computer code was used to solve the following conductive energy equation:

$$\rho_b C_b \frac{\partial T}{\partial t} = \nabla \cdot (k \nabla T) + \sum_{i=1,3} r_i h_{ri} M w_i + q_v \quad (17)$$

The symbols r_i , h_{ri} , and $M w_i$ represent the i^{th} reaction rate, reaction enthalpy, and the molecular weight of the adsorbed water and dry waste, respectively. “ q_v ” represents a background volumetric heat source based on radiological heating. Giaquinto estimated the decay heat in 26 kg of salt and 2 gallons of liquid to be 0.12 W and 0.17 W, respectively.

The bulk density of the waste material was taken from Figure D-1. The bulk specific heat of the waste, 2400 J/kgK, was determined by taking a weighted average of the specific heat of the components in the waste layer. The specific heat was assumed to be constant. The bulk thermal conductivity, k , is assumed to be constant at 0.4 W/mK in the processed salt layer and 0.3 W/mK in the processed liquid layer. The thermal conductivity was measured in Sandia Instrumented Thermal Ignition (SITI) experiment using the method discussed by Erikson. The parameters used in the drum chemistry model are given in Table D-9. The reactivity in both the processed waste layers was assumed to be the same. In other words, the reaction rate constants are the same, but the reaction enthalpy is based on the equilibrium product hierarchy predicted at 500 K and 1 atm as given Eqns. (1) and (3) in Table D-8.

Thermal Runaway Predictions of Drum 68660

Figure D-3.A shows the 2D axisymmetric mesh used to model Drum 68660. The axisymmetric mesh contains about 3000 elements. A mesh study was performed with a 12000-element mesh that predicted the same thermal runaway time. Radiological heating in the salt layer (0.12 W) and liquid layer (0.17 W) was used in this simulation. Figure D-3.B shows the temperature inside of Drum 68660 near thermal runaway after 70 days. At thermal runaway, about 3.4 kg of the waste was converted into gas, leaving 67.9 kg of material. The thermal runaway location was predicted to be about 0.41 meters above the bottom center portion of the drum. Using the same model with the radiological heating removed still resulted in thermal runaway of the drum in 75 days rather than 70 days.

Figure D-4.A shows axial temperatures along the center line, and Figure D-4.B shows radial temperatures from the center to outside edge of the drum. The radial temperatures is taken at a height of 0.41 m from the bottom of the drum. Figure D-4.C shows what the pressure would be inside the drum if the vent were clogged. The pressure rise is gradual before thermal runaway. Once thermal runaway starts, the pressure rise is dramatic as shown in Figure D-4.C. The temperature also increases dramatically once thermal runaway is reached. The pressure rise at thermal runaway is sufficient to cause the observed pressure burst. The maximum temperature within the drum is about 35 °C before thermal runaway. The spatially averaged temperature within the drum is about 29 °C, which is only a few degrees above the initial starting temperature of 27 °C. The drum wall temperature also increases slowly as shown in Figure D-4.C. The temperature increase is only about 1 °C before thermal runaway.

External heating

The adiabatic flame temperature for the waste in Drum 68660 at 1 atm pressure is 891 K (618 °C) as shown in Figure D-2.A. This is the temperature when the energy in the waste is used to heat up the decomposition products. The composition gases and condensed species at 1 atm and 891 K (618 °C) is 32.5 mole% H₂, 28.6 mole% H₂O, 9.1 mole% CO, 19.4 mole% CO₂, 5.4 mole% N₂, 1.2 mole% CH₄, 2.53 mole % MgO (s), 0.40 mole% CaCO₃(s), 0.055 mole% Fe₃O₄(s), and 0.77 mole% Na₂CO₃ (s). The *gas composition* at the adiabatic flame conditions are 33.8% H₂, 29.7% H₂O, 9.50% CO, 20.1% CO₂, 5.6% N₂, 1.27% CH₄, and other minor species. When these gases vent and mix with the external air, the adiabatic flame temperature increases. For example, Figure D-5 shows the adiabatic flame temperature as a function of the amount of mixed air. The condensed decomposition products were not used in these calculations. The adiabatic flame temperature is at a maximum temperature when the hydrogen and carbon monoxide concentration goes to zero. Figure D-5 implies that the external flame may have ranged between about 800 K and 1800 K. The exact temperature depends on factors such as heat loss to the surrounding and mixing with the external air.

The thermal runaway model of Drum 68660 was run with various external radiation boundary temperatures to determine the effect on external heating. Figure D-6 shows the thermal runaway time of an externally heated drum. This calculation was performed with the parameters in Table D-9. The thermal runaway time is fast when the exterior of the drum is heated. For example, at 1000 K, the thermal runaway time was calculated to be about 90 s.

Figure D-7 shows what might happen to a drum that is in close proximity of Drum 68660. The victim drum is shown in Figure D-7.A, and Drum 68660 is shown in Figure D-7.B. The victim drum begins thermal runaway 263 seconds after the breach of Drum 68660. This fast thermal runaway occurs in less than 5 minutes following the breach of Drum 68660. Only about 25 g of decomposition gases have evolved prior to the fast thermal runaway in Figure D-7. Contrast this to the 3.4 kg of decomposition gases that have evolved prior to the slow thermal runaway of Drum 68660. The victim drum is also heated on only one side, as the opposite side is hid from the view of the vented 68660 gases. A fast thermal runaway may not be able to sustain a burn since only a small amount to the waste material is preheated. The victim drum may show signs of heating on only one side of the drum, and the other side of the drum may look undamaged.

Summary and Conclusions

This memo presented a best estimate of the contents of Drum 68660, which breached on February 14, 2014 and resulted in a radiation leak at WIPP. We have made various assumptions regarding the composition. For example the Swheat Scoop® layer volume was probably between 0.08 and 0.1 m³, we chose 0.0912 m³ based on the X-rays of Drum 68660 prior to the event. The Swheat Scoop® was assumed to have 10% moisture. This is based on an estimate the ranged between 8-11% moisture. Recent measurements of the moisture content indicate that 10% is a good estimate. We also assume the bulk density of the Swheat Scoop® was 600 kg/m³ based on measurements at our laboratory. The patent indicates that the density ranges between 500-600 kg/m³. We assumed that the 2 gallons of decanted liquid had a molarity between 1 to 5 moles/L, and 3.3 moles/L is the most likely concentration. We assumed there were two gallons of 3.3 moles/L of triethanolamine used to neutralize the liquid nitric acid. The nitrate salt composition was assumed to be composed of 67.8 wt% Mg(NO₃)₂•6H₂O, 14.9 wt% NaNO₃, 10.3 wt% Ca(NO₃)₂•4H₂O, and 7.0 wt% Fe(NO₃)₃•9H₂O based on an analysis done by others. The composition of the Swheat Scoop® was assumed to be the same as wheat flour since it is a 100% wheat product. The heat of formation of the Swheat Scoop® was determined using the elemental composition along with the heat of combustion for wheat.

Various calculations were performed with the waste composition and included numerous thermodynamic point calculations at 1 atm and from temperatures ranging from 300-1000 K. We also performed adiabatic flame calculations with this mixture at 1 atm. The adiabatic flame temperature is around 900K and is hot enough to gasify the Swheat Scoop® to form a fuel rich gas consisting of 33 mole% hydrogen and 9% carbon monoxide. The waste was divided into two regions: 1) a processed salt layer and 2) a processed liquid layer. The contents of these two layers were determined by doing overall mass balances. We used the equilibrium composition at 500 K

to determine a simple three-step reaction mechanism to model the thermal runaway behavior of the waste in Drum 68660. The three reactions included a water desorption step with kinetics taken from the literature, a dry processed salt decomposition step, and a dry processed liquid decomposition step. The water desorption reaction was endothermic with the reaction enthalpy taken to be the latent enthalpy of evaporation, 2260 J/g (endothermic). The processed salt reaction was exothermic at 2820 J/g (exothermic). The processed liquid reaction was exothermic at -3160 J/g (exothermic). We also performed a similar analysis with a zeolite substituted for the Swheat Scoop® and determined the reaction to be endothermic.

We used a finite element model of Drum 68660 with a three-step reaction mechanism and with the waste decomposition kinetics adjusted to give thermal runaway in about 70 days. The kinetics for the water desorption reaction was taken from the literature. We used a background source of 0.12 W in the processed salt layer and 0.17 W in the processed liquid layer based on thermal decay energy produced from radioactive isotopes. The outer wall of the drum was exposed to a constant 300 K radiation boundary temperature. We also used 300 K for a free convection boundary. The predicted external drum temperature did not increase more than a degree during the 70-day thermal runaway event. We predict that the amount of waste converted into decomposition gases at thermal runaway was about 3.4 kg, which is about 5% of the mass of the waste in Drum 68660. A simulation was also performed with the radiological decay heat set to zero. For this simulation, thermal runaway occurred in 75 days rather than 70 days with the source.

Since the drum wall temperatures were relatively cool during pre-thermal runaway, we assess that the drum did not turn black until after ignition. Also, since the reaction mechanism was not pressure dependent, we assess thermal runaway could have occurred in Drum 68660 whether or not the drum was vented. Furthermore, the vented gases were probably fuel rich and once mixed with external air can increase in temperature up to 1800 K. We have also run the thermal runaway model with various external boundary temperatures. We have shown that if the external radiation temperature was 1000 K, the drum could ignite in about 90 seconds. We have also run a calculation showing the effects of thermal runaway of Drum 68660 on a close victim drum. The calculation indicates that the victim drum might ignite on the top edge of the waste. The victim drum would be a fast thermal runaway compared to the slow thermal runaway of Drum 68660. The victim drum waste will be close to the ambient temperature, and the thermal runaway may not be sufficient to burn much of the waste. Failure to propagate burning in drums undergoing fast thermal runaway may explain why radiation signatures measured in various WIPP filters appear as if the radiation source only came from Drum 68660.

Sibling drum 68685 is currently at Los Alamos and has a similar content to the processed nitrate salt layer in Drum 68660. Head gas has been monitored and the sibling drum temperature has not increased significantly. Calculations in the current work suggest that the external drum temperature would not increase appreciably before a thermal runaway event. Also, the thermal runaway is not only dependent on the reactivity of the waste, but also depends on the heat transfer characteristics of the waste. In the sibling drum, a 9.98 kg lead blanket is on top of the waste, which can act as a heat sink and can affect thermal runaway characteristics of the drum. A simple analysis with Drum 68660 with a higher air thermal conductivity (similar to lead) caused the thermal runaway time to increase substantially and the thermal runaway location to shift to the bottom of the drum. Thermal runaway may not occur in the sibling drum with different heat transfer characteristics. Future modeling could address this issue in more detail. Nevertheless, all of the calculations presented in the current work are consistent with observations regarding the WIPP radiation leak occurring on February 14, 2014.

Tables and Figures:

Table D-1. Parent and sibling drum mass balance

Name	Weight, kg	
Parent (585793)		
Nitrate salts	115.91	
Decant liquid (3.3 molar HNO ₃ with dissolved nitrate salts)	10.48	
lead blanket (on top of drum)	9.98	
68725 net weight	136.37	
External materials added to parent waste		
Neutralizer (3.3 molar triethanolamine)	7.97	
Room trash (tungsten glove, plastic bottle, etc.)	11.00	
Swheat (10% moisture)	71.34	
External material net weight	90.31	
Sibling (68660)		
Nitrate salts	26.16	Remediated salt layer
Swheat (3:1 Swheat to liquid ratio by volume)	13.63	
Decant liquid (3.3 molar HNO ₃ with dissolved nitrate salts)	10.48	Remediated liquid layer
Neutralizer (3.3 molar triethanolamine)	7.97	
Swheat (0.7:1 Swheat to salt ratio by volume)	13.03	
Room trash	11.00	Trash layer
68660 net weight	82.27	
Sibling (68685)		
Nitrate salts	89.75	
Swheat (0.7:1 Swheat to salt ratio by volume)	44.68	
Lead blanket	9.98	
68685 net weight	144.41	
Mass parent + Mass external materials	226.68	✓
Mass 68660 + Mass 68685	226.68	✓

Table D-2. Assumptions regarding Swheat Scoop® and neutralized liquids

Assumption	Source	Notes
Remediated layer volumes in both sibling drums (68660 and 68685)	Estimate from X-rays	X-ray of 68660 and 68685.
Swheat bulk density	Swheat patent (5,690,051 on 11/25/97) and measurements	We measured 550 kg/m ³ in small samples and 650 g/m ³ in larger samples. 600 g/m ³ is assumed to be the nominal density
Swheat moisture	Charles Neece (Pet Care Systems representative)	As shipped moisture content is 10-13%. In dry climates, this drops by 1-2%. The moisture content in NM is assumed to be 8-11 wt%.
Swheat:salt and Swheat: liquid volume ratio	Mass Balance and assumed volume ratio for Swheat:liquid.	The overall Swheat mass was determined by a parent to sibling mass balance. The volume ratio for the Swheat:liquids was assumed to be 3:1. The Swheat:nitrate salt volume ratio was calculated to be 0.7:1.
Neutralizer volume and molarity	Estimate	X-ray pictures showed a one gallon plastic neutralizer container in the trash layer. Two gallons of neutralize is a conservative estimate with molarity between 1-5 mols/L (3.3 mols/L used in the current work).
Molarity of nitric acid	Determined from amount of neutralizer.	Assumed to be the same as the neutralizer.
Nitrate salt composition	Kirk Weisbrod analysis	Determined from "stream analyzer" simulations assuming 1) analysis of source waste, 2) stream ratios stored in parent drum, and 3) amount of liquid retained with solid crystals.

Table D-3. Processed salts in 68660^a

Composition	Detailed	Simplified
	Mass, kg	Mass, kg
Dry wheat in Swheat	11.72	11.72
H ₂ O in Swheat	1.30	1.30
H ₂ O (with trace elements)	0.05	
Al(NO ₃) ₃ * 9H ₂ O	0.62	
Ca(NO ₃) ₂ * 4H ₂ O	2.48	2.70
KNO ₃	0.54	
Mg(NO ₃) ₂ * 6H ₂ O	16.30	17.74
NaNO ₃	3.58	3.89
Ni(NO ₃) ₂ * 6H ₂ O	0.02	
Pb(NO ₃) ₂	0.00	
(COOH) ₂	0.40	
Cr(NO ₃) ₃ * 9H ₂ O	0.03	
Fe(NO ₃) ₃ * 9H ₂ O	1.69	1.84
HNO ₃	0.40	
NaF	0.05	
Total	39.19	39.19

^aVolume of this layer is 0.053 m³

Table D-4. Processed liquids in 68660^{a,b}

Composition	Mass, kg
Dry wheat	12.26
H ₂ O in Swheat	1.36
H ₂ O in decant	3.13
HNO ₃ in decant	1.57
Nitrate salts ^b in decant	
Ca(NO ₃) ₂ * 4H ₂ O	0.54
Mg(NO ₃) ₂ * 6H ₂ O	4.27
NaNO ₃	0.54
Fe(NO ₃) ₃ * 9H ₂ O	0.43
TEA in neutralizer	3.73
H ₂ O in neutralizer	4.25
Total	32.08

^aRemediated liquid layer volume is 0.038 m³.

^bBased on measured solubility with composition based on most common salts.

Table D-5. Drum 68660 with zeolite instead of Swheat Scoop[®]

Composition	Mass, kg
Nitrate salts (solid)	
Ca(NO ₃) ₂ * 4H ₂ O	2.70
Mg(NO ₃) ₂ * 6H ₂ O	17.74
NaNO ₃	3.89
Fe(NO ₃) ₃ * 9H ₂ O	1.84
Dissolved nitrates in decant	
Ca(NO ₃) ₂ * 4H ₂ O	0.54
Mg(NO ₃) ₂ * 6H ₂ O	4.27
NaNO ₃	0.54
Fe(NO ₃) ₃ * 9H ₂ O	0.43
HNO ₃ in decant	1.57
H ₂ O in decant	3.13
TEA in neutralizer	3.73
H ₂ O in neutralizer	4.25
Analcite (representative zeolite)	172.91

Table D-6. Volumes and masses used to calculate zeolite mass

Volume of nitrate salts in both 68660 & 68685	0.137 m ³
Volume of nitrate salts in 68660	0.031 m ³
Liquids in 68660 (decant + neutralizer)	0.015 m ³
Volume of Analcite (1:1 in salts, 3:1 in liquids)	0.076 m ³
Volume of salts, liquids, analcite	0.122 m ³
Mass of salts, liquids, analcite	217.527 kg
Mass of Analcite	172.911 kg

Table D-7. Various oxygen balances and reaction energies in 68660

System	Oxygen Balance	Reaction Enthalpy, J/kg	
1) Remediated salt layer (salts, Swheat)			
dry ^a	-15.70%	-2.83E+06	exothermic
wet ^b	-15.66%	-2.66E+06	exothermic
2) Remediated liquid layer (acid, neutralizer, Swheat)			
dry ^c	-82.41%	-3.16E+06	exothermic
wet ^d	-59.96%	-1.58E+06	exothermic
3) Combined (salts, acid, neutralizer Swheat)			
dry ^c	-41.13%	-2.93E+06	exothermic
wet ^d	-35.34%	-2.17E+06	exothermic
4) Combined (salts, acid, neutralizer, zeolite)			
dry ^e	2.50%	2.33E+05	endothermic
wet ^f	2.41%	3.09E+05	endothermic

^a "dry" excludes 1.3 kg of water in Swheat in Table 3.

^b "wet" includes 1.3 kg water in Swheat. Thus, all the contents in Table 3 are considered.

^c "dry" excludes 8.74 kg of water in Swheat, decanted liquid, and neutralizer in Table 4.

^d "wet" includes all the contents in Table 4.

^e "dry" excludes 7.38 kg of water in the decanted liquid and neutralizer in Table 5.

^f "wet" includes all the contents in Table 5.

Table D-8. Possible reactions in 68660 at 1 atm and 500 K

System	Equation
Remediated salt layer:	
Dry: $C_{2.154}H_{8.647}O_{7.324}N_{1.202}Mg_{0.339}Na_{0.224}Ca_{0.056}Fe_{0.022} \rightarrow 3.38 H_2O + 0.452 CH_4 + 1.2 CO_2 + 0.6 N_2 + 0.036 H_2 + 0.0074 Fe_3O_4(s) + 0.283 MgCO_3(s) + 0.112 Na_2CO_3(s) + 0.056 CaMgC_2O_6(s) + 2.83 \times 10^6 J/kg$	(1)
Wet: $C_{1.592}H_{8.912}O_{5.673}N_{0.888}Mg_{0.25}Na_{0.166}Ca_{0.041}Fe_{0.016} \rightarrow 2.76 H_2O + 0.333 CH_4 + 0.884 CO_2 + 0.444 N_2 + 0.029 H_2 + 0.0055 Fe_3O_4(s) + 0.209 MgCO_3(s) + 0.0828 Na_2CO_3(s) + 0.041 CaMgC_2O_6(s) + 2.66 \times 10^6 J/kg$	(2)
Remediated liquid layer:	
Dry: $C_{3.989}H_{9.38}O_{4.956}N_{0.807}Mg_{0.109}Na_{0.042}Ca_{0.015}Fe_{0.007} \rightarrow 2.94 H_2O + 0.852 CH_4 + 0.785 CO_2 + 0.403 N_2 + 0.0414 H_2 + 2.207 C(s) + 0.00232 Fe_3O_4(s) + 0.094 MgCO_3(s) + 0.0208 Na_2CO_3(s) + 0.0149 CaMgC_2O_6(s) + 3.16 \times 10^6 J/kg$	(3)
Wet: $C_{0.956}H_{3.769}O_{1.946}N_{0.193}Mg_{0.026}Na_{0.01}Ca_{0.004}Fe_{0.002} \rightarrow 1.19 H_2O + 0.338 CH_4 + 0.325 CO_2 + 0.097 N_2 + 0.0163 H_2 + 0.259 C(s) + 0.000556 Fe_3O_4(s) + 0.0225 MgCO_3(s) + 0.005 Na_2CO_3(s) + 0.00358 CaMgC_2O_6(s) + 2.17 \times 10^6 J/kg$	(4)
Combined remediated salt and liquid layer (Swheat):	
Dry: $C_{2.947}H_{8.96}O_{6.308}N_{1.033}Mg_{0.24}Na_{0.146}Ca_{0.038}Fe_{0.016} \rightarrow 3.08 H_2O + 0.68 CH_4 + 1.08 CO_2 + 0.516 N_2 + 0.038 H_2 + 0.83 C(s) + 0.0052 Fe_3O_4(s) + 0.202 MgCO_3(s) + 0.073 Na_2CO_3(s) + 0.038 CaMgC_2O_6(s) + 2.93 \times 10^6 J/kg$	(5)
Wet: $C_{1.15}H_{4.72}O_{3.07}N_{0.4}Mg_{0.094}Na_{0.057}Ca_{0.015}Fe_{0.006} \rightarrow 1.6 H_2O + 0.37 CH_4 + 0.53 CO_2 + 0.2 N_2 + 0.02 H_2 + 0.11 C(s) + 0.002 Fe_3O_4(s) + 0.079 MgCO_3(s) + 0.028 Na_2CO_3(s) + 0.015 CaMgC_2O_6(s) + 2.17 \times 10^6 J/kg$	(6)
Combined remediated salt and liquid layer (zeolite):	
Dry: $Mg_{0.086}N_{0.32}H_{3.24}O_{7.13}Ca_{0.014}Na_{0.84}Fe_{0.006}C_{0.15}Al_{0.79}Si_{1.58} \rightarrow 1.62 H_2O + 0.16 O_2 + 0.137 CO_2 + 0.16 N_2 + 0.309 Al_2SiO_5(s) + 0.014 CaCO_3(s) + 0.0028 Fe_2O_3(s) + 0.43 SiO_2(s) + 0.086 Al_2MgO_4(s) + 0.422 Na_2O_5Si_2 - 2.33 \times 10^5 J/kg$	(7)
Wet: $Mg_{0.06}N_{0.23}H_{2.87}O_{5.34}Ca_{0.01}Na_{0.8}Fe_{0.004}C_{0.1}Al_{0.56}Si_{1.2} \rightarrow 1.44 H_2O + 0.11 O_2 + 0.097 CO_2 + 0.11 N_2 + 0.219 Al_2SiO_5(s) + 0.01 CaCO_3(s) + 0.002 Fe_2O_3(s) + 0.304 SiO_2(s) + 0.061 Al_2MgO_4(s) + 0.298 Na_2O_5Si_2 - 3.09 \times 10^5 J/kg$	(8)

Table D-9. Model parameters for 68660

Symbols	Description	Value	Units
$\ln(A_1), \ln(A_2), \ln(A_3)$	Natural logarithm of the pre-exponential	37, 40, 40	Ln(1/s)
$E_1/R, E_2/R, E_3/R$	Activation energies normalized by R	25000, 16493, 16493	K
$\sigma_1/R, \sigma_2/R, \sigma_3/R$	Standard deviation of E/R	2500,-500,-500	K
h_{r1}, h_{r2}, h_{r3}	Reaction enthalpy	-2260, 2830, 3160	J/g
$[H_2O_{a,liquid}]_0$	Initial adsorbed water in rem. liquid layer	12.8	kgmol/m ³
$[H_2O_{a,salt}]_0$	Initial adsorbed water in rem. salt layer	1.36	kgmol/m ³
$[waste_{liquid}]_0$	Initial dry waste in rem. liquid layer	4.01	kgmol/m ³
$[waste_{salt}]_0$	Initial dry waste in rem. Salt layer	3.85	kgmol/m ³
C	Specific heat	2400	J/kgK
k_{air}	Thermal conductivity of air layer	0.03	W/mK
k_{salt}	Thermal conductivity of rem. salt layer	0.4	W/mK
k_{liquid}	Thermal conductivity of rem. liquid layer	0.3	W/mK
k_{trash}	Thermal conductivity of trash layer	0.05	W/mK
ϵ_{drum}	Drum emmissivity	0.9	none
H_{conv}	Natural convection heat transfer coefficient	50	W/m ² K
$q_{v,liquid}$	Volumetric radiological heat in salt layer (0.12 W)	7.63	W/m ³
$q_{v,salt}$	Volumetric radiological heat in liquid layer (0.17 W)	2.26	W/m ³
T_{room}	Temperature of room	300	K
$\rho_{b, air}$	Bulk density of air layer	1.18	kg/m ³
$\rho_{b, salt}$	Bulk density of remediated salt layer	738	kg/m ³
$\rho_{b, liquid}$	Bulk density of remediated liquid layer	848	kg/m ³
$\rho_{b, trash}$	Density of trash layer	273	kg/m ³
$\rho_{tmd, salt}$	Theoretical maximum density of rem. salt layer	1394	kg/m ³
$\rho_{tmd, liquid}$	Theoretical maximum density of rem. liquid layer	1073	kg/m ³
$\phi_{o, liquid}$	Initial gas volume fraction in rem. liquid layer	0.47	m ³ /m ³
$\phi_{o, salt}$	Initial gas volume fraction in rem. salt layer	0.21	m ³ /m ³
V_{air}	Volume of air layer	0.0823	m ³
V_{salt}	Volume of remediated salt layer	0.053	m ³
V_{liquid}	Volume of remediated liquid layer	0.038	m ³
V_{trash}	Volume of trash layer	0.0403	m ³
$V_{gas(Trash, Liquid)}$	Gas volume in air and trash layer (0.08 + 0.03)	0.11	m ³

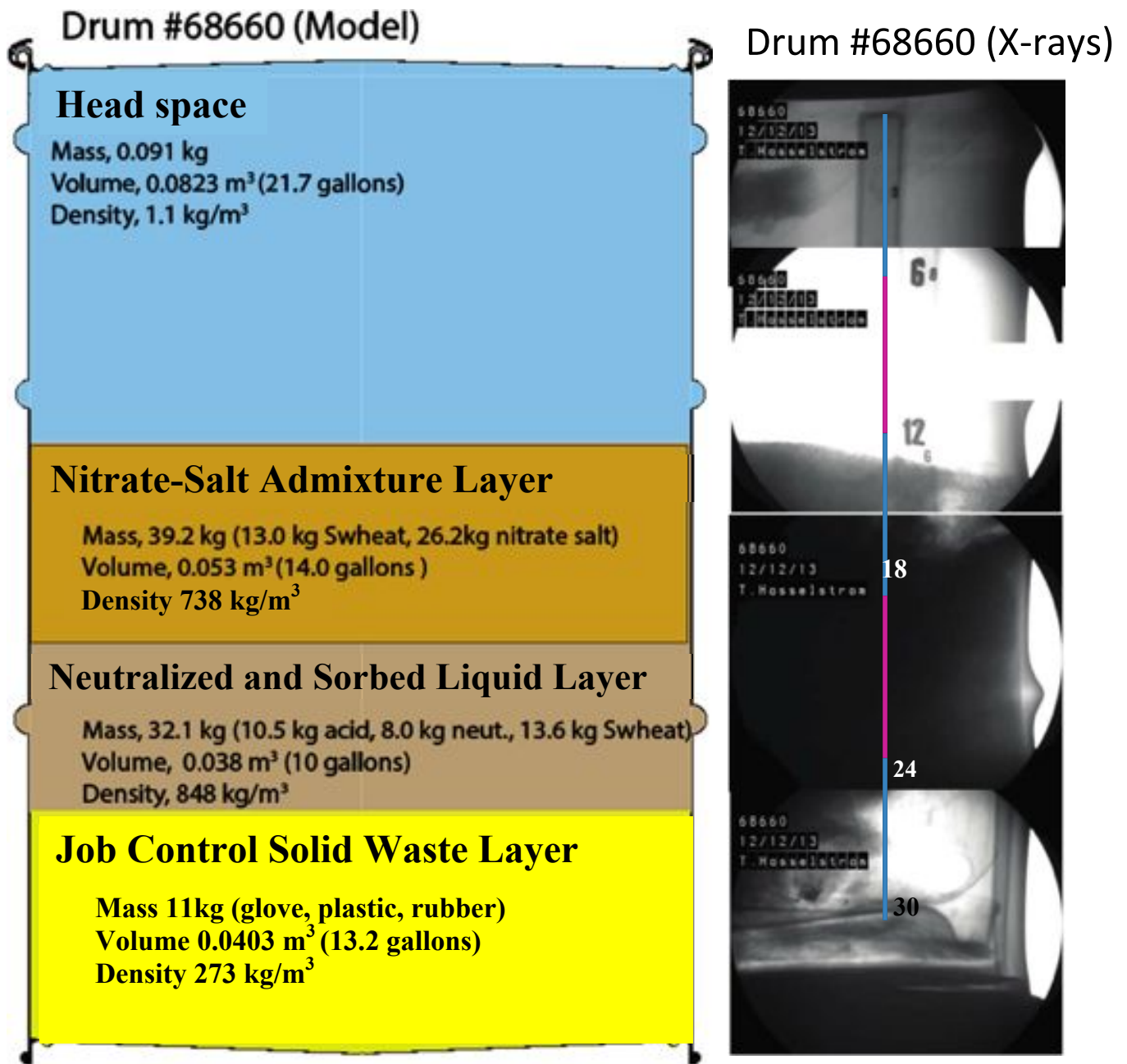
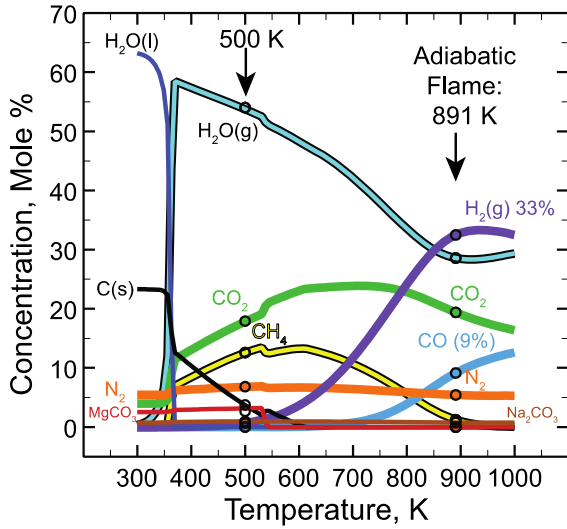


Figure D-1. TAT Model of Drum 68660 contents and distribution based on x-rays of Drum 68660

A) Waste composition with Swheat



B) Waste composition with zeolite

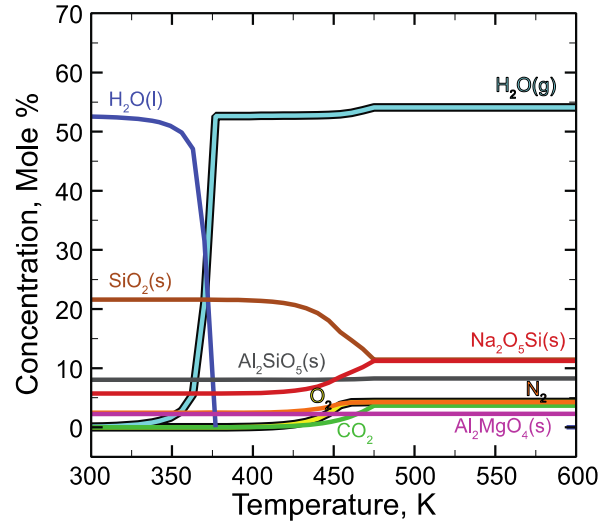


Figure D-2. Waste equilibrium composition at 1 atm for waste processed with A) Swheat Scoop® and B) zeolite.

A

B

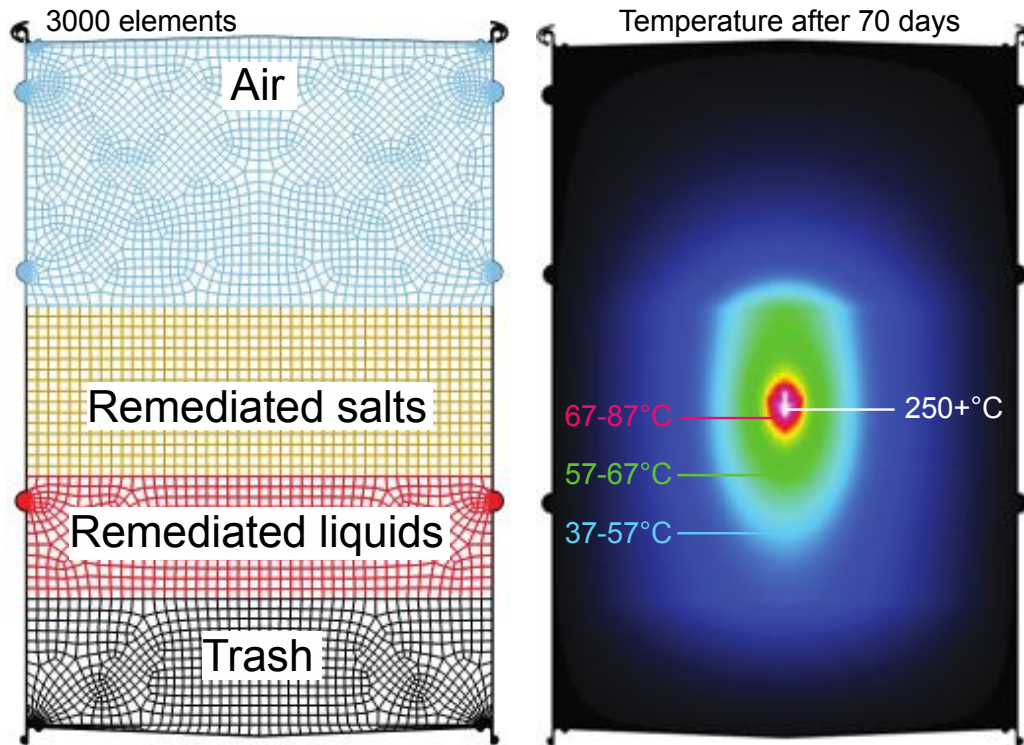


Figure D-3. A) 2D axisymmetric mesh with reflection about X axis and B) temperature profiles after 70 days. Model parameters are in Table D-9.

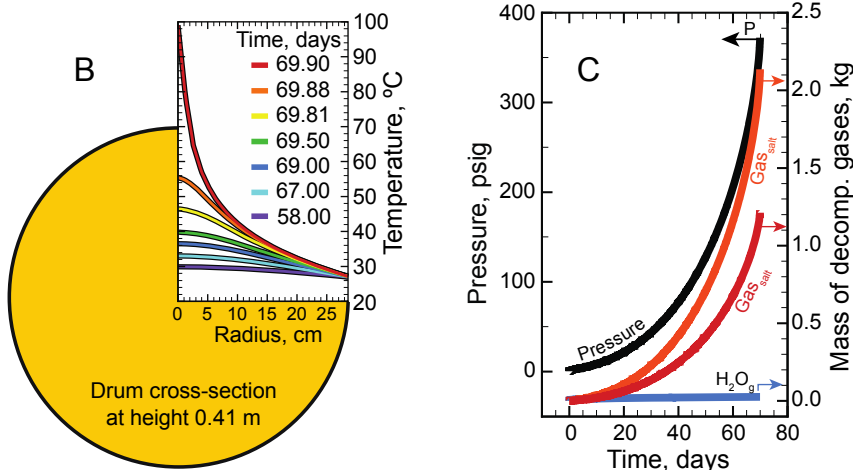
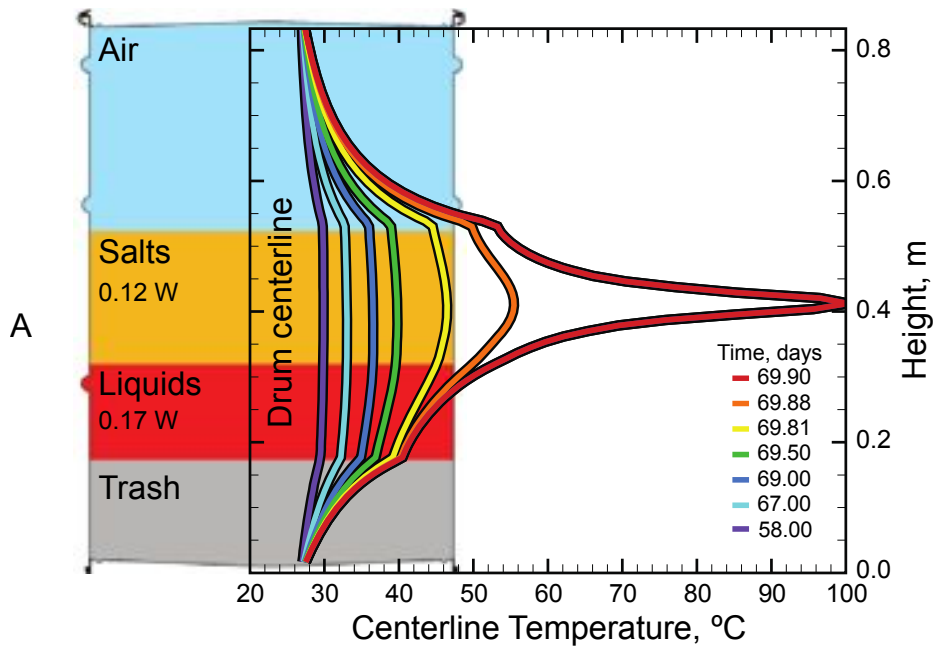


Figure D-4. A) Axial centerline temperature, B) radial temperatures at 0.41 m, C) pressure, and decomposition gas mass in drum #68660.

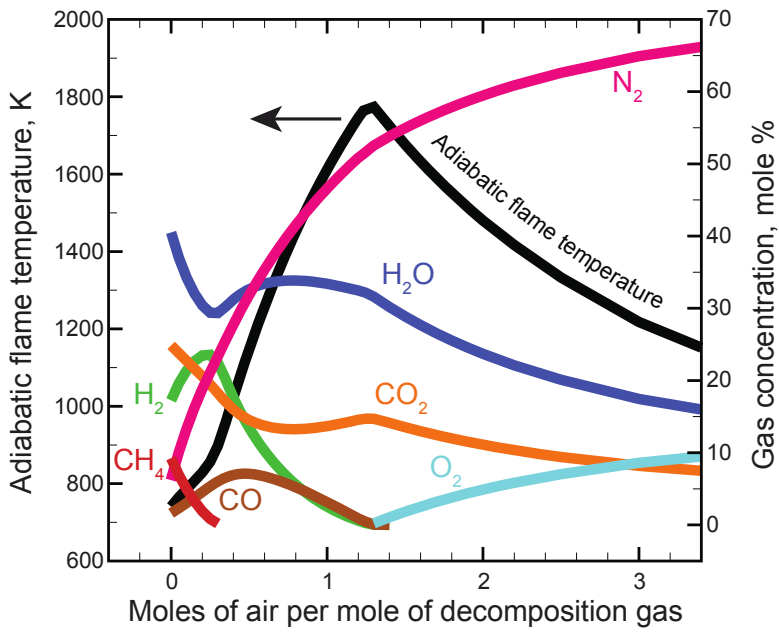


Figure D-5. Adiabatic flame temperature and gas compositions for various mixtures of air with the decomposition gases predicted from Drum 68660.

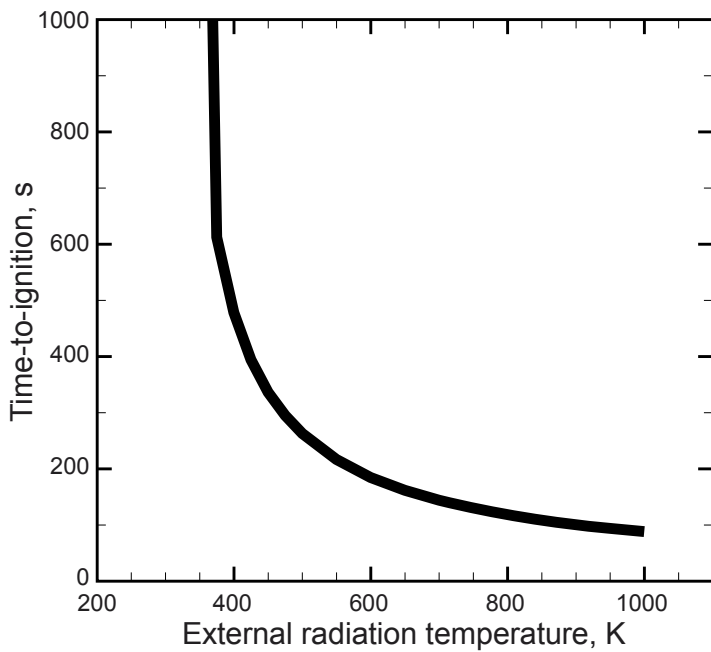


Figure D-6. Calculated thermal runaway time with a hot radiation boundary temperature.

A) Fast cookoff of victim drum

B) Slow cookoff of drum 68660

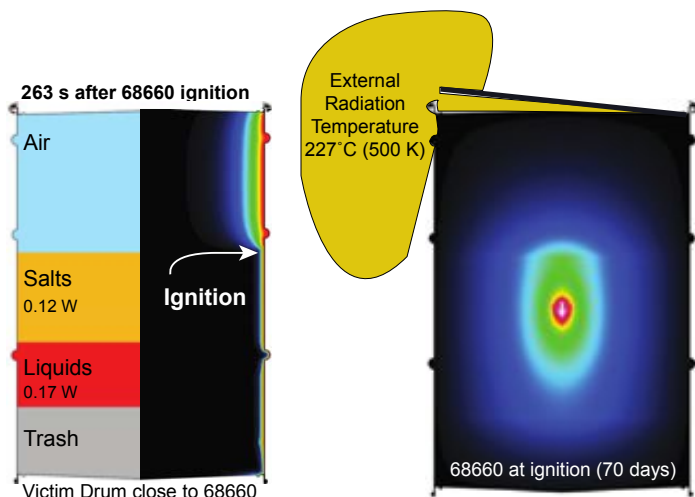


Figure D-7. The effect of thermal runaway of Drum 68660 on a nearby victim drum: A) fast thermal runaway of victim drum and B) slow thermal runaway of Drum 68660.

References

- Giaquinto, J., "Calculated decay heat in 68660," EMAIL sent to Minier on 11/19/2014. This calculation was based on mixing of the salts in the parent drum (S855793) before dispersal into the two sibling drums (68660 and 68685). The decay heat is based on 26 kg of salts and 2 gallons of liquid. The isotopes were Pu238, Pu239, Pu240, and Am241. The 26 kg of salts would have a total of 0.12 W produced from decay heat. The 2 gallons of liquid decant would have a total of 0.17 W produced from decay heat.
- CCP Radiography Data Sheet for Waste Container 68660.
- WIPP 2014 sharepoint site: Documents/LANL Documents/RTR (Drum Radiograph) video/68660.wmf
- Sladek, J. H., "Method for sorbing liquid using ground wheat grain litter: United States Patent, (November 25, 1997). See also WIPP 2014 sharepoint site: Reference Documents.
- Neece, C., Pet Care systems, telephone conversation with Hobbs, M. L. (August 25, 2014).
- Spilfyter Classifier/Neutralizer Reference Chart, www.npscorp.com/assets/resources/neutralizer-chart.pdf. This chart shows that 1 gallon of neutralizer will neutralize 0.5 gallons of 2.3 molar nitric acid.
- WIPP 2014 sharepoint site: Documents/Sandia Documents/Drum History/R16C4/R16-C4-68660.pdf
- Memo from Kenneth Hargis (khargis@lanl.gov) to David Hobbs (david.hobbs@srl.doe.gov), "Final Salt Estimate for 68660." (10/08/2014, 10:11 am).
- Veazey, G. W., Schake, A. R., Shalke, P. D., Romero, D. A., Smith, C. A., "Waste-Form Development for Conversion to Portland Cement at Los Alamos National Laboratory (LANL) Technical Area 55 (TA-55), LA-13125 (1996).
- Rafal, M., Berthold, J., Linz, D., "Introduction to OLI Electrolytes," OLI systems, Inc., www.olisystems.com/IntroElectrolytes.pdf (accessed 10/20/2014).
- Hobbs, M. L., Brundage, A. L., Yarrington, C. D., "JCZS2i: An Improved JCZ Database for EOS Calculations at High Temperature and Pressure," 15th International Detonation Symposium, San Francisco, CA (July 2014).
- Wiebenson W. E. Jr., Zwisler, W. H., Seely, L. B., and Brinkley, S. R., Jr., I Theoretical and mathematical formulations for the TIGER Computer Program, SRI publication under Contract No. DA-04-f200-AMC-3326(X) (1968).
- Cowperthwaite, M. and Zwisler, W. H., TIGER Computer program Documentation, SRI Publication No. Z106, Menlo Park, CA (1973).
- McBride, B. J. and Gordon, S., Computer Program for Calculation of Complex Chemical Equilibrium Compositions and Applications II. User's Manual and Program Description, NASA Reference Publication 1311, NASA Lewis research Center, Cleveland, Ohio (1996).

15. Supplies of organic materials, Part #502-274, wheat flour, page 14, www.leco.com (Accessed August 25, 2014).
16. Merrill, A. L., and Watt, B. K., "Energy Value of Foods...basis and derivation" Agricultural Research Services, Agricultural Handbook No. 74, U.S. Govt. Printing Office, Washington DC, (February 1973). The heat of combustion is found in Table 6 on page 6 of this document.
17. Hobbs, M. L. and Kaneshige, M. J., "Ignition experiments and models of a plastic bonded explosive (PBX 9502)," *The Journal of Chemical Physics*, **140**, 124203 (2014).
18. Notz, P. K., Subia, S. R., Hoopkins, M. M., Moffat, H. K., Noble, D. R., "SIERRA Multimechanics Module: Aria User Manual—Version 4.28" SAND2007-2734, Sandia National Laboratories, Albuquerque, NM (2013).
19. Erikson, W. W., Cooper, M. A., Hobbs, M. L., Kaneshige, M. J., Olkver, M. S., Snedigar, S., "Determination of thermal diffusivity, conductivity, and energy release from the internal temperature profiles of energetic materials," *International Journal of Heat and Mass Transfer*, **79**, 676-688 (2014).
20. Smith, J. A. "Mechanical Modeling of a WIPP Drum Under Pressure," Sandia National Laboratories memo to distribution, Albuquerque, NM (November 25, 2014).

MECHANICAL RESPONSE OF DRUM: MODELING OF DRUM BEHAVIOR WHEN PRESSURIZED

Summary

Mechanical modeling was undertaken to support the Waste Isolation Pilot Plant (WIPP) technical assessment team (TAT) investigating the February 14th 2014 event where there was a radiological release at the WIPP. The initial goal of the modeling was to examine whether a mechanical model could inform the team about the event. The intention was to have a model that could test whether scenarios with respect to the rate of pressurization. It was expected that the deformation and failure (inability of the drum to contain any pressure) would vary according to the pressurization rate. As the work progressed, there was also interest in using the mechanical analysis of the drum to investigate what would happen if a drum pressurized when it was located under a standard waste package. Specifically, would the deformation be detectable from camera views within the room.

A finite element model of a WIPP 55-gallon drum was developed that used all hex elements. Analyses were conducted using the explicit transient dynamics module of Sierra/SM to explore potential pressurization scenarios of the drum. These analyses show similar deformation patterns to documented pressurization tests of drums in the literature. The calculated failure pressures from previous tests documented in the literature vary from as little as 16 psi to 320 psi. In addition, previous testing documented in the literature shows drums bulging but not failing at pressures ranging from 69 to 138 psi. The analyses performed for this study found the drums failing at pressures ranging from 35 psi to 75 psi. When the drums are pressurized quickly (in 0.01 seconds) there is significant deformation to the lid. At lower pressurization rates the deformation of the lid is considerably less, yet the lids will still open from the pressure. The analyses demonstrate the influence of pressurization rate on deformation and opening pressure of the drums.

Analyses conducted with a substantial mass on top of the closed drum demonstrate that the drums will still open provided the pressure is high enough. Investigation teams should look for displaced drum lids when searching for drums that have pressurized and failed.

The mechanical modeling study for this program is summarized in the following memo. Following a brief introduction, there is a summary of a brief literature review of previous pressure testing of drums, an explanation of the model, presentation of the key results, some discussion, and concluding with a summary and key points.

Introduction

On February 14th 2014 there was a radiological release event at the Waste Isolation Pilot Plant (WIPP). An initial accident investigation report has been published which describes the event (U.S. DOE, 2014). An Accident Investigation Board (AIB) was created and as part of that board there is a Technical Assessment Team (TAT). The following work was conducted as part of Sandia National Labs (SNL) participation in the TAT's effort.

Initial images obtained from within WIPP discovered one drum that appeared open. An image of this drum (Drum 68660) is shown in Figure D-8.



Figure D-8. Drum 68660 in WIPP.

The following memo describes the mechanical modeling that was undertaken at SNL to support the TAT. The initial goal of this modeling was to examine whether a mechanical model could inform the team about the event and specifically what happened within Drum 68660. The intention was to have a model that could test scenarios with respect to the rate of pressurization. It was expected that the deformation and failure (inability of the drum to contain any pressure) would vary according to the pressurization rate. As the work progressed there was also interest in using the mechanical analysis of the drum to investigate what would happen if a drum pressurized when it was located under a standard waste package. Specifically, would the deformation be detectable from camera views within the room.

Review of Previous Drum Pressure Testing

An initial literature review was conducted to determine whether there was previous test data that could provide an indication of failure pressure and to provide results to benchmark the model developed for this work. Three studies were found that appeared relevant.

Los Alamos National Labs pressurization tests: A number of documents (Larranaga et al., 1998, Larranaga and Volz, 1998, Larranaga et al., 1999) appear to reference the same series of tests. Key points from this work are as follows:

1. The metal 55-gallon Open-Head drums tested in this work have the UN/DOT specification of 1A2/Y1.5/150. The WIPP drums modeled have the UN/DOT specification of 1A2/Y1.5/175. The difference is the wall thickness. The drums in the LANL study had a 1.2 mm nominal thick wall while the WIPP drum reportedly has a nominal wall thickness of 1.5 mm. A general internet search of drums suggests that some suppliers use the same lid thickness (1.5 mm) on both of these drums.
2. Failure pressures were similar for ½-full and ¾-full (with water) drums. Approximately 25-36 psi.
3. Failure pressures for cement filled drums was lower. Approximately 16-26 psi.
4. Drums failed near the bolt on the closure ring.
5. As quoted from LA-98-2541, “One interesting observation is the open-head drums appear to have vented at the above pressures immediately adjacent to the nut and bolt fastener on the ring.”

Savannah River pressurization tests: These tests were documented in Dykes and Meyer (1991). Key points from this work are as follows:

1. The objectives of this testing was to determine the minimum hydrogen concentration at which lid removal would occur and to investigate the maximum pressure and rate of pressure rise as a function of hydrogen concentration.
2. As quoted from the report, “variability in drum lid sealing and retaining ring closure” prevented them from establishing a relationship between pressure and hydrogen concentration. This suggests there is variability in the failure pressure.
3. Lids “blown” at pressures of 105-320 psi. Bulged at pressures of 69-138 psi.

Lawrence Livermore National Laboratory Fire Testing of 55 Gallon Metal Waste Drums: These tests were documented in Hasegawa et al. (1993).

Key points from this work are as follows:

1. Six tests were conducted using three different types of drums.
2. “Failure of the lid seals occurred in all of the drums early in the tests. Hot combustible gases vented from each drum and ignited. In three tests the lids blew off the drums ejecting some of the material from the drums.”
3. “Failure of lid seals will allow release of any toxic and/or radioactive materials and smoke contained in the drums.”

Model Development

Geometry:

The drum modeled was created from specifications of a Szolnok open head carbon steel drum, item CQ5508 (Szolnok, 2014). Drawings for the drum, lid, and bolt ring were obtained (see Appendix). Based on these drawings and some general assumptions a CAD file was created of the geometry. This file was used to create the meshes discussed below. The key assumption where the model differs from the actual geometry is in the ribs on the drum wall. Exact descriptions of those ribs are not detailed in on the drawings and the geometry of the ribs was simplified for speed of construction of the CAD geometry. The geometric differences of the ribs between the actual drum and that modeled are not considered significant with respect to the failure pressure and lid deformation behavior since they will mostly influence the circumferential stiffness of the drum. Figure D-9 shows an overview of the geometry created and a section of the drum CAD geometry.

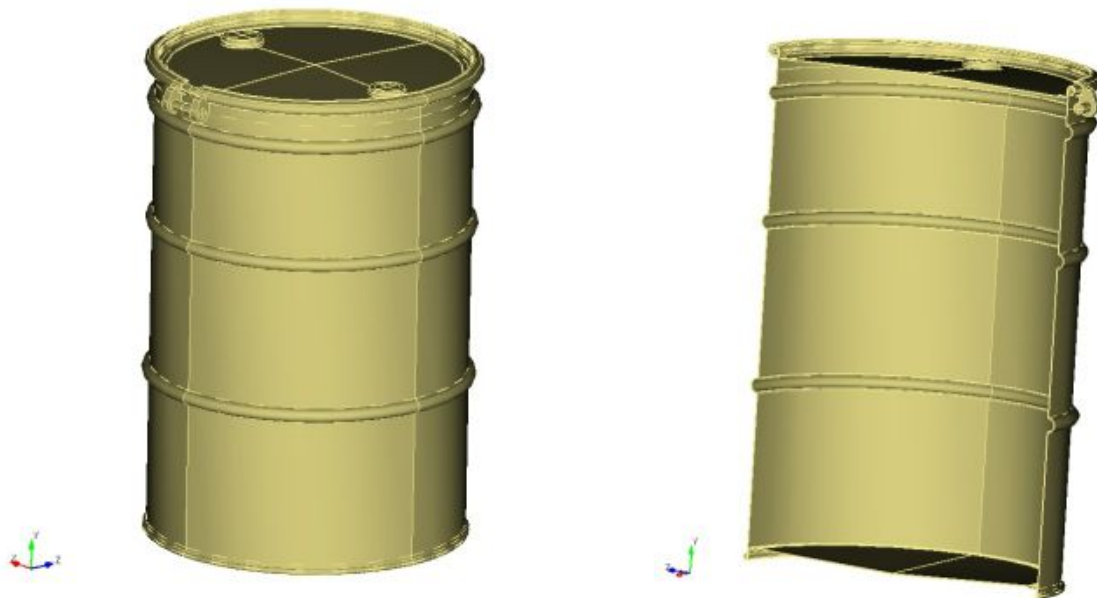


Figure D-9. Szolnok CQ5508 Drum CAD geometry

Material Properties:

An initial estimate of mechanical properties of the drum material was based on properties from Ludwig Sen, et al (1998) except the yield strength was lowered to 29.0e03 psi to more closely match published values (AK steel, 2014) of yield strength for ASTM A1008 steel used in these drums. Eventually, specimens were cut from the lid and closure ring of a drum obtained from LANL and tensile tests were performed on these specimens. The specimens tested from the drum lid were standard ASTM E8 sheet type specimen (ASTM, 2013). The specimens tested from the closure ring were ASTM E8 miniature specimens (ASTM, 2013).

There was not significant variation between each of the three specimens tested for each material. Figures D-10 and D-11 present the engineering stress-strain plots for the test data. The data for test 2 of each material was used in the analyses. For the closure ring data the material had a yield strength of 30.5e03 psi and for the drum lid material it had a yield strength of 40.0e03 psi. The ELASTIC_PLASTIC material model in Sierra/Solid Mechanics (Sierra Solid Mechanics, 2014) was used for the analyses. The hardening curves from the test data were implemented in the analyses for the elastic-plastic model. Figures D-3 and D-4 each have the initial assumed yield strength marked to demonstrate the difference between the initially assumed values and those of the tested properties from the drum obtained from LANL.

The initial analyses used the same properties for all material blocks in the model. Therefore, the drum body, lid, closure ring, and bolt all had the same properties (yield strength of 29.0e03 psi). The analyses run using the tested properties were run with the properties of the closure ring for the model closure ring and bolt, while the drum lid properties were used for the models drum body and the drum lid.

In all cases the gasket that is between the lid and the drum body lip is included in the analyses. However, it is modeled as steel. Modeling the gasket as a soft rubber presents computational difficulties. The gasket was included in the model to make sure the lid is seated accurately, but without the compliance of the rubber.

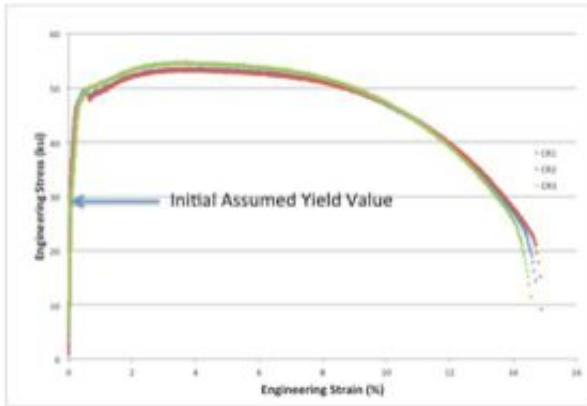


Figure D-10. Tested Closure Ring Engineering Stress-Percent Strain Curves for a drum obtained from LANL.

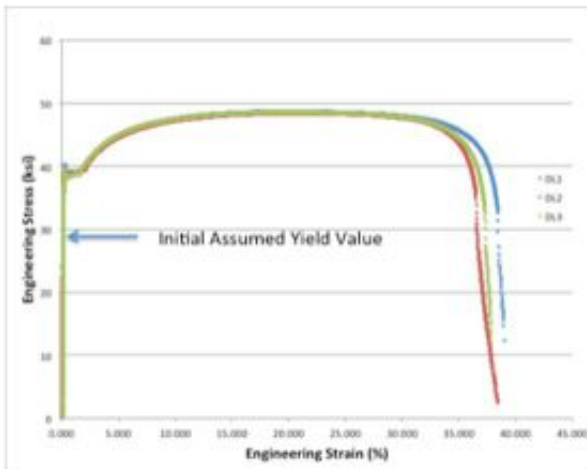


Figure D-11. Tested Drum Lid Engineering Stress-Percent Strain Curves for a drum obtained from LANL.

Analysis Approaches Explored:

The finite element meshes were created using Cubit (Cubit, 2014) and the analyses were performed using Sierra/SM (Sierra/Solid Mechanics, 2014).

Multiple analysis approaches were pursued initially to come up with an approach that could provide solutions within the accelerated timeframe and to maximize/optimize the potential solution methods. Options such as a full hex mesh, a hex-to-shell transition mesh, and pure shell mesh were pursued. In addition, the options for applying the preload to the drum closure ring to provide a tightly closed drum were pursued by both applying a closure strain to the closure ring and by displacing the flanges of the closure ring within the analysis and having the ring tighten due to the displacement; followed by securing the bolt (using the “tied” contact option in the code). Finally, the options of using either an implicit solver or performing an explicit transient dynamic analysis were pursued.

The advantage of using the implicit solver is that it can solve the analysis with larger time steps. This allows one to solve a problem over a much longer time frame than a transient dynamic analysis that takes many very small steps. However, the implicit solver can have trouble converging where there is significant contact. The problem of pressurizing a drum and having the solution run until the drum opens by the closure ring sliding over the lip of the drum body is a complex contact problem.

In the end, the full hex mesh using the explicit transient dynamic solutions was the only approach that yielded solutions under the current budget/time constraints. This approach provided a robust solution that has two main drawbacks. One, the turn-around time for analyses was slow, the solutions took 1-4 days of runtime. The model had more than 8-million elements with a time-step of approximately $2.3\text{e-}08$. Therefore, the turn-around time for analyses did not allow a substantial number of analyses. Second, due to the small time-step and duration of the event, only short duration events could be examined and consequently, what happens after the lid opens is beyond the reasonable duration of run-time. In addition, what happens after the drum lid opens is a very complex process that is beyond the fidelity of this model. This model does not include the contents under pressure and cannot account for the loss of pressure once the drum opens.

Modeling the closure of the drums is only an approximation of what the actual drums go through in the specified closure procedure. To have a more accurate representation of the drum closure preload for these analyses it would be best to have a measure of the strain in the closure ring once the drum is closed per the specified procedure. Since that was not available, the drum closure ring flanges were displaced to a position that resembled that of closed drums. However, small variations in this distance could potentially have a measurable influence on the preload of the closure ring (and opening pressure). In addition, the gasket between the drum lip and the lid likely changes the frictional characteristics between the parts and will have some influence on the opening pressure for these calculations. A coefficient of friction of 0.3 was modeled between all parts for these analyses.

Applied Loading:

A number of loading cases were explored for the analyses. For the pressurization two main cases were considered. Figures D-12 and D-13 present schematics of the two basic loading cases. The maximum pressure of the applied loadings varied some, but the shapes of the pressure curves were the same. For the analyses, this pressure was applied to the inside of the drum on the bottom, sidewall, and inside of the lid. When specific cases are discussed below, the maximum pressure will be specified. Figure D-12 shows what will be referred to as the “slow” loading case. For these cases the closure ring is closed in 0.005 seconds. Then the pressure is steadily increased until the time has reached 0.1 seconds. The other case (shown in Figure D-13), referred to as the “fast” load case the closure ring is closed in 0.005 seconds. Then the pressure is ramped quickly up to a “maximum” pressure at a total time of 0.015 seconds. Then, simulate pressure release, ramped back to zero in another 0.001 seconds (total time of 0.016 seconds). Some cases varying the time to maximum ramp pressure were also performed. Both of these pressure cases are purely hypothesized in nature, i.e. no chemistry effect should be inferred for these cases. They are used to understand structural performance differences that might present themselves from a short burst or a longer term loading.

The acceleration of gravity was applied in all of the cases presented below. In addition, the estimated weight of the contents (for Drum 68660) was included as a downward pressure on the bottom of the drums. For some analyses, a hydrostatic pressure on the sidewalls was applied to account for the contents applying pressure on the sidewalls. This was done because some of the testing at LANL (drums filled with cement) failed at lower pressures. However, for the analyses conducted with this study that included this hydrostatic sidewall pressure, the results were not affected. Therefore, further analyses did not include this loading.

Analyses were also conducted with a pressure force on the lid to account for the mass of the magnesium oxide (MgO). However, it should be noted that since this is applied as a pressure force down there are no inertial forces from this loading. The pressure to account for the weight of the MgO is 1.54 psi uniformly applied to the top of the drum. This is small compared to the internal pressure.

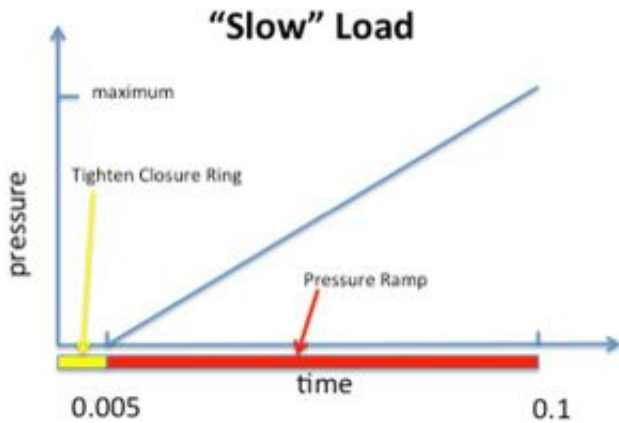


Figure D-12. Slower ramped loading form for analyses (referred to as “Slow” load)

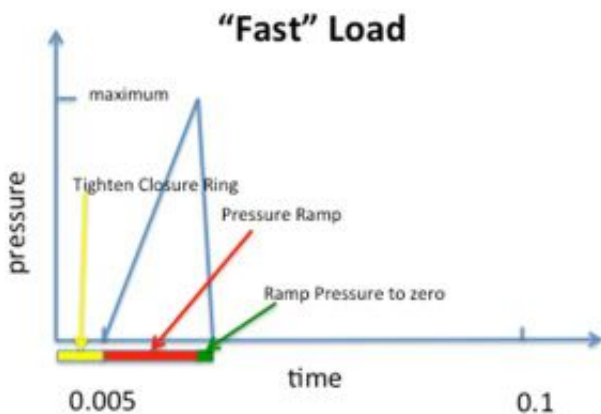


Figure D-13. Faster ramped loading form (and unloading) for analyses (referred to as “Fast” load)

Key Analysis Results

Since there is some subjectivity in the preload of the closure of the drums in these analyses (and most likely in actual drums) the predicted opening pressure also has some uncertainty. However, despite this issue there are a number of key results to present and conclusions that can be drawn from the result. In addition, results for the two different property sets (initially estimated properties and those from tests of a single drum from LANL) provide insight into potential variation in behavior such as deformation and failure pressure. Therefore, presented here are results of a number of the analyses performed for this study.

Using original mechanical property estimate and “fast” load case: For this case the maximum pressure load corresponds to 150 psi. The lid “pops” open at a pressure of approximately 75 psi. In the analysis the pressure continued to rise as the lid continued to come off. In an actual event, the pressure would be relieved once the drum opened. Analyses similar to this were run where the pressure was reduced to zero as soon as the lid “popped” open. In those cases the lid continued to open until the end of the analysis at 0.1 seconds. When the lid opens it has considerable velocity and one would not expect it to slow down within the 0.1 seconds of these analyses. Figure D-14 shows the drum with the Von Mises stress contours at the time the lid is opening (maximum contour represents yielding for the drum material). Note the large deformations of the lid. In addition, note the deformation near the closure-ring bolt. This lid deformation pattern is similar to the results from the testing at LANL (1998) with respect to the deformation pattern. Note that the separation of the closure ring from the lid is happening after the lid has opened. Since as stated above, the pressure is still being applied in the analysis which is likely not the case in an actual pressurization event (since the pressure would have been relieved) one cannot be certain whether the closure ring would actually separate from the lid.

Figure D-15 shows a comparison of one of the drums tested at LANL (Larranaga et al., 1999) and the results of the analysis at a similar deformation state. One can see the deformation patterns are similar. In addition, Figure D-16 shows a section from the analysis at the same point. There is actually a gap opened between the lid and the drum body lip where the closure ring gap is at the location of the bolt. This is where the drums lost pressure for the drums tested at LANL. In Figure D-16, one can see the seal would still be maintained at the opposite side of the lid because the closure ring is in contact with the drum body lip (in a real drum the gasket would protrude out of the closure ring). Also note as pointed out in Figure D-16 the discontinuity in the lid deformation patten near the plug location.

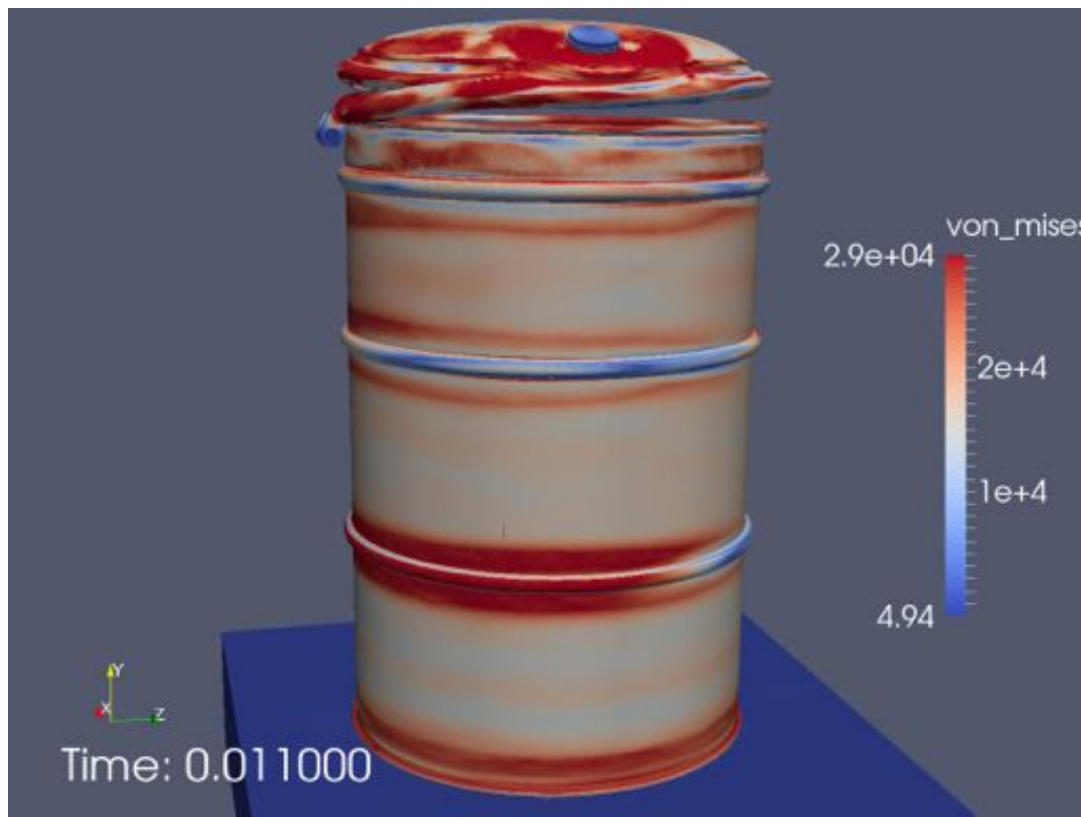


Figure D-14. Analysis results for case with original estimate of properties and “fast” loading.



Figure D-15. Comparison of tested drum at LANL (Larranaga et al., 1999) left, and analysis results, right.

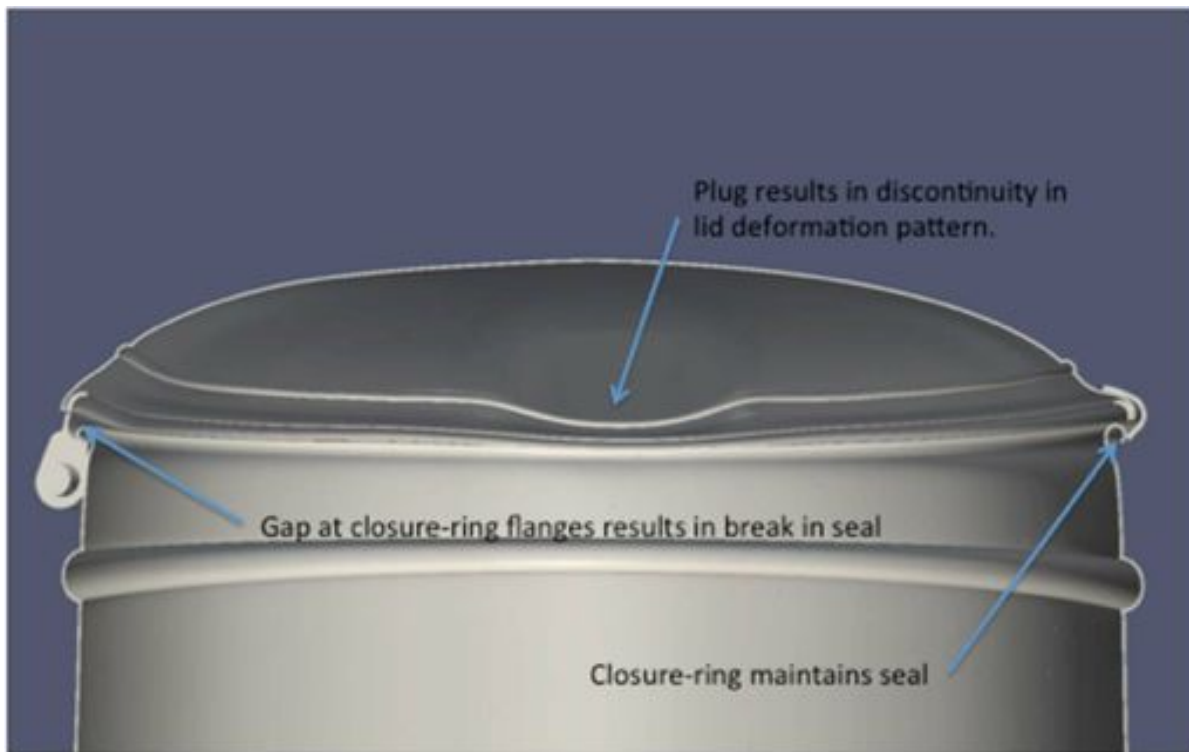


Figure D-16. Section showing lid deformation for initial property estimates and “fast” loading case.

Using original mechanical property estimate and “slow” load case: For this case the maximum pressure load corresponds to 50 psi. The lid “pops” open at a pressure of approximately 35 psi. In the analysis the pressure continues to be applied as the lid comes off. In an actual event, the pressure would be relieved once the drum is open. As discussed above, cases were run where the pressure was reduced to zero once the lid opened. However, the velocity of the lid is still high as the lid opens and it continues to move up until the analysis is complete at 0.1 seconds. Figure D-17 shows the drum with the Von Mises stress contours after the lid is open. In this “slow” loading case, one can see that there is less deformation of the lid when it opens than in the “fast” case. In addition, the lid opens in a gentler manner with the opening initiating away from the closure-ring bolt. Figure D-18 shows the lid from another view as it is opening. At a pressure of 30 psi the maximum deformation at the center of the lid is 2.6 inches and for the testing at LANL for a $\frac{3}{4}$ -full drum was measured at 2.8 inches. As pointed out above, the LANL tested drums were a thinner gauge material that could account for some of this difference.

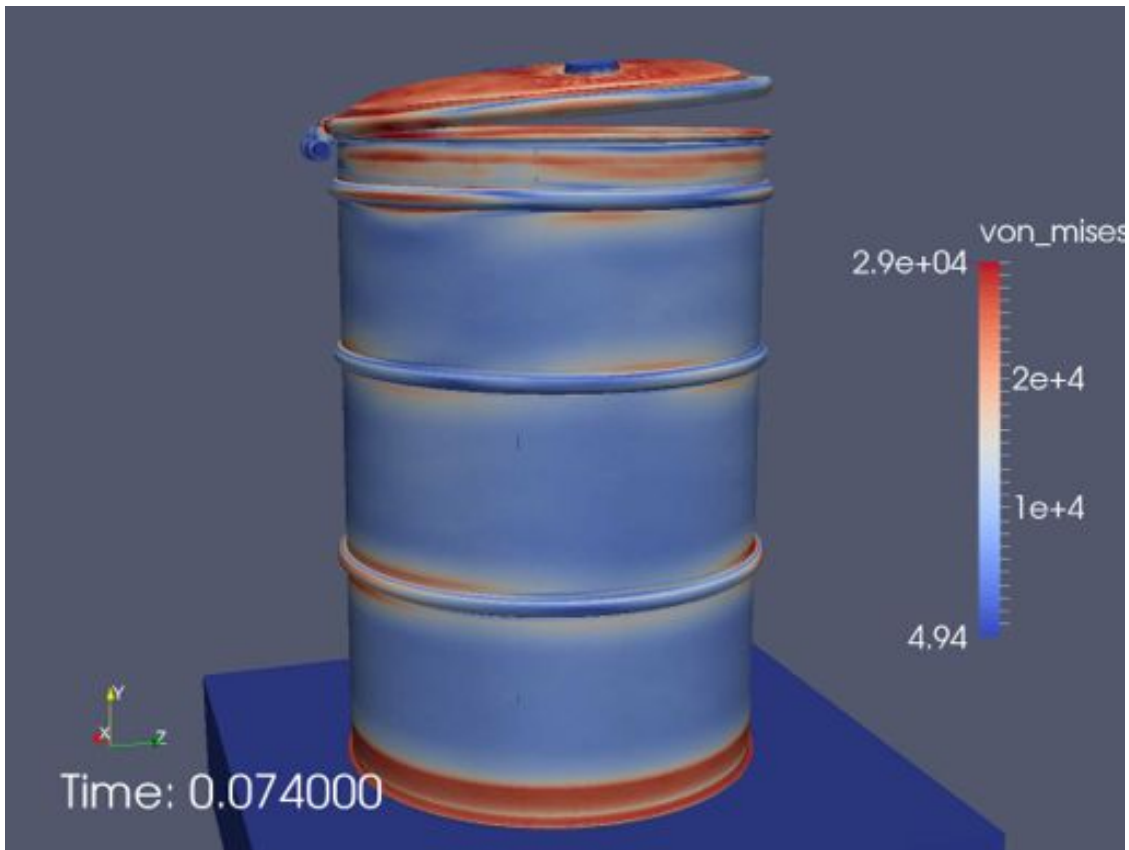


Figure D-17. Analysis results for case with original estimate of properties and “slow” loading.

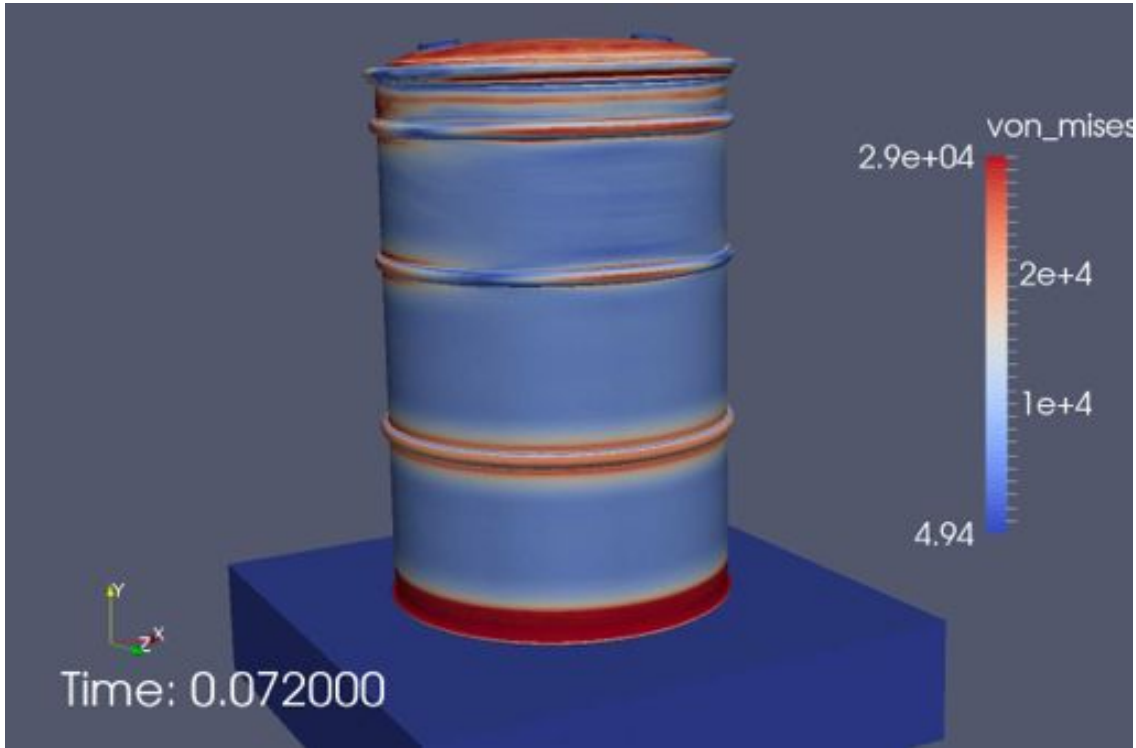


Figure D-18. As opening (Figure D-8 has it after it is open.)

Using original mechanical property estimates, “slow” load case, with surrogate drum on top: For this case a surrogate drum was placed directly on top of the drum. This case was to provide some insight as to what to look for if a drum under other waste packages was pressurized. The maximum pressure in this case was 50 psi. The drum opened at a pressure of approximately 46 psi. Once again, for this analysis the pressure continues to ramp up until 0.1 seconds. Figure D-19 shows the drum after it has opened. As expected, it takes a greater pressure to open the closure, but only an additional 11 psi.

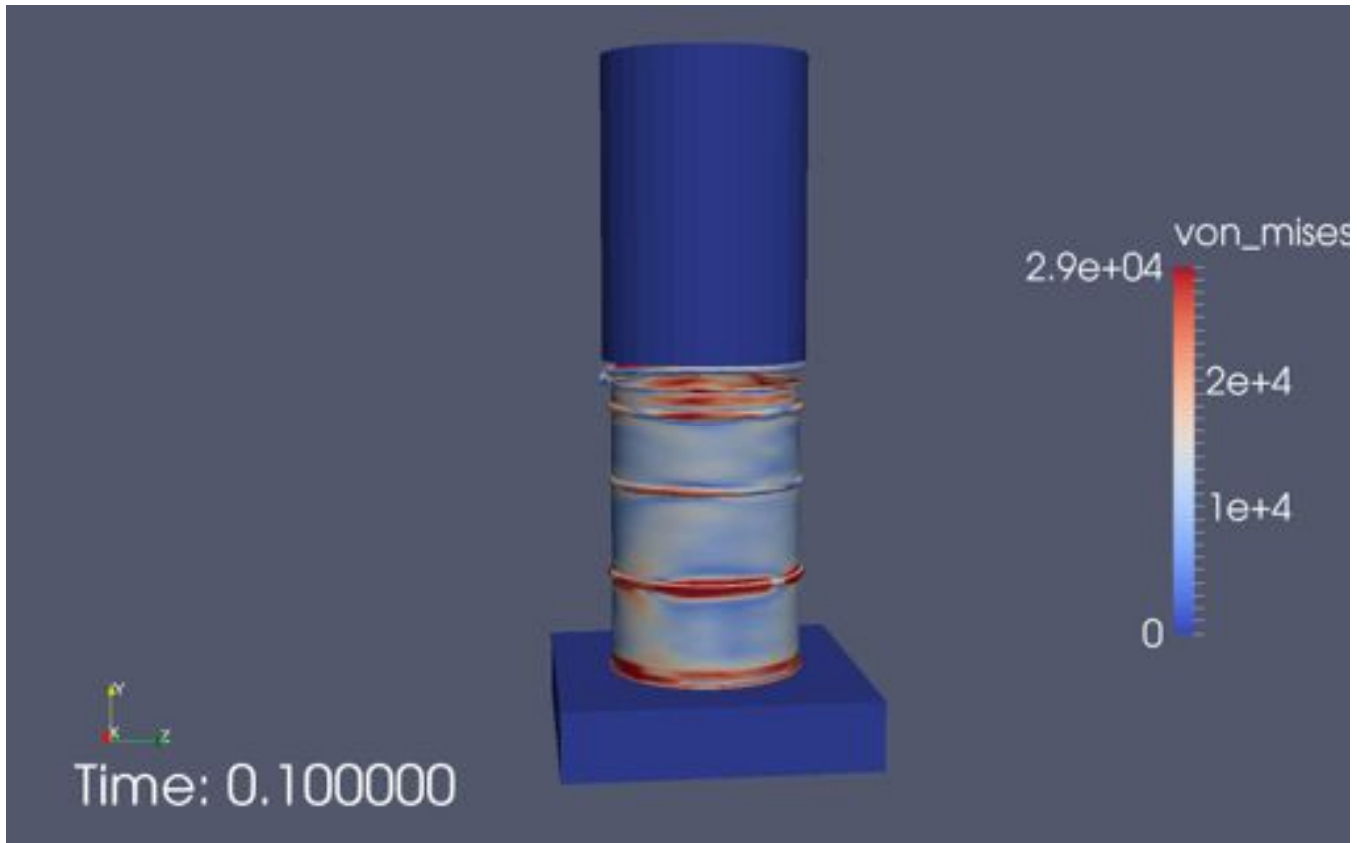


Figure D-19. Analysis results for case with original estimate of properties, “slow” loading, and surrogate cask on top.

Using test properties “fast” loading case: For this case the maximum pressure of the ramp was 75 psi. Results presented in Figure D-20. The deformation pattern of the lid as it opens is similar to the same loading case with the original estimated properties. The pressure when the drum lid pops off is approximately 75 psi, just as the case with the original estimated properties and the fast loading case.

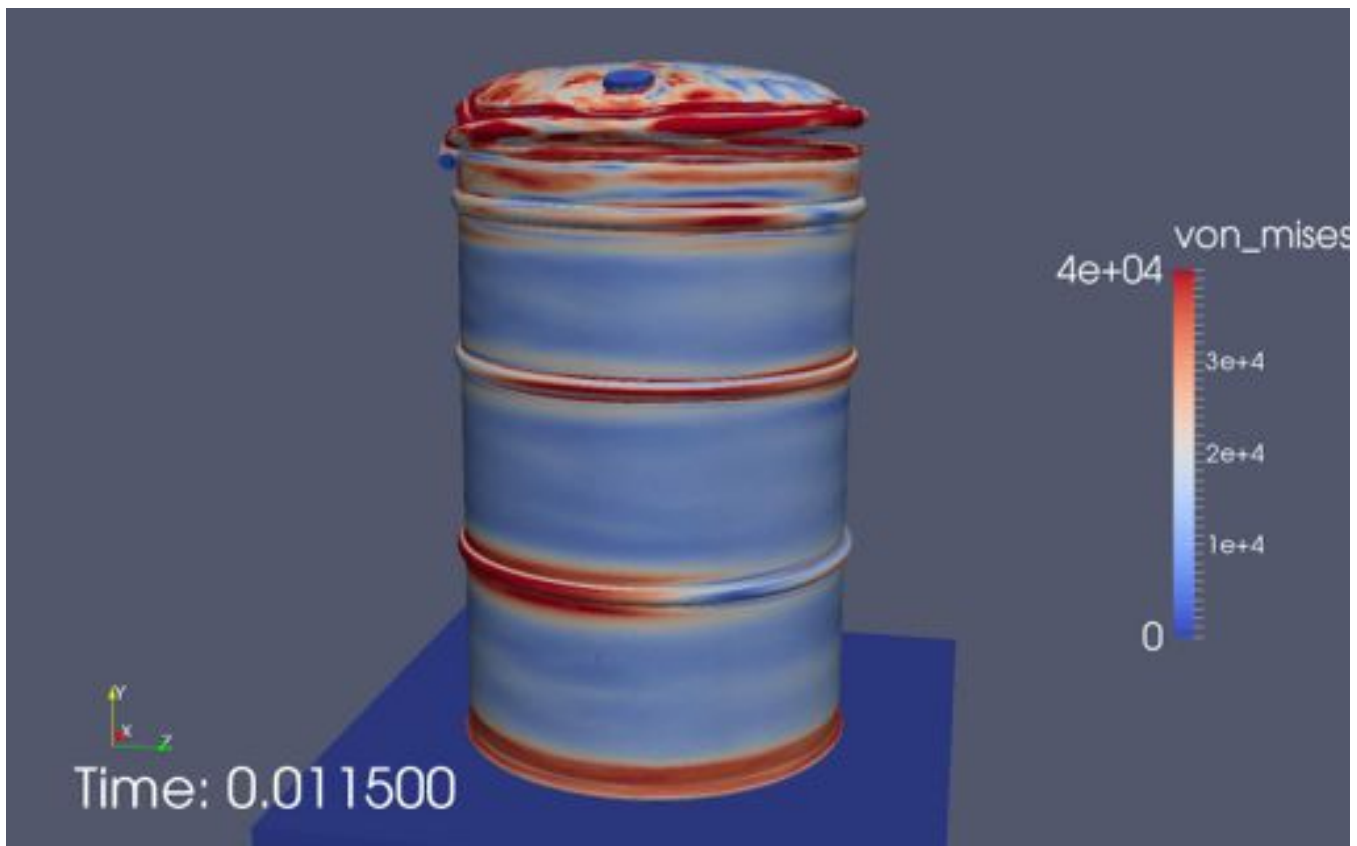


Figure D-20. Analysis results for case with test properties and “fast” loading.

Using test properties “slow” loading case: Initially, the “slow” loading case was repeated with the same maximum pressure for the ramp pressure (50 psi). However, with the test properties this case did not vent. Subsequently, it was re-run with a maximum pressure of 75 psi. This case did vent at a pressure of approximately 58 psi. See Figure D-21 (once again, the maximum contour represents yield for the drum material). The drum material for the test properties has a yield of 40.0e03 psi compared to the 29.0e03 psi used in the original estimate. See FigureD-11 showing the test properties and previous estimated yield. At a pressure of 30 psi the maximum deformation at the center of the lid is 2.2 inches and for the testing at LANL for a ¾-full drum was measured at 2.8 inches. . As pointed out above, the LANL tested drums were a thinner gauge material that could account for some of this difference.

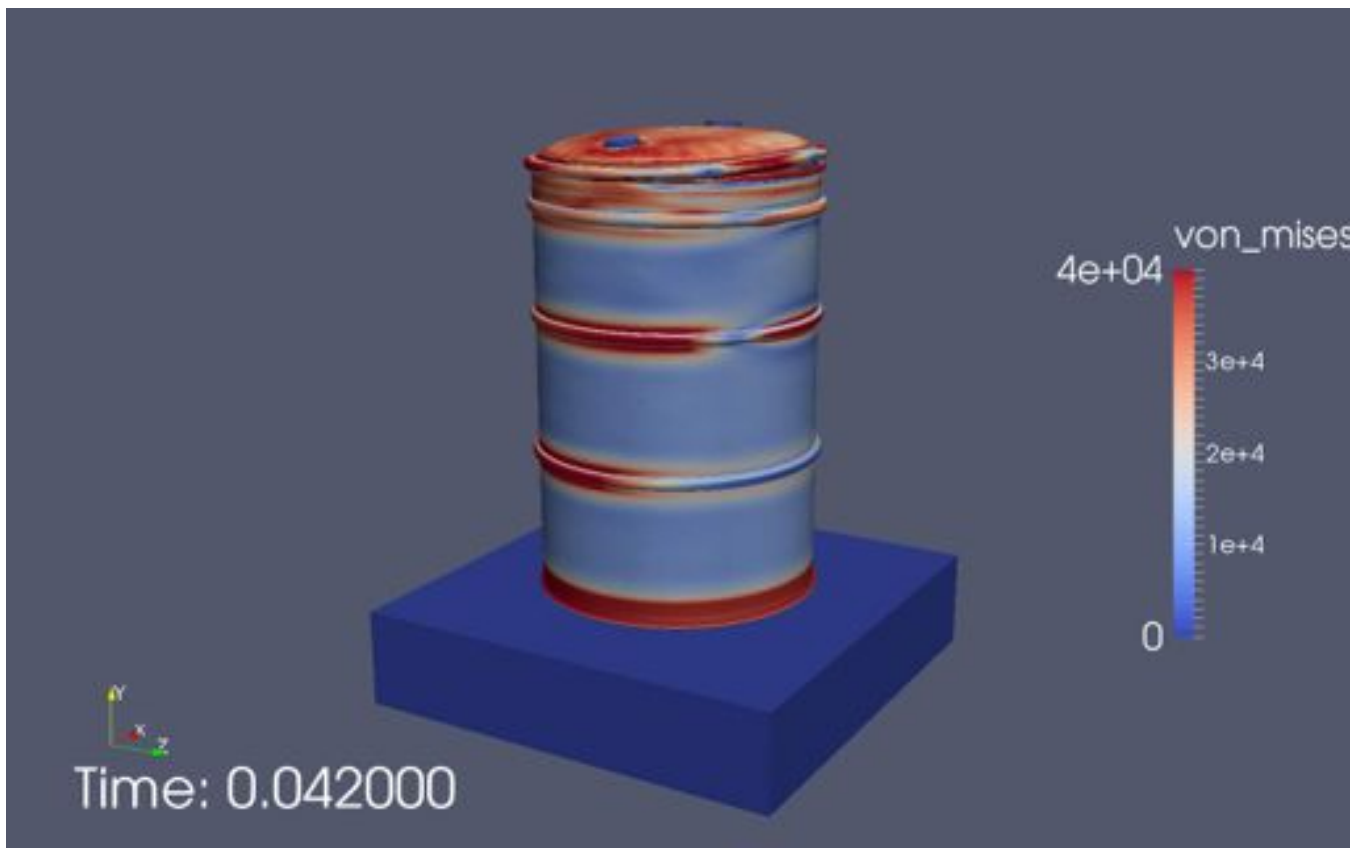


Figure D-21. Analysis results for case with test properties and “slow” loading.

Using test properties “slow” loading case, with surrogate drum on top: The first analysis run for this case had a maximum ramp pressure of 50 psi. That case did not result in the drum venting. See Figure D-22. The analysis was repeated with a max pressure of 75 psi. This case resulted in the drum venting at a pressure of approximately 67 psi (see Figure D-23).

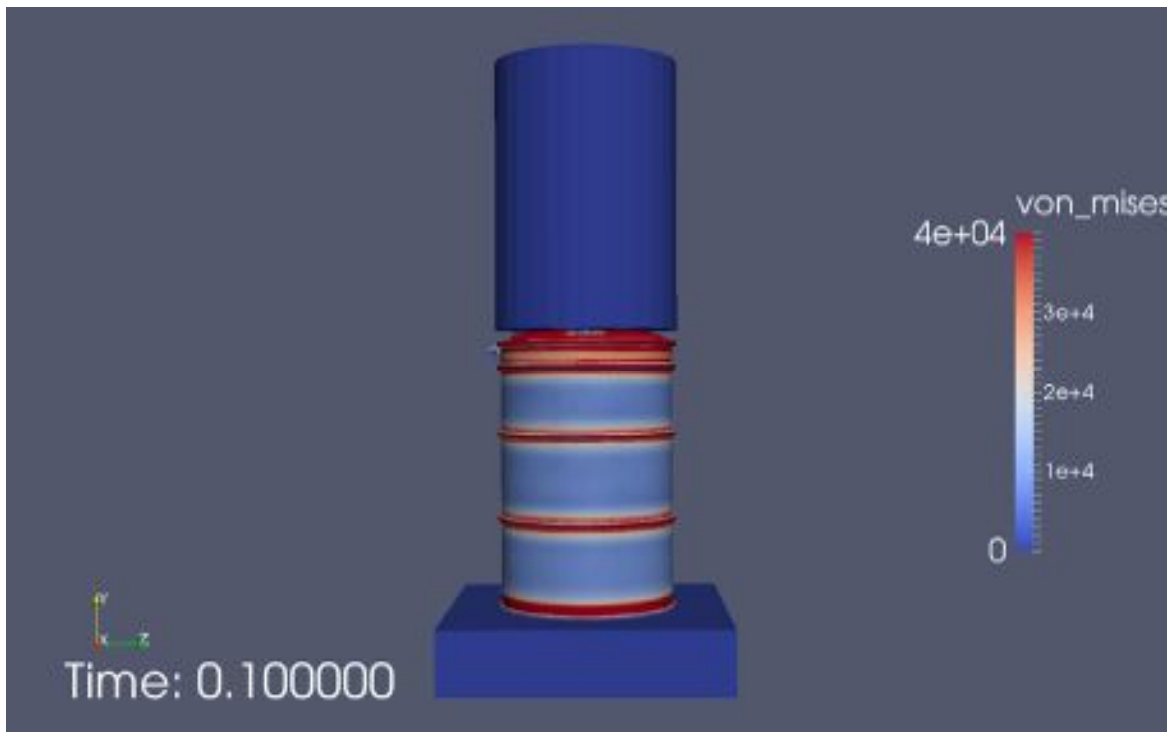


Figure D-22. Analysis results for case with test properties, “slow” loading with maximum ramp pressure of 50 psi, and surrogate cask on top.

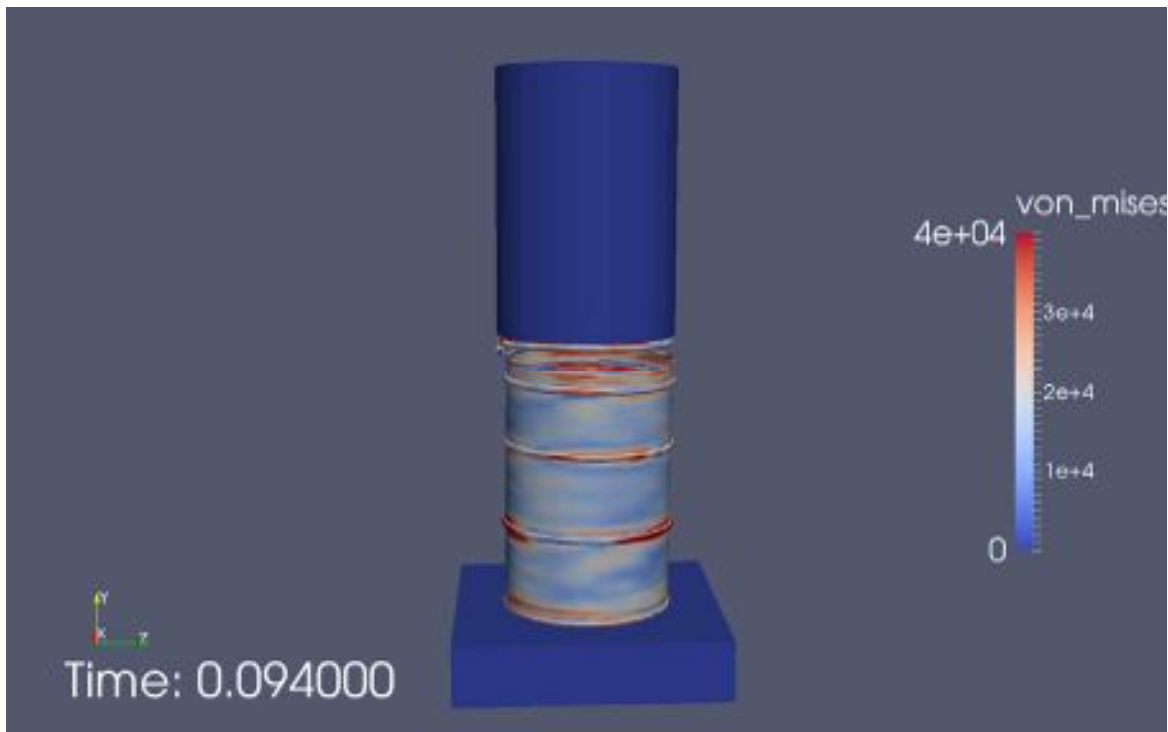


Figure D-23. Analysis results for case with test properties, “slow” loading with maximum ramp pressure of 75 psi, and surrogate cask on top.

Using test properties “fast” loading case, with surrogate drum on top: This case was run with a maximum ramp pressure of 75 psi and the drum did not vent (see Figure D-24).

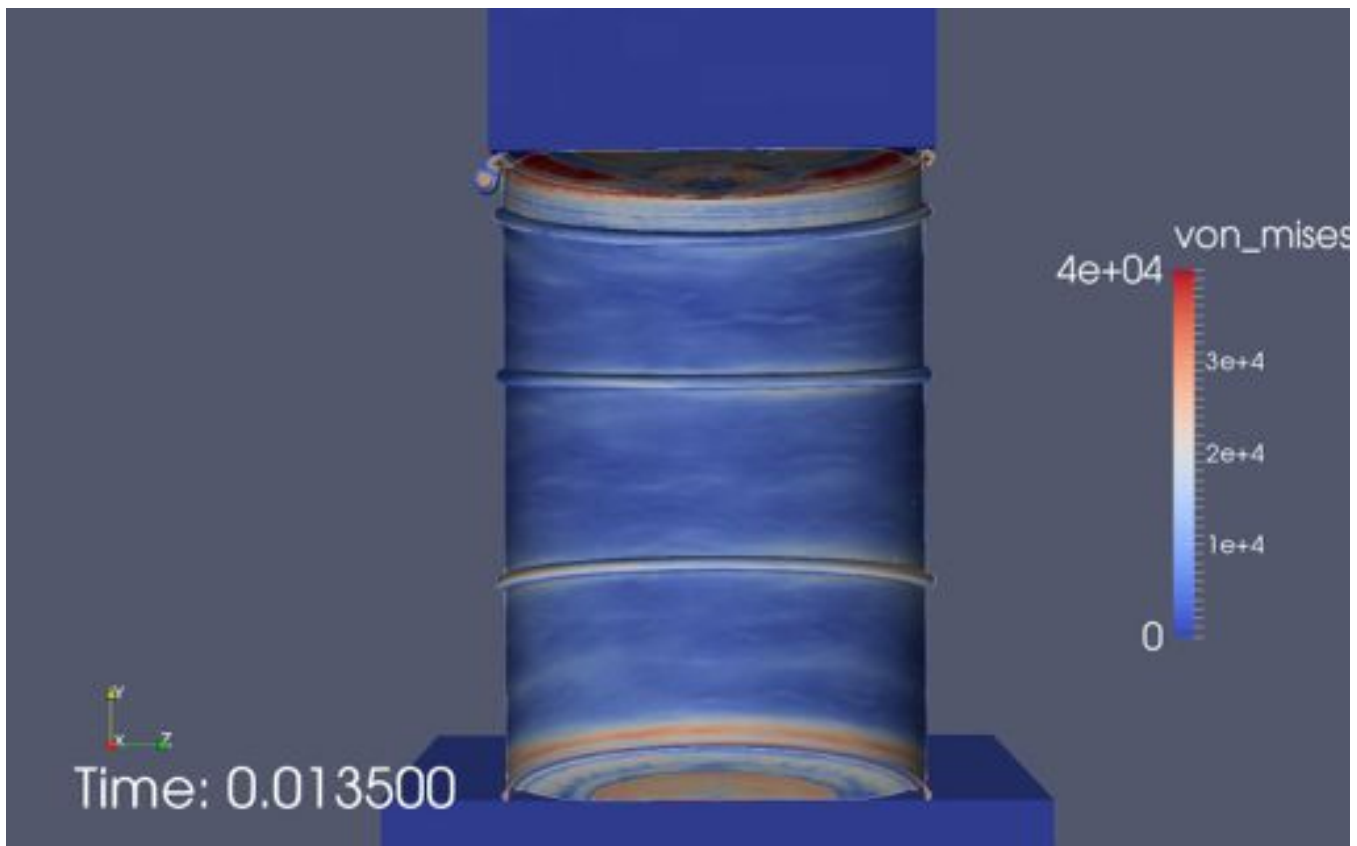


Figure D-24. Analysis results for case with test properties, “fast” loading with maximum ramp pressure of 75 psi, and surrogate cask on top.

Discussion

Further discussion of a number of topics are provided below.

Influence and significance of potential material property variation: The drums are required to meet minimum property requirements. This ensures a minimum strength of the drums. However, it does not preclude the manufacturer from using material that exceeds the minimum specified. For example, the minimum specified yield strength of the ASTM A1008 steel used for the drums is 29,000 psi. The tested value for the drum material tested and presented above is 40,000 psi. The strength of the drums likely varies and this could influence the failure (lid opening pressure) under pressure loads such as those examined in this study. However, as these analyses have shown, the failure modes would be similar. For the “fast” loading cases the opening pressure of the drum did not vary for the runs with the initial estimate for properties (based on the minimum specified tensile strength of the material) and the material properties from the drum obtained from LANL. For the “slow” loading case, the opening pressure varied from 35 psi to 57 psi. The maximum ramp pressure for the “slow” loading case had to be increased to get the drum to open during the analysis. Therefore, the rate of pressurization was also varied between the two analyses. See Table D-10 below for a summary of the analysis results.

Influence of MgO on the opening pressure and failure of the drums: The only analysis effort to account for the MgO on top of the drums was the inclusion of a uniformly distributed pressure across the top of the drums that accounted for the weight of the MgO. This resulted in a pressure of approximately 1.5 psi acting against the internal pressure. Therefore, it had relatively little influence on the resulting failure pressure. This does not account for any inertial forces that would be generated during a dynamic event. The MgO on top of the drums might have also influenced the location of the drum opening (e.g., if it is not evenly distributed across the top of the drum). However, no analyses were performed with anything other than a uniformly distributed load.

Influence of rate of pressurization and maximum ramp pressure: Analyses were conducted varying the time to maximum ramp pressure and the magnitude of maximum ramp pressure (See Figures D-12 and D-13). The results suggest that the relationship between the opening pressure and the time to maximum ramp pressure results in an increase in the opening pressure when the pressure ramps up at a higher rate. The opening pressures are a maximum for the cases where the time to maximum ramp pressure was 0.01 seconds. The analyses where this was extended to 0.015, 0.025, and 0.035 resulted in a significant decrease in the opening pressure. If the time to maximum ramp pressure was increased all the way to 0.1 seconds the opening pressure was the lowest of all the analyses (35 psi for the originally estimated properties). For analyses where the maximum ramp pressure was set at 150 psi and a time to maximum pressure of 0.01 seconds, there is significantly more deformation of the lid than when the time to maximum pressure is increased to 0.1 seconds. The pressurization in such a short time results in substantial deformation of the lid prior to the lid opening. Therefore, the deformation of the lid might provide an indication of the rate of the pressurization. See Table D-10 for a summary of the results.

Table D-10. Result exploring maximum ramp pressure vs. time to maximum pressure.

Material Property Set	Loading Case	Maximum Ramp Pressure (psi)	Time to Maximum Ramp Pressure (sec)	Lid Opening Pressure (psi)
Initial Estimate	fast	150	0.01	75
Initial Estimate	Slow	50	0.1	35
Initial Estimate	Slow (w/ surrogate drum)	50	0.1	46
Initial Estimate	Slow	150	0.1	38
Initial Estimate	fast	150	0.025	45
Initial Estimate	fast	75	0.015	45
Initial Estimate	fast	75	0.025	38
Initial Estimate	fast	75	0.035	38
Tested	fast	75	0.01	75
Tested	Fast (w/ surrogate drum)	75	0.01	n/a
Tested	slow	50	0.1	n/a
Tested	slow	75	0.1	57
Tested	Slow (w/ surrogate drum)	50	0.1	n/a
Tested	Slow (w/ surrogate drum)	75	0.01	66

Deformation of the lid and possible cause for the lid remaining open after pressurization: As discussed above, due to the small time-step of the analyses and the significant run-time associated with these analyses, performing analyses of a long enough duration to examine what happens after the lid opens was not completed for this study. However, there are two possible reasons for the lid remaining open after a pressurization event. One is that the lid undergoes plastic deformation during the pressurization, which results in permanent deformation of the lid. All of the analyses showed some plastic deformation in the lid. The analyses with a faster pressurization and especially the cases with the fast pressurization and highest value of ramp pressure have the most plastic deformation. The second reason the lid might not have closed after the pressurization event is that the closure ring is still under strain (preload); and if it only came partially off, there would be significant force where the bottom edge of the closure ring was crossing the lip of the drum. The lid could be essentially “cantilevered” from the supporting portion of the closure ring that is still seated on the drum body lip and at the intersection where the closure ring is crossing the drum body lip. There should be no expectation of a symmetric release or deformation of the lid. This would further prevent the lids from settling back into their original position.

An example of the permanent deformation of the lid can be seen from the tests conducted by LLNL shown in Figure D-25 (Hasegawa et al. 1993).

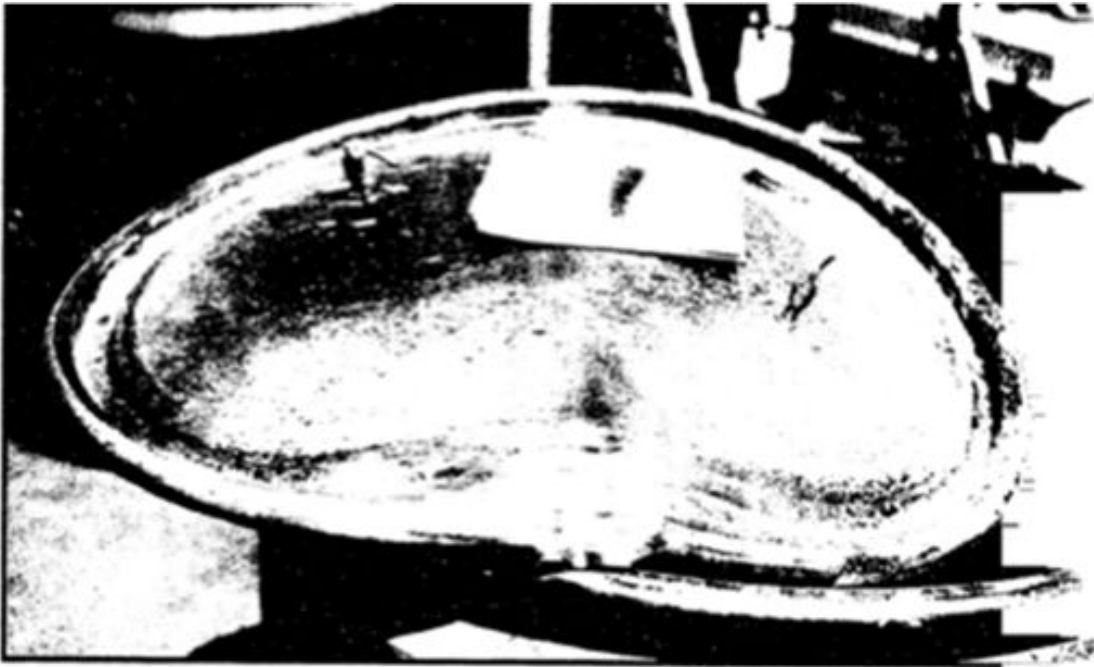


Figure D-25. Permanently deformed lid from fire test (reproduced from Hasegawa et al. 1993)

Drum geometric variations and lid closure preload and their influence on the results: Some analyses to examine the influence of drum geometric variations (thickness) and the influence of the closure ring preload were pursued. However, the initial analyses were not conclusive and due to time constraints the issues were not pursued further. The main reason for this is the lack of knowledge on the drum closure ring strain when closed per procedure. This likely has a significant influence on the calculated opening pressure from these analyses. Without a better understanding of the strain in the closure ring, it was not felt it was advisable to pursue some of these issues. There is uncertainty regarding how consistent the closure ring strain is from drum to drum. An improved understanding of this is advisable prior to pursuing further mechanical modeling with respect to predicting opening pressure.

Location of the initial drum opening and the orientation with drum plugholes: Some preliminary analyses were conducted investigating the orientation of the plugholes and the lid opening location. However, this was not pursued as a major area of investigation. However, it does appear that the plugholes could influence the location of the opening. For all of the analyses presented in this document, the lid was orientated in the same direction. Since the plugholes provide some stiffness to the lid, if the lid is rotated with respect to the bolt flanges on the closure ring, it might shift the location of the initial opening when the drum is over pressurized. Further investigation in the room of the accident should attempt to note the location of the drum plugholes.

Summary and Key Conclusions from Analyses

Over a relatively short period of time (several months) a finite element model of a WIPP drum was developed and analyses were conducted to support an investigation of the February 14th 2014 event. Uncertainty surrounding the closure ring tightness precludes some quantitative insights. However, a number of conclusions can be drawn from the study and are presented below:

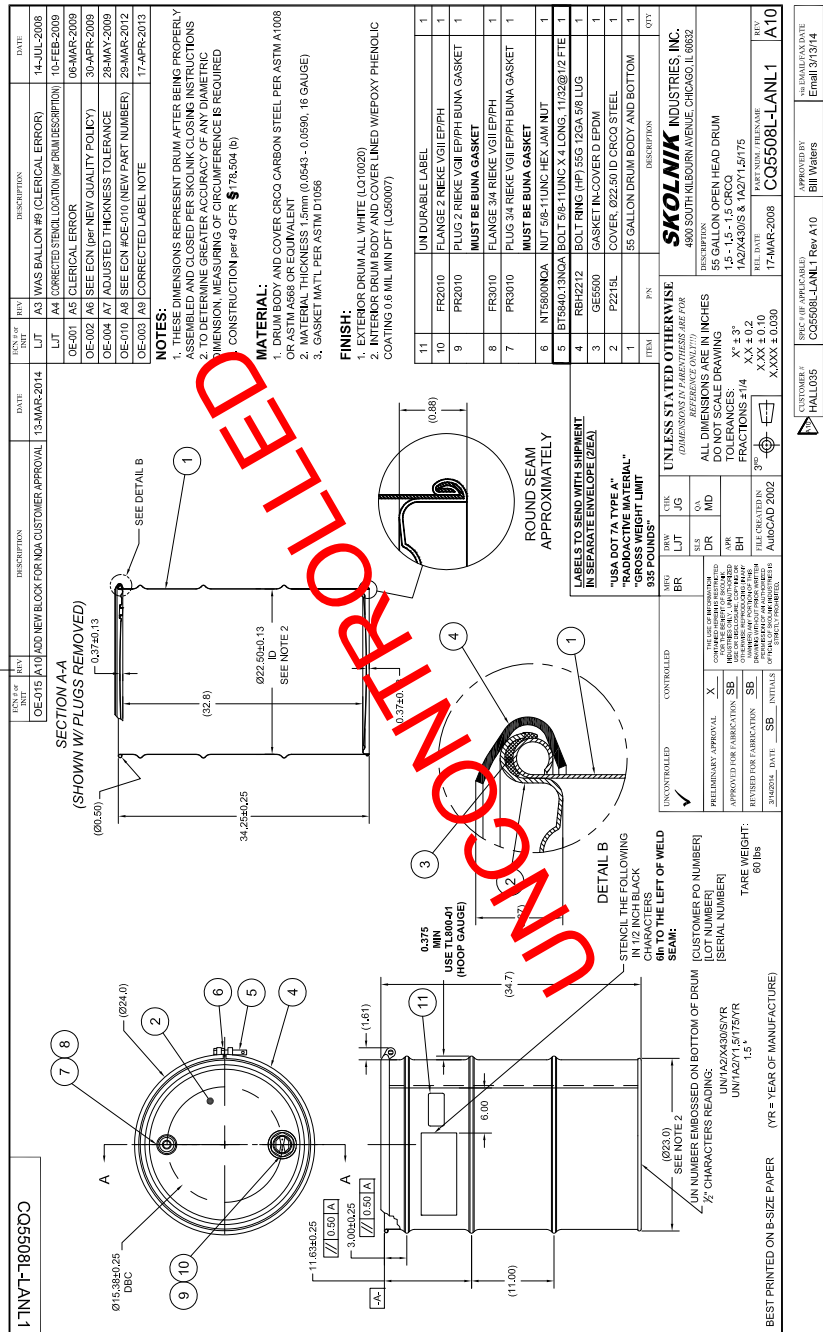
1. Analysis of pressurization of the drums show that the lid will open at pressures between 35 and 75 psi for cases analyzed here. This calculated failure pressure is of the same order as the manufacturer's specifications and previous pressurization test data. No analyses showed the drum rupture on its sidewall and one would not expect that to happen from this type of a pressurized event. Only a blast load that reached a high enough load to fail the metal sidewall prior to applying a load to the top or bottom of the drum could rupture the sidewall prior to the lid opening. The pressurization tests at LANL and Savannah River sites discussed above all resulted in failures at the top or bottom of the drums.
2. The deformation behavior of the lid and the subsequent venting varies depending on the rate of pressurization. The analyses show significant plastic deformation of the lid. A faster loading results in more deformation of the lid. Therefore, the lid will likely remain deformed after the event and not return to its pre-pressurization state.
3. The analyses suggest the initiation of the lid opening will occur at the opposite side of the bolt on the bolt closure ring. The orientation of the plugholes in the lid will likely have some influence on this. In addition, the tests at LANL and the analyses suggest for "fast" loading cases the lid will deform and begin to vent near the bolt ring when there is large deformation of the lid. This is prior to the lid ejecting off the drum.
4. Analyses examining a pressurization of a drum with a surrogate drum on top suggest that the drums could vent even with a large object on top of it. It takes a higher pressure to open the lid for these cases. The drums could also pressurize and not open the lid. Therefore, if the lid does not open and the pressure is not released, they could remain under pressure.

References

1. AKsteel, Cold Rolled Steels, Product Data Bulletin, http://www.aksteel.com/pdf/markets_products/carbon/AK_Cold_Rolled_PDB_2014061.pdf
2. ASTM E8, E8M-13a, Standard Test Methods for Tension Testing of Metallic Materials, ASTM International, West Conshohocken, PA, 2013, www.astm.org
3. Cubit, <https://www.cubit.sandia.gov>, 2014
4. Dykes, K.L., and Meyer, M.L., "TRU Drum Hydrogen Explosion Tests," WSRC-TR-90-165, Westinghouse Savannah River Company, Aiken, South Carolina, 1991.
5. Hasegawa, H.K., Staggs, K.J., and Doughty, S.M., "Fire Testing of 55 Gallon Metal Waste Drums for Dry Waste Storage, International Nuclear Information System (INIS), Volume 25, Issue 19, 1993.
6. Larranaga, M.D., Volz, D.L., and Bolton, F.N., "Pressure Effects and Deformation of Waste Containers," LA-UR-98-2541 Los Alamos National Laboratory, Los Alamos, NM, 1998.
7. Larranaga, M.D. and Volz, D.L., "Pressurized Drum Mitigation," LA-UR-98-2542, Los Alamos National Laboratory, Los Alamos, NM, 1998.
8. Larranaga, M.D., Volz, D.L., and Bolton, F.N., "Pressure Effects on And Deformation of Waste Containers," Fire Engineering, Volume 152, Issue 7, 1999.
9. Ludwigsen, J.S., Ammerman, D.J., and Radloff, H.D., "Analysis in Support of Residues in the Pipe Overpack Container, SAND98-1003, Sandia National Laboratories, Albuquerque, NM.
10. Sierra/SolidMechanics, Sierra/SolidMechanics 4.34 User's Guide, Sandia National Laboratories, Albuquerque, NM, 87185.
11. Skolnik, http://www.skolnik.com/product_sheet.php?product=CQ5508
12. U.S. Department of Energy, Office of Environmental Management, "Accident Investigation Report, Phase 1, Radiological Release Event at the Waste Isolation Pilot Plant on February 14, 2014," April 2014, http://www.wipp.energy.gov/wipprecovery/accident_desc.html.

Additional Information for Mechanical Response of Drum: modeling of drum behavior when pressurized

WIPP Drum Drawings



REV		DESCRIPTION	DATE	REV		DESCRIPTION	DATE	REV	DESCRIPTION	DATE
0E-015	A1	ADD NEW BLOCK FOR NDA CUSTOMER APPROVAL	13-MAR-2014	LIT	A3	WAS BALLON #9 (CLERICAL ERROR)	14-JUL-2008	LIT	A3	WAS BALLON #9 (CLERICAL ERROR)
0E-016	A1			LIT	A4	CORRECTED STENCIL LOCATION (PER RULES/DESCRIPTION)	10-FEB-2009	LIT	A4	CORRECTED STENCIL LOCATION (PER RULES/DESCRIPTION)
0E-001	A5			0E-001	A5	CLERICAL ERROR	06-MAR-2009	0E-001	A5	CLERICAL ERROR
0E-002	A5			0E-002	A5	SEE ECR FOR NEW QUALITY POLICY	30-APR-2009	0E-002	A5	SEE ECR FOR NEW QUALITY POLICY
0E-004	A7			0E-004	A7	ADJUSTED THICKNESS TOLERANCE	28-MAY-2009	0E-004	A7	ADJUSTED THICKNESS TOLERANCE
0E-010	A1			0E-010	A1	SEE ECR #02610 (NEW PART NUMBER)	29-MAR-2012	0E-010	A1	SEE ECR #02610 (NEW PART NUMBER)
0E-003	A9			0E-003	A9	CORRECTED LABEL NOTE	17-APR-2013	0E-003	A9	CORRECTED LABEL NOTE

NOTES: 1. THESE DIMENSIONS REPRESENT DRUM AFTER BEING PROPERLY ASSEMBLED AND CLOSED PER SKOLNIK CLOSING INSTRUCTIONS AND WITH THE DRUM OPEN TO ATMOSPHERIC PRESSURE. 2. ALL DIMENSION MEASUREMENTS OF CIRCUMFERENCE IS REQUIRED CONSTRUCTION PER 49 CFR § 178.504 (b)	MATERIAL: 1. DRUM BODY AND COVER: CRCO CARBON STEEL PER ASTM A1008 OR ASTM A568 OR EQUIVALENT 2. MATERIAL THICKNESS: 1.5mm (0.0643 - 0.0590, 16 GAUGE) 3. GASKET: MATL PER ASTM D1056	FINISH: 1. EXTERIOR DRUM ALL WHITE (LOT10200) 2. INTERIOR DRUM BODY AND COVER LINED W/ EPOXY PHENOLIC COATING 0.6 MIL MIN DFT (LQ50007)
--	---	--

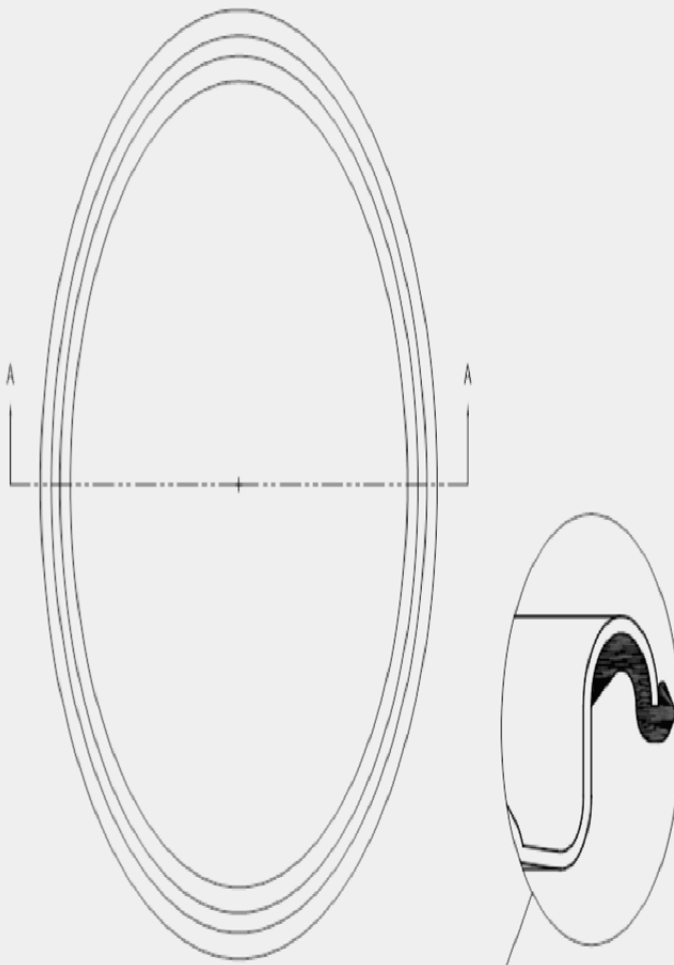
ITEM	PN	DESCRIPTION	QTY
11	FR2010	UNDURABLE LABEL	1
10	FR2010	FLANGE 2 RIEKE VGEI EPFH	1
9	FR2010	PLUG 2 RIEKE VGEI EPFH BUNA GASKET	1
8	FR3010	MUST BE BUNA GASKET	1
7	FR3010	FLANGE 3/4 RIEKE VGEI EPFH	1
6	FR3010	PLUG 3/4 RIEKE VGEI EPFH BUNA GASKET	1
5	NTS800NDA	NUT 5/8-11UNC HEX JAM NUT	1
4	REH2212	BOLT 5/8-11UNC X 4 LONG, 11/22@ 1/2 FTE	1
3	GE5600	GASKET IN-COVER D EPDM	1
2	P2215L	COVER, 022-501D CRCO STEEL	1
1		55 GALLON DRUM BODY AND BOTTOM	1

SKOLNIK INDUSTRIES, INC. 4900 SOUTH HILBOURN AVENUE, CHICAGO, IL 60632	
DESCRIPTION: 55 GALLON OPEN HEAD DRUM Q5508L-LANL1 1A2/A30/S 8 1A2/1.5/175	REL DATE: 17-MAR-2008 PART NDA FILE NAME: CQ5508L-LANL1 REV: A10

SPEC (IF APPLICABLE): CQ5508L-LANL1 Rev A10 CUSTOMER: HALL005 APPROVED BY: Bill Walters RE-RELEASE DATE: Email 3/13/14

SEE CHART / P22xx

REV	DESCRIPTION	DATE
A	RELEASE	01-DEC-2006



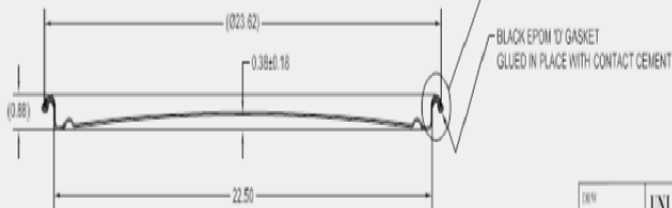
MATERIAL:

1. DRUM COVER CRCO CARBON STEEL PER ASTM A1008 OR ASTM A568 OR EQUIVALENT
2. MATERIAL THICKNESS 1.5mm (0.059, 18 GAUGE) OR 1.2mm (0.043 - 0.047, 18 GAUGE) OR 0.9mm (0.33 - 0.037, 20 GAUGE)
3. GASKET MAT'L PER ASTM D1056

FINISH:

1. DRUM COVER EXTERIOR PAINTED W/WHITE BASE WHITE OR EQUIVALENT

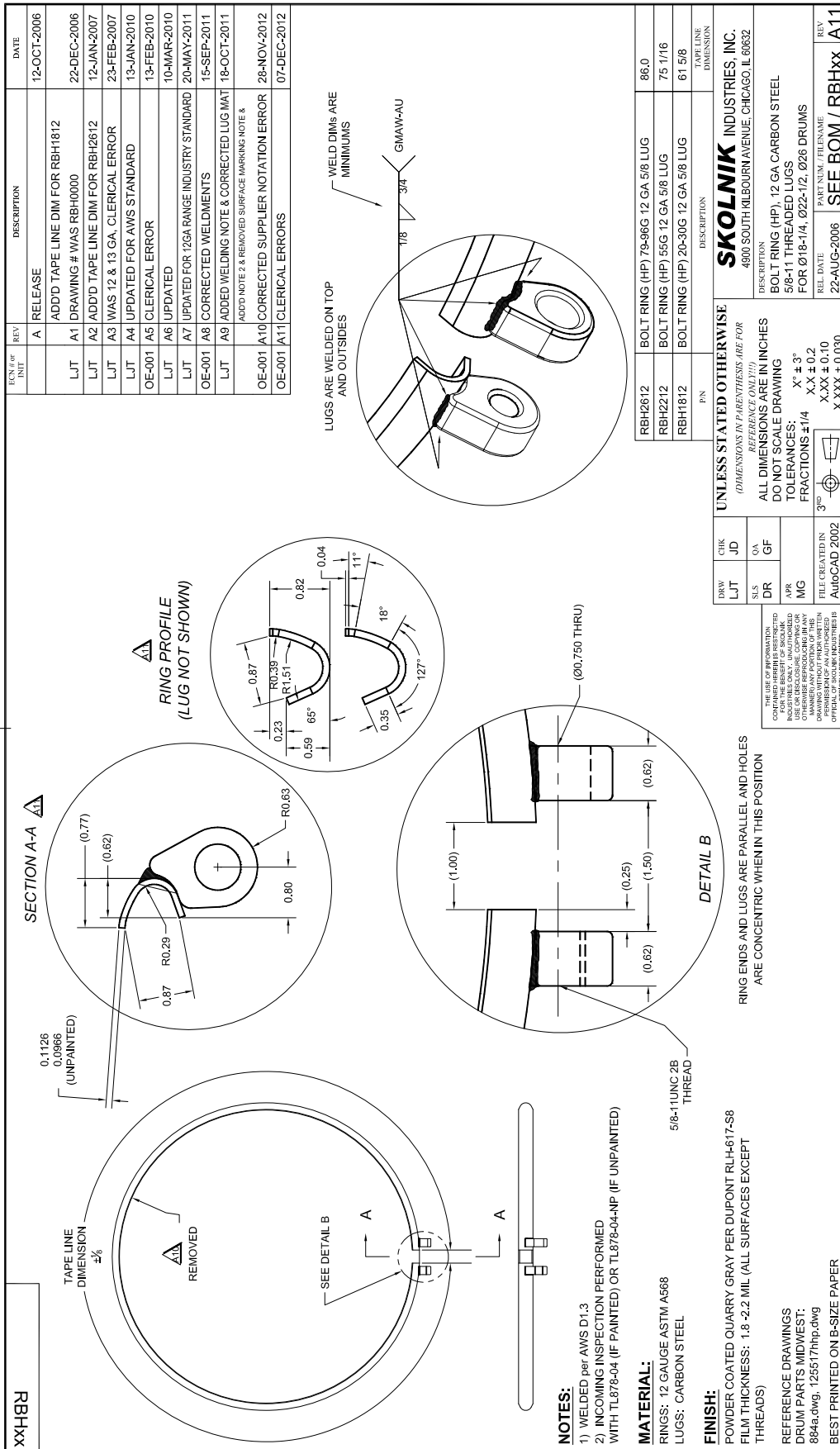
SECTION A-A



P2209KIT	55GalCvr0.9mmWhite/gskt
P2212KIT	55GalCvr1.2mmWhite/gskt
P2215KIT	55GalCvr1.5mmWhite/gskt

THE USE OF INFORMATION CONTAINED HEREIN IS LIMITED TO THE SPECIFIC PROJECT AND IS NOT TO BE REPRODUCED OR TRANSMITTED IN ANY FORM OR BY ANY MEANS, ELECTRONIC OR MECHANICAL, INCLUDING PHOTOCOPYING, RECORDING, OR BY ANY INFORMATION STORAGE AND RETRIEVAL SYSTEM, WITHOUT THE WRITTEN PERMISSION OF SKOLNIK INDUSTRIES, INC.

DESIGNED BY LJT	UNLESS STATED OTHERWISE REMOVE ALL BURRS BREAK ALL EDGES (R0.020 MAX) ALL DIMENSIONS ARE IN INCHES DO NOT SCALE DRAWING	SKOLNIK INDUSTRIES, INC. 4905 S. KILBOURN AVE., CHICAGO, IL 60632	
CHECKED BY LJT		DESCRIPTION COVER ASSEMBLY - 0225	WHITE W/ BLACK EPDM 'D' GASKET
APPROVED BY MS	TOLERANCES: X' ± 0.5' XX ± 0.1 XXX ± 0.03 X,XXX ± 0.005	REL. DATE 01-DEC-2006	PART NUMBER PREFIX SEE CHART / P22xx
FILE CREATED BY AutoCAD 2002	30°	REL. DATE 01-DEC-2006	REV A



THERMAL RESPONSE OF DRUM: EXPERIMENTAL OBSERVATIONS SUPPORTING THERMAL MODEL

Purpose

The purpose of the drum material heating experiment was to obtain insight into the possible thermal profiles experienced by the drums during the incident. Los Alamos drums are painted white. Some of the drums in room 7 had turned black when photographed following the release incident. The majority of the surface of Drum 68660 is now black (see Figure D-26). It is interesting to note that the lower portion of the drum (from the lowest rib to the bottom) appears to be white, while the rest of the drum is black. In addition, there is a transition from black through brown to white at this location. Finally, there is evidence of either peeling paint or a layer of material just above the bottom rib.



Figure D-26. Optical image of Drum 68660 taken after the breach.

The blackened appearance of the drum suggests that it may have been exposed to elevated temperatures, so a series of experiments was designed to assess the effect of elevated temperature on the drum material, and specifically on the paint. Specific questions include:

- What thermal conditions can cause the types of damage to the drum as observed in the photo?
- Can a set of temperature-time history boundaries for the drum be determined?

Experimental Details

Coupons were cut from a pristine drum obtained from Los Alamos. Samples were approximately 2 inches square. They were cut using an electric nibbling tool, and were obtained from the drum without damage to the paint. Coupons were labeled and photographed prior to exposure.

Samples were heated in air using several ovens. Exposure temperatures included 100°C, 200°C, 300°C, 400°C, 500°C, and 700°C. Coupons were placed in the oven and removed after various lengths of exposure. Samples were allowed to cool and then photographed to document their appearance.

The heating experiments were used to:

- Determine temperature required to turn paint from white to black;
- Establish general kinetics for color change;
- Bound upper temperature exposure for drum;
- Correlate model results of drum contents to coloration of drum to gain insight into characteristics of event within drum.

Observations and Results

Drums exposed to the lower temperatures (100°C – 200°C) did not exhibit any immediate color change. (Note: need to get exposure time information for the 100 & 200C coupons) At 300°C the paint underwent a gradual change in color upon heating (see Figure D-27). After 10 minutes the white paint has turned a light tan color. The paint continues to darken with exposure time. After 1 hour, the surface is a dark brown or black; after 2 hours the surface is black. Extended exposure of 4 hours resulted in a black surface, but without evidence of paint peeling.



Figure D-27. Metal drum coupons exposed to a temperature of 300C in air.

Samples exposed to a temperature of 400°C are shown in Figure D-28. Note that the reaction is much more rapid at this temperature. After 5 minutes, the paint is black. After 30 minutes peeling is observed.

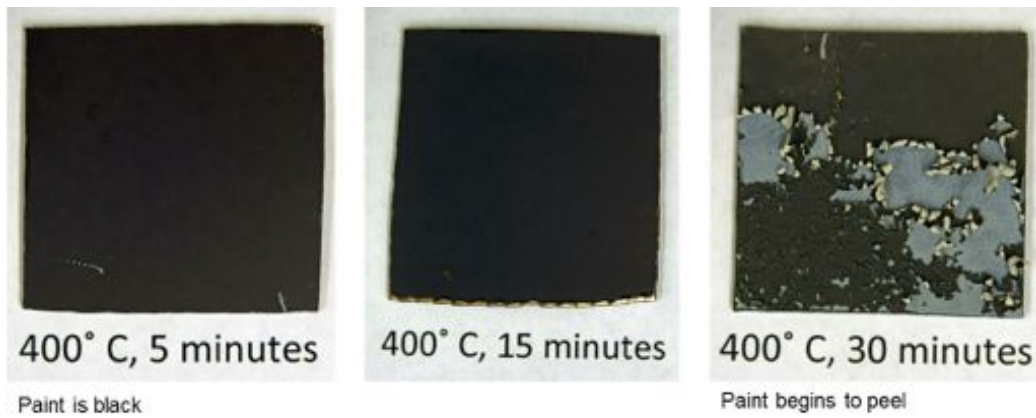


Figure D-28. Metal drum coupons exposed to a temperature of 400C in air.

At 500°C, the paint degradation is even more rapid. After 30 seconds, the surface is brown, and is black after one minute. After 2 minutes the surface starts to peel, and significant peeling is observed by 3 minutes.

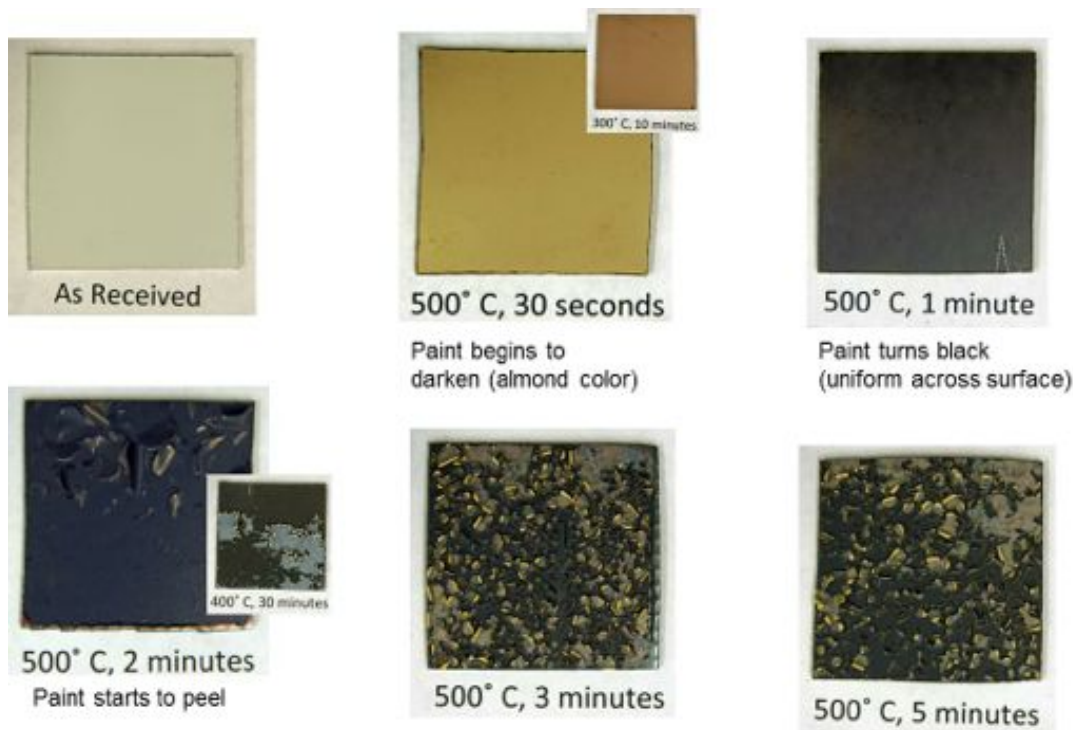


Figure D-29. Metal drum coupons exposed to a temperature of 500C in air.

Figure D-30 presents the results of the 700°C exposure. In this case, the paint is tan/brown after only 15 seconds, and black with evidence of peeling on the edge after 35 seconds.



Figure D-30. Metal drum coupons exposed to a temperature of 700C in air.

The images from the coupon heating study can be used to generate a “rough” description of the drum paint degradation kinetics. In this case, the images were analyzed, and the time to turn black and time to peel were estimated. The results are shown in Figure D-31 and listed in Table D-11. This figure plots time to blacken and time to peel (on a log scale) against the exposure temperature. The difference between the two (t_{\max} - maximum time at temperature) represents the maximum exposure of time at a given temperature without peeling. At the lower temperature (300°C), both the time to blacken and t_{\max} are on the order of hours. As the temperature increases, both values decrease. At 700°C the time to blacken and t_{\max} are on the order of seconds. t_{\max} decreases from over 2000 minutes at 300°C to 25 minutes at 400°C, and about 1 minute at 500°C. If we couple that information with time to blacken (60 minutes @ 300°C, 5 minutes @ 400°C, and 1 minute at 500°C), we can get a reasonable indication of the temperature bounds based on the response of the paint. It is likely that the drum temperature was between 300°C and 400°C and quite unlikely that it was as high as 500°C where the discoloration is observed on the external surface of the drum. While this analysis is not definitive, it does provide plausible bounds for the temperature based on observations in room 7.

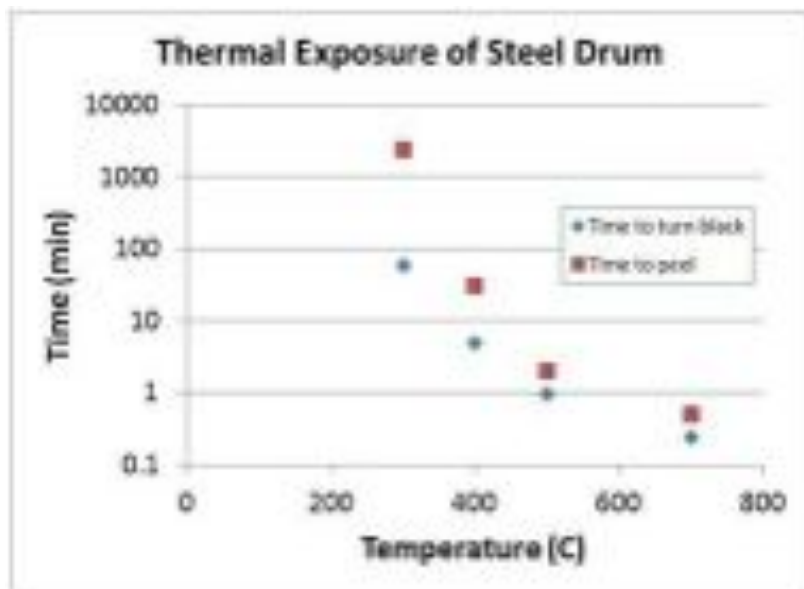


Figure D-31. Curves showing paint degradation kinetics. Time-to-blacken data are plotted as blue diamonds. Time-to-peel data are presented as red squares.

Table D-11. Paint degradation kinetics obtained from analysis of thermal test results.

Temperature	Time to Turn Black (min)	Time to Peel (min)	t_{\max} (min)
700	0.25	0.5	0.25
500	1	2	1
400	5	30	25
300	60	2400	2340

A second set of tests was performed. In these tests, drum coupons were heated with either a propane torch, or with an electric heat gun. The results are shown in Figure D-32. For the image in (a), the propane torch was directed at the painted surface, and was held for several minutes. During this test, the paint did not turn black. It eventually peeled from the metal surfaced, but it remained white throughout the exposure. For the sample in (b), the propane torch was directed at the back of the coupon (inside surface of the drum metal). In this instance, the paint turned black after only 5 seconds. The flame was in contact with the left side of the sample. A range of discoloration can be seen, ranging from black at the left edge to tan / white on the right edge. A third sample was heated using an electric heat gun (shown in Figure D-32c). The heat gun was directed at the exterior surface, and concentrated on the left edge of the sample. Exposure time was 7 minutes. This produced results that are similar to the sample in (b). Blackening of the paint was observed where the heat was concentrated, with a transition from black to white visible moving away from the heated air impact. While not conclusive, these results suggest that heating from the inside of the drum can produce the blackening observed in room 7. These results also suggest that temperature alone is not responsible for blackening of the paint. One can postulate that oxidizing conditions are required for the paint to darken.

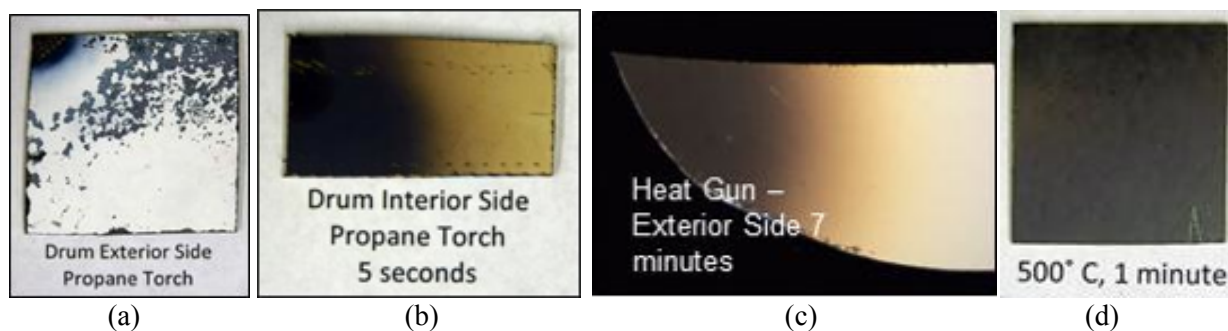


Figure D-32. Results of heating using a propane torch and heat gun.

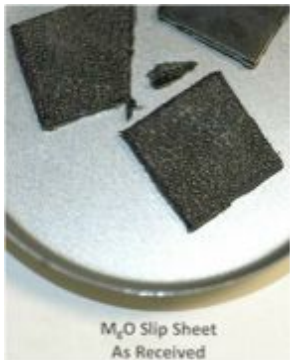
Polymer Thermal Tests

To determine the effect of elevated temperature on organics associated with WIPP drums, several samples were exposed to temperatures that resulted in blackening of the drum metals. Samples included the 7 pack reinforcing sheet, 7 pack slip sheet, MgO slip sheet, the MgO bag, and the stretch wrap used to wrap the drums. Samples were cut from pristine material, placed in aluminum weighing pans, and placed into a furnace. Exposure temperatures ranged from 400°C to 700°C. The exposure time was selected to match the time to blacken for the metals. The results of this test are shown in Figure D-33. The left column shows the as-received samples. Columns 2 and three depict samples exposed to 400°C and 500°C. Note that the exposure times are different for each temperature. The 400°C samples were exposed for 15 minutes (time for the metal to blacken at 400°C), and the 500°C samples were exposed for one minute. The reinforcing sheet and slip sheets charred at both temperatures. There is also evidence of melting with these samples. Both the MgO bag material and the stretch wrap were basically gone following exposure. It is not clear whether they burned or vaporized during the test. Flames were observed with the reinforcing sheet and slip sheet material during the 400°C test.

As Received

400C

500C



As Received



400C



500C

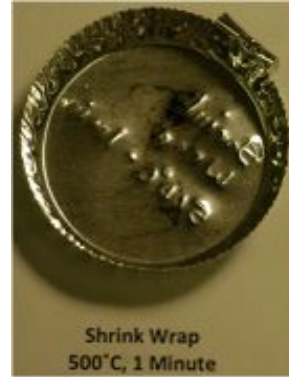


Figure D-33. Images of polymers exposed to elevated temperatures.

A second test was performed using some of the polymers to assess the difficulty of igniting the materials using a flame source. A paper match was used to “light” a thin piece of the polymer and the resulting flame was photographed. Figure D-34 shows images for the slip sheet materials, and for the reinforcing sheet. The MgO bag material was also ignited, but the resulting burning process was not photographed. In all cases, ignition of the material was quite facile, with only a few seconds of application of the match required to initiate burning. While burning, molten material dripped from the sample, and after a short period of time continued to burn in a molten pool below the sample. The MgO bag material, which is much thinner, initially melted and collapsed quite quickly, and then started to burn.

Summary on Plastic Material Response

Clearly, the organic materials associated with the WIPP drums are not stable at elevated temperatures. All of the materials burn readily and support a flame. As they burn, they drip molten plastic which continues to burn. The stretch wrap basically disintegrated, leaving little or no residue.

Executive Summary

The salt truck fire of February 5 introduced heating to the mine air and resulted in reduction of the total airflow through the mine during the process of personnel evacuation. Both of these effects have the potential to slightly diminish cooling to the waste array. The temperature increase in Panel 7 Room 7 (P7R7) air temperature during the fire was estimated to be less than 5 °C. Drum 68660 is inside the waste array and its interior would not be expected to respond to the small and temporary temperature increase of air at the waste array boundary. The convective coupling at the edge of the waste array is associated with very small heat flux so that the edge of the waste array would remain very near the temperature of the passing air even as the convection coefficient was diminished by reduced flow velocity. The magnitude of the P7R7 air temperature increase and the increase in temperature at the edge of the waste array associated with diminished flow could be small contributing factors to the incubation of an escalating reaction. However, these temperature increases are small compared to the temperature variations expected in the normal handling of the waste drums in the course of their prior storage, shipping, and handling to emplace at WIPP. Consequently, it is judged that these factors were not causal.

Given the energetic output predicted by the thermochemical runaway calculation for Drum 68660, the CFD calculation demonstrated that it is plausible that the drum's hot effluent in the cross-flow could reach much of the area known to be damaged. Other mechanisms such as combustion in the room, flame propagation, ember transfer, burning drips of melted polymer, and hot solid material ejected from the drum also may have contributed to the spreading of thermal damage. The potential contribution of those alternative mechanisms is consistent with REACH findings. Unknown flow characteristics, dependent upon geometry details that are altered in the aftermath, and unknown distribution of combustible and low-melting-point materials prior to the damaging event preclude the possibility of developing a precise description of thermal damage event.

Transient thermal analyses demonstrated that drum-to-drum propagation would require extremely energetic donor drums to significantly heat neighbor drums. Further, the thermochemical analyses demonstrating a plausible thermal runaway condition require isolation of the exothermic reaction within a region of low thermal diffusivity. Consequently, it is believed that the thermal stimulus leading to the pressurizing and failure of Drum 68660 was internal. The expulsion of energy and/or materials from Drum 68660 most likely initiated the observed damage to the surrounding area and not vice versa.

Introduction

On February 5, 2014, at approximately 10:48 AM, there was an underground fire in a salt hauler vehicle at the Department of Energy (DOE) Waste Isolation Pilot Plant (WIPP) near Carlsbad, New Mexico. An accident investigation board was appointed to investigate the accident. That investigation lasted from February 10, 2014 through March 8, 2014 and the findings are summarized in the resulting report^{cc}. Nine days after the truck fire event a radiological release occurred at the WIPP site on February 14, 2014. Because of the close proximity of the two events, a causal relationship was posited.

The truck fire occurred in the E-0 drift at the intersection with the drift and N-300. The fire was limited to the forward half of the vehicle and consumed two tires and most of the available combustible liquids as shown in Figure D-34.

^{cc} U.S. Department of Energy Office of Environmental Management Accident Investigation Report, *Underground Salt Haul Truck Fire at the Waste Isolation Pilot Plant February 5, 2014*, March 2014.



Figure D-34. Salt hauling truck after the fire

The occurrence of the February 14, 2014 radiation release in Panel 7 Room 7 (P7R7), less than 10 days after the February 5 salt haul truck fire, raises suspicion that the two events may be related. Figure D-35 shows a perspective view of the mine system indicating the location of the truck fire, the location at which the radiological release was first detected, and P7R7.

There are a number of ways that these two events could be related to each other, including heat and/or combustion products from the fire being transported into P7R7. Additionally, the flow of air through P7R7 was reduced for a period after the truck fire which potentially could have reduced the cooling of the waste array, leading to overheating of particular drums. Analyses for each of these potential scenarios follow.

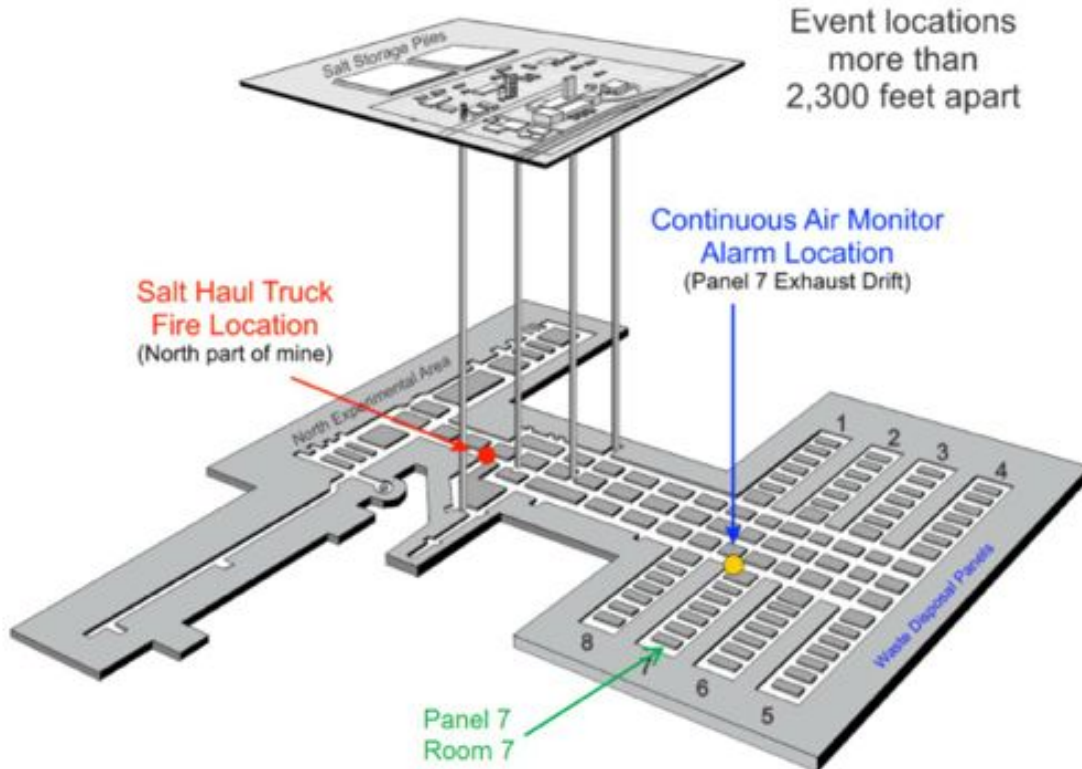


Figure D-35. Fire and radiological event locations

Specific Questions to be Addressed

This appendix documents analyses by the MgO bag sub team of the TAT assessing the plausibility of a number of different scenarios in which the MgO bags may have participated in or contributed to the radiological release event in P7R7 at WIPP. In addition to addressing the bag damage, several other questions were analyzed by this team.

The specific questions that are investigated here are

- Could the February 5 fire involving the Salt Haul Truck (SHT) have any significant influence on Panel 7 Room 7 resulting radiation release? Three possible mechanisms were considered:
 - Thermal: Did heating from the fire significantly heat the waste array?
 - MgO Reactions: Could CO₂ or H₂O from fire combustion products stimulate an exothermic reaction in the MgO on the waste array?
 - Did reduced flow through the waste array result in significant heating?
- Could the release from Drum 68660 alone have caused the damage observed to the MgO sacks and the slip sheets?
- Can the duration of the release event be estimated based on measured radiological data?

The following sections summarize analyses conducted by the MgO team to address the questions above, as well as several other related questions of interest. To address the questions above, simplifying assumptions had to be employed because there is significant uncertainty in the actual conditions within the room and waste pack, i.e. mass flows, waste-pack geometry, temperatures, etc. In many cases, the computed results from a numerical model will depend strongly on the boundary conditions. It is necessary to have well-known properties and boundary conditions to have high confidence in the computed results. One way of handling the large uncertainty in the specific problem is to rely on simplified or bounding analyses. Using bounding analyses, it may be feasible to develop some insight into the system response that could be used to demonstrate or eliminate the plausibility of specific physical mechanisms. Our approach for addressing the large uncertainty was to focus on assessing the plausibility of specific physical mechanisms, rather than attempting to compute an “exact” response. The level of detail in the analyses employed was limited by the tight time schedule for completing the project, which initially was expected to have been completed in October, 2014.

Influence of the February 5 Salt Haul Truck Fire

This analysis demonstrates that the truck fire could not have resulted in significant heating of P7R7. Reports^{dd} of undamaged materials with low melting points both in the waste array and nearer the truck location indicated that very high temperatures (>~130 °C) had not occurred anywhere near P7R7. Available data to support the analysis includes temperatures and air flow rates recorded by the mine’s Central Monitoring System (CMS).

Smoke was seen issuing from the salt handling shaft (SHS) confirming that there was outflow from that shaft after the fire. It is evident from recorded temperatures that the SHS was acting as an air supply prior to the fire. The analysis finds air mass flows for the air intake shaft (AIS) and SHS that balance friction losses with buoyancy differences associated with temperature differences in the two shafts while requiring the exit air temperature of the SHS to match the measurement. The recorded temperature of air leaving through the SHS was only around 30°F higher than the ambient air at the time of the fire. The analysis demonstrates that 62 °C is a conservatively high estimate of the air temperature at the base of the SHS. Given this upper bound on air temperature at the base of the SHS, further conservative assumptions are made regarding energy loss from air in transit to P7R7 and it is shown that the temporary increase in air temperature arriving at the waste array was less than 5 °C.

The ambient air temperature for early February used in the analysis was taken from historical data for the city of Carlsbad. The temperature recorded for air entering the SHS by the CMS was a few degrees colder than the

^{dd} Draft reports were shared by AIB analysts that included descriptions of materials proximal to but not melted by the fire. Analyses in this memo also utilize from AIB draft reports: pre-fire ventilation air flow rates of 142 kg/s, AIS and SHS shaft diameters of 6.25 and 3.05 m respectively, and 5 and 10 MW fire thermal output estimates.

historical data immediately prior to the fire. The effect of adjusting the ambient temperature prior to the fire downward (to agree with the CMS) would result in slightly higher estimates of the temperature at the base of the SHS and a negligible influence on the temperature estimated for P7R7.

THERMAL ANALYSIS OF FIRE INFLUENCE

Upcasting Through the Salt Handling Shaft During/After Fire

In normal operation the air inlet shaft (AIS) and salt handling shaft (SHS) are air supplies to the WIPP mine system. After the initiation of the fire of February 5 at WIPP the SHS reversed flow due to the buoyancy of the heated air at the lower end of the shaft. Figure D-36 below is visual evidence of the flow reversal.



Figure D-36. Smoke exiting the salt shaft^{ee}

Figure D-37 shows the recorded temperature near the top of the salt handling shaft from 10:00 a.m. on the morning of the February 5 through the next day. The vertical red line corresponds to the time of the onset of the fire (10:48). Prior to the fire the SHS is acting as an inlet to the mine system and the indicated temperature is in reasonable agreement with Carlsbad temperatures shown in Figure D-38. The CMS record indicates an upturn of the SHS exiting air temperature starting at 1102, just a few minutes after the ventilation mode was switched. In the hour following the fire onset, the temperature recorded near the SHS top increases approximately 20°F. This is evidently due to the flow reversal. The speed of the established, reversed flow was estimated to be about 9 m/s, for which the transit time for air entering the bottom shaft to arrive at the top would be approximately 72 s. Apparently the walls of the SHS, having been cold-soaked for days, cool the upcasting air but gradually the shaft wall warms up. After the first hour the temperature continues to rise about another 3°F over 12 hours. It appears that the fire is out in this interval but the flow is gradually warming as the walls of the shaft slowly warm due to mine-level warmer air passing. Just before midnight on the February 5, the flow reverses again due to adjustments made to the ventilation system.

An analysis was conducted to estimate airflow in the SHS after the fire. Flow velocities are estimated that balance the effects of buoyancy and friction for the flow conditions that were seen following the fire. Specifically, during

^{ee} U.S. Department of Energy Office of Environmental Management Accident Investigation Report, *Underground Salt haul Truck Fire at the Waste Isolation Pilot Plant February 5, 2014*, March 2014.

an interval of time after the fire, the air in the SHS is warmer than that in the AIS and there is a buoyantly driven flow out the SHS. The AIS supplies the SHS flow and the flow removed from the mine by the ventilation system. The buoyant force is balanced by friction losses in both shafts. Conservation of energy is considered for air flowing into the shafts and for geologic material constituting the shaft walls.

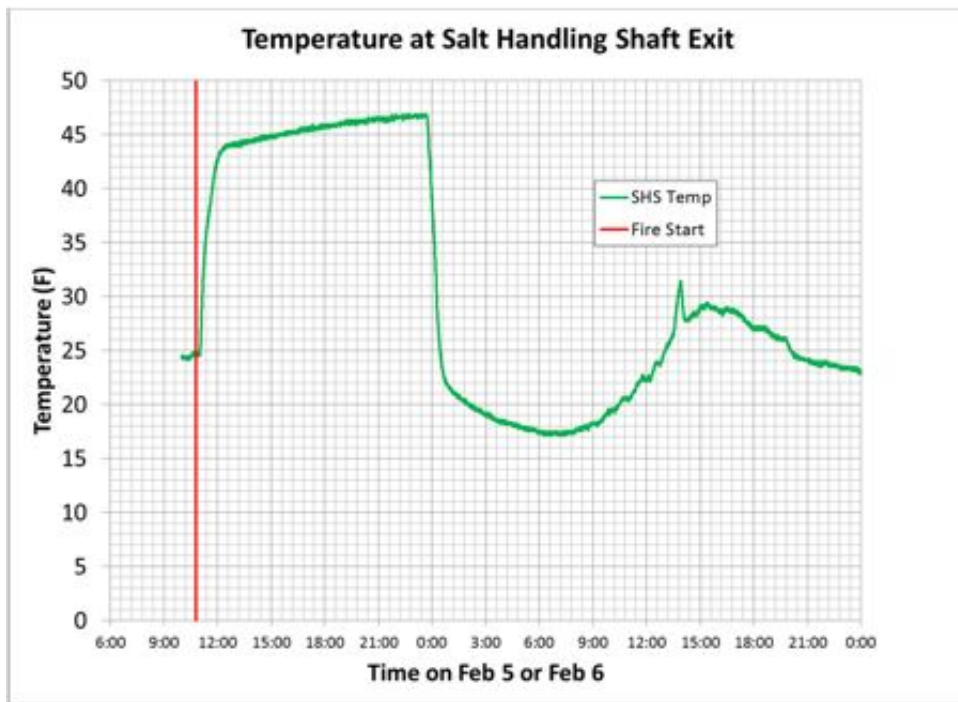


Figure D-37. Temperature near the top of the salt handling shaft on February 5 and 6

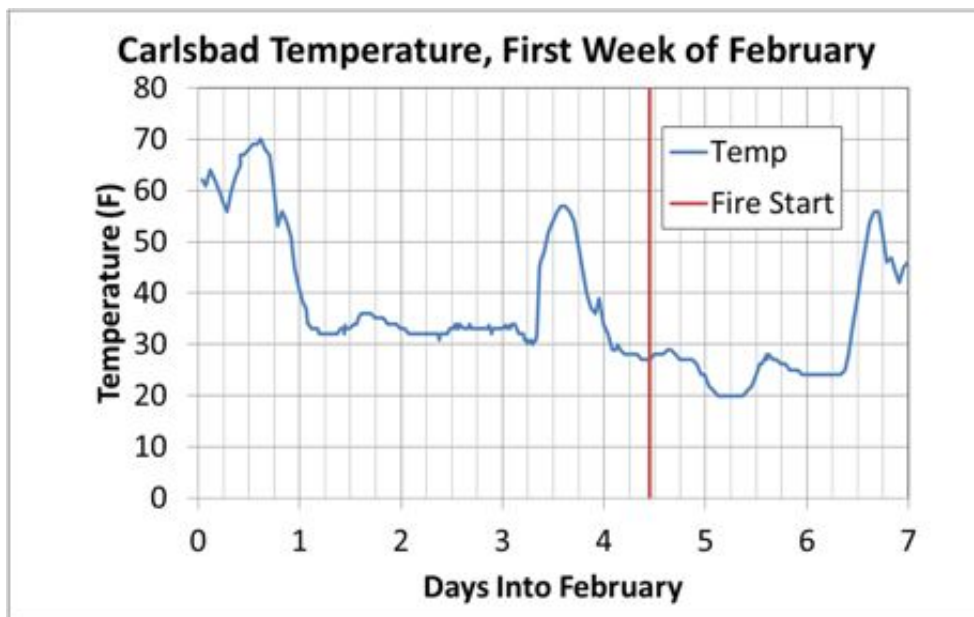


Figure D-38. Carlsbad temperatures in early February^{ff}

^{ff} http://www.wunderground.com/history/airport/KCNM/2014/2/5/DailyHistory.html?req_city=NA&req_state=NA&req_statename=NA
 This link provides hourly weather for February 5, 2014. The weather data was constructed by visiting each early day in February and electing the provision for comma-separated data export.

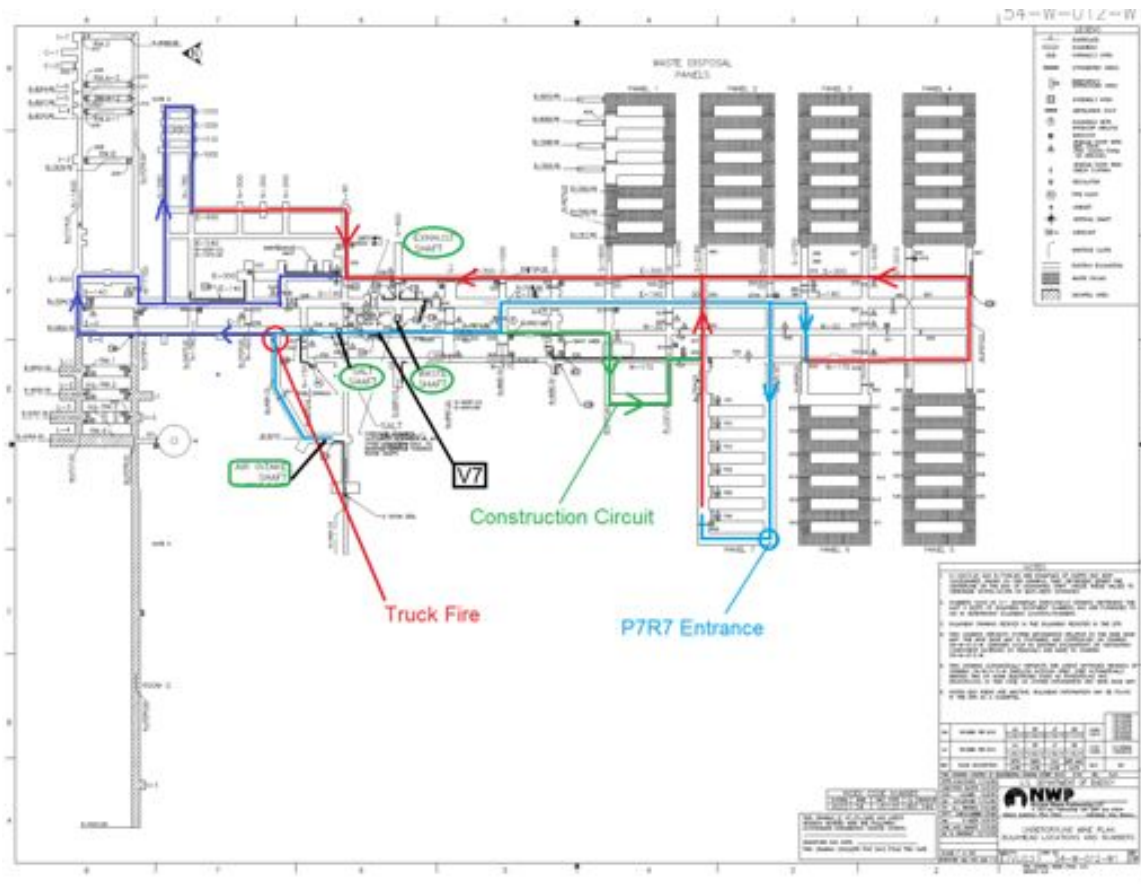


Figure D-39. Plan view showing principal mine relationships of air inlet shaft, truck fire, and P7R7

Figure D-39 shows principal flow circuits in the mine system. Approximately ten minutes after the fire started on February 5, the total flow through the mine system was reduced with the expectation of limiting the travel of smoke from the fire. The 142 kg/s pre-fire flow rate that will be used in the following analysis corresponds to the flow indicated by the CMS for V7 prior to the fire.

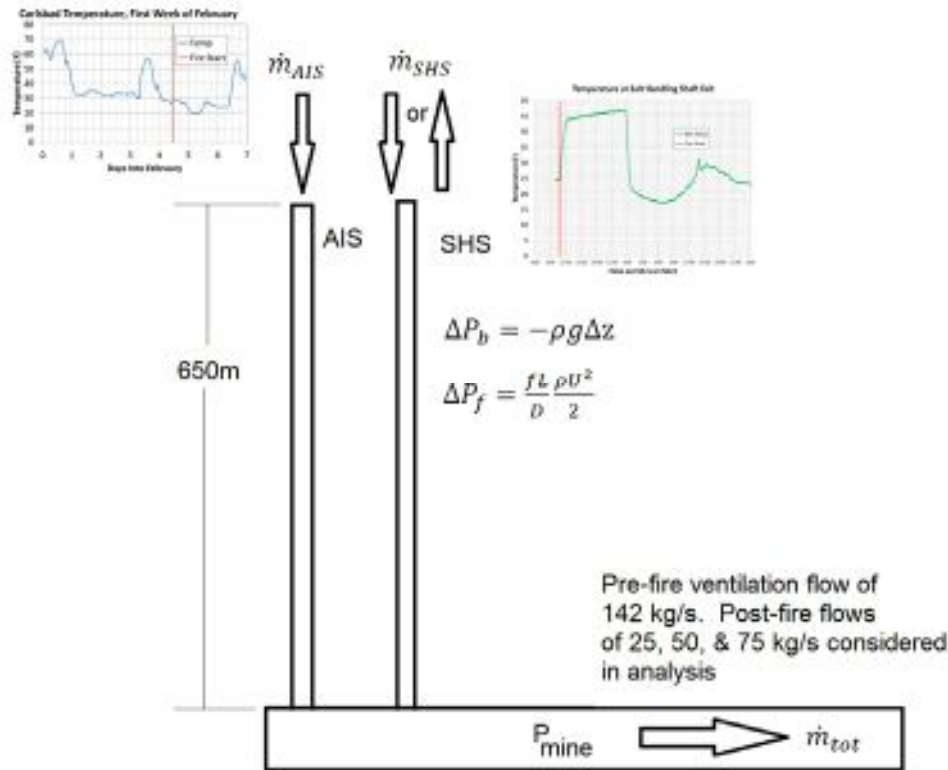


Figure D-40. WIPP flow model schematic

Flow Analysis

Figure D-40 shows a schematic rendering of the flow model. Some of the flow from the AIS went through the north circuit and energy deposited there could only help reduce heating in the direction towards Panel 7. However, for this analysis, the bulk of the flow heads south and the north circuit flow is neglected. The pressure change due to friction between two positions along an interval (Δz) of flow in a shaft is estimated as:

$$\Delta P_f = \frac{f \Delta z \rho U^2}{D} \quad (1)$$

The friction factor, f , was evaluated such that it satisfy the Colebrook formula. Properties of dry air were used for the analyses. Temperature dependent viscosity and thermal conductivity were included. The pressure change due to buoyancy force is:

$$\Delta P_b = -\rho g \Delta z \quad (2)$$

The AIS and SHS shafts were discretized into 40 vertical intervals and Eqs. 1 and 2 were applied to successive intervals in the direction of flow. At each segment the local density for air was calculated using the inlet temperature and pressure of the air. Heat exchange was considered between the flowing air and the bounding wall such that:

$$T_2 = T_W + (T_1 - T_W) \times \exp\left(-\frac{h \pi D \Delta z}{\dot{m} c_p}\right) \quad (3)$$

where T_W is the average of the wall temperature at the segment entrance and exit; T_1 and T_2 are the entrance and exit air temperatures; and \dot{m} is the mass flow rate. h is the convection coefficient and D the diameter. Equation (3)

is applied to one axial segment at a time (~16 m length) so the associated constant wall temperature of the model is reasonable. The total heat transfer between the air and the wall for the interval is then:

$$Q = \dot{m}C_p(T_2 - T_1) \quad (4)$$

Q was then applied as a uniform boundary flux for a simple finite difference model of transient radial conduction into or out of the geologic media forming the shaft wall. An annulus of material 1-m thick was considered which was divided into 40 radial segments^{eg}. Axial conduction was not considered and at the outside radius of the conduction system the boundary was considered adiabatic. Temperatures were associated with the 41 faces bounding the 40 radial layers for the midpoints of each of the 40 axial intervals. Consequently, each of the AIS and SHS had 1640 associated transient temperatures. Simple conduction with constant thermal conductivity was used to derive thermal resistance between successive layers. Any excess conduction in a layer (more energy in from the neighbor than out to the next neighbor) is available for increasing the local temperature. The resulting 3280 first-order differential equations were integrated through time using the Runge-Kutta method^{hh}. Figure D-41 shows a schematic representation of the transient radial conduction system that applies for each axial segment of the model.

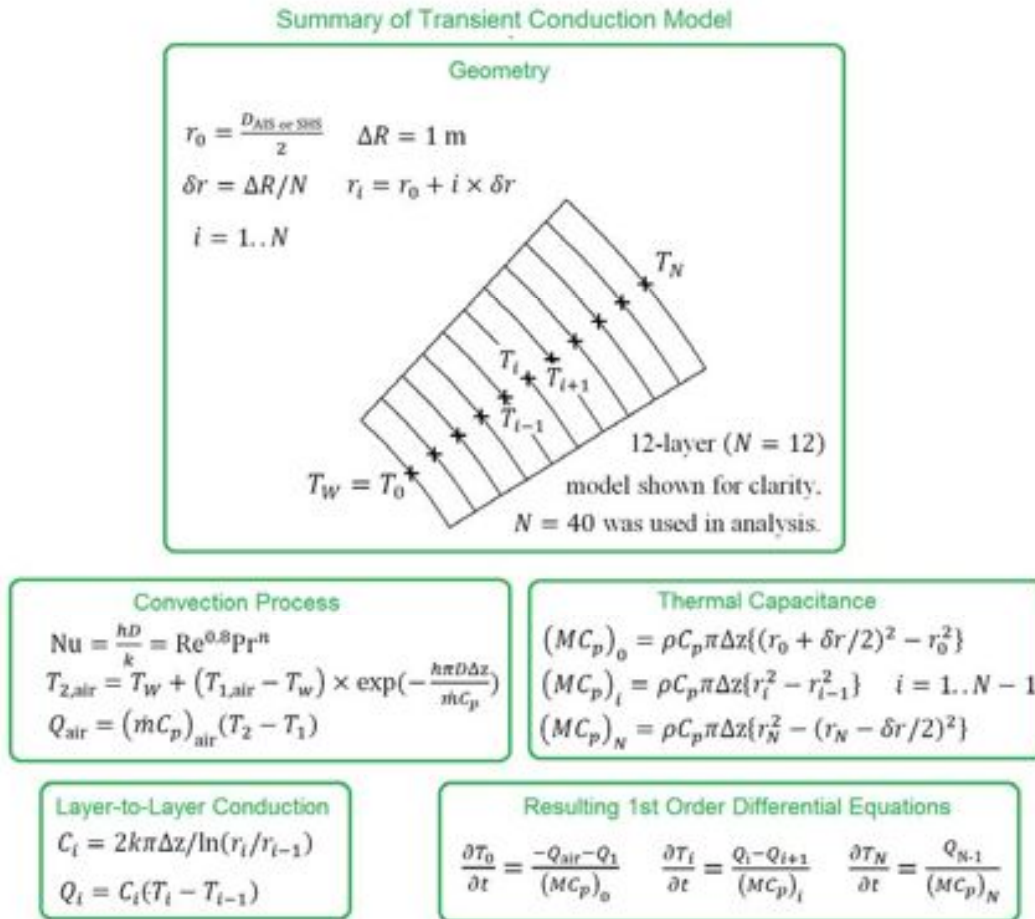


Figure D-41. Geometry of an axial segment in transient conduction model.

^{eg} A transient analytical solution for a semi-infinite material suddenly subjected to a convective heating boundary was examined to determine small response at about 1-m depth for 12 hours of heating. The choice is somewhat arbitrary but this thickness is sufficient to provide a boundary region in which the outer part only exhibits a small response relative to the surface temperature variations associated with the diurnal variation of the local weather.

^{hh} Felberg, E. NASA TR R-315 (1969).

The strata traversed by the shafts undoubtedly exhibit appreciable variation in thermal properties. Thermal properties of the lithosphere were taken as constant for convenience and representative of the earth in general. The analysis could possibly be improved by using depth-appropriate property adjustments along the shafts. The constant values of $k = 3\text{W}\cdot\text{m}^{-1}\cdot\text{K}^{-1}$, $\rho = 2800\text{ kg}\cdot\text{m}^{-3}$, and $C_p = 1000\text{ J}\cdot\text{kg}^{-1}\cdot\text{K}^{-1}$ were used for the properties of the earth forming the shafts. Nonetheless, the character of the system of ventilated shafts through geologic media is represented in the model and more precise specification of shaft wall properties would not be expected to significantly change the results.

A uniform initial temperature was assigned (275K, ~2 °C) to the conduction system and the integration was started at 12:00 a.m. on February 1 so that the first 4 and half days up to the fire onset were to establish an initialized condition for the material in the conduction system. The entrance air temperature for both shafts prior to the fire was that in Figure D-38.

The convective coefficient between the air and the shaft wall, h , was estimated using the Dittus-Boelter Equation:

$$\text{Nu} = \frac{hD}{k} = \text{Re}^{0.8} \text{Pr}^n \quad (5)$$

where the exponent on the Prandtl number is 0.3 when the air is cooled by the wall and 0.4 when it is heated. Prior to the fire, both shafts are inlets and the sum of their flows equals the ventilation system flowⁱⁱ which was taken to be constant at 142 kg/s. For either shaft the analysis steps from the surface to the mine successively applying all of Equations. 1-5 to march down the shaft. For these conditions the magnitude of the sum of the ΔP_f from Equation 1 is very much less than that of ΔP_b . Consequently, it was problematic to find a division of the mass flow that resulted in a matching pressure at the bottom ends of the shafts. The actual initial conditions for the rock were not known and the shafts having two different diameters result in different heating rates. Because the ΔP_f contribution to the pressure change going down the shaft was small, the equilibrium condition was fickle with regard to the unknown temperature distribution. So, rather than requiring precise agreement in pressure at the bottom of the two shafts, the flow was divided so that the total friction pressure drop was the same in both shafts assuming the same friction factor. That is:

$$\left(\frac{fL}{D} \frac{\rho U^2}{2}\right)_{SHS} = \left(\frac{fL}{D} \frac{\rho U^2}{2}\right)_{AIS} \quad (6)$$

Requiring the pressure to be the same on both ends of both shafts and their friction losses to be the same likewise requires that the integrated effect of buoyancy be the same for the two shafts (neglecting the small difference associated with exit losses of two different velocities). This result depends on the shaft diameters and results in the constant division of flow:

$$\dot{m}_{AIS} = \frac{\dot{m}_{tot} A_{AIS}}{\left\{ \sqrt{\frac{D_{SHS}}{D_{AIS}} A_{SHS} + A_{AIS}} \right\}} \quad (7)$$

and

$$\dot{m}_{SHS} = \dot{m}_{vent} - \dot{m}_{AIS} \quad (8)$$

The condition of Equation 7 was used to divide the flow until the time of the fire. For the diameters of 6.25 and 3.05 m, used to characterize the AIS and SHS, approximately 85% of the pre-fire total mass flow was through the AIS. After the fire, (\dot{m}_{AIS}) must supply both the ventilation flow (\dot{m}_{vent}) and the flow that goes up the salt

ⁱⁱ Several quantities used in the current analysis were taken from a preliminary analysis shared by AIB analysts. These include: the ventilation air flow rates of 142 and 54 kg/s, the shaft dimensions of 6.25 and 3.05 m diameter for the AIS and SHS, and 5 and 10 MW fire output estimates.

handling shaft (\dot{m}_{SHS}). Specification of flow past the SHS is poorly understood, so in the post-fire analysis \dot{m}_{vent} is treated as a parameter. Analyses are completed for 25, 50, and 75 kg/s flows.

The flow in the SHS and the temperature at its base are unknown. Newton's method was used to search on these two variables to find conditions that satisfy the requirements that the pressure at the mine level is the same for both shafts and the exiting air temperature for the SHS matches the record in Figure D-37. Solutions to the flow as formulated were not found until about 20 minutes after the 1048 report of the fire onset. (The solution conditions could not be met for the very lowest measured SHS outlet temperatures, by 1108 the measured outlet SHS temperature rose to about 29°F from the 25°F that was measured at 1048). The analysis stops at 11:13 PM on the evening of February 5.

Figure D-42 shows the predicted mass flow rate and temperature at the bottom of the SHS for the time interval between the fire onset and the end of the analysis. The model does not consider acceleration required to turn the airflow around. Predicting the flow reversal process is further complicated by the fact that buoyancy effects (Equation 2) handily exceed friction (Equation 1) and there is considerable uncertainty in the precise thermal conditions in the shaft.

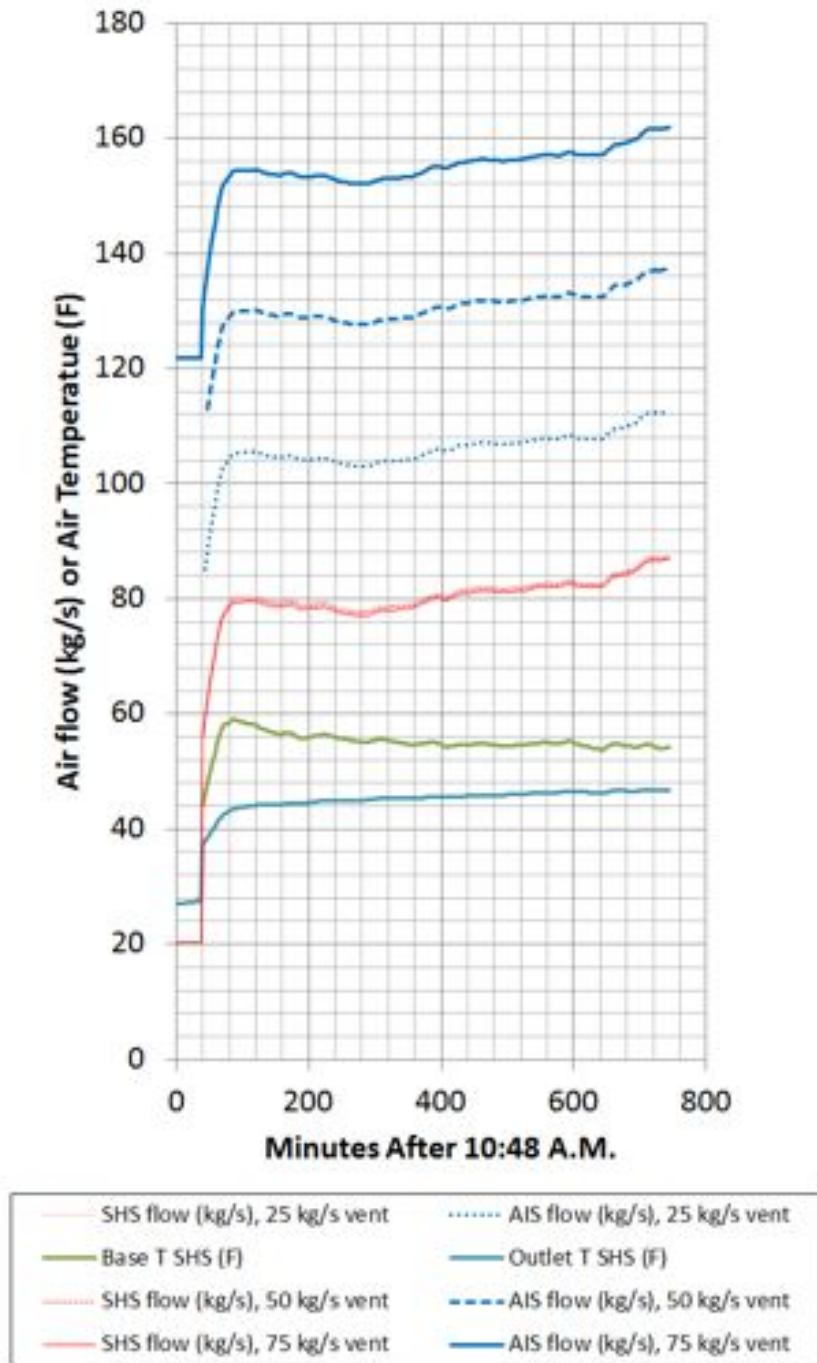


Figure D-42. Post-fire predicted mass flow rates and temperatures

The predicted mass flow rate in the SHS shown in Figure D-42 is fairly constant around 80 kg/s once the flow is established. The three red lines, corresponding to the different ventilation flows, are nearly indistinguishable. The calculated mass flow up the SHS falls slightly with higher ventilation flow because the increase in total flow in the AIS results in a slightly greater friction loss in that shaft. The three blue lines are the predicted flows for the AIS. As required by conservation, they are 25, 50, and 75 kg/s higher than the corresponding predictions for the SHS. The predicted inlet temperature for the air upcasting through the SHS is surprisingly low.

Figure D-43 shows the model-predicted temperatures of the air and the confining shaft wall at 1148. The model predicts that air arriving at the bottom of the AIS has been warmed by the shaft from about 28°F to 32°F. The SHS is warmer as required for the buoyancy difference to counter friction and exit losses.

It may have taken some time for the flow reversal to develop. The slowing of the mine ventilation system probably gave the flow reversal up the SHS a kick-start. As noted earlier, the temperature at the SHS exit begins to rise minutes after the ventilation mode adjustment was ordered. Just prior to switching to ventilation mode the predicted mean flow speed in the AIS is 3.1 m/s while that in the SHS is 2.15 m/s. Since the bottom of the SHS and AIS are relatively close, they should have experienced roughly the same transient pressure in response to switching to ventilation mode. Consequently, flow in the two shafts should have experienced approximately the same deceleration. So when the flow went from 142 kg/s to \dot{m}_{vent} kg/s, ignoring density variations, conservation requires:

$$(V_{AIS}A_{AIS} + V_{SHS}A_{SHS})\dot{m}_{vent} / 142 = (V_{AIS} - \Delta V)A_{AIS} + (V_{SHS} - \Delta V)A_{SHS} \quad (9)$$

where ΔV is the decrease in speed in both shafts. For the foregoing conditions, $\Delta V = 2.15$ m/s, just enough to stop the flow in the SHS, when $\dot{m}_{vent} = 37$ kg/s. While details of the transients in mine flow are not known, it seems plausible that the flow might have been arrested to $\dot{m}_{vent} < 37$ kg/s and the reversal initiated. The added bit of buoyancy due to the fire heating could then complete and sustain the reversed flow.

Figure D-43 shows the predicted vertical variation in the temperatures of the air and the walls in the two shafts an hour after the fire onset. The wall temperatures are primarily established by the 4 and half days of interaction with the ambient air prior to the February 14 fire (Figure D-38).

Figure D-44 shows predicted temperature profiles for radial depth into the shaft walls at one hour after the fire onset at the top and bottom ends of both the AIS and the SHS. For both locations of the AIS the wall temperature has been decreasing (it is lower than the temperature at greater radial depth) because the ambient temperature at the time of the fire was ~30°F lower than it had been the previous day (Figure D-38). At the bottom of the SHS the wall temperature is “turning around.” It is warming up because higher temperature air is entering that end of the SHS.

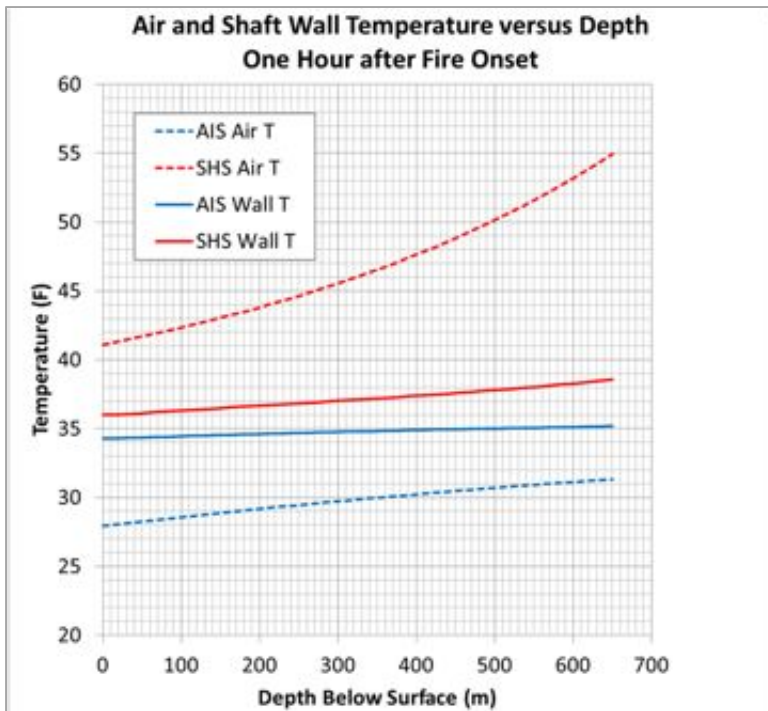


Figure D-43. Vertical temperature profiles: air and shaft wall temperatures in AIS and SHS one hour after fire onset

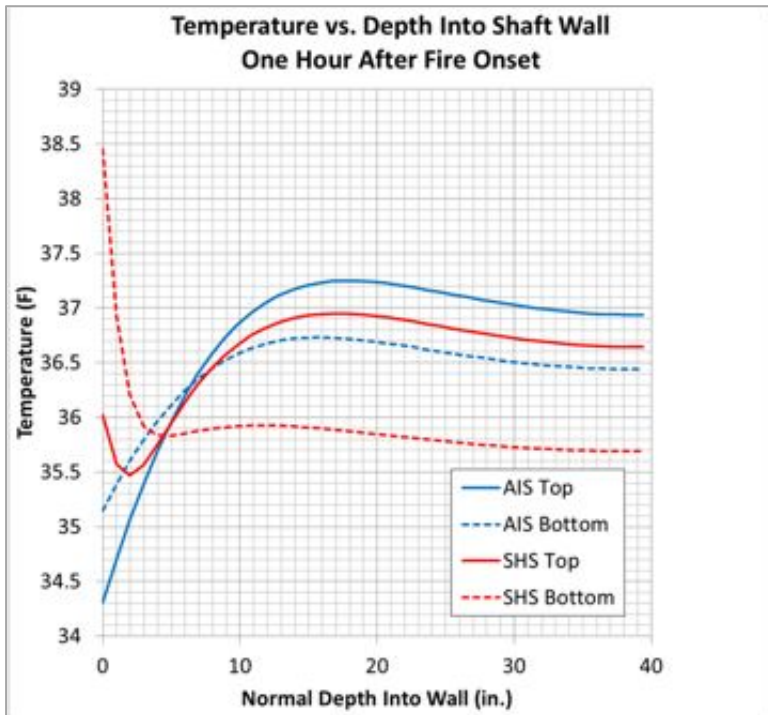


Figure D-44. Predicted temperature versus depth into wall at tops and bottoms of AIS and SHS one hour after fire onset

Alternate Flow and Temperature Estimates for the SHS

As noted in the previous discussion (Figure D-42), the temperatures predicted at the base of the SHS seemed low. The analysis of the previous section found the mass flow and temperature at the base of the SHS that allowed a pressure balance and matching of the temperature at the outlet of the SHS. The energy required of the fire to

arrive at the temperature required at the base of the SHS was not considered. In this section an alternate approach is considered in which energy from the truck fire, less losses, is added to the air flow from the AIS. Figure D-45 provides graphical solutions for conditions considered.

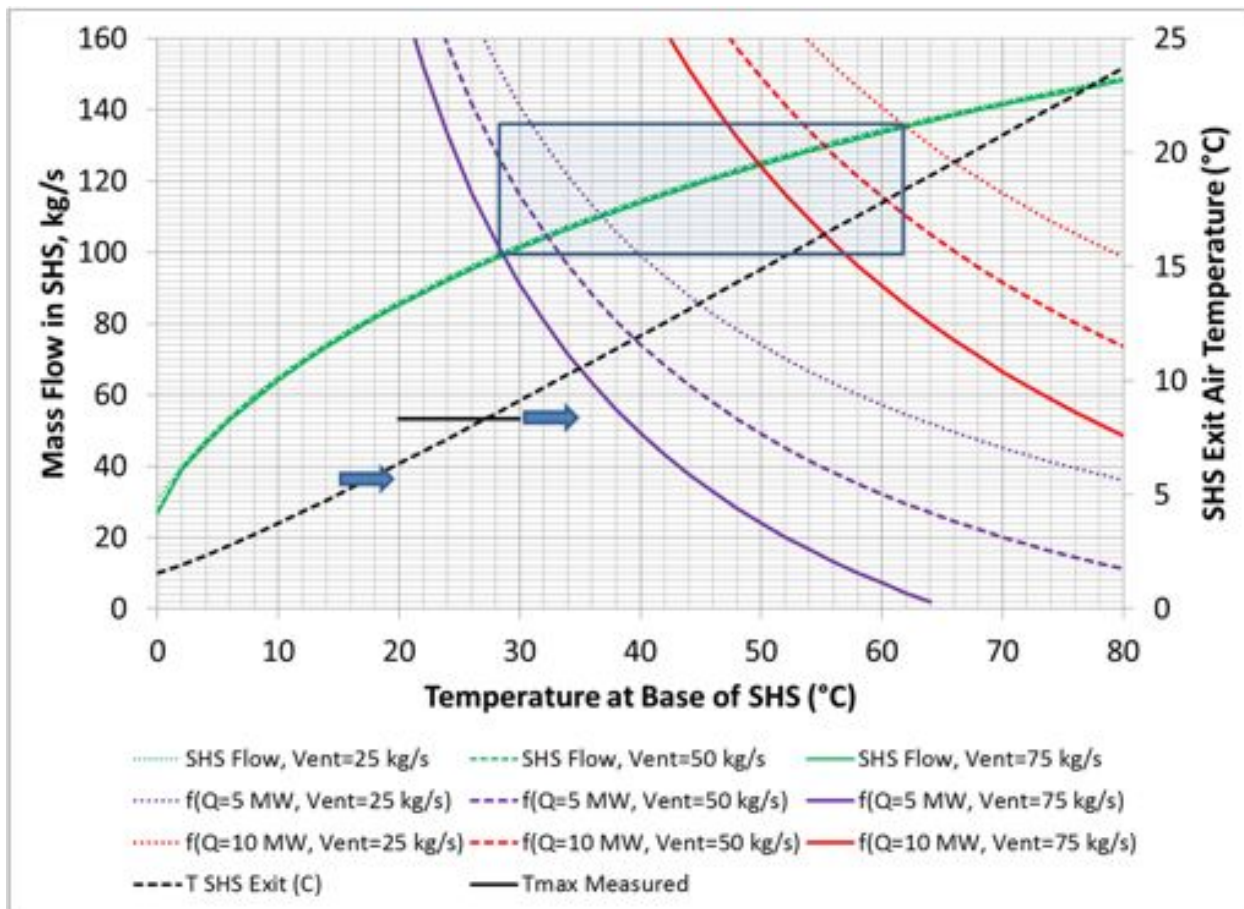


Figure D-45. Predicted buoyancy-driven flows and first-law consistent flow for specified SHS base temperatures

In Figure D-45, the green lines represent the mass flow calculated for the SHS using a specified temperature at the base of the SHS. The flow rate is that which satisfies the earlier momentum and energy equations for both shafts with the same pressure at their bases. The mass flow in the AIS is that of the SHS plus the ventilation flow. As before, the post-fire ventilation flow is 25, 50, or 75 kg/s. The wall temperatures of both shafts' are approximately those given in Figure D-43. The three green lines corresponding to the different ventilation flows are nearly indistinguishable, but are ordered appropriately. The calculated mass flow up the SHS falls slightly with higher ventilation flow because the increase in total flow in the AIS results in a slightly greater friction loss in that shaft.

The dashed black line (Figure D-45) is the estimated air temperature at the outlet of the upcasting SHS. The maximum measured SHS outlet temperature before the flow reverses again (11:13 PM on Feb 5, Figure D-37) is shown as the solid black line segment. The intersection with the dashed line at about 27 °C is the highest SHS base temperature that does not exceed the maximum measured temperature on the top end.

Details of the fire temperature spatial distribution are not considered, rather the region between the AIS and SHS is idealized as well-mixed and the air within as isothermal. Undoubtedly, a considerable temperature drop occurs in flow proceeding from the fire past the bottom of the SHS. Losses from radiation, in particular, would go up dramatically in high temperature regions. Consequently, the well-mixed average is expected to be between the hottest (near fire) and coolest (near SHS) parts of the actual system and thus constitutes a conservatively high estimate of the temperature at the SHS.

The red and purple lines are first-law consistent temperature predictions corresponding to fires of 10 and 5 MW thermal output. The dotted, dashed, and solid lines correspond to 25, 50, and 75 kg/s vent flow rates. The conservation of energy statement is:

$$Q_{\text{fire}} - Q_{\text{radiation}} - Q_{\text{convection}} = \dot{m}_{\text{AIS}} C_p (T_{\text{SHS}} - T_{\text{AIS}}) \quad (10)$$

where Q_{fire} is a specified thermal output of the fire (5 or 10 MW). Equation 10 is used to solve for \dot{m}_{AIS} for the two thermal powers and the varied ventilation rates as a function of T_{SHS} . Then

$$\dot{m}_{\text{SHS}} = \dot{m}_{\text{AIS}} - \dot{m}_{\text{vent}} \quad (11)$$

$Q_{\text{radiation}}$ and $Q_{\text{convection}}$ are energy losses due to radiation and convection. The region between the bottom of the AIS and SHS was approximated as a rectangular box 30' wide by 13' high by 300' long for which a mean beam length is $l = \frac{4V}{A} = 5.36$ m. The shaded box super-imposed on the Figure D-45 encloses the estimated range of base SHS air temperatures and resultant SHS flows corresponding to 5-10 MW fire output and 25-75 kg/s ventilation flows based on the solutions of Equation 10.

Conservatively small losses of energy from the air to the walls have been used. Larger estimates of $Q_{\text{radiation}}$ and $Q_{\text{convection}}$ would drive the shaded box in Figure D-45 along the predicted (green) mass flow line closer to the origin and closer to agreement with the initial analysis (for which the SHS exit air temperature was required to match the measurement). Additional water evaporated from confining walls and water and CO_2 from combustion would all enhance heat losses but are not considered in this model.

Soot from the fire would surely have been important in determining radiant losses from the hot products, but determining the transient and spatial variation of the soot properties is not practical. Moreover, the transient radiation through the varying conditions is not amenable to prediction. In addition to soot, H_2O and CO_2 would have been present and would have made contributions to radiation from gaseous products to the confining walls. To simplify the radiation prediction, only radiation from water vapor is considered here and only the water from the inlet air humidity is considered. That is, water added to the flow from combustion products is omitted. These very limiting assumptions still admit significant radiant losses and are sufficient to demonstrate that very significant cooling of the fire's products and the mixing air will occur before the flow reaches the SHS. Based on surface conditions at the time of the fire (~50% relative humidity and 27°F) the partial pressure of water vapor in the ambient air was about 0.00243 atm.

Figure D-46 provides emittance associated with water in a mixture of 1 atm total pressure. At the mean beam length of 5.36 m the path-partial-pressure product is 0.013 atm-m and from the figure, $\epsilon_{\text{H}_2\text{O}} = 0.075$ (marked with "+") at the low end of the temperatures presented. $\epsilon_{\text{H}_2\text{O}} \sigma T^4$ is an estimate of the mean radiant flux on the bounding surfaces so that:

$$Q_{\text{radiation}} = (2570 \text{ m}^2) \times \epsilon_{\text{H}_2\text{O}} \sigma (T^4 - T_{\text{wall}}^4) \quad (12)$$

where the area is the total surface area of the enclosing volume and the wall temperature, $T_{\text{wall}} = 20$ °C. The convection loss in Equation 10 was estimated as:

$$Q_{\text{convection}} = (2570 \text{ m}^2) \times h \times (T - T_{\text{wall}}) \quad (13)$$

where $h = 2 \text{ W} \cdot \text{m}^{-2} \cdot \text{°C}^{-1}$, a conservatively small convection coefficient.

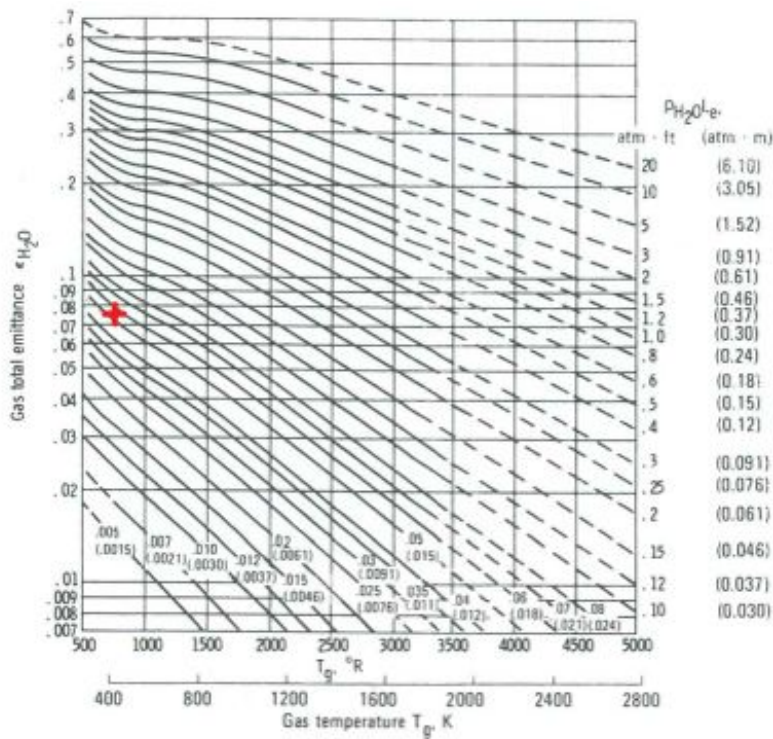


Figure D-46. Total emittance of water vapor^{jj}

In Figure D-45, the intersections of the red and purple lines with the green lines represent solutions to the conditions of conservation of energy per Equation 10 and the predicted mass flow balancing the buoyancy difference in the two shafts with friction losses. At the highest fire thermal output considered with the lowest ventilation rate (10 MW and 25 kg/s), this approach leads to an estimate of 62 °C for the temperature at the base of the SHS. Note that the predicted SHS outlet temperature at this condition is very substantially higher than the measurement given in Figure D-37. Consequently, 62 °C is a conservatively high estimate of the temperature at the base of the SHS. For the ventilation flows of 50 and 75 kg/s the estimated SHS base air temperatures are 55 °C and 50 °C.

Implications for Panel 7 Room 7 Thermal Disturbance

The previous section provides an analysis that demonstrates a temperature of less than 50, 55, or 62 °C at the base of the SHS during the fire depending upon the ventilation rate. The flow downstream of the base of the SHS in the mine subsequently divides and only a portion of it goes through P7R7. The flow path from the SHS base to P7R7 is approximately an additional 4200 feet (1280 m). To provide a simple means of estimating the decrease in air temperature between the SHS base and P7R7 consider flow in a tube of constant wall temperature and with a constant convective coefficient. The downstream temperature, $T(L)$, is given by:

$$\frac{T(L)-T_w}{T_1-T_w} = \exp\left\{\frac{-LPh}{\dot{m}C_p}\right\} \quad (14)$$

where L is the downstream distance and P is the perimeter of the flow channel, T_w is the wall temperature and T_1 is the entrance flow temperature. When h is based on the Dittus-Boelter Equation for large Reynolds number ($>10^4$), which is generally the case for flows of interest in this investigation, the magnitude of Equation 14

^{jj} Siegel, Robert, Howell, John R. "Thermal Radiation Heat Transfer" 4th ed. 2002. Taylor & Francis, New York, graph attributed to Hottel, H.C.: Radiant-Heat Transmission, in William H. McAdams (ed.), chap. 4, McGraw-Hill, New York, 1954.

increases with increasing mass flowrate. Consequently, for a given T_1 , a conservative estimate of $T(L)$ is realized by assuming a larger flow rate. A bounding estimate of the temperature at P7R7 is given by assuming that all of the ventilation flow remains in one flow passage in transit to P7R7. Assuming 25, 50, or 75 kg/s mass flow rates with 62, 55, and 50 °C values of T_1 proceeding 1280 m in a 9.1 m by 4.0 m (30 ft by 13 ft) of constant wall temperature of 20 °C results in an estimated temperatures at P7R7 of 24.5, 25.0, and 25.0 °C. While a stronger flow in Equation 14 predicts a larger response, the conservation of energy arguments from the previous section require lower T_1 for higher flow. The three conditions all result in about a 5 °C rise above the wall temperature. The Dittus-Boelter equation predicts a convective coefficient of 2.5-6.0 W/m²/K for the specified passage size and these three flow rates.

Conclusions of Thermal Analysis

This analysis demonstrates that very significant buoyancy-driven flow in the SHS resulted from the fire. Assumptions of the analysis were made to provide a conservatively high estimate of temperature at the base of the SHS. That the 62 °C estimate is an upper bound is strongly supported by the measured air temperature at the SHS exit. In fact for this temperature the predicted SHS exit temperature is well higher than the measurement. Conservatively small estimates of radiation and convection loss between the fire and the SHS base are sufficient to be consistent with the 62 °C estimate for a 10MW fire. Using the assumption that the entire flow proceeds from the base of the SHS to the waste array, results in a 5 °C predicted air temperature increase at the waste array.

HUMIDITY ANALYSIS

Humidity Increase in P7R7

The fire may have produced up to about 300 kg of H₂O products in 20 to 40 minutes. Figure D-47 is a plot of Carlsbad weather conditions in the time interval following February 5, 2014. At most the surface humidity was around 80% relative humidity at 30F at the time of the fire, which corresponds to a humidity ratio of 0.0027 kg moisture per kg of air.

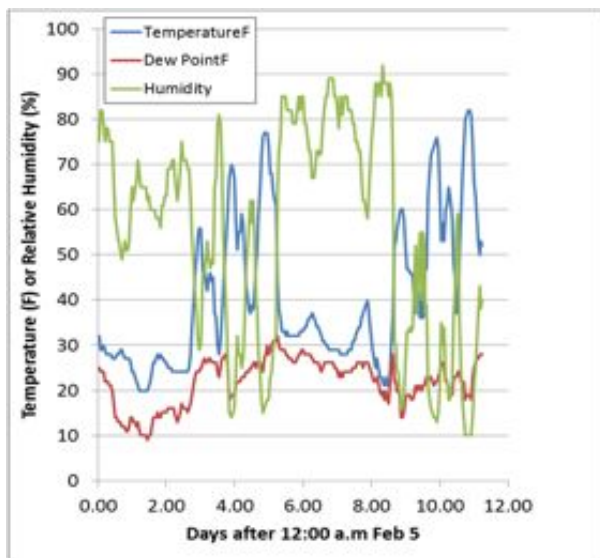


Figure D-47. Carlsbad weather conditions between fire and release events

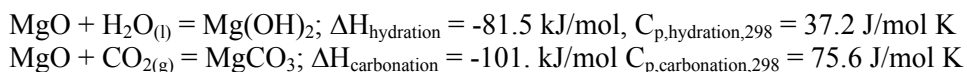
If 300 kg of water were produced in 20 minutes the production rate was 0.25 kg/s. Figure D-45 summarized conservative conditions for estimating a relatively high temperature at the base of the SHS. In order to be conservative in estimating the effect of humidity, consider the relatively low mass flow corresponding to the condition that matched the SHS outlet temperature, i.e., 53 kg/s up the SHS. Additional flow is associated with ventilation through the mine, but adding the 0.25 kg/s just to the 53 kg/s airstream would raise the humidity ratio to 0.0074. The humidity ratio for saturated 20 °C air is 0.01469. Therefore, at points away from the fire, there

would not be condensation on 20 °C walls. At distant points the air will be very near the salt wall temperature. If that is 20 °C, the 0.0074 humidity ratio corresponds to 51% relative humidity.

Note that the humidity discussion of the previous paragraph regards that of the incoming air as altered by water from the combustion process and does not consider mass transfer interactions with the mine surfaces. The vast surfaces of the mine and equilibrium with natural moisture at the boundary are likely determining factors for humidity in the mine. Nonetheless, disregarding the wall interaction, it is evident that the flow was not saturated by the water addition even when cooled back to mine temperatures.

Exothermic Reactions of H₂O and CO₂ with MgO

Because MgO hydration and carbonation generate heat, the likelihood of either reaction contributing to the February 14 radiation release from WIPP must be established. The relevant reactions are:



The magnitude of the enthalpies and heat capacities suggest that both hydration and carbonation could prompt temperature increases of several hundred °C, if reaction rates were not limited by: 1. slow reaction kinetics; 2. availability of H₂O or CO₂ including transport through the MgO bags, and/or; 3. heat transport away from the reaction site.

MgO hydration could occur by contact with liquid water or water vapor. Interviews with Sandians (L. H. Brush and C. R. Bryan) who did MgO kinetics analysis in the early 2000's, and a former Sandian (J. L. Krumhansl) who did earlier MgO kinetics analysis suggest that MgO hydration and carbonation are slow at the low temperatures and relative humidities prevalent in the WIPP. MgO carbonation is much slower than hydration^{kk}. Consequently, heat generation by MgO hydration is emphasized below.

Sandia^{ll} performed inundated and vapor hydration of MgO in the early 2000's. Note that these measurements were made on an earlier MgO provided by Premier Chemicals. The MgO used in P7R7 is a newer MgO with a smaller grain size. For the time being, the Premier MgO results are used to bound the reactivity of P7R7 MgO. Most MgO contains 1-3% CaO and 7-9% non-reactive silicate and aluminate impurities. Because hydration of CaO occurs very rapidly^{mmm}; it is unlikely that unhydrated CaO existed in the Room 7 MgO. CaO hydration is therefore neglected here.

MgO hydration rates increase with temperature and relative humidity. Temperatures in the unventilated room would not have exceeded 28°C, the ambient temperature in the repository. After the truck fire on February 5 the humidity in P7R7 might have been increased due to the H₂O generated by the truck fire that occurred on February 5. The results of Snider^{ll} (slide 22) indicate that the hydration rate of MgO at 25°C is ~ 0.1 mol%/day (RH = 95%) and 0.025 mol%/day (RH = 75%). Because the Premier MgO was replaced by a finer grained MgO with presumably a higher surface area, these rates are likely minimum values. This assumes that MgO hydration is a surface-controlled process and that higher surface areas will prompt higher reaction rates.

Therefore, for the purposes of bounding the process, we assume that the hydration rate of MgO in P7R7 is twice the Premier MgO values; Rate = 0.2 mol%/day (RH = 95%) and 0.05 mol%/day (RH = 75%). Assuming free access of H₂O (no H₂O barrier performance of bags) and negligible heat loss, a maximum temperature rise of between 1 and 4°C is predicted using the following equation:

$$\Delta T = 0.01 \text{Rate (mol\%/day)} H_{\text{hydration}} / C_{p,\text{hydration},298}$$

^{kk} A.C. Snider, personal communication

^{ll} Snider, A. C. Hydration of Magnesium Oxide in the Waste Isolation Pilot Plant, Mat. Res. Soc. Symp. Proc. Vol. 757, 2003

^{mmm} C. R. Bryan, personal communication

Possible temperature rises due to energy generation at these rates would easily be mitigated by heat losses to the air within the waste array and room. Consequently, these calculations suggest that MgO hydration is unlikely to have generated enough heat to melt the MgO bags.

Source of Damage to MgO Bags

A significant “footprint” of damage to the MgO bags and slip sheets was observed during the visual inspection of the waste pack array on May 30, 2014. The objective of the following analyses was to evaluate any heat/mass transport scenarios that may have contributed to the damage to the MgO bags and the slip sheets.

Potential for Thermal Damage to MgO Sacks

There are two plausible mechanisms by which the polypropylene super sacks could fail in the way observed in P7R7. They could either have 1.) ignited and burned or 2.) melted. Experiments show that the polypropylene readily ignites and sustains burning when exposed to even a small flame [Appendix D]. This is the most likely mechanism for the damage observed to the bags and may have been associated with ignition of hot materials ejected from Drum 68660. It is also possible for the bags to melt due to an external heat flux such as a convective flux from hot gases and/or a radiative flux from a flame at a distance. Figure D-48 shows a finite element model of the hexagonal blocks of MgO powder that was constructed to assess the combinations of incident heat flux and time required to heat the surface of the MgO to temperatures high enough to damage the polypropylene sacks.

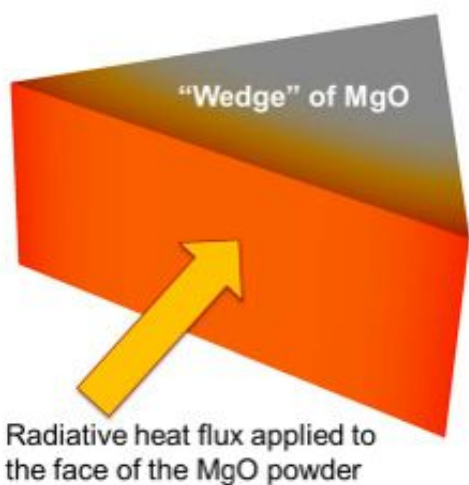


Figure D-48. Illustration of finite element model of MgO sack

The polypropylene material will melt at approximately 400K. It is expected to lose structural integrity at lower temperatures. Experiments to determine the point at which mechanical failure would occur due to the pressure of the MgO powder and elevated temperature were discussed. It was decided that these experiments would not be performed due to time constraints and the high flammability of the polypropylene material suggesting that it is likely the bags burned rather than melted.

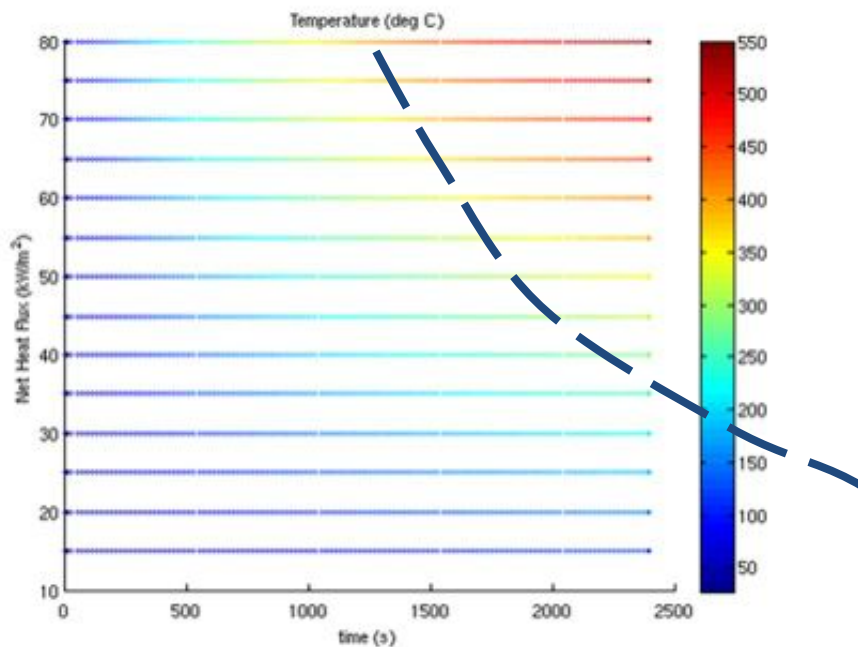


Figure D-49. Bag surface temperature as a function of incident heat flux and time

The predicted surface temperature as a function of net heat flux and time is summarized in Figure D-49. The dashed line indicates the relationship between the magnitude of the net heat flux and the approximate time for the bag to melt. For example, the polypropylene would melt after approximately 30 minutes of being subjected to a heat flux of 50 kW/m². This is the net heat flux which could consist of a combination of convective and radiative loads.

The damage footprint observed in P7R7 could be the result of multiple processes. It is possible that a fast release of flammable gases caused a fireball which damaged the MgO bags and ignited other combustible solids. These solids have been shown to be capable of sustaining flame once ignited and this flame could have propagated throughout the waste array. P7R7 was not inspected until several days following the release event. This flame propagation could have expanded the observed damage footprint over that time. Alternatively, the damage footprint observed in P7R7 could be the result of a sustained release of hot gases and other combustible materials from Drum 68660 over the course of several minutes. The validity of this second scenario is investigated here.

Accumulation of Flammable Gases within the Waste Array

One scenario in which the contents of the drums could have been heated by an external heat source was through the potential collection of flammable gases within the waste array and the subsequent ignition by an unidentified ignition source. To address this question, two scenarios were analyzed:

- Could heavier-than-air flammable gases “settle” within the voids of the waste array and subsequently been ignited?
- Could the air flow patterns within the room and waste array result in “stagnant” regions in which flammable gases (not restricted to heavier-than-air) could have collected within the voids of the waste array and subsequently been ignited?

To address the question of “heavier-than-air” gases, an estimate of the composition of the off-gas products of the chemical reactions within Drum 68660 were computed by Hobbs^m based on equilibrium of the products. In general, the dominate species of the products, which are assumed to have been vented from the drum, were H₂O, CO₂, CO, H₂, and CH₄. Based on these analyses, there were no heavier-than-air flammable gases venting from

^m Hobbs, M.L., “Cookoff modeling of a WIPP waste drum (68660),” memo to Distribution, December 15, 2014.

Drum 68660 that would have collected within the waste array. Consequently, because the expected venting gases are not heavier than air, it is unlikely that these gases would have accumulated within the waste array due to their density. More likely, these flammable gases would have mixed with the bulk air through the room and be advected from the waste array. Additionally, the lack of an identified source of ignition also makes this scenario unlikely.

The question of flammable gases accumulating within the waste array due to recirculation regions of the bulk flow was considered. The largest challenge in addressing this question is the lack of knowledge of the actual geometry of the waste boxes, drum assemblies, and MgO sacks, as well as the geometric configuration of these assemblies/boxes within the waste array and the room. An accurate characterization of the waste array geometry is a necessary input to a numerical model intended to compute flow within and through the waste array. Initial consideration of this scenario was limited to scoping calculations with highly-simplified geometry and physical assumptions. As the belief that the breach and release was more likely to have occurred due to internal chemical reaction and heating, the pursuit of this possible external heating scenario became a lower priority. More detailed, higher-fidelity numerical models capable of resolving the flow within the waste array between the waste boxes, drum assemblies, etc., were not developed. This scenario also lacks an identifiable source of ignition.

Computational Fluid Dynamics (CFD) Energy Transfer

For this scenario, the damage footprint in P7R7 is expected to loosely correspond to the spatial domain that experienced significantly elevated temperatures during the release event. A computational fluid dynamics (CFD) model was constructed to estimate the spatial extent of the damage consistent with conservation of mass, momentum, and energy for plausible drum emission scenarios.

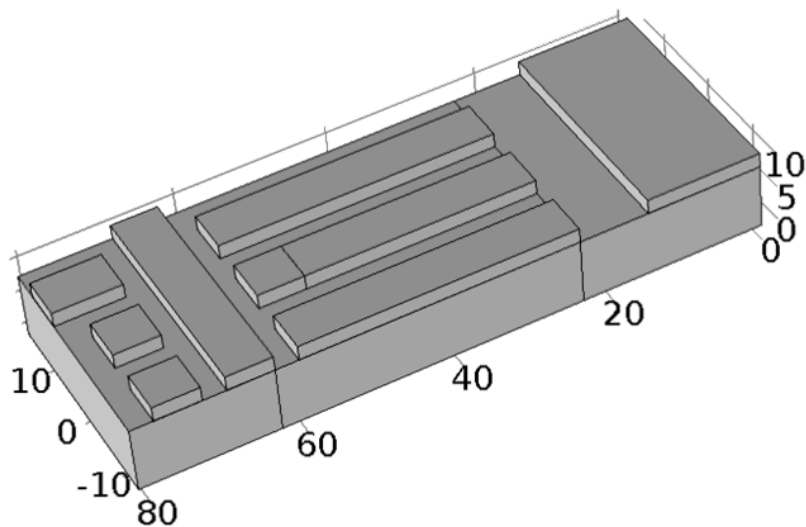


Figure D-50. Approximate geometry of waste array in P7R7 (dimensions in feet)

An approximate geometry (Figure D-50) is used for the CFD model. This simplification was made in order to reduce the mesh size and is justified by the fact that the precise arrangement of waste in P7R7 is uncertain. A consequence of this decision is that air flow through the waste array (expected to be near zero) is not simulated. The vast majority of the ventilation air flow is expected to go over and around the waste array. Additionally, because the geometry is approximate the simulation results are not expected to reproduce small-scale flow features.

There are a number of important parameters that are unknown, which limits the utility of the simulation results. It is recognized that results from the CFD model would be more useful if more information were available. With the limited data currently available, the CFD model predictions are useful in assessing whether a proposed release hypothesis is plausible given the known damage footprint and the constraints of mass, momentum, and energy conservation.

The event duration is also uncertain. Shorter events are less likely to cause extensive damage. Longer event times (minutes) are considered. The burn rate and energy release of the waste is unknown. This is important because the speed/pressure at which the combustion products exit the drum has a large effect on the size and shape of the resulting plume of hot gases. The model does not adequately capture the geometry changes or the transient emission of hot gases due to the bursting of Drum 68660. The model does not simulate the possible reaction or combustion of flammable gases exiting Drum 68660. Instead, it is assumed that hot air exits the drum at a specified rate and temperature. The flow rate is chosen based upon ‘reasonable’ estimates for release duration and the total mass of ejected material. The temperature is chosen based on the analysis of the drum contents and the thermal runaway modeling (Appendix D) to be between 1000 and 1700K. The consequence of not modeling the combustion of the gases is that the model does not predict which surfaces would be exposed to direct flame in a given release scenario. The model also does not include the additional heat potentially generated due to the combustion of other materials in P7R7 such as slip sheets and polypropylene super sacks. The heat transfer to the solid surfaces is treated in an approximate manner. Conduction into these solid bodies is not directly simulated by the CFD numerical model and thus the effects of the transient response of the solids can only be estimated. Two bounding cases for the heat transfer between the fluid and solids are considered. To establish an upper bound on temperatures within P7R7 heat transfer between the fluid and solids is neglected. To establish a lower bound on temperatures in P7R7 a convection boundary condition is used but the wall temperature is held fixed at the initial condition. The k-ε turbulence model is used in all cases.

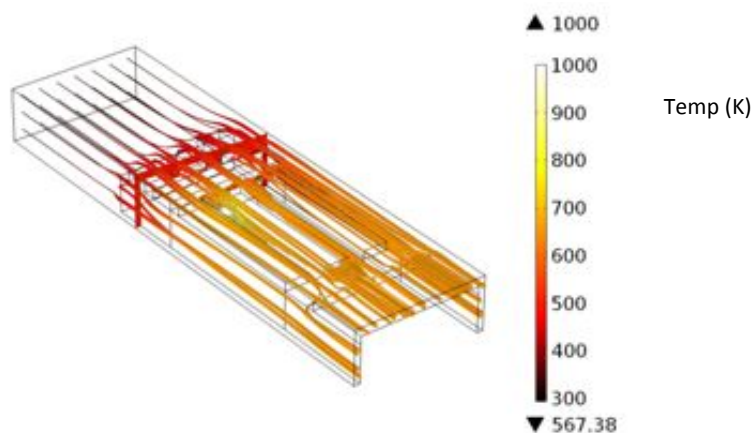


Figure D-51. Results of CFD simulation (upper temperature bound)

Because of the low residence time for air in P7R7 relative to the expected release duration, steady-state results are presented. This sustained release scenario is further supported by the discoloration and hardening of the MgO powder above Drum 68660 consistent with extended exposure to NO_x. The consequence of the above approximations and assumptions is that the results of the CFD analysis should currently be viewed as qualitative rather than quantitative. The ventilation flow rate through P7R7 was dramatically reduced when the HEPA filters were engaged in response to the release. This reduction in flow rate occurred approximately 10 minutes after the release event. Because the duration of the release event is unknown and is potentially greater than 10 minutes both the high (initial) and low ventilation flow rates are considered. Figure D-51 shows the results for a release temperature of 1000K and a hot-gas mass flow rate of 3.3 g/s during the high ventilation condition. Sufficiently elevated temperatures are observed over the entire damage footprint. While higher temperatures and faster release flow rates are possible, they would only serve to further increase the temperature predictions. These temperatures are expected to be an overestimate because heat losses to the walls and room contents are neglected. The high-bias of predicted temperature is expected to be especially pronounced further from the release location.

To establish a lower bound on the temperature environment in P7R7, heat losses to the walls and waste are overestimated. This is done by using a convection coefficient boundary condition but not allowing the wall temperature to increase. For the illustrated case the maximum release temperature of 1700K and release flow rate

of 33 g/s is used. Combined with the low ventilation flow rate these results are expected to represent the maximum temperatures achievable using this boundary condition.

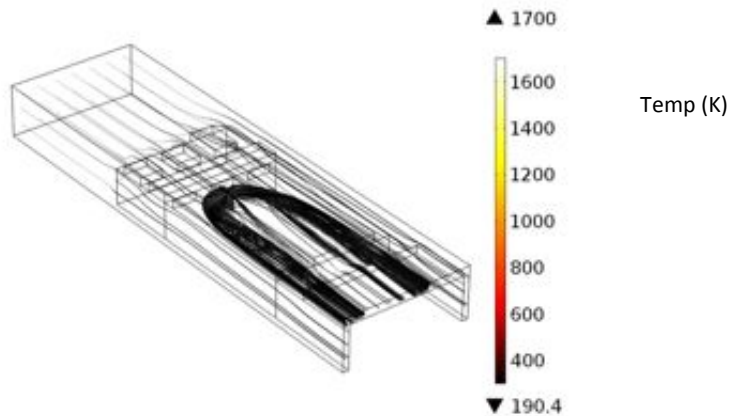


Figure D-52. Results of CFD simulation (lower temperature bound)

Figure D-52 shows temperatures over the damage footprint that would be too low to damage the polypropylene sacks thermally. The actual behavior at the interface between the air and solid surfaces is expected to be between the two responses predicted by the two boundary conditions considered. Because the temperatures predicted using the conservatively low boundary condition would be insufficient to cause the observed damage even in the most damaging release scenario and the temperatures predicted by the adiabatic condition would easily suffice for even the least damaging release scenario, we are forced to conclude that the damage observed in P7R7 may or may not have been solely caused by thermal effects. Further refinement of the upper and lower bounds may provide additional clarity but is not a high priority activity. It is expected that thermal effects contributed to the damage but were likely not the sole cause. Mechanisms such as combustion in the room, flame propagation, ember transfer, burning drips of melted polymer, and hot solid material ejected from the drum may also have contributed to the spreading of thermal damage. The potential contribution of those alternative mechanisms is consistent with REACH findings.

Reduced Ventilation

Examination of the waste array geometry (Figure D-53) reveals the waste containers to be very tightly packed. Many waste drums are contained in Standard Waste Boxes (SWBs), Standard Large Boxes (SLB2s) and 10-Drum Overpacks (TDOPs) further restricting airflow around the waste drums. These containers are vented to avoid pressurization in transit but the air within them is essentially stagnant and would be unaffected by changes to the ventilation in P7R7.

Drum 68660 is contained in a 7-pack. It is packaged closely with 6 other drums with polyethylene slip sheets above and below. The 7 drums are wrapped in cellophane further restricting air flow.



Figure D-53. Waste Face at Panel 7 Room 7

The surface temperature of a chemically active waste drum such as 68660 is expected to rise less than 1°C prior to thermal runaway (Hobbs¹⁴). This small temperature difference is not expected to drive significant natural convection currents which could be affected by changes to ventilation in P7R7. If reduced ventilation were sufficient to initiate a radiological release event, similar drums packaged in SWBs would have likely ruptured prior to February 14. Therefore, it is concluded that the reduction in ventilation in P7R7 due to the truck fire event would have had a negligible impact on the heat transfer environment of Drum 68660 and is unlikely to have contributed to the release event.

Duration of the Release

This analysis is an attempt to infer the duration of the release event. The analysis is in two parts: 1) the transient record from CAM151 is considered and 2) the activity of filters changed at stations A and B at the surface in the days following the release is examined.

The first part of the analysis looks at the transient record recorded by CAM151. Subsequent to completion of an initial analysis, it was learned that CAM151 stopped functioning around midnight of the day of the release. The analysis assumes perfect mixing of a representative sample of the material added to the ventilation air from the drum release. Turbulent diffusion in the flow-wise direction would stretch the time interval of a concentration passing CAM151. A calculation was performed that accounts for axial movement of the material due to diffusion. The analysis is complicated by the fact that the flow speed was promptly reduced by approximately a factor of 20 when the alarm was received. The signal from CAM151 endured for about 3300s. The analysis indicates that a continuous ten second release results in a signal shorter than the CAM151 data while the 100s release clearly produces a longer signal. The consequence of the CAM151 signal ending is that this diffusion analysis cannot be used to suggest an upper limit to an interval of material release at Drum 68660.

A plot of the relative activity of filters removed from Stations A and B at the surface in the days following the release shows a very dramatic decrease in the count rate for about one and half days. After that interval of rapid decrease the count rate decreases much more slowly. Due to the large volume of the mine system and the large distance between the release and the filters a period of a day or so (several air exchanges) would be expected to entirely clear a well-mixed gas from the mine. The sharp decrease in filter load after 1.5 days implies that significant release of material ended at some point before that. Filter load in days following the initial 1.5 days was likely associated with slower processes re-suspending material deposited on mine surfaces.

CAM151 Analysis Considering Turbulent Diffusion in the Flow-wise Direction

Figure D-54 shows the recorded signal from CAM151 which samples air leaving Panel 7. This sensor was the initial indication of the release on February 14. Based on Figure D-54, it appeared that radioactive contaminant passed CAM151 for approximately 3300s. Reynolds numbers associated with flows in mine corridors indicate turbulent flow conditions. In the presence of such turbulence the diffusion of a contaminant in the flow-wise direction is many orders of magnitude greater than diffusion in quiescent air. Consequently, if there were a release of short duration at the waste array the “signal” 600 feet away at CAM 151 would be “stretched.” This analysis attempted to demonstrate that the release event was of short duration.

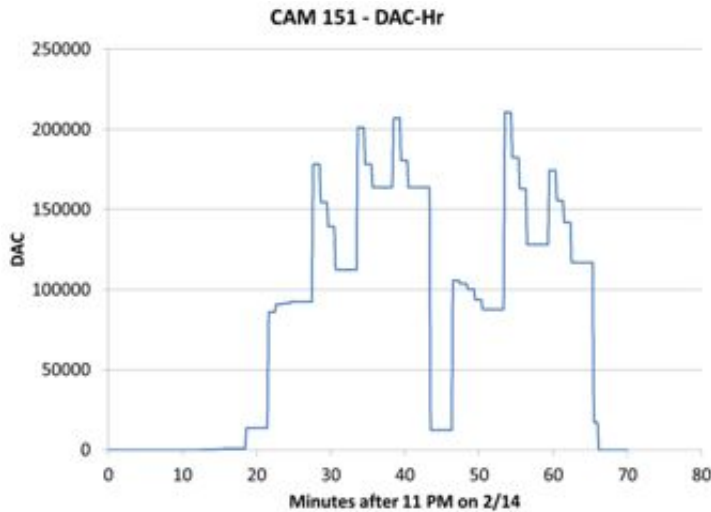


Figure D-54. Transient Count Record from CAM151^{oo}

A turbulent diffusion calculation was used to estimate the degree to which material released into the air in P7R7 would diffuse in the flow-wise direction before reaching CAM151. The ventilation data indicated that the airflow through Panel 7 dropped promptly when CAM151 sounded off (Figure D-55). This analysis uses superposition of an analytical solution to the 1-d advection/diffusion equation.

The concentration (Socolofsky & Jirka) from a small release diffused and advected in one direction is^{pp}:

$$C(x, t) = \frac{M}{\sqrt{4\pi Dt}} \exp\left(\frac{-(x-Ut)^2}{4Dt}\right) \quad (15)$$

In order to simulate a continuous constant release for an interval of time the total release can be divided into a series of N releases and the result of superposition used at the time and position of interest. Consider position L away from the constant source of duration T and represent the release as N small releases distributed over the time interval.

$$\dot{M} = \frac{M}{T} \quad (16)$$

$$C(L, t) = \sum_{i=1}^{N^*} \frac{M/N}{\sqrt{4\pi D\hat{t}_i}} \exp\left(\frac{-(L-U\hat{t}_i)^2}{4D\hat{t}_i}\right) \quad (17)$$

where

^{oo} U.S. Department of Energy Office of Environmental Management Accident Investigation Report, *Phase 1 Radiological Release Event at the Waste Isolation Pilot Plant February 14, 2014*, April 2014.

^{pp} S. A. Socolofsky and G. H. Jirka, "Chapter 2, Advective Diffusion Equation," [Online]. Available: <https://ceprofs.civil.tamu.edu/ssocolofsky/cven489/Book/Book.htm>.

$$\hat{t}_i = t - (i - 0.5)T/N, \quad (18)$$

D is the diffusion coefficient, M is the total mass released⁹⁹, and U is the flow speed.

$$N^* = \begin{cases} N & \text{for } t \geq T(1 - 1/[2n]) \\ \text{INT}\left(\frac{Nt}{T}\right) & \text{for } t < T \end{cases} \quad (19)$$

The variable upper limit on the summing allows for investigation of times less than the duration of the release.

The foregoing is sufficient to estimate $C(L, t)$ for constant conditions. In the present case the release is occurring during an initial interval of $U = U_1$ followed by an interval of $U = U_2$ that occurs when $C(L, t^*) > C_{\text{detect}}$. This time, t^* , could be less or greater than the release interval T . In any case, at t^* the spatial interval $0 < x < L$ has an existing concentration distribution and the speed changes abruptly to U_2 .

To continue past t^* in time we can represent the existing distribution as a spatially distributed series of releases that occurred at $t = t^*$. At position L for $t > t^*$:

$$C(L, t > t^*) = C_{\text{source}} + C_{\text{inventory}} \quad (20)$$

C_{source} is contribution from continued release at the source (this will be zero if the full release has occurred before t^*). If $t^* < T$ C_{source} is:

$$C_{\text{source}} = \sum_{i=N_1}^{N^*} \frac{M/N}{\sqrt{4\pi D \hat{t}_i}} \exp\left(\frac{-(L-U_2 \hat{t}_i)^2}{4D \hat{t}_i}\right) \quad (21)$$

where N_1 is time position of the first release to occur after t^* . The time after the flow slows is:

$$\tilde{t} = t - t^* \quad (22)$$

and the inventory in the pipe is represented as releases that occurred at \tilde{t} . So

$$C_{\text{inventory}} = \sum_{j=1}^J \frac{\delta x C(x_j, t^*)}{\sqrt{4\pi D \tilde{t}}} \exp\left(\frac{-([L-x_j]-U\tilde{t})^2}{4D \tilde{t}}\right) \quad (23)$$

where the “pipe” is broken into J segments and

$$\delta x = \frac{L}{J} \quad (24)$$

$$x_j = (j - 0.5)\delta x \quad (25)$$

⁹⁹ This one-dimensional system does not include the cross-sectional area so a unit of mass here is 1 gm/m². For each case studied a total of 1 gm/m² was released.

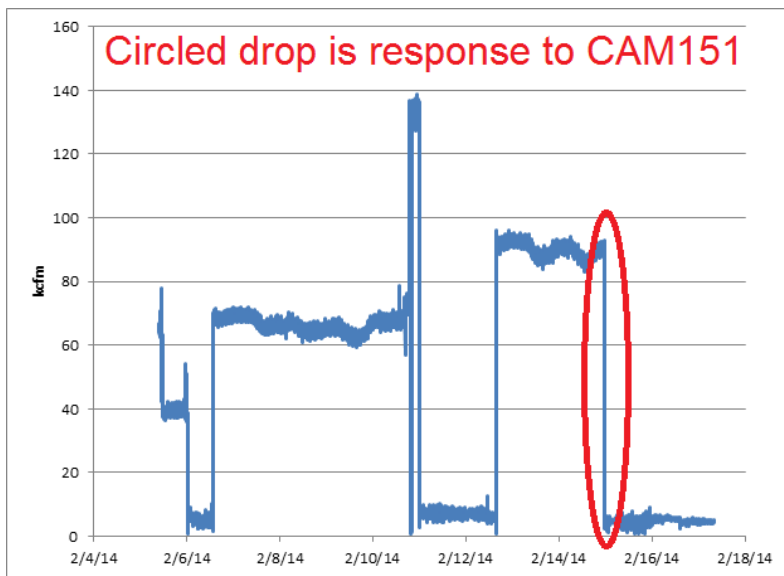


Figure D-55. Plot of panel 7 airflow from Ted Wyka supplied spreadsheet^{††} (Wyka)

Figure D-56 presents a graph of $D_{xx}/(Ud)$ from various investigators [3] for turbulent pipe flows where D_{xx} is the turbulent diffusivity. The following table also summarizes the diffusivity for the two flow conditions based on the air flowrates shown in Figure D-55.

Description	High Flow	Low Flow
Volumetric Flow	90.26 kcfm	4.35 kcfm
Mean flow Speed	0.872 m/s	0.0420 m/s
Reynolds Number	386,000	18,600
$D_{xx}/(Ud)$	0.121	0.263
D_{xx}	0.687	0.0721

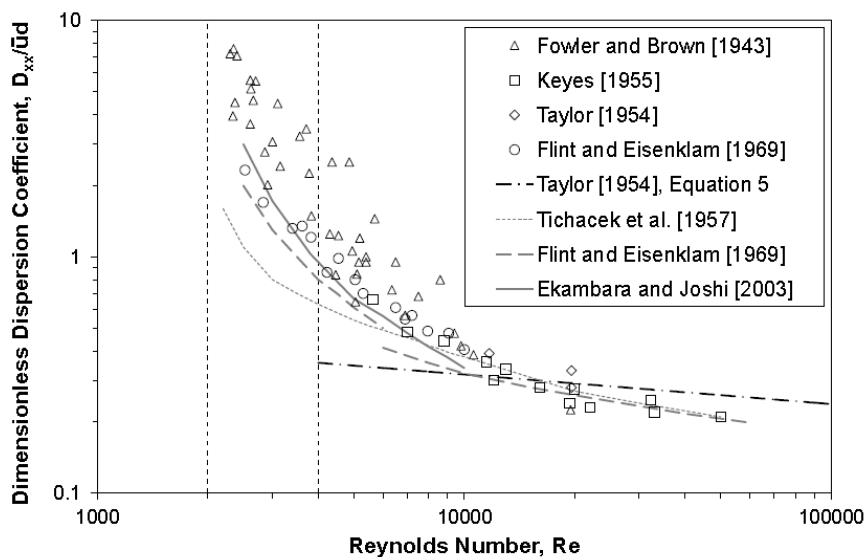


Figure D-56. Summary of flow-wise dispersion coefficients from various investigators^{SS}

^{††} T. Wyka, Email supplying underground airflow data at WIPP in response to action item generated at LANL meeting on Aug 18 and 19.

The superposition method was used to estimate the concentration history (in relative mass) at CAM151. An arbitrarily small detection concentration threshold was set at $1 \times 10^{-4} \text{ gm/m}^3$ times.

Figure D-57 shows the predicted concentration histories at CAM151 for release times of 10, 100, 300, and 1000s. At the time of detection the flow slows and the more complicated superposition solution (Equations 21 and 23) is used. For the short release times considered (10s and 100s) the whole release event has occurred before detection so $C_{\text{source}} = 0$. For the 300 and 1000s release times the character of the concentration estimate is rich and shows clear features due to both the inventory in the flow passage at t^* and the release that continues after t^* .

In all cases, the area under the predicted concentration curve conserves mass. That is:

$$U_2 \int_0^{8000s} C(L, t) dt = 1 \text{ gm/m}^2 \quad (26)$$

Based on the assumptions of this model and the recognition of a very slow flow speed *immediately* following detection, flow-wise dispersion is very significant. An enduring release, say greater 200s, would be stretched out for several thousand seconds by the time it has slowly traveled from Panel 7 to CAM151. A rapid release, on the other hand, will contaminate a shorter interval of flow in the passage. Further, a greater fraction of a rapid release will have occurred before detection at CAM151.

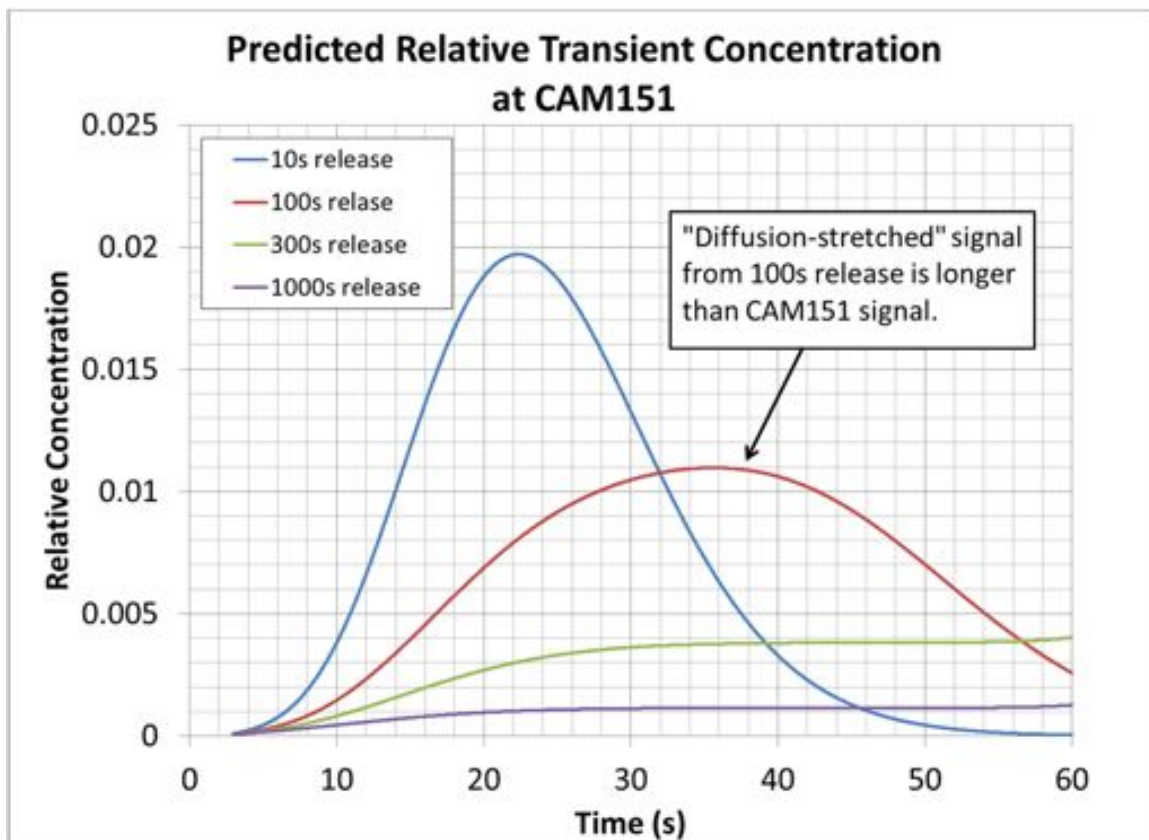


Figure D-57. Predicted transient concentration at CAM151 for various release time intervals

The signal from CAM151 endured for about 3300s. As shown in Figure D-57, the ten second release results in a signal shorter than the CAM151 data while the 100s release clearly produces a wider signal.

^{ss} J. Hart, I. Guymer, A. Jones and V. Stovin, "Longitudinal Dispersion Coefficients within Turbulent and Transitional Pipe Flow," in *Experimental and Computational Solutions of Hydraulic Problems*, 32nd International School of Hydraulics, pp. <http://link.springer.com/book/10.1007/978-3-642-30209-1> .

As noted earlier, this analysis is substantially discredited by the likelihood that the signal end in Figure D-54 is only due to the sensor stopping. Consequently, the radiological signal is not a clear indication of a short release duration from Drum 68660. Even if the release were very short, the deposition and resuspension of the contaminant that may occur is complicated. The foregoing idealization is the simplest possibility.

Analysis of Filters A and B Activity in Days Following the Release

Figure D-58 shows a plot of activity of filters for Stations A and B from the days after the release as documented on the Department of Energy website^{tt}. The source document alludes to multiple methods of the filter analysis. Figure D-58 presents the reported numbers without further consideration of the analysis method. The reported information gives time of analyzed filter removal. Figure D-58 shows the activity per day of filter residence presuming no delay between the removal and installation of successive filters. The scatter plot makes clear that the radioactivity load in the filters drops orders of magnitude in a few days’ time and then levels out. For the first couple of days the activity rate for Beta or Alpha at Station A and for Alpha at Station B drops by approximately an order of magnitude per day.

It appears from this data that any radioactivity released in the mine was confined to a short (<~1 day) interval of time. The actual processes conveying released material from P7R7 to the surface filters was complicated. For a contaminant that remains well-mixed in a volume, the concentration decreases ten-fold for every 2.3 (LN(10)) exchanges of air. Of course, the WIPP mine system did not remain well-mixed between the release site and the exits which would delay the dilution process. Consequently, significant release must have been confined to a period of time short relative to one day in for the “signal” at the filters to decay several orders of magnitude in just the first few days.

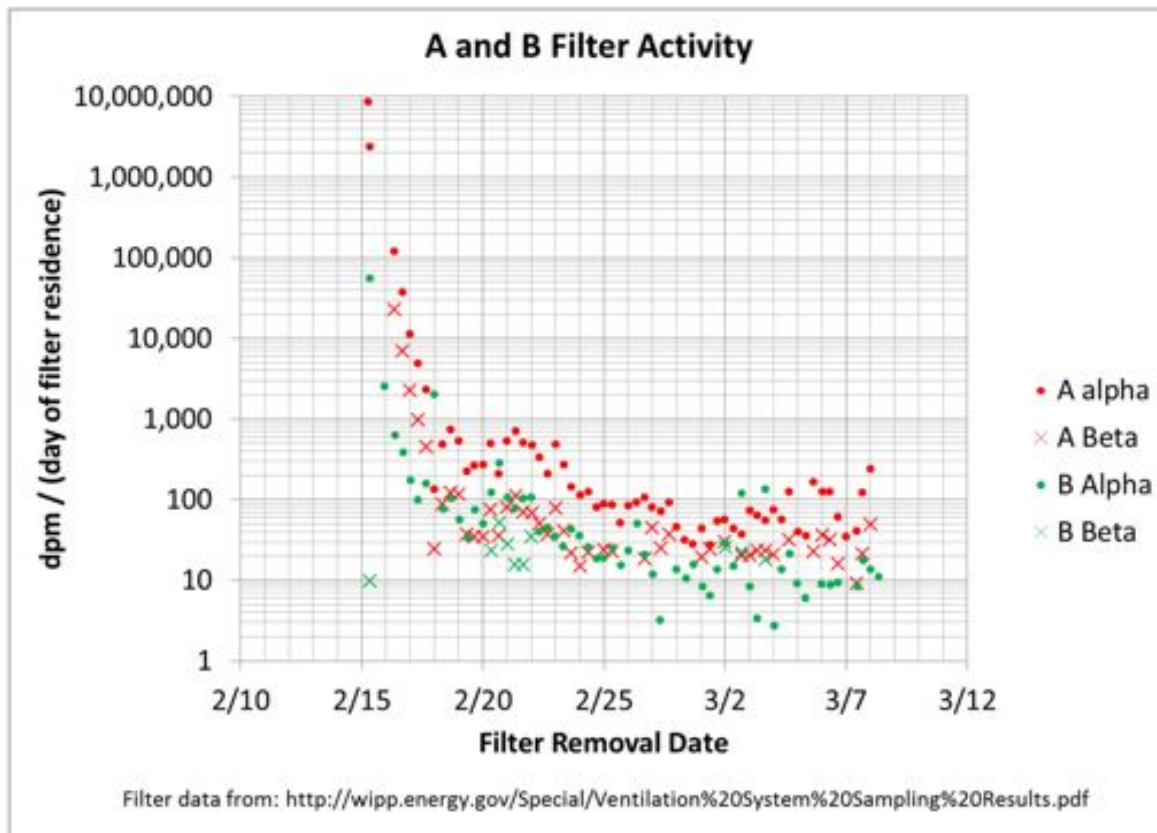


Figure D-58. Beta and alpha counts from filters at the surface in days following the release

^{tt} <http://wipp.energy.gov/special/ventilation%20System%20Sampling%20Results.pdf>

Conclusions

Thermal and humidity stimuli to the waste array resulting from the February 5 salt haul truck fire were considered and it appears that the release event of February 14 was not initiated by the fire. Other analyses examined the plausibility of important physics mechanisms that are consistent with the visual observations at the release site available through the early (May-June) inspections. It is plausible that hot issuing gaseous products from Drum 68660 spread to the approximate known damage footprint. However, as MgO bags were demonstrated to be flammable, it is not necessary that the hot eruption cover the extent of the damaged area. Nothing discovered in these analyses contradicts the hypothesis that exothermic reactions in Drum 68660 led to the release and the observed damage in the waste array.

APPENDIX E. DRUM CHARACTERIZATION INTEGRATED SUMMARY REPORT

DRUM HISTORY

Summary Conclusion

No evidence has been found to suggest Drum 68660 was processed, handled, transported, or stored any differently from other processed LANL MIN02 waste drums. A study of the physical and environmental effects this drum experienced during its lifetime was performed and documented to make this conclusion. Data were acquired from several sources, including Waste Characterization, Reduction, and Repackaging Facility (WCRRF) waste packaging reports, Real Time Radiographic (RTR) videos, Los Alamos spreadsheets prepared during their investigations, and conversations with multiple individuals. The timeline is being used to understand the sequence of events, and as input into the drum chemistry modeling efforts.

Also included was a determination of detailed inventory for the contents of the drum based on historical knowledge for the processes resulting the original MIN02 waste salts, WCRRF processing waste packages, post-processing RTRs, and Central Characterization Project (CCP) high efficiency passive neutron counter (HENC) used to perform non-destructive assays of the drums before placement into the WIPP repository. The drum inventory also supports the investigation into possible chemical reactions leading to the event.

Process history for recovery of plutonium

The MIN02 waste salts were produced during TA-55 evaporator operations which was used to minimize bulk volumes of anion exchange (AEX) effluents produced during the recovery of plutonium. Among the evaporator feed solutions relevant to this investigation generated from AEX effluent are the lean residue feed (LR), rich residue feed (RR), distillate solution feed (DS), or the filtrate from oxalate precipitation (OX) on the AEX plutonium effluent solution. The designator IXFS was used prior to LR/RR/DS to generally identify nitric acid ion exchange evaporator feed solutions. These designators were used as part of a naming convention to allow the evaporator feed that produced a certain bag of salt to be identified back to the process used to recover the plutonium. According to LANL documentation and procedures, 500-600 L of feed was reduced to 10-25 L of "bottoms". [MST-12 Procedure 485-REC-R00 and 485-REC-R01]. The "bottoms" were cooled to room temperature which produces the nitrate salts and a liquid supernate. The liquid was separated from the salts by filtration using a 200 mesh stainless steel screen. After filtration, the salts were vacuum dried. This process consisted of pulling air through the salts using house vacuum for approximately 15 minutes. After 1985 procedures were modified to allow for washing of the salts to meet an Economic Discharge Limit (EDL). Although it was not consistently documented it was felt by LANL personnel that it was likely that the nitrate salts produced in the 1980s onward were washed with concentrated or 7 M nitric acid as needed to meet the EDL. Nitrate salts produced from oxalate precipitation were washed with water. It was cautioned in the procedure to do this to prevent "...decomposition of any oxalic acid present in the salts and could result in pressurization of the sealed 55-gallon drum containing the salts." The "dried" salts were placed into a plastic bag and a grab sample, possibly from multiple places within the bag, was taken for americium and plutonium analysis prior to the bag being sealed. The sealed plastic bag was then double bagged, bagged out of the glovebox, and placed into a waste drum. These waste drums are the parents of the processed daughter drums produced during the recent campaign at LANL, a sub-set of which were placed in WIPP Panel 7 for permanent storage.

From the designators for the evaporator feeds general assumptions as to the make-up of the salts can be made.

First, when plutonium material is collected using anion exchange the liquid effluent contains most of the americium. Therefore when the liquid effluent is run through the evaporators it produces salts with high Am/SNM (Pu239 and Pu240) ratios. These are the LR and RR items from 1985 and forward. Before 1985 they are the IXFS items. When the Pu on the columns is removed and precipitated with oxalic acid the resultant liquids filtered off of the oxalate precipitates are very low in americium and the salts produced from evaporation have a low Am/SNM ratios. These salts have the OX or UOX designator in their sample identifiers. This information as well as historical analytical data for the salts was used for the evaluation for source term.

Secondly, typically 10 – 20% oxalic acid was used for the oxalate precipitation process. The excess oxalic acid remains in the solution sent to the evaporators. LANL analysis of the OX and UOX salts suggests that the majority of the oxalate does not precipitate upon evaporation. This means most of the oxalate remains in the post-evaporator liquid that was filtered off for processing by cementation. However, the salt's interstitial liquids would contain oxalate. Therefore, the amount of oxalate remaining with the nitrate salts depends upon how much liquid remains with the precipitated salts. This is considered to be a low weight percent of the total salt mass. This information assisted in the effort to identify and model possible chemical reactions during this investigation.

Thirdly, 1995 LANL characterization of LR, OX, and DS evaporator feed bottoms provided information as to the general chemical makeup of these salt types for use in the study of models for chemical reactivity.

Drum History

Drum 68660 was produced as part of the processing of parent drum S855793 (identified as drum S855793 in the WCRRF package). Radiography indicated the presence of liquid in the 55 gallon drum leading to the required processing. Two sibling drums were produced during processing, 68660 and 68685. Drum 68660 was shipped to WIPP. Drum 68685 remains at Los Alamos.

Figure E-1 depicts the processing and indicates the materials placed in each of the sibling drums. Drum 68660 received all of the observed 2 gallons of processed liquid (nitric acid, TEA, Swheat Scoop®), one process facility tungsten/bismuth/lanthanum-impregnated glovebox glove, job control solid waste (empty TEA bottles), and some of the processed nitrate/oxalate salts. The material is in three layers, and the drum is ~60% full. It should be noted that the WCRRF processing package for this parent drum recorded that glovebox gloves (plural) were added to 68660; however, a single glove was visually identified by an expert RTR operator at INL during review of the original RTR (See Addendum A to this appendix).

Drum 68685 received the remainder of the processed nitrate/oxalate salts (salts and Swheat Scoop®) as well as the lead blanket. It is approximately 85% full.

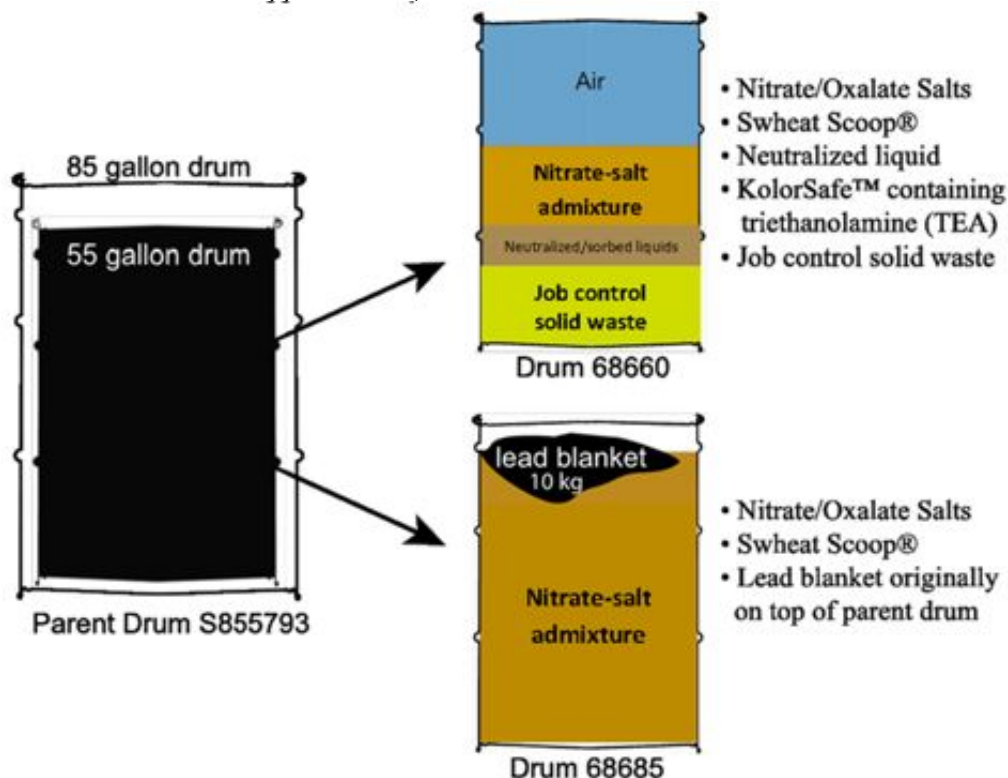


Figure E-1. Processing of parent Drum S855793 to produce sibling Drums 68660 and 68685

Figures E-2 and E-3 show the timeline for Drum 68660. Figure E-2 presents the data in flowchart form. Figure E-3 shows the actual timeline. Drum 68660 was produced December 4, 2013. It remained at Los Alamos until January 2014 when it was shipped to WIPP (January 28-29). It was placed in Room 7 Panel 7 two days later on January 31. On February 14, 2014, Drum 68660 breached and resulted in a radiation release.

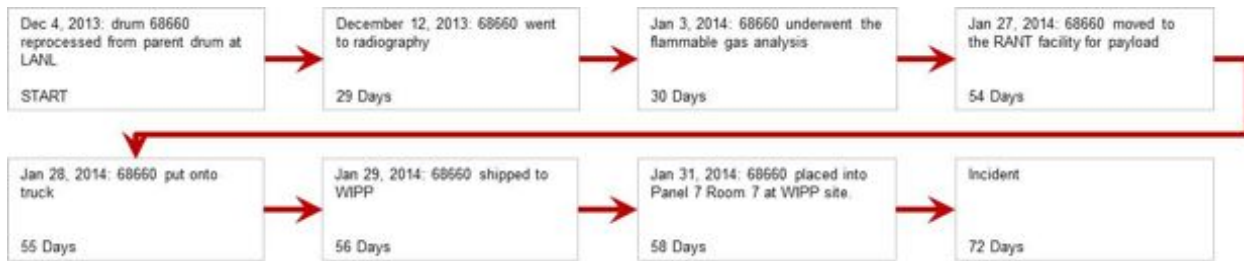


Figure E-2. Flowchart showing processing of Drum 68660

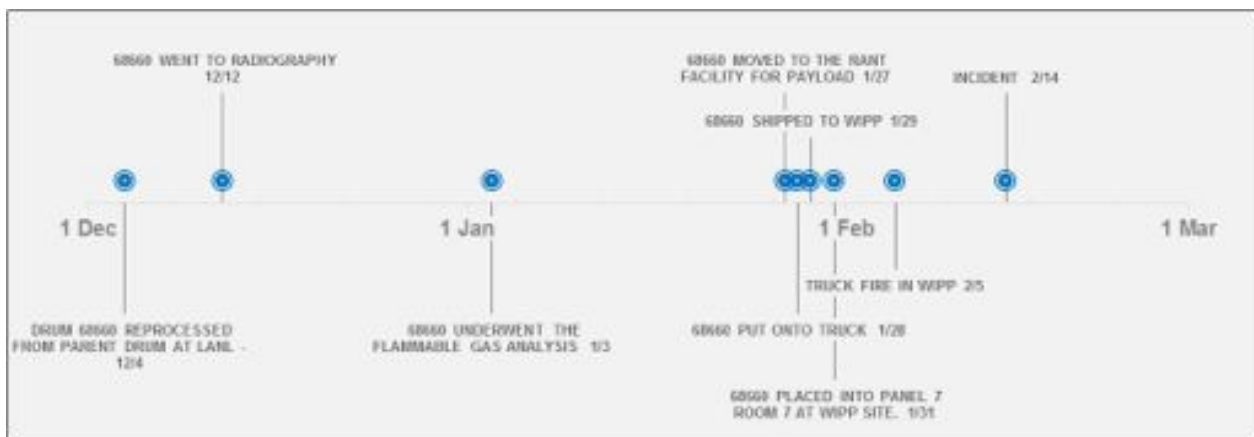


Figure E-3. Timeline for Drum 68660 from inception to the release event.

Drum Contents

Figure E-4 shows the assumed contents of Drum 68660. The yellow job control solid waste layer contains 5 kg of rubber and 6 kg of plastics. This layer also contains at least one glove of unknown composition (assumed to be tungsten-lined based on LANL information). The volume of the job control solid waste layer is 0.0403 m³ (13 gallons) and has a density of 273 kg-m⁻³. This layer is assumed to be nonreactive in the finite element model. The brown “Swheat Scoop®” layer is subdivided into two layers: 1) the processed liquid layer and the 2) nitrate salt layer. The detailed content of the drum was assessed by performing a mass balance for the parent (S855793) and both sibling drums (68660 & 68685). The major assumptions used in this analysis are shown in the bottom of Figure E-4.

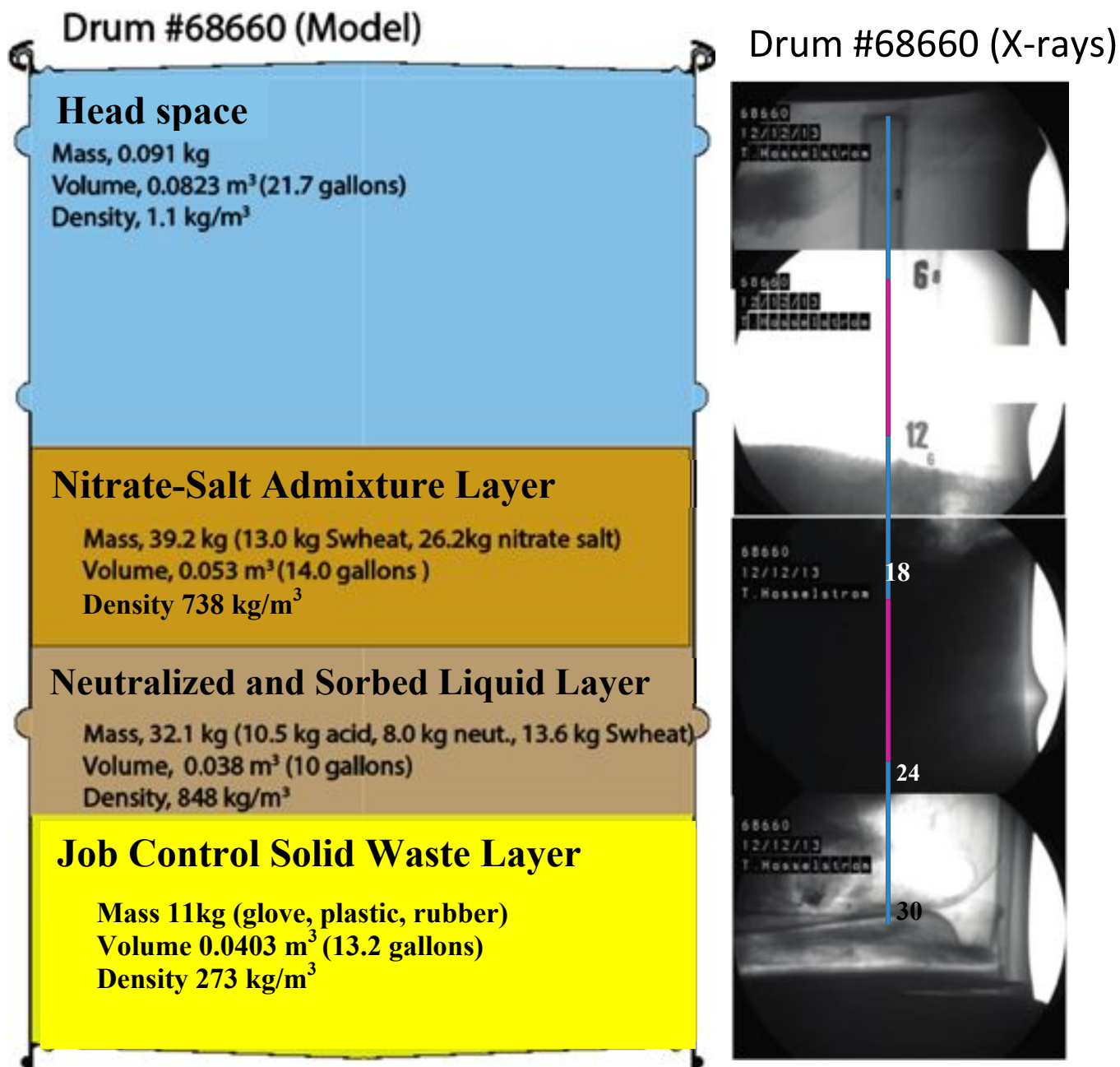


Figure E-4. TAT Model of Drum 68660 contents and distribution based on x-rays of Drum 68660

The content of Drum 68660 shown in Figure E-4 was determined with an overall material balance as given in Table E-1 using the assumptions listed in Table E-2. Table E-1 shows the net weight, which is the total mass minus the container mass composed of the drum steel, a plastic liner bag, and a fiberboard liner. The combined volumes of the processed layers were estimated from X-rays, which are partially shown in Figure E-4. The X-ray image in Figure E-4 was stitched together from an X-ray video and only shows the edge of Drum 68660. The combined processed salt and liquid layer volume probably ranges between 0.08-0.10 m³ since the layer interfaces are not sharp. The Swheat Scoop® bulk density is higher than the optimal density mentioned in the Swheat Scoop® patent (550 kg/m³) and is closer to 600 kg/m³ based on measurements of large quantities of Swheat Scoop®. The higher density is due to settling in the larger volumes. The Swheat Scoop® moisture content is typically between 10-13% at the manufacturing facility and loses about 2% moisture when it is shipped to dry environments such as New Mexico. This would make the moisture content range between 8 to 11% on a mass

basis. We have chosen 10% to be the moisture content in Swheat Scoop®. An overall mass balance was used to determine the total mass of Swheat Scoop® used to process the waste in the parent drum.

Two gallons of liquids were decanted from the nitrate salts in parent drum S855793. The two gallons of decanted liquids were composed of 3.3-molar nitric acid with dissolved nitrate salts. The two gallons of decanted liquids were neutralized with 2 gallons of 3.3-molar TEA making a total of 0.015 m³ (4 gallons) of liquid that was absorbed using Swheat Scoop®. The *Swheat Scoop® to liquid* volume ratio was assumed to be 3:1 based on experience in our laboratory where large amounts of Swheat Scoop® were required to fully absorb liquid. The remaining mass of Swheat Scoop® was mixed with the nitrate salts that were distributed between sibling drums 68660 and 68685 giving a *Swheat Scoop® to nitrate salt* volume ratio of 0.7:1. This ratio is lower than the specification of 1.2:1 for zeolite absorbents.

The 11 kg of nonreactive job control solid waste was added to the bottom of Drum 68660 and included a tungsten glove, at least one empty TEA bottle, and plastic bags. The “waste” above the job control solid waste layer in 68660 is subdivided into two reactive layers: a *processed liquid layer* directly above the job control solid waste layer and a *processed nitrate salt layer* above the processed liquid layer. The space above the processed nitrate salt layer is filled with air. The volume and density of each of these layers is given in Figure E-4. The estimated contents of the processed salt layer and processed liquid layer are given in Tables E-3 and E-4, respectively. Table E-3 has a detailed description of the composition of the nitrate salts. Weisbrod estimated the composition of the nitrate salts by starting with Veazey salt analysis. Weisbrod conducted a series of evaporation simulations using Stream Analyzer© from OLI Systems. Table E-3 also lists a simplified composition for the nitrate salts. Measured solubility data at our laboratory were used with this simplified composition to determine the amount of nitrate salts that were dissolved into the decanted liquid as shown in Table E-4.

Table E-1. Parent and sibling drum mass balance

Name	Weight, kg	
Parent (S855793)		
Nitrate salts	115.91	
Decant liquid (3.3 molar HNO ₃ with dissolved nitrate salts)	10.48	
lead blanket (on top of drum)	9.98	
68725 net weight	136.37	
External materials added to parent waste		
Neutralizer (3.3 molar triethanolamine)	7.97	
Room trash (tungsten glove, plastic bottle, etc.)	11.00	
Swheat (10% moisture)	71.34	
External material net weight	90.31	
Sibling (68660)		
Nitrate salts	26.16	Remediated
Swheat (3:1 Swheat to liquid ratio by volume)	13.63	salt layer
Decant liquid (3.3 molar HNO ₃ with dissolved nitrate salts)	10.48	Remediated liquid layer
Neutralizer (3.3 molar triethanolamine)	7.97	
Swheat (0.7:1 Swheat to salt ratio by volume)	13.03	
Room trash	11.00	Trash layer
68660 net weight	82.27	
Sibling (68685)		
Nitrate salts	89.75	
Swheat (0.7:1 Swheat to salt ratio by volume)	44.68	
Lead blanket	9.98	
68685 net weight	144.41	
Mass parent + Mass external materials	226.68	✓
Mass 68660 + Mass 68685	226.68	✓

Table E-2. Assumptions regarding Swheat Scoop® and processed liquid

Assumption	Source	Notes
Processed layer volumes in both sibling drums (68660 and 68685)	Estimate from X-rays	X-ray of 68660 and 68685.
Swheat bulk density	Swheat patent (5,690,051 on 11/25/97) and measurements	We measured 550 kg/m ³ in small samples and 650 g/m ³ in larger samples. 600 g/m ³ is assumed to be the nominal density
Swheat moisture	Charles Neece (Pet Care Systems representative)	As shipped moisture content is 10-13%. In dry climates, this drops by 1-2%. The moisture content in NM is assumed to be 8-11 wt%.
Swheat:salt and Swheat: liquid volume ratio	Mass Balance and assumed volume ratio for Swheat:liquid.	The overall Swheat mass was determined by a parent to sibling mass balance. The volume ratio for the Swheat:liquids was assumed to be 3:1. The Swheat:nitrate salt volume ratio was calculated to be 0.7:1.
Neutralizer volume and molarity	Estimate	X-ray pictures showed a one gallon plastic neutralizer container in the trash layer. Two gallons of neutralizer is a conservative estimate with molarity between 1-5 mols/L (3.3 mols/L used in the current work).
Molarity of nitric acid	Determined from amount of neutralizer.	Assumed to be the same as the neutralizer.
Nitrate salt composition	Kirk Weisbrod analysis	Determined from "stream analyzer" simulations assuming 1) analysis of source waste, 2) stream ratios stored in parent drum, and 3) amount of liquid retained with solid crystals.

Table E-3. Processed salts in 68660^a

Composition	Detailed	Simplified
	Mass, kg	Mass, kg
Dry wheat in Swheat	11.72	11.72
H ₂ O in Swheat	1.30	1.30
H ₂ O (with trace elements)	0.05	
Al(NO ₃) ₃ * 9H ₂ O	0.62	
Ca(NO ₃) ₂ * 4H ₂ O	2.48	2.70
KNO ₃	0.54	
Mg(NO ₃) ₂ * 6H ₂ O	16.30	17.74
NaNO ₃	3.58	3.89
Ni(NO ₃) ₂ * 6H ₂ O	0.02	
Pb(NO ₃) ₂	0.00	
(COOH) ₂	0.40	
Cr(NO ₃) ₃ * 9H ₂ O	0.03	
Fe(NO ₃) ₃ * 9H ₂ O	1.69	1.84
HNO ₃	0.40	
NaF	0.05	
Total	39.19	39.19

^aVolume of this layer is 0.053 m³

Table E-4. Processed liquids in 68660^{a,b}

Composition	Mass, kg
Dry wheat	12.26
H ₂ O in Swheat	1.36
H ₂ O in decant	3.13
HNO ₃ in decant	1.57
Nitrate salts ^b in decant	
Ca(NO ₃) ₂ * 4H ₂ O	0.54
Mg(NO ₃) ₂ * 6H ₂ O	4.27
NaNO ₃	0.54
Fe(NO ₃) ₃ * 9H ₂ O	0.43
TEA in neutralizer	3.73
H ₂ O in neutralizer	4.25
Total	32.08

^aRemediated liquid layer volume is 0.038 m³.

^bBased on measured solubility with composition based on most common salts.

Salt and Radiological Content in 68660

From the evaluation for source term there was an inference that the 14 individual salt bags in parent drum S855793 were mixed and processed with Swheat Scoop® as one batch prior to placement into the two sibling containers. From this finding the salt content can be determined accurately using the historical analytical data for each of the salt bags and the estimated mass of salts modeled to be in 68660 as described above. Table E-5 contains the material types, net weight of salts, and Pu and Am analytical information for each of the bags of MIN02 salts stored in parent container S855793 based on historical records.

Table E-5. MIN02 Salts in S855793 (Daughters 68660 and 68685)

Salt ID	MT	net (Kg)	Pu239 (g)	Pu240 (g)	Am241 (g)
10LALR1W	53	5.94	3.23	0.35	0.49
10LR5W1	53	4.8	0.47	0.05	0.12
10LR5E1	53	9.71	1.56	0.17	0.48
10LR16W1	53	8.6	2.20	0.20	0.50
10LR16E1	53	7.4	0.59	0.05	0.31
10LR17W1	53	7	0.71	0.06	0.40
10LR17E1	53	7.2	0.33	0.03	0.21
10RR18E1	52	9.68	4.08	0.25	0.39
10OX11W1-1	52	9.96	7.71	0.49	0.37
10OX11W1-2	52	10.97	8.49	0.54	0.41
10LR18E1	52	7.5	1.10	0.07	0.13
10LR18W1	52	12.93	2.13	0.14	0.39
10OX21E1	52	9.6	1.24	0.08	0.14
10OX21W1	52	15.1	2.27	0.15	0.08
Total		126.4	36.12	2.63	4.41

Nine bags of salts (71.08 Kg) were produced from lean residues anion exchange feeds ("W" designates washes and "E" designates effluents). One bag (9.68 Kg) from rich residue anion exchange feed. And, four bags (45.63

Kg) from the anion exchange plutonium effluent after oxalate precipitation. Mixing these materials then placing 26 kilograms of salts into 68660 as predicted by the WIPP TAT models would result in the following inventories of salt types and Pu and Am isotopes shown in Tables E-6 and E-7 below. Also included in Table E-3 is the heat generated in the salts from radiolytic decay for each of the isotopes based on the masses listed. The Decay Heat constants used were 1.9, 6.8, and 114 W/Kg for Pu239, Pu240, and Am241 respectively.

Table E-6. Inventory of Nitrate Salt Types in Drum 68660

LR Feed Salts (Kg)	RR Feed Salts (Kg)	OX Precip. Feed Salts (Kg)
14.6	2.0	9.4

Table E-7. Pu and Am Inventory and Radiolytic Heat Generation from the Salts in Drum 68660

Pu239 (g)	Pu240 (g)	Am241 (g)
7.43	0.54	0.91
Decay Heat (W)		
0.014	0.004	0.104

These inventory values are based on the data as measured at the time of generation of the parent. At the time of processing and generation of the daughter drums there was 2 gallons of free liquid recorded to be in the parent which separated from the wet vacuum dried salts. The number and identification of which salt bags this liquid separated from is unknown so it should be noted that the loss of liquid weight will have an impact on the weights listed for each of the salt types in Table E-5 and the Decay Heat estimates in Table E-6. Assuming 3.3M HNO₃ and a density of 1.12 g/mL, 2 gallons of liquid would weigh 8.5 Kg. This is 6.7% of the total salt mass and would therefore have to come from multiple bags of the salts as all but one contained salts weights less than this.

The 2 gallons of processed liquid mixed with Swheat Scoop® and bagged separately was placed into 68660. Shown in Table E-8 are the historical Am and Pu analysis of the liquids leftover after flash evaporation of the waste streams. These liquids were removed for disposal by cementation however the results would be analogous to the activities in the interstitial liquid present in the moisture content of the vacuum dried salts. Note that if liquids were to be observed within a salt bag during processing the operators would have classified it a “containerized” liquid. That liquid would have been drained from the bag and processed with Swheat Scoop® separately from the salts. No such comment was recorded in the records for the processing of S855793.

Table E-8. Am and Pu Activity Concentrations Analyzed in the Liquids Phases after Flash Evaporation

Liquid from Salt ID	Pu239 (Ci/L)	Pu240 (Ci/L)	Am241 (Ci/L)	Pu+Am (Ci/L)
10LALR1W	0.055	0.14	1.23	1.43
10LR5W1	0.009	0.02	0.35	0.39
10LR5E1	0.019	0.06	1.07	1.14
10LR16W1	-	-	-	-
10LR16E1	0.007	0.02	0.72	0.75
10LR17W1	0.006	0.02	0.64	0.66
10LR17E1	0.005	0.01	0.69	0.71
10RR18E1	0.032	0.14	0.64	0.81
10OX11W1-1	0.004	0.02	0.06	0.08
10OX11W1-2	-	-	-	-
10LR18E1	0.009	0.04	0.36	0.41
10LR18W1	0.010	0.04	0.49	0.54
10OX21E1	0.011	0.04	0.24	0.29
10OX21W1	0.012	0.05	0.11	0.17

Analytical information missing for two liquids (10OX11W1-2 is a duplicate of 10OX11W1-1). Missing data not considered to have a major effect on the evaluation for an estimate of total activity in the 2 gallons of processed liquid.

To create a working range of isotopic Pu and Am activities to consider for the processed liquid it was simply assumed first that all of the individually bagged salts contributed equally to the free liquid volume, then the seven salts with the highest level of interstitial liquid activities contributed equally to the free liquid volume, and lastly, for the low range, seven of the lowest activity liquids. For the liquids with missing activities it was assumed 10OX11W1-2 equaled that of 10OX11W1-1 and 10LR16W1 equaled that of 10LR5W1 which is reasonable as the first can be considered a duplicate sample based on its identifier and the other a feed stream similar to the known (LR wash), again based on the identifier. The ranges for Pu and Am mass inventory and the associated radiolytic heat generation are listed in Table E-9 below.

Table E-9. Ranges for Pu and Am Inventory and Radiolytic Heat Generation in Drum 68660 Processed Liquid

All Salts Contributed Equally		
Pu239 (g)	Pu240 (g)	Am241 (g)
5.92	0.48	1.18
Decay Heat (W)		
0.011	0.004	0.134
7 Highest Activity Salts Contributed Equally		
Pu239 (g)	Pu240 (g)	Am241 (g)
7.94	0.66	1.84
Decay Heat (W)		
0.015	0.005	0.209
7 Lowest Activity Salts Contributed Equally		
Pu239 (g)	Pu240 (g)	Am241 (g)
3.91	0.29	0.51
Decay Heat (W)		
0.007	0.002	0.059

Comparison of Attributes of 68660 to Other Drums in Waste Room 7 Panel 7

There are 55 LANL storage drums containing MIN02 waste salts in Waste Room 7 Panel 7. Using WCRRF processing packages and Real Time Radiographs a comprehensive listing of physical items and attributes for all LANL MIN02 drums in Waste Room 7 Panel 7 was made. Below is a listing of key attributes associated with 68660 compared to other LANL drums in the room.

- 21 drums contain processed liquid. The processed liquid in 68660 had a recorded pH of 0. Five other drums with processed liquids have recorded pH's of 3. The other 15 drums with processed liquid have no pH value recorded in the WCRRF paperwork.
 - 3 drums contain one or more tungsten/bismuth/lanthanum-impregnated glovebox gloves and processed liquids. Review of the RTR of Drum 68660 performed at LANL indicated that the glovebox glove was in the job control solid waste layer at the bottom of the drum physically separated from the neutralized liquid/Swheat Scoop® layer.^{uu}
 - 24 drums are from processed parents with some salts generated using oxalate precipitation. 11 of these drums have processed liquids (of these only 68660 contained a glovebox glove). Two drums in the room have an indeterminate salt makeup due to missing WCRRF processing packages.
 - 9 drums were 60% or less in fill volume (5 of these also contained processed liquid)
 - 11 drums resulted from the processing of parents with MT53 MT54 salt types
- Below is a series of tables listing combinations of key attributes compared to 68660.

^{uu} See Appendix E, Addendum A, "Expert Interpretation Of Real Time Radiograph Recordings," for details.

Table E-10. Drums with processed liquid in them and whose parents contained oxalate salts

Drum	Location	Oxalates Salts in Parent (~ 2 wt%)	Processed Liquid	Glovebox gloves	Drum % Full	Parent Initial PH
68545	13:3:B	Y (857 grams)	Y (5 gal)	N	100%	NR
68555	15:5:M	Y (1273 grams)	Y (7 gal)	N	60%	NR
68616	12:6:T	Y (990 grams)	Y (2 gal)	N	80%	NR
68629	5:1:T	Y (236 grams)	Y (1.1 gal)	N	90%	3
68654	5:1:T	Y (236 grams)	Y (8 gal)	N	90%	3
68655	5:1:T	Y (1073 grams)	Y (4 gal)	N	80%	NR
68660	16:4:T	Y (913 grams)	Y (2 gal)	Y	60%	0
68667	15:5:B	Y (832 grams)	Y (6 gal)	N	40%	NR
68672	3:3:T	Y (177 grams)	Y (3 gal)	N	80%	NR
68680	10:2:T	Y (572 grams)	Y (3 gal)	N	100%	NR
68687	15:5:B	Y (695 grams)	Y (3 gal)	N	100%	NR

Table E-11. Drums with processed liquids and glovebox gloves and whose parents contained oxalate salts

Drum	Location	Oxalates Salts in Parent (~ 2 wt%)	Processed Liquid	Glovebox gloves	Drum % Full	Parent Initial PH
68660	16:4:T	Y (913 grams)	Y (2 gal)	Y	60%	0

Table E-12. Drums with glovebox gloves

Drum	Location	Oxalates Salts in Parent (~ 2 wt%)	Processed Liquid	Glovebox gloves	Drum % Full	Parent Initial PH
68573	10:4:T	N	Y (7 gal)	Y	75%	NR
68660	16:4:T	Y (913 grams)	Y (2 gal)	Y	60%	0
68668	15:5:B	N	Y (3 gal)	Y	80%	3

Table E-13. Drums 60% full or less

Drum	Location	Oxalates Salts in Parent (~ 2 wt%)	Processed Liquid	Glovebox gloves	Drum % Full	Parent Initial PH
68512	10:6:B	N	N	N	50%	NA
68555	15:5:M	Y (1273 grams)	Y (7 gal)	N	60%	NR
68607	16:4:T	N	Y (0.12 gal)	N (RTR)	50%	NR
68609	13:3:B	Y (1273 grams)	N	N	40%	NA
68626	13:3:M	N	N	N	40%	NA
68649	15:5:M	N	Y (10 gal)	N	25%	NR
68660	16:4:T	Y (913 grams)	Y (2 gal)	Y	60%	0
68667	15:5:B	Y (832 grams)	Y (6 gal)	N	40%	NR
94152	15:5:B	N	N	N	50%	NA

SOURCE TERM

Drum 68660 was the source of the released radiological material.

Summary Conclusion

Based on the available photographic and video information, there is no evidence of involvement of any drum other than Drum 68660. This observation is supported by data from a series of non-destructive measurements made of the drum contents for acceptance into the WIPP facility and destructive analytical measurements obtained from a variety of sample locations in the facility, which includes debris from 15-5 and 16-4, surface smears, and constant air monitor (CAM) filters within WIPP as well as sampling of the Station A fixed air sampler (FAS) high efficiency particulate air (HEPA) filter. When this data set was compared to historical analytical data for the Pu and Am isotopic content for the processed wastes of the LANL drums stored in P7R7, it was determined to be consistent with a release from Drum 68660. Although when accounting for the analytical uncertainties inherent in the isotopic measurements, it cannot be concluded that no other drum contributed to the isotopic signature, from these data it can be stated that the dominant source of radioactivity was Drum 68660. Therefore, based on the evidence—photography and video; parent drum historical Uranium (U), Pu, and Am data for all LANL material types stored in P7R7; Central Characterization Program (CCP) gamma spectra for key LANL drums in P7R7 using high efficiency neutron counters (HENCs); and U, Pu, and Am isotopic measurements on post-event samples—it has been concluded that Drum 68660 was the source for the post-event radioactive contamination at the WIPP facility.

LANL Material Types and Panel 7 Drums' Salt Content

Visual evidence collected by the AIB positively identified a breached storage drum in Waste Room 7 of Panel 7 later identified as a LANL waste container. From storage records the container number was determined to be 68660. Using information documented in the Waste Characterization, Reduction, and Repackaging Facility (WCRRF) processing waste package it is recorded that 68660 and its sibling, 68685 (currently stored on the LANL reservation), were generated from the processing of parent waste container S855793 packaged in 1985 with 14 individual bags of legacy salts produced from the processing of LANL process waste streams consisting of plutonium material types (MT) 52 and 53. Early post-event sampling and analysis detected Pu240 content in the range of 7 weight percent or higher and Am241/Pu239 activity ratios from 15 to 26 from a number of remote sampling points. The concentration of Pu240 detected is consistent with LANL MT52 and MT53 or mixtures of those. Additionally, from discussions with LANL experts based on process knowledge and historical analytical data, it can be stated that MT53 and MT54 are more likely to contain higher levels of Am241 than those of MT42 and MT52 resulting in higher Am241/Pu239 activity ratios in those material types. Based on these very early analyses of key signature actinide isotopic ratios performed by the WIPP onsite laboratory and LANL analytical lab a release of radiological material from 68660 was confirmed. However, the WIPP TAT wanted to conduct a more exhaustive study that included all waste items in Panel 7 to determine whether 68660 was the sole contributor of the radiological material distributed throughout the facility for the final conclusion of source term.

All LANL material types (MT) contributing to the waste stored in Waste Room 7 Panel 7 with general descriptors for U, Pu, and Am content are shown in Table E-14 below.

Table E-14. Material Types (grams)

MT Code	Isotopic Description
12	Depleted U
42	> 60% Pu-242
51	< 4.00% Pu-240
52	4.00 < 7.00% Pu-240
53	7.00 < 10.00% Pu-240
54	10.00 < 13.00% Pu-240
81	Natural U

From this information it can be seen that a clear distinction of plutonium material types can be made based on the isotopic ranges shown.

In conjunction with this information a detailed listing of salt content for every LANL waste drum in Waste Room 7 was developed from LANL WCRRF waste packages and WIPP facility information for storage locations within the room. The information recorded in the WCRRF processing packages link each of daughter drums to a parent drum and provides specific data for each of the individual salt bags contained therein including net weight of the salts, material type, and grams of Special Nuclear Material (SNM). SNM consists of the weight sum for Pu239 and Pu240. Combined, these pieces of information were used to evaluate each item's key actinide isotopic signatures and to guide the sample isotopic analysis for data relating to source term in an effort to determine whether 68660 could be the sole contributor to the event as the early visual observations and analytical results would indicate.

Table E-15 contains the detailed listing with location of all LANL processed drums in Waste Room 7 Panel 7. Shown are the daughter and parent identifiers, the number of salt bags contained within the parent broken out by material type, and the percentage of SNM from material types other than MT52.

Table E-15. Processed LANL Waste Drums in Panel 7

Daughter	Parent	Bags: MT52:MT53:MT54	%SNM from MT other than 52
Location: R2C6			
68494	S910170 (missing WCRRF package)	-	-
68652	S852590	10:0:0	0%
Location: R3C1			
68614	S864662	12:1:0	5%
68623	S870381	11:0:0	0%
68671	S863789	10:0:0	0%
Location: R3C3			
68571	S846055	8:0:0	0%
68635	S832499	6:1:0 (plus one bag MT42)	15%
68636	S832499	6:1:0 (plus one bag MT42)	15%
68672	S853279	11:0:0	0%
Location: R5C1			
68541	S813676	4:0:0 (plus one bag MT42)	2%
68605	S822952	2:0:0 (plus one bag MT42)	34%
68629	S853326	9:0:0	0%
68654	S853326	9:0:0	0%
Location: R5C1, continued			
68655	S852590	10:0:0	0%
Location: R10C2			
68501	S910170 (missing WCRRF package)	-	-
68669	S853492	12:0:0	0%
68680	S863789	10:0:0	0%
Location: R10C4			
68573	S822952	2:0:0 (plus one bag MT42)	34%

Daughter	Parent	Bags: MT52:MT53:MT54	%SNM from MT other than 52
68578	S816837	4:0:0	0%
68647	S844689	6:3:0	22%
Location: R10C6			
68394	S841320 (missing WCRR package)	-	-
68395	S825902	4:0:0	0%
68422	S824208	2:0:0	0%
68423	S824208	2:0:0	0%
68424	S824208	2:0:0	0%
68510	S846055	8:0:0	0%
68511	S861975	9:0:0	0%
68512	S825902	4:0:0	0%
68513	S852883	10:0:0	0%
68577	S842181	3:0:0	0%
68582	S833481	8:0:2 (plus one bag MT51)	0.6%
68618	S825810	3:0:0	0%
Location: R12C6			
68616	S853771	12:0:0	0%
Location: R13C3			
68545	S846088	0:6:4 (plus 5 bags MT81 and 4 MT12)	100%
68548	S846088	0:6:4 (plus 5 bags MT81 and 4 MT12)	100%
68576	S825730	2:0:0	0%
68581	S816692	5:0:1	6%
68609	S852895	10:1:0	25%
68626	S832144	5:0:0	0%
68653	S833846	6:3:2	42%
68659	S853279	11:0:0	0%
68666	S845072	6:3:1	69%
Location: R15C5			
68328	S891513	13:0:0	0%
68459	S823004	4:0:0	0%
68555	S852895	10:1:0	25%
68649	S844689	6:3:0	22%
Location: R15C5, continued			
68667	S853492	12:0:0	0%
68668	S832150	5:0:0 (plus one bag MT42)	7%
68687	S870065	10:0:0	0%
94152	S842528	5:0:0	0%
Location: R16C4			
68333	S846107	8:0:0	0%
68607	S822952	2:0:0 (plus one bag MT42)	34%
68630	S818449	4:0:0	0%

Daughter	Parent	Bags: MT52:MT53:MT54	%SNM from MT other than 52
68660	S855793	7:7:0	26%
68670	S832150	5:0:0 (plus one bag MT42)	7%

LANL Historical Data for the Waste Salts

In addition to the information presented in Tables E-14 and E-15 historical data for Pu239, Pu240, and Am241 isotopes were obtained from LANL archived analytical records for the numerous bags of salt wastes contained in the parent drums that were processed. These data were obtained for the WIPP TAT through Kirk Veirs, a staff chemist at LANL. The pertinent data for these isotopes and drums of interest will be presented and discussed as arguments are made for groupings of drums for possible contribution to the radiological release. It should be noted that for this evaluation it was calculated that the radioactive decay of Pu241 to Am241 has minimal impact to the Am241/Pu239 activity ratios when comparing historical analytical records dating back to the 1980's to post-event sample analyses.

Unfortunately historical data and the WCRRF processing waste packages for S910170 and S841320, parent drums of 68494 and 68501, and 68394, respectively, could not be found in the archived records. One of those, 68494, can be ruled out as a contributor to the radiological release based on visual observations as discussed later. For 68501 and 68394 only the raw gamma spectra of the drums performed using a High Efficiency passive Neutron Counter (HENC) at the Central Characterization Project (CCP) in conjunction with the Fixed Energy Response Function Analysis with Multiple Efficiency (FRAM) software package analyses, as discussed below, was used for this source term evaluation.

FRAM Am241/Am243 Ratios and Post Event Pu and Am Isotopic Analytical Measurements

In LANL's July 2014 report "*Waste Isolation Pilot Plant Radiological Release: Phase I Report*" it was reported that the FRAM software code, developed at LANL to analyze pulse height spectra generated by high resolution gamma detectors, was used to extract Am241/Am243 mass ratios from raw gamma spectra data obtained by the CCP during handling and transport processes of all waste drums before emplacement in the WIPP facility. During LANL's Phase I investigation into the event the FRAM analysis of the HENC gamma spectra for 68660 and four other drums packaged in the same seven-pack storage platform was performed in an effort to determine whether the drum's radiological content would yield a unique signature for the gamma emitting isotopes and distinguish it from the others drums on the platform which contained salts solely from MT52. From this it was determined that a unique Am241/Am243 signature existed for 68660 when compared to those four MT52 drums packaged in the same storage platform placed in Column 16, Row 4. Inquiries into this revealed that in some instances to produce plutonium material meeting MT53 standards MT56 would be added. MT56 has a uniquely high Am243 concentration compared to other material types. This information was very useful for this study and from it, it was decided that having a measured ratio Am241/Am243 is highly desirable for source term. The WIPP TAT requested and obtained CCP gamma spectra for all waste drums in Waste Room 7 Panel 7 whose parent containers had processed waste salts from types MT53 and MT54 and as noted above for the daughter drums resulting from the processing of parent drums whose WCRRF packages and historical analytical data could not be found. These spectra were independently evaluated by both LANL and ORNL experts. The results of this evaluation are shown in Table E-16 below with the calculated average and uncertainties (2-sigma).

Table E-16. Waste Drum Am241/Am243 Content Based on FRAM Using CCP Gamma Spectra

Daughter	Location	Parent	FRAM (ORNL)		FRAM (LANL)		Average	
			Am241/Am243 (mass)	SD 2-sigma	Am241/Am243 (mass)	SD 2-sigma	Am241/Am243 (mass)	SD 2-sigma
Drums from parents containing MT52 plus MT53 and/or MT54								
68660	R16C4	S855793	482	66	476	62	479	90
68685	LANL		436	52	455	56	445	76
68581	R13C3	S816692	89984	55966	84706	40818	87345	69270
68653	R13C3	S833846	3836	608	4387	648	4111	889
68635	R3C3	S832499	969	102	1012	104	990	146
68636	R3C3		1188	174	1143	159	1166	236
68555	R15C5	S852895	318	76	229	63	274	99
68609	R13C3		283	74	260	73	272	104
68614	R3C1	S864662	682	249	667	206	675	323
68647	R10C4	S844689	1001	54	999	67	1000	86
68649	R15C5		1249	203	980	168	1114	264
68666	R13C3	S845072	1400	103	1402	116	1401	155
Drums from parents drums S841320 and S9100170 whose WCRR packages are missing								
68494	R2C6	S910170	302	27	318	29	310	40
68501	R10C2		298	17	325	28	312	33
68394	R10C6	S841320	3325	523	3159	605	3242	833
Drums from parents containing MT52 on seven-pack with 68660								
68333	R16C4	S846107	1029	77	1057	204	1043	218
68607	R16C4	S822952	18810	7655	15401	11132	17105	13510
68630	R16C4	S818449	47255	13659	42527	14540	44891	19949
68670	R16C4	S832150	77208	32492	85825	35650	81516	48235

From these results it can be seen that the drums have a measurably different Am241/Am243 mass ratio compared to Drum 68660 and also statistically similar ratios amongst all sibling pairs. It can be inferred from these statistically similar results obtained on a sibling pair that salt bags processed from the parent containers were mixed as one batch before placement into the daughter drums as the Am ratio is not expected to be similar between each salt bag and especially so for MT52 and MT53 as was in parent container S855793 (7 bags of MT52 and 7 bags of MT53 salts). This conclusion is further supported by the comparison of two independent efficiency responses that can be generated using FRAM. Using a set of gamma energies resulting from the decay of either Pu239 or Am241 an efficiency curve can be generated with the software. When these two independently generated efficiency curves overlap it can infer homogeneity of the material measured. This was the case for all sibling pairs listed in Table E-16. This is an important finding because it was not evident from the Energy Solutions waste operator interviews or information contained in the WCRRF waste packages how exactly the salts were split between sibling pairs. Note that results for these 4 sets of pairs do not infer it is known that similar operations were performed prior to distribution of other parent salts into daughter containers. All WIPP TAT post-event sample analyses details and results are reported separately in the SRNL and PNNL analytical reports. Only the measured Am241/Pu239 activity ratios, Am241/Am243 mass ratios, and Pu240/Pu239 mass ratios used for this study of source term are reported in Table E-17 below.

Table E-17. SRNL and PNNL Post-Event Am and Pu Ratios

Sample Type	Sample	Am241/Pu239 (activity)	Am241/Am243 (mass)	Pu240/Pu239 (mass)	
SRNL					
Airborne	FAS	26.1	444		
	CAM Filter #2	17.4	523	0.0770	
	CAM Filter #3	15.6	461		
	CAM Filter #4	15.8	505		
	CAM Filter #6	19.2	485		
	CAM Filter #7	17.9	495	0.0760	
	CAM Filter #8	22.2	466		
	CAM Filter #9	12.5	477		
	CAM Filter #11	12.1	493	0.0720	
	Panel 7 Swipes	Room 6	10.2		
Room 1		9.0			
Panel 7 debris	R15C5-replicate 1 debris	5.11	501		
	R15C5-replicate 2 debris	4.87	470		
	R15C5-replicate 3 debris	5.27	471		
	R15C5-replicate 4 debris	5.53	458		
	R15C5-replicate 5 debris	4.68	411		
	R15C5-replicate 6 debris	5.95	416		
	R15C5 (Total)	5.24	455	0.0752	
	R-15 C-5 SWB #1	5.45	455		
	R-15 C-5 SWB #2	11.1	509		
	PNNL				
	R-15 C-5 SWB	3.17	534		
	R-16 C-4 LIP	3.65		0.0780	
	14-0752c Smear 2 Upper Right	5.15			
	14-0752d Smear 3 Lower Left	1.95			
	14-0752k Velcro	2.73			
	14-0752fBottom Tape	1.94	467		
	14-0752g Top Tape	3.29	472		
	Smear 1 R16 upper left	2.68			
	Smear 2 R16 upper right	2.63			
Smear 3 R16 bottom left	2.03				
Smear 4 R16 bottom right	2.39				
Velcro backing R-16	3.31				
Subsample 14-0753 particulate vial	2.74				
Residual particles R-16	3.09		0.0777		

A cursory review of the data reveals that there is high variability for the Am241/Pu239 activity ratios. The general trend being that the lowest values are measured closest to the source and increases with distance from the source (R16 and R15, to room swipes, to CAMS, and to Station A FAS). As a note LANL and Carlsbad analytical laboratory measurements on the FAS also detected an Am241/Pu239 activity ratio in the range of 26. This

observed trend can be attributed to fractionation of the Am241 and Pu239 isotopes during the event and transport through the WIPP facility and out via the ventilation system. Given the different chemical and physical properties of the two elements the observed fractionation is to be expected. Another complicating factor to consider when using the Am241/Pu239 ratio for source term is the processing history for each of the individual produced salts. A salt's Am241 concentration is highly dependent on how the separation to recover plutonium was performed. When the plutonium material is processed using an anion exchange separation the liquid effluent contains most of the Am. When that liquid effluent is run through the TA-55 evaporators, it produces salt with high Am/Pu ratios. When an oxalate precipitation process is used Pu is precipitated with oxalic acid post ion exchange. The liquids filtered off of the oxalate precipitate are therefore very low in Am and when these liquids go through the evaporation process the resultant salts will be low in Am and therefore have low Am/Pu ratios. Being cognizant of which process was used to produce the waste salts being evaluated would have to be an important consideration if Am/Pu ratios are to be relied upon in the evaluation for source term.

Given the variability in the historical processing and post-event measured Am241/Pu239 ratios it was determined that although in a general sense the Am/Pu signature could be used to distinguish possible contributors to the event the Pu240/Pu239 and Am241/Am243 ratios are much more reliable signatures being the two dominate elements in the waste stream and the isotope pairs will behave chemically and physically similar negating any variability due to fractionation. Table E-18 lists the calculated simple averages of all the SRNL and PNNL measured Am and Pu ratios including the calculated 2-sigma deviation of the results. Also included are results bands with the low and high values shown for each based on this deviation at the 95% confidence level.

Table E-18. Calculated Average Pu and Am Ratios for all PNNL and SRNL Samples and their 2-sigma Uncertainties

Am241/Am243 (mass)	Standard Deviation (2- sigma)	Pu240/Pu239 (mass)	Standard Deviation (2- sigma)
475	62 (13%RSD)	0.0760	0.0044 (6%RSD)
low	high	low	high
412	537	0.0716	0.0804

From Table E-18, it can be seen that the variability in the data is acceptable for the measurement techniques used (gamma spectrometry for Am isotopes and quadrupole ICPMS for the Pu isotopes) and therefore, statistically, the samples can be attributed to a single source.

Systematic Evaluations and Discussions for Source Term

Drums with only MT52 salts

The first grouping of drums studied was that which were processed from parent drums with salts solely resulting from MT52 processing. A review of the historical analytical data revealed that all MT52 drums contained salts whose Pu240/Pu239 mass ratio was approximately 0.065 which is distinctly lower than the upper limit for Pu240 content for that material type (at 7 wt%). It is also measurably below any of the values analyzed on the post-event samples and the average listed in Table E-18 with a 2-sigma uncertainty. A review of the historical records also shows that the MT52 salts in this population of drums generally do have lower Am241 content and therefore lower Am241/Pu239 activity ratios compared to MT53 and MT54. Of course this cannot be said for every batch of MT52 salts in these drums due to the Am content being dependent on the factors described above. An example for the Pu ratio and generally low Am241 content in MT52 salts is given in Table E-19. These data were obtained from historical records for the individual salts in parent drum S842528. This drum was processed into drum 94152, location R15C5, and its sibling drum 94151 which was located in Panel 6. Shown in the table are the salt identifiers for each of the salt bags in the parent, the calculated Pu240 wt% and ratios for Pu240/Pu239 (mass) and Am241/Pu239 (activity) based on the historical analytical data for each of the salts. Some data are missing for

IXFS995 but based on the recorded Pu240 wt% the data can be assumed to be similar to the other salts in the drum. The total values are those calculated assuming all of the salts were mixed to make one batch then split into the two sibling drums.

Table E-19. Analytical Pu and Am Isotopic Data for MT52 Salts in S842528

Salt ID	Pu-240 (wt%)	Pu-240/Pu239 (mass)	Am-241/Pu239 (activity)
IXFS995	6.05		
994OX58	6.47	0.0692	1.04
990OX57	5.97	0.0635	1.05
IXFS988	6.02	0.0641	0.32
IXFS986	5.97	0.0635	0.17
Total		0.064	0.936

From what has been described above and the data in Table E-19, it can reasonably be concluded that the Pu and Am results measured cannot be attributed to drums whose radiological content is exclusively from MT52. This excludes 32 drums in Panel 7 for source term.

Drums with MT42 salts

The second grouping of drums studied contained those that had been processed from parent drums with salts resulting from process of MT52 as well as MT42. MT42 has a very high Pu242 content at > 60 wt%. All SRNL and PNNL analysis for plutonium isotopics included measurements for Pu242. This isotope was not detected in any sample. There are eight LANL waste drums in Panel 7 which were processed from parents with MT42 salts. Those drums are listed in Table E-20 below which is a condensed listing of Table E-15 showing only daughter drums whose parents contained MT42 salts.

Table E-20. LANL Processed Drums in Panel 7 Whose Parent Drums Contained MT42 Salts

Daughter	Parent	Bags: MT52:MT53:MT54	%SNM from MT other than 52
Location: R3C3			
68635	S832499	6:1:0 (plus one bag MT42)	15%
68636	S832499	6:1:0 (plus one bag MT42)	15%
Location: R5C1			
68541	S813676	4:0:0 (plus one bag MT42)	2%
68605	S822952	2:0:0 (plus one bag MT42)	34%
Location: R10C4			
68573	S822952	2:0:0 (plus one bag MT42)	34%
Location: R15C5			
68668	S832150	5:0:0 (plus one bag MT42)	7%
Location: R16C4			
68607	S822952	2:0:0 (plus one bag MT42)	34%
68670	S832150	5:0:0 (plus one bag MT42)	7%

Drums 68635, 68636, 68541, and 68605 are in locations in the panel for which AIB visual observations confirmed were not affected by the event. All of the MgO bags are observed to be intact in rows 2, 3, and 4 and there is no observable damage to any of the waste items. Based on these observations and the absence of Pu242 it was concluded that these particular drums were not contributors to the event. For the remaining drums in the table the MT42 SNM (Pu239 and Pu240) contribution is high enough that release of their material would have resulted

in gross levels of Pu242 in the debris field, swipes and airborne monitors/filters. Therefore these last remaining drums are also determined to not have contributed to the event based on post-event sampling and analyses.

Drums with MT12 and MT81 uranium

Drums 68645 and 69648 located in Row 13 Column 3 were processed from the same parent drum, S846088, which contained MT53, MT54, MT12, and MT81 salts. A review of the analytical records for those salt bags reveal that all of the MT53 and MT54 items have Pu240 greater than 8.9 wt% and therefore couldn't be responsible for the isotopics measured. Secondly, the drum contents are mixed MT12 and MT81 which are depleted and natural uranium. A listing of the salt bags processed from the parent is shown in Table E-21 below. Some of the items identifying information is either illegible or missing however this has no bearing on the listed material types present in the parent container. From this information it can be seen that these two daughter drums have thousands of grams of uranium content mixed with the Pu. All post-event measurements for uranium have been at the trace levels with isotopics slightly enriched in U235. Based on this information it can be concluded these drums were not contributors to the event.

Table E-21. Material Types in Parent Drum S846088

Salt ID	Net Wt. (Kg)	MT
LCU118N101	5.95	81
LCU12-895	6.29	53
LCU12-895	6.29	12
LCU12-895	6.28	81
UOX9-95NE1	14.32	53
LCU13103NE	1.59	53
LCU13103NE	1.59	12
LCU13103NE	1.59	81
LCU14119NE	1.88	54
LCU14119NE	1.87	81
<i>ILLEGIBLE</i>	13.31	54
-	14.31	12
-	14.31	81
UOX7-555A	13.99	53
-	4.09	53
-	4.09	12
NAX8-71NE1	26.82	54
UOX8-71NW1	14.55	54
LCU1170NW1	5.95	53
LCU1170NW1	5.95	12
LCU1513NW	7.16	54
LCU15132NW	7.16	12

Drum with MT51 salts

One drum in the panel, 68582 located in Row 10 Column 6, had a bag of MT51 salts documented in the WCRRF package to have been processed from the parent. The SNM in these are < 4 wt% Pu240. It was concluded that this drum cannot be attributed to the release due to the fact that only 0.6% of its SNM content is from MT54 and MT51 and the MT51 plutonium would "dilute" the MT54 contribution. Therefore the Pu240/Pu239 signature would be indicative to MT52 and below what was measured.

Drums missing WCRR processing packages and historical analytical data

FRAM analysis was used for evaluation for source term for drums 68501 (R10C2) and 68394 (R10C6) In the absence of historical analytical information and WCRRF processing records. Shown in Table E-16 above drum 68394 was analyzed using FRAM to have an Am241/243 ratio much higher than any of the sampled locations in the Waste Room and can be excluded based on this. Drum 68501 has a lower analyzed ratio averaging 312 +/- 33. Its exclusion from the source term can be confidently made based on this ratio and its 2-sigma uncertainty but since it is closer to the post-event average measured Am ratio than 68394 and no other data is available for evaluation, the Pu240/Pu239 ratio was also included in ORNL's FRAM analysis for it and its two sibling drums 68426 (stored at WCS) and 68494. From this evaluation the Pu240/Pu239 mass ratios were analyzed to be 0.022 (68426), 0.043 (68494), and below detection limits (68501). For the two sibling drums the ratio in the salt would be indicative of MT51. Heterogeneity of the Pu and Am isotopes in drum 68426 was noted based on the comparison of independently produced Am and Pu efficiency responses as described earlier. The very low Pu ratios analyzed in the two siblings of 68501 and plutonium gammas below detection in 68501 indicates a low overall Pu content. This additional plutonium information further supports exclusion of drum 68501 from source term.

Remaining drums with MT53 and MT54 salts

Remaining are eight drums which are listed in Table E-22 with location identified and the combined %SNM contribution from MT53 and MT54. Based on the %SNM contribution and the historical Am and Pu measurements for the salts in the parent drums, these have isotopic content that could be attributed to the radiological release.

Table E-22. Remaining Eight Drums with MT52:MT53:MT54 Salt Mixtures

Daughter	Parent	Bags: MT52:MT53:MT54	%SNM from MT other than 52
Location: R10C4			
68647	S844689	6:3:0	22%
Location: R13C3			
68581	S816692	5:0:1	6%
68609	S852895	10:1:0	25%
68653	S833846	6:3:2	42%
68666	S845072	6:3:1	69%
Location: R15C5			
68555	S852895	10:1:0	25%
68649	S844689	6:3:0	22%
Location: R16C4			
68660	S855793	7:7:0	26%

For these remaining eight drums a more thorough evaluation of their isotopic content is needed for evaluation of source term. Tables E-23 through E-28 lists the historical Am and SNM isotopic analyses for the salts contained in each of the parents which produced these drums. The total values listed are those calculated assuming all of the salts were mixed to make one batch then split into the respective daughter drums during processing. As discussed earlier statistically similar FRAM evaluations for Am241/Am243 supports mixing of the salts prior to processing with Swheat Scoop® and placement into the siblings.

Table E-23. Analytical Am and Pu Isotopic Data for Salts in S844689 (Daughters 68647 and 68649)

Salt ID	MT	Pu-240 (wt%)	Pu-240/Pu239 (mass)	Am-241/Pu239 (activity)
IXF1039	52	6.08	0.065	3.63
IXF1040	52	6.00	0.064	0.99
IXF1041	52	6.01	0.064	2.61
IXF1045	52	5.96	0.063	1.76
1038OX73NE	53	8.21	0.089	2.43
1038OX73NW	53	8.21	0.089	6.14
1042OX74NE	52	5.88	0.062	1.59
1042OX74NW	52	5.88	0.062	0.70
1043OX75NE	53	9.61	0.106	0.42
		Total	0.070	1.88

Table E-24. Analytical Am and Pu Isotopic Data for Salts in S816692 (Daughter 68581)

Salt ID	MT	Pu-240 (wt%)	Pu-240/Pu239 (mass)	Am-241/Pu239 (activity)
IXFS412FB	52	6.00	0.064	17.30
IXFS413FI	52	6.00	0.064	27.81
IXFS414FI	54	12.00	0.136	54.72
IXFS415FI	52	6.00	0.064	38.49
IXFS416FI	52	6.00	0.064	15.44
IXFS417FI	52	6.00	0.064	5.72
		Total	0.068	27.81

Table E-25. Analytical Am and Pu Isotopic Data for Salts in S852895 (Daughters 68555 and 68609)

Salt ID	MT	Pu-240 (wt%)	Pu-240/Pu239 (mass)	Am-241/Pu239 (activity)
OX180306NE	52	5.90	0.063	1.26
OX179305NW	52	6.10	0.065	2.40
LR308NW1	52	5.93	0.063	5.57
LR308NE1	52	5.94	0.063	8.03
DSL311NW1	52	6.21	0.066	3.70
OX181310NW	52	5.90	0.063	3.63
UOX181310NW	52	5.90	0.063	1.35
LR309NW1	52	5.99	0.064	6.83
LR309NE1	52	5.99	0.064	8.07
DSL311NE	52	6.21	0.066	3.98
UOX11313NW	53	9.64	0.107	3.07
		Total	0.074	3.90

Table E-26. Analytical Am and Pu Isotopic Data for Salts in S833846 (Daughter 68653)

Salt ID	MT	Pu-240 (wt%)	Pu-240/Pu239 (mass)	Am-241/Pu239 (activity)
IXFS-811-FA	52	6.00	0.064	12.36
OXF812-FA	52	6.00	0.064	18.49
IXFS-815-FA	53	9.09	0.100	18.36
IXFS-816-FA	52	5.27	0.056	10.31
IXFS818-FA	52	6.00	0.064	29.77
IXFS-819-FA	54	11.06	0.124	43.92
IXFS-820-FA	54	12.00	missing	missing
821OX40FC	52	6.00	0.064	6.10
IXFS-823-FA	53	9.75	0.108	25.51
IXFS-825-FA	52	6.00	missing	missing
IXFS-827-FA	53	9.89	0.110	7.69
IXFS-829-FB	52	6.50	0.070	15.61
		Total	0.084	18.67

Information missing for one bag each of MT54 and MT52 salts. Weight of salts is 4.6 and 5.9 Kg respectively. Missing data not considered to have a major effect on source term evaluation.

Table E-27. Analytical Am and Pu Isotopic Data for Salts in S845072 (Daughter 68666)

Salt ID	MT	Pu-240 (wt%)	Pu-240/Pu239 (mass)	Am-241/Pu239 (activity)
1077OX86FB	53	8.24	0.090	1.68
IXF1078	52	6.03	0.064	5.48
IXF1079	52	5.80	0.062	3.64
1080OX87FA	53	8.42	0.092	2.51
1081UOX-2	54	11.84	0.134	1.95
1082OX88	52	5.95	0.063	0.96
IXF1083	52	5.91	0.063	4.53
IXF1084NE	52	6.02	0.064	3.62
IXF1084NW	52	6.02	0.064	3.85
1085OX89SE1	53	9.53	0.105	1.90
		Total	0.084	2.49

Table E-28. Analytical Am and Pu Isotopic Data for Salts in S855793 (Daughter 68660)

Salt ID	MT	Pu-240 (wt%)	Pu-240/Pu239 (mass)	Am-241/Pu239 (activity)
10LALR1W	53	9.69	0.107	8.28
10LR5W1	53	9.69	0.107	13.70
10LR5E1	53	9.69	0.107	17.02
10LR16W1	53	8.14	0.089	12.41
10LR16E1	53	8.14	0.089	28.65
10LR17W1	53	8.14	0.089	30.76
10LR17E1	53	8.14	0.089	34.83
10RR18E1	52	5.82	0.062	5.25
10OX11W1-1	52	6.00	0.064	2.63
10OX11W1-2	52	6.00	0.064	2.63
10LR18E1	52	6.00	0.064	6.58
10LR18W1	52	6.00	0.064	9.97
10OX21E1	52	6.21	0.066	6.14
10OX21W1	52	6.21	0.066	1.97
Total			0.073	6.70

To further define the contents for this population of drums the measured Am241/Am243 for each of the drums determined using FRAM software code (Table E-16) was used in conjunction with the calculated Pu ratio for the mixed salts and WIPP TAT Am and Pu analytical measurements. Table E-29 is a summary of these data.

Table E-29. Daughters' Mixed Salts Pu240/Pu239 and Am241/Pu239 Ratios and FRAM Am241/Am243 Ratios

Ratio	Daughter								SRNL and PNNL
	6864 7	6858 1*	6860 9	6865 3	6866 6	6855 5*	6864 9*	6866 0*	Result Bands
Mixed Salts Pu240/Pu239 (mass)	0.0700	0.0680	0.0740	0.0840	0.0840	0.0740	0.0700	0.0730	0.0716 - 0.0804
FRAM Am241/Am243 (mass)	1000	58734	272	4111	1401	274	1114	479	412 - 537
Mixed Salts Am241/Pu239 (activity)	1.88	27.81	3.90	718.6	2.49	3.90	1.88	6.70	1.94 – 26.1

*Drums containing processed liquid

During WIPP TAT discussions the presence of processed liquids has been highlighted as an attribute of interest in regards to reactivity of drum contents. Because of these lines of inquiry the four drums in this grouping with processed liquids have been identified in the table.

From the data shown only Drum 68660 contains homogenized salts with both Am241/Am243 and Pu240/Pu239 mass ratios within the ranges of those measured in the post-event samples by SRNL and PNNL. The next closest match is sibling drums 68609 and 68555. These drums along with one other sibling, 68549 emplaced in Panel 6, were produced from parent S852895. The parent contained 11 salt bags, 10 containing MT52 (126 Kg total) and 1 containing MT53 (14 Kg total) salts. The Pu240/Pu239 mass ratios in the MT52 salts are around 0.06 while the MT53 salts have a ratio of 0.107. What drives the mixed salts, inferred by FRAM, to have a ratio stated is that

the MT53 SNM content makes up ~25% of the total therefore driving up the calculated ratio. The addition of a high confidence Am241/Am243 ratio was very important in this case for source term.

Based on this comparison and arguments put forth in this study, the release of radioactive contamination in WIPP can be attributed to Drum 68660.

APPENDIX E. ADDENDUM A. EXPERT INTERPRETATION OF REAL TIME RADIOGRAPHIC RECORDINGS

The following is an account by independent assessor Steve Tallman (Level III RTR, RTR SME, AMWTP-ITG-INL) of his full review of the Drum 68660 Real Time Radiograph (RTR) to determine whether the glove and neutralized liquid/Swheat Scoop® were in contact. Tallman's assessment is that the RTR shows a space between the glove and neutralized liquid/Swheat Scoop® in Drum 68660 but that a definitive statement that the glove and liquid waste were or were not in contact cannot be made based solely on the RTR.

Summary Review of LANL Containers by Steve Tallman– 11/19/2014

I completed a review of RTR Recordings for 11 LANL containers, and completed answering a set of questions on some specific and general comments about these containers at the request of DOE's Mr. Roger Claycomb:

1. How many gloves in 68660? There was one glove confirmed, could see the fingers and cuff.
2. Are gloves in direct contact with the waste? There was no evidence of a separate horsetail, which would provide a layer of plastic. There is some space between the S3000 solid waste and glove, in my opinion, there doesn't look like there is any contact.
3. Are gloves in bottom of 68660 separately bagged? No evidence of a horsetail, in my opinion it was indeterminate on whether the glove was bagged.
4. In looking at other drums, was it standard practice to bag things separately? In my review of the other containers listed below, there were some indications of horsetails in the waste, mostly in the levels that held the S3000 solid waste. There were indications that some of the solids had been packaged separately, because you can see the rounded corners of some of the individual packages, and some separation within the waste on some of the containers.
5. Look at 68685- compare and contrast with 68660 - waste stream looked similar. Drums were inspected on different RTR systems, which make the waste look different, but there is a mixed combination of debris and solids waste in both. A brief description of each container is provided below.

I reviewed RTR Recordings for a total of 11 containers. Quite a bit of time was spent on the recordings for containers 68660 and 68685, in looking for detailed information. The recordings for the other containers were reviewed to confirm the waste was similar, and to provide a brief description of the waste contents. In general, all of the containers appeared to be the same waste stream; S3000 solid waste with a mixture of debris waste present. The look and density of the waste appears to be consistent. A brief description of each container;

Container ID Brief description

68660 - The container has a liner, plastic bag with horsetail (rest of reviews, description shortened to just horsetail), a small amount of debris waste on top, PPE, then layers of solid waste. At bottom, one glove, finger/cuff observed, debris waste, rigid liner lid, large small mouthed poly bottle, small pieces of metal debris. One area of dense debris adjacent to glove, couldn't tell what it is, other than confirm it is debris, and one small horsetail seen, coming up the side of the container, in the solids waste

68685 (sibling to 68660) - This container was inspected on a higher energy system than the other containers. The container has a liner, horsetail, quite a bit of plastic waste on top, what looks like lead pieces folded/stacked, solids waste, and small debris pieces mixed in with solids. Some of the solids waste has individual horsetails noted, for indication of separate bags.

68501 - The container has a liner, horsetail, solid waste, that is individually bagged, smaller horsetails, shape of the packages, some small debris mixed in with solids, rigid liner lid in with waste.

68511 - The container has a different packaging configuration - a pipe over-pack component (POC) with packaging to hold POC in place, waste looked to be bulk loaded into POC, plastic debris, small bags of solid waste.

68541 - The container has a liner, horsetail, lead sheet on top, layers of solid waste, and a small amount of miscellaneous debris waste on bottom.

68494 - The container has pieces of lead sheet cut up, an area of solid waste, denser near the top of the waste, small amount of debris waste at bottom.

68555 - This container has a liner, horsetail, pieces of lead sheet, layer of solid waste, rigid liner lid buried in solid waste.

68573 - This container has a liner, horsetail, layers of solid waste, with small pieces of debris mixed in, individual bags of waste, based on shape and appearance, no small horsetails evident, rigid liner lid buried, debris waste on bottom, lead/plastic.

68605 - This container has a liner, horsetail, solids waste with small amount of debris mixed in.

68607 - This container has a liner, horsetail, lead sheet/pieces, plastic debris, and bags of solid waste, based on shape/appearance.

68668 - This container has a liner, horsetail, lead sheet, solid waste, lead debris, and rigid liner lid at bottom.

APPENDIX E. ADDENDUM B.

In addition to Drum 68660 the RTR's on file were used for the assessment of the following LANL waste drums to visually document their inventory and attributes.

For the two siblings 68494 and 68501 there was no WCRRF processing package available. The RTR was used to document drum contents from the processing of their parent S910170.

For drum 68541 and siblings 68573, 68605, and 68607, the WCRRF processing package recorded that all of these were packaged with processed liquid. In the comment section it was also written that a pair of glovebox gloves was included as additional waste material added to the daughters. However it was not documented into which drum the glovebox gloves were added to.

It was recorded that drum 68511 contained a "lead" glove but it was not clearly documented as being put into the drum.

By inventory of items and attributes, 68668 is the closest match to 68660. No oxalate salts though.

Lastly, 68555 and 68680 have approximately the same mix of Material Types, oxalate salts and adsorbed free liquids as 68660.

Drum ID	RTR Operator Observations	Additional notes
68501	Liner, Horsetail – inner bag Solids, plastic bag ~50% utilized Homogeneous solids Plastic lid Fiberboard liner plastic liner bag Bottom appears to be dry Plastic bags	No WCCR package
68494	10/28/13 Scrap lead – flat piece ~100% utilized Horsetail – plastic liner bag Homogeneous solids Plastic bags at bottom of drum Fiberboard liner plastic liner bag Bottom appears to be dry Able to verify only one horsetail at the top – single layer confinement	No WCCR package Lead is at the top of the drum
68494R	Liner & liner bag Horsetail at top Scrap lead Homogeneous solids Bottom of container Fiberboard liner, no lid, liner bag Appears to be dry ~95% utilized – one layer containment	Replicate scan of the drum.
68541	Hasselstrom Liner – no lid, bag, horsetail of the bag Scrap lead	

Drum ID	RTR Operator Observations	Additional notes
	Homogenous solids Bottom of drum Horsetail for plastic bag Fiberboard liner Another horsetail for plastic bag ~70% utilized Appears to have two layer confinement	
68573	Simmons Rigid liner with no lid Plastic liner bag & horsetail Homogenous solids Leaded rubber glove A bunch of pairs of leaded rubber gloves Fiberboard rigid liner No lid No liquid Whole bunch of leaded rubber gloves at the bottom ~75% utilized One layer confinement	Frame captures to show gloves
68605	Simmons Rigid liner – no lid Horsetail Homogeneous solids Plastic bag, horsetail, homogenous solids Fiberboard liner Bottom of drum, bottom of liner appear to be dry ~95% utilized, two layers confinement	
68607	Simmons Rigid liner no lead Plastic liner, horsetail Plastic containers, scrap lead, homogenous solids Bottom of drum Fiberboard liner, no lid Appear to be dry ~55% utilized, two layer confinement	Empty bottles & lead on top of salts
68511	Maestas Center pipe overpack Liner is vented Vent for POC Rigid liner & liner bag inside POC Liner sleeve inside POC Homogeneous solids Metal hardware (scrap metal) Bottom of drum Plastic sheeting 90 mil liner Bottom appears to be dry	

Drum ID	RTR Operator Observations	Additional notes
	~50% utilized	
68668	Simmons Rigid liner, no lid Plastic liner bag with horsetail Scrap lead (flattened sheets) Homogenous solids Plastic bag, horsetail Plastic bags, horsetails Bottom of drum Leaded rubber gloves 90 mil liner lid Fiberboard liner Bottom of drum, bottom of liner appear to be dry ~70% utilized Two layers of confinement	Lead is near the top Operator repeated plastic bags and horsetails (indicating multiples) Gloves were at the very bottom of the drum (look like they may be in contact with salt) Noted pretty thick sheet of lead (leaded window?)
68555	Simmons Rigid liner, no lid Plastic liner bag with horsetail Center of drum Plastic bag, horsetails Scrap lid, homogenous solids, plastic bags Bottom of drum 90 mil plastic liner lid Plastic containers Bottom of drum, bottom of liner appear to be dry 50% utilized Two layers of confinement	
68680	Maestas Liner Horsetail plastic liner bag Plastic bags Homogenous solids Scrap lead Bottom of drum Scrap metal Plastic bags Plastic lid Fiberboard liner Bottom of drum, bottom of liner appear to be dry	
68685	Simmons Scrap lead Plastic horsetail Homogenous solid Bit more scrap lead Plastic bags (plural) horsetail Bottom of drum Plastic bag	Lead is on top of the waste

Drum ID	RTR Operator Observations	Additional notes
	Homogenous solid Fiberboard rigid liner – no lid Another horsetail for another plastic bag Bottom of drum, bottom of liner appear to be dry ~85% utilized Two layers of confinement Some scrap metal at top of drum	

APPENDIX F. REACTION CHEMISTRY AND HYPOTHESES

SUMMARY

This document provides a review of the possible chemical reactions that could have occurred in Drum 68660 based on the available information on the contents of the drum. These findings are derived from evaluating the available chemical literature and preliminary results from probative laboratory testing. Key conclusions include the following:

- The combination of the acidic free liquid from the parent drum and TEA during neutralization and subsequent sorption onto the Swheat Scoop® material as well as the combination of acidic nitrate salts and Swheat Scoop® created a potentially reactive mixture of fuels (Swheat Scoop® and TEAN) and oxidizers (nitrate salts and nitric acid).
- The drum was a complex, heterogeneous mixture of materials with the potential for multiple reaction sites and reaction chemistries.
- Possible chemical reactions involving the sorbent and the neutralization reagent included hydrolysis, oxidation, and nitration.
- Biological reactions may have occurred at low temperatures (<80 °C) and were more likely to have occurred in the processed liquid fraction due to the higher water content and neutral or near-neutral pH.
- The presence of TEAN in the neutralized free liquid added a potentially reactive compound to the region of the drum containing the neutralized liquid/Swheat Scoop® mixture.
- The localized water content likely played a key role in the reactivity of the TEAN/Swheat Scoop® and the metal nitrate/Swheat Scoop® mixtures.
- The interface of the neutralized liquid/Swheat Scoop® and the nitrate salts/Swheat Scoop® layers may have played an important role in forming a localized region of high reactivity.

Based on these key conclusions, we hypothesize that a sequence of exothermic chemical reactions led to a thermal runaway system, which resulted in radiological material being released from Drum 68660.

INTRODUCTION

This document provides a discussion on the nature of the reactive chemicals that were added to the waste Drum 68660, the possible reactions that could occur between the reactive compounds, and the effects that key parameters may have on the reaction chemistry. Based on information from the chemical literature and recent experimental results, we have developed a hypothesis of how a series of exothermic reactions led to a runaway system and resulted in contents of the drum being released into the mine.

The Center for Chemical Process Safety (CCPS) of the American Institute of Chemical Engineers (AIChE) identifies the important factors affecting chemical stability as temperature, the nature and concentrations of the reactants, the nature and concentrations of impurities or other compounds present, solvent, air when air-sensitive compounds are present, and confinement. [CCPS 1995]

According to the CCPS, the hazards of any chemical system depend on 1) the potential energy of any chemical reactions that can occur between constituents, 2) the rates of any potential reactions, and 3) the process equipment. The first potential energy includes both possible exothermic and endothermic reactions. The second, reaction rates, includes rates for all of the possible reactions in the system such as exothermic reactions between an oxidant and a fuel and endothermic reactions including phase changes such as the evaporation of water or melting of salts. The third involves designing a process or equipment to ensure that “any heat generated can be adequately removed during normal operations and any gas production must be managed.” [CCPS 1995]. To prevent a thermal runaway event in a potentially chemically reactive system, the system must be able to dissipate any heat produced at a rate that will prevent increases in temperature sufficient to support additional or accelerated chemical reaction rate(s).

Temperature is a very important parameter as it controls the rate at which a chemical reaction occurs. As a general

rule of thumb, a 10 °C increase in temperature results in an increase in the reaction rate by a factor of between 2 and 4. Thus, as exothermic reactions proceed and the temperature of the system rises, the rates of reactions increase. As temperatures increase, the chemical system reaches activation energies allowing additional reactions to occur.

Industrial wastes containing both organic and inorganic materials are complex systems where various interrelated biological and chemical reactions can result in potential combustion [Hogland 2003]. While degradation processes can be both chemically and microbiologically mediated, biological reactions typically predominate at temperatures below 65 °C [Storm 1985]. Chemical oxidation of solid waste has been reported to be slow at temperatures of 30 °C, which is the temperature in the underground rooms at the WIPP facility [Moqbel 2010]. However, as the temperature increases, chemical oxidation will increase.

The nature of the reactants is critical as this defines the system's potential energy and the potential to produce gaseous products and pressurized conditions in storage containers. Included in the CCPS' list of systems meriting consideration are mixtures of organics and oxidizers other than oxygen such as nitrates and nitrites. The reactants' concentrations are important since reaction rates are roughly proportional to those concentrations. Impurities can have catalytic effects by reducing activation energies, increasing reaction rates, and decreasing reaction onset temperatures. Solvents are important as they may promote material transport, serve as diluents, and serve as heat sinks due to refluxing. Confinement may cause the reaction rate to increase due to pressure increases or by allowing product gases to participate in secondary reactions.

DESCRIPTION OF REACTIVE CHEMICALS IN DRUM 68660

Nitrate salt residues from plutonium processing facilities at the Los Alamos National Laboratory (LANL) were removed from the original drums and repackaged for disposal in Waste Isolation Pilot Plant (WIPP) near Carlsbad, NM. Free liquids containing water, nitric acid and dissolved metal nitrates were drained from the parent steel drum and plastic bags and neutralized (pH approximately 7) with a mixture of triethanolamine and water commercially known as Kolorsafe®. The neutralized liquids were then sorbed onto an organic wheat-based sorbent (Swheat Scoop®) and placed in a new drum lined with a PVC bag. The remaining moist, still acidic, nitrate salts from the parent drum were mixed with additional Swheat Scoop® and a portion of this mixture was placed in the same drum as the neutralized nitric acid/Swheat Scoop® mixture.

After filling the drum to about 60% of capacity, the PVC bag was taped closed, the drum lid installed, and the drum removed from the glove box. The combination of the nitrate salt residues, organic sorbent and neutralizing agent represents a potentially reactive chemical mixture. Following is a description of the various reactive drum components and possible reaction chemistry that could lead to sustainable chemical reactions and, ultimately, to a thermal runaway system.

Metal Nitrate Salts

Nitrate salt wastes were produced at LANL from the recovery and purification of plutonium [Clark 2015]. The resulting nitric acid solutions contained a number of metal ions and were concentrated through evaporation until the nonvolatile salts in the evaporator were close to saturation. The concentrated solution was poured into a water-cooled tray and flash-crystallized to produce solid nitrate salts. After filtration to remove the bulk of the acidic supernatant liquid, the nitrate salts were washed with concentrated nitric acid and vacuum dried. [Haagenstad 2012] The nitrate salts would contain residual supernatant liquid as well as water from the waters of hydration in the crystallized salts. Salts derived from oxalate filtrates were washed with water and not with nitric acid because nitric acid would accelerate decomposition of any oxalic acid presents in the salts and could result in pressurization of the sealed 55-gallon drums containing the salts with oxalate. [Haagenstad 2012]

The nitrate salt waste that was repackaged into Drum 68660 was taken from Drum S855793. Drum S855793 was generated in October 1985 and reported to contain 14 bags of nitrate salts, four of which resulted from an oxalate precipitation process. Documentation of the original, detailed chemical composition of the nitrate salt waste

contained in Drum 68660 does not exist. Analysis of the nitrate salt samples taken from two un-processed drums, produced in 1980 and 1981, respectively, indicated the following elements were present, Na, Mg, K, Ca, Al, Fe, Pb, Cr, Ni, Zn, and U. Although the nitrate content of each sample was similar, the concentrations of metals varied considerably. For example, the sodium and calcium concentrations varied by factors of 2.8 and 300, respectively [Drake 2014]. The variation in elemental composition is not unexpected given the variety of materials processed in the plutonium processing facilities at the Los Alamos National Laboratory. The metal nitrate salts in Drum 68660 would be expected to be largely comprised of the alkali (Na, K) and alkaline earth (Mg, Ca) elements with lower amounts of other transition metal (Fe, Cr, Ni, Zn), main group (Al, Pb), and actinide (U) elements.

Oxalate was used in the plutonium processing operations at LANL and would have been a component in residues sent for evaporation and formation of salts. Oxalate is decomposed to carbon dioxide in 0.1–6 M nitric acid and in the presence of metal catalysts such as manganese and vanadium. [Nash 2012] Typically, the solutions are heated to about 100 °C to increase the rate of decomposition. After storage of the parent drum containing nitrate salts for just over 28 years at ambient conditions, the concentration of oxalate in the nitrate salts is not known. However, given the acidity and length of time, the oxalate concentration would be expected to be much lower than when the salts were first generated. [WIPP 2014]

Oxalate is also an effective chelating ligand for many metal ions. The formation of metal chelates with oxalate, which when solubilized, may act as a catalyst of the oxidation of organics. However, metal oxalates can have relatively low solubility in aqueous systems. If the metal oxalate salt precipitates from solution, the concentration of metal ion remaining in solution is decreased and the catalytic activity is reduced. Metal oxalates likely formed during the original evaporation/crystallization operation but, in all likelihood, underwent decomposition reactions during the 28+ year storage time of the parent drum to produce carbon dioxide and corresponding metal oxide. The metal oxide formed during this process could also serve as a catalyst for the oxidation of organic compounds in the matrix.

Absorbent

The Swheat Scoop® line of absorbents produced by Pet Care Systems (Detroit Lakes, MN) is derived from the whole grain of wheat [Sladek 1997; *Swheat Scoop* 2014]. Wheat kernels consist of three parts, (1) the bran or outer shell of the kernel, (2) the endosperm, which represents most of the mass (80-85%) of the kernel and (3) the germ which is the embryo or sprouting section of the kernel, which represents the smallest part (2-3%) of the kernel. The endosperm consists of starch (83%), proteins/enzymes (13%), fats (1.5%), dietary fibers (1.5%), and minerals (0.5%). The bran, which represents about 13 -15% of the kernel mass, is complex mixture of cellulose, lignin, pentosans and polymers based on xylose and arabinose that are tightly bound to proteins. Thus, starch comprises about 65-70% by mass of the entire wheat kernel. The next most common class of compounds is proteins/enzymes, which comprise about 14% of the mass of the wheat kernel. [Sramkov 2009]

According to the manufacturer, the production process exposes the starch of the grain from the inside the kernel of the wheat, which serves as the clumping agent upon contact with liquids. [*Swheat Scoop* 2014] Starch consists primarily of two polymers, amylose and amylopectin [Koehler 2013]. Amylose is a spiral polymer of D-glucose units with the idealized structure shown in Figure F-1. Amylopectin is a highly branched polymer of D-glucose units with the idealized structure in Figure F-2.

Given the high weight fraction of starch in the sorbent, starch would be expected to serve as the predominant fuel component in the processed drums. Consequently, the two principal chemical components of starch, amylose and amylopectin would be the most likely candidates to undergo oxidation and possibly nitration reactions.

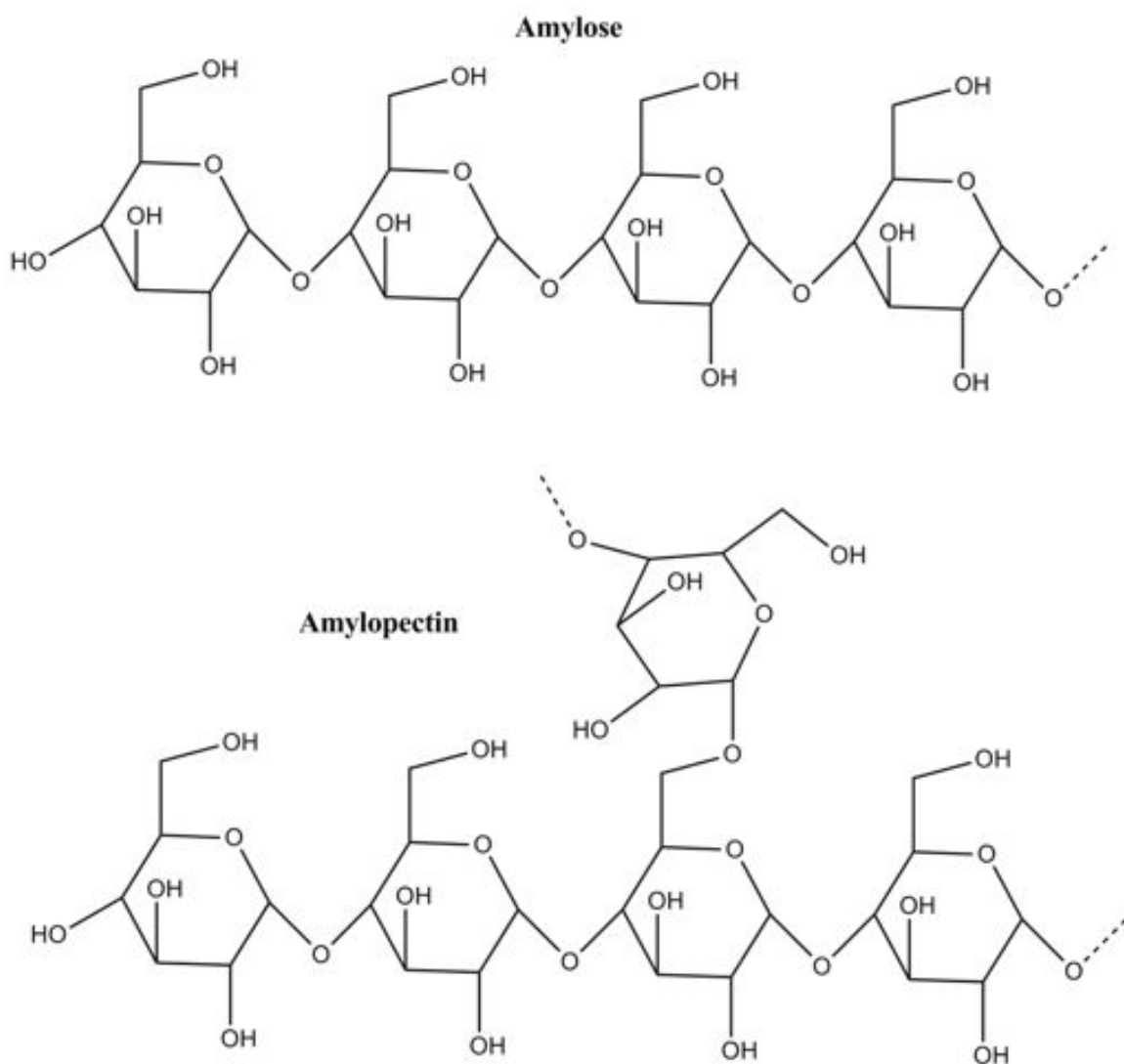


Figure F-1. Schematic representations of amylose and amylopectin

In addition to starches, the Swheat Scoop® sorbent also contains cellulose, proteins/enzymes, lipids, minerals, cellulose, lignin and other polymeric carbohydrates. Proteins are large molecular weight molecules consisting of amino acids. Lipids are a large, diverse group of naturally occurring organic compounds that feature limited solubility in water, but high solubility in non-polar organic solvents. Examples of lipids include long-chain carboxylic acids, waxes, phospholipids, terpenes and steroids. Cellulose is a linear, high molecular weight polymer of 1,4-linked glucose units and is the major structural component of the primary cell walls of plants. Lignin is a complex polymer of aromatic alcohols and another component of cell walls of plants. According to the manufacturer, Swheat Scoop® is known to harbor an indigenous natural microbial population. This microbial inoculum is the source of the product enzymes claimed in the patent that degrade animal residues and associated odorous aromatic compounds [Williams 2014]. Note, all of the organic compounds present in the Swheat Scoop® sorbent would be subject to and could participate in oxidation and nitration reactions provided that the conditions are met such that the chemical reactions will proceed at a measurable rate.

Neutralization Reagent

LANL has reported that during the processing operations with the nitrate salt wastes, any free liquid that was found in the parent drum was poured into a tub and the pH measured by Hydrion® pH strips [Clark 2015]. If the pH was not close to a neutral pH value, a neutralizing chemical, sodium carbonate or a commercial acid-neutralizing product Spilfyter® Kolorsafe®, aqueous triethanolamine (TEA) with the pH indicator alizarin, was

added until the pH was neutral. The neutralized liquid was then combined with the absorbent and placed into a new drum. Neutralization of nitric acid with TEA produces the protonated nitrate salt, hydrogen triethanolammonium nitrate (TEAN).

TEA is a viscous organic compound that features a tertiary amine and three primary alcohol groups. The amine and alcohol function groups are nucleophilic and serve as Lewis bases by donating a pair of electrons to form chemical bonds. [Dow 2014] TEA melts at 21.6 °C and exhibits high thermal stability as evidenced by a boiling point of 335.4 °C. [Lange's 1985] TEAN melts at 80 °C is reported to begin exothermic (heat producing) decomposition with the release of gaseous products at 250 to 325 °C when heated at 175 °C s⁻¹ under 1379 kPa (200 psi) of Ar [Cronin 1988]. Gases released included CO₂, N₂O, CO, NO, NH₃, and HCN. This mixture of nitrogen oxide oxidants, N₂O and NO, and the fuels, CO, NH₃, and HCN, are also potentially a reactive mixture particularly if confined. In addition, the gaseous nitrogen oxides can react with the fuel constituents in the waste mixture particularly if confined. Thus, protonation of TEA to produce the protonated nitrate salt results in a more thermally unstable chemical compound whose decomposition products can participate in secondary exothermic reactions. TEA has been reported to be a sensitizer for energetic compounds (including explosives) such as nitroaromatics (TNT) and some nitroamines (RDX). Although TEA is believed to have played an important role in various possible reaction pathways leading to the drum release, it did not serve as a sensitizer in the manner described above, as no organic compounds were present in the drum that could be considered mono-molecular explosives. Instead, it is believed that TEA facilitated various decomposition reaction pathways in both the free-base form (TEA) and as its nitrate salt (TEAN).

The presence of TEA/TEAN could serve several roles in the release event:

- TEA forms complexes with metal ions. TEA is a polyfunctional ligand capable of bonding through its nitrogen and/or oxygen atoms to form complexes with a variety of metal ions [Fowkes 2006; [Neilsen 1972; Allen, 2002; Yilmaz 2002]. Yilmaz and his coworkers [Yilmaz 2002] used simultaneous thermogravimetric and differential thermal analysis (TG/DTA) to determine the thermal stability of metal/TEA complexes. Results indicated that exothermic onset temperatures were as low as 114 °C, which is considerably below the decomposition temperature of TEA and TEAN. Thus, the formation of metal-TEA complexes could reduce the onset temperature (i.e., activation energy) for the decomposition of TEA and TEAN.
- Because of the relatively low melting point, TEAN could reach a liquid state, producing a localized region of increased transport of this and other potentially reactive species, as well as providing a matrix for reaction chemistry.
- TEAN in the neutralized free liquid and associated organic material also could serve as a microbial substrate [Kaplan 1984]. Both TEAN and TEA can be biodegraded both anaerobically and aerobically in a variety of media [Kaplan 1984; Williams 1982]. Formulations that contain di- or triethanolamine compounds can be readily biodegradable. Such formulations have become contaminated with microorganisms capable of degrading these substances unless an addition (e.g. biocide) is added to the formulation to prevent this occurring [West 1996].

POSSIBLE REACTION CHEMISTRY

In this section we discuss possible reaction chemistries and physical conditions leading to a thermal chemical reaction sequence. As previously described, Drum 68660 contained a complex chemical mixture of organics from the Swheat Scoop® sorbent, an organic nitrate salt (TEAN), potentially oxalic acid, as well as nitric acid, and a variety of acidic alkali, alkaline earth, transition metal, main group metal, and actinide nitrate salts. Given this complex mixture, the predominant exothermic chemical reactions include hydrolysis, oxidation and nitration of the organic constituents of the Swheat Scoop® and TEAN. Radiolysis of the carbohydrates and other organics produces organics that would be more susceptible to oxidation and nitration.

Chemical Hydrolysis and Oxidation of Organics

The hydrolysis of carbohydrates serves to break the polymer chains of the D-glucose units into smaller glycosidic units and increases the number of reactive centers. The neutralized liquid/ Swheat Scoop® region of the drum likely has a higher water content than that in the nitrate salt/ Swheat Scoop® region. However, the neutral or near-neutral pH would reduce the likelihood of chemical hydrolysis in neutralized liquid/ Swheat Scoop® layer in the drum. It is likely that chemical hydrolysis would be more prevalent in the drum layer containing the moist nitrate salts/ Swheat Scoop® mixture due to the acid (pH 0) content. The presence of nitric acid in the liquid portion of the nitrate salts fraction of the MIN02 waste will facilitate both chemical hydrolysis and oxidation of carbohydrates. [Morrison 1975] The oxidation of d-glucose to d-glucaric acid is reported to occur in dilute nitric acid at 55–60 °C. [Loudon 1995] Hydrolysis can occur at low temperature and is an exothermic reaction. Consequently, hydrolysis combined with biodegradation of the Swheat Scoop® would likely have contributed to heating of the drum contents beginning from the time that Drum 68660 was assembled.

Oxidation of carbohydrates proceeds through a complex series of reactions ultimately producing carbon dioxide and water as shown in equation 1. Initially, the alcohol and aldehyde groups of the carbohydrates are converted to hydroxy ketones and carboxylic acids. Hydroxy ketones generally rearrange to produce the corresponding aldehydes. For example, 5-hydroxymethylfurfural is reported to be a reaction product from the oxidation of cellulose. [Zhou 2015] As oxidation proceeds, the ring structure of d-glucose unit is cleaved, producing four or five-carbon carboxylic acids such as shown in Figure F-2 for glucose. Finally, the low molecular weight carboxylic acids are converted into carbon dioxide and water.



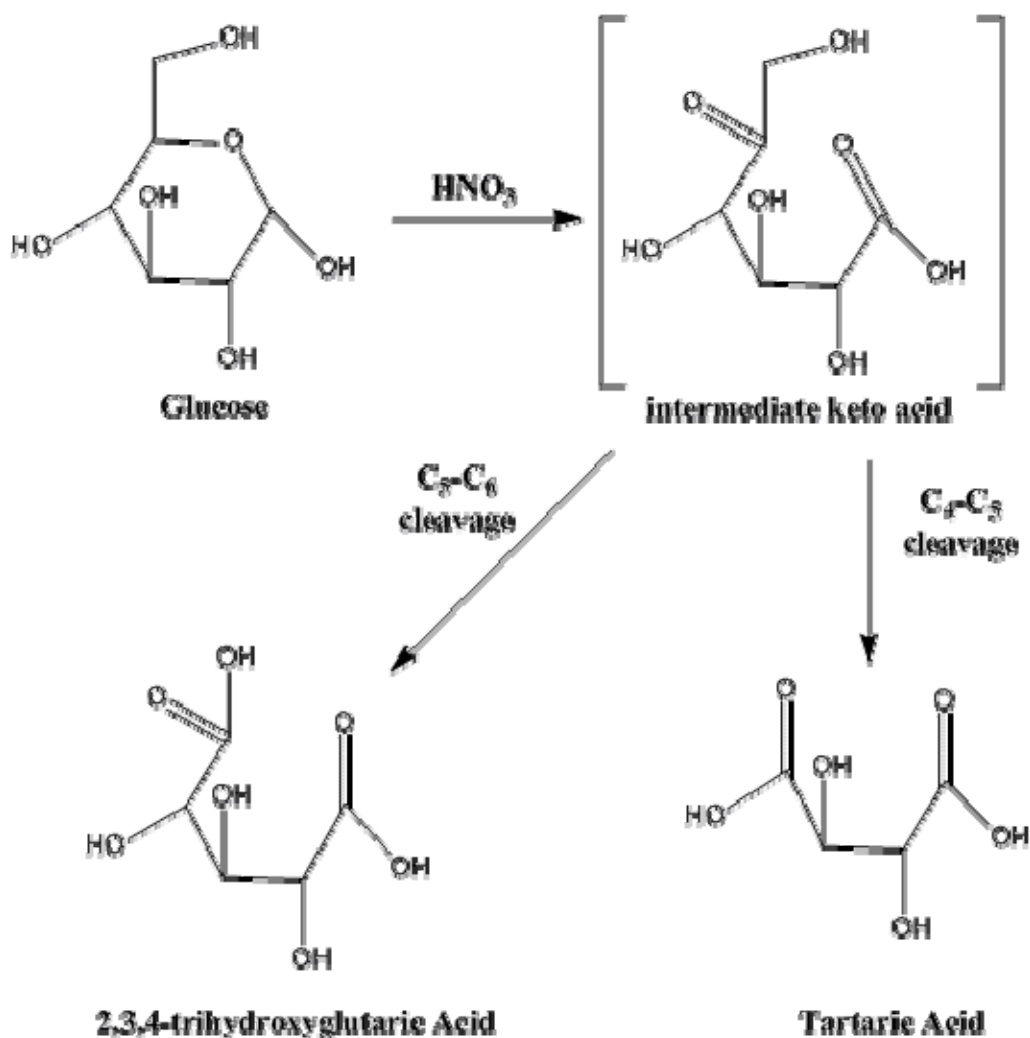


Figure F-2. Oxidation of Glucose to Produce Trihydroxyglutaric Acid and Tartaric Acid

Although there are no direct studies on the reaction of nitrate salts with **Sweet Scoop®** and TEA-neutralized nitric acid and the effects of the other waste constituents on the thermal sensitivity of these potentially reactive nitrate and organic mixtures, a number of studies have been performed to assess the reactivity of wheat constituents (e.g., cellulose) and similar compounds (e.g., sucrose^{vv} and amine- and carboxylate-based complexants). For example, Beitel investigated the explosivity and combustibility of various organics with nitrate-rich Hanford salt cake waste and nitrate salts [Beitel 1977; Beitel 1976a; Beitel 1976b; Beitel 1976c]. Scheele and coworkers investigated the reactions of amine-based complexants, carboxylate-based complexants, cellulose, and sucrose with nitrate and/or nitrite salts and simulated Hanford nitrate-rich wastes [Scheele 1995; Scheele 2005; Kim 2005; Scheele 2007; Scheele 2008], and the Bureau of Mines investigated the reactivity and explosivity of amine- and carboxylate-based complexants with nitrate and/or nitrite salts [Turner 1994b; Turner 1994a].^{ww} Findings from these studies revealed that mixtures of nitrates and organics having many constituents can have lower onset temperatures than that of pure mixtures indicating the possibility of synergistic and catalytic effects of the constituents. Also, the production of gases generated in these studies include those reported in recent headspace gas samples taken from processed MIN02 waste drums at LANL and 10-gal drum tests at SNL.

^{vv} Sucrose is a disaccharide containing glucose and fructose. Although sucrose is not a major constituent of **Sweet Scoop®**, the starch, cellulose and other complex carbohydrates in **Sweet Scoop®** are comprised of polymerized units of d-glucose. Thus, the reaction chemistry of sucrose can provide valuable insight into the possible reaction chemistry of **Sweet Scoop®**.

^{ww} See Appendix A for more details about the conditions and findings from these studies.

Furthermore, Desai, et al. reported that the addition of metal nitrates to amylose produced a system that is unstable well below that of pure amylose (280 °C) [Desai 1972]. In this study, the mixture of magnesium nitrate and amylose exhibited the highest reactivity with the mass loss initiating at about 50 °C. The authors attributed the reactivity to thermal decomposition of the metal nitrate forming nitric oxide which reacts and degrades the amylose. Previously, Gordon and Campbell reported that magnesium nitrate decomposes at relatively low temperature to generate nitric acid vapors and nitrous (NO₂) fumes. [Gordon 1955] Recent laboratory experiments at SNL and LANL have shown that mixtures of metal nitrates including sodium nitrate, magnesium, calcium, and ferric nitrate, and Swheat Scoop® exhibit exothermic reactions occurring at temperatures well below 100 °C. [SNL testing reported in Appendix G; Leonard 2014] Since these metal nitrates are known to be present in the MIN02 waste stream, we conclude that combining metal nitrate salts with Swheat Scoop® may produce a reactive mixture that can decompose organic compounds in the Swheat Scoop®.

Since oxalate is a potential constituent of the Drum 68660 we also considered the reaction chemistry of oxalate and nitric acid/nitrate salts. It is well known that oxalate reacts with nitric acid and metal nitrates to produce carbon dioxide. [Nash 2012] This reaction has been used to decompose oxalic acid in a variety of solutions at the Savannah River Site. Generally, the nitric acid concentration must be above 2 molar for the rate of reaction to be sufficiently rapid for the decomposition to proceed to completion with a few hours. Evidence also exists that oxalate reacts with nitrate salts. For example, differential scanning calorimetry (DSC) and TGA measurements by Turner and Miron found that sodium oxalate reacts with sodium nitrate, sodium nitrite, and equimolar sodium nitrate and nitrite beginning at temperatures ranging from 230 to 322 °C [Turner 1994a]. Exothermic behavior was observed at much lower temperatures, between 105 and 130 °C, when sodium hydroxide was added to a mixture containing 60 mass% sodium oxalate mixture [Turner 1994b]. Thus, if neutralized liquid within the drum were alkaline as a result of an excess of Kolorsafe®, the processed liquid/ Swheat Scoop® mixture may have exhibited increased reactivity at lower temperature.

Reaction products from reactions of carbohydrates with nitrate salts and nitric acid include carbon dioxide (CO₂), nitrous oxide (N₂O), molecular nitrogen (N₂), water (H₂O), and the formation of low molecular weight aldehydes and carboxylic acids as well as aldehyde and carboxylic acid functional groups on the carbohydrate polymers. Evidence for low temperature oxidation reactions is provided by the detection of elevated carbon dioxide and nitrous oxide levels in headspace gas samples taken from a number of drums by LANL stored at ambient temperatures. [Clark 2015] Since abiotic and biotic pathways produce similar reaction products, it is not possible to determine which pathway predominates in the waste drums at low temperatures. Biotic pathways, if present, would diminish as the temperature inside the drum increased and stop upon reaching temperatures near 80 °C.

Biological Hydrolysis and Oxidation

Possible biotic pathways for hydrolysis and oxidation of organics in Drum 68600 include both aerobic and anaerobic respiration (denitrification). Aerobic respiration requires oxygen and may have occurred when the drum was initially assembled and oxygen was present. However, with time and assuming the waste bags retain their integrity, oxygen will be depleted and anaerobic respiration will become the predominant biotic pathway. This sequence appears possible based on preliminary findings from recent testing at Sandia National Laboratories (SNL). In these tests, a 3:1 mixture of Swheat Scoop®:water was placed within a 10-gallon carbon steel drum and allowed to stand undisturbed for a period of time. After seven days, analysis of a sample of the gas removed from the headspace of the drum showed that the gas was comprised of two parts carbon dioxide and 1 part nitrogen and no measureable oxygen. After two more days, the carbon dioxide concentration had continued to increase and had displaced all of the nitrogen with still no measurable oxygen. (Appendix G) However, in drums containing liquids with nitrate salts, carbon dioxide was produced, but at much lower rates.

Another example of biological oxidation of organics in a low moisture environment was that reported by Francis et al. at Brookhaven National Laboratory (BNL) [Francis 1996]. This work investigated microbial degradation of the organic constituents of transuranic (TRU) waste under conditions expected at the WIPP repository. Gas

generation was observed from the microbial degradation of mixed cellulose, plastic and rubber materials (polyethylene, polyvinylchloride, neoprene, hypalon, and leaded hypalon). It was found that more gas was produced in samples containing nutrients, especially excess nitrate, relative to those without a nutrient addition. More recently, Francis reported biodegradation of natural and synthetic organic compounds in low- and intermediate-level wastes (L/ILW), and TRU wastes under aerobic and anaerobic conditions results in the production of gases such as CO₂, N₂O, N₂, H₂, H₂S, and CH₄ as well as HT, ¹⁴CO₂, ¹⁴CH₄, CH₃T, ¹⁴CH₃T [Francis, 2013].

While the exact composition of Drum 68660 is not known, the Swheat Scoop® component is an excellent organic substrate suitable for microbial growth. Swheat Scoop® samples examined at the Savannah River National Laboratory (SRNL) were found to have a diverse microbial population including viable fungi, yeast, and bacteria. [Brigmon 2014] This microbial activity was confirmed through microscopic and culture techniques. Cultures of Swheat Scoop® samples went anaerobic in 1-2 days indicating potential for similar activity in the drums. By day 4 of the culture some hydrogen production was detected. Since yeasts are evident from microscopic examination alcohol production may be possible as well.

The microbial digestion process most likely would begin with bacterial hydrolysis of the Swheat Scoop® in order to break down insoluble organic polymers, such as carbohydrates, through enzyme activity (e.g. amylase) and make them available for other bacteria [Sivaramakrishnan 2006]. Typically acidogenic bacteria then would convert the sugars and amino acids into CO₂, H₂, NH₃, and organic acids. Acetogenic bacteria then convert the organic acids into acetic acid, along with additional CO₂, H₂, and NH₃. Finally, methanogenic bacteria convert these products to CH₄ and CO₂ [O'Keefe 2000]. These biological pathways are exothermic and would contribute to heating of the drum contents. Due to the limited availability of oxygen, the system would quickly move into anaerobic processes. The expected anaerobic processes would most likely not exceed 80 °C due to limited nutrients in the semi- closed and static system.

Handling and shipping of the drum may have helped biological activity by mixing and aerating the contents.. Note, the radiation level in this drum (≤ 17.8 Ci) is not sufficiently high to inhibit biotic reactions [Caldwell 1988]. The described microbial activity could also have caused varying degrees of organic matter functionalization and solubilization, leading to increased chemical reactivity.

Recent results from a 10-gallon drum test at SNL suggests high metabolic activity occurs in a mixture of water and Swheat Scoop® as evidenced by relatively rapid gas (CO₂) production and depletion of N₂ and O₂ at ambient temperature. However, mixtures of Swheat Scoop® and either acidic nitrate salts or TEA-neutralized nitric acid containing dissolved nitrate salts exhibit reduced CO₂ production and N₂/O₂ depletion suggesting that biological activity is significantly reduced and possibly inhibited. Thus, we hypothesize that while biological reactions may have contributed to initial drum heating and some transformation of the Swheat Scoop® components into more reactive species, chemical reactions were the predominant contributor to drum heating.

Nitration of Organics

Organic compounds are well known to undergo nitration in which the nitro group, NO₂, attaches to a carbon atom (C-nitration), a nitrogen atom (N-nitration), or an oxygen atom (O-nitration) of the organic compound [Olah 1989]. The introduction of the nitro group into organic compounds can be accomplished by ionic, radical ion and free radical reactions. The most common method, which is widely used in the chemical industry, is an ionic reaction in which the nitronium ion, ⁺NO₂, is generated in-situ or added as a preformed reagent. In-situ generation of the nitronium ion to affect nitration of alcohols, amides or nitroaromatics is usually accomplished at high nitric acid concentrations (>80% aqueous nitric acid) or in a mixture of concentrated nitric and sulfuric acids [Olah 1989].

The formation of nitrate esters and nitramines in nitric acid mixtures is strongly dependent on the concentration of the nitric acid or the concentration of the “mixed acid” solutions (nitric and sulfuric acids), depending on which

reagents are used for the nitration. For instance, ethylene glycol may be nitrated with “mixed acid” to yield ethyleneglycol dinitrate (EGDN) if the water content in the nitrating mixture is <15%. [Roth 1958] If the water concentration is greater than 15% little or no nitration occurs. This is due to the fact that alcohol and amine nitrations are equilibrium reactions and it is necessary to keep the concentration of the acids very high to push the equilibrium to the nitrated species. The mixed acid acts as both a nitronium ion (NO_2^+) source and as a dehydrating agent, as the formation of nitrate esters or nitramines also gives water as a product species. If the concentration of the mixed acid is too low, the equilibrium lies towards the starting alcohols or amines.

Nitration can also occur if nitrous acid (HNO_2) is present. If present, nitrous acid can hydrolyze in concentrated nitric acid solutions to produce the nitrosonium ion, NO^+ . The nitrosonium ion is electrophilic and reacts with organic compounds to produce a nitroso product which then is rapidly oxidized by nitric acid to produce the corresponding nitro compound. Nitrous acid is the other reaction product of the nitrosonium oxidation resulting in the potential for the reaction to become autocatalytic. [Elias 2010]

The liquids associated with the solid nitrate salts in Drum 68660 were not neutralized and may have been highly acidic. The nitric acid concentration of the liquid as well as the quantity of liquid associated with the nitrate salts mixed with the Sweat Scoop® are both likely to be heterogeneously distributed in the drum.. The free liquid recovered from the parent drum of Drum 68660 was reported to have a pH of zero, which indicated an acid concentration of at least 1 M. According to operating procedures, these acidic liquids were neutralized to pH 7 before sorbing onto the Sweat Scoop® kitty litter. However, documentation that the liquids were neutralized and records of the final solution pH do not exist. Nevertheless, the nitric acid concentration, whether the liquid associated with the nitrate salts, or in the neutralized liquid, is not sufficiently concentrated to produce the nitronium ion at ambient conditions. Consequently, it is very unlikely that extensive nitration of the organics in Drum 68660 occurred at low temperatures.

Radiolysis Reactions

The presence of ionizing radiation from radioactive decay of transuranic elements in the waste could also facilitate reactions between the chemicals inside the nitrate salt waste drums. Although the radioactivity content is relatively low in TRU waste drums, the alpha particles emitted by plutonium and americium isotopes in the waste have energies in excess of 5 MeV. These particles have limited range, but will deposit considerable energy in their path with the potential to produce reactive radical and ionic species. The radioactive decay will also provide heat to the drum. However, the concentrated tracks containing these reactive species ensure that most recombine rather than reacting with other solutes, and alpha radiolysis typically has less damaging effects on organic species in solution than gamma radiolysis. [Mincher 2014]

Possible radiolytic reactions include the radiolysis of water, nitrate, and organic compounds. In addition to the organic sorbent and TEA/TEAN, the waste drums contain plastic materials, primarily polyethylene (PE) and polyvinyl chloride (PVC). The major gaseous products from the radiolysis of organic compounds (e.g., cellulose) and plastics is hydrogen with smaller amounts of carbon dioxide, carbon monoxide, water, methane, and oxygen. [Molecke 1980] Plastics often become more brittle with irradiation, due to cross linking reactions that produce higher molecular weight, unreactive polymer species. Other organic compounds are well known to undergo a variety of reactions upon exposure to ionizing radiation. In studies where water is present, hydroxyl radicals, $\bullet\text{OH}$, hydrated electrons, and $\bullet\text{H}$ atoms are formed which will react with organics in addition to direct interactions with ionizing radiation. These radicals often react by H-atom abstraction, to produce carbon-centered radicals. These carbon-centered radicals may then undergo many other reactions, including cross linking with each other as for the polymers above. In another example, in the radiolysis of glucose in water, the reaction of the $\bullet\text{OH}$ radical predominates to form glucosyl radicals by H atom abstraction. The glucosyl radicals further react to produce ketone and carboxylic acids. [Diehl 1978] The nature of the products depends greatly upon the oxygen content of the system. Carbon-centered radicals add oxygen to form peroxy radicals, which then typically decompose to give oxidation products such as acids and ketone. In the absence of oxygen, a wider variety of products is possible. [Alfazzi 1997]

In the presence of proteins, the formation of ketones is reduced likely by reactions with more reactive centers such as carbon atoms bonded to a heteroatom nitrogen or sulfur. Thus, the carbohydrates, proteins and lipids in the Swheat Scoop® absorbent would be expected to undergo radiolytic reactions upon exposure to ionizing radiation from the transuranic elements. A wide variety of products are to be expected, but all at low concentrations.

Gamma radiolysis of a solution of the hydrochloride salt of TEA has been reported to produce equal molar yield of acetaldehyde and diethanolamine [Schwarz 1982]. Because of the high water content in these experiments, the initiating reaction was judged to be the reaction of the TEA with either the •OH or •H produced by radiolysis of water. Acetaldehyde has a boiling point of 20.2 °C and, therefore, would be expected to be easily volatilized and would be detected in the gases evolved from a drum.

Radiolysis of nitrate would be expected to produce nitrite, NO₂⁻, and oxygen, the nitro radical, •NO₂, and the nitrate radical, •NO₃. Nitrite would not be expected to a strong nitration reagent, but nitrite salts are known to thermally react with organic carboxylate- and amine-complexants [Scheele 1995]. Nitrous acid, HNO₂, is a strong nitrating agent under acidic condition. The •NO₂ and •NO₃ radicals are very reactive and would be expected to react with organic compounds at relatively low temperatures to produce nitrated organics. However, the low curie content of the drum (≤ 17.8 Ci) limits this reaction pathway being a major reaction because only very small concentrations of these reactive species are generated [Giaquinto 2014].

In general, head space gas analysis of processed waste drums at LANL has indicated that the major gaseous products are carbon dioxide and nitrous oxide and not molecular hydrogen [Leibman 2014]. Hydrogen is measureable, but at very low concentrations in the majority of the samples. Since H₂ is a major organic species radiolysis product, the low hydrogen concentration in the headspace gas samples is evidence that radiolytic reactions are not a predominant reaction pathway in those drums.

Other Factors That Can Influence Reaction Chemistry

In addition to the heat produced from exothermic chemical reactions, heat was also produced by radioactive decay of the plutonium and americium. Heat produced from these two sources could be stored in the nitrate salts raising the temperature of the salts. The melting points of pure, anhydrous sodium nitrate, potassium nitrate, and calcium nitrate salts are 306.8, 334, 561 °C, respectively. [Weast 1984] Except for the alkali metal nitrates (Na, K), metal nitrates are usually present as hydrated salts that contain between 2 and 12 molecules of water. The melting points of the hydrated metal nitrate salts are much lower than the anhydrous metal nitrates (see Table F-1). From Table F-1, several of the hydrated metal nitrate salts melt well below 100 °C. Furthermore, the melting point of TEAN is 80 °C.

Table F-1. Melting Points of Selected Hydrated Metal Nitrates [Weast 1984]

Salt	Melting Point (°C)
Mg(NO ₃) ₂ 2H ₂ O	129
Mg(NO ₃) ₂ 6H ₂ O	89
Ca(NO ₃) ₂ 4H ₂ O	39.7 (α); 42.7 (β)
Al(NO ₃) ₃ 9H ₂ O	73.5
Fe(NO ₃) ₃ 6H ₂ O	35
Cr(NO ₃) ₃ 6H ₂ O	60

Upon melting, these melt liquids offer the opportunity to wet the surface of the Swheat Scoop®, providing the possibility of a more intimate dispersion of the nitrates and TEAN into the Swheat Scoop® particles. The increased dispersion may offer increased reactivity of the mixture. There are reports of mixtures of TEAN/hydroxylammonium nitrate, urea (or other organic fuel) and water serving as a liquid monopropellant with low

melting points. [Garner 1997; Zabala 1992; Lee 2001; Daniel 1997] In one study [Garner 1997] the decomposition of the liquid propellant was quite significant at 100-148 °C and that the decomposition gases catalyzed further decomposition of the organic fuel.

If temperatures within the drum resulted in the evaporation of water from the metal nitrates, formation of anhydrous metal nitrates could occur within regions of the drum. Although the melting points of the pure nitrate salts of sodium, potassium, and calcium range from 306.8 to 561 °C, eutectic mixtures of the salts could form that melt at appreciably lower temperatures. Upon melting, the nitrate salts would be expected to react much more rapidly with the organic absorbent and neutralizer, resulting in highly exothermic reactions such as oxidation and nitration of the organics. As the reactions proceed, more heat would be generated along with the formation of product gases. The product gases could catalyze further oxidation and decomposition, build pressure in the vessel and also increase the surface area of the Swheat Scoop®, creating more reactive surfaces for the oxidation/nitration/decomposition reactions. There are reports that metal nitrate salt mixtures can oxidize other transition metals present in the drum such as lead, cobalt, iron, tin and copper to their respective oxides at elevated temperatures. [Eweka 1996; Kerridge 1991] These transition metal oxides could also serve as catalysts for oxidation and nitration of organics. [Kerridge 1991]

There are several published studies describing the use of metal nitrate mixtures as heat storage medium. [Bradshaw 2008; Breidenbach 2012] The premise is that these mixtures have a high latent heat of fusion so they may be able to store and transport heat efficiently. The high heat of fusion allows the liquid to transport a large amount of heat and release it upon solidification. The melting temperatures of the mixtures reported in these papers were as low as 82.3 °C [Cordaro 2012] and could be lower if there are multiple nitrate salt components in the matrix such as that reported for the MIN02 waste stream.

These nitrate salts also form low-melting eutectics with organic compounds such as acetamide or butyramide, confirming that eutectics or low-melting mixtures with organic compounds, such as TEAN, are possible. [Nikolic 1992; Eweka 1999] This work supports the idea that nitrate salt mixtures would be able to absorb a significant amount of latent heat from various hydrolysis, and abiotic/biotic reactions of the organic compounds in the matrix. This would act as a temperature limiter on the system, much like water. The salt mixture would absorb a significant amount of energy, keeping the temperature of the system stable at the melting point of the eutectic.

Once all of the eutectic mixture had transitioned to the liquid phase however, the system would not only be free to increase in temperature, but the resulting molten salt would act as a highly efficient heat transfer system. Gravity induced flow would transport hot molten salt from upper portions of the system to lower regions.

If the molten salt encountered temperatures low enough to solidify, the large heat of fusion would result in significant local heating. In addition, with the melting of the mixture, the oxidation and decomposition reaction rates would increase significantly because the reactions are proceeding in the liquid phase or at the liquid/solid interface. If the temperature rises above the decomposition temperature of the nitrate salts or the TEAN mixture, a significant amount of additional heat would be generated along with decomposition gases.

Once a system reaches a temperature at which the reactants have the necessary activation energy for a particular chemical reaction, the reaction will proceed. The rate of the reaction is governed by the system conditions. Typically, reaction rates increase by a factor of two to three for every 10 °C rise in temperature [CCPS 1995]. Thus, as chemical reactions proceed and heat is released and retained within the drum, the contents will increase in temperature resulting in faster reaction rates. Faster reactions lead to increased energy released driving internal drum temperatures higher and can eventually reach thermal runaway. As the temperature increases, additional oxidation reaction pathways or autocatalytic or self-catalyzing reactions can occur potentially with faster reaction rates and faster heat generation rates.

Reactivity Considerations for the Nitrate Salts/Swheat Scoop® Mixture

The moist nitrate salts, which were mixed with Wheat Scoop® without the addition of the neutralizing agent contain an unknown quantity of acidic liquid. This liquid would be located on the surface of salts and occluded within the salt crystals. Nitrate salts can be highly hygroscopic and contain significant water in the crystalline matrix.

The liquid contained in the nitrate salts is comprised of nitric acid and dissolved metal ions. Metal ions include the alkali (Na, K), alkaline earth (Mg, Ca), transition metal (Fe, Cr, Ni), main group (Pb, Al) and actinides (Pu, Am). The nitric acid concentration could range from a low of 0.01 M to greater than 1 M (see discussion above). This range of nitric acid concentrations in the moist nitrate salts increases the reactivity of metal nitrates toward the oxidation of organic components in the Wheat Scoop® compared to metal nitrates at or neutral pH. The relatively high acid concentration would reduce, but not eliminate, biotic reaction as these pathways are favored at near- neutral conditions.

The liquid most likely available to interact with the Wheat Scoop® sorbent matrix is that at or near the surface of the nitrate salts. Thus, penetration of the liquid from the nitrate salts into the Wheat Scoop® matrix would be much more limited compared to the case in which drained, free liquid is mixed with the Wheat Scoop® matrix. Consequently, the nitrate salt/ Wheat Scoop® mixture would have a more heterogeneous distribution of liquid within the nitrate salt/ Wheat Scoop® mixture compared to that obtained by mixing neutralized liquid and Wheat Scoop®.

Reactivity Considerations for the Neutralized Liquid/Swheat Scoop® Mixture

The presence of TEAN in the neutralized liquid/ Wheat Scoop® mixture added an additional fuel source in this layer of Drum 68660. The neutralized liquid fraction contains much higher liquid content than the nitrate salt fraction, which allows for increased transport of dissolved chemical species into the Wheat Scoop® sorbent matrix. Thus, a much more intimate mixture of the neutralized liquid and the Wheat Scoop® particles would be expected compared to the nitrate salt/Sorbent mixture. Note, since the pH of the neutralized liquid is near neutral, the nitrate would be expected to be less reactive than when present under acidic conditions such as that in the moist nitrate salts that were not neutralized.

Upon sorption of the neutralized liquid into the sorbent, the water content in the Wheat Scoop® could be increased to a level that facilitates biotic reactions including hydrolysis, oxidation and respiration of the organic polymers. Hydrolysis of the organic polymers increases the number of potentially reactive alcohol functional groups that subsequently could undergo oxidization or nitration. It is likely that any biological reaction would begin under aerobic conditions, but through the consumption of oxygen and release of carbon dioxide, the system will proceed to anaerobic condition. Note, however, the biological activity is likely reduced by the presence of nitrate salts as previously discussed.

Reactive Considerations at the Interface of the Neutralized Liquid/Swheat Scoop® and the Nitrate Salts/Swheat Scoop® Fractions

Assembly of Drum 68660 featured a layer of neutralized free liquid sorbed onto Wheat Scoop® followed by a layer of nitrate salts mixed with Wheat Scoop®. Thus, there is a region in the drum in which the two mixtures are in physical contact and likely partially mixed. The total surface area of this interfacial region is not known. However, it is likely that the interfacial region is greater than the geometrical surface area representing two completely level layers of solids in contact with each other.

The consistency of the neutralized liquid/Swheat Scoop® mixture in Drum 68660 was not reported. In preparing neutralized liquid/Swheat Scoop® mixtures for the 10-gallon drum tests at SNL, it was reported that the mixtures were dough-like. Thus, upon transfer of the neutralized liquid/Swheat Scoop® mixture into Drum 68660, these solids are likely to form an irregularly shaped layer since the mixture was not likely to have been free flowing. The solids containing the nitrate salts/Swheat Scoop® mixture would then fill in open voids, if present, around the neutralized liquid/Swheat Scoop® solids. The resulting mixture would have a higher

interfacial surface area than two layers of level solids.

If the neutralized liquid/Swheat Scoop® mixture formed a domed- or column-shaped region, this region would then be largely surrounded by the nitrate salts/Swheat Scoop® solids. Such a situation may serve to thermally insulate a region of the neutralized liquid/Swheat Scoop®. Thus, heat produced from exothermic reactions in neutralized liquid/Swheat Scoop® mixture could be retained leading to higher localized temperatures. The nitrate salts/Swheat Scoop® layer could also be serving as a conduit to remove water vapor (an excellent heat sink) from the neutralized liquid/Swheat Scoop® region.

Drum Configuration

Drum #68660 consisted of the following in order of addition, (1) vented carbon steel drum with vented PVC bag and fiber-board liner inserted within the PVC bag, (2) a bottom layer of job-control solid waste consisting of plastic bags, an empty Kolorsafe® bottle cut into two pieces and a glove-box glove, (3) 2 gallons of free liquid reported to have a pH of 0 that had been neutralized with Spilfyter® Kolorsafe® (50% triethanolamine/50% water) and absorbed onto Swheat Scoop® kitty litter, and (4) moist nitrate salts mixed with Swheat Scoop®. The neutralized liquid/Swheat Scoop® mixture was placed on top of the job-control solid waste followed by the nitrate salts/Swheat Scoop® mixture.

The RTR record confirmed that the drum was filled to approximately 65% capacity with no visible free liquid. The heterogeneous distribution of liquids sorbed into the Swheat Scoop® and surfaces of metal nitrate salts makes the drum a collection of nanometer, micrometer, and millimeter-scale chemical reactors. There is no active mixing in these reactors, although there would be some limited amount of mixing when the drum was being physically moved.

Chemical reactions will occur at or near the surfaces of solids where water/liquid is present or where reactive gases are released. Transport of reactive species and products is controlled by diffusion. In the event that conditions resulted in the melting of the nitrate salts, the resulting liquid phase would provide for increased transport of reactive species and reaction products. There are also a number of interfaces within the drum including, (1) neutralized liquid/Swheat Scoop® mixture and moist salt/Swheat Scoop® mixture, (2) neutralized liquid/Swheat Scoop® with job-control solid waste, (3) neutralized liquid/Swheat Scoop® and fiber-board liner, (4) moist salt/Swheat Scoop® mixture and fiber-board liner, and (5) moist salt/Swheat Scoop® mixture and PVC bag. Of these five types of interfaces, the interface between the neutralized liquid/Swheat Scoop® mixture and the moist nitrate salt/Swheat Scoop® mixture represents the more likely location for chemical reactions.

KEY CONCLUSIONS

Based on the discussion presented above concerning the chemicals assembled into Drum 68860, the physical configuration of the drum contents, and the possible reaction chemistry, the TAT concludes the following:

- The combination of the acidic free liquid from the parent drum and TEA during neutralization and subsequent sorption onto the Swheat Scoop® material as well as the combination of acidic nitrate salts and Swheat Scoop® created an incompatible mixture of fuels (Swheat Scoop® and TEAN) and oxidizers (nitrate salts and nitric acid).
- The drum was a complex, heterogeneous mixture of materials with the potential for multiple reaction sites and reaction chemistries.
- Possible chemical reactions involving the sorbent and the neutralization reagent included hydrolysis, oxidation, and nitration.
- Biological reactions may have occurred at low temperatures (<80 °C) and were more likely to have occurred in the processed liquid fraction due to the higher water content and neutral or near-neutral pH.
- The presence of TEAN in the neutralized free liquid added a potentially reactive compound to the region of the drum containing the neutralized liquid/Swheat Scoop® mixture.
- The localized water content likely played a key role in the chemical reactivity of the TEAN/Swheat

Scoop® and the metal nitrate/Swheat Scoop® mixtures.

- The physical configuration at the interface of the neutralized liquid/Swheat Scoop® and the nitrate salts/Swheat Scoop® layers may have played an important role in forming a localized region of high reactivity.

Using the key conclusions listed above, we propose the following conditions and sequence of chemical reactions that led to a runaway reaction system and release of drum contents into Room 7 of Panel 7 in the WIPP facility. A combination of exothermic chemical reactions and radioactive decay heat heated the drum contents in localized regions of the drum which evaporated free liquid and waters of hydration in the nitrate salts. Chemical reactions continued until a runaway reaction occurred or heated up the liquid fraction containing TEAN so that the TEAN decomposition reaction began leading to a thermal runaway condition. During heating the partial pressure of nitric acid in the vapor phase was increased, which led to increased oxidation of the organic compounds in the Sweat Scoop®. Heat from the exothermic chemical reactions continued to increase the temperature of the drum contents, which in turn increased the reaction kinetics, the production of gaseous products, and also initiated chemical reactions with higher activation energies. At this stage, a self-sustaining condition was achieved such that the dissipation of heat to surrounding regions of the drum could not keep up with that produced by the exothermic chemical reactions. Heat and gas production ultimately proceeded at such a rate to pressurize the drum and overcome the venting and drum ring enclosure.

REFERENCES

1. **[Alfassi 1997]**. Alfazzi, The chemistry of free radical: Peroxyl radicals, Wiley 1997
2. **[Allen 2002]**. Allen, F., The Cambridge Structural Database: a quarter of a million crystal structures and rising. Acta Crystallographica Section B, 2002. 58(3 Part 1): p. 380-388.
3. **[Beitel 1976a]**. Beitel, G. Sodium Nitrate Combustion Limit Tests. 1976. ARH-LD-123. Atlantic Richfield Hanford. Richland, Washington.
4. **[Beitel 1976b]**. Beitel, G.A. Final report on investigation of stability of organic materials in salt cake. 1976. ARH-LD-126. Atlantic Richfield Hanford Company. Richland, WA.
5. **[Beitel 1976c]**. Beitel, G.A. Chemical stability of salt cake in the presence of organic materials. [Detonation hazard]. 1976. ARH-LD-119. Atlantic Richfield Hanford Company. Richland, WA.
6. **[Beitel 1976d]**. Beitel, G. A. Sodium nitrate combustion limit tests. ARH-LD-123. Atlantic Richfield Hanford Company. Richland, WA. <http://www.osti.gov/scitech/servlets/purl/7186506>.
7. **[Beitel 1977]**. Beitel, G.A. Exothermic potential of sodium nitrate salt cake. 1977. ARH-LD-163. Atlantic Richfield Hanford Company. Richland, WA.
8. **[Bradshaw 2008]**. Bradshaw, R.W. and N.P. Siegel, "Molten Nitrate Salt Development for Thermal Energy Storage in Parabolic Trough Solar Power Systems." ES2008 Energy Sustainability 2008. 2008, ASME: Jacksonville, Florida USA. p. 1-7.
9. **[Breidenbach 2012]**. Breidenbach, N., et al. "Overview of Molten Salt Storage Systems and Material Development for Solar Thermal Power Plants." ASES Solar 2012. 2012. Freiburg, GE: American Solar Energy Society.
10. **[Brigmon 2014]**. Brigmon, R. Environmental Biotechnology II. Laboratory Notebook. SRNL-NB-2012-00014. Pages 146-147. November 21, 2014.
11. **[Buggeln 2002]**. Buggeln, R. and R. Rynk. 2002. Self-Heating In Yard Trimmings: Conditions Leading To Spontaneous Combustion Compost Science & Utilization, 10: 162-182 [
12. **[Caldwell 1988]**. Caldwell, D.E., R. C. Hallet, M. A. Molecke, E. Martinez, B. J. Barnhart. 1988. Rates of CO₂ Production From the Microbial Degradation of Transuranic Wastes Under Simulated Geologic Isolation Conditions. CONTRACTOR REPORT SAND87- 7170 Unlimited Release UC-70
13. **[CCPS 1995]**. Guidelines for Chemical Reactivity Evaluation and Application to Process Design. 1995, New York: American Institute of Chemical Engineers - Center for Chemical Process Safety.
14. **[Clark 2015]**. Clark, D.L.; Funk, D.J. Waste Isolation Pilot Plant (WIPP): Chemical Reactivity and Recommended Remediation Strategy for Los Alamos Remediated Nitrate Salt (RNS) Wastes. 2015. Los Alamos, NM. LA-CP-15-20082.

15. **[Cordaro 2012]**. Cordaro, J.G., et al., “Thermodynamic Properties of Molten Nitrate Salts.” Preprints of Symposia - American Chemical Society, Division of Fuel Chemistry (2012), 57(1), 47-48.
16. **[Cronin 1988]**. Cronin, J.T.; Brill, T.B. “Thermal Decomposition of Energetic Materials 29 – The Fast Thermal Decomposition Characteristics of a Multicomponent Material: Liquid Gun Propellant 1845”, *Combustion and Flame*, 1988, 74, 61 -89.
17. **[Daniel 1997]**. Daniel, K.J., et al., Investigation of ignition of liquid propellant in reservoir in regenerative liquid propellants gun trials. *Defense Science Journal*, 1997. 47(2): p. 185-192.
18. **[Deihl 1978]**. Diehl, J.F.; Adam, S.; Delincee, H.; Jakubick, V. “Radiolysis of Carbohydrates and Carbohydrate-Containing Foodstuffs”, *J. Agricultural and Food Chemistry*, 1978, 26(1), 15 – 20.
19. **[Desai 1972]**. Desai, D.H.; Patel, C.K.; Patel, K.C.; Patel, R.D.; “The Effect of Some Nitrate Salts on the Thermal Behavior of Amylose”, *Starch*, 1972. 24(2), 42-45.
20. **[Dow 2014]**. Company, D.C., Ethanolamines. 2014, Dow Chemical Company.
21. **[Drake 2014]**. R. Drake, “Analytical Results from the Area G Nitrate Salt Samples Submitted to C-AAC”, memorandum to N. Sauer, CAAC-14-23, May 22, 2014.]
22. **[Elias 2010]**. Elias, G.; Mincher, B.J.; Mezyk, S.P.; Cullen, T.D.; Martin, L.R. Anisole nitration during gamma- irradiation of aqueous nitrite and nitrate solutions: free radical versus ionic mechanisms. *Environ. Chem.* 2010, 7, 183 – 189.]
23. **[Eweka 1996]**. Eweka, E.I., and D.H. Kerridge, Molten sodium nitrite-sodium nitrate-potassium nitrate eutectic: The reactions and spectra of iron (III), cobalt (II), nickel(II) and copper (II) compounds. *Thermochim. Acta*, 1996. 290: p. 133-138.
24. **[Eweka 1999]**. Eweka, E.I. and D.H. Kerridge, Solution chemistry of molten amide-nitrate eutectics. *Chem. Papers*, 1999. 53(1): p. 11-15.
25. **[Fowkes 2006]**. Fowkes, A. and W.T.A. Harrison, (Nitrate-[kappa]2O,O')bis(triethanolamine-[kappa]4N,O,O',O'')lanthanum(III) dinitrate. *Acta Crystallographica Section C*, 2006. 62(6): p. m232-m233.
26. **[Francis 1996]**. Francis, A.J., J. B. Gillow, and M. R. Giles. Microbial Gas Generation Under Expected Waste Isolation Pilot Plant Repository Conditions. 1996. CONTRACTOR REPORT SAND96-2582 Unlimited Release UC-721.
27. **[Francis 2013]**. Francis, A.J. 2013, Microbial Transformations of Radioactive Wastes: Implications on Gas Generation and Radionuclide Speciation. Proceedings FORGE Symposium, Luxembourg 5 to 7 February 2013. Pgs. 37-40
28. **[Garner 1997]**. Garner, J.S., J.S. Oxley, and J.L. Smith, Thermal stability of HAN-based liquid gun propellant. *J. Therm. Anal.*, 1997. 49(3): p. 1315-1319.
29. **[Giaquinto 2014]**. Giaquinto, personal communication, October 28, 2014.
30. **[Gordon 1955]**. Gordon, S.; Campbell, C. “Differential Thermal Analysis of Inorganic Compounds – Nitrates and Perchlorates of the Alkali and Alkaline Earth Groups and Their Subgroups”, *Analytical Chemistry*, 1955, 27(7), 1102-1109.
31. **[Haagenstad 2012]** Haagenstad, M. “Legacy TA-55 Nitrate Salt Wastes at TA-55—Potential Applicability of RCRA D001/D002/D003 Waste Codes.” February 29, 2012. Los Alamos, NM. ENV-RCRA-12-0053.
32. **[Hogland 2003]**. Hogland, W. , and M. Marques. 2003. Physical, biological and chemical processes during storage and spontaneous combustion of waste fuel. 40:53–69
33. **[Kaneshige 2014]**. M.J. Kaneshige, email correspondence to D.L. Wilson, December 8, 2014
34. **[Kaplan 1984]**. Kaplan, D. L., Riley, P. A., Emerson, D. J., and Kaplan, A. M. 1984. "Degradation of Ammonium Nitrates in Aqueous and Soil Systems", *Environ. Sci. Technol.*, 18:694-699.
35. **[Kerridge 1991]**. Kerridge, D.H. and W.M. Shakir, Molten lithium nitrate-potassium: the reactions of aluminum, gallium and thallium. *Thermochim. Acta*, 1991. 182(1): p. 107-122.
36. **[Kim 2005]**. Kim, D.-S., et al., Tc Reductant Chemistry and Crucible Melting Studies with Simulated Hanford Low-Activity Waste. 2005. PNNL-15131.
37. **[Kissinger 1957]**. Kissinger, H.E., Reaction Kinetics in Differential Thermal Analysis. *Anal. Chem.*, 1957. 29(11): p. 1702-1706.
38. **[Koehler 2013]**. Koehler, P.; Wieser, H. “Chemistry of Cereal Grains”, Chapter 2 in *Handbook on Sourdough Biotechnology*, Gobbetti, M.; Ganzle, M., Eds. Springer Science, New York, 2013, pp 11 – 45.

39. **[Lange's 1985]**. *Lange's Handbook of Chemistry*, 13th Edition, Dean, J.A., Ed.; McGraw-Hill, New York, 1985, page 7-657.
40. **[Lee 2001]**. Lee, H.-S. and T.A. Litzinger, Thermal composition of HAN-based liquid propellants. *Combust. And Flame*, 2001. 127(4): p. 2205-2222.
41. **[Leibman 2014]**. C. Leibman, D. Martinez, J. Coons, K. Weisbrod, "Headspace Gas Sampling and Analysis of LANL TRU Wast Drums/SWBs", presented to Technical Assessment Team, July 21, 2104.
42. **[Leonard 2014]**. P. Leonard, E. Hartline, M. Sandstrom, G. Brown, "APTAC and TAM Experiment Summary", Los Alamos National Laboratory, working draft, December 2014.
43. **[Loudon 1985]**. Loudon, G. M. *Organic Chemistry*, 3rd Edition, Benjamin/Cummings Publishing Co., Inc., Redwood City, CA, pp 1350 - 1351.
44. **[Mincher 2014]**. Mincher, B.J. et al. "The Radiation Chemistry of CMPO: Part 2. Alpha Radiolysis" Solvent Extraction and Ion Exchange, 2014, 32 167-178.
45. **[Mogdel 2010]**. Moqbel, S.D. Reinhart, R-H. Chen. 2010. Factors influencing spontaneous combustion of solid waste. *Waste Manag.* 30: 1600–1607
46. **[Molecke 1980]**. Molecke, M.A. "Gas Generation from Transuranic Waste Degradation", Scientific Basis for Nuclear Waste Management, Volume 2, Northrup, Jr., C.J.M., Ed., Plenum Press, NY, 1980, 569 – 575.
47. **[Morrison 1975]**. Morrison, R.T.; Boyd, R.N. *Organic Chemistry*, 3rd Edition, Allyn and Bacon, Inc., Boston, MA, pp 1075 – 1077.
48. **[Nash 2012]**. Nash, C.N., "Literature Review for Oxalate Oxidation Processes and Plutonium Oxalate Solubility", Technical Report SRNL-STI-2012-00003, Rev. 0, Savannah River National Laboratory, Aiken, SC, January 2012 and references reported therein.
49. **[Nielsen 1972]**. Nielsen, K., R.F. Hazell, and S.E. Rasmussen, The Crystal Structure of Di-triethanolamine-Ni(II)- dinitrate. *Acta Chemica Scandinavica*, 1972. 26: p. 889-896.
50. **[Nikolic 1992]**. Nikolic, R., G. Ristic, and M. Todorovic, Binary eutectics of acetamide with organic nitrates: thermophysical properties relevant to heat storage. *Solar Energy Materials and Solar cells*, 1992. 28: p. 59-69.
51. **[O'Keefe 2000]**. O'Keefe, D. M., R.L. Brigmon, and D.P. Chynoweth. 2000. Influence of methane enrichment by aeration of recirculated supernatant on microbial activities during anaerobic digestion. *Bioresource Technol.*, 71:217-224.
52. **[Olah 1989]**. Olah, G.A., Malhotra, R., Narang, S.C. *Nitration Methods and Mechanisms*, VCH Publishers, Inc., New York.
53. **[Roth 1958]**. Roth, J., F.S. Stow, and D.L. Kouba, Kinetics of ethylene glycol nitration. *Ind. Eng. Chem.*, 1958. 50(9): p. 1283-1288.
54. **[Saldek 1997]**. Sladek, J.H. Method for Sorbing Liquid using Ground Wheat Grain Litter. U.S. Patent 5,690,052, November 25, 1997.
55. **[Scheele 1995]**. Scheele, R.D., et al. Organic Tank Safety Project: Preliminary Results of Energetics and Thermal Behavior Studies of Model Organic Nitrate and/or Nitrite Mixtures and a Simulated Organic Waste. 1995. PNL-10213. Pacific Northwest Laboratory. Richland, Washington.
56. **[Scheele 2005]**. Scheele, R.D., et al., Thermal Stability Studies of Candidate Decontamination Agents for Hanford's Plutonium Finishing Plant Plutonium-Contaminated Gloveboxes. 2005. PNNL-15410.
57. **[Scheele 2007]**. Scheele, R.D., et al. Evaluation of Exothermic Reactions from Bulk Vitrification Melter Feeds Containing Cellulose. 2007. PNNL-16677. Pacific Northwest National Laboratory. Richland, WA.
58. **[Scheele 2008]**. Scheele, R.D., B.K. McNamara, and L.M. Bagaasen. Thermal Flammable Gas Production from Bulk Vitrification Feed. 2008. PNNL-17491. Pacific Northwest National Laboratory. Richland, WA.
59. **[Schwarz 1982]**. Schwarz, H.A. "Chain Decomposition of Aqueous Triethanolamine", *J. Phys. Chem.*, 1982, 86, 3431 – 3435.
60. **[Shewry 2013]**. Shewry, P.R., et. al "Natural Variation in Grain Composition of Wheat and Related Cereals", *J. Agricultural and Food Chemistry*, 2013, 61, 8295 – 8303.
61. **[Sivaramakrishnan 2006]**. Sivaramakrishnan, S. , D. Gangadharan, K. M. Nampoothiri, C. R. Soccol, and A. Pandey. 2006. α -Amylases from Microbial Sources – An Overview on Recent Developments. *Food Technol. Biotechnol.* 44 (2) 173–184
62. **[Sramkova 2009]**. Sramkov, Z., Gregova, E.; Sturdik, E. "Chemical Composition and Nutritional Quality of Wheat Grain", *Acta Chimica Slovaca*, 2009, 2(1), 115 – 138.

63. **[SRNL 2014]**. SRNL report with DSC data
64. **[Storm 1985]**. Storm, P., 1985. Identification of thermophilic bacteria in solid-waste composting. *Appl. Environ. Microbiol.* 50: 906–913.
65. **[Sweat Scoop 2014]**. Sweat Scoop® Natural Clumping Litter – Why It Works, <http://www.sweatscoop.com/>, accessed 11/10/2014.
66. **[Turner 1994a]**. Turner, D.A. and Y. Miron. Testing of Organic Waste Surrogate Materials in Support of the Hanford Organic Tank Program - Final Report. 1994. WHC-MR-0455. Westinghouse Hanford Company. Richland, WA.
67. **[Turner 1994b]**. Turner, D.A. and Y. Miron. Testing of Organic Waste Surrogate Materials in Support of the Hanford Organic Tank Program - Final Supplementary Report. 1994. WHC-MR-0455 Supplement 1. Richland, Washington.
68. **[Weast 1984]**. Handbook of Chemistry and Physics, R. C. Weast, Ed., 65th Edition, CRC Press, Boca Raton, FL, 1984.
69. **[West 1996]**. West, R.J., and S. J. Gonsior. 1996. Biodegradation of triethanolamine. *Environmental Toxicology and Chemistry.* 15, 472–480.
70. **[Williams 1982]**. Williams, G.R. and A. G. Calley. 1982. The Biodegradation of Diethanolamine and Triethanolamine by a Yellow Gram-negative Rod. *Journal of General Microbiology*, 128, 1203-1209.
71. **[Williams 2014]**. Personal Communication: Bob Williams, LANL
72. **[WIPP 2014]**. “Waste Isolation Pilot Plant Radiological Release: Phase I Report, Los Alamos National Laboratory WIPP Recovery Team, Internal Report to the Director, July 25, 2014
73. **[Yilmaz 2002]**. Yilmaz, V.T., Y. Topcu, and A. Karadag, Thermal decomposition of triethanolamine and monoethanolethylenediamine complexes of some transition metal saccharinates. *Thermochimica Acta*, 2002. 383(1–2): p. 129-135.
74. **[Zabala 1992]**. Andrio Zabala, J.A., A. Gonzales Oejo, and L.A. Vidal Rodriguez, Compositions for gel-type permissible explosives, and their manufacture. 1992: Germany.
75. **[Zhou 2015]**. Zhou, K., et al., Hydrolysis of cellulose catalyzed by novel acidic ionic liquids. *Carbohydr. Polym.*, 2015. 115: p. 49-53.

APPENDIX F. ADDENDUM A. EXPERIMENTAL DETAILS AND FINDINGS FOR TESTS INVESTIGATION REACTION CHEMISTRY OF NITRATES AND ORGANIC COMPOUNDS

In Beitel's combustibility studies, he packed a small open aluminum capsule with 1 g of the test mixture on top and ignitor mixture of 20 wt% charcoal/80% sodium nitrate that he ignited with a heated nichrome wire and he determined the nature of the test mixtures reaction. He found that simulated Hanford salt cake/sugar mixtures reacted energetically at 25% sugar, but at 10% sugar no combustion occurred. (Beitel 1976d) In studies to evaluate the effectiveness of sucrose as a denitrating agent for Hanford wastes, Scheele and coworkers (Kim et al. 2005) using TG/DTA found that sucrose began to react exothermically with nitrate and nitrite in a simulated alkaline Hanford waste principally composed of nitrate and nitrite salts but with percent or slightly less levels of a variety of constituents. The gases N_2O , CO_2 , and CO were observed in sealed container tests indicating oxidation; the formation of the reactive oxidants NO and NO_2 cannot be discounted because of the tests being performed in sealed containers permitting back reaction with sucrose.

Scheele and coworkers determined the thermal reactivity of a variety of cellulosic materials and nitrates both as neat mixtures and with other salts present. These studies provided insights into the effects of temperature, other mixture constituents, and aging during room temperature storage. In studies supporting plutonium (Pu) glovebox decontamination operations, Scheele et al. (Scheele et al. 2005) used TG/DTA and ARC to study the thermal reaction sensitivities of cotton and cotton/nylon cloths saturated with nitric acid-based decontamination agents and neutralized with sodium hydroxide or sodium carbonate. In cloths containing dried sodium hydroxide neutralized solutions of 1 M HNO_3 and ceric and cerous nitrates, the ARC observed reaction onsets as low as room temperature. The age of the dried cloths affected thermal sensitivity with the ability of the cloth to sustain self-sustaining reactions increasing at lower temperatures up to 114 days and decreasing for a 149 days old cloth. 100% cotton cloths containing a sodium hydroxide-neutralized solution of HCl , NH_4F , citric acid, nitric acid, and proprietary buffering agents, supported a self-sustaining reaction beginning at 120 °C while the unneutralized cloths began to react at 70 °C indicating increased susceptibility at acidic conditions.

In studies investigating the use of cellulose to denitrate a Hanford waste, Scheele and coworkers using 10 to 50 mg-scale TG/DTA and 1 to 6 g ARC studies found that a simulated waste mixed with cellulose begins to react at a lower temperature than a neat mixture of sodium nitrate and cellulose suggesting catalytic behavior by other waste constituents [Scheele 2007; Scheele 2008]. Mixtures of cellulose and sodium nitrate with cellulose to nitrate ratios ranging from 75 to 1300% of stoichiometric cellulose had reaction onset temperatures ranging from 190 to 220 °C depending on sample mass. A 1.24 g neat mixture of sodium nitrate and 75% of the predicted stoichiometric amount of sodium nitrate to fully denitrate (C:N molar ratio = 0.75:1) exhibited a limited reaction at 220 °C. A mixture with an excess of cellulose (C:N = 13) showed a self-sustaining reaction at 270 °C, while a larger 2.5 g mixture exhibited limited reaction at 220 °C. A 1-g cellulose, 0.24-g $NaNO_3$ mixture with a C:N ratio of 13 showed exothermic behavior at 190 °C that raised or where cellulose itself exothermically decomposes in a sealed container but the temperature to reaction failed to sustain itself above 200 °C, another 10 °C temperature increase started a. A second self-sustaining reaction began at 210 °C and continued to 240 °C; after the ARC heated the sample to the point at which it failed to sustain itself but at which each successive 10 °C temperature increase started another reaction that eventually sustained itself at 265 °C, a final self-sustaining reaction that led to self-heating rates of >1000 °C min^{-1} began. In another experiment, a 1-g sample of cellulose-containing simulated waste (C:N = 0.75) began a self-sustaining reaction at 115 °C that increased the sample's temperature about 3 °C and after being heated to 125 °C but died after heating the sample about 3 °C. The sample began a self-sustaining reaction or series of reactions at 125 °C that self-heated the temperature to 450 °C, where the experiment was stopped. The mass spectroscopy-measured residual gases from cellulose-containing simulated waste included N_2O , NO , H_2O and CO_2 ; it is likely that most NO_x produced reacted with organics in the simulated waste since the experiments were performed in sealed containers. These experiments indicate that the oxidation reactions between cellulose and nitrate and/or nitrite can begin at lower temperatures when other compounds such as metal ions are present. Using Kissinger's method (Kissinger 1957) and the DTA results for 290 °C-onset reaction, the activation energy (E_a) and Arrhenius pre-exponential (A) were 186 kJ $mole^{-1}$ and $3 \times 10^{14} s^{-1}$, respectively.

Although not strictly germane, Scheele and coworkers' studies to determine the reactivity of nitrate- and organic-rich Hanford wastes provides additional insights into the effects of other waste constituents. (Scheele et al. 1995) These studies investigated the thermal stability of 2, 6, and 10 mass% total organic carbon admixtures of nitrate and/or nitrite with the sodium salts of acetate, citrate, ethylenediaminetetraacetate (EDTA), and hydroxyethylethylenediaminetriacetate (HEDTA) and a simulated organic complexant-containing Hanford waste. The neat mixtures began reacting between 180 and 290 °C as measured by the ARC which is often below the melting point of the nitrate and/or nitrite salt. A 0.7 g sample simulated organic-and nitrate-rich Hanford waste containing a variety of metal salts and complexants began a self-sustaining reaction near 120 °C or much lower than would have been predicted based on the admixtures of the pure reactants. This initial reaction could not sustain itself beyond 140 °C but restarted again after being heated to 150 °C; a larger sample size likely could have sustained the reaction. This reduction in onset temperature suggests that the constituents in the waste had a synergistic effect that possibly could include catalysis by the metal ion constituents. The gaseous products from these reactions included CO₂, N₂O, H₂O, and NH₃ depending on the organic.

APPENDIX G: SUMMARY OF REACTIVITY TESTING

The TAT commissioned a limited set of thermal analytical experiments conducted at various scales in an attempt to answer several key questions that remained after the review of preliminary results from the analysis of samples taken from P7R7. The questions included but were not limited to:

- Could key incompatible constituents (namely Swheat Scoop®, Kolorsafe®, HNO₃, and the presence of reactive metals such as Fe and Pb), mixed together as part of the processing of wastes contained within Drum 68660, lead to runaway reactions capable of explaining the observed damage within P7R7?
- If so, was it possible to determine whether the runaway reactions that led to the contamination release initiated within the neutralized and sorbed liquid waste or whether they more likely originated within the nitrate salt waste admixture?
- Can either chemical oxidation or biological oxidation reactions be eliminated as possible initiators of the excursion event in P7R7?

To address these questions, experiments were undertaken at various scales, including

1. bench-scale thermogravimetric and differential thermal analysis (TG/DTA) and accelerating rate calorimetry (ARC) tests
2. small-scale tests using the Sandia Instrumented Thermal Ignition (SITI) apparatus
3. medium scale (10-gallon drum) thermal runaway tests.

Summaries of the sets of experiments are provided below.

INTRODUCTION

Bench-scale Thermal Analytical Experiments

In support of the TAT's efforts, the Pacific Northwest National Laboratory (PNNL) performed a probative set of thermoanalytical experiments to determine the thermal reaction sensitivities of simulated wastes and individual constituents expected in Drum 68660. Simultaneous TG/DTA and ARC were used to determine the thermal sensitivities of simulated waste constituents and their mixtures with Swheat Scoop®. Kolorsafe®, an aqueous solution of triethanolamine (TEA), was used to neutralize the liquid waste fraction. Swheat Scoop®, an organic kitty litter, was used to absorb the neutralized liquid waste fraction as well as the free, interstitial, and occluded nitric acid solution in the salt waste fraction. The constituents and mixtures tested were selected based on the nominal TRU-waste composition, the chemicals and materials used for processing the TRU-wastes put into Drum 68660, and PNNL's previous reaction thermal sensitivity studies of similar nitrate and organic mixtures such as cellulose and sodium nitrates.

Small-scale Thermal Analytical Experiments

The SITI small-scale slow thermal runaway apparatus was used to investigate thermal decomposition reactions in mixtures of materials associated with Drum 68660 that are candidates for mid-scale (10-gallon) drum tests or that are outside the scope of the 10-gallon drum tests. Heat release and thermal runaway were measured as the mixtures were heated to compare reactivity of different mixtures. The different mixtures represented binary parameter studies (changing one variable at a time to evaluate its effect). The results were also used to determine thermal properties and to support refinement of hypothetical reaction mechanisms and thermal runaway models.

10-Gallon Drum Experiments

A series of sub-scale (10-gallon) drum experiments was conducted to characterize the reactivity, heat generation, and gas generation of mixtures of chemicals believed to be present in the Drum 68660 at a scale expected to be large enough to resemble the environment in that drum but small enough to be practical, safe, and cost effective.

These tests were intended to observe, in a controlled environment and with suitable diagnostics, the behavior of mixtures of Swheat Scoop®, Kolorsafe®, nitric acid, and various metal salts in order to determine whether they could support reactivity that could result in thermal runaway or whether some other ingredient or event would be necessary to explain the damage observed in R7P7. This set of experiments was intended to provide a framework to postulate realistic, data-supported hypotheses for processes occurring in a “68660-like” configuration, not to prove definitively what actually occurred in 68660.

EXPERIMENTAL

Bench-Scale TG/DTA & ARC Experimental

Salient points from the series of bench-scale thermal analytical experiments employing TG/DTA and ARC tests are provided here.^{xx}

This section provides 1) the basis for the experimental approach, 2) the instruments and methods, and 3) a description of the test materials used in the bench-scale experiments, their preparation, and some chemical and physical characteristics.

Experimental Strategy

The experimental strategy was to use the approach recommended by the Center for Chemical Process Safety (CCPS) of the American Institute of Chemical Engineers (AIChE) for evaluating chemical reaction process hazards (CCPS 1995). The basic strategy was to use thermoanalytical methods to identify potentially reactive and energetic materials and determine whether they had the potential for thermally initiated reactions. TG/DTA and ARC were used for this study to determine the thermal sensitivities of simulated Drum 68660 waste constituents and mixtures.

The waste constituents in Drum 68660 that had the greatest potential to exhibit significant thermal reactivity were 1) the product(s) from the neutralization of the acid constituents in the acidic liquid waste, 2) the mixture of the neutralized liquid fraction and Swheat Scoop®, 3) the mixture of nitric acid (HNO₃) and Swheat Scoop® (HNO₃/Swheat Scoop®) arising from adding Swheat Scoop® to the moist acidic salt fraction to absorb free, interstitial, and occluded acidic liquids, and 4) the metal nitrate salts (MNO₃) mixed with Swheat Scoop® (MNO₃/Swheat Scoop®). The product of the neutralization of the liquid waste fraction's nitric acid was expected to be hydrogen (H) and metal (M) salts of triethanolamine nitrate, which are referred to as HTEAN and (H,M)TEAN, respectively, in this appendix. The processed liquid waste fraction should be a mixture of (H,M)TEAN and Swheat Scoop® [(H,M)TEAN/Swheat Scoop®]. The first three types were tested.

Instruments

A Seiko 320 simultaneous TG/DTA and ARC was used to determine the thermal sensitivities of the tested surrogate waste mixtures. TG/DTA measures mass changes and temperature differences between the sample and a reference material, which was alumina in this test. The TG/DTA was located in a fume hood on a marble slab to minimize disruptive vibrations.

^{xx} Complete descriptions of the experiments and results are contained in this document: Scheele, R. D., et al. "Preliminary Investigations of the Thermal Stability of Wastes Present in Waste Drum that Breached while in WIPP." February 2015. PNNL-24125.

In this use, the DTA provided a qualitative measure of whether an observed reaction produced heat (exothermic) or required heat (endothermic). Static room air or an ultra-high purity (UHP) Ar purge and a heating rate of 5 °C/min were used for the TG/DTA experiments; a heating rate of 10 °C/min was used once.

The ARC operated as an adiabatic calorimeter in a heat/wait/search mode using sample sizes ranging from 2.5 to 8 g in a nominal 10-ml sample container. In the heat/wait/search mode, the ARC begins at an operator-selected temperature, equilibrates for an operator-selected time at temperature, and then monitors the sample's temperature to determine whether the sample is self-heating. If no self-heating is observed (heating rate > 0.01 °C/min), the temperature is increased an operator-selected amount and the heat/wait/search process repeated until the ARC observes self-heating, whereupon the ARC enters its adiabatic mode, maintaining the calorimeter temperature at the same temperature as the sample self-heats. The ARC is sealed, so all product gases are retained in the container. The ARC measures self-heating rate, pressure, and pressure change rate.

Test Material Preparation

The materials prepared for testing were simulated waste solutions and the simulated processed wastes 3.5 M HNO₃/Sweat, HTEAN, (H,Pb)TEAN, (H,Pb,Fe)TEAN, HTEAN Sweat Scoop®, (H,Pb)TEAN/ Sweat Scoop®, (H,Pb,Fe)TEAN Sweat Scoop®, HNO₃/HTEAN/ Sweat Scoop®, and HTEAN/TEA/ Sweat Scoop®. The simulated waste solutions prepared were 3.5 M HNO₃, Pb(NO₃)₂-saturated 3.5 M HNO₃, and Fe-saturated Pb(NO₃)₂-saturated HNO₃. This section provides details on the methods used to prepare test samples. In addition to the mixtures, unscented Sweat Scoop® was tested.

Simulated Waste Solutions and TEAN Preparations

To prepare materials representative of components of the liquid waste fraction in Drum 68660, we first prepared solutions of 3.5 M HNO₃, Pb(NO₃)₂-saturated 3.5 M HNO₃, and Pb(NO₃)₂- and Fe-saturated HNO₃, used Kolersafe® to neutralize these solutions to prepare the (H,M)TEANs, and then used Sweat Scoop® in a 3:1 volume ratio based on LANL procedures (Clark and Funk 2015) to absorb the Kolersafe®-neutralized solutions.

The 3.5 M HNO₃ was prepared from ultrapure-grade concentrated HNO₃ and deionized water. The Pb(NO₃)₂ used to prepare the Pb(NO₃)₂-saturated 3.5 M HNO₃ was Baker Analyzed ACS reagent grade. The prepared combination lead nitrate- and iron- (Pb, Fe) saturated HNO₃ solution was prepared by treating Johnson Matthey Electronics grade 99.2% .-48 mesh iron metal (Fe) powder with the prepared Pb(NO₃)₂-saturated 3.5 M HNO₃.

In the neutralization step, the TEA in Kolersafe® reacted with the solution's cations and nitrate to form soluble or insoluble salt(s) of TEAN. To imitate that step, Kolersafe® was used to neutralize 1) 3.5 M HNO₃ to produce hydrogen TEA nitrate (HTEAN), 2) Pb-saturated HNO₃ to produce a mixture of HTEAN and lead TEAN [(H,Pb)TEAN], and 3) (Pb,Fe)-saturated HNO₃ to produce a mixture of (H,Pb)TEAN and iron TEAN, [(H,Pb,Fe)TEAN]. TG/DTA was used to test Sweat Scoop® mixtures containing 3.5 M HNO₃. In one case enough Kolersafe® was added to the system to neutralize the acid to neutral conditions, and in another a 25% excess of Kolersafe® was added to test the effect of over neutralization on reactivity.

PNNL's Analytical Services Laboratory titrated the 3.5 M HNO₃ and Pb(NO₃)₂-saturated 3.5 M HNO₃ solutions with Kolersafe®. The equivalence point for the HNO₃ mixture was pH 4. The equivalence points for the Pb/HNO₃ were pH 2.5 and pH 5.5; the former was for the hydrogen ion and the latter was for the Pb. This indicated that adjusting the pH to 7 required more Kolersafe® than necessary to neutralize the hydrogen ion and the Lewis acid metals to their equivalence point. The titration of the lead solution showed that one of the constituents would complex with the TEA and thus increase the fuel burden in the liquid waste fraction.

Sweat Scoop® Mixture Preparations

For these bench-scale experiments, 3 volumes of Sweat Scoop® were added to 1 volume of solution to absorb the simulated liquid waste fraction of Drum 68660. To eliminate or reduce physical factors such as sample uniformity, before thermoanalytical testing, the Sweat Scoop®-containing materials were powdered with a coffee grinder.

In our early TG/DTA testing, Swheat Scoop® was placed into the sample pan followed by addition of the solution. In early ARC testing, the mixtures of Swheat Scoop® with HNO₃ and Kolorsafe®-neutralized solutions were prepared by first adding the Swheat Scoop® to the ARC-bomb using a funnel and then adding the liquid to the Swheat Scoop® and mixing using a stainless steel rod that would fit through the 6.4-mm sample-container neck. This likely did not produce homogeneous mixtures although the liquid transferred throughout the Swheat Scoop®. Later, premixed samples were used in both TG/DTA and ARC testing.

After several approaches for drying, simple passive air drying at room temperature proved to be the most effective and fortuitously the most representative of how a waste would likely dry after generation and during storage. It took about 10 and 3 days to dry to equilibrium liquid content for the 3.5 M HNO₃/ Swheat Scoop® and (H,Pb,Fe)TEAN/ Swheat Scoop® mixtures, respectively.

Small Scale SITI Experiments

Salient points from a series of small-scale thermal analytical experiments employing the SITI apparatus are provided here.^{yy}

The SITI apparatus, illustrated in Figure G-1, is typically used to study slow thermal runaway of energetic materials. As a sample is heated, thermal decomposition reactions generate heat, which is observed with a grid of thermocouples in the middle of the sample, and gas, which is observed as headspace pressure.

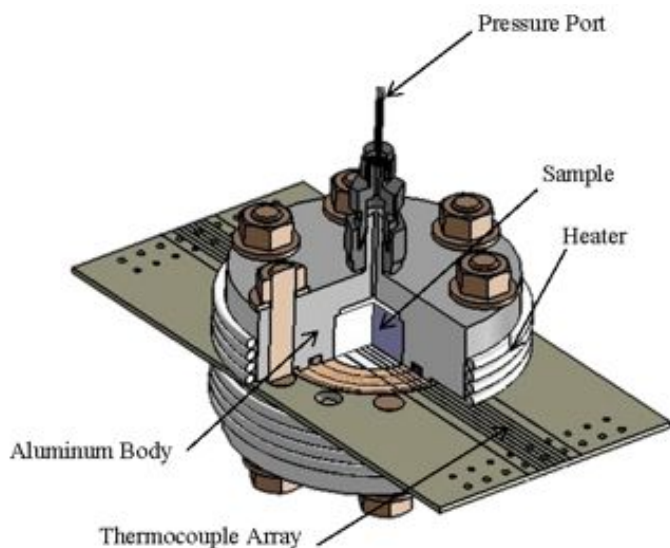


Figure G-1. Cutaway illustration of the Sandia Instrumented Thermal Ignition (SITI) experiment. Insulation is not shown.

The specimen is 25.4 mm diameter and 25.4 mm tall, separated into two halves between which the thermocouple grid is placed. Nine thermocouple wires provide spatially resolved temperature measurements from the center to the edge of the specimen. The body is aluminum, and the assembly is encased in insulation to approximate an isothermal (uniform) boundary condition on the sample. The thermocouple wires are sealed inside a Kapton gasket, and the assembly is sealed gas tight with o-rings, enabling measurement of pressurization. Tests can also be run fully vented.

^{yy} Refer to SAND2015-0861R for a complete description of experiments and results.

Heat is provided by a resistive rope heater wrapped around the assembly and controlled by a feedback temperature controller. Typically a material is studied by heating to a number of different set point temperatures and observing thermal decomposition and thermal runaway. Alternatively, the temperature can be ramped continuously from ambient to thermal runaway. A method has been developed to derive thermal properties (specifically thermal diffusivity) from linear ramp data. Other temperature profiles are possible.

Test Matrix Summary

Table G-1 lists the tests performed and details of the materials and other test conditions. The table provides brief result statements for the tests conducted. In general for the SITI testing:

- Tests were vented.
- Heating rate was 5 °C/min.
- Swheat Scoop® was included.

Table G-1 uses the following abbreviations:

DI – Deionized

NNA - Neutralized Nitric Acid: 3.3M Nitric Acid + Kolorsafe® to pH 7, equal volumes

ONNA – Over-neutralized Nitric Acid: 3.3M Nitric Acid + Kolorsafe® to pH 7, equal volumes, plus 5.26 ml Kolorsafe® per 100 ml final solution.

UNNA - Under-neutralized Nitric Acid: 3.3M Nitric Acid + Kolorsafe® to pH 7, equal volumes, plus 5.26 ml 3.3M nitric acid per 100 ml final solution.

Table G-1. Summary of tests and test parameters. Swheat Scoop® used in all tests. Unless noted, all tests were vented and heated at 5 °C/min.

Test	Date	Liquid	Salts	Notes / Results
Exp386	10/20/14	Tap Water	None	Sealed
Exp387	10/27/14	DI Water	None	2 °C/min to study low temperature reactions. Small exotherm.
Exp388	10/30/14	NNA	None	Two exotherms after water vaporized.
Exp389	11/4/14	DI Water	None	No exotherm until end of ramp.
Exp390	11/7/14	NNA	Na and Mg nitrates	One exotherm after water vaporized—temperatures to 600 °C.
Exp391	11/11/14	UNNA	Na and Mg nitrates	Compatibility test with UNNA and Mg and Na nitrates.
Exp392	11/12/14	UNNA	Na and Mg nitrates	Compare under-neutralized acid to neutralized in Exp390.
Exp394	11/18/14	ONNA	Na and Mg nitrates	Too much salt used due to density measurement error. Strong effect on phase change. Launched top insulation.
Exp395	11/20/14	ONNA	Na and Mg nitrates	Same as Exp394.
Exp396	11/24/14	ONNA	Na and Mg nitrates	Compare over-neutralized acid. Large exotherm and lots of gas.
Exp397	11/25/14	ONNA	LANL SA mix	Compatibility test with LANL Stream Analyzer mix and ONNA.
Exp398	11/26/14	ONNA	LANL SA mix	LANL salt estimate. Most TCs failed early. Slow (not energetic) build to thermal runaway and slow burn.
Exp399	12/3/14	ONNA	Na and Mg nitrates	Pulled vacuum to draw off water, but it didn't work.
Exp400	12/4/14	N/A	Remains of Exp397	Attempted to ignite, but did not work
Exp401	12/8/14	ONNA	LANL SA mix	Ramp and hold at 105 °C. Water did not fully vaporize after 4 hours. No thermal runaway. Re-heated to 105 C and held for >4 hours with no thermal runaway.

Test	Date	Liquid	Salts	Notes / Results
Exp402	12/10/14	ONNA	LANL SA mix	Ramp and hold at 110 °C. No thermal runaway after about 5 hours.
Exp403	12/11/14	None	LANL WB-4 mix w/out 0.2% water	Exotherm or phase change starting around 66C.
Exp404	12/12/14	None	LANL WB-4 mix w/out water, Pb, or Cr	Exotherm started around 71 °C.
Exp405	12/15/14	None	LANL WB-4 mix w/out water, Pb, or Cr	Open SITI. 2 °C/min. No thermal runaway up to 290 °C. Material expanded significantly.
Exp406	12/16/14	None	LANL WB-4 mix w/out water, Pb, Cr, or oxalic acid	Attempted plume thermal runaway, but test was very energetic
Exp407	12/17/14	None	LANL WB-4 mix w/out water, Pb, Cr, Ca, or oxalic acid	No eutectic, still some exothermic activity at low temperature, but thermal runaway at higher temperature.
Exp408	12/19/14	None	LANL WB-4 mix w/out water or Fe nitrate	Low temperature reactions are suppressed or masked and thermal runaway occurs at higher temperature.
Exp409	12/22/14	None	LANL SA mix w/out liquid	Compare to LANL SA mix w/liquid and WB-4 mix w/out. Appearance of boiling, perhaps from water from Mg nitrate.
Exp410	12/23/14	None	LANL WB-4 mix w/out water, Pb, or Cr	Same as Exp404, but 2 °C/min.
Exp411	1/6/15	None	LANL WB-4 mix w/out water, Pb, or Cr	Same as Exp404 and Exp410, but 1 °C/min.

Medium Scale (10 gallon) Tests

Salient points from a series of medium-scale 10-gallon drum thermal runaway experiments are provided here.^{zz}

An instrumented 22-gauge steel, 10-gallon drum was down-selected as the preferred test vehicle. Part number P/N N110FRC-U 10-gallon drums were obtained from General Container Corp for this purpose. Holes for Swagelok thermocouple pass-throughs were drilled and sealed at SNL. The drums are unlined steel, but a polyethylene (PE) liner was used to prevent gross contact between the drum walls and interior contents. The PE liner was pierced to allow passage of the thermocouples into the drum contents. Physical dimensions of the drum are inside diameter 14” and inside height 15.5”. A total of six drums were prepared. Two were planned as relative control examples. Drum A used a combination of only water and Swheat Scoop® in a 1:2 ratio (volume to volume) in a single uniform layer. This control was to exhibit the behavior of wet Swheat Scoop® with no acid or nitrate salts present. Drum B consisted of neutralized nitric acid and Swheat Scoop® in a 1:2 ratio (volume to volume) in a single uniform layer. This control is to exhibit the behavior of wet Swheat Scoop® in the presence of triethanolammonium nitrate (TEAN), the product of nitric acid and Kolorsafe® liquid acid neutralizer with no free acid or nitrate salts present. Four additional experiments were prepared, envisioned as pairs to elucidate the effects of non-functioning vents and the presence of small amounts of lead respectively. Drums C and D consisted of a bottom layer containing neutralized acid absorbed on Swheat Scoop® in a 1:3 (liquid: Swheat Scoop®) volume ratio and a top layer of acid-wet mixed sodium and magnesium nitrate salts combined with Swheat Scoop® in a 1:1.2 (salt:Swheat Scoop®) volume ratio. Drum D contained a small amount of lead nitrate, which was not added to Drum C. Drums A, B, C, and D were equipped with vents open to the atmosphere for the duration of the experiment. Drums E and F, identical in constituents to Drums C and D, respectively, were equipped with pressure transducers, and the open vent was eliminated; a gas sampling valve was used to collect

^{zz} Refer to SAND2015-0866 R for a complete description of experiments, determination of sample contents, and results.

headspace gas. While a gasket was used to improve the seal of the lids used on all drums, no particular effort was made to ensure that the seal on E and F was gas-tight to a specific pressure. Thermocouples were placed as shown in Figure G-2.

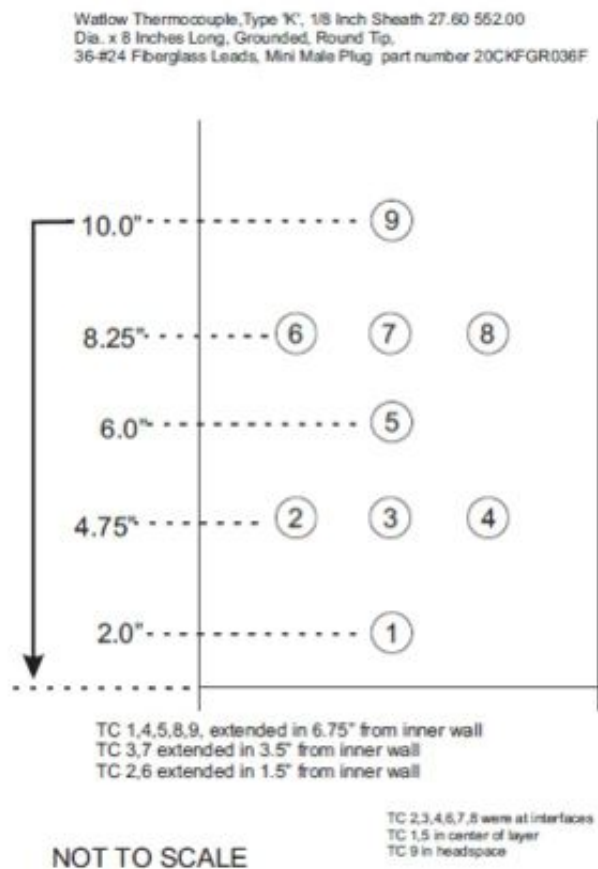


Figure G-2. Thermocouple placement during Medium Scale experiments.

General procedure

A metal nitrate salt mixture was prepared, then slurried up in 2 L of a previously salt-saturated nitric acid solution. The resulting mixture was allowed to sit for 24 hours, then the liquid decanted. Less than 2 L of liquid was recovered from each mixture in this method. The total volume of the recovered liquid was brought to 2 L with the salt-saturated nitric acid solution used to prepare the initial slurry. The recovered liquid was then brought to a neutral pH (~5-7) via the addition of Kolorsafe® liquid acid neutralizer. The resulting neutralized liquid (a solution of water, metal nitrate salts, and triethanolammonium nitrate) was then mixed with Sweat Scoop® in a 3 to 1 Sweat Scoop® to liquid ratio (by volume) and placed in the bottom of the drum. Thermocouple 1 was positioned to be roughly in the center of this layer, and thermocouples 2, 3, and 4 were adjusted so that they were positioned just at the top of this layer (so that they would be in the interface between this bottom layer and the next). The solid residue, nitric acid wetted mixed metal nitrate salts, was then broken up with a metal scoop (upon standing, the layer tended to consolidate significantly) and mixed with Sweat Scoop® in a 1.2 to 1 Sweat Scoop® to nitrate salt ratio (by volume). This mixture was then added on top of the first layer. Thermocouple 5 was positioned to be roughly in the center of this layer, and thermocouples 6, 7, and 8 were adjusted so that they were positioned just at the top of this layer (so that they would be at the interface between this top layer and the empty head-space at the top of the drum). Thermocouple 9 was positioned in the void head-space in the top portion of the drum. The drum liners contained a significant amount of excess material past the top of the drum contents and the top lip of the drum. This excess was trimmed off with scissors, providing less than 6 inches of excess material above the drum lip. The excess material was folded down but not twisted or secured. The drum

tops were then attached using a clamping band. The drums were then wrapped in thermal insulation and placed in a firing pad, thermocouple and pressure sensor leads connected, and data acquisition started.

Temperature was recorded for each thermocouple in one minute increments and recorded via a data-logger. Data was recovered from the data-logger daily. Pressure measurements were captured using digital pressure transducers. A gas sample from the headspace of each drum was collected daily.

Drums were loaded on 11/14/2014 and 11/17/2014. The observation period ran until 1/13/2015 for a total of 57 days.

Six test drums were prepared. Four of the drums were allowed to vent if gas formed; two were not.

- A. Swheat Scoop® + water/single layer: 8 L water + 16 L Swheat Scoop® (8 kg water + 10.3 (±0.1) kg Swheat Scoop®)
- B. Neutralized acid and Swheat Scoop®/single layer: (4 (±0.1) L 3.3 M nitric acid+ 4 (±0.1) L Kolorsafe® liquid acid neutralizer + 10.3 (±0.1) kg Swheat Scoop®)
- C. Two layers, vented:
 - Neutralized acid bottom layer: 2 L decanted liquid + 974 ml Kolorsafe® liquid acid neutralizer + 8 L (5 kg) Swheat Scoop®.
 - metal nitrate salt upper layer: 5.4 (±0.1) kg magnesium nitrate hexahydrate + 1.9 (±0.1) kg of sodium nitrate + interstitial liquid + 3.2 (±0.1) kg Swheat Scoop®.
- D. Two layers with lead, vented:
 - Neutralized acid bottom layer: 2 L decanted liquid + 913 ml Kolorsafe® liquid acid neutralizer + 8 L (5 kg) Swheat Scoop®
 - metal nitrate salt upper layer with lead: 5.4 (±0.1) kg magnesium nitrate hexahydrate + 1.9 (±0.1) kg of sodium nitrate + interstitial liquid + 3.2 (±0.1) kg Swheat Scoop® + 0.0032 kg lead (II) nitrate.
- E. Two layers, no vent:
 - Neutralized acid bottom layer: 2 L decanted liquid + 962 ml Kolorsafe® liquid acid neutralizer + 8 L (5 kg) Swheat Scoop®.
 - metal nitrate salt upper layer: 5.4 (±0.1) kg magnesium nitrate hexahydrate + 1.9 (±0.1) kg of sodium nitrate + interstitial liquid + 3.2 (±0.1) kg Swheat Scoop®.
- F. Two layers with lead, no vent:
 - Neutralized acid bottom layer: 2 L decanted liquid + 923 ml Kolorsafe® liquid acid neutralizer + 8 L (5 kg) Swheat Scoop®.
 - metal nitrate salt upper layer with lead: 5.4 (±0.1) kg magnesium nitrate hexahydrate + 1.9 (±0.1) kg of sodium nitrate + interstitial liquid + 3.2 (±0.1) kg Swheat Scoop® + 0.0032 kg lead (II) nitrate.

RESULTS AND DISCUSSION

Thermal Analytical Bench-Scale Testing

Thermal Behavior of Swheat Scoop®

The TG/DTA evaluations of Swheat Scoop® in Ar and air found that after the sorbed water was evaporated, Swheat Scoop® decomposed endothermically beginning near 150 °C and exothermically in air at the same temperature.

Thermal Behavior of 3.5 M Nitric Acid/ Swheat Scoop®

The mixture of 3.5 M HNO₃/ Swheat Scoop® was tested as simulating a portion of the salt/ Swheat Scoop® waste fraction. The other waste components were dissolved nitrate salts and the solid salts, with the former being distributed in the Swheat Scoop®.

To determine the thermal reactivity of this surrogate waste, we analyzed undried 3.5 M HNO₃/ Swheat Scoop® using both TG/DTA and ARC. We analyzed “dried” 3.5 M HNO₃/ Swheat Scoop® using ARC alone. Figure G-3 compares the measured self-heat rates measured by ARC for the three 3.5 M HNO₃/ Swheat Scoop® experiments. For the two dried sample experiments, energetic gas-producing thermal runaways occurred and ruptured the sample containers, terminating the experiments. Figure G-4, Figure G-5, and Figure G-6 provide pictures of a new container and the two ruptured containers and illustrate the power of the thermal runaway reaction that occurred as a result of a self-propagating reaction starting near room temperature under adiabatic conditions; the initial reactions were observed immediately after starting the experiment. For the two dried samples, after the containers rupture, no real additional measurements exist; the experiments self-terminate.

Figure G-3 illustrates that moisture or a significant heat sink mitigated or prevented a low temperature reaction from self-heating to a temperature at which a thermal runaway reaction occurred. Direct comparison is difficult because of differences in the sample sizes and the amounts of reactants. We cannot say whether aging affected the thermal reaction profile beyond the effect of reducing the moisture content.

Our ARC and TG/DTA experiments indicate that unneutralized HNO₃ will react exothermically with Swheat Scoop® starting at temperatures near room temperature. If dried for 16 hours or 7 days, the mixture is capable of self-heating to a temperature where a vigorous and energetic thermal runaway occurs.

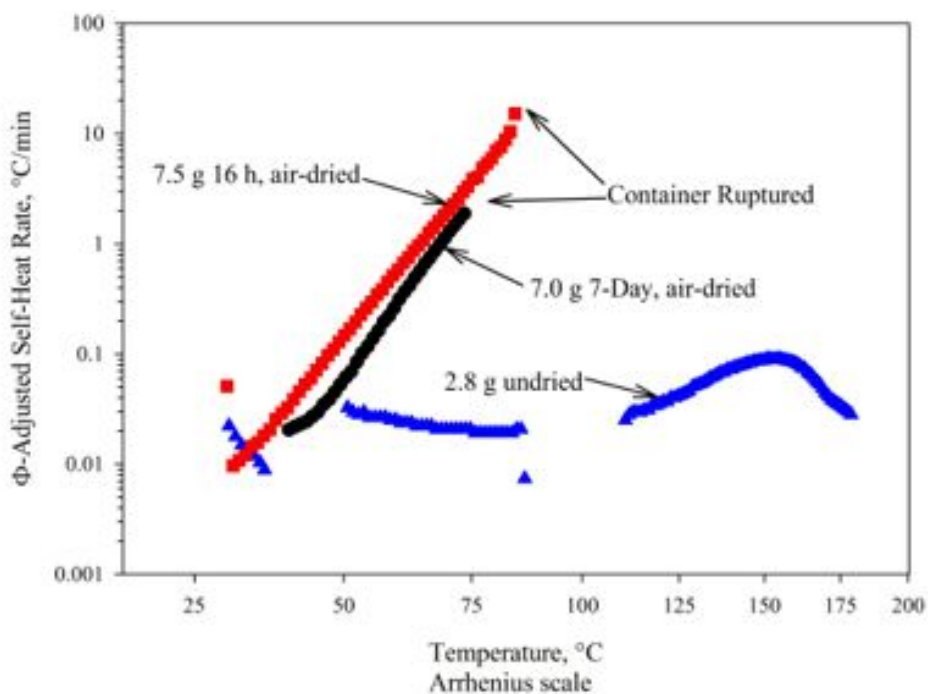


Figure G-3. Comparison of ARC-measured self-heating rates for undried and dried 3.5 M HNO₃/ Swheat Scoop®.



Figure G-4. New Bomb



Figure G-5. ARC Bomb after 7.5 g 16 h dried 3.5 M HNO₃/Swheat Scoop® Experiment



Figure G-6. ARC Bomb after 7 g 7-day dried 3.5 M HNO₃/Swheat Scoop® Experiment

Thermal Behavior of (H,M)TEAN

The TG/DTA and ARC were used to determine the thermal sensitivities of the prepared (H,M)TEANs. Since behaviors were similar, this section uses the behavior of (H,Pb,Fe)TEAN to describe the TEAN behavior.

The TG/DTA identified similar behaviors with an initial reaction occurring after thermal drying near 150 °C. After this reaction started, a second reaction, whose detailed character was unobservable because of its vigor, occurred; the gas release drove the TG beam down rapidly, and the instrument responded rapidly, essentially losing the data. When a TEAN decomposes, it does so in two reaction steps with the second being extremely vigorous.

As shown in Figure G-7, the ARC observed exothermic reactions below 100 °C for a sample dried at 50 °C for 2 days in an Ar glovebox that could not self-heat the mixture. At 125 °C, the TEAN began to self-heat, which led to a vigorous thermal runaway reaction at 215 °C that ruptured the sample container.

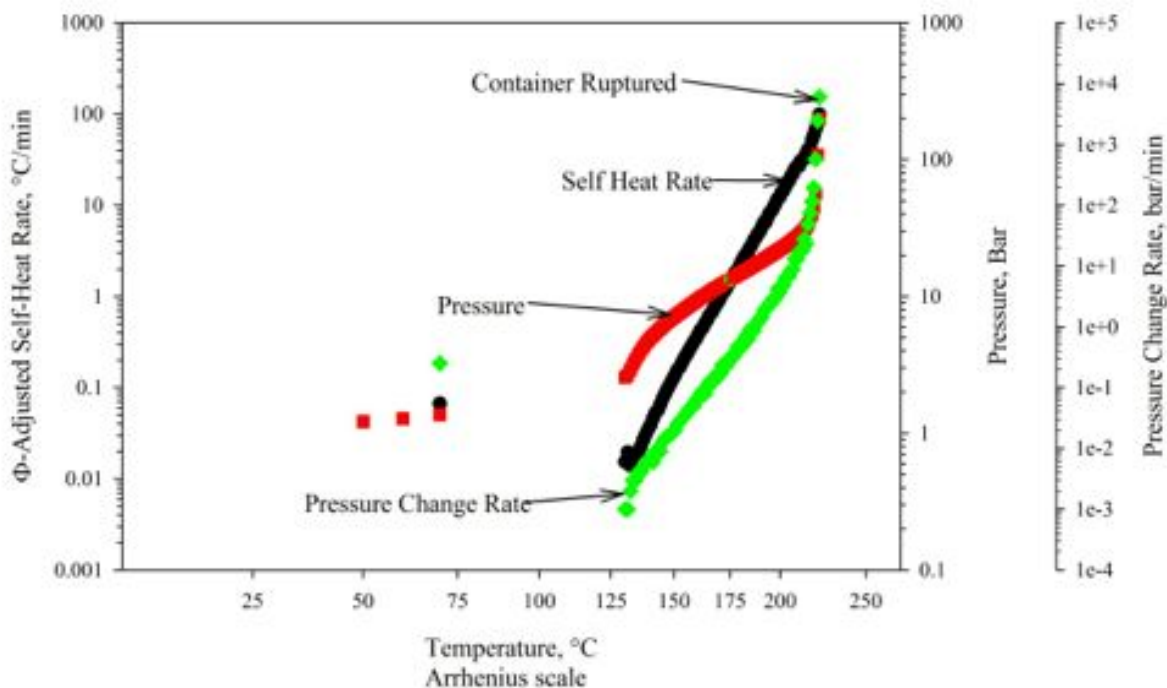


Figure G-7. ARC-measured thermal behavior of 3.5 g dried (H,Pb,Fe)TEAN after drying at 50-60 °C for 2-4 hours.

This ARC experiment confirmed the results of the TG/DTA analyses of the TEANs, which found significant and rapid exothermic reactions in the 210 °C range. This ARC analysis suggested that a TEAN could decompose exothermically at temperatures <100 °C even for a material that had been exposed to 50 °C for 2 days in Ar. This ARC analysis also indicated that if heated to 130 °C under adiabatic conditions or conditions where the heat dissipation rate was slower than the heat-production rate, the TEAN could self-heat to thermal runaway. Applying the CCPS rule-of-thumb of an operating temperature >50 °C away from the ARC-observed onset temperature (assuming that the lower exotherms were spurious) indicates that the sustained temperature of (H,Pb,Fe)TEAN should be less than 80 °C. (CCPS 1995)

Thermal Behavior of (H,M)TEAN/ Swheat Scoop®

In general, these studies indicate that mixing (H,M)TEAN with Swheat Scoop® reduces the vigor of the TEAN decomposition reaction. TG/DTA was able to measure the thermal behavior of a (H,M)TEAN/ Swheat Scoop® while unable to measure (H,M)TEAN's thermal behavior above 210 °C.

TG/DTA testing of partially- neutralized 3.5 M HNO₃ and neutralized 3.5 M HNO₃ with added TEA mixed with Swheat Scoop® found subtle differences between the two and HTEAN/ Swheat Scoop®. The 210 °C-onset reaction observed for partially neutralized HNO₃ mixture appears to have faster kinetics than either of the other two, and the mixture with 25% excess of TEA mixture appears to have slower kinetics.

The thermal behavior of (H,Pb,Fe)TEAN/ Swheat Scoop® were used to illustrate the thermal sensitivities of the (H,M)TEAN/ Swheat Scoop® mixtures. TG/DTA in Ar and air and ARC were used to determine the thermal behavior of (H,Pb,Fe)TEAN/ Swheat Scoop®. The (H,Pb,Fe)TEAN/ Swheat Scoop® used for TG/DTA was dried 11 days at room temperature. The sample used for the ARC was a 7-g sample dried at 50 °C for 5.5 hours with air blowing into the ARC sample container.

The TG/DTA experiments in combination showed that (H,Pb,Fe)TEAN/ Swheat Scoop® is susceptible to exothermic reactions initiated by temperatures as low as 90 °C although more obvious for the experiment done in

air. A second exotherm starts near 200 °C, leading to a series of rapid exothermic reactions. The significant exothermicity in Ar indicated that even if all the available oxygen from air were consumed and anaerobic conditions existed, the reaction would continue either through decomposition of the TEAN or by reaction of the nitrate in the TEAN with the Sweat Scoop®. Additional experiments would be required to differentiate the mechanism.

The ARC experiment presented in Figure G-8 provided some interesting results with the container rupturing as a result of a runaway thermal reaction. The ARC detected heating rates at 45 and 55 °C, but the exotherms were unable to continue to raise the temperature of the sample. Unsustainable exotherms were detected at 100 and 110 °C, but at 125 °C a self-sustaining gas producing reaction began, which self-heated to 210 °C, whereupon the reaction accelerated and ruptured the sample container terminating the experiment.

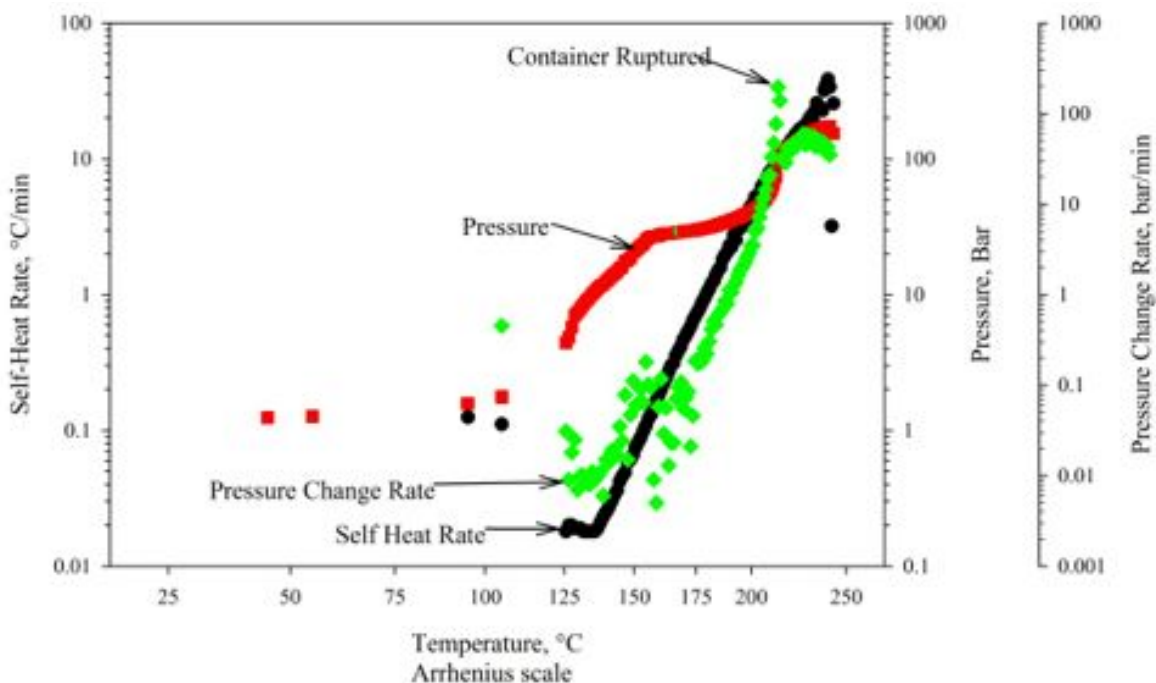


Figure G-8. ARC-measured thermal behavior of 7 g of (H,Pb,Fe)TEAN/ Sweat Scoop® dried at 50 °C for 5.5 hours in bomb.

Small-Scale Testing using SITI

Summaries of select tests are provided in this section to provide insight into the information obtained and interpreted from the tests. Two general types of experiments were performed, ones with nitric acid neutralized to varying degrees with Kolorsafe® neutralizer and ones with no added free liquid. Results indicated that reactivity was greater in the dry mixture and that Fe nitrate and Ca nitrate played significant roles in thermal runaway behavior, whereas Pb nitrate, Cr nitrate, and oxalic acid did not. Within mixtures with liquid, little exothermic behavior was observed with Sweat Scoop® and water, but adding neutralized acid and nitrate salts resulted in significant reactivity and thermal runaway. This behavior was either suppressed or masked by liquid water, and thermal runaway occurred after the water had fully vaporized, although it is not clear whether thermal runaway occurred quickly because of the relatively high wall temperature at the end of the vaporization process.

Exp386

Exp386 is a baseline test and consisted of Sweat Scoop® and water and was sealed. As shown in Figure G-9, the pressure and temperatures increased until about 250 °C and 120 psig, at which point the pressure held steady while the temperatures indicated an exothermic event. The source of this event is unknown. Subsequently, the pressure exceeded the measurement range, causing the pressure signal to stop rising at about 2500 psi. The vessel seal subsequently failed, resulting in steam escaping rapidly, as shown in Figure G-10a. During the cool down, a

large endothermic process occurred, the source of which is unknown. Figure G-10b shows the contents of the vessel after the experiment. The charred remnants indicate that the Swheat Scoop® was oxidized despite having no exposure to air.

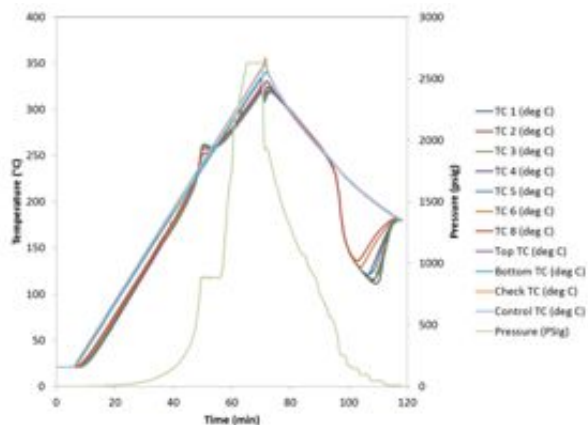
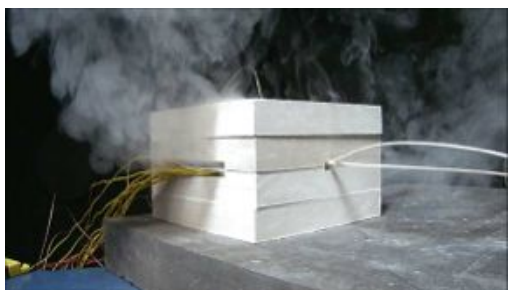


Figure G-9. Exp386 temperature and pressure data. Contents were Swheat Scoop® and water. The vessel was sealed.



(a)



(b)

Figure G-10. (a) Exp386 video frame showing steam escaping after vessel seal failure. (b) Exp386 post-test debris.

Exp 388

Exp388 was also a baseline test and contained Swheat Scoop® and neutralized acid. It was vented and run at 5 °C/min. It exhibits exothermic activity that starts at the end of the water vaporization, slows, and then accelerates again after the water is vaporized (Figure G-11). The internal temperatures remained at about 97 °C during the water vaporization, slightly higher than in Exp387 because of dissolved TEAN from the neutralized nitric acid. The two exothermic events correspond to exhaust jets in the video, as shown in Figure G-12. Before, between, and after the jets, a stream of smoke or steam was visible, but not during most of the water vaporization.

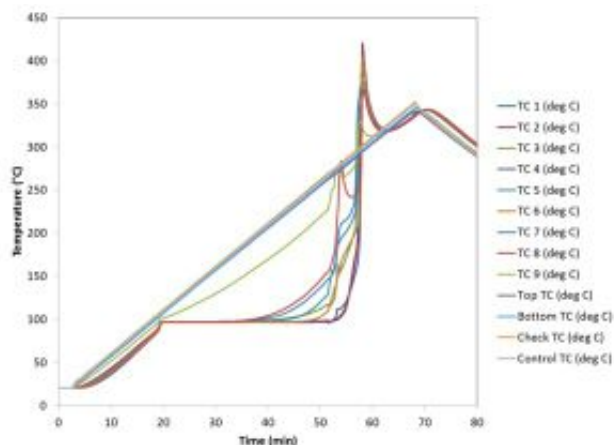


Figure G-11. Exp388 temperature data. Contents were neutralized acid and Sweat Scoop®.

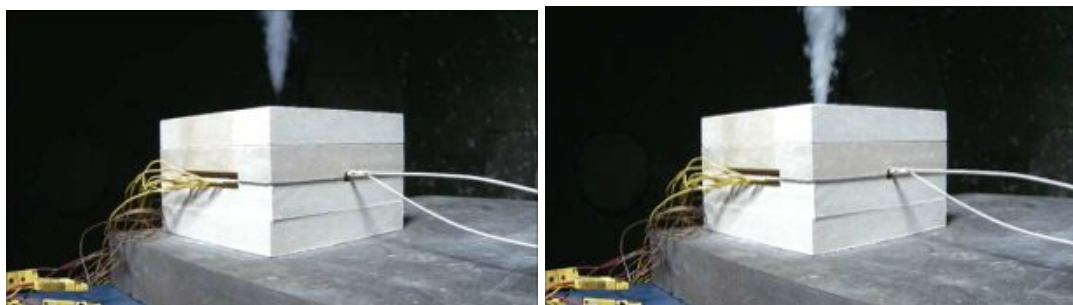


Figure G-12. Frames from Exp388 video showing two jets

Figure G-13 shows the post-test contents of the experiment. Although charred, the substantial amount of material remaining indicates that the exothermic event does not consume all of the reactants.



Figure G-13. Exp388 post-test residue

Exp390

This experiment was conducted with the nitrate salts added. The temperature data from Exp390 shown show an exotherm after vaporization of water that reaches 600 °C, higher than the exotherm in Exp388 and starting at a lower temperature (although this may be related to differing amounts of liquid – the moisture content was about 28% in Exp390 and 48% in Exp388). The exotherm occurs at about 51 minutes, when the boundary temperature is about 258 °C, whereas in Exp388 the initial exotherm occurred at about 52 minutes when the boundary temperature was about 270 °C but quenched and was followed by a stronger exotherm at 57 minutes when the boundary temperature was about 294 °C. The video showed a pressure-burst release followed by a decaying jet that was more energetic than the jets seen in Exp388. These observations suggest that adding sodium and magnesium nitrates enhances reactivity relative to Sweat Scoop® and neutralized acid, although this may be due to the simultaneous reduction in the amount of liquid. The post-test debris is essentially identical to previous tests.

Except for the outer two thermocouples, which are often dominated by the vessel wall, the internal temperatures ranged between 100 °C and 107 °C during the vaporization of water. The shift upward relative to Exp387, Exp388, and Exp389 is apparently due to dissolved Mg and Na nitrate salts, in addition to TEAN.

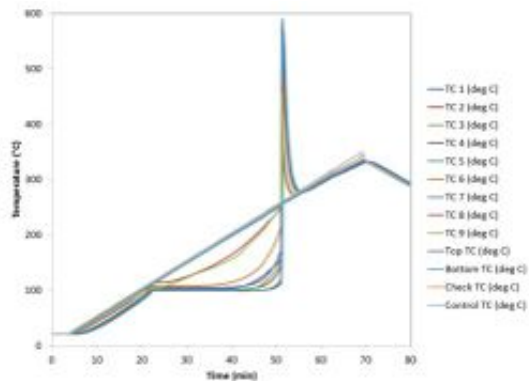


Figure G-14. Exp390 temperature data. Contents were neutralized acid, Swheat Scoop®, magnesium nitrate hexahydrate, and sodium nitrate.

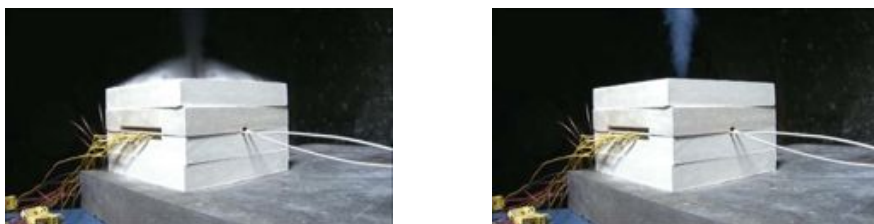


Figure G-15. Images from video of Exp390. Left: pressure-burst event accompanied by loud report, and right: decaying jet that followed the pressure-burst event.



Figure G-16. Exp390 post-test residue.

Exp396

Exp396 was the same as Exp394 and Exp395 (over-neutralized acid, Swheat Scoop®, and Mg and Na nitrates) except with the correct amount of nitrate salts (same as Exp390 and Exp392). As seen in Figure G-17, the effect was that the normal water vaporization returned followed by an exothermic event. In fact, a closer look at the data and the video indicates that there were two exothermic events, although the first was abrupt and the second was gradual. These results are virtually identical to Exp390 (Swheat Scoop®, neutralized acid, and nitrate salts), and similar to Exp392 (Swheat Scoop®, under-neutralized acid, and nitrate salts). Both Exp392 and Exp396 exhibited two exothermic events, although they were different in timing. The post-test debris show that as usual, charred material remained after the test.

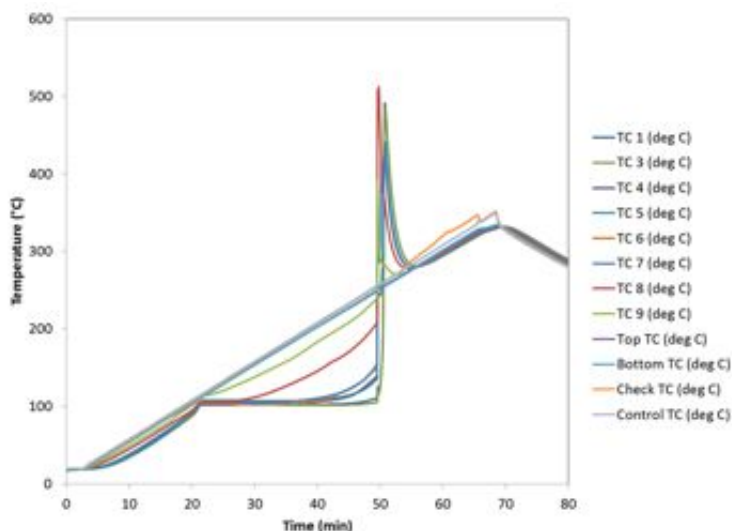


Figure G-17. Exp396 temperature data. Contents were over-neutralized acid, Swheat Scoop®, magnesium nitrate hexahydrate, and sodium nitrate.



Figure G-18. Image from video of Exp396.

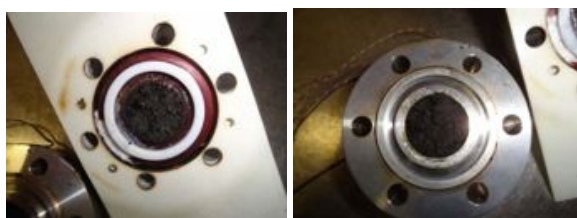


Figure G-19. Post-test debris from Exp396.

Exp401

In another attempt to investigate the effect of removing water, Exp401 consisted of a ramp-and-hold at 105 °C. It was heated to 105 °C because the vaporization process was observed to occur between 100 °C and 105 °C in previous tests, presumably due to dissolved salts in the water. Based on the water vaporization observed in other tests, the water was expected to boil off rapidly and the dry material was expected to undergo thermal runaway soon after. After about 4 hours, the internal temperatures approached the boundary temperature but did not show any signs of exothermic reaction, so the heat was turned off. The next day, the test was continued, and after another 4 hours, the temperature was ramped again at 5 °C/min until thermal runaway. The temperature data show two strong exothermic events around the end of the water vaporization, and the video shows two corresponding jets being released, leaving the test assembly intact.

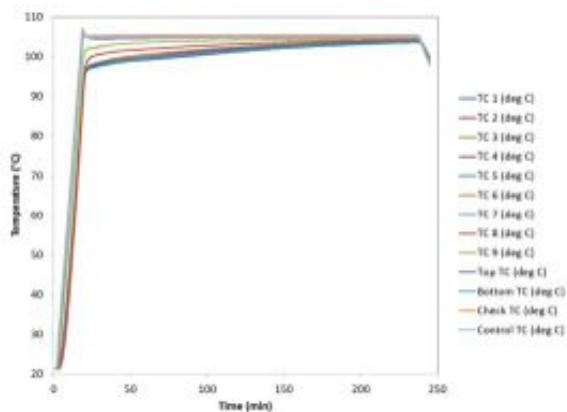


Figure G-20. Exp401 initial ramp and hold at 105 °C.

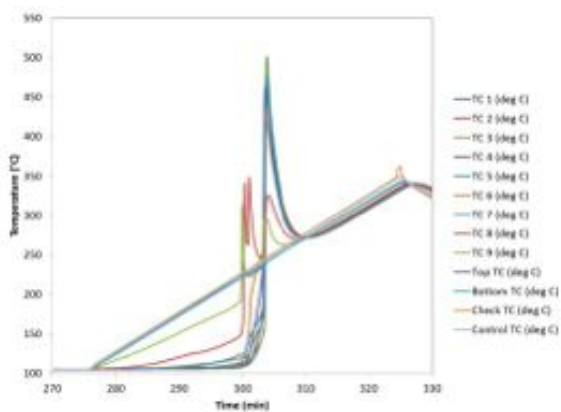


Figure G-21. Exp401 second part - reheated and held at 105 °C for about 4 hours, then heated at 5 °C/min.



Figure G-22. Image from video of Exp401.

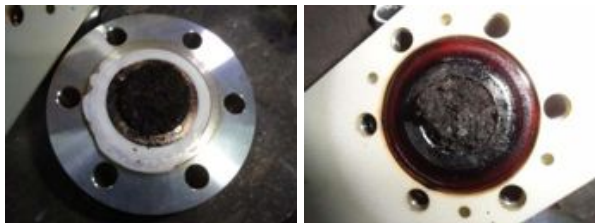


Figure G-23. Post-test debris from Exp401.

Exp403

In December, 2014, the TAT received a report from LANL about TAM (Thermal Activity Monitor) and APTAC (Automatic Pressure Tracking Adiabatic Calorimeter) measurements on certain mixtures of materials believed to be present in Drum 68660. These mixtures contained various ratios of aluminum nitrate nonahydrate, calcium nitrate tetrahydrate, potassium nitrate, chromium nitrate nonahydrate, iron nitrate nonahydrate, water, magnesium nitrate hexahydrate, nitric acid, sodium nitrate, sodium fluoride, nickel nitrate hexahydrate, lead nitrate, oxalic acid, and Swheat Scoop®. They did not contain Kolorsafe®. The results showed exothermic activity in APTAC starting at 55 °C in mixtures composed principally of magnesium nitrate hexahydrate, Swheat Scoop®, sodium nitrate, calcium nitrate tetrahydrate, and iron nitrate nonahydrate. It was found that removing iron nitrate nonahydrate effectively stopped the exothermic activity altogether, demonstrating the likely important role of iron nitrate nonahydrate. Although these experiments did not explore the effects of TEA/TEAN from Kolorsafe®, they demonstrated that low temperature reactions occur in mixtures of dry constituents alone.

Based on these results, Exp403 was run with a dry version of the LANL WB-4 mixture, the details of which are listed in Table G-2. Listed are the mass percentages for the original WB-4 mixture and the version used in Exp403. For Exp403, the 0.2% water was omitted and the Swheat Scoop® to salt ratio was adjusted to approximately 1.26:1 by volume. The density of Swheat Scoop® was assumed to be 0.55 g/cc and that of the salt mixture was assumed to be 1.0 g/cc. The mass percentages calculated from measured masses are listed in

Appendix A of SAND2015-0861R. The most notable difference between the mixture used in Exp403 and WB-4 is the Swheat Scoop® to salt ratio.

Table G-2. LANL WB-4 mixture and Exp403 target mass percentages.

Substance	LANL WB-4	Exp403
Ca(NO ₃) ₂ *4H ₂ O	8.4	6.63
Cr(NO ₃) ₃ *9H ₂ O	0.1	0.079
Fe(NO ₃) ₃ *9H ₂ O	5.7	4.50
Mg(NO ₃) ₂ *6H ₂ O	20.6	16.3
NaNO ₃	36.7	29.0
Pb(NO ₃) ₂	1.9	1.50
(COOH) ₂	1.4	1.11
H ₂ O	0.2	
Swheat Scoop®	25	40.9

LANL reported that the WB-4 mixture exhibited exothermic activity starting at 55 °C and 100 °C in APTAC. Figure G-24 shows the start of an exothermic event around 55 °C, as the difference between the internal and external temperatures drops to zero. The exothermic activity varies but continues until thermal runaway begins around 190 °C.

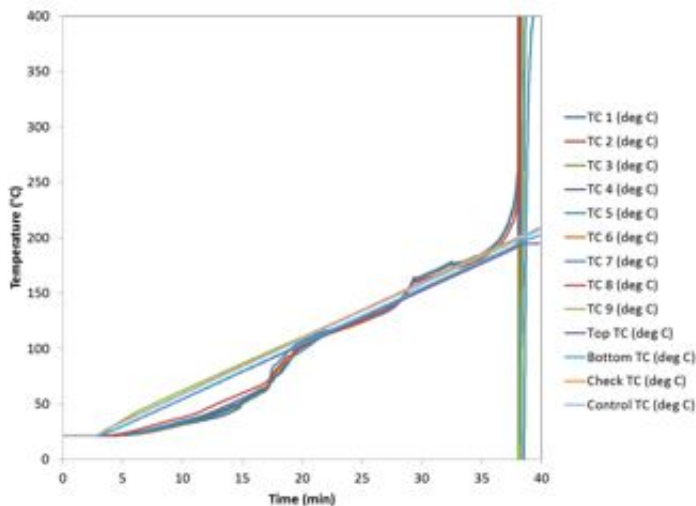


Figure G-24. Temperature data from Exp403. Contents were based on the LANL WB-4 mix: Ca nitrate, Cr nitrate, Fe nitrate, Mg nitrate, Na nitrate, Pb nitrate, oxalic acid, and Swheat Scoop®. No liquids were added.



Figure G-25. Image from video of Exp403.

As shown in Figure G-25, the thermal runaway in Exp403 was more energetic than Exp401; in Exp403, damage was done, as the top insulation block was blown completely off the test assembly.

Figure G-26 provides photographs of the equipment after the test, showing that the o-ring failed, allowing gases to escape, and that material also was ejected through the top vent.



Figure G-26. Post-test images from Exp403. The left image shows that a substantial amount of material was expelled through the vent. The right image shows that the O-ring failed.

Medium Scale (10 gallon) Tests

Drums A and B contain 1:2 liquid to Swheat Scoop® ratios (all ratios are volume to volume with ± 200 mL accuracy) as this was the ratio referenced in both process documents and interviews with personnel preparing Drum 68660. However, the intent of this process was to absolutely prevent the occurrence of any free liquid that would cause rejection of the drum from WIPP and require reprocessing. During the assembly of A and B, it was noted that water combined with Swheat Scoop® in the desired ratio to yield a moist (but not excessively wet) material, in the combination of neutralized acid (Drum B) in the concentrations listed above, resulted in a material that left behind an oily residue. This residue is conjectured to be the product of neutralization: TEAN in solution with water.

When salt-saturated nitric acid was neutralized and sorbed onto Swheat Scoop®, it was found that a 1:2 liquid to Swheat Scoop® ratio was insufficient to eliminate all free liquid. Additional Swheat Scoop® was added in portions until no free liquid was visible. The final ratio used was close to 1:3 liquid to Swheat Scoop®. This same ratio was used in Drums C, D, E, and F for immobilization of the neutralized salt saturated acid solutions. For all liquid/ Swheat Scoop® mixtures, the final mixture was a moist, almost doughy mass with a faint wheat (bread) odor. The combination of acid-wet mixed metal nitrate salts with 1:1.2 (salt: Swheat Scoop®, the salt/ Swheat Scoop® mixture used in the top layer of the drums) produced a moist, but not free flowing material more akin to damp sand.

The acid concentration of entrained liquid in 68660 was unknown but hypothesized as between 1 and 3.3 M. The concentration of acid in the liquid decanted from the simulant mixtures was ~ 1.5 M, which was within the expected concentration range for Drum 68660. The amount, in both mass and volume, of sodium and magnesium salts that would be required to saturate 3.3 M nitric acid solution was significantly underestimated. Saturation of 3 L of 3.3 M nitric acid solution yielded almost 4 L of salt saturated solution that contained only 2.48 M nitric acid. This became further diluted when introduced to the mixed metal salts as part of simulant preparation. The large amount of water associated with the magnesium nitrate contributed significantly to this effect.

The difference between the amount of liquid decanted from simulant mixture C and that recovered from simulant mixtures D, E, and F is attributed to expected variances in implementation of a procedure. The experimental data does not suggest that the presumably higher liquid content in the mixed metal salt portions of D, E, and F resulted in a difference in behavior between C and the remainder of the mixed salt simulants.

Figures G-27 and G-28 show recorded temperatures for the duration of the experiment. Figure G-27 shows all thermocouples (and the pressure reading) for Drum F. Figure G-28 shows readings from thermocouple 3 (see Figure G-2 for thermocouple placement) for each drum and a temperature reading for the firing pad (Drum A Pad, equivalent to the environmental condition surrounding each drum). Only these two examples are shown due to the nature of the data collected: there was no deviation of drum internal temperature away from ambient (as measured

by the pad thermocouples) greater than the limits of discrimination for any of the thermocouples measured. In addition, both sealed drums (E and F) did not register a deviation from atmospheric pressure of more than 1 psi.

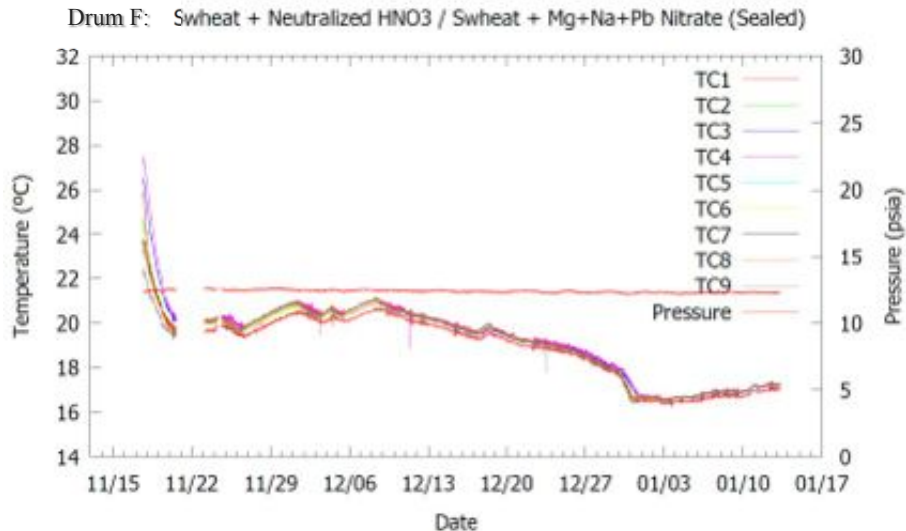


Figure G-27. Temperature data collected for Drum F over the course of the experiment. Thermocouples correspond to the arrangement shown in Figure G-2.

Thermocouples recorded for Drum E contained significant amounts of noise and were consistently lower than ambient temperature for a significant portion of the observation period. This appears to be due to a systematic equipment bias associated with the data-logger channel they were recorded on. The issue was repaired 12/22 and from that point on it is clear that Drum E was tracking with the ambient temperature in agreement with the remaining five drums.

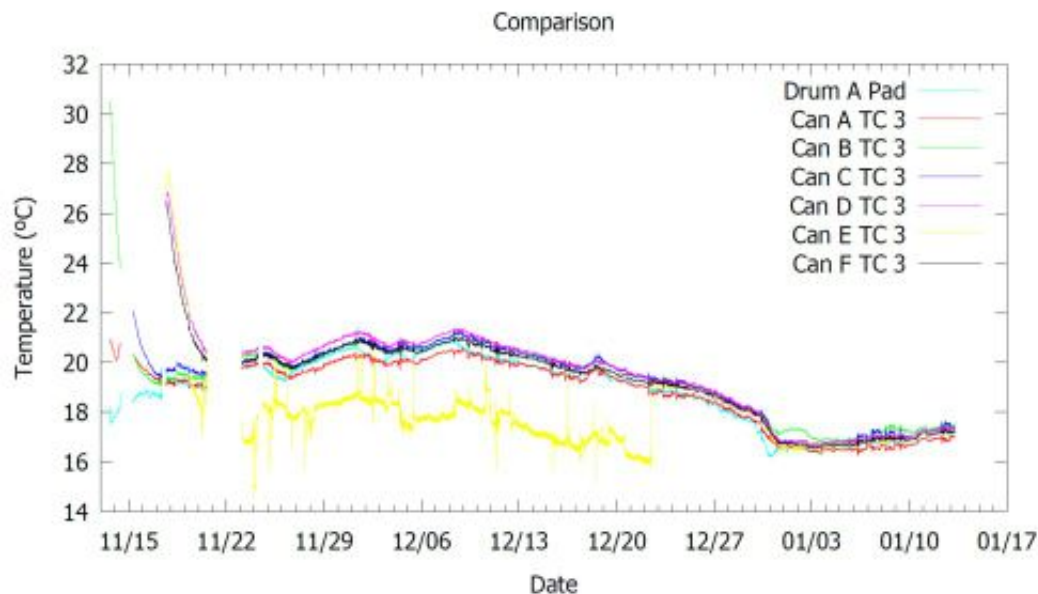


Figure G-28 Comparison of thermocouple 3 for each drum over the course of the experiment. “Drum A Pad” was the name given to the thermocouple measuring the ambient temperature immediately outside Drum A.

Headspace gas samples were collected and analyzed intermittently: early in the experiment samples were taken daily during the week. At the end of the overall observation period, two samples were taken: one on 12/22/2014 and a final one on 1/5/15. No headspace gas samples were taken following the final sample collected 1/5/15.

Headspace gas was collected into evacuated cylinders attached to the drum vent. For sealed drums (E and F) the vent was sealed with a quarter-turn manually operated valve. Headspace gas samples were analyzed on a GCMS for N₂, O₂, CO₂, NO, and N₂O, typically within two days of being collected. While gas samples were collected every day, every other sample collected was analyzed. If significant changes in results were found between consecutively analyzed samples, the intervening sample would be analyzed to determine whether the collection and sampling rate needed to be changed to capture critical information. All headspace gas samples and “air control” samples were injected at the same pressure: 25±2 torr. Headspace gas samples were analyzed on an Agilent 7890A GC coupled with an Agilent 5975C triple axis mass spectrometer using an Agilent PoraBondQ capillary column and helium carrier gas. Samples were analyzed and compared with a 12-component gas calibration standard for detector response of specific analytes. Air control samples (from ambient atmosphere) were injected at the same pressure as the analytes (25 ±2 torr) and provide a measure of day-to-day same-operator/same-instrument scatter and a comparison for overall headspace gas content, since only the species of interest were analyzed (N₂, O₂, CO₂, NO, and N₂O). The amount of sample passing through the detector (total counts) for air was used as a total content standard for the pressure injected; the same volume and pressure of sample injected at the same temperature should contain the same number of molecules. The % composition of the analytes of interest (as mol fraction) for each drum and their total content compared to the air control sample are presented in SAND2015-0866 R. The results for Drum C are shown below to provide representation of the data and results collected.

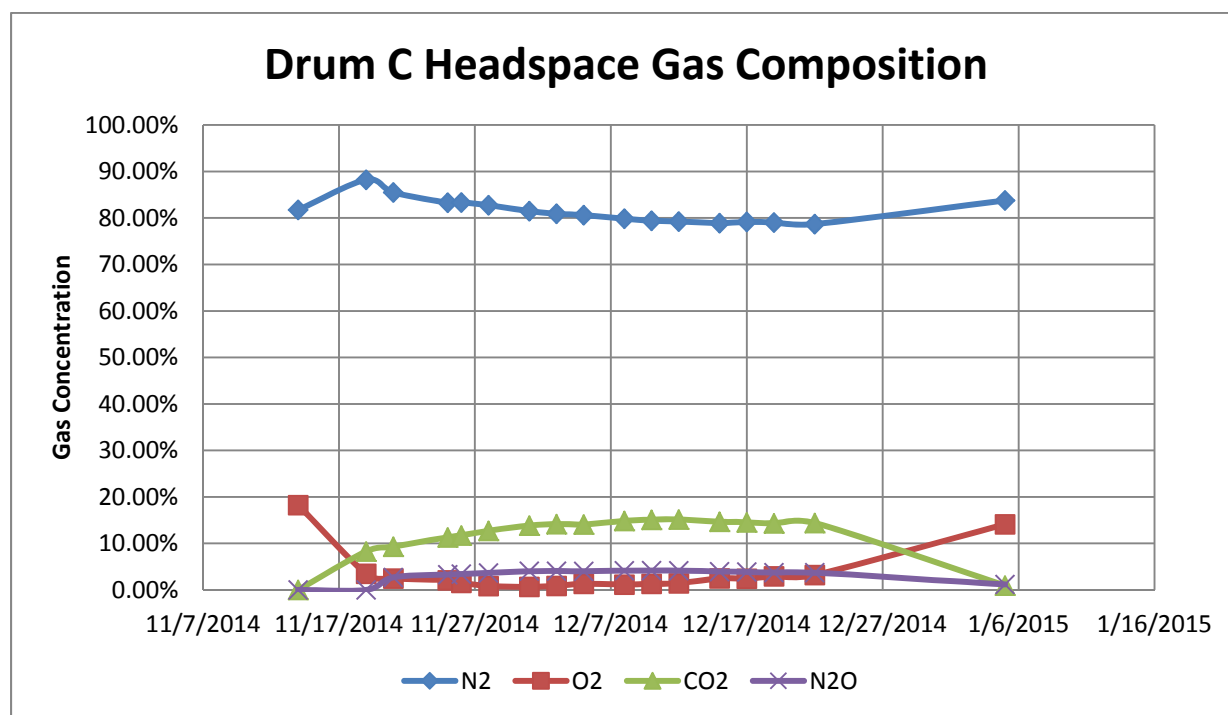


Figure G-29. Drum C headspace gas composition as a function of time.

Table G-3. Drum C headspace gas composition data.

Date	N2	O2	CO2	N2O	Total compared to air
11/14	82%	18%	0%	0%	99%
11/19	88%	3%	8%	0%	88%
11/21	86%	2%	9%	3%	107%
11/25	83%	2%	11%	3%	100%
11/26	83%	2%	12%	3%	99%
11/28	83%	1%	13%	4%	94%
12/1	81%	1%	14%	4%	99%
12/3	81%	1%	14%	4%	98%
12/5	81%	1%	14%	4%	110%
12/8	80%	1%	15%	4%	100%
12/10	79%	1%	15%	4%	97%
12/12	79%	1%	15%	4%	99%
12/15	79%	2%	15%	4%	105%
12/17	79%	2%	15%	4%	98%
12/19	79%	3%	14%	4%	94%
12/22	79%	3%	14%	4%	97%
1/5	84%	14%	1%	1%	93%

There was a lack of measurable heat evolution in any configuration examined. Whether this was a result of a lack of significant exothermic reactions occurring in the matrix or of efficient heat dissipation from the system to its surroundings is unknown. Steps were taken to reduce thermal communication between the pad and the drum contents (drums wrapped in insulation, placed on foam insulation pads, top-covered with foil-lined foam), but the close tracking of interior drum content temperature with ambient pad temps indicated that even at the center of the drum (thermocouple # 3), thermal communication was good at the time-scale of ambient pad temperature change. For this reason, the only definitive statement that can be made is that if an exothermic reaction was active, it did not produce enough heat to overcome dissipation to the environment.

In contrast, headspace gas analysis provided insight into the potential chemical and biological processes active in the different configurations and material sets investigated. Drum A contained only water and Swheat Scoop®. This combination of materials provided the most robust headspace gas activity of all the materials studied. It has been noted that Swheat Scoop® contains active biological organisms that will colonize both Swheat Scoop® constituents and adsorbed favorable nutrients, such as TEAN. The rapid evolution of CO₂ in Drum A is consistent with an aerobic oxidation process. One matter of note in Drum A is that while it appeared that CO₂ completely displaced other headspace gas constituents in a matter of days, total detector count for these samples fell to almost 50% of the control sample, indicating presence of significant (almost 50%) species in the headspace gas that were not captured in the analysis. Since both analyte and air control samples were injected at the same pressure, if all species were accounted for, total detector count should be the same.

While this presents a significant question regarding the actual, active processes in Drum A, its impact to the investigation as a whole is reflected in comparison of overall Drum A gas production to the rest of the experimental group. In short, Drum A presented a headspace gas profile unique to water/ Swheat Scoop® not seen in the other material sets. As a control, this provides negative information that is nonetheless cogent: the apparent biological processes active in Drum A (and possibly Drum B) were not seen in the other drums.

Drum B contained neutralized nitric acid (4 L of 3.3 M nitric acid neutralized with 4 L of KolorSafe® liquid acid neutralizer) adsorbed on Swheat Scoop®. The mixture in Drum B exhibited CO₂ development that appears to be similar to that seen in Drum A. The difference between these two systems was that the gross constituents of Drum

B headspace gas remained the same species: N₂, O₂, CO₂. The headspace gas in Drum B produced detector counts similar to the air control for the entire length of the experiment (average 99 ± 5%). It may be important to note that the absolute amount of CO₂ developed in Drum B appeared to be similar to that produced in Drum A (that is, about 50% of the total free volume in the headspace was occupied by CO₂ in both Drum A and Drum B). This suggests that whatever biological or chemical pathway was active in CO₂ evolution in Drum A may also have been active in Drum B. This also suggests that whatever process in Drum A led to the anomalous headspace behavior (that is, almost 50% of the headspace gas was not detected or identified with the GC/MS analysis used) was *not* active in Drum B. In addition, trace analysis of both Drum A and Drum B headspace gas indicated the presence (< 0.1%) of typical, expected fermentation products such as ethanol and isopropanol. Neither Drum A nor Drum B showed any traces of NO, N₂O, or possible nitration products such as methyl nitrate or methyl nitrite.

Drums C and D exhibited similar enough behavior that they can be addressed as a repetition of a single experiment. There was no detectable difference in either their temperature or headspace gas data. This suggests that the lead nitrate present in Drum D had no appreciable impact on the observed behavior. It is important to note that only ambient temperature behavior was observed in these experiments; if a constituent had had a significant, perhaps even dominant, effect at raised temperature, this experiment would not have borne that out. The behavior of Drum C and Drum D was in marked contrast to that seen in Drum A and Drum B. In Drum C and Drum D, what appeared to be initial consumption of O₂ was balanced with CO₂ production, with CO₂ comprising no more than 20% of the total headspace gas volume. At three days into the experiment, N₂O, interpreted as a marker for either nitrate salt oxidation of organics or nitrate salt decomposition, appeared. This species was not detected over the period of observation for either Drum A or Drum B. While Drum C and Drum D were equipped with vents and thus had gas phase communication with the surrounding environment, it is unclear how much equilibration occurred over the course of the experiment or what the rate of exchange between interior and ambient atmosphere was. The reduction in CO₂ and N₂O and rise in both O₂ and N₂ at the end of the experiment are interpreted as these species equilibrating to their ambient atmospheric concentrations. This suggests that the processes resulting in CO₂ and N₂O evolution had, at that point, either halted or slowed such that the drum internal headspace was once again dominated by the characteristics of the external atmosphere rather than the result of internal reactions. Trace (< 0.1%) amounts of methyl nitrite and methyl nitrate along with various low molecular weight ketones and esters (anticipated hydrolysis products) were detected in both Drum C and Drum D. These species were not detected in Drum A or Drum B. It is unclear whether the methyl nitrite and methyl nitrate were products (or byproducts) of nitrate salt nitration of Swheat Scoop® constituents or whether they were simply released as fragments of existing species or over what time frame they were produced (the trace analysis was a snapshot taken at roughly the mid-point of the observation period).

Drums E and F exhibited similar enough behavior that they will be addressed as repetition of a single experiment, similar to Drums C and D. Drum E and drum F were distinct from the other drums in that they were sealed without an open vent. Access to the headspace was through a manually operated quarter-turn valve that was opened only during headspace gas sampling. The lids on all the drums were sealed with a rubber gasket and clamped with a locking band. While secure, the seal formed by this arrangement was not confirmed to be gas tight. The temperature data recorded for Drum E was both noisy and anomalously low compared both to Drum F and to all the other drums, until 12/22/2014. At this time, the thermocouple leads for Drum E were removed and reattached, at which point the discrepancy was eliminated. From this point on, the temperature in Drum E tracked well with both the other drums and the internal temperature of the firing pad in which the experiment was performed. Much like Drum C and Drum D, Drum E and Drum F differed from each other only in that Drum F contained a small amount of lead nitrate, while Drum E did not. The close agreement between Drum E and Drum F in headspace gas activity suggests that they were virtually identical to each other, and their similarity to Drum C and Drum D suggests that venting had little effect on the overall chemistry that occurred in all four drums. The only significant difference between Drums C/D and Drums E/F was that Drum E and Drum F did not trend back to atmospheric content levels in O₂ and N₂ as Drums C/D did toward the end of the experiment. Given that Drum E and Drum F were effectively isolated from the surrounding atmosphere, this is not surprising. This also lends further credence to the proposition that significant gas-forming reactions had either slowed or halted by the end of the observation period (@ 6 weeks).

SUMMARY & CONCLUSIONS

Key findings of reactivity testing include:

1. Simulated constituents and mixtures of components of key waste fractions in Drum 68660 (Swheat Scoop®, Kolosafe®, various nitrate salts and nitric acid) were capable of producing low temperature reactions near ambient temperatures that can eventually lead to thermal runaway.
2. Nitrate salts of Ca, Mg, Na, and Fe were found to further catalyze reactivity of mixtures and drive down onset temperatures of exothermic reactions; the presence of Pb, Cr, or oxalic acid did not have an appreciable effect on reactivity.
3. Moisture present in test systems acted as a heat sink for low temperature reactions, suggesting thermal runaway within Drum 68660 would not have occurred prior to local evaporation of entrained water. Additionally, there would likely have been little indication of self-heating outside Drum 68660 prior to the excursion event. The presence of water during reactivity testing either suppressed or masked the ability to detect and monitor self-heating at temperatures below 100°C.
4. Rapid pressure increases measured during experiments exhibiting thermal runaway illustrated that reactive incompatible mixtures studied could easily overcome vented systems.
5. Gas evolution within Swheat Scoop®/water and Swheat Scoop®/acid neutralized systems was significant but was significantly suppressed with the presence of high concentrations of metal nitrate salts. This suggests that biological activity was not likely an important factor in the initiation of the thermal runaway that occurred in Drum 68660.

Experimental observations from bench-scale TG/DTA and ARC studies that support key findings include:

- During ARC tests, overnight and 7-day dried mixtures of 3.5 M nitric acid and Swheat Scoop® began to self-heat immediately upon initiation of the experiment (between 30 and 40 °C) and under adiabatic conditions led to a rapid, energetic thermal runaway reaction at 80 °C with sufficient gas and heat production to rupture the spherical sample container rated to over 300 bar. The samples were passively dried at room temperature (15 – 18 °C) in air. This mixture was used to simulate the treated salt waste fraction within Drum 68660.
- During ARC tests, the mixture of Kolosafe® (aqueous triethanolamine) and nitric acid, used to simulate a major constituent in the liquid waste fraction in Drum 68660, will produce triethanolamine nitrate (HTEAN) salts that thermally decompose, and eventually initiate an energetic, gas-producing, thermal runaway reaction when heated under adiabatic conditions to between 125 and 150 °C.
- Mixing Sweat with MTEAN slows the MTEAN decomposition rate.
- ARC testing of TEAN and TEAN/ Swheat Scoop® mixtures, used to simulate the liquid waste fraction in Drum 68660, identified exothermic reactions occurring at temperatures below 100 °C and observed self-sustaining reactions starting at 125 to 150 °C that eventually led to thermal runaway.
- TG/DTA testing of (H,Pb,Fe)TEAN/ Swheat Scoop® in air produced exothermic reactions below 100 °C.
- TG/DTA testing indicated that addition of PbTEAN to HTEAN reduces the onset temperature of the initial exothermic reaction.
- TG/DTA testing shows that neutralized HNO₃ with excess Kolosafe® slightly alters the thermal exothermic reaction profile and slows the TEAN/ Swheat Scoop® exothermic reaction.
- TG/DTA testing indicates that under-neutralization of nitric acid by Kolosafe® slightly alters the thermal exothermic reaction profile and slightly accelerates the TEAN/ Swheat Scoop® exothermic reaction.
- The Chemical Center Process Safety of the AIChE has published rules-of-thumb for using TG/DTA- and ARC-measured reaction onset temperatures to establish safe process operating temperatures. The CCPS

indicates that processes should be safely managed if a TG/DTA-measured onset temperature is within 100 °C or if an ARC-measured onset temperature is within 50 °C of the process temperature.

Experimental observations from small-scale SITI studies that support key findings and provide insight into possibilities for large-scale drum results include:

- Comparison with Los Alamos National Laboratory (LANL) results:
 - Extrapolation of low temperature exothermic reactions over a range of heating rates suggests these may occur near ambient temperature, with Swheat Scoop®, Mg nitrate, Na nitrate, Fe nitrate, and Ca nitrate.
 - Ca nitrate and Fe nitrate both have strong effects on thermal runaway temperatures. Fe nitrate has a significant role in low-temperature reactions.
 - Pb, Cr, and oxalic acid have little effect on thermal runaway of the dry mixtures.
- Exhaust gases do not easily ignite.
- Confinement matters. Reaction rates drop dramatically when temporary clogs release.
- Vaporization of water has a strong effect on exothermic reactions in all mixtures.
- Thermal properties have been estimated. Thermal properties vary primarily with presence of moisture. Addition of salts to Swheat Scoop® has a lesser effect on thermal properties than water.
- In most cases, materials are not entirely consumed during combustion. Solid residue with similar total volume is left behind.
- Temperatures were as high as 400-600 °C in thermal runaway with mixtures that include liquid. Measured temperatures reached as high as ~300 °C in dry mixtures. Thermal runaway was more localized and exhibited more rapid heating rates than in the wet mixtures.
- Neutralized acid and Swheat Scoop® is more reactive than Swheat Scoop® and water.
- Adding Mg and Na nitrates to Swheat Scoop® and neutralized acid increases reactivity, although this may be due to reduction in the amount of liquid present.
- No mixtures studied to date react as energetically as a detonation of a conventional explosive.
- Thermal runaway is scale dependent. The SITI small-scale tests exhibited phenomena believed to have occurred in Drum 68660 despite the absence of the scaling factor.
- Thermal runaway events, including some substantially energetic ones, demonstrate that venting can be overcome by rapid gas generation, although the vent in these experiments was not scaled to the vent used on WIPP drums.

Experimental observations from medium-scale 10 gallon studies that support key findings include:

- Drum B had an odor described as “rotted apple cider”, again attributed to bacterial or fungal activity. In addition, there were a number of either bacterial or fungal colonies visible as white fibrous masses on the top of the Swheat Scoop®/neutralized acid mixture. The wet Swheat Scoop® mixture had darkened slightly in visual appearance and settled about 2 inches (slightly less than in Drum A).
- Drums C, D, E, and F all had similar appearance and odor. No significant notable odor. The Swheat Scoop®/mixed metal salt top layer appeared to have lightened in color compared with the as-prepared sample. The bottom Swheat Scoop®/neutralized acid layer appeared to have significantly darkened, consolidated, and solidified compared with the as-prepared sample..
- All drums exhibited significant corrosion (rust) on both the interior walls of the drum and the interior of the drum lid. In some cases it appeared that corrosion products may have flaked off of the lid interior and fallen down onto the surface of the top layer.
- The mixture of neutralized acid, sodium nitrate, magnesium nitrate, and Swheat Scoop® used in the experiments was insufficient to generate any measurable temperature rise in the configuration and scale used.

The close tracking of internal drum temperature with the temperature of the firing pad the drums were located in indicates that drum contents were not sufficiently thermally isolated from the surrounding environment. The thermal data developed in these experiments should not be taken as supporting the supposition that the material sets used do not produce exothermic reactions at ambient temperature. Heat loss to the environment was not sufficiently controlled by the insulation to allow for any conclusive statements about heat generation or thermal run-away.

- Mixtures of water/ Swheat Scoop® (Drum A) and TEAN/water/ Swheat Scoop® (Drum B) exhibit similar amounts and rates of CO₂ evolution. However, the anomalous behavior observed in the water/ Swheat Scoop® system headspace gas composition precludes a strong statement that identical reactions are occurring in the TEAN/water/ Swheat Scoop® system. All of the full, layered mixtures that contain neutralized acid adsorbed on Swheat Scoop® in the bottom layer and mixed metal salts and Swheat Scoop® in the top layer exhibit similar headspace gas behavior. This behavior is not consistent with what was observed in either water/ Swheat Scoop® or neutralized acid/ Swheat Scoop® mixtures.
- We attribute the significant evolution of CO₂ in the water/ Swheat Scoop® and neutralized acid/ Swheat Scoop® mixtures predominantly to biological processes. We believe that the headspace gas data developed supports the assertion that these same processes are not as active in the mixtures containing the metal nitrate salts.

REFERENCES

1. CCPS. 1995. Guidelines for Chemical Reactivity Evaluation and Application to Process Design. American Institute of Chemical Engineers - Center for Chemical Process Safety, New York.
2. Clark, DL, and DJ Funk. 2015. Waste Isolation Pilot Plant (WIPP): Chemical Reactivity and Recommended Remediation Strategy for Los Alamos Remediated Nitrate Salt (RNS) Wastes (Working Draft). Los Alamos National Laboratory. LA-CP-15-20082.
3. Scheele, R. D., et al. "Preliminary Investigations of the Thermal Stability of Wastes Present in Waste Drum that Breached while in WIPP." February 2015. PNNL-24125.

Supporting Data

The densities of the processed salt and liquid layers as determined in the thermal modeling section were 738 and 848 kg/m³, respectively. The specific heat was also assumed to be 2400 J/kgK. The thermal conductivities of the processed salt and liquid layers using a thermal diffusivity of 0.0015 cm²/s are 0.3 and 0.4 W/mK, respectively. These thermal conductivities were used in the thermal modeling section.

ATTACHMENT 1. TAT MEMBER QUALIFICATIONS

SAVANNAH RIVER NATIONAL LABORATORY

WILSON, DAVID L.

CURRENT POSITION

Associate Laboratory Director, National Security Directorate, Savannah River National Laboratory, Aiken, SC

PERTINENT PROFESSIONAL EXPERIENCE

- 23 years of forensics experience
 - Director, FBI Terrorist Explosive Device Analytical Center
 - Deputy Assistant Director, DHS National Technical Nuclear Forensics Center
 - Chief FBI Chemical-Biological Sciences Unit
 - Chief, FBI Hazardous Materials Response Unit

SPECIALIZATION/EXPERTISE

- Hazardous materials collection
- Chemical, biological and radiological material characterization
- Forensic microscopy

EDUCATION

- M. S., Botany, University of Tennessee
- B. A., Biology, University of Tennessee

MARRA, JOHN E.

CURRENT POSITION

Laboratory Fellow & Chief Research Officer, Savannah River National Laboratory, Aiken, SC

PERTINENT PROFESSIONAL EXPERIENCE

- 28 years' experience in the government nuclear industry including both technical and management of nuclear waste treatment and policy issues.
- Recent Experience
 - Chair, NNSA High-Performance Research Reactor Convert Program Independent Strategic Review Committee
 - Member, NNSA Y-12 Uranium Processing Facility Red Team Review Committee
 - Member, DOE-SC New Brunswick Lab Committee of Visitors
 - Member, DOE-NE Fukushima Accident Recovery Team
- Past-President of The American Ceramic Society (ACerS) and Past-Chair of the ACerS Nuclear & Environmental Technology Division

SPECIALIZATION/EXPERTISE

- Radiochemical separations in complex matrices and treatment of contaminated waters
- Nuclear fuel reprocessing and separation of transuranic elements
- Nuclear waste processing and processing, including both low- and high-level wastes streams
- Application of advanced materials to the Nuclear Fuel Cycle

EDUCATION

- Ph.D., Ceramic Engineering, The Ohio State University (1987)
- B.S., Ceramic Engineering and B.A., Chemistry, The New York State College of Ceramics at Alfred University (1983)

BRIDGES, NICHOLAS J.**CURRENT POSITION**

Principal Scientist, Savannah River National Laboratory, Aiken, SC

PERTINENT PROFESSIONAL EXPERIENCE

- 7 years' experience in the government nuclear industry. Recently:
- Graduate studies involved formulation of novel energetic materials centered around quaternary ammonium

SPECIALIZATION/EXPERTISE

- Radiochemical separations and purification and plutonium recovery
- Nuclear forensic
- Actinide chemistry

EDUCATION

- Ph.D., Chemistry, The University of Alabama
- B.S., Chemistry, Tennessee Technological University

HOBBS, DAVID T.**CURRENT POSITION**

Senior Advisory Scientist, Savannah River National Laboratory, Aiken, SC

PERTINENT PROFESSIONAL EXPERIENCE

- 30 years' experience in the government nuclear industry. Recently:
- Member, Hanford Waste Treatment Plant Criticality Chemistry Expert Review Team
- Member, DOE Review Team for Review of Water Treatment Facilities at Fukushima
- Member, IAEA Review Panel for the Treatment of Low- and Intermediate-Level Nuclear Wastes
- Member, DOE Technical Expert Group Reporting to Assistant Secretary of Energy for Environmental Management
- Member, DOE Science Panel Reporting to Secretary of Energy on Fukushima Accident
- Technical Lead for the Development of ⁹⁰Sr and Actinide Separation Processes at Savannah River Site

SPECIALIZATION/EXPERTISE

- Radiochemical separations in complex matrices and treatment of contaminated waters
- Nuclear fuel reprocessing and separation of transuranic elements
- Inorganic ion-exchange materials for separations and deliver of therapeutic metals and isotopes
- In-situ and Ex-situ spectroscopic techniques for the characterization of novel materials and determination of trace component in extreme environments

EDUCATION

- Ph.D., Inorganic Chemistry, Vanderbilt University
- B.S., Chemistry, University of North Carolina, Chapel Hill

HUNTER, CHARLES H.**CURRENT POSITION**

Manager, Atmospheric Technologies, Savannah River National Laboratory, Aiken, SC

PERTINENT PROFESSIONAL EXPERIENCE

- 35 years in applied meteorology mainly for the nuclear industry. Recently:
- Member, DOE Meteorology Coordinating Council
- Member, DOE Committee on Consequence Assessment and Protective Actions
- Member, American Nuclear Society Standards Committee: 3.11 – Meteorological Monitoring Guidance for Nuclear Facilities; 2.14 – Atmospheric Modeling for Routine Emissions; 2.15 – Atmospheric Modeling for Accidental Releases.
- Lead expert witness for modeling and assessment of environmental damages in DOJ lawsuit related to a major chlorine release from train derailment in Graniteville, South Carolina

SPECIALIZATION/EXPERTISE

- Atmospheric dispersion and fate of chemical and radionuclide emissions
- Emergency response hazards consequence assessments - requirements, applications and systems.
- Meteorological forecasting for facility operations and safety
- Climate analyses supporting nuclear design and operational safety

EDUCATION

- M.S., Meteorology, Florida State University
- B.S., Physics, University of Virginia

VINER, BRIAN J.**CURRENT POSITION**

Senior Scientist, Savannah River National Laboratory, Aiken, SC

PERTINENT PROFESSIONAL EXPERIENCE

- Ten years' experience modeling the atmospheric dispersion or airborne particles.
- Knowledge of behavior and processes involved in various dispersion models including Lagrangian, Gaussian and advection/diffusion models.
- Modeling of tritium oxide deposition processes to determine an appropriate deposition velocity for dispersion models at SRNL.
- Modeling of airborne releases to support sampling projects carried out by field monitoring teams.
- Two years spent on the SRS Emergency Response Operations team as a dispersion modeling specialist.

SPECIALIZATION/EXPERTISE

- Numerical modeling of airborne particles.
- Numerical modeling of meteorological processes.
- Boundary-layer meteorology, including turbulence characterizations and plant/land/atmosphere interactions.

EDUCATION

- M.S. and Ph.D., Agricultural Meteorology, Iowa State University, Ames, IA
- B.S., Meteorology, Iowa State University, Ames, IA

WALTER, STEVEN R.

CURRENT POSITION

Fellow Scientist, Savannah River National Laboratory, Aiken, SC

PERTINENT PROFESSIONAL EXPERIENCE

- 46 years' experience as analytical and physical chemist. Recently:
- Savannah River National Laboratory
- Rocky Flats Plant
- Motorola Inc.
- Celanese Chemical Co.
- Core Laboratories
- Texas Instruments

SPECIALIZATION/EXPERTISE

- Study of chemical airborne signatures to locate and monitor nuclear weapon related activities
- Development and construction of analytical instruments

EDUCATION

- Ph.D., Physical Chemistry, University of Arizona
- B.S., Chemistry, University of North Texas

YOUNG, JOHN E.

CURRENT POSITION

Fellow Technical Advisor, Analytical Development, Savannah River National Laboratory, Aiken, SC

PERTINENT PROFESSIONAL EXPERIENCE

- 35 years' experience in commercial and defense nuclear operations
- Has led 15 incident evaluations involving hazardous, toxic, and radioactive materials
- Developed and implemented a novel technique for measuring trace levels of uranium in PUREX solutions by laser induced fluorescence
- Configured and deployed DOE's first high-rad mixed waste analytical capability for volatile organics
- Led the organics section of the CERCLA (Superfund) characterization efforts for the L-Area Oil & Chem basin waste site with completely automated regulatory data packages with 100% validation of data
- Led the radiological rollback initiatives for SRNL AD, successfully identifying and remediating 17 contaminations to complete the rollback that remains in effect
- Principal investigator to resolve flammability safety issues in the TRU drum Vent and Purge System which led to the development and implementation of the "Intrinsically Safe Sampling Dome" to safely sample TRU drum headspace without subjecting the sampling team to potentially explosive drum condition/geometry
- Technical Lead for FBI examinations in the Radiological Evidence Examination Facility at SRNL. Led SRNL AD efforts for RCRA investigation of a mixed waste facility for the FBI. Has been the principal examiner for FBI nuclear forensics examinations for all of the cases that SRNL has supported involving non-natural radioisotopes in 1999
- Task Leader for Inductively Coupled Plasma-Emission Spectrometry for trace metals determination at SRNL

SPECIALIZATION/EXPERTISE

- Law Enforcement Support, including FBI case examination support, Hazardous Materials Response Unit training support, and Domestic Nuclear Detection Office – Laboratory Lead for Reach back Spectroscopy
- Nuclear Material Detection, including local, state, and national technical support

EDUCATION

- B.S., Chemistry, University of South Carolina

LAWRENCE LIVERMORE NATIONAL LABORATORY

HART, BRADLEY R.

CURRENT POSITION

Director, Forensic Science Center, Lawrence Livermore National Laboratory, Livermore (LLNL), CA

PERTINENT PROFESSIONAL EXPERIENCE

- 15 years' experience conducting research in topics related to chemical analysis, synthesis, materials science and forensics
- Director of the Forensic Science Center, overseeing forensic research and real-world sample analysis efforts covering chemical, biological, nuclear, explosive and human forensics
- Developed and implemented plans for broadly-scoped forensic analysis laboratory capabilities for use both in the US and overseas
- Manage ISO-17025 certified forensic analysis capability supporting multiple Federal agencies and international treaty organizations

SPECIALIZATION/EXPERTISE

- Experimental determination of chemical fate and transport in environmental systems
- Real-world forensic collection and analysis experience
- Forensic chemical and explosives analysis method development and implementation
- Development and implementation of sample collection and preservation methods
- Chemical threat agent synthesis and analysis

EDUCATION

- Ph.D., Chemistry, University of California, Irvine
- B.S., Chemistry, University of Kansas

KOESTER, CAROLYN J.

CURRENT POSITION

Deputy Director, Forensic Science Center, Lawrence Livermore National Laboratory (LLNL), Livermore, CA

PERTINENT PROFESSIONAL EXPERIENCE

- 20+ years' experience in analysis of trace contaminants in environmental matrices
- Author of over 20 publications, including contributing to Analytical Chemistry's biannual Environmental Analysis review from 1995–2005
- Principal Investigator, since 2007, for LLNL's CWA Reference Laboratory in support of the U. S. Environmental Protection Agency's Environmental Response Laboratory Network (ERLN)
- Deputy Principal Investigator for LLNL's Organization for Prohibition of Chemical Weapons (OPCW) designated laboratory

SPECIALIZATION/EXPERTISE

- Subject matter expert on sampling and analysis protocols
- Operation of and data interpretation from gas chromatography/mass spectrometry and liquid chromatography/mass spectrometry
- Integration and interpretation of data from multiple analytical techniques to identify unknown compounds
- Interaction with personnel to assist them in standing-up capabilities to analyze CWAs; development of new analysis methods; and conduct of research with CWA in support of preparedness for processing efforts
- Implementation of quality assurance/quality control practices for ISO-certified analyses

EDUCATION

- Ph.D., Analytical Chemistry, Indiana University
- B.S., Chemistry, Hope College

ALCARAZ, ARMANDO.**CURRENT POSITION**

Senior Scientist, Lawrence Livermore National Laboratory, Livermore (LLNL), CA

PERTINENT PROFESSIONAL EXPERIENCE

- 30 years' experience at LLNL's working on National Security programs. Recently:
- Chemical Detection of Chemical Warfare Agents and Neuro-Toxins with various analytical instrumentation
- Chemical Detection of High Explosives and Nuclear Processing Chemicals with various analytical instrumentation
- On-site Field Chemical Analysis Experience for Treaty Verification
- Oversee ISO-17025 certification of CWA explosives and Rad/Nuc analysis methods
- Lead sessions at the OPCW CWC Workshops
- Served as a National Laboratory lead for OPCW CWC activities

SPECIALIZATION/EXPERTISE

- Principal Investigator for the International OPCW Designated laboratory at LLNL for 15 years
- Interacted and participated in International CW workshops, NATO conferences and On-site Trial Inspections for the detection of Chemical Weapons
- Evaluate and developed analytical protocols for the isolation and identification of CW related compounds using various analytical techniques

EDUCATION

- M.S. Chemistry, San Jose State University, San Jose, CA
- B.A. Chemistry, San Jose State University, San Jose, CA

GRANT, PATRICK M.**CURRENT POSITION**

Chemist, Livermore National Lab, Livermore, CA

PERTINENT PROFESSIONAL EXPERIENCE

- 40 years of experience in DOE national labs:
- LLNL Forensic Science Center – General forensic analyses, WMD analytes, special operations, extraordinary samples & investigations
- LLNL FSC – Program manager & POC for FBI and other LEA & IC forensic projects
- LLNL Nuclear Chemistry Division – Analyst & Radiochemistry Coordinator for NTS underground nuclear explosions
- LANL Group CNC-11 – Radioisotope production for nuclear medicine and other applications
- Charter member and steering committee of several former FBI Scientific Working Groups
- Fellow of the American Academy of Forensic Sciences & editorial board of the *Journal of Forensic Sciences*

SPECIALIZATION/EXPERTISE

- General sample prep, radiochemical separations, applications of nuclear & atomic spectrometry
- Project coordination and sample analyses for unusual IC, homeland security, & LEA forensic investigations
- WMD, HE, and general (criminalistics) forensic analyses
- Route nuclear forensic analyses and assessments

EDUCATION

- Ph.D., Chemistry, University of California, Irvine
- B.S., Chemistry, University of California, Santa Barbara

PAGORIA, PHILIP F.**CURRENT POSITION**

Deputy Scientific Capabilities Leader, Physical Life Sciences, Lawrence Livermore National Laboratory, Livermore, CA

PERTINENT PROFESSIONAL EXPERIENCE

- 29 years' experience in energetic materials synthesis and characterization
- Group Leader of the Energetic Materials Synthesis Group of the Energetic Materials Center
- LLNL High Explosives Safety Committee Chairperson
- Forensic analysis of high explosives
- Home-made explosives synthesis, testing and analysis

SPECIALIZATION/EXPERTISE

- Synthesis and formulation of Energetic compounds
- Synthetic Organic Chemist
- Safety in working with high explosives

EDUCATION

- Ph.D., Chemistry, Washington University
- B.S., Chemistry, MacMurray College

SUTTON, MARK.**CURRENT POSITION**

Associate Program Leader for Nuclear Energy, Lawrence Livermore National Laboratory, Livermore, CA

PERTINENT PROFESSIONAL EXPERIENCE

- 19 years of experience in the nuclear industry. Recently:
- 9 years of experience on DOE's Yucca Mountain Project
- Lead for all work at LLNL associated with US nuclear energy
- Lead for Used Fuel Disposition Campaign work at LLNL
- Member of the International High Level Radioactive Waste Management Committee
- Laboratory QA Point of Contact for DOE-NE5 work
- Radiological Dispersal Device (RDD) Migration Decontamination, Fate and Transport research at LLNL
- Peer reviewer for Canadian Nuclear Waste Management Organization
- Peer reviewer for several journals and DOE's Nuclear Energy University Program
- Deputy Group Leader, Experimental Nuclear and Radiochemistry

SPECIALIZATION/EXPERTISE

- Radiochemistry associated with the nuclear fuel cycle, from mining to disposal
- Analytical chemistry
- CBR response and recovery

EDUCATION

- Ph.D., Environmental Radiochemistry, Loughborough University, UK
- B.S., Chemistry, Loughborough University of Technology, UK

OAK RIDGE NATIONAL LABORATORY

BAKER, MICHAEL L.

CURRENT POSITION

Director, Office of Integrated Performance Management, Oak Ridge National Laboratory, Oak Ridge, TN

PERTINENT PROFESSIONAL EXPERIENCE

- 30 years of experience leading nuclear research and development projects, managing research operations, and leading mission support organizations.
- Co-leads the strategic and business planning process at ORNL in support of the ORNL science mission.
- Responsible for implementation of the Contractor Assurance System, Performance Management, Requirements Management, Records Management, and the Quality Program.
- Member of the Operations Committee at the Pacific Northwest National Laboratory (PNNL). The Operations Committee is a subcommittee to the PNNL Board of Directors.
- Served as Deputy Director for Environment, Safety, Health, and Quality (ESH&Q), responsible for environmental protection, safety and health, radiological protection, and occupational medicine.
- Led the ORNL Safety Services Division, responsible for developing the health and safety agenda for ORNL.
- Led the Technology Development Division at the Y-12 National Security Complex including 150 scientists, engineers, technical support and administrative staff.

SPECIALIZATION/EXPERTISE

- Extensive experience leading research and development projects related to nuclear weapons secondary materials, material sciences, chemical processing, environmental engineering, and process modeling.
- Research focus on actinide recovery and chemical processing including development of new chemical processing technologies, modeling of actinide recovery operations, and production support.
- Additional focus on development of waste treatment technologies for DOE nuclear weapons processing facilities.
- Experience leading large technical and mission support organizations.
- Experienced leading Laboratory-level event investigations.

EDUCATION

- M.S., Environmental Engineering, University of Tennessee
- B.S., Chemical Engineering, University of Tennessee

BRITT, PHILLIP F.**CURRENT POSITION**

Director, Chemical Sciences Division, Oak Ridge National Laboratory, Oak Ridge, TN

PERTINENT PROFESSIONAL EXPERIENCE

- 27 years' experience in kinetics and mechanisms of high temperature organic reactions and quantitatively analysis of complex reaction mixtures
- Published over 150 peer reviewed manuscripts and preprints
- Leads a research Division of over 150 scientists, technical support, administrative staff, postdoctoral researcher associates, and graduate students
- Program manager for U.S. DOE, Office of Science, Basic Energy Sciences, Chemical Sciences, Geosciences, and Biosciences Division programs
- Led Macromolecular Nanomaterials group at the Center for Nanophase Materials Sciences
- Fellow of the American Chemical Society

SPECIALIZATION/EXPERTISE

- Extensive experience in leading multi-disciplinary research and development teams
- Integration and interpretation of data from multiple analytical techniques to identify unknowns
- Elucidation of mechanisms of pyrolysis reactions of organic compounds
- Expertise in analytical techniques including gas chromatography/mass spectrometry, thermal gravimetric analysis coupled with mass spectrometry analysis of the evolved gases, liquid chromatography, NMR, SEM-EDS, and FTIR

EDUCATION

- Ph.D., Organic Chemistry, University of Texas at Austin, Austin, TX
- B.S., Chemistry, James Madison University, Harrisonburg, VA

DAVISON, BRIAN H.**CURRENT POSITION**

Chief Scientist for Systems Biology and Biotechnology, Oak Ridge National Laboratory, Oak Ridge, TN

PERTINENT PROFESSIONAL EXPERIENCE

- Over 30 years of experimental and modeling expertise in bioprocessing and industrial microbiology
- Led ORNL and DOE initiatives in Systems Biology and Bioenergy
- Over 130 publications and patents

SPECIALIZATION/EXPERTISE

- Bioconversion of biomass
- Non-aqueous Biocatalysis
- Bioprocessing, mass transfer and separations in multiphase bioreactors
- Biomethanogenesis

EDUCATION

- B.S.E., Chemical Engineering, with honors, University of Rochester, Rochester, NY, 1979.
- Ph.D., Chemical Engineering, California Institute of Technology, Pasadena, CA, 1985.

GIAQUINTO, JOSEPH

CURRENT POSITION

Group Leader, Nuclear Analytical Chemistry and Isotopics Laboratories, Oak Ridge National Laboratory, Oak Ridge, TN

PERTINENT PROFESSIONAL EXPERIENCE

- 23 years of analytical laboratory experience performing and leading destructive characterizations on high level radioactive materials and matrices.
- Manager of four specialized radiochemistry and mass spectrometry laboratories and 21 professional chemists and radiochemical technicians.
- Responsible for a diverse portfolio of analytical work in the areas of transuranium isotope chemistry and production, fuels cycle R&D, radiological environmental management, and nuclear forensics, non-proliferation and safeguards for nuclear materials.
- Current projects include the detailed destructive characterizations of spent nuclear fuels specimens and development of separation methodologies for the measurement of lanthanide and actinide isotopic distributions in transuranic materials in support of ORNL's heavy isotope Cf-252 and Pu-238 production programs as well as high precision quantifications of trace impurities in nuclear materials using novel separation techniques and isotope dilution mass spectrometry.

SPECIALIZATION/EXPERTISE

- Analytical chemistry related to nuclear disciplines including radiochemical separations and high precision measurement methodologies.
- Elemental mass spectrometry and radiological counting techniques
- Expert in numerous analytical and radiochemical techniques and protocols with emphasis in mass spectrometry and the chemistry of the lanthanide and actinide elements.

EDUCATION

- B.S., Chemistry, University of Florida
- Naval Nuclear Propulsion Systems, U.S.N (2-year graduate level studies)

TICKNOR, BRIAN

CURRENT POSITION

Research and Development Staff Scientist, Nuclear Analytical Chemistry and Isotopics Laboratories, Oak Ridge National Laboratory, Oak Ridge, TN

PERTINENT PROFESSIONAL EXPERIENCE

- 12+ years' experience with custom built and commercial mass spectrometers
- 4+ years' experience with isotope ratio mass spectrometry
- Current projects include bulk analysis of environmental samples for the IAEA NWAL, analytical chemistry support for Stable Isotope sales at ORNL, and a variety of other projects in the fields of nuclear forensics, nuclear non-proliferation, and nuclear safeguards

SPECIALIZATION/EXPERTISE

- Inorganic/elemental mass spectrometry
- Isotope ratio analysis using multi-collector inductively coupled plasma and thermal ionization mass spectrometry
- High resolution actinide and lanthanide isotope ratio measurements

EDUCATION

- B.S., Chemistry and History, Furman University, 2002
- Ph.D., Physical Chemistry, University of Georgia, 2008
- National Research Council Postdoctoral Fellow, Space Vehicles Directorate, Air Force Research Laboratory, 2008-2010

PACIFIC NORTHWEST NATIONAL LABORATORY

SCHWANTES, JON M

CURRENT POSITION

Senior Scientist, Pacific Northwest National Laboratory, Richland, Washington

PERTINENT PROFESSIONAL EXPERIENCE

- Over 20 years' experience as a radiochemist working in areas related to the environment, super-heavy element chemistry and physics, astrophysical nucleosynthesis, science based stockpile stewardship, and nuclear forensics.
- Part of the confirmatory team for the discovery of element 111
- Lead a team of researchers in 2009 that identified the oldest known reactor-produced plutonium in the world
- Authored or coauthored 64 peer-reviewed journal articles
- Technical Point of Contact for his Laboratory to the Department of Homeland Security's National Technical Nuclear Forensics Center
- Serves as the Lead for the Destructive Assay Users Group for the Institute for Nuclear Materials Management (INMM)
- U.S. National Committee Representative to the International Union of Pure and Applied Chemistry (IUPAC)
- Co-Chair of the Exercise Task Group for the Nuclear Forensics International Technical Working Group (ITWG)

SPECIALIZATION/EXPERTISE

- Nuclear forensics
- Nuclear and radioactive source attribution
- Chemical process modeling
- Nuclear detection
- Ultra-trace actinide analytical techniques

EDUCATION

- Ph.D., Civil (Environmental) Engineering, Texas A&M University
- M.S., Chemical Oceanography, Texas A&M University
- B.S., Marine Sciences, Texas A&M University

MINETTE, MICHAEL JAMES

CURRENT POSITION

Senior Project Manager, Pacific Northwest National Laboratory, Richland, Washington

PERTINENT PROFESSIONAL EXPERIENCE

- Thirty years' of project management experience in the mining and nuclear industries
- Project manager of the Hanford Plutonium Finishing Plant contaminated equipment removal and incinerator demolition projects
- Project manager for the PNNL technology development efforts with the Hanford Waste Treatment Plant construction efforts
- Hanford Plutonium Finishing Plant project manager and decontamination cognizant engineer that worked with PNNL to determine thermochemical hazards associated with Hanford Plutonium Finishing Plant plutonium-contaminated gloveboxes decontamination wastes
- Has received over 31 major project awards for managing nuclear projects

SPECIALIZATION/EXPERTISE

- Twenty Three years of managing nuclear projects and over thirty years as a project manager
- Professional Project Manager (PMI) and Licensed Professional Engineer (State of Washington)
- Expert in nuclear waste packaging and the safety waste processes for controlling nitric acids and organic wastes
- Author on four major papers on the thermal stability of nitric acid nuclear waste streams
- Author on over forty nuclear papers and reports

EDUCATION

- B.S., Mining Engineering, Montana College of Mineral Sciences and Technology
- MBA Finance, San Diego State University
- Project Management Certification Program, Washington State University and the Project Management Institute
- Project Manager Development Program, Pacific Northwest National Laboratory University
- Project Manager Training Program, Fluor Corporation
- Past Board Member of the Washington State University Project Management Educational Advisory Board
- Past Project Management Instructor, Washington State University

ATKINSON, DAVID ALAN**CURRENT POSITION**

Senior Research Scientist, Pacific Northwest National Laboratory, Richland, Washington

PERTINENT PROFESSIONAL EXPERIENCE

- 25+ years' of experience in the DOE laboratory system involved with technical challenging trace detection and analytical chemistry projects
- Extensive experience in designing instrumentation and developing detection methodologies for a variety of materials of interest to national security (e.g. explosives, illicit drugs, and chemical warfare agents)
- Co-developed a suite of methods for organic analysis of highly radioactive acidic waste streams
- Manages the business development aspects of a large and diverse portfolio (>\$25 million) related to chemical, biological, and explosives threat detection and mitigation
- Experience includes building teams to successfully execute large, multi-disciplinary research efforts (e.g. Explosives Detection LDRD Initiative, Center for Ion Mobility Spectrometry)

SPECIALIZATION/EXPERTISE

- Organic detection methodology, including sampling, instrumentation, and data reduction flow-sheet development of novel processes to address technical problems in the DOE complex
- All stages of technology development, from fundamental research through application development to field deployment
- Internationally known in the area of ion mobility spectrometry and explosives detection
- Developing analytical methods for deployment into difficult environments

EDUCATION

- Ph.D., Chemistry, Washington State University
- M.S., Chemistry, Washington State University
- B.S., Polymer Science, Pennsylvania State University

SCHEELE, RANDALL DUNSTAN**CURRENT POSITION**

Staff Scientist, Pacific Northwest National Laboratory, Richland, Washington

PERTINENT PROFESSIONAL EXPERIENCE

- 40 years' experience in the government nuclear industry. Recently:
- Led project for Fuel Cycle Energy Research & Development project and PNNL internal research project on nitrogen trifluoride-based volatile fluoride spent nuclear fuels reprocessing concept
- Led projects to determine thermochemical hazards associated with the use of cellulose and sucrose to denitrate Hanford radioactive wastes
- Led project to determine thermochemical hazards associated with Hanford Plutonium Finishing Plant plutonium-contaminated gloveboxes decontamination wastes
- Led project to determine the thermochemical hazards of Hanford's ferrocyanide-containing high level radioactive wastes
- Led project to determine the thermochemical hazards of Hanford's Organic Tank high level radioactive wastes
- Led miscellaneous projects to assess thermochemical hazards of radioactive wastes with various organics to be used in proposed waste management processes

SPECIALIZATION/EXPERTISE

- Radiochemical separations and purification nuclear waste processing and plutonium recovery
- Flow-sheet development of novel processes to address technical problems in the DOE complex
- Actinide Chemistry, Physical Properties and Reaction Chemistry
- Radionuclide immobilization (actinides, radioiodine)
- Application of thermoanalytical methods (thermogravimetric analysis, differential thermal analysis, differential scanning calorimetry, accelerating rate calorimetry) to assess the thermochemical hazards of wastes and waste management approaches
- Capture of volatile radioiodine during nuclear fuels reprocessing and waste management operations

EDUCATION

- B.S., Chemistry, Pacific Lutheran University
- 40+ h graduate chemistry credits

BEISWENGER, TOYA NICOLE**CURRENT POSITION**

Research Scientist, Pacific Northwest National Laboratory, Richland, Washington

PERTINENT PROFESSIONAL EXPERIENCE

- 5 years' of experience in electron microscopy for particle characterization
- Current work includes analyzing environmental samples utilizing FT-IR Spectroscopy

SPECIALIZATION/EXPERTISE

- Automated Scanning Electron Microscopy
- Transmission Electron Microscopy
- Field Emission Scanning Electron Microscopy

EDUCATION

- M.S., Environmental Science, Washington State University
- B.S., Biology, Southeastern Louisiana University

BUCK, EDGAR

CURRENT POSITION

Senior Research Scientist, Pacific Northwest National Laboratory, Richland, Washington

PERTINENT PROFESSIONAL EXPERIENCE

- Program Manager for the Used Fuel Disposition Project at Pacific Northwest National Laboratory looking at radiolysis effects on spent nuclear fuel.
- Co-authored a special issue in the MRS Bulletin on actinide spectroscopy and the Chapter on Uranium for the 3rd edition of the Chemistry of the Actinide and Transactinide Elements.
- Held scientific leadership roles over time, including DARPA radioisotope battery project, colloidal migration studies, and the PNNL Tc-metal waste form project.
- Lead author on the Waste Form and In-drift Colloids-Associated Radionuclide Concentrations: Abstraction and Summary, MDL-EBS-PA-000004 for the Yucca Mountain Repository License Application.
- Conducted data interpretation for the Hanford Waste Treatment Project intermittently for more than 8 years and worked for the Tritium Readiness Program conducting Post-Irradiation Analysis of target components for more than 7 years.
- Currently teaches a graduate level course in electron microscopy at WSU Tri-Cities.
- Over 60 publications in the open literature.

SPECIALIZATION/EXPERTISE

- Knowledgeable in the interaction of electron beams with matter, electron and x-ray instrumentation, and materials science with an emphasis on radioactive materials.
- Expertise in the long-term behavior of nuclear materials; including oxide spent nuclear fuels, borosilicate glass and ceramic waste forms, radio-colloids, and materials for tritium production.
- Expert in ultramicrotomy of materials.
- Expert in electron energy-loss spectroscopy of nuclear materials using the electron microscope.
- Application of Microscopy (Optical, SEM, TEM) to material science problems.

EDUCATION

- Ph.D. Materials Science, University of Birmingham, United Kingdom

COFFEY, DEBORAH S**CURRENT POSITION**

Senior Quality Engineer, Pacific Northwest National Laboratory, Richland, Washington

PERTINENT PROFESSIONAL EXPERIENCE

- Current Quality Representative for the WIPP TAT effort at PNNL
- Former Deputy Quality Manager, WIPP, Sandia National laboratory

SPECIALIZATION/EXPERTISE

- Quality Assurance Program implementation and compliance

EDUCATION

- M.S., Resource Ecology, University of Michigan – Ann Arbor
- B.S., Biology, Chemistry, University of Michigan – Flint

FRAGA, CARLOS G**CURRENT POSITION**

Senior Research Scientist, Pacific Northwest National Laboratory, Richland, Washington

PERTINENT PROFESSIONAL EXPERIENCE

- Senior Research Scientist in the Chemical and Biological Signature Science Group at Pacific Northwest National Laboratory (PNNL)
- Joined PNNL after 12 years as an U.S. Air Force officer
- Managed and performed research dealing with the sampling, detection, and fate of chemical weapon related compounds
- Led a 13-member radiochemical separations group that processed samples for subsequent analyses of radionuclides using various radiation detectors and mass spectrometers
- Co-hosted two symposium on chemical forensics at the American Chemical Society's (ACS) national meetings in Denver (2011) and Indianapolis (2013)
- Taught chemistry at the Air Force Academy including a course on chemical weapons (CW)

SPECIALIZATION/EXPERTISE

- Development of chemometric and two-dimensional chromatographic methods for the analysis of trace organic compounds in complex mixtures
- Chemical forensics for sourcing CW agents and explosives
- Published six peer-reviewed papers in chemical forensics for the DHS Chemical Forensics Program including a paper demonstrating for the first time the use of chemical forensics on a CW agent

EDUCATION

- Ph.D., Analytical Chemistry, University of Washington
- M.S., Chemistry, University of Illinois
- B.S., Chemistry, United States Air Force Academy

GASSMAN, PAUL LAWRENCE

CURRENT POSITION

Research Scientist, Pacific Northwest National Laboratory, Richland, Washington

PERTINENT PROFESSIONAL EXPERIENCE

- 25 years of research experience for DOE - including the following topical areas:
- Geochemical research in contaminant mobilities in subsurface environments, including radionuclide mobilities as affected by mineralogy and co-disposed organic chelates.
- Field campaigns at Hanford, in Texas and in Mexico examining site suitabilities for long term disposal of vitrified nuclear wastes, EPA compliance by coal-fired power plants, and environmental considerations for Mexico's petroleum industry (PEMEX).
- Co-developed an exemplar library of uranium compounds to aid identification of uranium containing phases in the subsurface sediments of Hanford using laser induced fluorescence spectroscopy.
- Co-developed an exemplar library of liquids of select organic compounds using quantitative infrared spectroscopic techniques.
- Supported projects in the Environmental Molecular Sciences Laboratory at PNNL using fluorescence,, infrared and Raman spectroscopies to develop electrochemical sensors for detecting nerve agents, development of improved filtration systems for water treatment plants, development of new understandings of incipient organic aerosol formation during combustion.
- Supported method development for detecting low volatility chemicals from nuclear fuels reprocessing using infrared reflection absorption techniques.
- Recent work has included providing an improved understanding of technetium (Tc) incorporation in glasses using Raman spectroscopy to aid disposal of Hanford's Tc containing wastes through vitrification

SPECIALIZATION/EXPERTISE

- Geochemistry
- Soil and Environmental sciences
- Fluorescence and Laser-Induced Fluorescence Spectroscopy
- Vibrational Spectroscopies (Infrared and Raman)
- Analytical Chemistry
- Nuclear Forensics and Nuclear Non-Proliferation

EDUCATION

- M.S., Soil and Environmental Sciences, Virginia Polytechnic Institute and State University
- B.S., Geological Sciences, Virginia Polytechnic Institute and State University

GREENWOOD, LARRY R

CURRENT POSITION

Laboratory Fellow, Pacific Northwest National Laboratory, Richland, Washington

PERTINENT PROFESSIONAL EXPERIENCE

- 40 years' experience in Nuclear Physics research and applications
- Team Leader for Radioanalytical Applications Team and Radiomaterials Chemistry Team at PNNL
- Physicist in Chemical Technology Division 1970 to 1990 at Argonne National Laboratory
- Postdoctoral appointments at Argonne National Laboratory and Northwestern University working with the Nuclear Data Project at Oak Ridge National Laboratory

SPECIALIZATION/EXPERTISE

- Reactor dosimetry for research and commercial nuclear reactors and accelerator neutron sources
- Lead scientist of a certified radionuclide laboratory for the International Monitoring System of the Comprehensive Test Ban Treaty Organization
- FLC and R&D 100 Award for the development of Cs-131 brachytherapy seeds with IsoRay
- Consultant to the International Atomic Energy Agency for the development of the International Reactor Dosimetry File 2002 and the International Reactor Dosimetry Fission Fusion file
- Developed the SPECTER computer code for the calculation of fundamental radiation damage in irradiated materials and the STAYSL_PNNL code for neutron spectral adjustment

EDUCATION

- Ph.D., Nuclear Physics, Rice University
- B.S., Physics and Math, Rice University

JOHNSON, TIMOTHY J

CURRENT POSITION

Senior Research Scientist, Pacific Northwest National Laboratory, Richland, Washington

PERTINENT PROFESSIONAL EXPERIENCE

- PI and lead scientist for spectroscopic studies for national security and environmental applications
- Project development & management of >20M\$
- Constructed a quantitative infrared high-resolution infrared database with spectra of > 500 of species for remote and in situ gas detection.

SPECIALIZATION/EXPERTISE

- Infrared Gas-phase Spectroscopy Signatures
- Raman Spectroscopy – Solid & Liquids
- Atmospheric Measurement Campaigns
- Advanced Fourier Transform Infrared (FTIR) Spectroscopy

EDUCATION

- Ph.D., Chemical Physics, Washington State University
- B.A., Chemistry, Carleton College

KROGSTAD, EIRIK JENS**CURRENT POSITION**

Staff Scientist, Pacific Northwest National Laboratory, Richland, Washington

PERTINENT PROFESSIONAL EXPERIENCE

- 32 years' experience in isotopic and trace element mass spectrometry at university and national lab positions
- Managed five mass spectrometry laboratories; establishing or responsible for major upgrades at four of them

SPECIALIZATION/EXPERTISE

- Operation, redesign/rebuild, software design, and maintenance of TIMS (single- and multi-collector), magnetic sector ICP-MS (single- and multi-collector), and quadrupole ICP-MS instruments.
- Method development in MC-ICP-MS, TIMS, LA-ICP-MS
- Laser ablation ICP-MS and/or LA-LIBS-ICP-MS for isotope ratio or elemental analysis
- Development of lanthanide and actinide separation methods
- Isotope dilution mass spectrometric analyses of lanthanides, actinides and other elements.

EDUCATION

- Ph.D., Geochemistry, State University of New York at Stony Brook
- B.S., Geology, Western Washington University

MCNAMARA, BRUCE K**CURRENT POSITION**

Senior Research Scientist, Pacific Northwest National Laboratory, Richland, Washington

PERTINENT PROFESSIONAL EXPERIENCE

- Chemical and physical studies related to tank waste characterization
- NMR investigation of technetium and actinide metals for tank waste characterization

SPECIALIZATION/EXPERTISE

- Fluorination reactions of actinyl species for separations
- fundamental investigations of hydrated UO₂
- commercial spent fuel
- Analytical radiochemistry
- Radiochemical separations

EDUCATION

- Ph.D., Physical Chemistry, Purdue University
- B.S., Chemistry, University of Massachusetts

MEIER, DAVID E**CURRENT POSITION**

Senior Research Scientist, Pacific Northwest National Laboratory, Richland, Washington

PERTINENT PROFESSIONAL EXPERIENCE

- 10 years of experience in Nuclear Forensic Sciences
- Project manager of Plutonium Processing Project at PNNL
- Laboratory manager of WIPP laboratory at PNNL

SPECIALIZATION/EXPERTISE

- Radiochemical separations
- Plutonium reprocessing and purification
- Nuclear forensics
- Neutron activation analysis and isotope production

EDUCATION

- Ph.D., Radiochemistry, University of Missouri
- B.S., Chemistry, Lincoln University

POOL, KARL N**CURRENT POSITION**

Analytical Support Operations Lead, Pacific Northwest National Laboratory, Richland, Washington

PERTINENT PROFESSIONAL EXPERIENCE

- Project management and integration of all NC&E analytical chemistry activities at PNNL
- Manage the operational systems necessary to facilitate laboratory activities to include the NC&E's policy on record keeping and retention, the standardization of laboratory reporting formats, management of laboratory supplies, equipment and chemicals and management of waste handling, analysis and disposal activities for waste generated from analytical support activities
- Provide technical direction to Hot Cell technicians in the preparation and analyses of sample materials
- PNNL representative and former acting chairman for the Hanford Analytical Services Quality Assurance Requirements Document (HASQARD)

SPECIALIZATION/EXPERTISE

- Lead scientist for 325 Hot Cell analytical services

EDUCATION

- B.S., Chemistry, Washington State University
- Management of Polychlorinated Biphenyls Disposal Training, National Environmental Training Office

TONKYN, RUSSEL G**CURRENT POSITION**

Staff Scientist, Pacific Northwest National Laboratory, Richland, Washington

PERTINENT PROFESSIONAL EXPERIENCE

- 22 years research as PNNL staff member, 1 year as a Post Doc
- 3 years Post-Doctoral work at Brookhaven National Lab

SPECIALIZATION/EXPERTISE

- Gas phase chemical physics—ion molecule chemistry, kinetics
- Photoelectron spectroscopy, VUV generation, assorted laser spectroscopy techniques
- Catalytic and plasma-catalytic treatment of diesel exhaust for NO_x processing
- FTIR and FT-Raman spectroscopy of gases, liquids and solids

EDUCATION

- Ph.D., Physical Chemistry, University of Wisconsin at Madison
- B. A., Chemistry, Reed College

SODERQUIST, CHUCK Z**CURRENT POSITION**

Senior Research Scientist, Pacific Northwest National Laboratory, Richland, Washington

PERTINENT PROFESSIONAL EXPERIENCE

- 31 years' experience in radiochemistry, in both commercial and government laboratories
- Author or co-author of 35 journal articles and PNNL reports, and 3 patents

SPECIALIZATION/EXPERTISE

- Radioanalytical separations and counting, ranging from low environmental levels up to irradiated fuel and high level waste
- Hanford tank waste chemistry and analysis
- Spent nuclear fuel chemistry
- Actinide chemistry and actinide separations
- Inorganic synthesis

EDUCATION

- M.S., Chemistry, Central Washington University
- B.S., Chemistry, Northwest Nazarene College

SWEET, LUCAS**CURRENT POSITION**

Staff Scientist, Pacific Northwest National Laboratory, Richland, Washington

PERTINENT PROFESSIONAL EXPERIENCE

- 6 years of experience in the government nuclear industry

SPECIALIZATION/EXPERTISE

- X-ray crystallography
- Optical spectroscopies, Raman, infrared, and UV/Vis
- Actinide chemistry

EDUCATION

- Ph.D., Chemistry, Texas A&M University
- B.S., Chemistry, Lake Forest College

WAHL, JON H**CURRENT POSITION**

Senior Research Scientist, Pacific Northwest National Laboratory, Richland, Washington

PERTINENT PROFESSIONAL EXPERIENCE

- 20 years of experience in ultra-trace organic collection and detection.
- Led projects to characterize forensic-related sampling protocols
- Led projects to characterize a variety of USG related interests
- Authored or co-authored of over 30 peer-reviewed publications, numerous conference presentations, book chapters, and U. S. patents

SPECIALIZATION/EXPERTISE

- Advanced separation techniques
- Ultratrace analysis for chemical warfare agents (and pre/post and degradation products), biological, explosives, and other signature compounds of interest to USG

EDUCATION

- Ph.D., Analytical Chemistry, Michigan State University
- B.S., Chemistry, Michigan Technological University

SANDIA NATIONAL LABORATORIES

SHOEMAKER, PAUL

CURRENT POSITION

Senior Manager, Sandia National Laboratories/Carlsbad (SNL/C), NM

PERTINENT PROFESSIONAL EXPERIENCE

- 24 years' experience managing high-profile programs at Sandia National Laboratories. Recently:
- Leader of Sandia's work in support of DOE on matters associated with the Waste Isolation Pilot Plant (WIPP)
- Total of 9 years managing Sandia's work in support of WIPP
- Previously served as Deputy Chief Operating Officer for Sandia's Nuclear Weapons Strategic Management Unit
- Previous to that, served as leader of Sandia's strategic planning group in the Laboratories' executive office

SPECIALIZATION/EXPERTISE

- Management of technical activities related to nuclear waste management
- Placement of those and other Sandia technical activities in strategic context
- Maintenance of productive working relationships with officials within DOE/EM, DOE/NE, DOE/Office of Science, and NNSA

EDUCATION

- MPAff, Lyndon B. Johnson School of Public Affairs, University of Texas at Austin
- B.S., Physics, New Mexico Institute of Mining and Technology, Socorro, NM

MINIER, LEANNA

CURRENT POSITION

Manager, Energetic Materials Dynamic & Reactive Explosives Technologies Group

PERTINENT PROFESSIONAL EXPERIENCE

- 24 years' experience energetic material degradation reactive processes and kinetics, focus on science underlying performance and compatibility, and determination of aging and slow-reactive mechanisms of energetic materials.
- 10 years' experience managing research in the area of energetic material science
- Active in Joint Munitions Program, Joint Army Navy NASA Air Force program and multiple other programs for past 25 years

SPECIALIZATION/EXPERTISE

- Focus on leading programs involving intentional and highly coupled efforts between experiment and modeling to develop the physics underlying the relationship between energetic material properties and their performance, reliability and safety.

EDUCATION

- Ph.D. Chemistry, New Mexico Technical Institute of Mining & Technology, Socorro, NM
- M.S. Chemistry, New Mexico Technical Institute of Mining & Technology, Socorro, NM
- B.S. Biology, New Mexico Technical Institute of Mining & Technology, Socorro, NM

BEPPLER, CHRISTINA

CURRENT POSITION

Senior Member of Technical Staff, Explosives Technologies Group, Energetic Materials Characterization

PERTINENT PROFESSIONAL EXPERIENCE

- 2 years' experience directing the mass spectrometry facilities for Sandia's Explosives Components Facility. Recently:
- Use of state-of-the-art quadrupole-time of flight (QTOF) mass spectrometry to identify non-volatile degradation products

SPECIALIZATION/EXPERTISE

- Analytical chemist leading state-of-health chemical and material evaluations of energetic materials
- Studies involving planning work and analyzing data from diverse chemical and material analysis techniques

EDUCATION

- Ph.D. Analytical Chemistry, Washington State University, Pullman, WA
- B.S. Chemistry, University of New Mexico, Albuquerque, NM

HIGHTOWER, SHAUN**CURRENT POSITION**

Senior Member of Technical Staff, energetics Characterization Organization, Test Operations Engineer & Laboratory Coordinator

PERTINENT PROFESSIONAL EXPERIENCE

- First year as a Senior Member of Technical Staff in the Energetic Characterization department at Sandia National Laboratories. Recently:
- 7 years' experience working in laboratories specializing in Forensic Chemistry
- Expert witness in forensic chemistry in New Mexico and Federal courts

SPECIALIZATION/EXPERTISE

- Expert in forensic chemistry

EDUCATION

- M.S. Analytical Chemistry, New Mexico State University, Las Cruces, NM
- B.S. Biochemistry, New Mexico State University, Las Cruces, NM

KANESHIGE, MICHAEL**CURRENT POSITION**

Distinguished Member of Technical Staff, Explosives Technologies Group

PERTINENT PROFESSIONAL EXPERIENCE

- 15 years' experience on hazards of energetic materials with a focus on thermal ignition and response of energetic materials to abnormal thermal and mechanical environments.
- Principal Investigator of the Energetic Material Hazards projects within the Joint DoD-DOE Joint Munitions Program and the Sandia Weapon Systems Engineering Assessment Technologies program
- Active member of the Sandia Explosives Safety Committee, chair of the Explosives Technologies Group Safety Review Board, author of the Explosives Technologies Group Training and Qualification program, and instructor of the explosives section of Sandia's Engineering Guide to Nuclear Weapons Development, Production, and Stockpile class.

SPECIALIZATION/EXPERTISE

- Explosives Technologies
- Energetic Materials
- Predictive Modeling

EDUCATION

- Ph.D. Mechanical Engineering, California Institute of Technology, Pasadena, CA
- M.S. Mechanical Engineering, California Institute of Technology, Pasadena, CA
- B.S. Mechanical Engineering, University of Illinois, Urbana-Champaign, IL

HOBBS, MICHAEL**CURRENT POSITION**

Principal member of the technical staff

PERTINENT PROFESSIONAL EXPERIENCE

- His work has involved numerical simulation of the physics related to fossil fuel energy conversion, polymer decomposition, propellants, explosives and pyrotechnics. Recently:
- First author for over 15 journal publications and delivered more than 30 presentations at national and international symposia

SPECIALIZATION/EXPERTISE

- Three decades of experience modeling thermal behaviors of materials and reactive processes

EDUCATION

- Ph.D. Chemical Engineering, Brigham Young University, Provo, UT
- M.S. Chemical Engineering, Brigham Young University, Provo, UT
- B.S. Chemical Engineering, Brigham Young University, Provo, UT

SMITH, JEFFERY**CURRENT POSITION**

Principal Member of Technical Staff, Computational Structure Mechanics & Applications, Computational Structural Mechanics & Apps.

PERTINENT PROFESSIONAL EXPERIENCE

- 15 years' experience in structural mechanics. Recently:
- Current work includes examining the mechanical effects of abnormal accidents on components and systems
- Principal Investigator for a validation and verifications program for modeling bolted connections

SPECIALIZATION/EXPERTISE

- Structural mechanics

EDUCATION

- Ph.D. Civil Engineering, University of Kansas, Lawrence KS
- M.S. Civil Engineering, University of Kansas, Lawrence KS
- B.S. Civil Engineering, University of Kansas, Lawrence KS

REDMOND, JIM**CURRENT POSITION**

Senior Manager, Solid Mechanics & Shock Physics, Engineering Sciences Center

PERTINENT PROFESSIONAL EXPERIENCE

- More than 10 years' experience managing structural mechanics departments. Recently:
- Senior Manager of Solid Mechanics and Shock Physics, an organization of ~70 professional staff dedicated to furthering the understanding of structures subjected to extreme environments
- Led teams providing engineering analysis support in response to national emergencies

SPECIALIZATION/EXPERTISE

- Structural mechanics

EDUCATION

- Ph.D. Mechanical Engineering, North Carolina State University, Raleigh, NC
- M.S. Aerospace Engineering, North Carolina State University, Raleigh, NC
- B.S. Aerospace Engineering, North Carolina State University, Raleigh, NC

ROSENBERG, DAVID**CURRENT POSITION**

Senior Member of Technical Staff, Explosives Technologies Group, Energetic Materials Characterization Org.

PERTINENT PROFESSIONAL EXPERIENCE

- 15 years' experience in energetic material synthesis, compatibility, and thermal sensitivity of energetic materials for the DoD and DOE. Recently:

SPECIALIZATION/EXPERTISE

- Energetic material synthesis

EDUCATION

- Ph.D. Organic Chemistry, University of Nebraska, Lincoln, NE
- B.S. Chemistry, Adams State University, Alamosa, CO, *Cum Laude*

SORENSEN, N. ROBERT**CURRENT POSITION**

Distinguished Member of Technical Staff, Materials Reliability Department

PERTINENT PROFESSIONAL EXPERIENCE

- 33 years of experience in materials science including aqueous and atmospheric corrosion, materials degradation, materials reliability, and failure analysis. Recently: Manages programs on PV reliability and Predictive Materials Aging and Reliability.

SPECIALIZATION/EXPERTISE

- Materials Degradation, Materials Reliability, Failure Analysis

EDUCATION

- Sc.D. Materials Science, Massachusetts Institute of Technology, Cambridge, MA
- B.S., Metallurgical Engineering, University of Utah, Salt Lake City, Utah.

XIONG, YONGLIANG**CURRENT POSITION**

Principal Member of Technical Staff, Repository Performance

PERTINENT PROFESSIONAL EXPERIENCE

- 12+ years as specialized in providing key technical evaluations at the WIPP site for determining the actinide solubility's, technical basis behind the magnesium oxide engineered barrier, and solubility of other compounds and minerals potentially impacting the long-term repository performance of the WIPP site.
- Responsible for actinide solubility calculations by using the FMT code for Compliance Re-certification Application (CRA) Performance Assessment (PA) for WIPP.
- Responsible for the establishment of uncertainty range of actinide solubility predictions based on actinide oxidation state models of +III, +IV, and +V oxidation states, for FMT code.

SPECIALIZATION/EXPERTISE

- Geochemistry, engineered barriers for radioactive waste disposal, actinide chemistry

EDUCATION

- Ph.D. Geochemistry, University of Idaho, Moscow, ID
- M.S. Geology, University of Alberta, Edmonton, Canada
- M.S. Geosciences, China University, Wuhan, China
- B.S. Engineering Geosciences, China University, Wuhan, China

BRADY, PATRICK**CURRENT POSITION**

Senior Scientist, Geoscience Research & Geosciences, Climate & Consequences Effect Center

PERTINENT PROFESSIONAL EXPERIENCE

- Led waste form chemistry effort for Yucca Mountain, measured radionuclide uptake by Culebra Dolomite for WIPP, have published several dozen peer-reviewed journal articles, book chapters, and books on geochemistry.

SPECIALIZATION/EXPERTISE

- Environmental chemistry, mineral surface chemistry, geochemistry, radioactive waste disposal.

EDUCATION

- Ph.D. Geochemistry, University of California, Berkeley, CA
- M.S. Geochemistry, Northwestern University, Evanston, IL
- B.S. Geology, Northwestern University, Evanston, IL

LARSEN, MARVIN**CURRENT POSITION**

Principal member of Technical Staff, Thermal Sciences & Engineering

PERTINENT PROFESSIONAL EXPERIENCE

- 28 years of experience at Sandia in thermal sciences and weapon effects modeling
- NEST and JTOT emergency response support spanning 25 years including development of weapon (nuclear and dirty bomb) effects modeling and foam mitigation technologies
- Principal thermal model developer for risk assessments and development for SST, SGT, and MGT (bomb trucks).
- Application of finite element thermal models to support weapons programs and satellites

SPECIALIZATION/EXPERTISE

- Radiation Heat Transfer
- Weapons Effects
- Predictive Thermal Modeling

EDUCATION

- Ph.D. Mechanical Engineering, University of Texas, Austin, TX
- M.S. Mechanical Engineering, Southern Methodist University, Dallas, TX
- B.S. Mechanical Engineering, South Dakota School of Mines and Technology, Rapid City, SD

TENCER, JOHN**CURRENT POSITION**

Senior Member of Technical Staff, Thermal Sciences and Engineering

PERTINENT PROFESSIONAL EXPERIENCE

- 1 year experience performing analysis of abnormal thermal environments for weapons safety

SPECIALIZATION/EXPERTISE

- Radiation Heat Transfer

EDUCATION

- Ph.D. Mechanical Engineering, University of Texas at Austin, Austin, TX
- M.S. Mechanical Engineering, University of Texas at Austin, Austin, TX
- B.S. Mechanical Engineering, University of Tennessee, Knoxville, TN

HOGAN, ROY

CURRENT POSITION

Distinguished Member of Technical Staff, Thermal Sciences & Engineering Dept.

PERTINENT PROFESSIONAL EXPERIENCE

- 27 years' experience in heat transfer and thermal sciences with a focus on finite element modeling and numerical simulations in a wide range of thermal applications. Recently:
- Active leader and team member on projects developing advanced strategies for full-system safety analyses of weapons subjected to abnormal thermal environments
- Principal investigator for Advanced QMU Methods project developing improved methods for quantifying uncertainty in complex weapons safety analyses
- Co-developed and taught Sandia in-house course: "Finite Element Method for Heat Transfer Problems"
- Previous Chair of the ASME Heat Transfer Division

SPECIALIZATION/EXPERTISE

- Heat Transfer and Thermal Sciences
- Numerical Modeling and Simulation
- Full-system Safety Analyses of Nuclear Weapons in Abnormal Thermal Environments

EDUCATION

- Ph.D. Mechanical Engineering, Texas A&M University, College Station, TX
- M.S. Mechanical Engineering, Louisiana Tech University, Ruston, LA
- B.S. Mechanical Engineering, Louisiana Tech University, Ruston, LA

LEIGH, CHRISTI

CURRENT POSITION

General Technical Manager, Repository Performance Department

PERTINENT PROFESSIONAL EXPERIENCE

- 33 years of experience at Sandia in nuclear reactor safety and radioactive waste disposal
- Performed a decision analysis to address the issue of hydrogen gas build up in transportation containers.
- Wrote the first mixed waste inventory report and the mixed waste treatment report for Congress
- Developed the screening analysis used to determine the radionuclides to track in performance assessment for Yucca Mountain
- Performed analysis of MgO emplacement strategies that supported WIPP's emplacement of compacted waste from INEEL.

SPECIALIZATION/EXPERTISE

- Fate and transport of contaminant materials
- Geochemistry of brine systems
- Systems Analysis, Decision Analysis, Performance Assessment

EDUCATION

- Ph.D. Chemical Engineering, University of New Mexico, Albuquerque, NM
- M.S. Chemical Engineering, Stanford University, Palo Alto, CA
- B.S. Chemical Engineering, Arizona State University, Tempe AZ

**ATTACHMENT 2. WASTE ISOLATION PILOT PLANT (WIPP) FEBRUARY 14, 2014 EVENT
TECHNICAL ASSESSMENT TEAM (TAT) CHARTER**

Waste Isolation Pilot Plant (WIPP) February 14, 2014 Event Technical Assessment Team (TAT) Charter

Background

On February 14, 2014, an event at the Waste Isolation Pilot Plant (WIPP) resulted in the release of radioactive material. It is essential that the Department's response to the event be safe, scientifically sound, and conducted with a sense of urgency.

In accordance with the requirements of DOE Order 225.1B, *Accident Investigations*, an Accident Investigation Board (AIB) was appointed on March 4, 2014, to investigate the radiological event.^{aaa} The scope of the AIB's investigation includes but is not limited to "identifying all relevant facts, determining direct, contributing, and root causes of the event, developing conclusions, and determining judgments of need to prevent recurrence. The scope of the investigation is to include DOE programs and oversight activities."^{bbb}

The AIB's Phase 1 Investigation Report concluded that the direct cause of the event was the "breach of at least one transuranic (TRU) waste container in the underground which resulted in airborne radioactivity escaping to the environment downstream of the HEPA filters."^{ccc} The Phase 1 Investigation Report noted that "the exact mechanism of container failure . . . is unknown at this time and must be determined once access to the underground is restored. This will be investigated in Phase 2."^{ddd}

Charter

DOE is establishing a Technical Assessment Team (TAT) to complement the AIB investigation, to aid in a comprehensive technical review of the mechanism(s) and chemical reactions that resulted in the release of radioactivity, and to plan and conduct a sampling, analysis, and assessment process to determine the causal mechanism(s) and chemical reactions that resulted in the waste container failure and release of radioactive material. The TAT will draw upon the technical and scientific capabilities of the Savannah River National Laboratory, the Pacific Northwest National Laboratory, the Sandia National Laboratories, the Oak Ridge National Laboratory, and the Lawrence Livermore National Laboratory.

To achieve the most technically definitive analysis of samples and materials collected at WIPP and elsewhere, as well as characterization and assessment of the WIPP release event, the TAT will plan and execute its work using accepted forensic science and analytical chemistry, including traceability, quality control and assurance, and peer review. The TAT will operate in recognition that its actions, findings, and conclusions will be considered by the AIB as part of its investigation, thoroughly documenting the collection, analysis, and maintenance of the sampled materials.

The activities of the TAT will be coordinated, as appropriate, with the ongoing investigative efforts of the Carlsbad Field Office and the Los Alamos Field Office.

^{aaa} An Accident Investigation Board was appointed by Matthew Moury, Deputy Assistant Secretary, Safety, Security, and Quality Programs, U.S. Department of Energy (DOE) Office of Environmental Management (EM) on February 27, 2014, to investigate the airborne release of radioactive material from the underground at the WIPP on February 14, 2014. The appointment letter was revised on March 4, 2014.

^{bbb} Memorandum from Matthew Moury, Deputy Assistant Secretary for Safety, Security, and Quality Programs, U.S. Department of Energy (DOE) Office of Environmental Management (EM), to Theodore A. Wyka, Board Chairperson, Chief Nuclear Safety Advisor, entitled "Radiological Incident into the February 14, 2014 Event at the Waste Isolation Pilot Plant" (March 4, 2014).

^{ccc} Phase 1 Accident Investigation Report Radiological Release Event at the Waste Isolation Pilot Plant on February 14, 2014 (April 2014), at ES-6.

^{ddd} Id.

Scope of Activities and Description of Duties

The TAT will develop a structured, well-planned program of sample identification and collection, data analysis, and interpretation/evaluation. Specifically, the TAT will assess the potential causal mechanism(s) and will use this assessment to identify high priority analysis targets to guide the development of the sampling and analysis plan. The TAT will also develop and execute the plan for the analysis and management of materials from the WIPP site and elsewhere, ensuring the traceability and reliability of all work performed.

To ensure the integrity of laboratory analyses, all laboratory work will meet standards set by the forensic laboratory community. Specifically, laboratories conducting analyses of materials recovered from WIPP will demonstrate the following:

- Appropriate facilities for materials receipt, processing, analysis and, as appropriate, archival.
- Robust quality control/quality assurance program.
- Analytical staff with documented training and demonstrated competencies.
- Process management and documentation by a scientist with experience to interpret the analytical results.
- Administrative and technical peer review prior to finalization of any report.

The TAT will provide the level of rigor and credibility that is appropriate to assess the potential causal mechanism(s) and will contribute to the technical basis needed to develop and implement a WIPP recovery plan.

Membership and Organization

The TAT will be chaired by Savannah River National Laboratory and will be comprised of TAT members representing the Savannah River National Laboratory, the Pacific Northwest National Laboratory, the Sandia National Laboratories, the Oak Ridge National Laboratory, and the Lawrence Livermore National Laboratory. The TAT may employ consultants as needed. The TAT chairperson will be responsible for assigning and coordinating tasks in order to take full advantage of the inter-laboratory team capabilities and expertise. The TAT chairperson will coordinate with the AIB Chair and report to the Deputy Under Secretary for Management and Performance. The Deputy Under Secretary for Science and Energy will serve as the Technical Task Monitor of the TAT.

Coordination and Reporting

The TAT will establish an agreement with Los Alamos National Laboratory defining areas of responsibility and authority. The TAT will have independent authority to plan and execute the analysis of samples it receives from WIPP and elsewhere.

The TAT will provide the Deputy Under Secretary for Management and Performance, the Deputy Under Secretary for Science and Energy, and the Deputy Under Secretary for National Nuclear regular progress updates and a final report. The TAT will coordinate its efforts with the AIB and provide its final report to the AIB. The TAT will focus on timely completion of its work and reporting of results, with the goal of providing meaningful results before the end of this fiscal year. As with any investigation, testing of the hypotheses and analysis of processes may not lead to a definitive conclusion, however, eliminating hypotheses and processes from further consideration can be equally important for informing decisions about future WIPP operations.

**ATTACHMENT 3. WASTE ISOLATION PILOT PLANT EVENT TECHNICAL ASSESSMENT TEAM
PROJECT PLAN**



Waste Isolation Pilot Plant Event Technical Assessment Team Project Plan

David L. Wilson

July 2014

DRAFT 2014-08-04

SRNL-RP-2014-00775

Revision 0



DISCLAIMER

This work was prepared under an agreement with and funded by the U.S. Government. Neither the U.S. Government or its employees, nor any of its contractors, subcontractors or their employees, makes any express or implied:

4. warranty or assumes any legal liability for the accuracy, completeness, or for the use or results of such use of any information, product, or process disclosed; or
5. representation that such use or results of such use would not infringe privately owned rights; or
6. endorsement or recommendation of any specifically identified commercial product, process, or service.

Any views and opinions of authors expressed in this work do not necessarily state or reflect those of the United States Government, or its contractors, or subcontractors.

Printed in the United States of America

**Prepared for
U.S. Department of Energy**

Keywords: TRU, transuranic, drum,
WIPP, Waste Isolation Pilot Plant

Retention: *Permanent*

Waste Isolation Pilot Plant Event Technical Assessment Team Project Plan

David L. Wilson

June 2014

APPROVALS

AUTHORS

David L. Wilson Date
Savannah River National Laboratory

Bradley R. Hart Date
Lawrence Livermore National Laboratory

Michael L. Baker Date
Oak Ridge National Laboratory

Jon M. Schwantes Date
Pacific Northwest National Laboratory

Paul E. Shoemaker Date
Sandia National Laboratories

REVIEWER

Michael Knotek, Deputy Under Secretary for Science and Energy Date
United States Department of Energy

APPROVAL

Terry A. Michalske, Director Date
Savannah River National Laboratory

David Klaus, Deputy Under Secretary for Management and Performance Date
United States Department of Energy

TABLE OF CONTENTS

<u>LIST OF ABBREVIATIONS</u>	266
<u>1.0 INTRODUCTION</u>	267
<u>2.0 APPROACH</u>	268
<u>2.1 WIPP TAT ORGANIZATION, ROLES AND RESPONSIBILITIES</u>	269
<u>2.1.1 WIPP TAT ORGANIZATION</u>	269
<u>2.1.2 WIPP TAT ROLES AND RESPONSIBILITIES</u>	270
<u>3.0 PRIMARY TECHNICAL ASSESSMENT AREAS</u>	270
<u>3.1 SITE ASSESSMENT AND SAMPLING (WBS 2.0)</u>	270
<u>3.2 ANALYSIS AND CHARACTERIZATION (WBS 3.0)</u>	270
<u>3.3 TRU DRUM PROCESSES AND PRACTICES (WBS 4.0)</u>	271
<u>3.4 MECHANISM, HYPOTHESIS, AND TECHNICAL INTEGRATION (WBS 5.0)</u>	271
<u>3.5 PROJECT INTEGRATION AND COMMUNICATION (WBS 1.0)</u>	271
<u>3.6 TAT LOGIC FLOW</u>	272
<u>4.0 COMMUNICATION AND COORDINATION</u>	272
<u>5.0 SCHEDULE AND SPEND PLAN</u>	272
<u>6.0 REFERENCES</u>	272
<u>ATTACHMENT 1: WIPP TAT Leaders and Qualification Summaries</u>	273
<u>ATTACHMENT 2: TAT Scope Overview by Laboratory</u>	276

LIST OF ABBREVIATIONS

AIB	Accident Investigation Board
CBFO	Carlsbad Field Office
DOE	Department of Energy
EM	Office of Environmental Management
LASO	Los Alamos Field Office
LANL	Los Alamos National Laboratory
LLNL	Lawrence Livermore National Laboratory
ORNL	Oak Ridge National Laboratory
PNNL	Pacific Northwest National Laboratory
SNL	Sandia National Laboratories
SRNL	Savannah River National Laboratory
TAA	Technical Assessment Area
TAT	Technical Assessment Team
TRU	Transuranic
SRNS	Savannah River Nuclear Solutions, LLC.
WIPP	Waste Isolation Pilot Plant

1.0 INTRODUCTION

On Friday, February 14, 2014, an incident in the underground repository at the Department of Energy (DOE) Waste Isolation Pilot Plant (WIPP) near Carlsbad, New Mexico resulted in the release of radioactive material from at least one transuranic (TRU) waste container into the environment. WIPP is a deep geologic repository, mined out of a thick bed of salt, for the disposal of TRU waste generated primarily from the clean-up of DOE sites. No personnel were determined to have received external contamination; however, twenty-one individuals were identified through bioassay to have low level amounts of internal contamination, and trace amounts of radioactive material were detected off-site following the incident.

On February 27, 2014, the Deputy Assistant Secretary for Safety, Security, and Quality Programs, DOE Office of Environmental Management (EM), formally appointed an Accident Investigation Board (AIB) to investigate the radiological release in accordance with DOE Order 225.1B, *Accident Investigations*.

The radiological event at WIPP presents significant technical and mission challenges for DOE. It is essential that the Department's response to the event be safe, scientifically sound, and conducted with a sense of urgency. On May 27, 2014, DOE established this Technical Assessment Team (TAT) to aid in a comprehensive technical review of the event.

DOE established the TAT to plan and conduct analyses and assessments to determine the mechanism(s) and chemical reactions that resulted in the drum failure and release of material in WIPP. The TAT's efforts will provide technical underpinning to the Department's determinations regarding the WIPP radiological event. The TAT will draw upon the technical and scientific expertise of the Department's national laboratories to form its core leadership team (Savannah River, Pacific Northwest, Sandia, Oak Ridge, and Lawrence Livermore National Laboratories).

The TAT will have independent authority to direct activities within its charter. The TAT's efforts will support and be effectively coordinated with the ongoing efforts of the DOE AIB. The TAT will report directly to the DOE Deputy Under Secretary for Management and Performance. The Deputy Under Secretary for Science and Energy will serve as the Technical Task Monitor of the TAT.

2.0 APPROACH

Actions taken at the outset of any investigation will directly influence the investigation's outcome. The disciplined application of well-vetted methods is essential to ensure that probative materials are properly documented, collected, and maintained and analyzed. Maintaining the integrity of these materials is essential if valid and defensible interpretations are to be made from subsequent laboratory analyses. Effective integration with ongoing WIPP site assessment efforts and the AIB will be a priority.

The TAT core leadership team will be comprised of representatives nominated by SRNL, SNL, ORNL, LLNL and PNNL. The team will draw upon the technical and scientific expertise of the Department's national laboratories, and other sources outside the Department, as required to complete its charter.

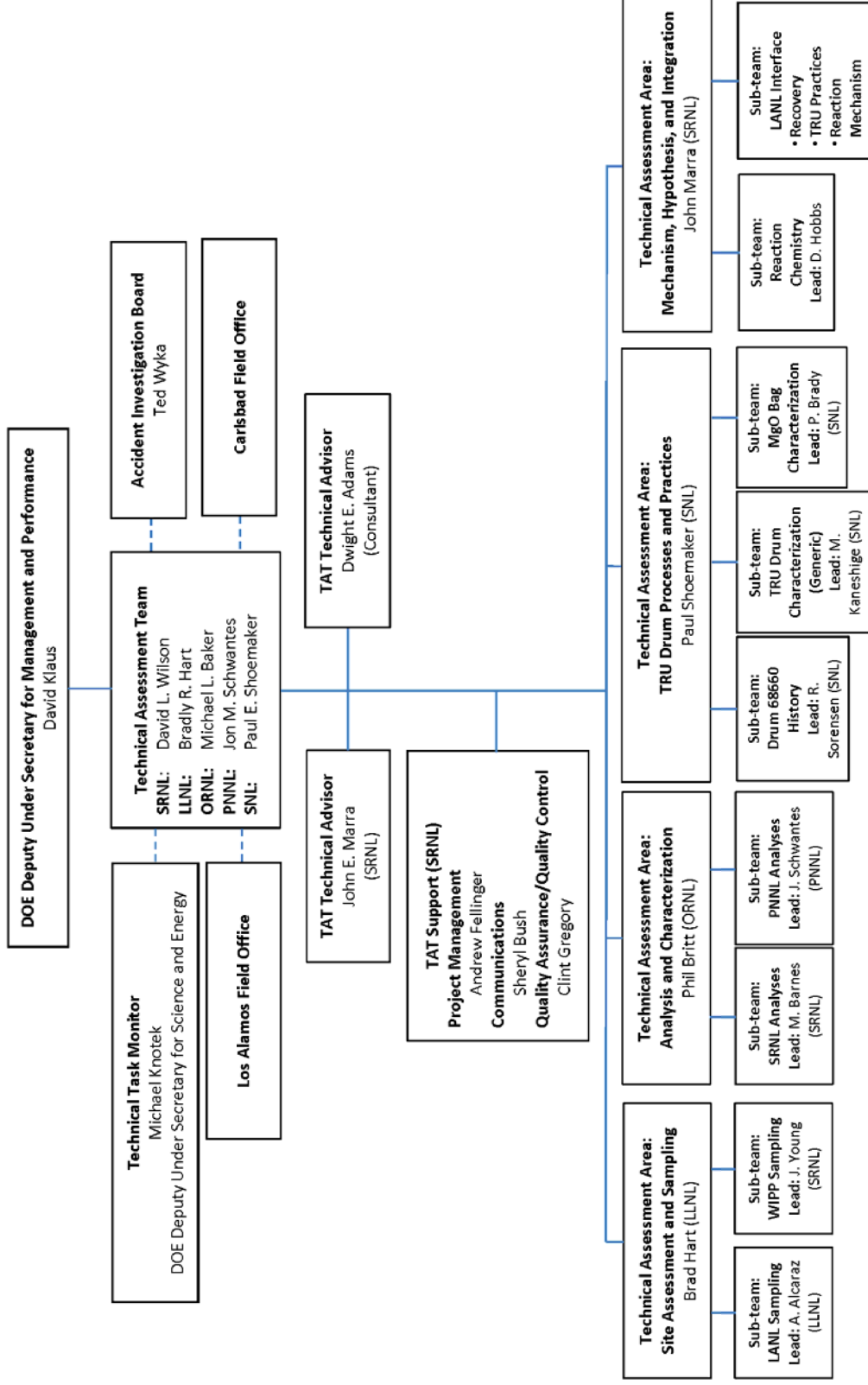
The TAT will identify discovery, sampling, analytical, and experimental objectives required to provide information and data sufficient to make assessments of the mechanism(s) and chemistry that resulted in the WIPP release event. Hypotheses and lines of inquiry will be developed to guide the TAT's efforts, and the TAT will organize itself based on those lines of inquiry.

To achieve the most technically definitive and defensible analysis of samples and materials collected at WIPP and elsewhere, as well as characterization and assessment of the WIPP release event, the TAT will plan and execute its work using accepted principles of forensic science and analytical chemistry, including traceability, quality control and assurance, and peer review. The TAT's National Laboratory team approach will provide the level of technical rigor and credibility that the Department will need to assess the event.

The TAT is mindful of implications of the WIPP release and the urgency associated with gaining an understanding of the event. The TAT will focus on timely completion of its work and reporting of results, with the goal of providing meaningful results by the end of fiscal year 2014. It is understood that TAT findings may lead to further exploration of waste handling processes and waste acceptance recommendations for placement in WIPP. As with any investigation, testing of the hypotheses and analysis of processes may not lead to a definitive conclusion with a direct effect on the outcome of the broader investigation; however, eliminating hypotheses and processes from further consideration can be equally important for informing decisions about future WIPP operations.

2.1 WIPP TAT ORGANIZATION, ROLES AND RESPONSIBILITIES

2.1.1 WIPP TAT ORGANIZATION



Key:
 ----- Dotted Line=Coordination
 _____ Solid Line=Reporting

2.1.2 WIPP TAT ROLES AND RESPONSIBILITIES

1. Technical Assessment Team

The TAT is responsible for overall management and direction of TAT activities, including organization, tasks, budget, communication and interface with DOE Headquarters and WIPP stakeholders.

2. Technical Assessment Area (TAA) Leads

The responsibility of each TAT Technical Assessment Area Lead is to develop work plans in collaboration with the sub-team leads in the TAA, coordinate and oversee the work of the sub-teams in the TAA, integrate and reconcile the outputs of the sub-teams, and provide integrated reports to the Technical Assessment Team leadership.

3. TAA Sub-team Leads

The responsibility of each TAA sub-team lead is to manage the work plans, schedules, assignments, performance, and integrated reporting of sub-team results to the TAA lead.

Attachment 1 contains a list of WIPP TAT leaders and summaries of their qualifications.

3.0 PRIMARY TECHNICAL ASSESSMENT AREAS

3.1 SITE ASSESSMENT AND SAMPLING (WBS 2.0)

The TAT will perform site assessments of affected locations and develop and direct strategies for sample identification, collection and preservation. Lawrence Livermore National Laboratory will take the lead in this Technical Assessment Area (TAA). Two sub-teams will focus on sample collection from the following sample collection locations.

- Waste Isolation Pilot Plant (WIPP) Sampling
- LANL Sampling as well as sampling elsewhere as required, including Waste Control Specialists (WCS) in Andrews, Texas.

The scope of the Assessment and Sampling TAA includes:

- developing guidance for sampling at WIPP
- developing guidance for sampling at LANL, WCS and elsewhere as required
- coordinating with AIB, LANL and the Project Reach Team to execute sampling
- coordinating with the Analysis and Characterization TAA for in-mine characterization and development of sample handling and management requirements.

3.2 ANALYSIS AND CHARACTERIZATION (WBS 3.0)

The TAT will draw upon national laboratory expertise and experience to develop and implement a strategy for sample characterization, analysis, and interpretation to provide data to the Mechanism, Hypothesis, and Technical Integration TAA (see 3.4 below). The Oak Ridge National Laboratory will take the lead in the Analysis and Characterization TAA.

The scope of the Analysis and Characterization TAA encompasses

- developing and executing a plan for the analysis and management of materials from the WIPP site, and potentially other sites, ensuring the traceability, quality and reliability of all work performed
- assessing potential causal mechanisms and using those assessments to identify high priority analysis targets to guide the development of sampling plans
- producing objective and scientifically defensible interpretation of data garnered from analyses performed within the scope of this effort.

Sub-teams in this TAA will

- coordinate with the Site Assessment and Sampling TAA for in-mine characterization and development of sample handling and management requirements
- develop and implement sample handling and management procedures.
- develop analytical plans, coordinate directed analyses at selected laboratories, and produce peer-reviewed reports to TAT Leadership
- develop and implement analytical quality assurance requirements that ensure the integrity, quality and defensibility of laboratory analyses.

3.3 TRU DRUM PROCESSES AND PRACTICES (WBS 4.0)

Sandia National Laboratories will take the lead in the TRU Drum Processes and Practices TAA. The TAA will assemble relevant information and familiarize the TAT with the waste form processes history and materials related to containers in WIPP, LANL and Texas.

Three sub-teams will conduct work in this TAA:

- The Drum 68660 History sub-team will focus on the life-cycle of the drum emplaced in WIPP for which there is definite visual evidence of a breach, including delineation of its origin, contents, packaging, shipment and handling, ambient conditions experienced, and life span.
- The TRU Drum Characterization sub-team will focus on questions to be answered about generic TRU waste drums, such as what pressures (or pressure histories, i.e., quasi-static, rapid pressurization, or blast) could cause the observed drum failure. The answers may help determine what type of event was responsible, e.g., a slow generation of gases (possibly at low temperature), thermal runaway, smoldering reaction, combustion reaction. The answers also may help describe what kind of precursor might be observed before another event.
- The MgO Bag Characterization sub-team will investigate aspects of the bags that contain magnesium oxide (MgO) in the WIPP underground, many of which emplaced in Room 7 of Panel 7 have been disrupted. Question to be answered here may include what mechanisms are capable of making the MgO bags disintegrate (i.e., match the observations; what temperatures, chemicals, or other exposures could cause significant weakening; and how much weakening is necessary for a bag to fail. The answers may help explain whether one drum could be responsible for the observed failures or whether multiple drums must have been involved and how (i.e., through heat generation only, or generation of hot gases, or certain chemicals).

3.4 MECHANISM, HYPOTHESIS, AND TECHNICAL INTEGRATION (WBS 5.0)

Savannah River National Laboratory will lead the Mechanism, Hypothesis, and Technical Integration TAA. Sub-teams in this TAA will evaluate potential reaction mechanisms and chemistry that could explain the WIPP release and associated observations; use available data and analyses from other TAAs to determine whether the WIPP event was due to a single drum (Drum 68660) failure or whether additional drums were involved; and present options to guide future inspection, sampling, and analysis programs to prove or disprove postulated reactions.

3.5 PROJECT INTEGRATION AND COMMUNICATION (WBS 1.0)

The TAT will be organized and led in accordance with the structure depicted in 2.1.1 above. Technical and project reporting protocols will be established and implemented to maintain the integrity of the TAT's efforts and conclusions. The Savannah River National Laboratory will be responsible for the overall coordination and direction of TAT activities, management of tasks and budget, and communication and interface with headquarters and WIPP stakeholders.

3.6 TAT LOGIC FLOW

The TAT will develop a process flow chart depicting its efforts and decision points. This document will be maintained separately and updated as work progresses

4.0 COMMUNICATION AND COORDINATION

The Savannah River National Laboratory is responsible for the overall coordination and direction of TAT activities, including communication and interface with headquarters and WIPP stakeholders.

The TAT has aligned and integrated its efforts with those of the DOE Accident Investigation Board (AIB). AIB representatives have membership on TAT sub-teams, and directly support TAT planning and work execution.

The TAT has established an agreement with LANL defining areas of responsibility and authority.

The TAT will provide regular progress updates and a final report to the Deputy Under Secretary for Management and Performance, and the TAT will coordinate reported information with the DOE AIB.

5.0 SCHEDULE AND SPEND PLAN

The efforts of the TAT are in large part exploratory. Modifications to tasks and work scopes will certainly be required to address the operational and analytical challenges presented by the WIPP release event. Despite this uncertainty, the TAT has established the goal of providing initial findings by the end of the fiscal year.

Initial funding of \$935K has been allocated for TAT efforts in June 2014. Additional funding is being identified to continue work. See Attachment 2: Initial TAT Scope by National Laboratory.

Funding estimates by laboratory supporting work through FY14 will continue to be refined based on TAT operational priorities and requirements.

Details of WIPP TAT project management are maintained separately.

6.0 REFERENCES

U.S. Department of Energy Office of Environmental Management. *Accident Investigation Report: Phase 1 Radiological Release Event at the Waste Isolation Pilot Plant on February 14, 2014*. April 2014.

Morton, A. S., DOE-SR, to Temple, J. W., SRNS. *Management and Operating Contract DE-AC09-08SR22470: Waste Isolation Pilot Plant (WIPP) Event Technical Assessment Team*. Enclosure 1: "Team Introduction." May 27, 2014.

ATTACHMENT 1: WIPP TAT LEADERS AND QUALIFICATION SUMMARIES

TECHNICAL ASSESSMENT TEAM

David L. Wilson

Associate Laboratory Director, National Security Directorate
Savannah River National Laboratory

M.S., Botany

Retired FBI Senior Executive, former Chief of the FBI's Chemical, Biological Radiological Nuclear Sciences Unit
23 years of forensics experience including nuclear forensics

Bradley R. Hart

Director, Forensic Science Center
Lawrence Livermore National Laboratory

Ph.D., Organic Chemistry

Expertise in organic chemistry and chemical forensics

Michael L. Baker

Director of Integrated Performance Management
Oak Ridge National Laboratory

M.S., Environmental Engineering; B.S., Chemical Engineering

30 years of experience leading nuclear research and development projects, managing research operations, and leading mission support organizations.

Jon M. Schwantes

Senior Research Scientist & Technical POC to the National Technical Nuclear Forensics Center
Pacific Northwest National Laboratory

Ph.D., Civil Environmental Engineering, M.S., Chemical Oceanography, B.S., Marine Sciences

+20 years' experience in Radiochemical and Analytical Laboratories

Paul E. Shoemaker

Senior Manager, Defense Waste Management Programs Group
Sandia National Laboratories

Master of Public Affairs; B.S., Physics

24+ years managing high-profile programs at Sandia, with ~7 years managing the scientific analyses and technical advice at the WIPP, Carlsbad, NM

TECHNICAL ASSESSMENT AREA LEADS

Brad Hart

Director, Forensic Science Center
Lawrence Livermore National Laboratory

Ph.D., Organic Chemistry

Expertise in organic chemistry and chemical forensics

Phil Britt

Director, Chemical Sciences Division
Oak Ridge National Laboratory

25+ years in kinetics and mechanism of organic reactions and quantitative analysis of complex organic mixtures

Paul Shoemaker

Senior Manager, Defense Waste Management Programs

Sandia National Laboratories

Master of Public Affairs; B.S., Physics

24+ years managing high-profile programs at Sandia, with ~7 years managing the scientific analyses and technical advice at the WIPP, Carlsbad, NM

John E. Marra

Associate Laboratory Director, Science & Technology Directorate

Savannah River National Laboratory

Ph.D., Materials Science

25+ years nuclear process experience including 10+ years in nuclear operations

SUB-TEAM LEADS

Armando Alcaraz

Senior Research Scientist

Lawrence Livermore National Laboratory

M.S. Analytical Chemistry

Expertise in analytical chemistry with emphasis on the forensic analysis of complex organic and environmental samples.

John Young

Advisory Scientist, Analytical Development

Savannah River National Laboratory

B.S., Chemical Engineering

30+ years nuclear process experience, FBI sampling and protocol expertise

Mark Barnes

Director, Analytical Development

Ph.D., Chemical Engineering

20+ years nuclear analytical technique development and process sampling support.

Jon M. Schwantes

Senior Research Scientist (PI)/Technical POC to the National Technical Nuclear Forensics Center

PhD Civil Environmental Engineering, MS Chemical Oceanography, BS Marine Sciences

+20 years' experience in Radiochemical and Analytical Laboratories

Dr. N. Robert Sorensen (expertise in corrosion and material compatibility issues)

Distinguished Member of Technical Staff; Sandia National Laboratories

33+ years of experience studying materials degradation phenomena and failure analyses for weapon components, satellites, and energy systems. Expertise in corrosion issues and material compatibilities.

Dr. Michael Kaneshige (expertise in thermal response of energetic materials)

Distinguished Member of Technical Staff; Sandia National Laboratories

Ph.D., Mechanical Engineering

15+ years at Sandia as expert on hazards of energetic materials with a focus on thermal ignition (thermal runaway) and response of energetic materials to abnormal thermal and mechanical environments. He is frequently sought out for consultation on accidents involving energetic materials including the 2010 BP Deepwater Horizon spill in the Gulf of Mexico.

Pat Brady

Senior Scientist

Sandia National Laboratories

Assistant Professor of Civil and Environmental Engineering at New Mexico Institute of Mining and Technology,
Socorro, New Mexico

Ph.D., Geochemistry

20+ years' experience

Expertise in geochemistry, water treatment, enhanced oil recovery, nuclear waste disposal, and climate change

David Hobbs

Senior Advisory Engineer [Scientist]

Savannah River National Laboratory

Ph.D., Chemistry

30+ years' experience.

Expertise in actinide science and nuclear separations.

ATTACHMENT 2: TAT SCOPE OVERVIEW BY LABORATORY

SAVANNAH RIVER NATIONAL LABORATORY

- Provider senior-level TAT leadership and project support, including the services of an independent consultant.
- Lead the development of hypotheses for potential mechanisms and reactions.
- Lead development of methods to ensure that samples are thoroughly documented, collected appropriately, and properly maintained.
- Develop sampling plans and provide on-site leadership at WIPP, LANL for sample collection.
- Support development of enhanced sampling and WIPP site characterization capabilities.
- Develop transport model for WIPP Panel-7 to assess source term concentrations
- Develop and oversee the execution of a TAT Analytical Quality Plan.
- Triage, store and distribute samples for TAT analyses.
- Conduct analysis of WIPP samples as required, provide analysis reports, help generate SOPs for specific WIPP operations and review TAT documents.
- Oversee the technical peer review of reports.
- Travel to TAT meetings as required.

LAWRENCE LIVERMORE NATIONAL LABORATORY

- Lead the Site Assessment and Sampling TAA
- Provide evaluations of methods that are essential to ensure that samples are thoroughly documented, collected appropriately, and properly maintained.
- Support development of hypotheses for potential mechanisms and reactions.
- Conduct analysis of WIPP samples, provide analysis reports as required.
- WIPP and LANL collection operations and sample documentation and management
- Support technical and peer review of plans and reports
- Travel to TAT meetings to review and discuss assessment plans.

OAK RIDGE NATIONAL LABORATORY

- Lead the Analysis and Characterization TAA and coordinate activities with other TAAs
- Provide evaluations of analytical and quality plans
- Help generate SOPs for specific WIPP operations and review TAT documents
- Provide analytical services if required based on analytical plans
- Support in the technical peer review of reports
- Travel to TAT and TAT sub-team meetings as required
- Provide support to the TRU Drum Process and Practices TAA and the Mechanism, Hypothesis and Technical Integration TAA

PACIFIC NORTHWEST NATIONAL LABORATORY

- Lead the Analysis Sub-Team
- Provide evaluations of quality plans and analytical from other laboratories..
- Develop and execute an analytical plan for initial samples collected from WIPP
- Support development of hypotheses for potential mechanisms and reactions.
- Support the technical peer review of reports
- Travel to TAT meetings to review and discuss assessment plans.

SANDIA NATIONAL LABORATORY

- Lead the TRU Drum Processes and Practices TAA
- Develop testing matrix for contents of breached drum and surrounding MgO.
- Support development of sample requirements
- Support development of hypotheses for potential mechanisms and reactions.

- Provide evaluations of analytical and quality plans.
- Support determination of laboratories where the specified analyses can best be performed.
- Provide modeling of 68660-like 55-gallon, filtered drum structural mechanics to simulate drum integrity and behavior when subjected to adverse thermal and pressure environments.
- Support characterization of the source term required to result in HEPA filter contamination.
- Lead investigation into TRU drum process history
- Travel to TAT meetings as required.